Synthesis, characterisation, process simulation and multiobjective optimisation of biomass-derived renewable polyesters: An integrative study toward a sustainable polymer industry

Thesis submitted in accordance with the requirements of the University of Liverpool for the degree of Doctor in Philosophy

by

Mónica Lomelí Rodríguez

August 2017

“Love the animals, love the plants, love everything.
If you love everything, you will perceive the divine
mystery in things. Once you perceive it, you will begin
to comprehend it every day. And you will come at last
to love the whole world with an all-embracing love.”

-Fyodor Dostoevsky

“Every experience has its elements of magic.”

- Hermann Hesse

“Cualquier destino, por largo y complicado que sea,
consta en realidad de un sólo momento: el momento
en que el hombre sabe para siempre quién es.”

- Jorge Luis Borges

Acknowledgements

This long and winding road would have been impossible without the support of many people throughout it. I want to firstly thank my supervisor Professor Tony López-Sánchez, for always trusting and supporting me since day one, mentoring me and allowing me to pursue different projects within my PhD. To my supervisor at Universidad Iberoamericana Ciudad de México, Dr. Martín Rivera-Toledo, I have admired you since my undergraduate years that it has been an honour to be taken under your wing and to work with you in the process simulation and optimisation work of my PhD. Thank you very much! To the Postdocs in Tony's group: Dr. Thomas Davies, thank you so much for your unconditional support, time, guidance and all our nice chats. Dr. Annarita Noschese, thanks a lot for your help during the last period of my PhD, your friendship and always making me laugh. Dr. Solène Cauët, thank you for teaching me NMR. I am very grateful to all of you.

To the very nice and lovely people from Becker Industrial Coatings Ltd, who taught me everything I know about polyester processing, and allowed to me to use their facilities throughout all my PhD. Dr. Chris Lowe, Dr. Omer Erdemli, Rob Mulholland and Cian Bartlam, thank you so much for every single day you helped me. Special thanks to my co-supervisor Sue Willis, you have been an incredible mentor, I've learnt a lot from you more than I can tell and have always been there for me and interested in my work.

My beloved students, without you this would have never become a reality. Maria Jiménez, my dear girl, you started with me since the very beginning and gave me strength and confidence to carry on, thank you for learning by my side and not panicking! Miguel Martín, thank you so much for your scientific curiosity, leadership, commitment and hard work. Zahara Nasim, thanks for trusting me in supporting you to deliver your project and being such a nice student. Clément Gueret, dear boy, your work was so valuable as it was so new and great, thanks a lot! Raúl Corpas, you performed the most unpredictable reactions, you did it amazingly, and your sweetness made my days better! I love and miss you guys and will always be in my heart. Thank you as well for the uncountable number of samples taken every half an hour! All of you shaped this project and committed to it as your own.

To my family: Mum and Dad, Maocita and Papito, you have given to me everything in this world: Honesty, hard work, integrity, courage, passion, humbleness. I love you with all my heart and will always try to emulate you as the amazing human beings you are. Papito, you are the best chemical engineer ever, and you are the most integral person I've ever met. You are the person I admire the most. Maocita, you are simple the most incredible woman that could inhabit this world. Your intelligence and big heart make the perfect combination. I owe you what I am. Marthi, hermanito, my sister and best friend, you know you mean everything to me and I love you till the stars fall down from the sky. You are one of a kind. Two of us forever and ever! Skelter, my cute and soft bunny, your mere existence has brought me joy and happiness, my sweet fluffy love.

To Victor Juarez: You are the love of my life and I'd have gone mad without having you with me. You embraced my PhD and your love, patience, understanding and support were my pillars. Sorry for being a pain some days. You are my very best and we make the greatest team ever!

To all JALS research group, wish you guys all the best in your future. My dear friends and also brothers, Dr. Nor Azam Endot and Ali Bashal, you mean a lot to me and you were my strength during the gloomiest days, and always trusted me and knew how to put a smile on my face. I will miss the falafel and Vine Court days. Aldo Reyes, Dr. Joel McGlone, Nadiah Mohamad Noh, and Liqaa Majdal, thanks for all those nice days. I will miss you so much! To my grandparents, cousins, uncles and aunties, along with my friends back home: All of you are part of who I am; I love you, thank you very much. To my professors at Universidad Iberoamericana: Rubén, Jorge, Grace, Lorena, Javier, Andrea, Toño, Alberto, you were fundamental to enhance my love for my career and embrace the responsibility it implies towards society. Many thanks.

Finally, thank you John, Paul, George and Ringo, for being a source of inspiration since I can remember. Thank you Liverpool, a place that certainly feels like home now.

Abstract

Global warming, climate change and pollution are the greatest challenges of the 21st century. The high-scale exploitation of traditional fossil feedstocks and an unsmart anthropogenic usage of these resources have prompted the rise of environmental, health and economic problems which are affecting every cohabitant of the planet. We must act quickly from several fronts, as individuals and professionals, to mitigate this threat.

The objective of this PhD thesis was to produce a complete research study in the field of polyesters derived from biomass feedstocks, by integrating knowledge from polymer chemistry, polymer reaction engineering and process engineering. Previous research in the area of biopolymers has been mainly focused in their synthesis and characterisation whereas the process and reaction engineering work remains scarce. A thorough systematic framework was therefore developed, which was comprised not only by the renewable polymer synthesis and characterisation, but also by kinetic modelling, simulation and optimisation tools, prompting the scale up and real application of these polymers and providing tangible and useful information to academia, polymer industry and policy makers. My intention is that this research framework could be applied to other biomass-based polymers. It is imperative to develop a sustainable, green and clean industry that will positively impact our everyday life as plastics are one of the largest sources of pollution and are present in so many different applications.

The polyesters in this thesis were constituted by the biomass-derived monomers succinic acid (SA), 2,5-furandicarboxylic acid (FDCA) and either 1,3-propanediol (PDO) or 1,5-pentanediol (PTO). Isosorbide (IS) was studied as an extra monomer to enhance the original physical properties of the base polyesters. The intended application of the polyesters is coil coatings, as the research study was done in collaboration with Becker Industrial Coatings Ltd, located in Speke, Liverpool. One of the sustainability initiatives of the company is the development of biobased resins, which prompted the analysis of different formulations and process conditions throughout the industrial partnership.

The overall approach for the research study could be divided into two sub studies; on the one hand, the experimental synthesis and characterisation and on the other hand, the kinetic modelling using the mathematical software MATLAB and subsequent process simulation and optimisation using Aspen Plus, a well-known process simulator. Firstly, the synthesis of the polyesters was performed through a two-step process which involved

esterification as the first stage and polycondensation as the second one. The process variables studied during the syntheses were the temperature (210, 220 and 230 °C) and FDCA/SA molar ratio. The later was varied between 0 and 100 mol% FDCA to provide complete polyester libraries with different molecular weights, and therefore, thermal and mechanical properties, by only varying the bio-derived diol structure and composition. The new biomass-derived polyesters were characterised by nuclear magnetic resonance (^{1}H NMR), gel permeation chromatography (GPC), differential scanning calorimetry (DSC), thermal gravimetric analysis (TGA) and common mechanical testing for paint resins, such as microhardness, impact resistance and flexibility. These physical properties are fundamental to determine the most suitable coating application. The paint characterisation methods were performed by Beckers research staff.

For the process engineering analysis, the first step is to estimate the kinetic parameters that will define the polymerisation process. We therefore carried out the modelling of the reactions by fitting three polyesterification kinetic models to our experimental data in terms of carboxylic acid concentration. The predictions of the models were obtained on ordinary differential equations (ODEs) defined by the reaction rate equations implemented in the MATLAB while the experimental data were regressed using the weighted-sum-of squares.

After the estimation of the kinetic parameters, we then proceeded with the process simulation and optimisation in Aspen Plus. The objectives were to define the best environmental, cost and performance-efficient operation conditions for the industrial production of these renewable polymers, considering different types of industrial chemical reactors, such as a batch reactor and plug flow reactor (PFR). The ε-constraint method was followed to solve the multiobjective optimisation problem, considering two objective functions that maximise the number average molecular weight M_n and simultaneously minimise the heat duty Q of the reactor. The efficient operation points are reported for each case through the construction of Pareto frontiers and the performance of the polymers was compared to that of petroderived polyethylene terephthalate (PET) in terms of sustainability indicators.

In addition to the choice of monomer and whether it is renewable, process intensification can generate great advantages in terms of energy consumption, capital cost savings and investment in equipment. The process intensification was achieved by simulating the polyesterifications in a reactive distillation column and a divided wall column.

Finally, in order to improve the thermal and mechanical properties of the base polyesters, isosorbide was incorporated in different compositions. Moreover, a brief research study about itaconic acid (IA) polyesters was conducted, which opens the possibility for developing new polymers by post-polymerisation functionalisation.

Important conclusions were obtained as a result of the systematic framework followed. The characterisation results showed that the molecular weight, glass transition temperature (T_g), microhardness and impact resistance increased as the FDCA concentration of the polyester increased. Overall, the resulting properties could be tuned accordingly by varying the processing conditions to obtain weight average molecular weights (M_w) between 1100 and 10700 Da and T_g in the range of –48 °C to 18 °C. The use of vacuum during the second stage led to an increase of M_w of about 5000-6000 Da. The properties of the finished paints are benchmarked to industrial standards. In general, the resins bearing 70 or 85 mol% FDCA had the higher molecular weights and greater mechanical performance.

The process simulation results suggested that the optimum process temperatures for the bioderived polyesters were in the range of 190 °C to 215 °C for all compositions whereas for PET was 269 °C. Interestingly, the polymerisation is not sensible to the type of reactor configuration, which allows a flexible and cost-effective operation. The results concluded that the production of biomass-derived polyesters releases less CO_2, 60% less in respect to PET. The production of PET presented the highest energy consumption and CO_2 release among all the polymers studied. Regarding the process intensification, the concept was proven as the reactive distillation was the most energy efficient configuration among all. The energy intensity for reactive distillation was decreased between 7% and 46%, compared to the conventional batch and PFR configurations.

The polyester structure modification with isosorbide led to increments in T_g from 5 °C to 40 °C. The isosorbide resins achieved the best physical properties among all the bioderived polyesters in the study, matching or enhancing those of the Becker's reference resin.

The overall results provide a good basis for the implementation of biomass-derived polymers in large scale, as they could be more environmentally friendly than petrochemical-derived ones and are therefore a strong support for industry to embrace renewable feedstocks.

TABLE OF CONTENTS

List of Figures

List of Tables

List of Schemes

List of Abbreviations and Symbols

EPA	Environmental Protection Agency
EEA	European Environmental Agency
HVLV	High-value-low-volume
LVHV	Low-value-high-volume
LCF	Lignocellulose feedstock
PLA	polylactic acid
PHA	polyhydroxyalkanoates
PBSA	poly(butylene succinate-co-adipate)
PBAT	poly(butyrate adipate-co-terephthalate)
DOE	Department of Energy
SA	succinic acid
PES	poly(ethylene succinate)
PPS	poly(propylene succinate)
PBS	poly(butylene succinate)
PPS	poly(propylene)
PET	poly(ethylene terephthalate)
FDCA	2,5-furandicarboxylic acid
HMF	5-hydroxymethyl furfural
PBT	poly(butylene terephthalate)
PBF	poly(ethylene 2,5-furandicarboxylate)
PEF	poly(ethylene 2,5-furandicarboxylate)
ROP	ring-opening polymerisation
IA	itaconic acid
PIA	poly(itaconic acid)
PDO	1,3-propanediol
PTO	1,5-pentanediol
BDO	1,4-butanediol
THFA	tetrahydrofurfuryl alcohol
FA	furfuryl alcohol
IS	Isosorbide
MWD	Molecular weight distribution
M_n	Number average molecular weight
M_w	Weight average molecular weight
Đ	Dispersity
DP_n	Degree of polymerisation
PFR	Plug-flow reactor
CSTR	Continuous stirred tank reactor
TPA	Terephthalic acid
EG	Ethylene glycol
BHET	bishydroxyethyl terephthalate
MOO	Multiobjective optimisation
PPS	poly(1,3-propylene succinate)
PPF	poly(1,3-propylene 2,5-furandicarboxylate)
PPFPS	poly(1,3-propylene 2,5-furandicarboxylic acid-co-1,3-propylene succinate)
PPeS	poly(1,5-pentylene succinate)
PPeFS	poly(1,5-pentylene 2,5-furandicarboxylate-co-1,5-pentylene succinate)

PPeFIS	poly(1,5-pentylene-2,5-furandicarboxylate)-*co*-(1,5-pentylene-succinate)-*co*-(isosorbide-2,5-furandicarboxylate)-*co*-(isosorbide-succinate)
PPeIS	poly(1,5-pentylene succinate-co-isosorbide succinate)
PPFIS	poly(1,3-propylene-2,5-furandicarboxylate)-*co*-(1,3-propylene-succinate)-*co*-(isosorbide-2,5-furandicarboxylate)-*co*-(isosorbide-succinate)
PPeSIa	poly(1,5-pentylene itaconate-co-1,5-pentylene succinate)
PPeIa	poly(1,5-pentylene itaconate)
b_0	Initial excess of the hydroxyl group concentration
n	Reaction order with respect to the diol
m	Reaction order with respect to the diacid
k	Kinetic coefficient
K	Equilibrium constant
K_{e0}	Equilibrium ionisation constant at zero conversion
k_h	Rate constant hydrolysis of ester bonds
E_a	Activation energy, $kJ \cdot mol^{-1}$
B-SA	Bound segment succinic acid
T-SA	Terminal segment succinic acid
B-FDCA	Bound segment FDCA
T-FDCA	Terminal segment FDCA
B-PTO	Bound segment 1,5-pentanediol
T-PTO	Terminal segment 1,5-pentanediol
B-PDO	Bound segment 1,3-propanediol
T-PDO	Terminal segment 1,3-propanediol
W	Water
GWP	Global warming potential, $kg \cdot kg^{-1}$
R_{SEI}	Specific energy intensity, $kBTU \cdot kg^{-1}$
RME	Reaction mass efficiency, $kg \cdot kg^{-1}$
MI	Mass intensity, $kg \cdot kg^{-1}$
RD	Reactive distillation
DW	Divided wall
BTU	British thermal unit
LCA	Life cycle analysis

List of Publications

1. Lomelí-Rodríguez, M.; Rivera-Toledo, M.; López-Sánchez, J.A., Process Intensification of the Synthesis of Biomass-Derived Renewable Polyesters: Reactive Distillation and Divided Wall Column Polyesterification. *Industrial & Engineering Chemistry Research* **2017**, 56, (11), 3017-3032.

2. Lomelí-Rodríguez, M.; Rivera-Toledo, M.; López-Sánchez, J. A., Optimum Batch-Reactor Operation for the Synthesis of Biomass-Derived Renewable Polyesters. *Industrial & Engineering Chemistry Research* **2017,** 56, (2), 549-559.

3. Lomelí-Rodríguez, M.; Martín-Molina, M.; Jiménez-Pardo, M.; Nasim-Afzal, Z.; Cauët, S. I.; Davies, T. E.; Rivera-Toledo, M.; Lopez-Sanchez, J. A., Synthesis and kinetic modeling of biomass-derived renewable polyesters. *Journal of Polymer Science Part A: Polymer Chemistry* **2016,** 54, (18), 2876-2887.

4. Ciriminna R., Lomeli-Rodriguez M., Carà P.D., Lopez-Sanchez J.A., Pagliaro M. Limonene: a versatile chemical of the bioeconomy. *Chemical Communications* **2014**, 50, (97), 15288-15296.

List of Conferences

1. **3rd International Conference on Chemical and Polymer Engineering (ICCPE'17).** Rome, Italy, June 8th-10th 2017.
   Oral Presentation
2. **STEM for Britain 2017 competition**. London, UK, March 13th 2017.
   Poster Presentation
3. **International Conference of Sustainable Bioplastics.** Alicante, Spain, November 10th-11th 2016
   Oral Presentation
4. **Macro UK RSC Young Research Meeting (YRM).** Liverpool, UK, April 5th, 2016.
   Oral Presentation

CHAPTER 1

Introduction

1. Introduction

In the following sections, an overall background of the different research fields involved in the present PhD thesis are presented, starting with biomass transformations towards platform chemicals and specifically, the monomers used throughout this study. Next, a brief overview of previous studies on polyesters based on such monomers is described, closing the current status in the area. The introduction is then complemented with general aspects of kinetics of polyesterification, chemical reactors, process simulation and optimisation. The introduction is thus aligned with the systematic framework followed herein, whose methodology is a result of the integration of polymer chemistry, modelling and process engineering tools, positioning this PhD thesis in a wider context of both fields of biomass-derived polymers, reaction and process engineering.

1.1 Biomass as a potential feedstock for fuels and chemicals

1.1.1 Background

The worldwide environmental impact of anthropogenic activity, fossil fuel usage and polluting activities has resulted in climate change being one of the greatest challenges of the 21st century.[1] This problem is further compounded by numerous phenomena such as the extreme fluctuation in oil prices, the dependence of commodity and engineering materials, global warming, fossil fuel depletion, and waste disposal.[2] Biomass arises as a sustainable and even obvious source for energy and materials that could contribute to the mitigation of greenhouse-gas emissions. According to the European Renewable Energy Directive,[3] biomass is defined as the biodegradable fraction of products and waste from agriculture, forestry, fishery and aquaculture, as well as the biodegradable fraction of industrial and municipal waste.

Biomass is carbon neutral, renewable, widely available and features a closed cycle, which means that the release of CO_2 generated in the transformation of chemicals and fuels is recaptured by plants via photosynthesis.[4] Therefore, biomass has the potential to replace fossil feedstocks as a carbon source for the production of fuels, polymers and a large variety of bulk and fine chemicals.[5] The use of renewable feedstocks has been identified as one of the principles of green chemistry, defined by the U.S. Environmental Protection Agency (EPA) as "The utilisation of starting materials that are renewable rather than depletable. The source of renewable feedstocks is often agricultural products or the wastes of other processes;

the source of depletable feedstocks is often fossil fuels such as petroleum, natural gas or coal, or mining operations."[6] The European Environmental Agency (EEA) projected in 2006 that up to 15% of the energy demand could be covered by bioenergy based on European sources by 2020.[7] In America, the U.S. Department of Energy has set goals to derive 25% of U.S. chemical commodities from biomass by 2030.[8]

It is imperative though to distinguish the type of biomass suitable for large-scale production. During the early 2000's, edible or first generation biomass, in the form of simple sugars, starch and vegetable oils, led to considerable concerns because of the food *vs.* fuel competition which brought along other issues as deforestation and threats to biodiversity as land was used to harvest corn crops for ethanol production.[4] Lignocellulosic or second generation biomass, however, which is mainly waste plant biomass, is non-edible and therefore does not face the food *vs*. fuel debate. Lignocellulosic materials incorporate agricultural residues, energy crops, wood residues and municipal paper waste.[9] Third generation biomass is derived from waste vegetable oils, microbes or microalgae.[10] Other types of biomass not falling into these categories include manure, sewage sludge and food waste.[10]

Lignocellulose is a natural polymer composed of three primary units: 40-50% cellulose, 20-40% hemicellulose and 10-30% lignin.[11] Cellulose is a crystalline polysaccharide composed of glucose units linked by β-1,4-glycosidic bonds[5] whereas hemicellulose presents an amorphous structure made of five (β-D-xylose, α-L-arabinose) and six-carbon (β-D-mannose, β-D-glucose, α-D.galactose) sugars and/or uronic acids (α-D-glucuronic, α-D-4-*O*-methylgalacturonic and α-D-galacturonic acids).[12] The recalcitrant nature of lignocellulosic biomass is given by lignin, whose cross-linked amorphous structure is synthesised by the random polymerisation of three primary phenyl propane monomers, which are bonded together through several C-O-C and C-C interunit linkages.[13] The structural units of hemicellulose and the chemical structures of cellulose, hemicellulose and lignin are shown in **Scheme 1** and **Scheme 2**, respectively.

Lignocellulosic biomass sources have become increasingly important in efforts to decrease the dependence of the chemical industry on traditional petrochemical feedstocks. **Figure 1** shows the broad range of biomass feedstocks available along with their conversion routes. The versatility of lignocellulosic biomass towards the production of value-added

chemicals and fuels creates great expectations towards a bio-based economy, and therefore, toward the industrial-scale implementation of biorefineries.

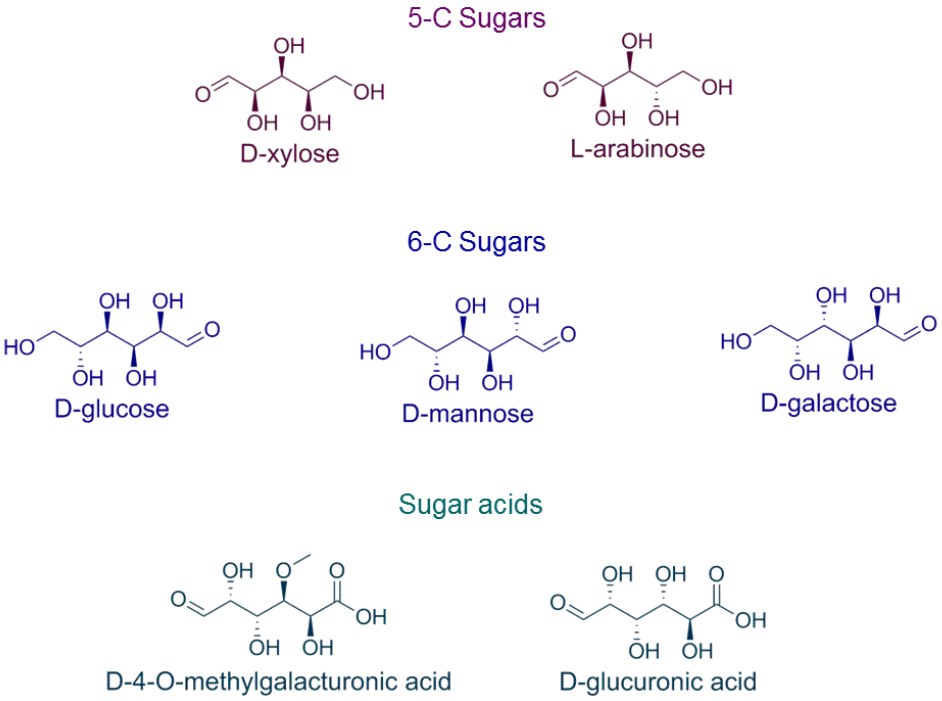

Scheme 1. Structural units of hemicellulose.

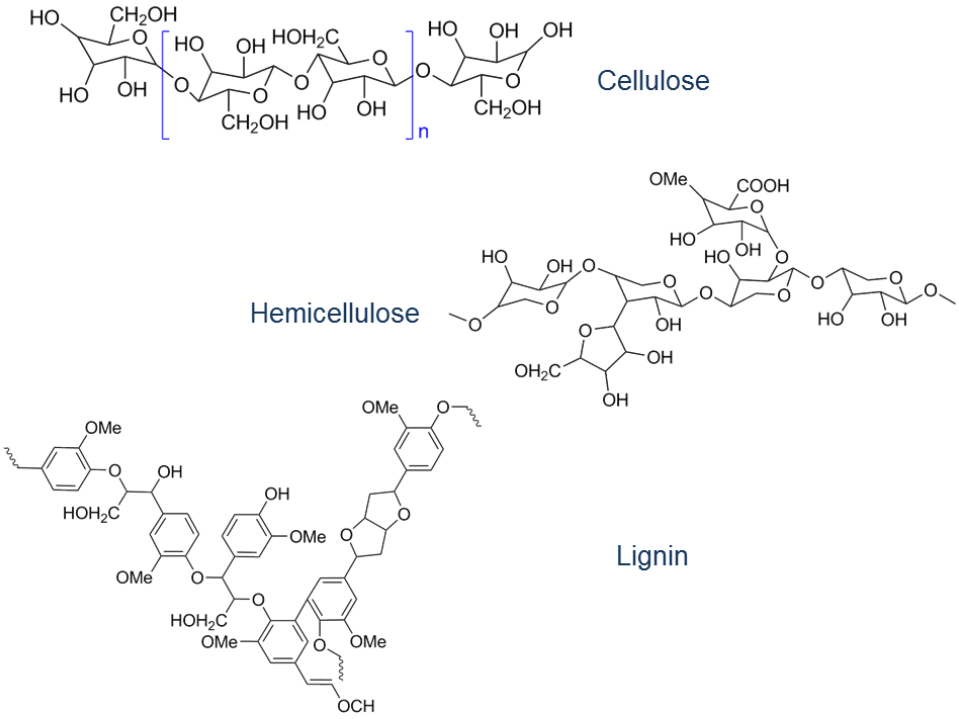

Scheme 2. Chemical structures of cellulose, hemicellulose and lignin.[5]

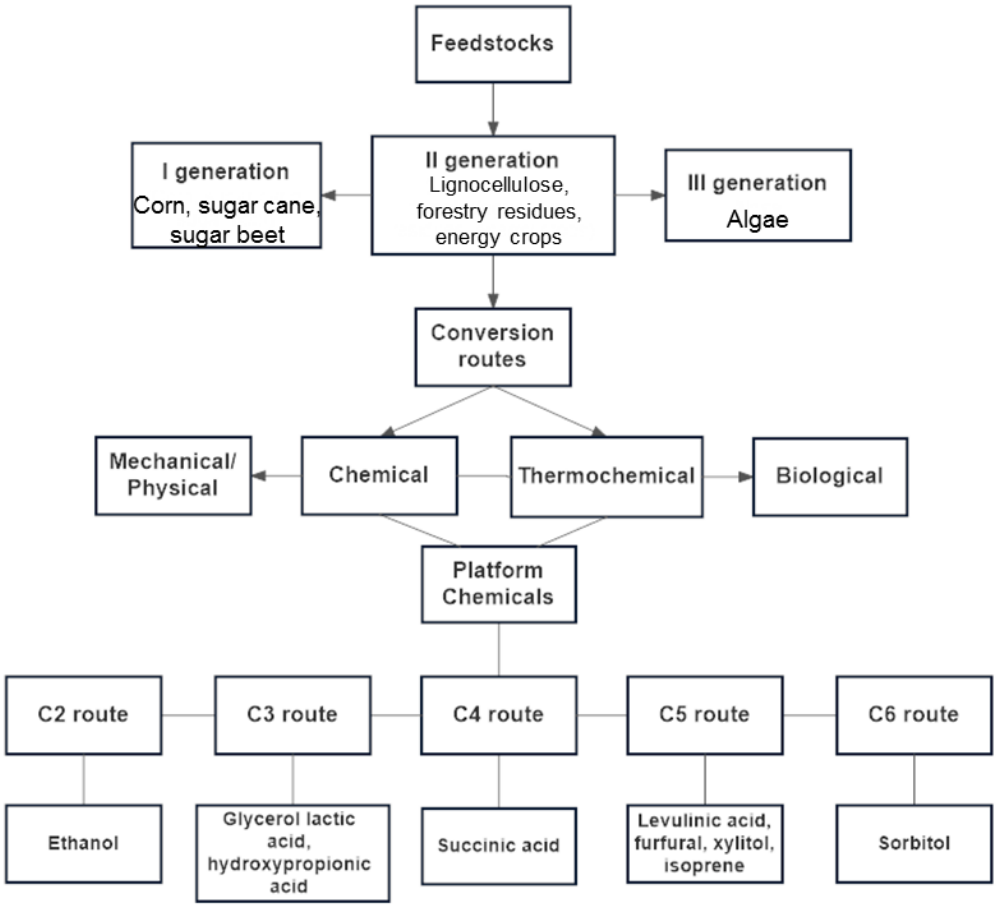

Figure 1. Biomass feedstocks and their conversion processes, adapted and modified from Fiorentino, et al.[5]

1.1.2 The Biorefinery Concept

Biorefinery describes a network of integrated bioconversion processes of biomass to value-added products. The concept was advocated by the International Energy Agency in analogy to the petroleum-based refinery concept.[14] In the modern biorefinery, polysaccharides and lignin enter the biorefinery and are fractioned and converted into transportation fuels, chemicals and direct energy.[15] Biomass is converted to fuels by pyrolysis and gasification, whereas the transformation to platform molecules and chemical building blocks is achieved through fermentation or chemo-catalytic routes, preferably by using one-pot syntheses with novel and green heterogeneous catalysts which decrease the number of required reaction steps.[16] **Section 1.3** focuses on the most important bioderived chemicals that are or could potentially be used as monomers for polymer synthesis.

A lignocellulosic biorefinery scheme is shown in **Figure 2**.[17] The main goal of a biorefinery is to produce the right portfolio of high-value-low-volume (HVLV) and low-

value-high-volume (LVHV) products.[18] Both of them are indispensable for the technology and processes to succeed as profitability is enhanced by the HVLV products while the LVHV help to meet the global energy demands.[18] Kamm, et al.[19] and Van Dyne, et al.[20] described three different types of biorefineries:

- Phase I biorefinery: This early type of biorefinery uses grains as feedstock and has fixed processing capabilities; therefore process flexibility is disregarded. The typical example is dry ethanol milling technology, as it converts grains to ethanol, carbon dioxide and feed coproducts.
- Phase II biorefinery: In this plant, process flexibility is allowed so the production is aligned to market demands.[18] A wet milling process is a phase II biorefinery example as it is able to produce a range of products such as starch, high fructose corn syrup, ethanol, and corn oil. Phase II biorefineries facilitate the connection of industrial production lines to existing agricultural production units. An example of this approach is the integrated production of biodegradable bioplastics.[19]
- Phase III biorefinery: Phase III represents the most advanced biorefinery and is currently under research and development. This biorefinery can use varied biomass feedstocks and processing methods to produce a mix of higher value chemicals for the industrial market place.[20] Examples of this phase are whole-crop, green and lignocellulose feedstock (LCF) biorefineries.[18] Efforts are being made towards the development of successful LCF biorefineries. This is because of the variety of raw materials that could be processed (straw, reed, grass, wood, and paper waste) and also, the conversion products have a good position with both the petrochemical and biobased product markets.[19] Lignocellulosic biomass has higher amount of oxygen and lower fractions of hydrogen and carbon with respect to petroleum sources; hence, the presence of oxygen provides valuable physical and chemical properties to the product.[21]

The final objective is the operation of an integrated biorefinery, which would combine thermochemical and sugar platforms to produce electricity, bioproducts from different conversion platforms and conversion of bio-oil, the product of biomass pyrolysis.[18] Thereby, mass and energy integration in a biorefinery scheme is accomplished by combining process integration, energy and greenhouse analysis and life cycle assessment (LCA) for investigating

environmental impacts and material and energy inventories throughout a process.[22] An interesting example of an integrated biorefinery featuring heat integration, and synergetic material product integration is the production of biodiesel from *Jatropha curcas*, where the required thermal and electrical energy are generated from residues of the crop.[22] Similarly, Coma and coworkers[10] presented an integrated organic waste biorefinery featuring the co-processing of different waste streams, which included the hydrothermal co-liquefaction of polyethylene and polypropylene waste.

1.2 Current status and classification of bioderived polymers

Polymers are part of the everyday life and are present in a wide variety of applications across different industries; however, they come along with environmental, sustainability and economic problems that have been arising as a result of the excessive use and production of plastics and polymers. They therefore represent a feasible area for renewable sources to be considered.[23] Consequently, biobased and sustainable polymers are one of the main drivers towards the materials and energy revolution the world is facing.

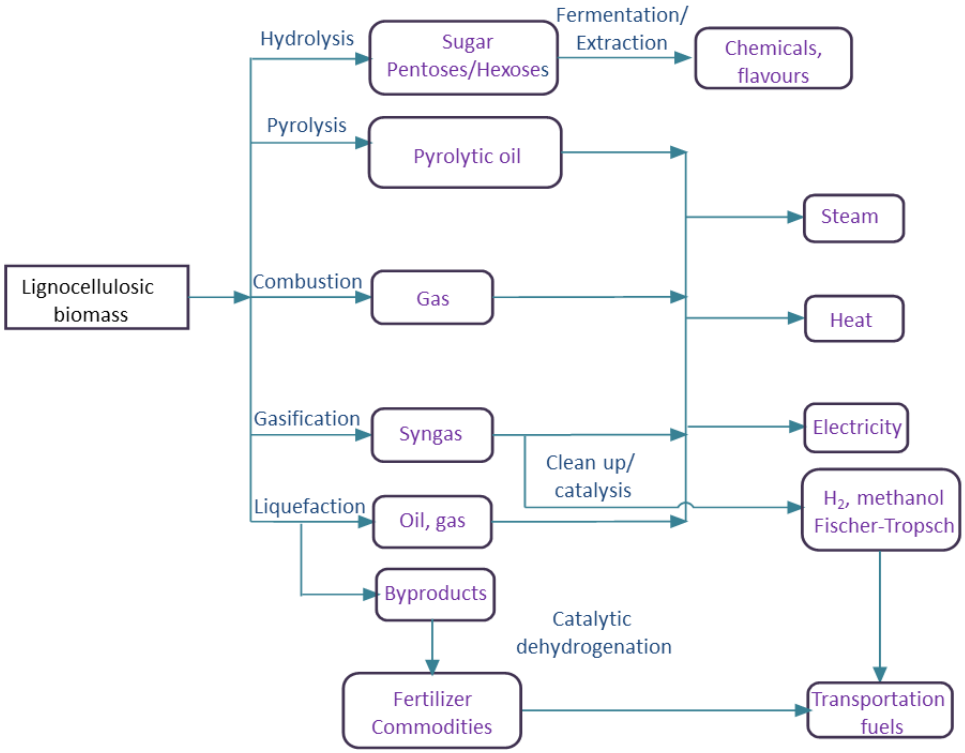

Figure 2. Lignocellulosic biomass refinery scheme, adapted and modified from[17]

One of the principal motivations is the huge size of the polymers market nowadays, being biobased polymers a key player within it. According to the European Bioplastics Agency, biopolymers currently represent about one per cent of the about 300 million tonnes of plastic produced annually.[24] The global production capacity of biopolymers is predicted to grow to approximately 6.1 million tonnes in 2021.[24] **Figure 3** shows the current and projected worldwide production capacities of biopolymers.

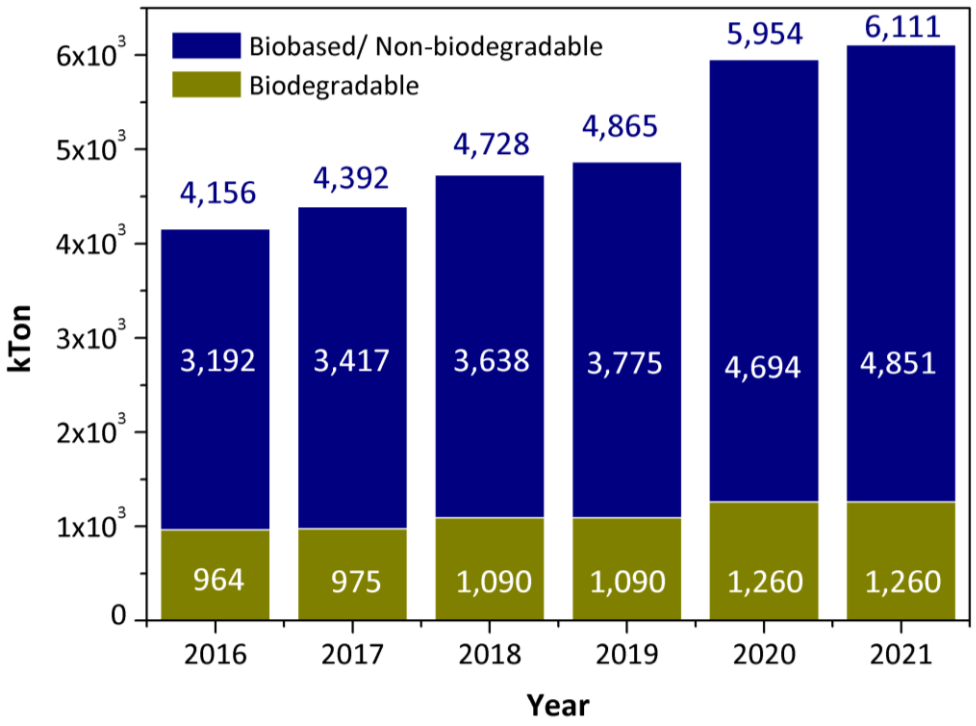

Figure 3. Global production of biopolymers, adapted and modified from the European Bioplastics Agency.[24]

1.2.1 Classification of bioderived polymers

The concept of biopolymers is broad as they could fall in the following main groups:[25]

- Renewable polymers, produced from a natural resource which can be regenerated at the time, through natural or biological processes.
- Biodegradable polymers, designed to degrade upon disposal by the action of living organisms, which can come from non-renewable sources (petrochemical-based). Thus, not all biodegradable polymers are bio-based.

Biobased polymers can be classified into four categories according to their method of production, as summarised in **Figure 4**:[26]

- **Category 1** Polymers directly extracted from biomass such as starch, cellulose and chitin.
- **Category 2** Polymers produced by classical chemical synthesis from biomass monomers such as polylactic acid (PLA) and biopolyethylene.
- **Category 3** Polymers produced directly by natural or genetically modified organisms such as polyhydroxyalkanoates (PHA).
- **Category 4** Polymers whose monomers are obtained from petrochemical-based monomers such as poly(caprolactone) (PCL), poly(butylene succinate-co-adipate) (PBSA) and poly(butyrate adipate-co-terephthalate) (PBAT).

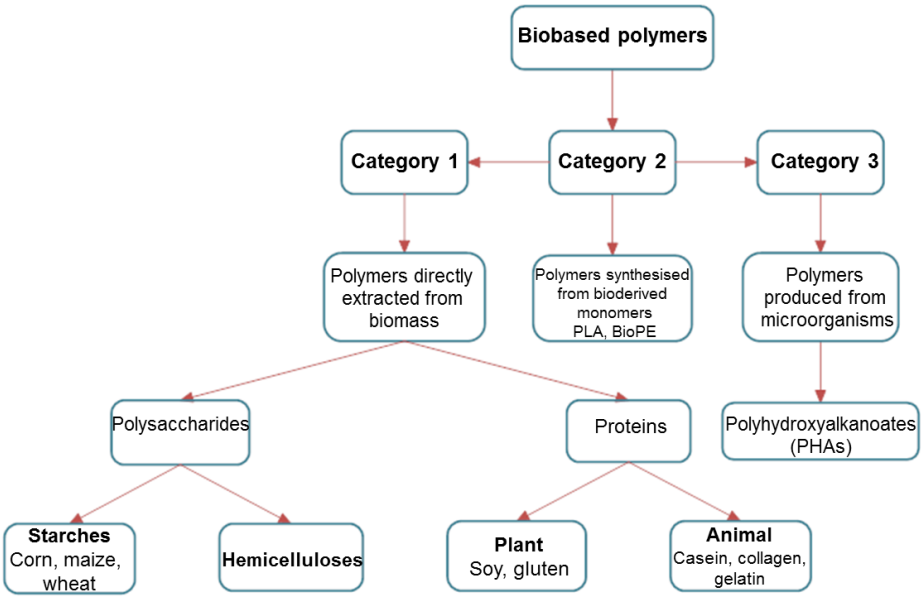

Figure 4. Classification of biobased polymers based on their origin and method of production, adapted and modified from Robertson.[26]

1.3 Biomass-derived monomers and polyesters

As previously described, there is an increasing motivation for the development and positioning of biomass-derived compounds in industry. The European Technology Platform for Sustainable Chemistry (SUSCHEM) has estimated that the share of bio-based chemicals will grow globally from the 3-4% in 2010 to approximately 30% by weight in 2050.[27]

In 2004, the U.S. Department of Energy (DOE) released a pioneer report which identified twelve building blocks that could be biologically or chemically produced from carbohydrates.[28] The DOE's down selection was made considering the existing petrochemical

models for the building blocks, chemical data, market data and the feasibility of conversion of these building blocks to secondary chemicals or derivatives.

Since the so called DOE's "Top 10" list was released, several advances and technology improvements have been accomplished for certain chemicals; therefore, they remain as part of what is known as the updated version of the original list: "Top 10 revisited".[29] Nonetheless, some of the compounds included in the original list were not considered anymore since research and development have been stalled and attention focused on other candidates. Some other criteria were decisive to gather the final list, such as market volume, technology applicable to chemicals or its role in a comprehensive biorefinery concept. The original and revisited lists are summarised in **Table 1.**

Table 1. Top chemicals derived from biomass according to DOE: 2004 and 2014[28, 29]

2004	2014
1,4-diacids (Succinic, fumaric, malic)	Ethanol
2,5-furandicarboxylic acid	Furans
3-hydroxypropionic acid	Glycerol
Aspartic acid	Biohydrocarbons
Glucaric acid	Lactic acid
Glutamic acid	Succinic acid
Itaconic acid	Hydroxypropionic acid/aldehyde
Levulinic acid	Levulinic acid
3-hydroxybutyrolactone	Sorbitol
Glycerol	Xylitol
Sorbitol	
Xylitol/Arabinitol	

Renewable, bioderived monomers can be classified based on their biomass origins:[30]

o Oxygen-rich biomass-derived monomers; for example, carboxylic acids, polyols, dianhydroalditols and furans.

o Hydrocarbon-rich biomass derived monomers such as vegetable oils, fatty acids, terpenes and terpenoids.

o Hydrocarbon monomers such as bio-ethene, bio-propene and bio-isoprene.

o Non-hydrocarbon monomers like carbon dioxide.

In the following subsections, the bio-based monomers that build the core of the present project are presented in terms of properties, petrochemical and biological routes, production levels and market volume, highlighting their current role in the synthesis of biomass-derived polyesters. These analyses are based on recent reviews on the production of renewable polymers from lignocellulosic monomers.[21, 23, 31, 32]

1.3.1 Dicarboxylic acids

1.3.1.1 Succinic acid

Succinic acid (SA) is praised as one of the key bioderived monomers and has a strong presence in the market as it is an important building block for biomass-derived polyesters and is a precursor to other bulk chemicals such as 1,4-butanediol, γ-butyrolactone, tetrahydrofuran and adipic acid.[23] SA is an intermediate of the citric acid cycle and one of the fermentation end-products of anaerobic metabolism.[33] **Scheme 3** summarises the use of succinic acid as platform chemical. It is observed that most derivatives are produced through hydrogenation using a wide diversity of heterogeneous and homogeneous catalytic routes.[34]

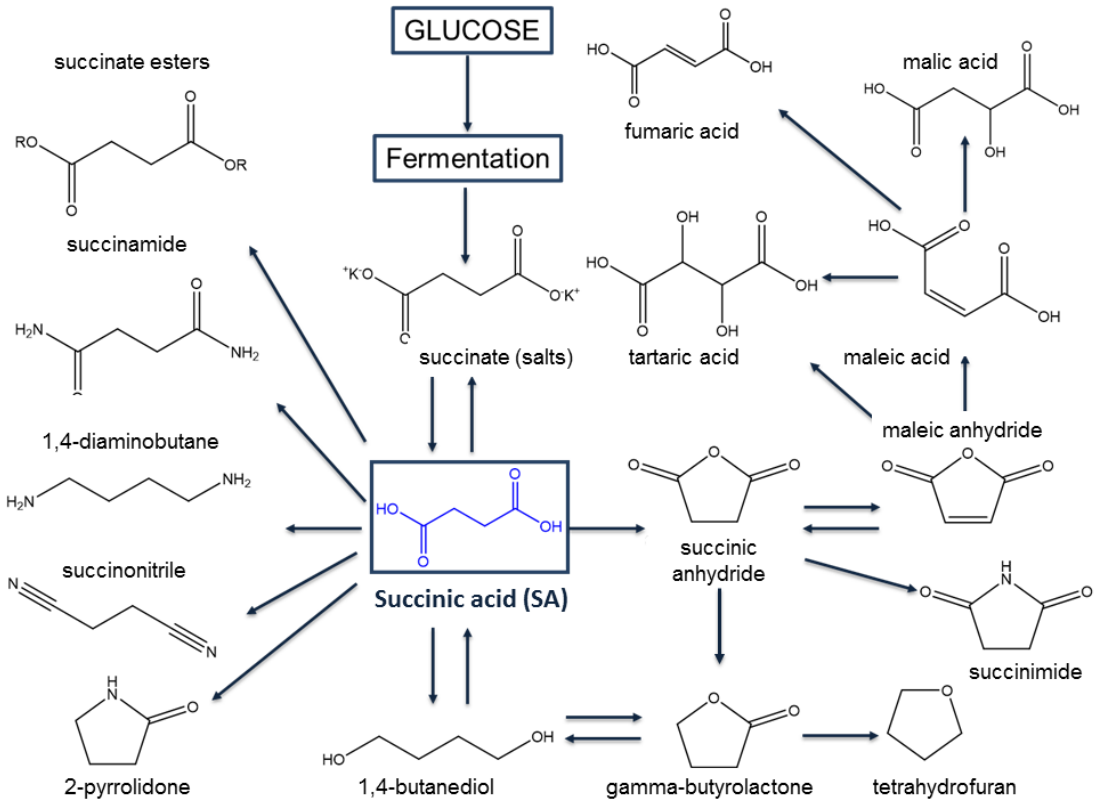

Scheme 3. Succinic acid derivatives.[34]

The current chemical pathway for the production of succinic acid starts from n-butane through maleic anhydride. SA is obtained by hydrogenation of maleic anhydride followed by hydration toward succinic acid. The catalyst and process conditions for the hydrogenation of maleic anhydride give conversions of 98-99% to succinic anhydride, using a Ni/Zr/Al/Si alloy as catalyst.[35] Other industrial production routes include oxidation of paraffins which lead to a mixture of dicarboxylic acids, followed by the separation of succinic acid, and production from acetylene, carbon monoxide, and water in acid media under a pressure of 3-49 MPa, and a temperature range of 80-250 °C.[36]

The fermentation production of SA from biomass has attracted considerable interest as part of the implementation of the biorefinery concept.[36] SA is produced via fermentation of different glucose sources by natural or genetically modified microorganisms.[37] The most promising bacterial strains for succinic acid production include *Actinobaccilus succinogenes, Anaerobiospirillum succiniciproducens, Mannheimia succiniciproducens, and E. coli* since they produce succinic acid in considerable yields.[36]

Theoretical calculations demonstrate that the production of SA via fermentation has a competitive cost against conventional, petrochemical routes, exemplified by using the Reverdia case, the resulting process of the joint venture of DSM and Roquette, as the theoretical basis. It was concluded though that there is room for improvement in terms of the yeasts used, reduction of water usage, and elimination of separation/purification steps.[38]

Continuous work has been done to improve the actual biomass-derived process. For instance, Morales, et al.[39] recently investigated the effect of metabolic engineering in combination with several upstream (pH level) and downstream (reactive extraction, electrodialysis and ion exchange) conditions on the production of succinic acid from sugar beet and lignocellulosic residues. It was found that *E. coli* strains with high sugar resistance coupled with reactive extraction was the most economically viable technology, whereas *E. coli* with resistance at the acidic pH level in the fermentation also with reactive extraction was identified as the best option in terms of environmental performance. In an alternative approach, succinic acid was produced from a different biomass platform, namely levulinic acid via a non-fermentative, one-step and metal-free process using trifluoroacetic acid as catalyst and hydrogen peroxide with 60% yield of SA.[40]

The market value of microbial production of SA is expected to reach $1.1 billion by 2020, compared to $115.2 million in 2013.[21] Currently, some companies are producing biomass-derived SA. Myriant employs grain sorghum grits and the Reverdia process simultaneously produces ethanol and SA.[31] The Reverdia's yeast-based process uses *a S. cerevisiae* strain to produce succinic acid.[41] The main advantage of this process is the cost reduction of the acidic pH fermentation, which eliminates the need of adding a base to control the pH and further recovery of the succinic salt, as done in the bacteria-based fermentation.[42]

Various polyesters can be synthesised via polycondensation of succinic acid or succinic acid diesters with diols, mostly poly(alkylene succinates).[21] Poly(ethylene succinate) (PES), poly(propylene succinate) (PPS) and poly(butylene succinate) (PBS) are the most studied polyesters of succinic acid. PBS is a biodegradable polyester synthesised via transesterification or direct condensation of SA with 1,4-butanediol.[32] PBS is likely to substitute some conventional polymers such as polypropylene (PP) or poly(ethylene terephthalate) (PET) because of its mechanical properties and crystallisation behaviour.[32, 43] The current annual market volume of PBS is around 40 kton,[32] so different companies have pioneered the production of bioderived PBS, such as Showa with Bionolle™,[44] Mitsubishi's

bioPBS™[45] and AmberWorks, a joint venture between NatureWorks and BioAmber, to explore the production of 100% renewable PBS polyesters.[46] Bionolle™ is currently being used in agriculture (pots, trash bags), fishery (nets) and common household (bottles, gloves, foamed tubes, pegs) applications,[47] whereas bioPBS™ has been used in biodegradable moulding, coated paper and flexible packaging.[48]

1.3.1.2 2,5-furandicarboxylic acid

The bioderived diacid monomer with the most potential in the market is 2,5-furandicarboxylic acid (FDCA), which is a high value derivative from 5-hydroxymethyl furfural (HMF), itself an important chemical platform obtained from the dehydration of C5 and C6 sugars.[29] Extensive reviews on HMF synthesis, process technologies, properties and applications were gathered by Van Putten,[49] Rosatella, et al.,[50] and more recently, Mukherjee, et al.[51] **Scheme 4** highlights the importance of HMF as a platform chemical to synthesise different molecules.

FDCA is mainly produced by the selective oxidation of HMF, over a wide variety of heterogeneous metal catalysts.[52-58] The metal-free conversion of HMF to FDCA has also been recently reported.[59] FDCA has been called "The sleeping giant"[60] because of its potential as a source of chemicals and polymers, which has been extensively reviewed.[61]

Because of its industrial importance, recent years have seen an important development in synthesis routes and production methods of FDCA. Although it is primarily synthesised from HMF, its production from pentoses such as furfural[62] or 5-chloromethyl furfural[63] has gained attention. Several industries have patented FDCA production pathways, such as DuPont, Canon, ADM and Avantium's[64-66] well-known YXY technology, which relies on the catalytic dehydration of carbohydrate feedstock to produce methoxymethylfurfural followed by the catalytic oxidation of the latter in acetic acid to synthesise FDCA.[67] The Canon patent describes the production of FDCA from the oxidation of HMF with a metal permanganate in an alkaline media whereas the other patents focus in the oxidation of HMF derivatives in an acetic acid medium.

Commercial production of FDCA will soon come to a reality, as Avantium announced in 2016 a joint venture with BASF for the production of FDCA through Avantium's YXY technology, with a projected annual capacity of 50 ktons.[68]

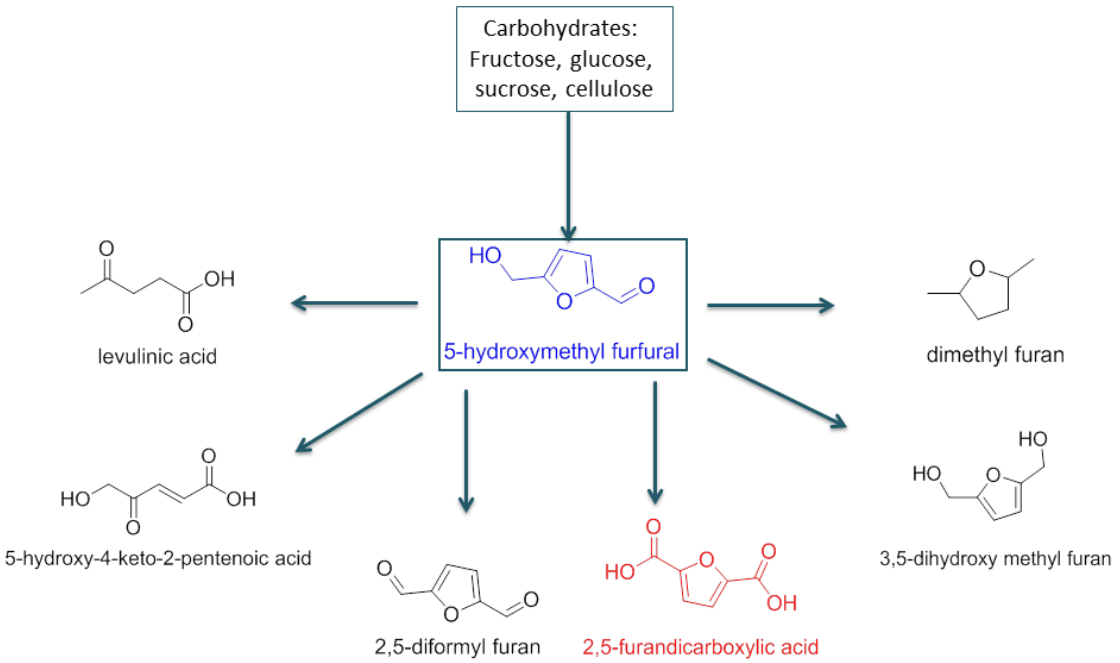

Scheme 4. 5-hydroxymethyl furfural (HMF) and its derivatives.[50]

FDCA is envisioned as a replacement for terephthalic acid in the synthesis of PET and poly(butylene terephthalate) (PBT),[69] and has already been patented for the production of poly(butylene 2,5-furandicarboxylate) (PBF).[70] Poly(ethylene 2,5-furandicarboxylate) (PEF) shows greatly improved barrier and mechanical properties, higher glass transition temperature, reduced oxygen permeability and slower chain mobility than its terephthalic acid counterpart.[71] **Table 2** lists relevant physical properties information for PET and PEF, as presented by Burgess, et al.[71]

Starting with the early work of Moore,[72] FDCA has been subject to extensive research over the last years with a drive to develop it as a green chemical building block for polyesters.[73-82] The synthesis of potentially 100% renewable FDCA copolyesters with different biomonomers has been explored as well, mainly with succinic acid[78, 83-88] although some work has been done with copolyesters of FDCA with lactic acid[89] and isosorbide or its derivatives.[90-92] The synthesis of PBSF, a copolyester synthesised from 1,4-butanediol (BDO), succinic acid and FDCA is shown in **Scheme 5**, as reported by Wu, et al.[84] Lately, the Bikiaris group has extensively studied the thermal properties of FDCA polyesters, such as poly(octylene furanoate),[93] along with thermal degradation of different polyfuronoates.[94, 95] Thiyagarajan, et al.[96] studied the application of different isomers of FDCA, namely 2,4-

FDCA and 3,4-FDCA, and found no relation between the position of the carboxylic acid groups with regard to molecular weight and thermal stability.

Table 2. Physical property information for amorphous PEF and PET[71]

Polymer	Structure	T_g[a], °C	T_m[b], °C	T_d[c], °C
PEF	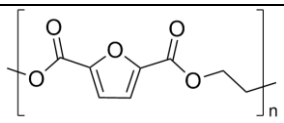	85	211	389
PET	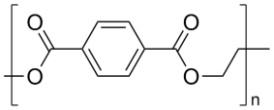	76	247	413

a: Glass transition temperature; b: Melting temperature; c: Thermal degradation temperature

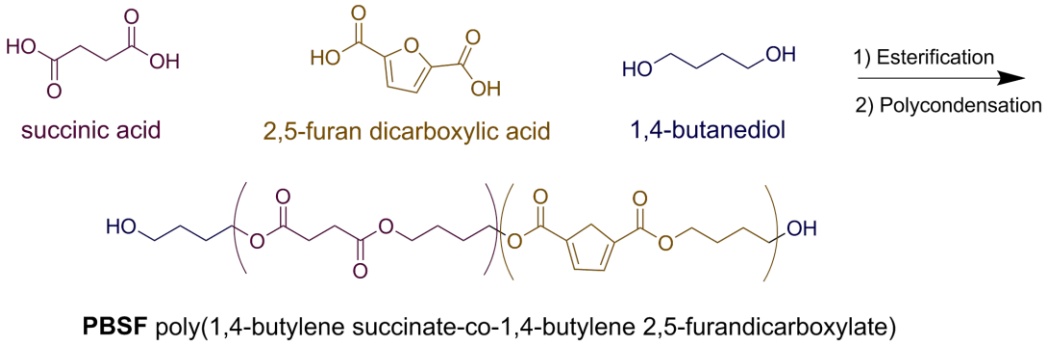

Scheme 5. Synthesis of PBSF via two-step polycondensation of SA, FDCA and BDO.[84]

Conventional polycondensation is not the only methodology followed for the synthesis of FDCA-based polyesters. Pfister, et al.[97] reported the two-step synthesis of poly(butylene 2,5-furandicarboxylate) (PBF) starting with the formation of cyclic oligoesters by esterification followed by polymerisation via ring-opening polymerisation (ROP). Recently, copolyesters of FDCA, succinic acid and 1,4-butanediol were synthesised by ROP using two different catalytic systems: chemical, with tin dioctanoate and enzymatic, using *Candida antarctica* lipase B.[98]

The potential of polyesters based on FDCA is steadily increasing and their industrialisation and commercialisation will eventually become a reality. Papageorgiou, et al.[99] and Vilela, et al.[61] recently reviewed the current status and latest progress of polyfuranoates. The total addressable market for FDCA polyesters with current end use markets is around 44 kton.[100]

1.3.1.3 Itaconic acid

Itaconic acid (IA), also known as methylene succinic acid, has the potential to be a key building block for producing both commodity and specialty chemicals and was included in the original DOE's top chemicals from biomass list.[28] **Scheme 6** shows itaconic acid and its primary derivatives.

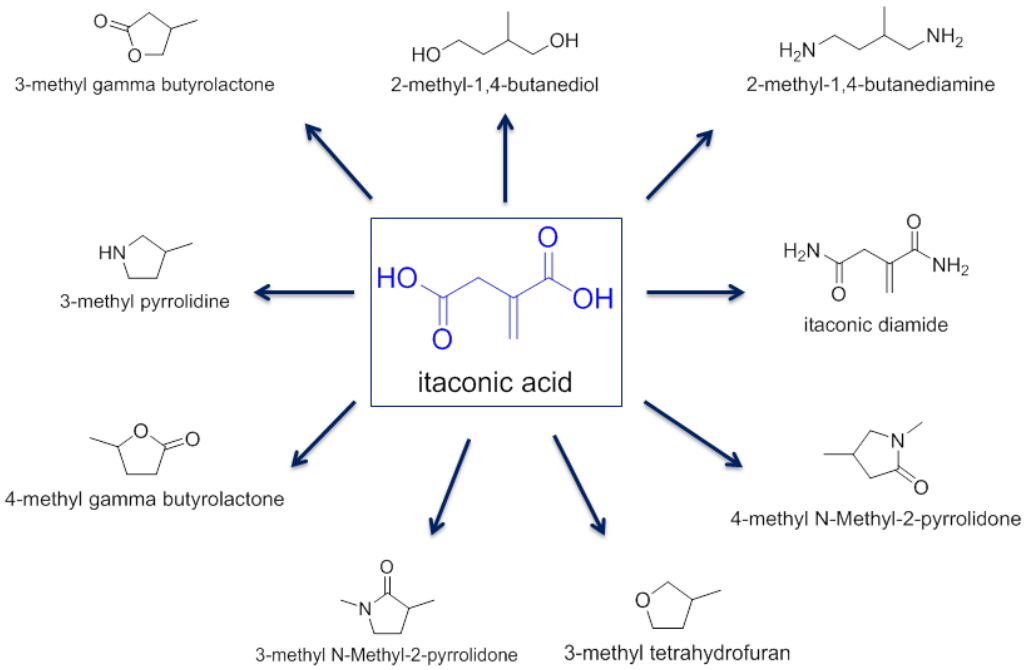

Scheme 6. Itaconic acid as a platform chemical for bioderived products.[28]

Currently, itaconic acid is produced on an industrial scale through fermentation with *Aspergillus terreus* from carbohydrates like sucrose, glucose and xylose.[101] The American company Itaconix produces itaconic acid by fermentation using this strain. The biological production from other fungi species, *Ustilago maydis,*[102] has also been reported. Synthesis can be accomplished via citric acid, although its industrial production is not promisingly envisioned.[103] The most interesting feature of IA is the presence in its structure of the methylene group along with two carboxylic acid groups. The α,β-unsaturated double bond could be subjected to addition polymerisation, which gives an interesting feature coupled with the dicarboxylic acid functionality and enables the use of IA in bioderived plastics, adhesives, elastomers and coatings.[21, 104]

The worldwide production of IA is estimated to be around 80 ktons per year, and it is expected to grow by 5.5% every year between 2016 and 2023.[101] The current drawback of the

biological production of itaconic acid on an industrial scale is production costs,[105] namely associated with the need of improvement of microbial catalysts, control of operating environment, and increase of yields and productivities, which is considered in a long-term perspective.[28] The crucial factor that affects the yields of itaconic acid is the substrate used, where focus has been moving away from glucose towards the usage of other sources such as molasses, corn syrup hydrolysates or wood.[23]

Itaconic acid may serve as a replacement for petrochemical-based acrylic or methacrylic acid and could be used in the manufacture of fibres, coatings, adhesives and binders.[30]

The most well-known polyester of itaconic acid is its homopolyester, poly(itaconic acid) (PIA). The production of PIA was patented in 1962[106] and is currently commercially available from Itaconix Corporation.[21] Apart from PIA, polyesters bearing itaconic acid units and other monomers have been reported; for instance, with ethylene glycol,[107] 1,4-butanediol,[108] succinic acid,[109, 110] glycerol,[111] 3-methyl-1,5-pentanediol,[112] lactic acid,[113] and sorbitol.[109] The synthesis of copolyesters from itaconic acid, succinic acid and isosorbide is depicted in **Scheme 7**.

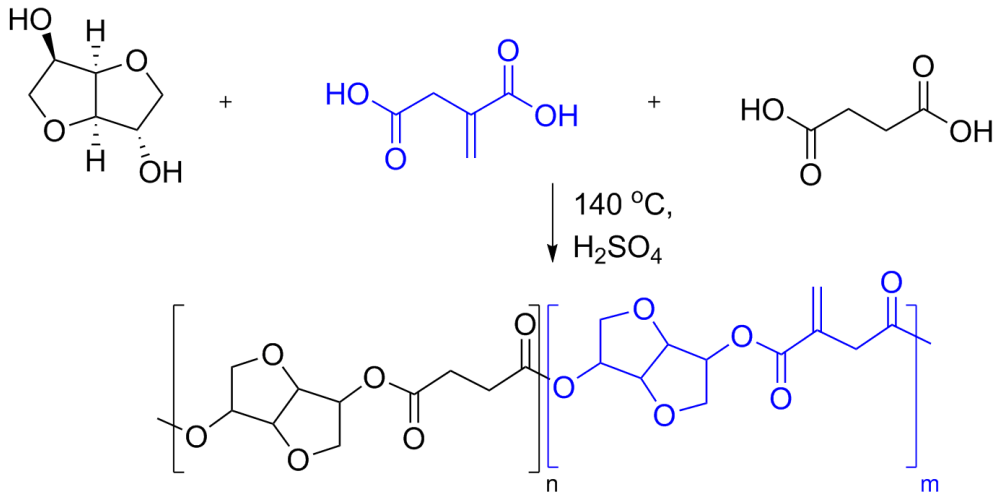

Scheme 7. Synthesis of a copolyester from isosorbide, itaconic acid and succinic acid.[110]

Besides the main application of itaconic acid-based polyesters as an alternative to methacrylates, another interesting recent field is the post-polymerisation modification through the *exo*-chain double bond.[101, 114] In this regard, several poly(alkylene itaconates) namely based on 1,12-dodecanediol, 1,20-icosanediol and 1,4-cyclohexane dimethanol were

subject to post-polymerisation functionalisation using Michael additions.[115] Lv, et al.[116] used ADMET polymerisation to synthesise a polyester based in di(10-undecenyl itaconate) and further functionalised it with different mercaptans. Similarly, polysulfides were obtained via thiol-Michael addition of unsaturated polyesters based on dimethyl itaconate polyesters[117] whereas Farmer, et al.[118] recently synthesised itaconate unsaturated-polyesters and post-functionalised them via a microwave-assisted Michael addition of 1,3-dicarbonyls, acetylacetone and dimethyl malonate.

The presence of the vinyl group expands the frontiers of itaconic acid-based polyesters in different markets and applications, enabling a productive platform for post-polymerisation modifications, such as Michael-additions with different kinds of nucleophiles, among others.[101]

1.3.2 Polyols

1.3.2.1 1,3-propanediol

Nowadays, the conventional chemical processes for the synthesis of 1,3-propanediol (PDO) are through the hydration of acrolein and hydroformilation of ethylene oxide.[119] In the Shell process, PDO is obtained from the reaction of ethylene oxide with carbon monoxide and hydrogen.[120] However, the process conditions include high temperature, high pressure, and complex catalysts.[120] Bioengineering routes are therefore desirable: in this vein, glycerol is the major feedstock for the synthesis of 1,3-propanediol.[29] Bioglycerol is a by-product which is obtained in great amount from the soap manufacturing process, microbial fermentation, and hydrogenolysis; and in terms of biomass routes, through enzymatic transformation of glycerol.[119] Glycerol is an interesting building block within the biorefinery concept, as many compounds could be derived from it, as presented in **Scheme 8**. Fermentation of glycerol to produce 1,3-propanediol has been reported using bacteria of the Enterobacteriaceae family such as *Citrobacter freundii,*[121] *Klebsiella pneumonia,*[122, 123] *Enterobacter, Clostridium,*[124-126] *Lactobacillus and Bacillus* species.[127] Optimisation of the fermentative process relies on dealing with the inhibitions of both substrate and products.[128]

Industry has taken a step forward on the production of biomass-derived PDO. Traditionally, PDO is obtained in a two-step process: yeast fermentation followed by the bacterial transformation to PDO.[129] An improved one-step biological production of PDO

from a fermentable carbon source by a single microorganism has been patented by Dupont and Tate & Lyle Bioproducts resulting in the commercial biomass-derived glycol Susterra™.

As PDO is extensively used in the manufacture of polyesters, the global demand is expect to reach 150 ktons by 2019, compared to the demand of 60.2 kton in 2012.[119]

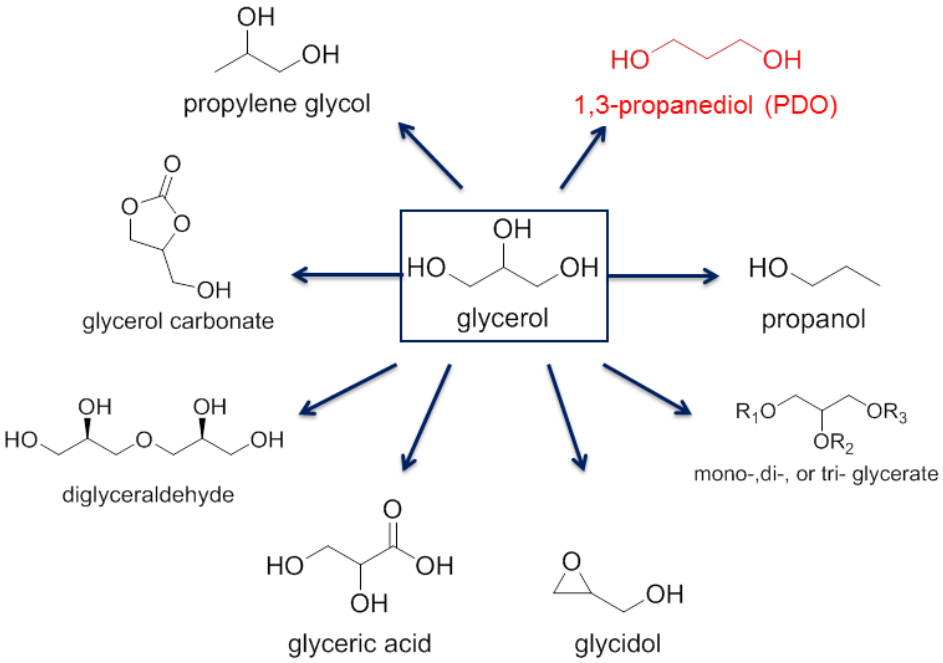

Scheme 8. Derivatives of glycerol.[28]

1.3.2.2 1,5-pentanediol

The synthesis of 1,5-pentanediol (PTO) relies in the hydrogenolysis of furfural and a number of its derivatives, such as tetrahydrofurfuryl alcohol (THFA) and furfuryl alcohol (FA).[32, 130, 131] The selective hydrogenolysis of THFA to PTO has been explored over a number of metal catalysts with different conversion and selectivities.[132-138] **Scheme 9** highlights the importance of hydrogenolysis and hydrogenation of furfural.[139]

Agricultural raw materials, such as corncobs, oat hulls and bagasse are the main source of furfural.[140] It is produced on an industrial scale (300 kton·y^{-1}) by hydrolysis of hemicellulose with a projected annual growth rate of 11.9%.[141] During the production process, the hemicellulose is firstly hydrolysed to pentose consisting mainly of xylose, which is then dehydrated into furfural.[142]

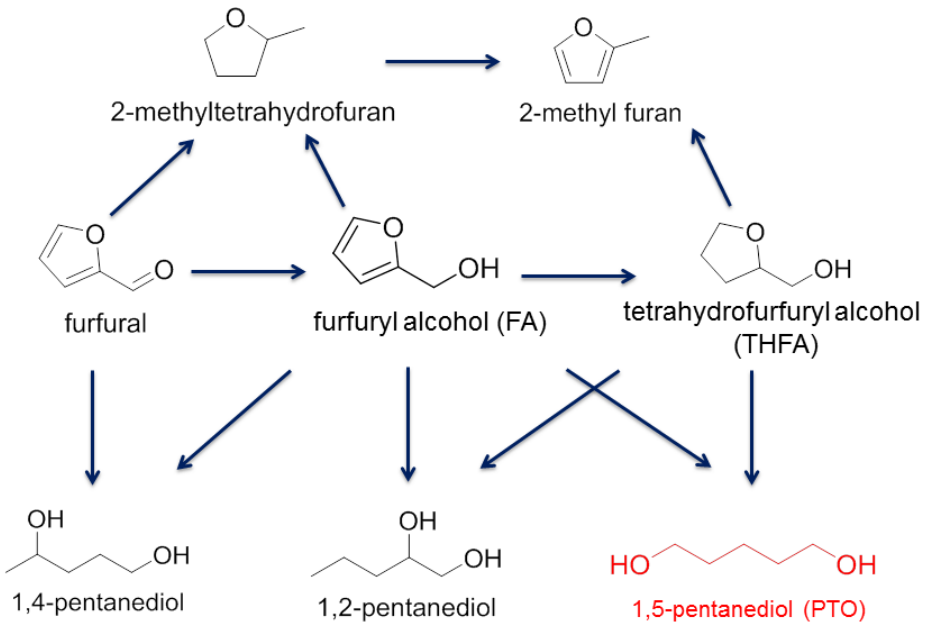

Scheme 9. Hydrogenation and hydrogenolysis of furfural.[139]

Early studies reported a two-step process where the intermediate ω-hydroxyvaleraldehyde is synthesised from THFA followed by the hydrogenation to 1,5-pentanediol using copper chromite as catalyst, although the selectivity was only 70%.[143] In particular, the Tomishige group has explored Rh/SiO_2 catalysts modified with ReOx, MoOx and W, presenting selectivities to 1,5-pentanediol above 94%.[132, 133] More recently, Li, et al.[138] reported the use of $Ir\text{-}VOx/SiO_2$ catalysts at 80 °C achieving a PTO selectivity above 80%. The analysis of the hydrogenolysis of THFA has been extended through density functional theory (DFT) simulations of feasible ring-opening mechanisms to study the role of Mo using a MoO_3 catalyst with Rh nanoparticles.[137] Comprehensive reviews on the reaction mechanisms of selective catalytic hydrogenolysis have been compiled providing an overview of current progress in the development of catalysts.[130, 144] The direct transformations from furfural[139, 145, 146] or FA[147] to PTO have recently been reported providing the first steps towards a more efficient, quicker production of PTO. A recent review points out the advances and development in the area of catalytic transformation of biomass toward C5 alcohols.[148]

Apart from furfural and furfuryl alcohol, the hydrogenation/reduction of glutamic acid represents another transformation pathway to PTO.[21, 28, 103] This process is however at an initial stage since new catalysts must be developed to obtain high yields of the desired products.

The literature describing the synthesis of polyesters using 1,5-pentanediol as a main building block is still limited. Recently, polyesters synthesised from FDCA with 1,5-pentanediol were reported, with a melting temperature of 94 °C.[81] Buchholz, et al.[149] synthesised aliphatic copolyesters of adipic acid, 1,5-pentanediol and 2-butyl-2-ethyl-1,3-propanediol and proved to be degradable by enzymatic action (**Scheme 10**). Tang, et al.[112] first copolymerised a polyester containing itaconic acid, 3-methyl-1,5-pentanediol and maleate units to prepare further cross-linked polymers. Using photopolymerisation as an alternative methodology, furfural-based polyesters have been synthesised from 2-furanacrylic acid molecules with 1,5-pentanediol.[150] Our recent work with 1,5-pentanediol focused on the batch-reactor simulation and multiobjective optimisation of copolyesters with SA and FDCA,[88] followed by the process intensification of the polyesterification reaction.[151]

1,5-pentanediol has also been considered as a biomass-derived platform chemical, since the production of benzene-toluene and xylene (BTX) along with liquefied-petroleum gas (LPG) was successfully accomplished via catalytic conversion of PTO under low-temperature and atmospheric-pressure conditions.[152]

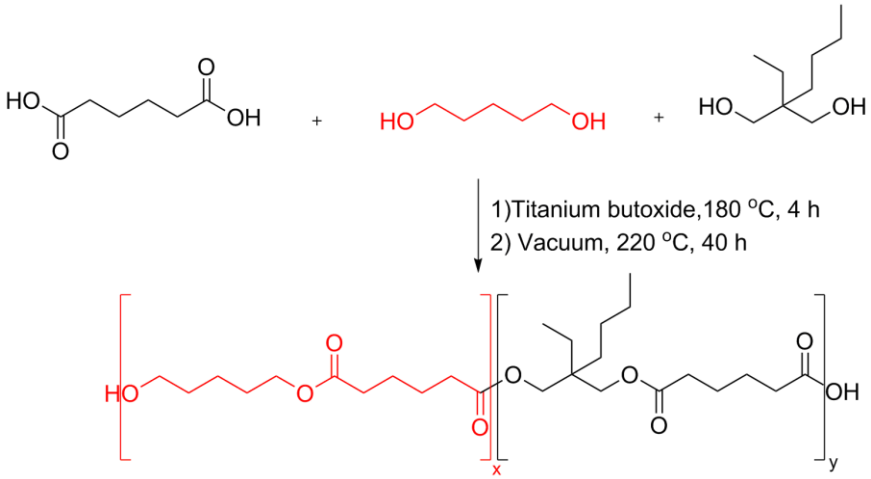

Scheme 10. Polycondensation of copolyesters of adipic acid, 1,5-pentanediol and 2-butyl-2-ethyl-1,3-propanediol.[149]

1.3.2.3 1,4:3,6-dianhydrohexitols: Isosorbide

Depending on the chirality, three isomers of the 1,4:3,6-dianhydrohexitols sugar diols exist, namely isosorbide, isomannide and isoidide[153] and their structures are depicted in **Scheme 11**. Isosorbide, also known as 1,4:3,6-dianhydro-D-glucitol is a molecule conformed

by two *cis*-connected tetrahydrofuran rings with secondary hydroxyl groups in the 2- (*endo*) and 5- (*exo*) positions.[154]

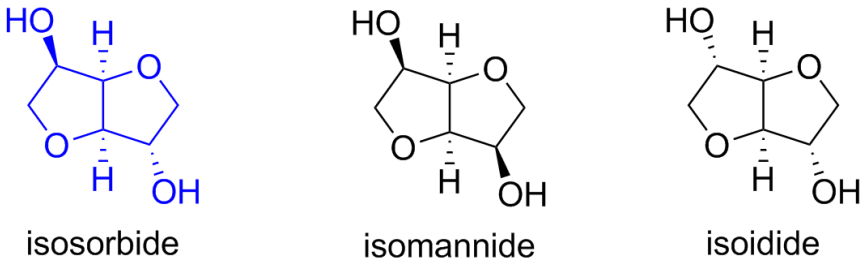

Scheme 11. Structures of the 1,4:3,6-dianhydrohexitols.[153]

The synthesis of dianhydrohexitols is based on the extraction of starch from cereals which is later degraded into *D*-glucose and *D*-mannose by enzymatic action. The sugars are then subjected to hydrogenation to give *D*-sorbitol and *D*-mannitol[153] which are finally dehydrated to obtain isosorbide and isomannide, respectively. Sorbitol can be converted to isosorbide via sorbitan by performing a two-fold dehydration reaction.[154] **Scheme 12** shows all the intermediates found in the isosorbide production from polysaccharides.[154] Nevertheless, due to the food production debate, it is imperative to find alternative sources to starch, for example, lignocellulosic biomass, which includes wood, straw and biowaste.

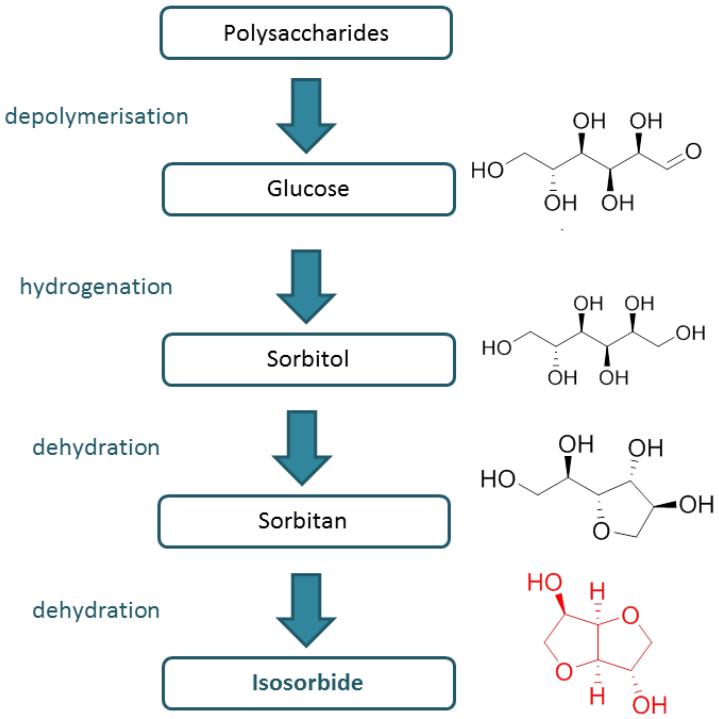

Scheme 12. Reaction pathway for the production of isosorbide.[154]

Research on polyesters based on 1,4:3,6-dianhydrohexitols has focused on isosorbide because it is the only one available industrially among the three isomers. Isomannide is less reactive than isosorbide and isoidide, despite being the most reactive isomer, is produced from L-idose which is rarely encountered in biomass.[153]

Roquette is the world leader in the production of isosorbide, with an annual production capacity of 20 kton. The intended application of the high purity grade isosorbide, POLYSORB P is the synthesis of polyesters.[155]

Several researches have studied the incorporation of isosorbide into the synthesis of bioderived polyesters due to its rigidity, which confines higher glass transition temperatures to the polymer, leading to enhanced mechanical strength and thermal stability,[156] as shown by Storbeck, et al.[90] Charbonneau, et al.[157] patented the synthesis of copolyesters containing isosorbide blocks, coupled with different diacid moieties, in a temperature range of 260-300 °C and salts of Li, Ca, Mg, Mn, Ti, Sn or Ge as catalysts. The amount of monomer depended on the properties and final composition desired. Other patent studies include the work done by Lee, et al.[158] where polyesters with improved impact strength were obtained by polymerisation of isosorbide and 1,4-cyclohexanedimethanol with terephthalic acid. Moreover, Germroth, et al.[159] produced polyesters by firstly obtaining an aqueous solution of isosorbide which was fed to a reactor, followed by glycols and dicarboxylic acids fed into the aqueous solution with the final formation of copolymer and polycondensation.

PET, one of the polymers with the largest market share, including bottles, film and other moulded commodity products has also been synthesised with isosorbide. For example, Abid, et al.[160] synthesized PET by melt polycondensation of dimethyl terephthalate, ethylene glycol and isosorbide, resulting in amorphous copolymers with different compositions. In order to overcome the inherent low reactivity of the isohexides, as well as the decolourisation of the isosorbide-based polyesters, Bersot, et al.[161] proposed a novel catalytic combination of antimony oxide with Li or Mg which gave higher reaction rates and less yellowish issues during isosorbide-based PET synthesis. Gioia, et al.[162] synthesised polyesters based on recycled PET, succinic acid and isosorbide for powder coating applications (**Scheme 13**) whereas in another study, the incorporation of 1,4-cyclohexanedimethanol to isosorbide-containing PET overcame the low reactivity problem, achieving M_n of 25,400 Da.[163]

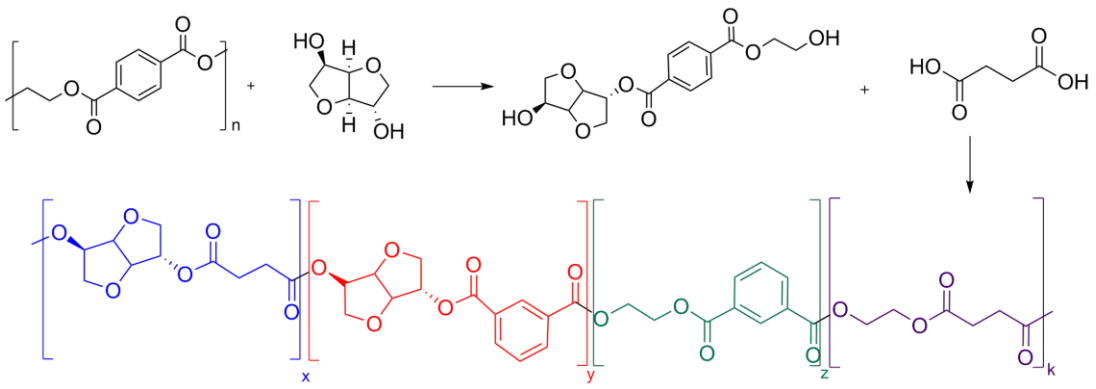

Scheme 13. Chemical recycling of PET with isosorbide and polymerisation with succinic acid.[162]

Besides PET, isosorbide has been incorporated into other well commercialised polyesters. Sablong, et al.[164] studied the synthesis of PBT with isosorbide by solid-state polymerisation, which resulted in higher molecular weights and less coloured polymers compared to conventional melt polycondensation. Likewise, Lavilla, et al.[165] reported the modification of PBT polyesters with other carbohydrate-based bycyclic diols apart from isosorbide, isomannide and isoidide. The authors obtained higher molecular weights and compositions closer to the feed with isomannide and isoidide-modified polyesters, although isosorbide increased the glass transition temperature more efficiently. Similarly, PBS was modified with 5-10 mol% isosorbide, showing that the glass transition temperature increased as the mol% isosorbide increased; the polymers however exhibited a reduced ability to transreact because of the lower reactivity of the isosorbide hydroxyl group in the *endo* position.[92]

Isosorbide has been incorporated into different polyesters based in a variety of biomass-derived monomers, mainly citric acid,[166] lactic acid,[167] succinic acid,[110, 168-170] sebacic acid,[169, 171] and itaconic acid.[110] Wu, et al.[172] transformed the secondary hydroxyls of isosorbide into carboxylate functionalities to develop a new bio-derived monomer, isoidide dicarboxylic acid, in order to overcome the low reactivity inherent to isosorbide while the rigidity is retained. This diacid was reacted either with ethylene glycol, 1,4-butanediol or 1,10-decanediol.

Few types of polyester have been reported with isomannide[173, 174] or isoidide.[174] Okada, et al.[174] studied the biodegradability of polyesters from isomannide or isoidide and different dichloride acids, such as succinyl, adipoyl and sebacoyl dichlorides. The polyesters had

molecular weights between 9 and 34 kDa, and the authors reported that all the polymers based on isoidide were scarcely biodegradable whereas only the polyester based on isomannide and sebacoyl dichloride showed enzymatic biodegradability.

1.4 Polymer reaction engineering

1.4.1 Synthesis of polyesters

Polyesters are among the most targeted and interesting polymers due to their great variety of properties, such as heat and chemical resistance, good electrical properties and enhanced processability, which also enables them to present fibre forming ability and biocompability.[23] Furthermore, their versatility during synthesis and compounding allows them to be processed by injection moulding, extrusion and blow moulding, expanding the application fields, from commodities such as bottles up to high performance thermoplastics in the electronics or automotive industries.

Generally, a polyester is a polymer that contains ester functionality repeated in the polymer chain and can be synthesised via the direct esterification of diacids and diols, self-esterification of hydroxyacids, transesterification of diols with carboxylic acid esters, and even by the reaction of acid chlorides with diols or by ring opening polymerisation of lactones.[175] The first polyesters were synthesised by Roy Kienle in 1926.[176]

The synthesis of polyesters is achieved through a step-growth mechanism.[177] Step-growth polymerisation involves the slow build-up of polymer chains from monomers, dimers and trimers.[178] There are other polymerisation mechanisms, such as chain polymerisations, which take place by a rapid addition of molecules to a growing chain end. An example of this mechanism is the synthesis of polyolefins.[177]

Polycondensation is a type of step-growth reaction, during which a small molecule is eliminated, such as water or alcohol.[179] There are two routes for the synthesis of linear, condensation polymers from polyfunctional compounds: The A-R-B route and the A-R-A-B-R'-B route. The former starts from a monomer with two unlike functional groups suitable for polycondensation (polycondensation of hydrocarboxylic acids) whereas the latter starts from two different monomers, each possessing a pair of identical reactive groups that can react with each other.[180] In this case, R represents an alkyl or aryl group to which the two functional groups A and B are attached.[181]

The synthesis of polyesters followed in the present work fall in the A-R-A-B-R'-B category, as they are formed from the polycondensation of diols with dicarboxylic acids, as shown in **Scheme 14**. Contrarily, if one of the monomers used in the polycondensation is a tri- or multifunctional species, the polymerisation will result in a branched polymer. The degree of branching can be controlled by the amount of triol added relative to diol.[177]

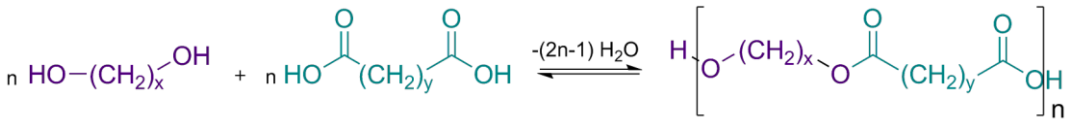

Scheme 14. Polycondesation reaction between a diol and dicarboxylic acid.[180]

In most step-growth reactions, the final conversion, and hence the average molecular weight, is limited by the reaction equilibrium; therefore the removal of the byproduct is essential to lower the rate of the reverse reaction.[182] This implies that the operation is carried out at high temperatures and reduced pressures to remove the condensation products. Some type of polyesters however, such as alkyd resins, do not need to be synthesised under reduced pressure because the final products have relatively low-molecular weight.[183] It is common practice to add xylene to the reactants to facilitate water removal by azeotropic distillation, as performed in the present work, and will be fully described in **Chapter 2**.

1.4.2 Fundamentals of step-growth polymerisation

As defined by Rudin[183] and Allcok,[177] step-growth polymerisation exhibits the following features:

- Equal reactivity hypothesis: It is assumed that the functional group on the end of a monomer has the same reactivity as that on a polymer regardless the size of the chain. This postulate is further described in **1.4.3**.
- A high conversion of functional groups is necessary to produce high-molecular-weight polymers, so the molecular weight steadily increases during the reaction.
- Monomer units can react with each other or with polymers of any size: hence any two molecules can react with each other.
- The monomer disappears at an early stage of the polymerisation.

- The existence of a broad molecular weight distribution in the later stages of the step-growth reaction, whereas in chain polymerisation, the reaction mixture contains only monomer and high polymer at any stage.

As pointed out before, if the functional groups are located in the same molecule, the polymerisation is considered to be A-R-B type. These functional groups will remain equimolar throughout the reaction. If P_m and P_n refer to polymer molecules having *m* and *n* monomeric units, the polymerisation can be described by equation 1[181, 184]

$$P_m + P_n \leftrightarrow P_{m+n} + W \qquad m,n=1,2\ldots \tag{1}$$

Where *W* is the condensation product and P_{m+n} is a polymer of length $(m+n)$ produced from the reaction between P_m and P_n.

In the case of A-R-A-B-R'-B polymerisation, the oligomeric molecules present are distinguished by their end groups, depicted in **Figure 5**.

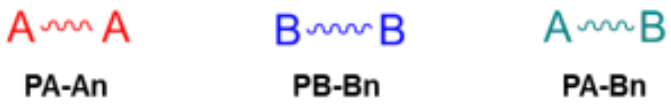

Figure 5. End groups in A-R-A-B-R'-B polymerisation.

By analogy with A-R-B polymerisation, the chain growth steps for A-R-A-B-R'-B can be represented by the following equations[184]

$$\begin{aligned} P_{A-Bm} + P_{A-Bn} &\leftrightarrow P_{A-B(m+n)} + W \\ P_{A-Am} + P_{B-Bn} &\leftrightarrow P_{A-B(m+n)} + W \\ P_{A-Bm} + P_{B-Bn} &\leftrightarrow P_{B-B(m+n)} + W \\ P_{A-Am} + P_{A-Bn} &\leftrightarrow P_{A-A(m+n)} + W \end{aligned} \tag{2}$$

If the monomers are present in equimolar ratio, the set of reactions above are reduced to equation 1.

1.4.3 The equal reactivity hypothesis

Consider the following reactions of carboxylic and dicarboxylic acids, as described by Gupta[181]

$$H-\ (CH_2)_n-COOH+C_2H_5OH \xrightarrow{HCl} H-(CH_2)_n-COOC_2H_5+H_2O \quad (3)$$

$$COOH-\ (CH_2)_n-COOH+C_2H_5OH \xrightarrow{HCl} \quad (4)$$

$$COOC_2H_5-(CH_2)_n-COOH+H_2O$$

The reaction rate coefficients are evaluated through the following expression:

$$r_e=\frac{d[COOH]}{dt}=k_A[COOH][H^+] \quad (5)$$

Where r_e is the rate of esterification, *[COOH]* represents the total concentration of the carboxylic acid groups and $[H^+]$ is the concentration of protons liberated by HCl. **Table 3** shows the calculated rate constants for the esterification of carboxylic acids.[181] These results primarily suggest the reactivity of molecules does not depend on the size of the molecule for chain length n>8. Second, for larger molecules, the rate constant is independent of whether there are one, two, or more carboxylic acid groups per molecule.

Based on the experimental results in **Table 3**, further kinetic studies will assume all the rate constants are independent of chain length. This postulate is known as the equal reactivity hypothesis.

There are however some step-growth mechanisms in which the equal-reactivity hypothesis does not hold accurately.[181] Kuchanov, et al.[185] found that the hydroxyl activity increased with increasing chain length in the solution polycondensation of terephthalates with benzoyl chloride in tetrahydrofuran. The authors determined that the degree of solvation of functional groups and the local values of the dielectric constant of the medium could be responsible for the changes in the rate constant of the chemical reactions. Park[186] proposed a model for the chain dependence of the reaction rate constant, which predicted that the molecular weight could reach infinity for a finite time of the reaction. Similarly, the molecular weight distribution arising from the condensation of divinylbenzene and p-cresol differed from that predicted on the basis of the theory of equal reactivity.[187] The authors then assumed that each *ortho* site on *p*-cresol was between two and four times as reactive as that on monosubstituted cresol, which provided a calculated distribution in better agreement with the experimental data.[187]

Table 3. Rate constants for the esterification of carboxylic acids in excess of ethanol[181]

Chain length (n)	k_a x 10^4 (L·mol^{-1}) monocarboxylic acid	k_a x 10^4 (L·mol^{-1}) dicarboxylic acid
1	22.1	-
2	15.3	6.0
3	7.5	8.7
4	7.45	8.5
5	7.42	7.8
6	-	7.3
8	7.5	-
9	7.47	-
Higher	7.6	-

1.4.4 Kinetics of step-growth polymerisation

It has been shown that the rate constant of polyesterification reactions is independent of the molecular size. Hence, it is possible to determine the concentration of functional groups; for example, by titration of unreacted carboxylic acid groups during the reaction.[177]

Flory[188] showed that if any molecule is picked randomly from the reacting mixture, the probability *P* that it will have chain length *n* in terms of the conversion of the limiting functional group *p* is

$$P(n) = p^{n-1}(1-p) \quad (6)$$

Consumption of *n* monomer to form the polymer chain requires *n-1* independent chain-linking reactions, each with probability *p*. The distribution in equation 6 is called the most probable distribution (MPD) or Schulz-Flory Distribution.[182] Stockmayer[189] extended Flory's distribution to branched chain polymers, although this analysis is out of the scope of the present study.

As conversion p increases toward 1, the mole fractions of small molecules decrease while the mole fractions of larger molecules increase. If the total number of molecules remaining at conversion p is defined by N and N_0 is the initial number of monomer molecules, then $N=N_0(1-p)$ the mole fraction of the n-mer is

$$x(n) = \frac{N_n}{N_0(1-p)} \tag{7}$$

Recalling the Schulz-Flory distribution and since $x(n)=P(n)$, the number of moles of n-mer is

$$N_n = N_0 p^{n-1}(1-p)^2 \tag{8}$$

and the weight fraction of the n-mer is

$$w(n) = \frac{N_n(nw_m)}{N_0 w_m} = \frac{N_0(1-p)^2 p^{n-1} n}{N_0} = (1-p)^2 p^{n-1} n \tag{9}$$

Where w_m is the molecular weight of the repeating unit.[182]

Performing polymerisation modelling could address important problems in industry, as it requires the integrated use of thermodynamics, kinetics, reactor design and transport phenomena. Such problems are mainly related to operator training, process control, troubleshooting, process optimisation and monitoring.[190]

Chapter 5 provides a detailed analysis on kinetic modelling of polyesterification reactions, along with the kinetic fitting of different models to the experimental data generated in the present study.

1.4.5 Molecular weight and molecular weight distributions of condensation polymers

The repeating unit of each polyester molecule contains one structural unit from the diol and one structural unit for the acid, as depicted in **Scheme 15**.

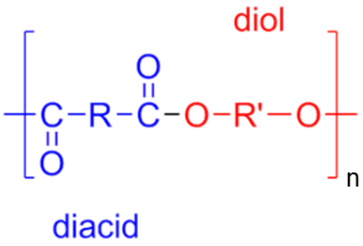

Scheme 15. Structural units of a polyester.

Structural units are never removed from the system. The total number of structural units present at all times thus is a constant and is equal to the initial number of molecules.[177] This is expressed by the following equation

$$\frac{N_{structural\ units}}{V} = [COOH]_0 \tag{10}$$

Where $[COOH]_0$ is the concentration of carboxylic acid in the beginning of the reaction and V is the volume of the reaction mixture. The average degree of polymerisation of the system, DP_n, is defined as the average number of structural units per molecules. Hence,

$$DPN = \frac{[COOH]_0}{[COOH]} = \frac{1}{1-P} \tag{11}$$

Where P is the conversion. P could we written as

$$P = \frac{[COOH]_0 - [COOH]}{[COOH]_0} \tag{12}$$

which is known as the Carothers equation.[178] $[COOH]$, which is the concentration at any time t could be then expressed as

$$[COOH] = [COOH]_0(1-P) \tag{13}$$

If a polymer is fractionated into various chain lengths, the weight of polymer in each fraction w_n is given by the molecular weight of each chain length M_n times the number of molecules of each length[191]

$$w_n = M_n N_n \tag{14}$$

If each chain has the same monomer units, the equation is expressed as

$$w_n = m_0 n N_0 \tag{15}$$

The molecular weight distribution (MWD) is expressed as weight fraction versus molecular weight (w_i vs. M_i). The MWD is characterised using moments of the distribution, which are used to characterise polymer properties: number-average molecular weight ($\bar{M}_n$), weight-average molecular weight ($\bar{M}_w$) and z-average molecular weight ($\bar{M}_z$),[192] as described below

$$\bar{M}_n = \frac{\sum w_i M_i}{\sum w_i} \tag{16}$$

$$\bar{M}_w = \frac{\sum w_i {M_i}^2}{\sum w_i M_i} \tag{17}$$

$$\bar{M}_z = \frac{\sum w_i {M_i}^3}{\sum w_i {M_i}^2} \tag{18}$$

Generally, $\bar{M}_w > \bar{M}_n$ because M_w emphasises larger molecules whereas M_n calculations emphasises equally all molecules.[177] The breadth of molecular weight distribution is commonly characterised by the ratio between M_w and M_n and is called dispersity (Đ). Step-growth polymerisations typically produce polymers with dispersity values in the range of 2 to 5.[192] Values of 1.05 correspond to very narrow distributions, for example those obtained from some anionic polymerisations,[177] whereas a dispersity of 3 means that there is a wide distribution of polymer sizes.[193]

The importance of the molecular weight distribution relies on the strong dependence it keeps with some key polymer properties, as well as with the average molecular weight. For example, a polymer in the low-molecular weight range may exhibit poor physical properties, such as mechanical strength. Contrarily, a polymer in the very high range of molecular weight might not be desirable either, because the bulk viscosity of the polymer would make processing extremely difficult[177] and would compromise the safety of the operation.[177] Variations in MWD among polymer batches, for example, could be reflected in injection moulding behaviour, because of possible melt elasticity variations.[194]

A typical differential representation of the molecular weight distribution is depicted in **Figure 6**. The ordinate shows the weight fraction of the polymer in an infinitesimal interval around the specified value of *M*. The area under the curve thus represents the weight fraction of polymer with specified values of molecular weight.[177]

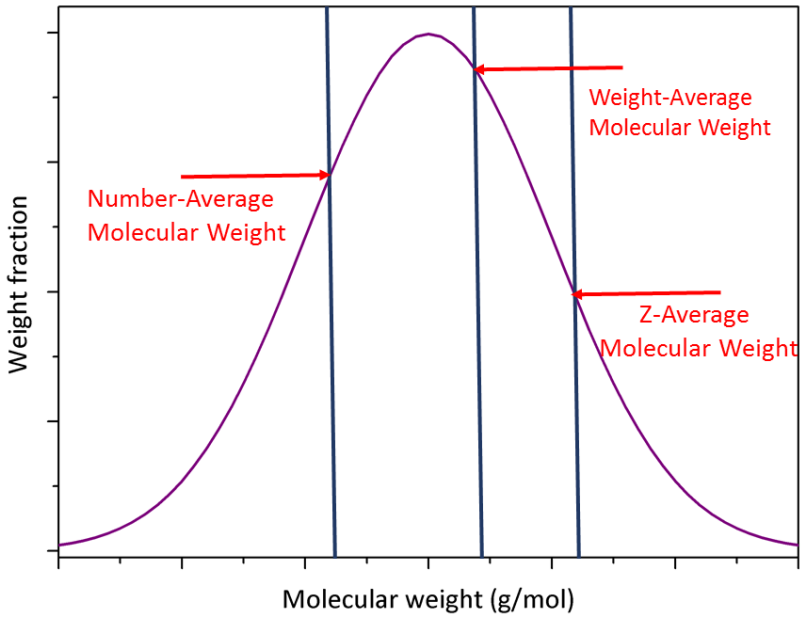

Figure 6. Typical molecular weight distribution for a polymer.[192]

1.4.5.1 Determination of molecular weight

A variety of methods are available for molecular-weight determination. The number-average molecular weight can be determined by end-group analysis and colligative properties (Depression of freezing point, elevation of boiling point, lowering of solvent vapour pressure and development of an osmotic pressure) measurements, whereas weight-average molecular weight can be calculated by light-scattering.[181] Currently, the most popular and widely used method to calculate molecular weights and molecular weight distributions is size exclusion chromatography, namely known as gel permeation chromatography (GPC). The method is basically based on the separation of macromolecules according to their size, and requires the polymer to be in solution.[177] The principle of the method could be described by having a mixture of small and large molecules deposited at one end of a column packed with porous beads (0.1-100 μm). An initial concentration gradient causes diffusion of polymer into the bead, although the large molecules cannot penetrate the beads.[195] The smaller molecules will enter the openings of the pores and tend to dissolve in the pure solvent that is immobilised there, and therefore travel slowly throughout the column.[181] A continuous flow of solvent sweeps the large molecules along and reverses the concentration gradient for the small ones so that they now diffuse back out of the beads.[195] Molecules then travel at different speeds and emerge from the column at different times, resulting in separation by molecular

weight.[181] Eventually, large molecules will emerge first and the small ones will emerge last.[195]

1.4.6 Polymerisation reactors

As many other reactions, polymerisations can be carried out in batch and continuous reactors: Batch, tubular (Plug-flow reactors, PFR) and continuous stirred tank reactors (CSTR).

1.4.6.1 Batch Reactors

A batch reactor does not have in- or out-flow of reactants or products while the reaction takes place.[196] The general mole balance of species *i* in a reaction volume *V* for a batch reactor is defined as

$$\frac{dN_i}{dt} = r_i V \tag{19}$$

Chapter 6 of the present thesis focuses on the batch-reactor process simulation of polyesterification, while **Chapter 7** presents the simulation in PFR.

1.4.6.2 Continuous Stirred Tank Reactors (CSTR)

CSTR is a commonly encountered reactor configuration in industry. The CSTR is normally operated at steady state and is considered to be well-mixed; therefore, any spatial variations in concentration, temperature or reaction rate are disregarded.[196] The design equation for a CSTR is given by the following equation

$$V = \frac{F_{i0} - F_i}{-r_i} \tag{20}$$

The molar flow rate *F* of species *i* can be defined in terms of the molar concentration *Ci* and the volumetric flow rate *v*[196]

$$F_i = C_i v \tag{21}$$

In a single CSTR, monomer and other reactants of the polymerisation are continuously fed into the reaction vessel while the polymer and the rest of the reaction mixture are removed.[195] The residence time distribution of a CSTR is broader than that of a batch reactor, whose all contents would have the same residence time as they are introduced and removed from the reactor at the same times.[183] A cascade of CSTRs would approach the operation of a plug-flow reactor.

Industrially, the production of PET proceeds firstly by the direct esterification of terephthalic acid (TPA), which is mixed with ethylene glycol (EG) and reacted to give bishydroxyethyl terephthalate (BHET) in a train of CSTR's.[184] This is done to overcome the limited solubility of TPA. The vapours leaving the various reactors are collected and separated in a single fractionator, with the final step being the polymerisation of BHET to form PET.[184] A flowsheet of the process is depicted in **Figure 7**.

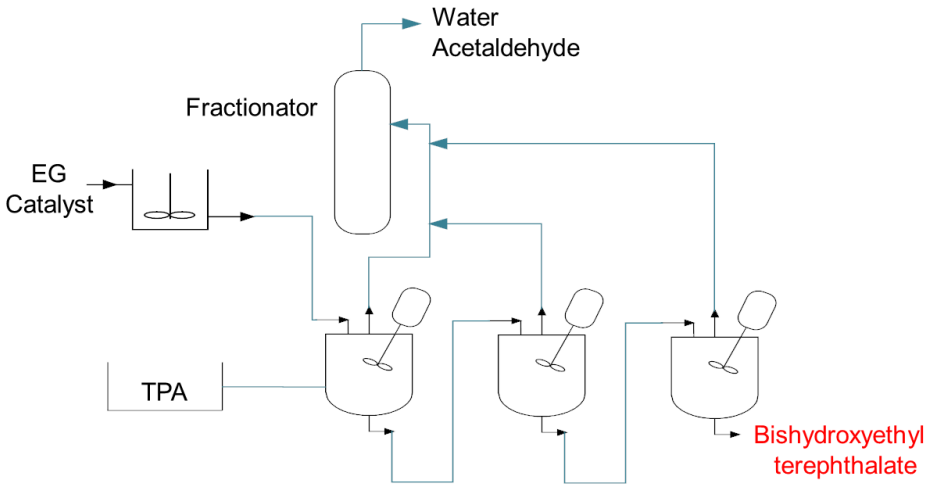

Figure 7. Flowsheet for the direct esterification of terephthalic acid (TPA) for the formation of bishydroxyethyl terephthalate, adapted and modified from Gupta.[184]

1.4.6.3 Plug-Flow Reactors (PFR)

A PFR consists of a cylindrical pipe and is operated at steady state.[196] A general representation of a tubular reactor is depicted in **Figure 8.** The design equation of a PFR in terms of the molar flow rate F of component i is defined by equation 22[196]

$$\frac{dF_i}{dV} = \nu_i(-r_A) \tag{22}$$

Where F_i is the molar flow rate of component i, V is the reactor volume, ν_i is the stoichiometric coefficient of component i (positive for products and negative for reactants), and r_A is the reaction rate for limiting reactant A.

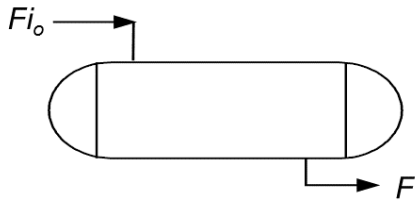

Figure 8. Tubular reactor.

The flow is considered turbulent so there is no radial variation on the concentration, but only axial; hence, the tubular reactor can be referred as a plug-flow reactor. Generally, the material at the tube centre will be at higher temperature than the reaction mixture at the tube wall. The temperature increases with the reactor's radius, because of the convention heat transfer.[183] The relatively high viscosities of polymeric species at intermediate conversions have limited the use of plug-flow reactors in polymer production.

An important application of tubular reactors is the production of high pressure, low density polyethylene,[183] although step-growth polymerisation have been described as well.[184, 197] In this vein, the V.K. tube (Vereinfacht Kontinuierliches Rohr) reactor has been reported for the nylon 6 polymerisation.[192, 198-201] The V.K. reactor is a vertical tube reactor in which internal gratings facilitate uniform heating and a nearly flat velocity profile of the reaction mass.[201] It is normally modelled as a train of 2 continuous stirred reactors (CSTR), to account for water removal, followed by a PFR, since the agitation is vigorous during the first two stages, leading to a very viscous final product.[201] The V.K. tube is said to be the first industrial reactor choice for the production of nylon 6.[200] **Figure 9** shows a schematic representation of the V.K. tube. In the present work, **Chapter 7** describes the plug flow reactor simulation for the polyesterification reactions considered.

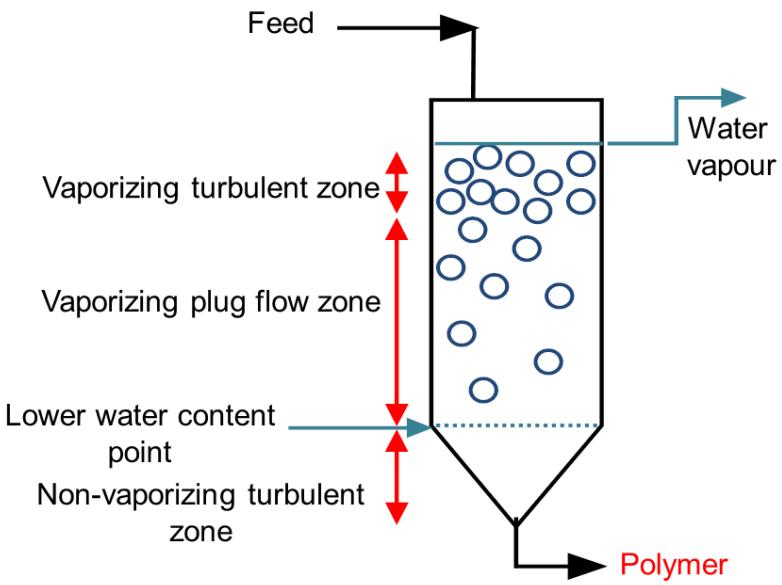

Figure 9. Industrial V.K. tube, adapted and modified from Agrawal, et al. [201]

1.5 Process simulation and optimisation

1.5.1 Simulation of chemical processes

The primary objective of polymerisation reactor modelling is to develop mathematical equations that are capable of explaining the polymerisation rate and predicting product properties accurately.[202] Process modelling could collaborate to produce the most efficient, economical and quality processes possible[190] because they can be implemented for process simulation, design, optimisation and control.[202]

Process simulation is a fantastic tool that allows chemical engineers to analyse process flowsheets, and mainly predict the performance of such processes.[203] All the required information is contained in a mathematical model in the form of equations that calculates material and energy balances coupled with phase equilibrium, transport and kinetic equations; it could also consider equipment sizing and profitability analysis.[203] There are currently several available commercial process simulation programs, such as Aspen Plus and CHEMCAD.[204]

There are well-defined steps in building a simulation in any process simulator:[204]

1. **Specification of components.** Choosing the components that will be included in the mass balance.

2. Selection of physical property models. Selecting a thermodynamic model that accurately represents the system. This will allow calculation of physical properties and phase equilibria of the studied system. In the case of polymers, where not only pure monomers and the final polymer but also segments need to be considered, group contribution methods are used so the physical properties can be determined from the constituent atoms, groups and bonds.[204] Detailed explanation of the group contribution methods used in the present work is presented in **Chapter 6**.

3. Identification of unit operations. Setting up of models that represent unit operations connected by mass and energy streams, such as reactors, columns, heat transfer equipment, rotating equipment, mixers or splitters, among others.

A diagram of a typical simulation programme is depicted in **Figure 10**.

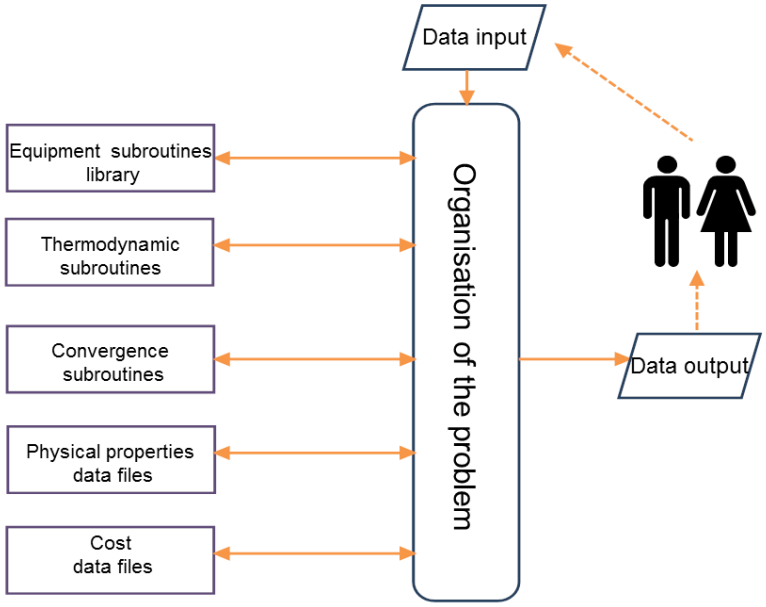

Figure 10. A typical simulation problem, adapted and modified from Towler, et al.[204]

Regarding polyesterification process simulations, previous research has focused on different polyester systems such as the reaction of maleic anhydride with 1,2-propanediol in a semi-batch reactor,[205] the reaction of glycerol and adipic acid,[206] the production of poly(3-hydroxybutyrate) by bacterial fermentation[207] and the evaluation of the process and greenhouse balance of the production of PEF from fructose via the furan pathway.[208]

One should be cautious as simulation must only be considered as a model of the process it represents with limitations determined by the assumptions made to simplify the mathematical model, the extent of knowledge about the process and the capabilities of the computing package.[209] **Chapter 6** presents the process simulation of the synthesis of biomass-derived polyesters in Aspen Plus.

1.5.2 Optimisation of chemical processes

The optimisation of chemical processes has its origin in the linear programming at the beginning of the 1960s.[210] Optimisation refers to obtaining the values of decision variables, which correspond to the maximum or minimum of one or more objective functions.[211] Thus, the main goal is to select the best alternative to some process response criteria.[210] The optimisation of a process brings on the minimisation of the operating costs, the energy consumption and the contaminant emissions, or to the maximisation of the yields and operation productivity.[210]

In an optimisation problem it is important to identify the independent characteristics that lead to different results, (independent variables) and the variables that make possible the measurement of the relative excellence of a solution (dependent variables). The set of interactions between the dependent variables that conduce to a response is known as objective function.[210] Generally, the control or manipulated variables in a polymerisation reactor are polymerisation temperature, pressure, concentration and feed rate of monomers as well as heat transfer variables, such as feed temperature of the monomers, available heat transfer area, or flow rate of the cooling-heating fluid.[212] Moreover, the objective functions of a polymerisation reactor will generally fall into the following categories: Molecular property specifications, safety, reactor and environmental constraints, and economic objectives.[212]

In the specific case of polymers, it is well-known that tackling the desired thermal and mechanical properties depends strongly on achieving a high molecular weight and a narrow molecular weight distribution, so optimal reactor operating conditions must be guaranteed.[213] Along with the final quality of the synthesised polymers, the reduction of production costs needs to be considered when implementing the polymerisation process. To achieve these goals, process optimisation represents a powerful tool for effectively designing efficient industrial operations.[214]

1.5.2.1 Multiobjective optimisation (MOO)

In chemical engineering, the presence of several conflicting objectives to be optimised simultaneously is commonly observed in practice; for example, capital investment versus operating cost; cost versus safety; quality versus recovery and cost; and environmental impact versus profitability.[211] As a result, multiobjective optimisation (MOO) rises as a suitable tool to simultaneously find the optimal solutions (Maximising/minimising) of two or more opposing objective functions.

MOO techniques can be employed to deal with the simultaneous and opposing performance objectives commonly found in polymerisation reactions. This methodology is based upon finding a set of equally good solutions, known as Pareto optimal solutions. Along the Pareto frontier, no point is better than the other solutions with respect to all objective functions.[215] Hence, there is no single solution which leads to the designation of a set of points that fit a definition of an optimum operating point.[216] Several MOO methods are commonly used in engineering fields, an excellent and comprehensive review of which was published by Marler and Arora.[216]

Within the field of multiobjective optimisation of polymerisation reactors, considerable work has been done on both the free-radical[213-215, 217] and step-growth mechanisms.[218-223] As is well-known, polyesterification falls in the latter category, as originally established by Flory[188] and studied extensively by Kumar and Gupta.[181, 184] Research on optimisation of polyester production has mainly focused on the maximisation of the population of desired functional groups while minimising residence time,[222] minimising the concentration of methyl ester and residence time in the case of the transesterification step of PET from dimethyl terephthalate (DMT),[218] and the minimisation of undesired side products, namely diethylene glycol, vinyl ester and acid end groups in the synthesis of copoly(ethylene-polyoxyethylene terephthalate).[223]

The specific use of several optimisation and multioptimisation techniques in polymerisation problems has been reviewed, namely on polymer production, design and polymer production scheduling.[224] A representation of a general set of objectives, decision variables and constraints for MOO in polymer processing is shown in **Figure 11**. **Chapter 6** contains a detailed description of multiobjective optimisation methods and polymerisation cases, along with the MOO optimisation results obtained in Aspen Plus for the synthesis of biomass-derived polyesters.

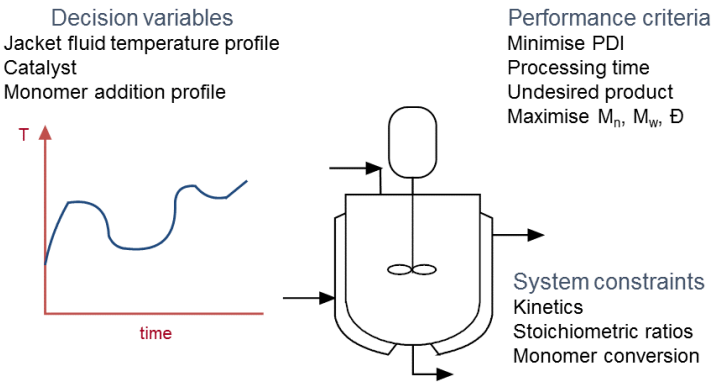

Figure 11. Set of objectives, decision variables and constraints for multi-objective optimal control in polymer processing, adapted and modified from Mitra.[224]

Overall structure of the project

The overall outline of the thesis is depicted below. The flowchart on the left shows the first sub-study, consisting in the lab-synthesis of the biomass-derived polyesters, followed by the corresponding characterisation methods to determine their physical properties (^{1}H NMR, GPC, DSC, TGA and paint characterisation). The experimental procedure determined the influence of process variables in the final product, such as type of monomers, temperature and monomer molar ratio. The experimental data acquired during this study, namely the concentration profiles of the functional groups involved (dicarboxylic acid, diol and ester), enabled the implementation of chemical engineering tools to develop an integrative research framework in the fields of polymer science, process and reactor engineering. The second sub-study, depicted below on the right flowchart, firstly entailed the estimation of kinetic parameters of each of the polymerisation systems, which were used along with the experimental data for the simulation of an industrial-scale polymerisation. This industrial problem was then optimised to determine the most efficient process conditions in terms of economics, polymer properties and sustainability.

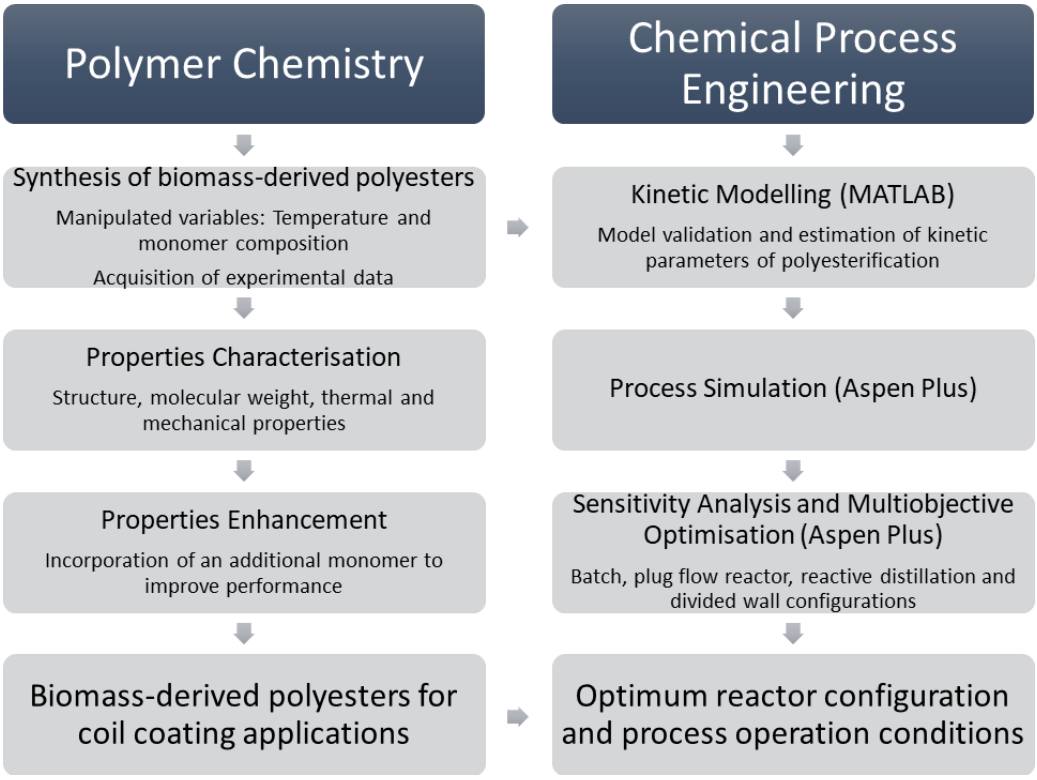

CHAPTER 2

Experimental and Characterisation Methods

2. Experimental and Characterisation Methods

2.1 Introduction

The present chapter describes the experimental procedures for the synthesis of biomass-derived polyester resins intended for coil coating applications, along with the analytical methods and characterisation techniques employed.

Firstly, all the monomers and reagents are listed, followed by the definition of the different polyesters synthesised. Second, the general experimental procedures are described. These methodologies were based on a two-step process: polyesterification and polycondensation. The polycondensation stage (second stage) was accomplished via azeotropic distillation for most of the cases, although some polymers' syntheses were vacuum-driven as well, as specified later. It is then proceeded with some processing considerations and the troubleshooting guide which were in place in case of failure during experimentation. Next, the purification methods for the polyesters are described. Finally, the specifications of the different characterisation methods are included.

2.2 Materials

The following reagents and solvents were used as received: Succinic acid (SA) (>99%, Acros Organics), 1,3-propanediol Susterra™ (PDO) (>99%, Dupont Tate & Lyle Bioproducts), 1,5-pentanediol (PTO) (99%, Acros Organics), 2,5-furan dicarboxylic acid (FDCA) (>98%, Manchester Organics), itaconic acid (IA) (99%, Acros Organics), isosorbide (IS) (98%, Acros Organics), $SnCl_2$ (Alfa Aesar, 98%), KOH in methanol (0.1 M, Sigma-Aldrich), KOH in ethanol (0.5 M, Sigma-Aldrich) xylene (Analytical grade, Fisher Scientific), methanol (HPLC grade, Fisher Scientific), phenolphthalein (99%, Sigma-Aldrich), chloroform (Analytical grade, Fisher Scientific), hexane (Analytical grade, Fischer Scientific), diethyl ether (Analytical grade, Fisher Scientific).

2.3 Experimental procedure for the synthesis of biomass-derived polyester for coil coatings

2.3.1 General polymerisation procedure

Polyesterification reactions were performed at two different scales: 250 mL and 500 mL. The choice of scale depended on the mol% FDCA in the feed, because the bulk viscosity of the system increased as the mol% FDCA was increased. Hence, all the polyesters bearing

furanic content above 50 mol% were synthesised at the 500 mL scale. The different scales also facilitated cleaning and recovery of the product, while minimising the use of solvents. Despite working with two different volumes, the geometry of the stirrer and the shape of the reactor (round-bottom) were the same in both configurations, as well as the nitrogen flow rate. (No flowmeter was in place but the nitrogen flow in a glycerol reservoir was set to 2 bubbles·s^{-1}.

The 250 mL reactions were performed in a four-neck round-bottom flask whereas the 500 mL experiments were done in a glass reactor with a 5-neck lid. The reactor was fitted with an overhead stirrer, thermocouple, sampling port, a Raschig-ring packed column and a distillation condenser. The condenser is essential for removing water and reducing loss of glycols. Nitrogen was bubbled continuously through a gas inlet to ensure the removal of water and an inert system. The reactor was heated with a heating mantle from Electrothermal™ (CMU05000/CE, 280 W) for the 500 mL scale and from WISD (WHM-C10B) for the small scale. The temperature was monitored through a digital temperature controller (MC810B for 500 mL and WHM12093 for 250 mL) coupled to the mantel. The actual reactors are shown in **Figure 12** and **Figure 13**.

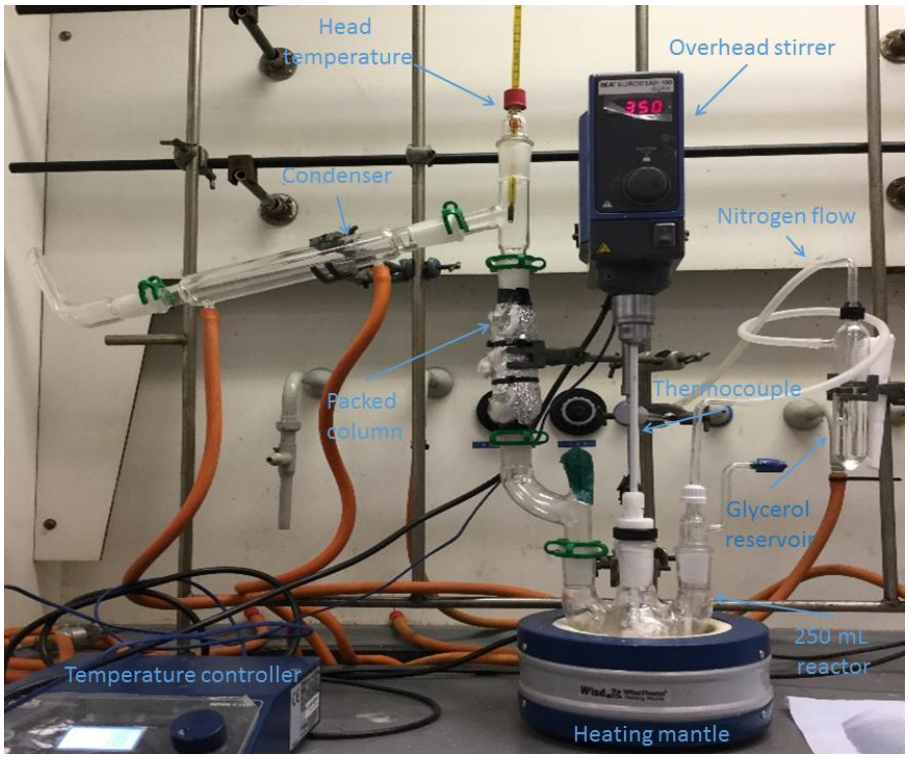

Figure 12. Four-neck round bottom flask used for the 250 mL polymerisation during the first stage (polyesterification).

The syntheses were performed following a two-stage process: esterification and polycondensation, described in the following steps:

1. First, the required amount of monomers was charged into the reactor: glycols (80-160 g), FDCA (30-160 g), SA (30-100 g), prior to heating and stirring. Liquids were weighed in first, followed by glycols then acids. In the case of copolyesters with both diacids, FDCA and the glycol(s) were mixed first and heated to 150 °C, followed by the addition of succinic acid after reaching that temperature.

Figure 13. Glass wall reactor with 5-neck lid used for the 500 mL polyesterifications during the second stage (polycondensation).

2. The reactor was then heated up to the corresponding process temperature (210-230 °C for the kinetic analysis presented in **Chapter 5**) of each particular reaction and continuously stirred at 350 rpm. The temperature was raised slowly whilst the monomers melt and not brought above 200 °C immediately to minimise the loss of glycols at early stages of the reaction. The temperature at the condenser head remained in the range of 95-100 °C while the reaction water was monitored and driven off via the condenser.

3. As the head temperature began to drop, the temperature could be increased slowly to the process temperature. The starting point of the reaction (t=0) was considered when all the

monomers were solubilised, which meant that the reaction mixture was homogeneous and achieved the clear point. The esterification reaction was completed after 2 hours, as most of the water had been removed and the head temperature was back to ambient temperature.

4. The polycondensation reaction was continued by azeotropic distillation using a Dean-Stark trap, adding 3 wt% xylene as azeotropic agent under atmospheric pressure for 5 hours to increase the molecular weight and remove residual diol. The xylene was added below 180 °C and the temperature could be then brought swiftly to the process temperature. Once at the desired temperature, the xylene should be undergoing a steady reflux. The Dean-Stark trap is shown in **Figure 14.**

5. The polymerisation was monitored every half an hour by acid value determination, which is later described in **Section 2.7.1.** After 7 hours of polymerisation, the acid value was below 5 $mg_{KOH} \cdot g_{polyester}^{-1}$ meaning the reaction reached the end point. The reactor was then cooled down and the polyester recovered.

Figure 14. Dean-Stark trap used for the azeotropic distillation during the polycondensation stage. The Dean-Stark trap was used for the polycondensation stage in both 250 and 500 mL scales.

The purpose of the azeotropic solvent is to aid in the removal of water formed during the condensation reaction. The reflux solvent and water volatilise together and liquefy in the condenser placed above the reaction vessel. A separator or Dean-Stark trap below the condenser collects this liquid mixture, and the azeotrope solvent is returned to the reactor.[225]

A flowsheet of the semi-batch polyesterification (first stage) process is depicted in **Figure 15**. This flowsheet is the same for the two scales, as the polyesterification stage is carried out in the same way by using a Rashig-ring packed column.

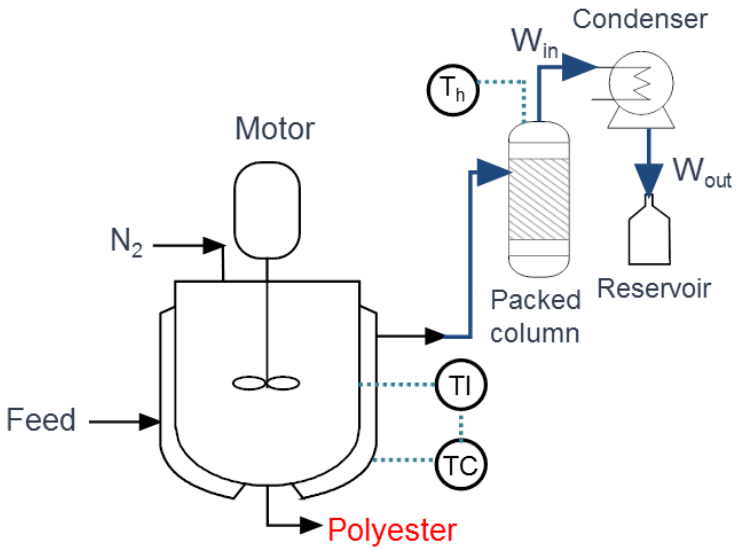

Figure 15. Process flowsheet of the semi-batch polyesterification process (first stage) for the 250 mL and 500 mL scales.

2.3.2 Vacuum-driven polycondensation

As a proof of concept, some polyester resins where alternatively synthesised by applying vacuum during the second stage or polycondensation, after all the water of esterification has been released. This alternative configuration was pursued in order to compare the processing methods in terms of key final polymer properties, such as molecular weight, dispersity and thermal properties. For this configuration, the system reactor was coupled with a distilling head, a diaphragm pump (MZ 2C NT, Vacuubrand) and a vacuum controller (CVC 3000 controller, Vacuubrand). A cold trap (B45 Rodaviss joint, JY valve) was placed in an 1800 mL-tall foam dewar with liquid nitrogen to prevent vapours from entering the vacuum pump where they would condense and lead to severe contamination and damage. **Figure 16** shows the actual vacuum-set up. The vacuum was set to 300 mbar for the remaining 5 hours of processing time and the joints were perfectly sealed with Parafilm to avoid any leakages. **Table 9** summarises the polyesters synthesised using this configuration.

Figure 16. Vacuum-driven polycondensation stage.

2.3.3 Biomass-derived polyesters for coil coatings

Tables 4-8 summarise the different biomass-derived polyesters synthesised, including the reaction conditions. Within these polyesters, poly(propylene succinate) (PPS), poly(propylene 2,5-furandicarboxylate) (PPF) and poly(pentylene 2,5-furandicarboxylate) (PPeF) have been previously synthesised by other researchers.[75, 81, 226, 227] All the other polyesters presented herein are completely novel. The polyesters are classified according the type of glycol in their structure. Detailed synthetic procedures for each family of polyesters are described in the following subsections. **Schemes 16-20** show the corresponding chemical structures of the biomass-derived polyesters synthesised in the present study.

The polyesters' nomenclature is based on the diol used (1,3-propanediol or 1,5-pentanediol), the diacid molar ratio (FDCA:SA) and in some cases, the molar proportion of isosorbide or itaconic acid present. For a typical polyester name, the first *P* refers to the suffix *poly*, followed either by *P* or *Pe*, if synthesised with 1,3-propanediol or 1,5-pentanediol, respectively. Next, if the polyesters bear F_x, this indicates the presence of FDCA in *x* mol%. Similarly, S_y refers to succinic acid present in *y* mol%. Finally, if *I* or *Ia* are found in the nomenclature, the polyesters contain isosorbide and itaconic acid units, respectively, with subscripts indicating their mol%. For example, $PPeF_{15}I_{10}S_{85}$ refers to a polymer synthesised from 1,5-pentanediol, 15 mol% FDCA, 10 mol% isosorbide and 85 mol% SA

Table 4. Synthesised biomass-derived polyesters with 1,3-propanediol

1,3-propanediol (PDO)						
No.	**Acronym**	**Name**	**T,[a] °C**	**Mol% FDCA**	**Mol% SA**	**r[b]**
1	PPS	poly(1,3-propylene succinate)	210-230	-	100	1.1
2	PPF	poly(1,3-propylene 2,5-furandicarboxylate)	210-230	100	-	1.6
3a	$PPF_{15}PS_{85}$	poly(1,3-propylene 2,5-furandicarboxylic acid-co-1,3-propylene succinate)	210-230	15	85	1.5
3b	$PPF_{30}PS_{70}$			30	70	
3c	$PPF_{70}PS_{30}$			70	30	
3d	$PPF_{85}PS_{15}$			85	15	

[a] Reaction temperature, [b] molar ratio diol:diacid.

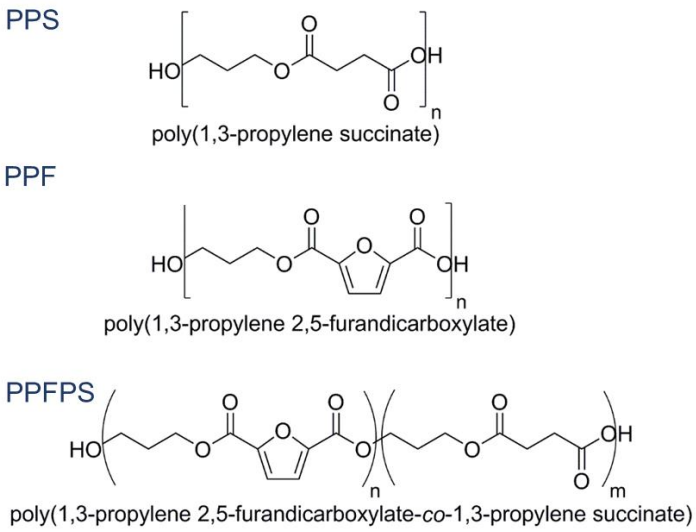

Scheme 16. Chemical structures of 1,3-propanediol-based polyester resins (**1-3**).

Table 5. Synthesised biomass-derived polyesters with 1,5-pentanediol

1,5-pentanediol (PTO)						
No.	**Acronym**	**Name**	**T,[a] °C**	**Mol% FDCA**	**Mol% SA**	**r[b]**
4	PPeS	poly(1,5-pentylene succinate)	210-230	-	100	1.05
5	PPeF	poly(1,5-pentylene 2,5-furandicarboxylate)	210-230	100	-	1.3
6a	$PPeF_{15}S_{85}$	poly(1,5-pentylene 2,5-furandicarboxylate-co-1,5-pentylene succinate)	210-230	15	85	1.3
6b	$PPeF_{30}S_{70}$			30	70	
6c	$PPeF_{70}S_{30}$			70	30	
6d	$PPeF_{85}S_{15}$			85	15	

[a] Reaction temperature, [b] molar ratio diol:diacid.

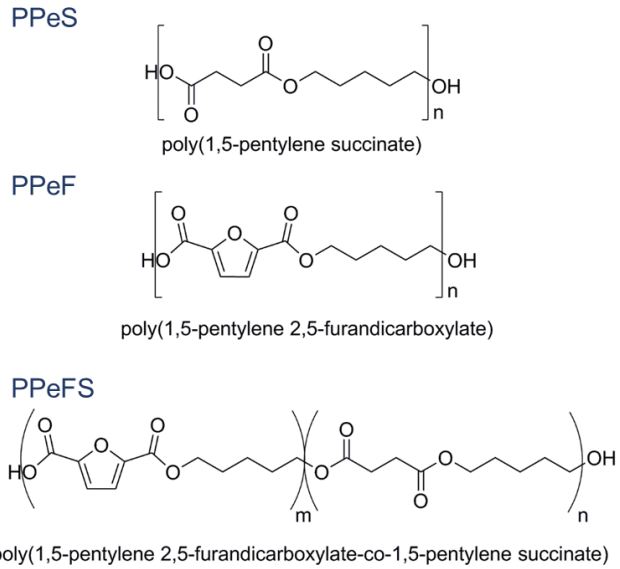

Scheme 17. Chemical structures of 1,5-pentanediol-based polyester resins (**4-6**).

Table 6. Synthesised biomass-derived polyesters with 1,3-propanediol and isosorbide

No.	Acronym	Catalyst[a]	T[b], °C	Mol% FDCA	Mol% IS[c]	r[d]
			Isosorbide			
			1,3-propanediol			
7a	$PPF_{15}I_{30}S_{85}$				30	
7b	$PPF_{15}I_{60}S_{85}$	$SnCl_2$	215	15	60	1.5
7c	$PPF_{15}I_{70}S_{85}$				70	
8a	$PPF_{30}I_{30}S_{70}$				30	
8b	$PPF_{30}I_{60}S_{70}$	$SnCl_2$	215	30	60	1.5
8c	$PPF_{30}I_{70}S_{70}$				70	
9a	$PPF_{70}I_{10}S_{30}$				10	
9b	$PPF_{70}I_{30}S_{30}$	$SnCl_2$	215	70	30	1.5
9c	$PPF_{70}I_{50}S_{30}$				50	
10a	$PPF_{85}I_{10}S_{15}$				10	
10b	$PPF_{85}I_{30}S_{15}$	$SnCl_2$	215	85	30	1.5
10c	$PPF_{85}I_{50}S_{15}$				50	

[a] 0.02 mol%$SnCl_2$/mol diacid [b] Reaction temperature, [c] Isosorbide, [d]Molar ratio diols:diacids

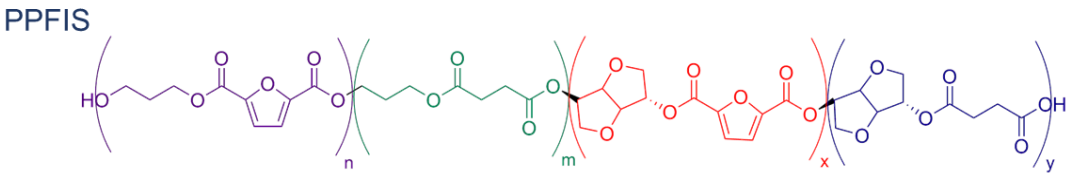

Scheme 18. Polyesters from 1,3-propanediol, isosorbide, succinic acid and FDCA (**7-10**).

Table 7. Synthesised biomass-derived polyesters with 1,5-pentanediol and isosorbide

No.	Acronym	Catalyst[a]	T[b], °C	Mol% FDCA	Mol% IS[c]	r[d]
			1,5-pentanediol			
11a	$PPeI_{10}S$				10	
11b	$PPeI_{30}S$				30	
		$SnCl_2$	215	-		1.3
11c	$PPeI_{50}S$				50	
11d	$PPeI_{60}S$				60	
12a	$PPeF_{15}I_{10}S_{85}$				10	
12b	$PPeF_{15}I_{30}S_{85}$				30	
12c	$PPeF_{15}I_{50}S_{85}$	$SnCl_2$	215	15	50	1.3
12d	$PPeF_{15}I_{60}S_{85}$				60	
12e	$PPeF_{15}I_{70}S_{85}$				70	
13a	$PPeF_{30}I_{10}S_{70}$				10	
13b	$PPeF_{30}I_{30}S_{70}$				30	
13c	$PPeF_{30}I_{50}S_{70}$	$SnCl_2$	215	30	50	1.3
13d	$PPeF_{30}I_{60}S_{70}$				60	
13e	$PPeF_{30}I_{70}S_{70}$				70	
14a	$PPeF_{70}I_{10}S_{30}$				10	
14b	$PPeF_{70}I_{30}S_{30}$	$SnCl_2$	215	70	30	1.3
14c	$PPeF_{70}I_{50}S_{30}$				50	
15a	$PPeF_{85}I_{10}S_{15}$				10	
15b	$PPeF_{85}I_{30}S_{15}$	$SnCl_2$	215	85	30	1.3
15c	$PPeF_{85}I_{50}S_{15}$				50	

[a] 0.02 mol%$SnCl_2$/mol diacid [b] Reaction temperature, [c] Isosorbide, [d]Molar ratio diols:diacids

PPeFIS

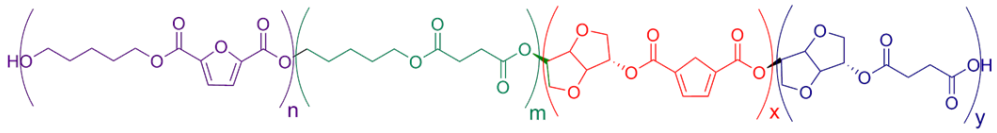

Scheme 19. Polyesters from 1,5-pentanediol, isosorbide, succinic acid and FDCA (**12-15**).

Table 8. Synthesised biomass-derived polyesters with itaconic acid (IA)

No.	Acronym	Catalyst	T,[c] °C	Mol% IA	r[d]
16a	$PPeSIa_5$			5	
16b	$PPeSIa_{10}$	$Ti(OBu)_4$[a]	190	10	1
16c	$PPeSIa_{15}$			15	
17	PPeIa	$SnCl_2$[b]	160	100	1
18	PPIa	$SnCl_2$[b]	160	100	1

[a] 0.05 weight% $Ti(OBu)_4$/total charge, [b] 0.5 mol% $SnCl_2$/mol_{IA} [c]Reaction temperature, [d] Molar ratio diols:diacids

PPeSIa

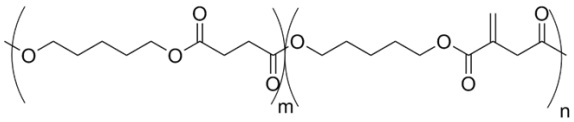

PPeIa

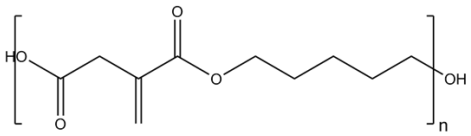

PPIa

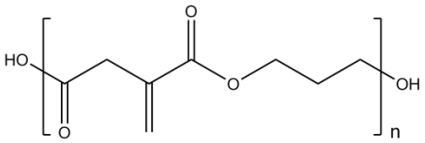

Scheme 20. Polyesters from itaconic acid with 1,5-pentanediol and succinic acid (PPeSIa,**16**); 1,5-pentanediol (PPeIa,**17**) and. 1,3-propanediol (PPIa, **18**).

Table 9. Polyesters synthesised by application of vacuum during polycondensation

No.	Polyester
3a	$PPF_{15}PS_{85}$
6a	$PPeF_{15}S_{85}$
3b	$PPF_{30}PS_{70}$
6b	$PPeF_{30}S_{70}$
7a	$PPF_{15}I_{30}S_{85}$
7b	$PPF_{15}I_{50}S_{85}$
12c	$PPeF_{15}I_{30}S_{85}$
12d	$PPeF_{15}I_{50}S_{85}$
13b	$PPeF_{30}I_{30}S_{70}$

2.3.3.1 Synthesis of polyester 1: PPS

1. To a 250 mL 4-neck round-bottom flask equipped with an overhead stirrer, was added 80 g (1.047 mol) of 1,3-propanediol (PDO) and 112 g (0.95 mol) of succinic acid.

2. The reactor was heated up to different reaction temperatures: 210, 220 or 230 °C and was continuously stirred at 350 ppm. The esterification stage was completed after 2 hours when all the water had been released and the head temperature on top of the distillation column was back to ambient temperature.

3. The polycondensation reaction was carried out by azeotropic distillation by changing the packed column to a Dean Stark trap, adding 3 wt% xylene as azeotropic agent under atmospheric pressure for 5 hours.

4. The reaction was then cooled down and the polymer was poured into glass containers for further characterisation. Samples were taken every 30 minutes.

^{1}H NMR ($CDCl_3$, δ/ppm, 400 MHz): PPS, 4.26 (t, 4H, -C**H**2- CH2- CH2- CH2- C**H**2-); 2.63 (s, 2H,-O-C**H**2-C**H**2-O-); 1.98 (m, 2H, -CH_2- C**H**$_2$- CH_2).

Scheme 21 depicts the reaction conditions (time and temperature) during polyesterification and polycondensation, listed as 1) and 2), respectively. The bold number in the right-hand side of the arrows (product) indicates the particular polymer synthesised,

which is named according to **Tables 4-8**. In this specific case, PSS or polyester **1**, was defined in **Table 4**. All the polyesters are depicted in a similar fashion in **Schemes 22-32**.

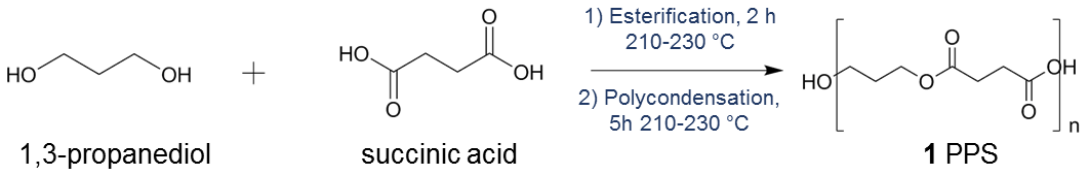

Scheme 21. Synthesis of polyester **1**, PPS.

2.3.3.2 Synthesis of polyester 2: PPF

1. To a 500 mL single wall glass reactor with a 5-neck lid equipped with an overhead stirrer, was added 80 g (1.047 mol) of PDO and 112 g (0.95 mol) of FDCA.

2. The reactor was heated up to different reaction temperatures: 210, 220 or 230 °C and was continuously stirred at 350 ppm. The esterification stage was completed after 2 hours when all the water had been released and the head temperature on top of the distillation column was back to ambient temperature.

3. The polycondensation reaction was carried out by azeotropic distillation by changing the packed column to a Dean Stark trap, adding 3 wt% xylene as azeotropic agent under atmospheric pressure for 5 hours.

4. The reaction was then cooled down and the polymer was poured into glass containers for further characterisation. Samples were taken every 30 minutes. **Scheme 22** shows the synthetic procedure.

^{1}H NMR ($CDCl_3$, δ/ppm, 400 MHz): PPF, 7.35 (s, 2H, H_3, H_4, furan ring); 4.39 (t, 4H, - C**H**$_2$- CH_2- C**H**$_2$-); 1.80 (m, 2H, -CH_2- C**H**$_2$- CH_2-).

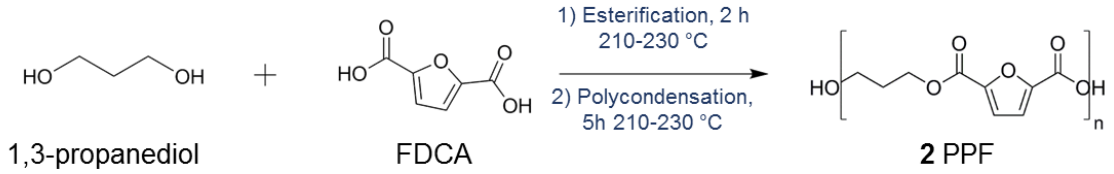

Scheme 22. Synthesis of polyester **2**, PPF.

2.3.3.3 Synthesis of polyesters 3: PPFPS

This experimental procedure was followed for all polyesters by adjusting the ratio of the monomers accordingly. The exact quantities are available in **Appendix A**.

1. In a typical polymerisation to synthesise polyester **3a**, to a 250 mL 4-neck round-bottom flask equipped with an overhead stirrer, was added 91 g (1.2 mol) of PDO and 19 g (0.12 mol) of FDCA.

2. The reactor was heated up to 150 °C and 80 g of succinic acid (0.68 mol) was added. The temperature was increased to the corresponding process temperature: 210, 220 or 230 °C and was continuously stirred at 350 ppm. The esterification stage was completed after 2 hours when all the water had been released and the head temperature on top of the distillation column was back to ambient temperature.

3. The polycondensation reaction was carried out by azeotropic distillation by changing the packed column to a Dean Stark trap, adding 3 weight% xylene as azeotropic agent under atmospheric pressure for 5 hours.

4. The reaction was then cooled down and the polymer was poured into glass containers for further characterisation. Samples were taken every 30 minutes. **Scheme 23** shows the synthetic procedure.

^{1}H NMR ($CDCl_3$, δ/ppm, 400 MHz): PPFPS, 7.27 (s, 2H, H_3, H_4, furan ring); 4.50 (t, 4H, - C**H**$_2$- CH_2-C**H**$_2$-FDCA); 4.24 (t, 4H, -C**H**$_2$- CH_2- C**H**$_2$-SA); 3.78 (m, 2H,O-CH_2-CH_2-C**H**$_2$-OH);2.63 (s, 2H, -O-C**H**$_2$-C**H**$_2$-O-, succinic acid); 2.17 (m, 2H, O-CH_2- C**H**$_2$- CH_2-O); 1.87 (m, 2H,O -CH_2- C**H**$_2$- CH_2-OH).

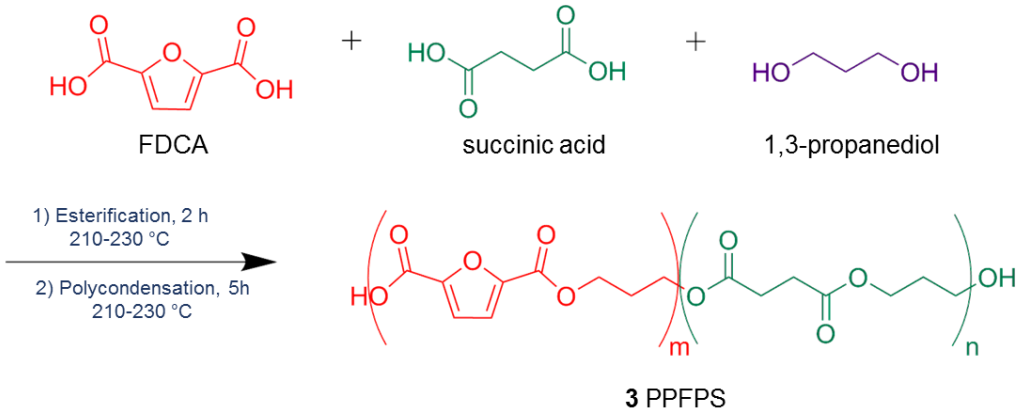

Scheme 23. Synthesis of polyester **3**, PPFPS.

2.3.3.4 Synthesis of polyester 4: PPeS

The experimental procedure followed correspond to that described in **Section 2.3.3.1** using 1,5-pentanediol as diol instead of 1,3-propanediol and adjusting the ratio of the monomers accordingly. **Scheme 24** shows the synthetic procedure.

^{1}H NMR ($CDCl_3$, δ/ppm, 400 MHz): PPeS, 4.09 (t, 4H, -C**H**$_2$- CH_2- CH_2- CH_2- C**H**$_2$-); 2.62 (s, 2H,-O-C**H**$_2$-C**H**$_2$-O-); 1.66 (m, 4H, -CH_2- C**H**$_2$- CH_2- C**H**$_2$- CH_2-); 1.44 (m, 4H, -CH_2- CH_2- C**H**$_2$- CH_2- CH_2-).

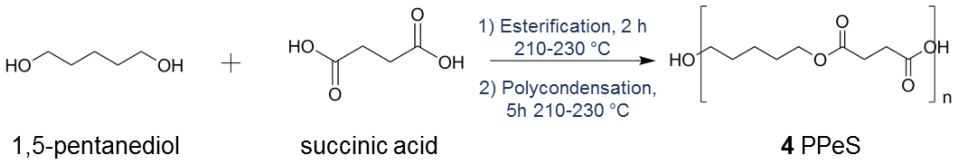

Scheme 24. Synthesis of polyester **4**, PPeS.

2.3.3.5 Synthesis of polyester 5: PPeF

The experimental procedure followed correspond to that described in **Section 2.3.3.2** using 1,5-pentanediol as diol instead of 1,3-propanediol and adjusting the ratio of the monomers accordingly. **Scheme 25** shows the synthetic procedure.

^{1}H NMR ($CDCl_3$, δ/ppm, 400 MHz): PPeF, 7.2 (s, 2H, H_3, H_4, furan ring); 4.35 (t, 4H, -C**H**$_2$- CH_2 - CH_2 - CH_2-C**H**$_2$-); 1.84 (m, 2H, -CH_2- C**H**$_2$- CH_2- C**H**$_2$-CH_2-); 1.55 (m, 4H, -CH_2- CH_2- C**H**$_2$- CH_2- CH_2-).

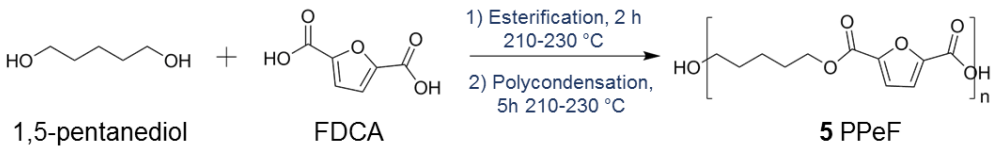

Scheme 25. Synthesis of polyester **5**, PPeF.

2.3.3.6 Synthesis of polyester 6: PPeFS

The experimental procedure followed correspond to that described in **Section 2.3.3.3** using 1,5-pentanediol as diol instead of 1,3-propanediol for all polyesters and adjusting the ratio of the monomers accordingly. **Scheme 26** shows the synthetic procedure.

^{1}H NMR ($CDCl_3$, δ/ppm, 400 MHz): PPeFS, 7.2 (s, 2H, H_3, H_4, furan ring); 4.36 (t, 4H, - C**H**$_2$- CH_2 - CH_2 - CH_2-C**H**$_2$-FDCA); 4.11 (t, 4H, -C**H**$_2$- CH_2- CH_2- CH_2- C**H**$_2$-SA); 2.62 (s, 2H, -O-C**H**$_2$-C**H**$_2$-O-, succinic acid); 1.84 (m, 2H, -CH_2- C**H**$_2$- CH_2- C**H**$_2$-CH_2-); 1.68 (m, 4H, -CH_2- C**H**$_2$- CH_2- C**H**$_2$- CH_2-); 1.57 (m, 4H, -CH_2- CH_2- C**H**$_2$- CH_2- CH_2-).

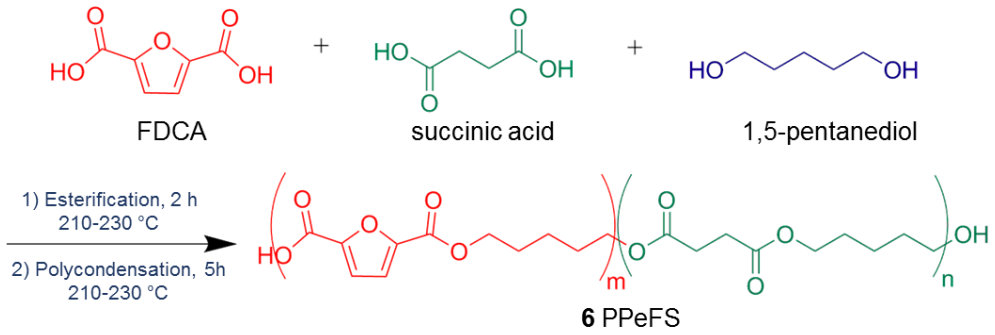

Scheme 26. Synthesis of polyester **6**, PPeFS.

2.3.3.7 Synthesis of polyesters 7-10: PPFIS

This experimental procedure was followed for all polyesters by adjusting the ratio of the monomers accordingly. The exact quantities for each polyester are available in **Appendix A**. **Scheme 27** shows the synthetic procedure, including the catalyst used (0.02 mol% relative to the diacids).

1. In a typical polymerisation to synthesise polyester **7a**, to a 250 mL 4-neck-round bottom flask equipped with an overhead stirrer, was added 59 g (0.77 mol) PDO, 48 g (0.33 mol) of isosorbide and 17 g (0.11 mol) of FDCA.

2. The reactor was heated up to 150 °C and 74 g (0.62 mol) of succinic acid and $SnCl_2$ were added. The temperature was increased to 215 °C and was continuously stirred at 350 ppm. The esterification stage was completed after 2 hours when all the water had been released and the head temperature on top of the distillation column was back to ambient temperature.

3. The polycondensation reaction was carried out by azeotropic distillation by changing the packed column to a Dean Stark trap, adding 3 wt% xylene as azeotropic agent under atmospheric pressure for 5 hours.

4. The reaction was then cooled down and the polymer was poured into glass containers for further characterisation. Samples were taken hourly.

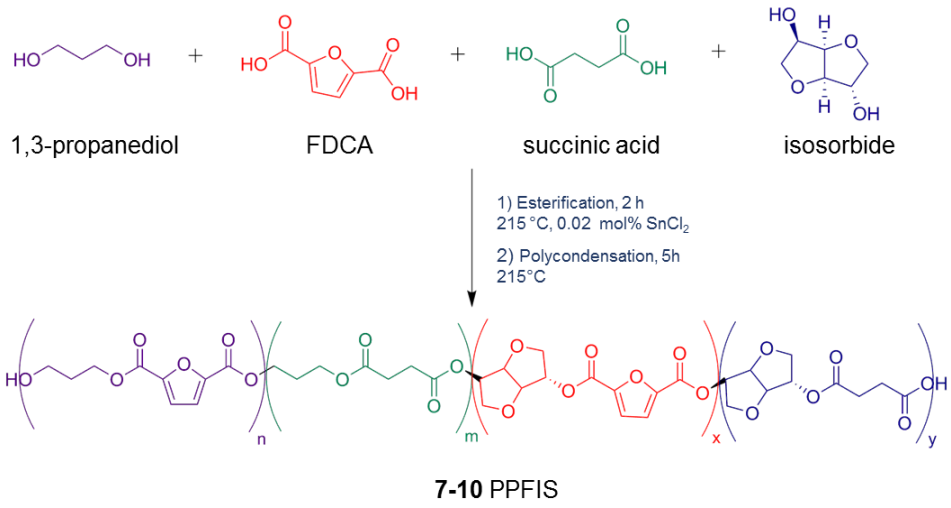

7-10 PPFIS

Scheme 27. Synthesis of polyesters **7-10**, PPFIS.

2.3.3.8 Synthesis of polyester 11: PPeIS

1. In a typical polymerisation to synthesise **11a**, to a 250 mL 4-neck-round bottom flask equipped with an overhead stirrer, was added 89 g (0.86 mol) of 1,5-pentanediol (PTO) and 14 g (0.09 mol) of isosorbide.

2. The reactor was heated up to 150 °C and 86 g (0.73 mol) of succinic acid and $SnCl_2$ (0.02 mol% relative to the diacids) were added. The temperature was increased to 215 °C and was continuously stirred at 350 ppm. The esterification stage was completed after 2 hours when all the water had been released and the head temperature on top of the distillation column was back to ambient temperature.

3. The polycondensation reaction was carried out by azeotropic distillation by changing the packed column to a Dean Stark trap, adding 3 weight% xylene as azeotropic agent under atmospheric pressure for 5 hours.

4. The reaction was then cooled down and the polymer was poured into glass containers for further characterisation. Samples were taken hourly. **Scheme 28** shows the synthetic procedure.

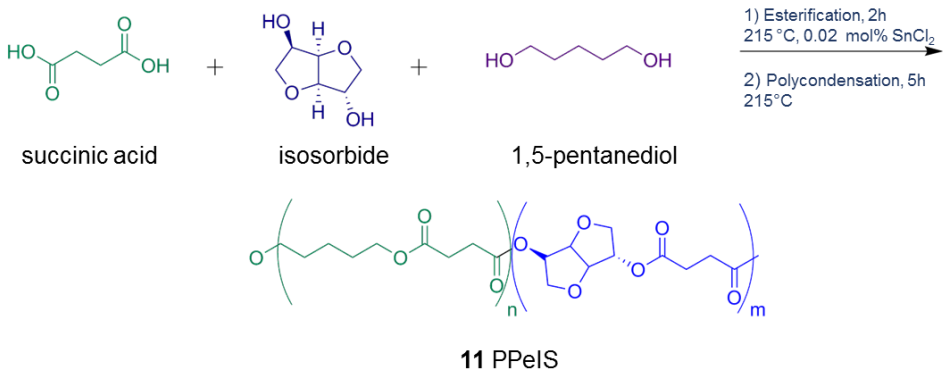

Scheme 28. Synthesis of polyester **11**, PPeIS

2.3.3.9 Synthesis of polyesters 12-15: PPeFIS

The experimental procedure followed correspond to that described in **Section 2.3.3.7** using 1,5-pentanediol as diol instead of 1,3-propanediol for all polyesters and adjusting the ratio of the monomers accordingly. **Scheme 29** shows the synthetic procedure.

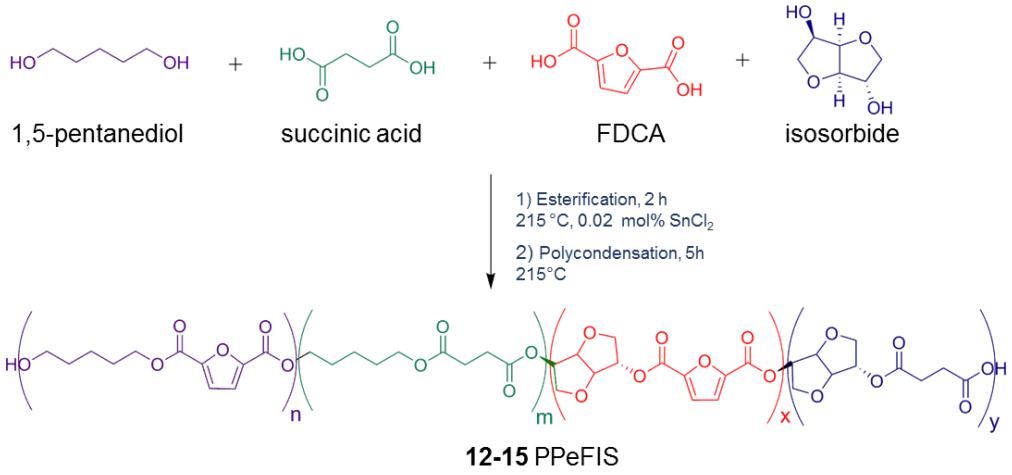

Scheme 29. Synthesis of polyesters **12-15**, PPeFIS.

*2.3.3.10 Synthesis of PPeSIa_5 (**16a**)*

The synthesis of polyester **16**, PPeSIa was achieved by following the experimental procedure proposed by Teramoto, et al.[108]

1. To a 250 mL 4-neck-round bottom flask equipped with an overhead stirrer, was added 89 g (0.85 mol) of 1,5-pentanediol, 11 g (0.085 mol) of itaconic acid and 90 g (0.76 mol) of succinic acid.

2. The reactor was heated up stepwise to 190 °C and when the clear point was reached, approximately at 160 °C, $Ti(OBu)_4$ (0.05 weight% relative to the total charge) was added. The reactor was continuously stirred at 350 ppm. The esterification stage was completed after 2 hours when all the water had been released and the head temperature on top of the distillation column was back to ambient temperature.

3. The polycondensation reaction was carried out by azeotropic distillation by changing the packed column to a Dean Stark trap, adding 3 weight% xylene as azeotropic agent under atmospheric pressure for 5 hours.

4. The reaction was then cooled down and the polymer was poured into glass containers for further characterisation. Samples were taken every 30 minutes. **Scheme 30** shows the synthetic procedure.

^{1}H NMR ($CDCl_3$, δ/ppm, 400 MHz): PPeSIa, 6.32 (s, H, =C**H**$_2$-); 5.71 (s, H,=C**H**$_2$) 4.09 (t, 4H, -CO-C**H**$_2$-CH_2-SA); 2.62 (s, 2H,-O-C**H**$_2$-C**H**$_2$-O-); 3.30 (d,2H,-O-CO-C**H**$_2$-); 1.66 (m,2H,O-CO-CH_2-C**H**$_2$-C**H**$_2$-CH_2-CH_2); 1.42 (m, 2H, O-CO-CH_2-CH_2-CH_2-C**H**$_2$-CH_2); 3.33 (m, 2H, O-CO-CH_2-CH_2-CH_2-CH_2-C**H**$_2$).

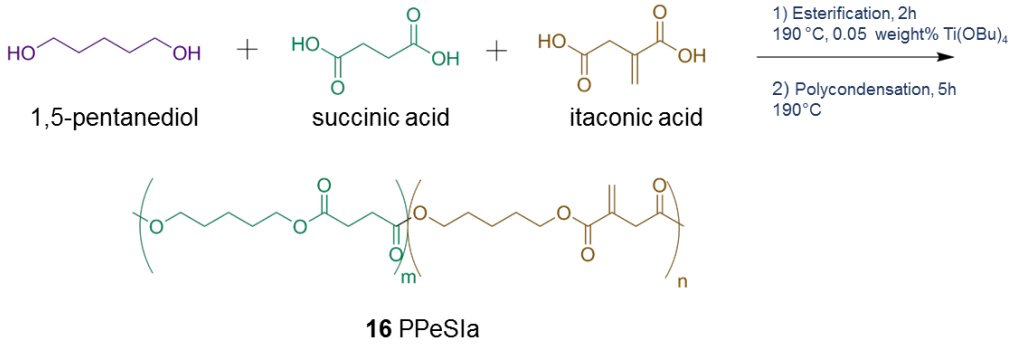

16 PPeSIa

Scheme 30. Synthesis of polyester **16**, PPeSIa

*2.3.3.11 Synthesis of PPeIa (**17**)*

The syntheses of polyesters **17** and **18**, PPeIa and PPIa, respectively were achieved by following the experimental procedure proposed by Dai, et al.[111]

1. To a 250 mL 4-neck-round bottom flask equipped with an overhead stirrer, was added 94 g (0.90 mol) of 1,5-pentanediol, 129 g (0.99 mol) of itaconic acid, 0.5

mol%/$mol_{itaconic\ acid}$ of $SnCl_2$ as catalyst and hydroquinone (0.5 weight% relative to the total charge) as a free radical polymerisation inhibitor.

2. The reactor was heated up stepwise to 160 °C and was continuously stirred at 350 ppm. The esterification stage was completed after 2 hours when all the water had been released and the head temperature on top of the distillation column was back to ambient temperature.

3. The polycondensation reaction was carried out by azeotropic distillation by changing the packed column to a Dean Stark trap, adding 3 weight% xylene as azeotropic agent under atmospheric pressure for 5 hours.

4. The reaction was then cooled down and the polymer was poured into glass containers for further characterisation. The polyester was purified according to section **2.6.2**. **Scheme 31** shows the synthetic procedure.

^{1}H NMR ($CDCl_3$, δ/ppm, 400 MHz): PPeIa, 6.24 (s, H, =C**H**$_2$-); 5.82 (s, H,=C**H**$_2$) 4.01-4.08 (t, 4H, -CO-C**H**$_2$-CH_2-); 3.30 (d,2H,-O-CO-C**H**$_2$-); 1.58 (m,2H,O-CO-CH_2-C**H**$_2$-C**H**$_2$-CH_2-CH_2); 1.33 (m, 2H, O-CO-CH_2-CH_2-CH_2-C**H**$_2$-CH_2); 3.3 (m, 2H, O-CO-CH_2-CH_2-CH_2-CH_2-C**H**$_2$).

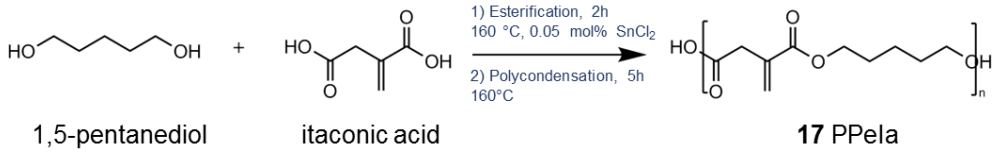

Scheme 31. Synthesis of polyester **17**, PPeIa.

*2.3.3.12 Synthesis of PPIa (**18**)*

The experimental procedure followed correspond to that described in **Section 2.3.3.11** using 1,3-propanediol instead of 1,5-pentanediol for all polyesters and adjusting the ratio of the monomers accordingly.

^{1}H NMR ($CDCl_3$, δ/ppm, 400 MHz) 6.22 (s, H, =C**H**$_2$-); 5.84 (s,H,=C**H**$_2$) 4.08-4.16 (t, 4H, -O-C**H**$_2$-C**H**$_2$-O); 3.32-3.44 (d,2H,-O-CO-C**H**$_2$-CH_2); 1.91 (m,2H,O-CO-CH_2-C**H**$_2$-).

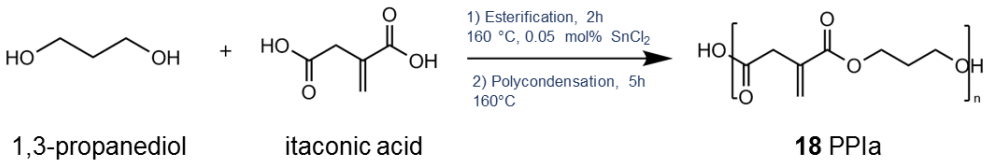

Scheme 32. Synthesis of polyester **18**, PPIa.

2.4 Process development of polyesterification with FDCA: Processing of polyesters 2, 3, 5, and 6.

Successful polymerisation and copolymerisation of FDCA were obtained following some method development. The range of operation temperatures were chosen according to published results[74, 75, 84] and our previous experience. This experience was based on initial polymerisation trials which showed that processing above 230 °C promoted gelation and difficulties during the determination of acid value because of the insolubility of the resin in the titration solvents. Processing below 210 °C on the other hand, was not enough for full dissolution of FDCA, so the clear point could not be reached, leading to the formation of hot spots.

Optimal diol:diacid ratio was determined through an iterative process. Polymerisations were carried out at 220 °C starting at a diol:diacid molar ratio of 5:1, going down to 3:1, 2:1, 1.8:1 and finally 1.3:1, 1.3:1, 1.5:1, 1.6:1 for polyesters **5**, **6c-6d**, **3c-3d** and **2**, respectively. These ratios were in agreement with previous works on FDCA-based polyesters.[75, 84] In polymerisation attempts with lower diol:diacid molar ratios, FDCA did not dissolve and the reaction mixture was a white paste that would burn under heating rather than polymerise.

It was also found that proper dispersing of the FDCA powder is crucial to avoid the formation of hot spots. When all reagents were added together, areas of high FDCA concentration would form in the early stages of the polymerisation at the bottom of the reactor where mixing was insufficient. It was found that a preliminary step of mechanical mixing of the diol and FDCA followed by heating up to 150 °C before the addition of succinic acid overcame the diffusion limitation provoked by the poor solubility of FDCA.

During these preliminary studies it was found that special considerations did not need to be applied for the succinic acid-rich systems, such as PPS (**1**), PPeS (**4**),

$PPF_{15}PS_{85}$/$PPeF_{15}S_{85}$ (**3a,6a**) and $PPF_{30}PS_{70}$/$PPeF_{30}S_{70}$ (**3b,6b**). The polymerisation mixtures were still processable with a diol to succinic acid ratio as low as 1.05.

2.5 Troubleshooting

Table 10 provides a quick guide of common problems encountered during the processing of polyester resins, including the possible causes and potential solutions. These techniques were applied accordingly when needed and provided a fundamental tool during process development in order to achieve a successful polymerisation in terms of safety, properties and aesthetics of the final polyester resins and delimit the final operation procedure to be followed further on.

Table 10. Troubleshooting guide, causes and solutions during the processing of polyester resins

Problem	Possible Cause	Suggested Solution
Poor resin colour	Poor agitation	Improve agitation, and/or modify baffles, as the initial charge may easily collect on them.
	Hot spots	Improve agitation and assure full solubility of raw materials.
Processing time too long	Contaminants	Proper storage of raw materials.
	Poor agitation	Improve agitation and/or increase the rate of nitrogen to aid removal of water of esterification.
	Inadequate heat supply	Ensure the equipment is well insulated and that the reaction mixture is 75% volume capacity of the vessel.
High glycol losses	Inefficient condenser	Use condensers with packed columns. Wrap the condenser with insulation tape to reduce heat loss.
	Temperature too high	Very high temperature may increase glycol loss. Reduce the heat applied.
Resin gelation	Improper ratio of raw materials	Double check weights of monomers and test solubility and compatibility of monomers before processing.
	Glycol loss	Reduce the heat applied.

2.6 Purification of polyester resins

The final product of the polyesterification reaction may contain different chain length oligomers as well as remaining diol or any other side-reaction product that may interfere in the characterisation methods. In order to remove these undesired compounds, a purification of the final resin is required.

The purification method to be used on the resin depends on the concentration of the diacids used and its final physical state. The purification is based on the solubility of the resins in different solvents. The aim is to dissolve everything but the resin, washing away other compounds.

For a complete characterisation of the resin, 5 g of non-purified resin was weighed in a 100 mL beaker. Smaller beakers may be used, but the risk of overflowing and splashing while drying is high.

2.6.1 Purification of PPS (1), PPeS (4, 11), polyesters with 15/85 (3a, 6a, 7, 12) or 30/70 (3b, 6b, 8, 13) FDCA/SA molar ratio

1. Fill the beaker up to a 10% of its total height with hexane, stir magnetically and ensure that the solvent does not evaporate and that the resin is completely dissolved in it (no lumps or regions with different density).
2. Once this mixing is achieved, top up with methanol. To ensure an efficient contact of the hexane-dissolved resin phase with methanol a gentle stirring may be applied. After this, cover with Parafilm and allow settling and cooling down in ice. This stirring shall never create a suspension. Once there are to different phases observed (1-2 h), remove the largest amount of the above phase (disposing it in the solvent container). Remove the rest of this phase with a syringe, drawing out the minimum amount possible of the denser phase.
3. Vacuum-dry overnight in the oven at 50ºC. Maximum allowed temperature is 55ºC, otherwise the boiling of the liquid resins will be too abrupt and the resin will overflow the beaker.

2.6.2 Purification of polyesters with 70/30 FDCA/SA molar ratio (3c, 6c, 9 and 14) and polyesters with itaconic acid (16-18)

The same procedure in **2.6.1** is followed, but chloroform is used instead of hexane as the solvent in step 1.

2.6.3 Purification of polyesters with 85/15 FDCA/SA molar ratio (3d, 6d, 10 and 15)

1. Fill the beaker up to a 10% of its total height with chloroform, stir magnetically and ensure that the solvent does not evaporate and that the resin is completely dissolved in it (no lumps or regions with different density).
2. Once the mixing is achieved, top up with methanol, cover with Parafilm and allow to settle for about 1-2 h. When the non-purified resin is completely solid and brittle, the mixture is usually a white suspension. The drying requires filtering under vacuum. Use a Büchner flask connected to a vacuum pump. Place a filter paper the size of the funnel on it and dampen with methanol. Turn the vacuum pump on and carefully pour the suspension onto the paper avoiding the sides. If any washing is required, use methanol. Once the surface of the solid on the paper is cracked and as dry as possible, turn the pump off, empty them onto a watch glass and cover with a punctured tinfoil.
3. Vacuum-dry overnight in the oven at 50ºC. Maximum allowed temperature is 55ºC, otherwise the boiling of the liquid resins will be too abrupt and the resin will overflow the beaker.

2.6.4 Purification of polyesters PPF (2) and PPeF (5)

The same procedure in **2.6.3** is followed, but diethyl ether is used instead of chloroform as the solvent in step 1.

2.7 Characterisation of polyester resins

2.7.1 Acid Value (AV) determination

The acid value allows the calculation of carboxylic acid content in the polyester resin and is used to monitor progress, end point and consistency of polyester resins. It allows the determination of polyesterification kinetics as well.

2.7.1.1 Acid value solution

Fill a 1L screw-top bottle with a 50:50 v/v solution of xylene and methanol and 0.5% phenolphthalein. This should be brought to a pink end point with 0.1 M KOH in methanol.

2.7.1.2 Method

1. Measure resin sample into a 250 mL wide-necked conical flask and record weight (xylene can be added after weighing to aid dissolution). Then dissolve in roughly 50 mL acid value solution, with gentle warming and swirling if required. Weight of sample is dependent on the stage of the reaction. Less resin is needed for a sample taken at a higher acid value (earlier in the reaction) (~2g) as it stops unnecessarily long titrations. Increased accuracy is needed for acid values ≤10 (~4-5g).

2. Titrate against 0.1M KOH and record the end point. The AV is then calculated by the equation below

$$AV = \frac{MW_{KOH} M_{KOH} V_{titre}}{Sample\ weight} \tag{23}$$

Where MW is the molecular weight of KOH (56.1 $g \cdot mol^{-1}$), M is the molar concentration of KOH (0.1 M) and AV is the acid value ($mg_{KOH} \cdot g_{polyester}^{-1}$).

The schematic representation of the acid value determination is depicted in **Figure 17.**

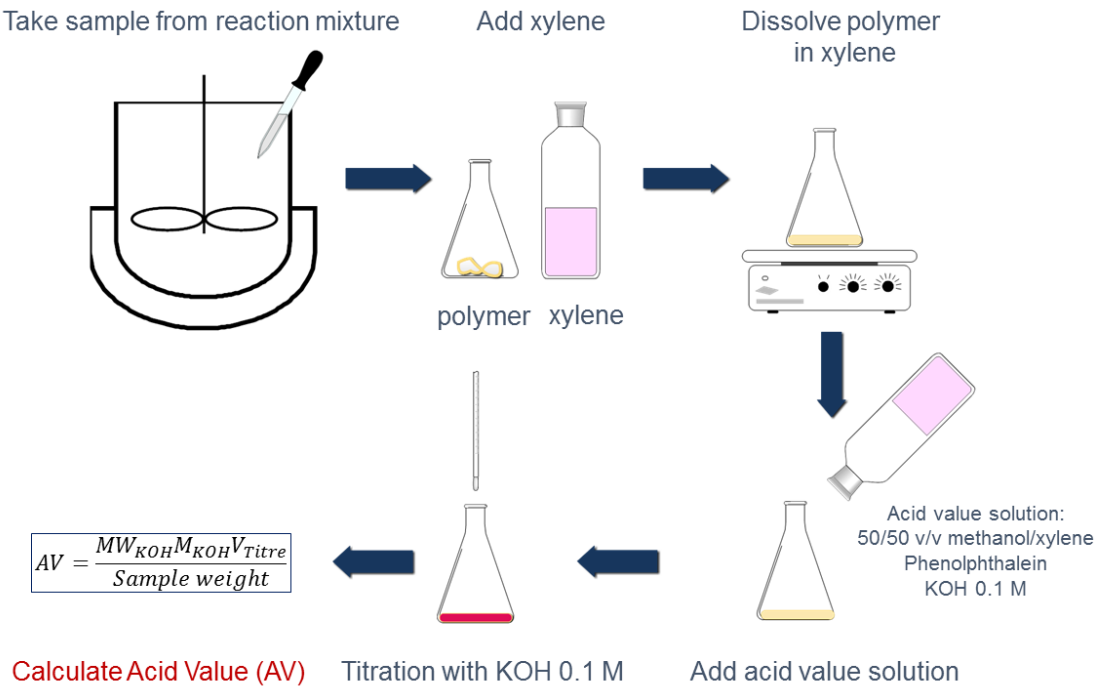

Figure 17. Acid Value (AV) determination.

2.7.2 Hydroxyl Value (OHV) determination

2.7.2.1 Preparation of acetylating solution

Into a dry 250 mL volumetric flask, add ethyl acetate (150 mL, analytical grade) and perchloric acid (1.2g, 70%) and then cool the flask in ice. Measure out 50 mL acetic anhydride, and slowly add 8 mL dropwise into the chilled ethyl acetate and allow the solution to stand for 30 minutes. Add extra ice to keep the solution cool. Add the remaining anhydride dropwise and dilute to the mark with ethyl acetate. The resulting solution should be pale straw in colour. It is stable for 3 months.

2.7.2.2 Method

1. Weigh 3g (approx.) base resin into a clean, oven dried 150 mL conical flask with a ground glass neck joint and record weight of resin. Add approximately 25 mL ethyl acetate and gently warm with swirling until the resin is fully dissolved (can be left overnight).

2. 2 'blank' flasks should also be made up, containing approximately 25 mL ethyl acetate only.

3. Accurately add 5 mL acetylating solution to all flasks, taking great care over consistency of additions, stopper flask and leave to stand for a minimum 30 minutes.

4. Add approx. 5 mL deionised water and 10 mL pyridine and again stopper and allow to stand for a minimum 30 minutes.

5. Titre the solution with 0.5M KOH, using phenolphthalein as indicator, to the end point and record. The OH value is calculated using the equation below

$$OHV = \frac{MW_{KOH} M_{KOH(} V_{blank} - V_{titre})}{Sample\ weight} \quad (24)$$

Where V_{blank} is the average titre from "blank" flasks.

The importance of OHV relies on its big impact in the molecular weight. However, the OHV determination is not accurate and is also time-consuming.

2.7.3 ^{1}H Nuclear magnetic resonance (NMR)

2.7.3.1 Background

The basis of NMR is the resonance interaction between a high frequency field and the nuclei of a compound placed in an external magnetic field. The nuclei of some isotopes having a spin quantum number of ½ possess a magnetic moment produced by the spin of the nucleus. Examples are ^{1}H, ^{11}B, ^{19}F, ^{31}P, ^{35}Cl, and ^{79}Br. Isotopes with both the number of neutrons and protons being even do not have any nuclear magnetic moment and cannot be detected by this technique. When electromagnetic radiation of a right frequency (resonance frequency) is passed through the substance, it is absorbed by the nuclei which shift from a lower to a high energy level.[209]

The measurement of the field strengths required for resonance of various protons in a molecule provides useful information; for instance, the number of different absorptions, namely signals or peaks, which imply how many different types of protons are present. Furthermore, the intensities of the signals indicate how many protons of each type are present, while the splitting of the signals gives information about nearby protons.[228]

Protons in a molecule are partially shielded from the magnetic field, and this shielding depends on each proton's environment. Hence, protons in different environments within a molecule absorb the radiation at different magnetic field strengths. The NMR spectrometer then was originally developed to vary the magnetic field and a plot a graph of energy absorption as a function of the magnetic field strength, which is known as nuclear magnetic resonance spectrum. Higher values of the magnetic field are toward the right (upfield) and lower values are toward the left (downfield).[228] A block diagram of a NMR spectrometer is depicted in **Figure 18**.

The variations in the positions of NMR absorptions are called chemical shifts, which are defined as the difference in parts per million (ppm) between the resonance of the proton being observed and tetramethylsilane (TMS), which is the widely used NMR reference compound and whose protons are absorbed at a higher field strength than most hydrogens bonded to carbon or other elements.[228]

In general, the number of NMR signals corresponds to the number of the different types of protons present. Protons referred as chemically equivalent are located in identical chemical

environments. The area under the peaks is proportional to the number of hydrogens contributing to that peak.[228]

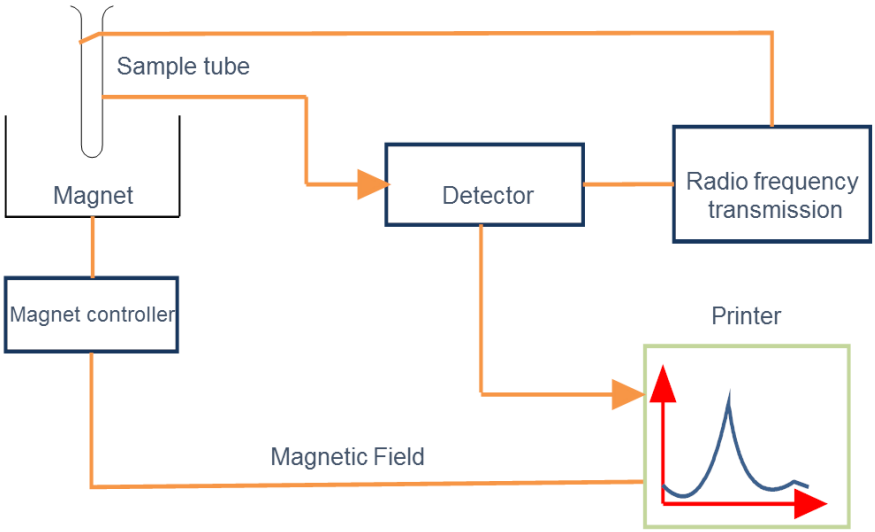

Figure 18. Simplified block diagram of a NMR spectrometer, adapted and modified from Wade.[228]

2.7.3.2 Method

^{1}H NMR measurements were performed on a Brucker NMR spectrometer (400 MHz). Deuterated chloroform ($CDCl_3$) or dimethyl sulfoxide (DMSO) were used as solvents for all samples and were purchased from Sigma-Aldrich. Chemical shifts are reported in parts per million (ppm) δ relative to tetramethylsilane, referenced to the chemical shifts of residual solvent resonances.

2.7.4 Gel Permeation Chromatography (GPC)

2.7.4.1 Background

As explained in the introduction, the gel permeation chromatography method (GPC) provides a separation based upon molecular size, carried out with a liquid substrate.[209] In GPC, the mixture of different-size polymers and oligomer molecules is eluted in a solvent through a column of porous particles. The smaller particles can enter the pores and be retarded, whereas the larger molecules are swept through.[177] A schematic representation is shown in **Figure 19**.

In GPC molecules are separated according to their hydrodynamic volume. Their molecular weights and molecular weight distribution can be determined from the measured

retention volume (RV) by means of a calibration curve (log Molecular weight vs RV), which must be set up with the aid of a number of standards of known molecular weight.[229]

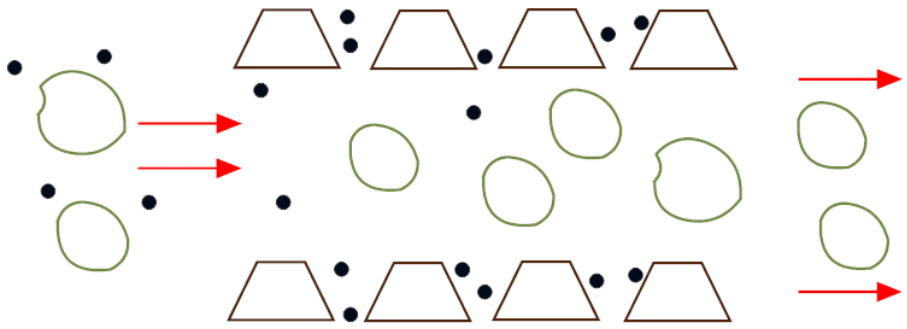

Figure 19. GPC: Molecules eluted in a liquid phase through a column of porous particles, adapted and modified from Allcock, et al.[177]

The use of GPC for the measurement of molecular weights relies on ensuring that the elution time along the column is reproducible for two different specimens on the same polymer that have the same molecular weight and molecular weight distribution (MWD). This is fulfilled by GPC equipment by maintaining the same flow rate of the eluting solvent through the column as well as keeping the size of the tunnels within the stationary particles the same. A mechanical pump is usually employed to force the sample and the elution solvent through the columns at pressures of up to 1000 to 4000 psi and at a rate of 2 to 3 mL/min. The eluent passes through a detector after passing the column system. A commonly used detection method is differential refractive index measurements, where a refractometer measures the difference in refractive index between the eluted solution and the pure solvent. MWD plots can be yielded from a plot of the refractive index difference as a function of time.[177] Another means of detection for conventional GPC is the ultraviolet absorption, where a spectrometer is set to a particular wavelength and the absorbance is thus monitored as a function of elution time.[229] A block diagram representation of GPC apparatus is depicted in **Figure 20**.

2.7.4.2 Method

Gel permeation chromatography (GPC) was carried out on an Agilent 1260 Infinity equipped with two Agilent ResiPore Organic 250 x 4.6 mm columns, a guard column and a refractive index detector. The eluent was tetrahydrofuran (THF) at a flow rate of 0.3 mL·min^{-}

[1]. Molecular weights and dispersity were calculated using a conventional calibration with polystyrene standards.

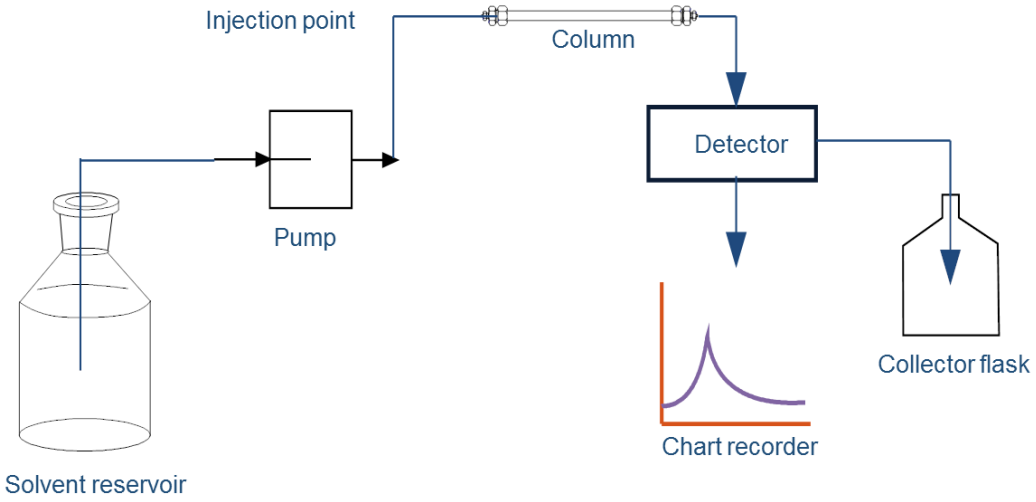

Figure 20. Schematic diagram of a gel permeation chromatography apparatus, adapted and modified from Allcock, et al.[177]

2.7.5 Differential Scanning Calorimetry (DSC)

2.7.5.1 Background

Differential scanning calorimetry (DSC) is a technique for measuring the response of polymers to heating. DSC can be used to study the thermal transitions of a polymer, such as melting of a crystalline polymer or the glass transition temperature (T_g).[230]

The glass transition is the temperature range where the amorphous part of a polymer changes from a hard, rigid state (Below T_g) to a rubbery state (Above T_g).[231] The T_g could be affected by several factors, such as heating rate, morphology or molecular weight.[232] The T_g is considered a second-order thermodynamic transition since there is no transfer of heat, but only the heat capacity changes, whereas in a first-order transition, there is a transfer of heat between the system and surroundings and the system undergoes a volume change, as it happens during melting.[233]

The common set-up of DSC consists of a measurement chamber and a computer. Two pans, the sample pan and the reference pan, are heated in the chamber. The computer is used to monitor the temperature and regulate the rate at which the temperature of the pan changes. This rate change for a given amount of heat will differ between the two pan, and depends on

the composition of the material and phase changes.[230] A schematic representation of DSC equipment is shown in **Figure 21**.

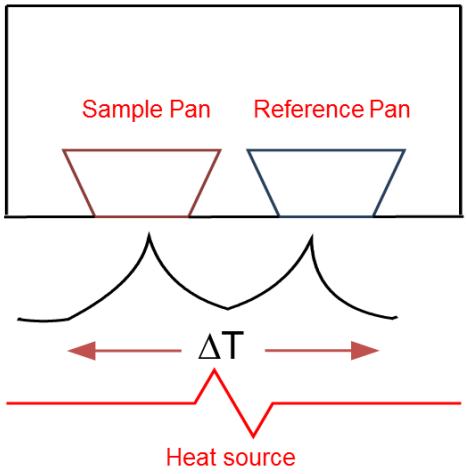

Figure 21. Schematic diagram of DSC, adapted and modified.[234]

2.7.5.2 Method

The differential scanning calorimetry measurements were performed using a TA Instruments Q2000 analyser with a RC590 cooling system using a standard heat-cool-heat method. The temperature range was -50 °C to 200 °C. Both the heating and cooling rates were 10 °C/min in N_2. The amount of sample was approximately 6±0.1 mg. The samples were deposited in Tzero aluminium pans. The glass transition temperatures reported are the midpoint of a temperature range, bounded by the tangents to the two flat regions of the heat flow curve.

2.7.6 Thermal gravimetric analysis (TGA)

2.7.6.1 Background

Thermogravimetric analysis is a technique in which the mass of a substance is monitored as a function of temperature or time as the sample is subjected to a controlled temperature program in a controlled atmosphere. TGA, thus, measures a sample's weight as it is heated or cooled in a furnace.[235]

The equipment consists of a sample pan supported by a precision balance. That pan resides in a surface and is heated or cooled during the experiment. The mass of the sample is monitored during the experiment and a sample purge gas controls the sample environment as it flows over the sample and exits through an exhaust.[235]

2.7.6.2 Method

The thermal stability of the polyesters was determined by thermogravimetric analysis (TGA) using TA Instruments Q5000 equipment under N_2 atmosphere. The samples were placed in aluminium pans and heated from room temperature to 550 °C at a rate of 10 °C/min. This method was chosen upon previously reported ones for polyesters in the literature.[74, 75, 170]

The actual equipment used is shown in **Figure 22**.

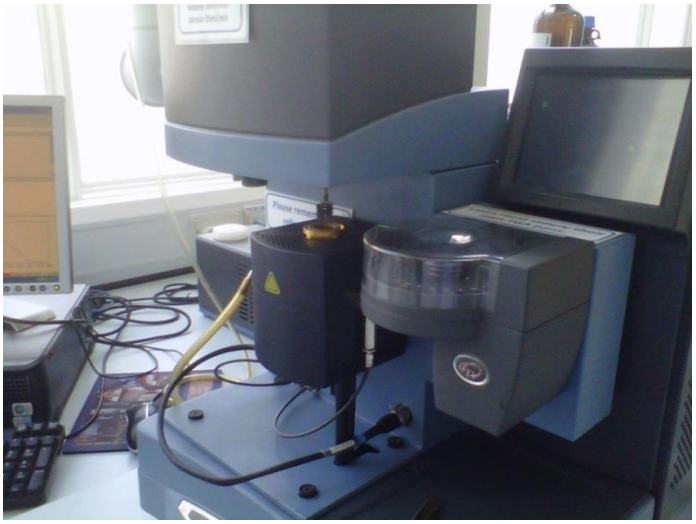

Figure 22. TGA equipment used for the characterisation of biomass-derived polyesters.

2.7.7 Paint testing protocol

Representative polyester samples were evaluated using a white polyester resin protocol for coil coatings. These analyses were done by our industrial partners, Becker Industrial Coatings Ltd, at their research facilities in Speke, Liverpool. The specification of the white formulation protocol cannot be disclosed.

The performance of the resins was compared to that of reference and standard resins used internally by Becker Industrial Coating Ltd. The white paint protocol was chosen because there was no colour match requirement. If the pigment dispersion and colour stability were parameters to be assessed, then a dark brown paint should have been tested as well, in order to allow the resin to be assessed at the extremes of pigment loading.

Coatings were applied at 18-20 microns directly onto a smooth metal substrate (steel) and cured in an oven for 40 seconds to reach a peak metal temperature of 224-232 °C.

The following physical testing was carried out on the metal panels:

- **Rapid Deformation** EN 13523-5(2001) Part 5 or ASTM D2794-93

This test method covers a procedure for rapidly deforming by impact a coating film and its substrate and for evaluating the effect of such deformation. Impact is understood as the number of inch-pounds (kilogram-meters) required to produce cracking in the deformed coating.[236]

- **Erichsen** EN 13523-6 (2002) Part 6 or ASTM D1474

Indentation hardness measurements have proven to be useful in rating coatings on rigid substrates for their resistance to mechanical abuse, such as that produced by blows and scratching. This method consists of applying a load to the surface of a coating by means of a pyramidal shaped diamond and converting the measurements of the resultant permanent impression to a hardness number.[237]

- **Pencil Hardness** EN 13523-4 (2001): Part 4 or ASTM 3363-00

This part describes the procedure to assess the relative hardness of an organic coating on a metal substrate, by means of pencils of known hardness. The hardest lead which does not scratch the coating for a minimum of 3 mm length determines the degree of hardness. Pencil hardness is defined as the resistance of the coating surface to scratching when a pencil with a specified dimension, shape and hardness of the lead is pushed across the surface.[238]

- **Gloss (60^{o})** EN 13523-2 (2001) or ASTM D523-89(1999)

This test method covers the measurement of the specular gloss of nonmetallic specimens for glossmeter geometries of 60, 20, and 85°. Gloss is associated with the capacity of a surface to reflect more light in some directions than in others. The directions associated with specular reflection normally have the highest reflectance. Measurements by this test method correlate with visual observations of surface shininess made at roughly the corresponding angles.[239]

- **Coating Thickness** EN 13523-1 (2001): Part 1 or ASTM D1186-9.

This standard provides the procedures for determining the thickness of an organic coating on a metallic substrate, using electrical measuring devices.[240]

- **MEK Resistance** ECCA - T11 (1999) or ASTM D5402-93(1999).

This practice describes a solvent rub technique for assessing the solvent resistance of an organic coating that chemically changes during the curing process. Coatings that chemically change during the curing process, such as polyesters, become more resistance to solvents as they cure. Rubbing with a cloth saturated with the appropriate solvent is one way to determine when a specific level of solvent resistance is reached.[241]

- **Micro-indentometry** ISO 14577-1.

Hardness has typically been defined as the resistance of a material to permanent penetration by another harder material. This norm has been prepared to enable the user to evaluate the indentation of materials by considering both the force and displacement during plastic and elastic deformation.[242]

- **Glass transition temperature** ASTM E1356-98.

This test method involves continuously monitoring the difference in heat flow into, or temperature between, a reference material and a test material when they are heated or cooled at a controlled rate through the glass transition region of the test material and analysing the resultant thermal curve to provide the glass transition temperature.[243]

- **T – Bend Flexibility** No Crack / No Removal: EN 13523-7 (2001) Part 7 or ASTM D4145.

Coatings on precoated sheet are subjected to stresses when fabricated into products by roll forming, or other deformation processes. These stresses can exceed the flexibility or adhesive strength of the coating, resulting in fracture of the coating which exposes the substrate, or in the loss of adhesion of the coating to the substrate. This test method describes a procedure for determining the flexibility and adhesion of coatings on metallic substrates that are deformed by bending when the sheet is fabricated into building panels or other products. [244]

CHAPTER 3

Properties of biomass-derived polyesters with 1,3-propanediol: PPS, PPF and PPFPS

3. Properties of biomass-derived polyesters with 1,3-propanediol: PPS, PPF and PPFPS

This chapter presents the properties' characterisation of biomass-derived polyesters based on 1,3-propanediol (PDO), 2,5-furandicarboxylic acid (FDCA) and succinic acid (SA): PPS (Polyester **1**), PPF (**2**) and PPFPS (**3**). The final application of these polyesters is coil coatings. The objective of this chapter is to determine the relationship between the composition and structure of the bio-polyesters with their final properties.

3.1 Introduction

One of the many applications of polyesters is in coatings. Data up to 2013 showed that the global paints and coatings demand increased steadily 5.4% annually, with sales of coatings reaching 41.75 million tons.[245] The distribution of the volume across the different end use markets is depicted in **Figure 23**, which highlights that architectural coatings represent the largest market share with 40%.

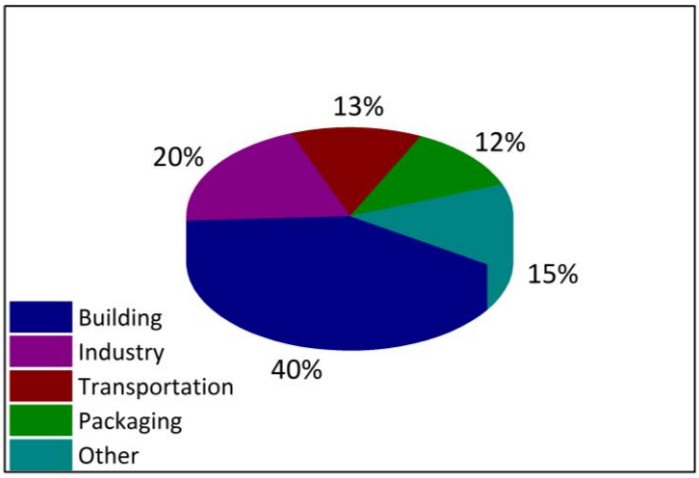

Figure 23. Global paints and coatings demand in 2013.[245]

There are several application methods for coating different substrates, which depend mainly on the geometry of the article to be painted, the type of paint, and environmental constraints.[175] These methods include spraying techniques, such as electrostatic spraying, immersion painting, flow coating, electrodeposition and coil coating.

Specifically for polyesters, the coil coating method is widely used. In this process, a coil of steel is unrolled and passes through two or more rollers impregnated with paint. The

steel sheet passes across a high temperature oven where the paint is dried and then cooled and recoiled.[175] The resulting coated metal is sufficiently robust to enable it to be post-formed and fabricated into building construction panels or casings for domestic appliances or other end uses without damaging the protecting paint layer.[246] The method is particularly popular with the construction, the automotive and electrical appliances industries.[247] A typical coil coating line is shown in **Figure 24**.

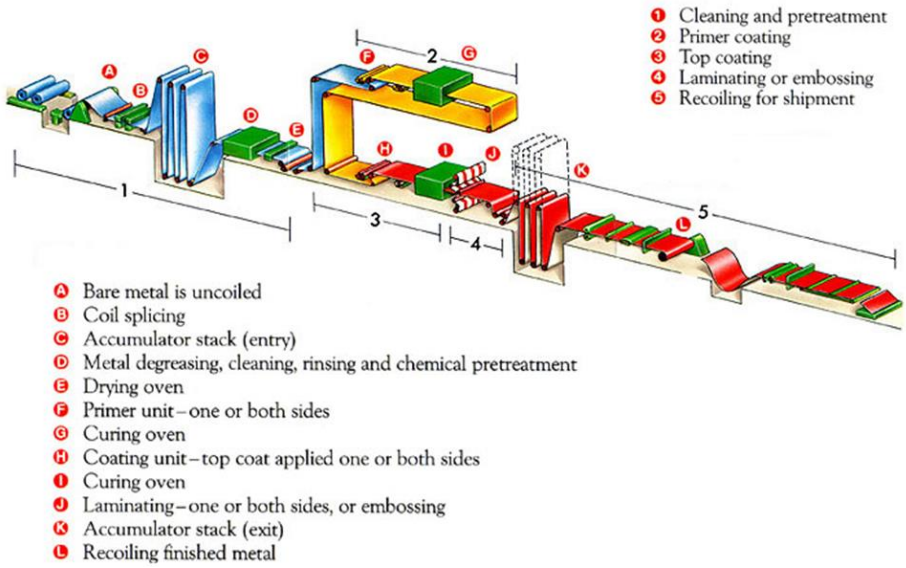

Figure 24. Schematic representation of a typical coating line, adapted and modified.[248]

Coil coatings comprise liquid paint in a polyester matrix in a wide range of colours and finishes that can be applied to continuous steel or aluminium strip.[249] This paint application process intends to reduce the environmental impact by minimising paint waste and making use of excess solvents.[249] The European Coil Coating Association (ECCA) has stated in its 2012 report that coil coating is "the most efficient, the most reliable and the most environmentally friendly means of applying a high quality paint finish to metal surfaces."[250]

3.1.1 General properties of polyester resins

Linear high molecular weight polyesters (>20000 Da) cannot be used in paints and coatings. The M_n of most polyesters used for industrial coatings range from 2000 to 6000 Da.[175] Polyester coatings are characterised as well by their excellent flexibility and adhesion to metal, and they show great versatility in terms of composition and structure by the use of various dicarboxylic acids and diols which lead to linear or branched structures, and acid or hydroxyl functionalities.[251]

To obtain a good balance of the required properties, it is normal for the polyester to contain a mixture of aromatic and aliphatic diacids. The mechanical properties of the coating are a function of the resin composition, its structure, its molecular weight and the ultimate crosslinking depending on the hydroxyl value and crosslinking concentration. In general, the aliphatic constituents tend to reduce T_g and aromatics tend to do the opposite. This control, together with the hydroxyl value, means resins can be developed for specific end uses.[175]

3.1.2 Biomass-derived polyester coatings

As part of the biomass-derived polymers trend in several applications across industry, the future in polyester coatings relies on the usage of monomers sourced from bioderived, renewable feedstocks.[246] Currently, the most common polyester resins used for coatings are prepared from diacids such as terephthalic acid, isophthalic acid (IPA), phthalic anhydride (PA) and AA. The polyalcohols include difunctional neopentyl alcohol (NPG), ethylene glycol (EG) or polyfunctional compounds, including glycerol, among other compounds with functionalities exceeding two.[252] There has been an increasing amount of research regarding the use of biomass derived building blocks in coating applications, studying their feasibility in terms of mechanical (impact), thermal (T_g) and chemical (OH and acid end groups) properties in order to be competitive against the typical polyesters from fossil sources.[253]

Noordover, et al.[254] reported the synthesis of linear and branched polyesters via polycondensation from isosorbide and succinic acid to yield hydroxyl and carboxylic acid functional polymers. Moreover, terpolyesters from succinic acid, isosorbide and either 2,3-butanediol or 1,3-propanediol have glass transition temperatures suitable for coating applications. Improved mechanical properties and enhanced chemical resistance were shown by branched polymers when compared to linear polymers. Likewise, the authors published another study where thermosetting polyesters based on isosorbide and succinic acid are analysed, along with their performance with several curing agents. [255]

Another approach of biobased polyesters suitable for coatings was pursued by Jasinska, et al.,[256] where they successfully synthesised unsaturated biobased polyesters via a titanium (IV) n-butoxide catalysed bulk polycondensation using isosorbide, maleic anhydride and succinic acid as the renewable monomers.

The polyesterification from renewable or recycled materials for coatings applications has been studied as well. The direct incorporation of isosorbide into polyesters by a chemical

recycling process was reported by Gioia, et al.[162] who performed the combination of the chemical recycling of PET with isosorbide and succinic acid, where the biomonomer is inserted in the final polymer chain providing a polymer derived from recycled materials and renewable resources suitable for coating applications.

Furan building blocks, an interesting family of carbohydrate-derived monomers, have been also included in coating formulations, particularly FDCA or its dimethyl-ester derivative, dimethyl-2,5-furandicarboxylate. Gubbels, et al.[257] described the synthesis and properties of polyesters intended for coatings based on this derivative. The furanic block was transesterified with 2,3-butanediol, glycerol or pentaerythritol. Likewise, in an extension of the work previously done, the same research group evaluated linear and branched bio-based semi-aromatic polyesters for both solvent-based and powder coating applications.[252] They proved the suitability of the branched resins as potential candidates for solvent-based and powder coating applications, especially where impact resistance was not critical to quality.

Furthermore, another approach towards renewable based coatings is using alkyd polyesters derived from seed oils. Argyropoulos, et al.[258] developed seed oil based monomers, controlling the molecular weight and functional groups present and further convert them to polyesters via condensation.

Similarly, citric acid has been considered as a monomer for polyester coatings synthesis. It has been tested as a functionality increasing agent for coating applications in polyesters with isosorbide and succinic acid, assessing its thermal stability during polyester modification and curing.[259]

It is likely that the use of biopolymer coatings will extend to high performance applications and advanced coating systems, including optoelectronics, chemical or biological sensors and industrial applications.[260]

3.2 Experimental procedure

The polyesters considered in this chapter are summarised in **Table 11**, which resembles the information in **Table 4** in **Chapter 2**. The chemical structures are shown in **Scheme 33**. Polyesters **3a** ($PPF_{15}PS_{85}$) and **3b** ($PPF_{30}PS_{70}$) were alternatively synthesised by applying vacuum during the polycondensation stage. The experimental details for each polyester are available in **Appendix A**.

Table 11. Biomass-derived polyesters with PDO, FDCA and SA

No.	Acronym	Mol% FDCA	Mol% SA	r[a]	T, °C
1	PPS	-	100	1.1	
2	PPF	100	-	1.6	
3a	$PPF_{15}P_{8S}$	15	85		210-230
3b	$PPF_{30}PS_{70}$	30	70	1.5	
3c	$PPF_{70}PS_{30}$	70	30		
3d	$PPF_{85}PS_{15}$	85	15		

[a]Molar ratio diol:diacid

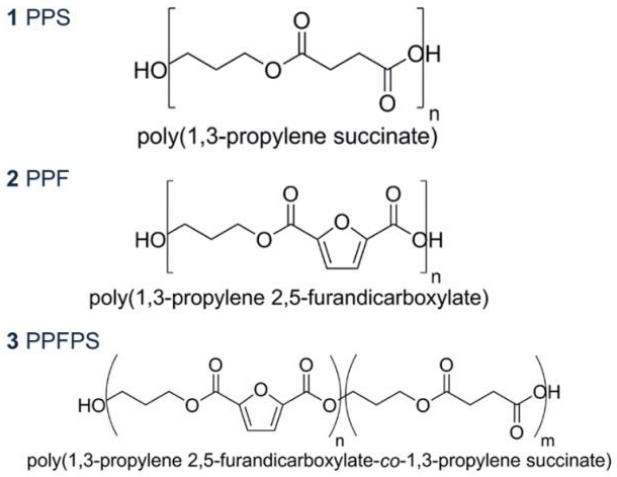

Scheme 33. Chemical structures of polyesters **1-3** derived from SA, FDCA and PDO.

3.3 Characterisation results

3.3.1 ^{1}H NMR

The structures of polyesters PPS, PPF and PPFPS (**1-3**) were confirmed by ^{1}H NMR. The chemical shifts are listed in **Table 12** and the chemical structures with their corresponding assignments are depicted in **Scheme 34** and **Figure 25**. To support the analysis, the ^{1}H NMR spectra of the monomers are shown in **Figure 26**. The chemical shift associated with the furan ring (*a*) appears at 7.20 ppm whereas the chemical shift of CH_2 in the SA unit (*b*) appears at 2.63 ppm for **1** and at 2.64 ppm for **3**. Both FDCA and SA are

completely incorporated as a single peak is observed for each one. The formation of the polyesters is confirmed by the protons adjacent to FDCA (*f*) at 4.50 ppm, SA (*g*) at 4.26 ppm and the appearance of a new shift at 2.11 ppm (*i*) demonstrates the formation of the copolyesters as it indicates that the esters of FDCA and SA are chemically bonded. The spectra suggests that some unreacted 1,3-propanediol might be present as its peaks are distinguishable at chemical shifts of 3.70-3.78 ppm (*c*) (C**H**$_2$-OH) and 1.81-1.88 ppm (*d*) (C**H**$_2$-CH$_2$OH). The peaks around these chemical shifts might correspond to the formation of single or dual-side reacted diols, as the syntheses for **2** and **3** were performed with excess of diol. Assignment *d* transforms into *h* (1.98-2.01 ppm) and *e* (2.25 ppm) when attached to succinic acid or FDCA, respectively.

Table 12. Assignment of chemical shifts of polyesters PPS, PPFPS and PPF

Polyester	Assignment of chemical shifts ($CDCl_3$, δ/ppm)								
	a	**b**	**c**	**d**	**e**	**f**	**g**	**h**	**i**
PPS (1)	-	2.63	3.70	1.88	-	-	4.26	1.98	-
PPFPS (3)	7.20	2.64	3.78	1.87	2.25	4.50	4.26	2.01	2.11
PPF (2)	7.20	-	3.78	1.81	2.25	4.50	-	-	-

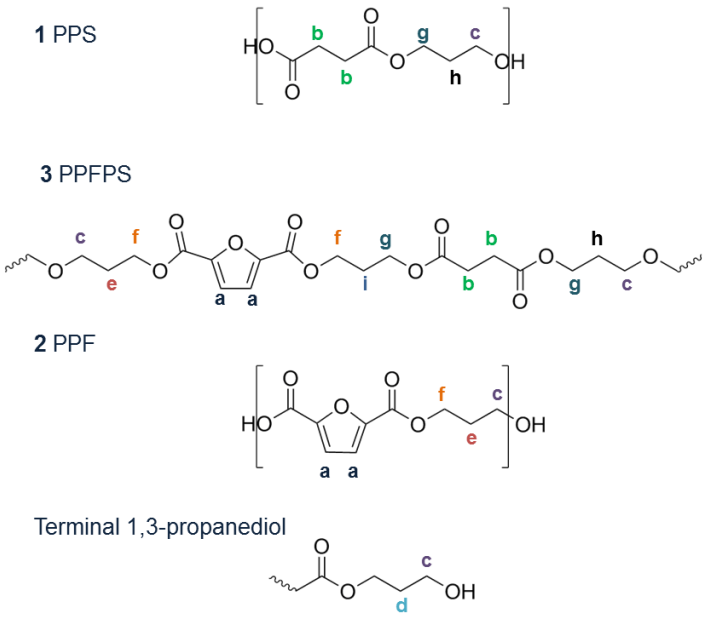

Scheme 34. ^{1}H NMR assignments for polyesters **1-3** and terminal 1,3-propanediol.

The chemical shifts align with previous work on 1,3-propanediol-based polyesters with FDCA[85, 227] and succinic acid.[226] There are however unidentified shifts at 2.01 ppm for the furan polyester **2** and at 2.17 ppm for **3d**, which are believed to correspond to the formation

of one-side reacted species as the excess of diol might prompt the formation of different oligomeric species.

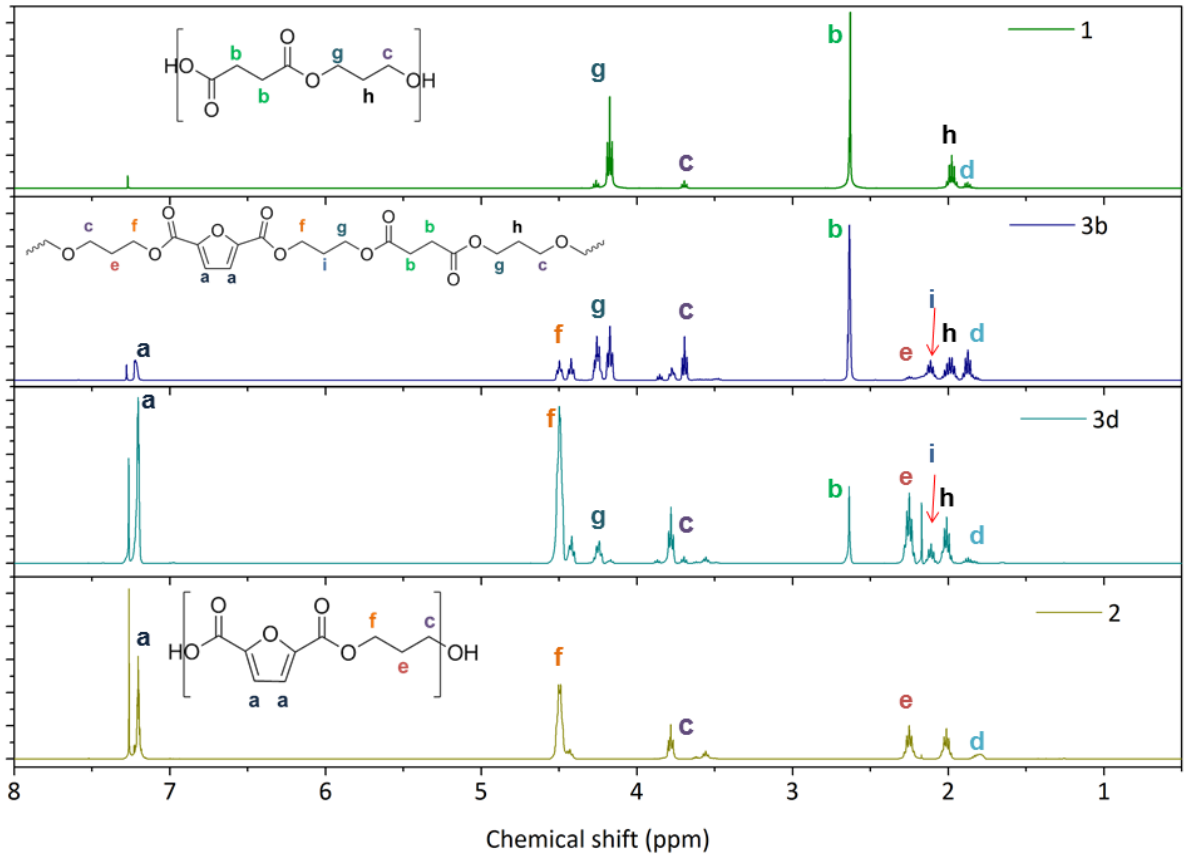

Figure 25. ^{1}H NMR spectra of PPS (**1**), $PPF_{30}PS_{70}$ (**3b**), $PPF_{85}PS_{15}$ (**3d**) and PPF (**2**).

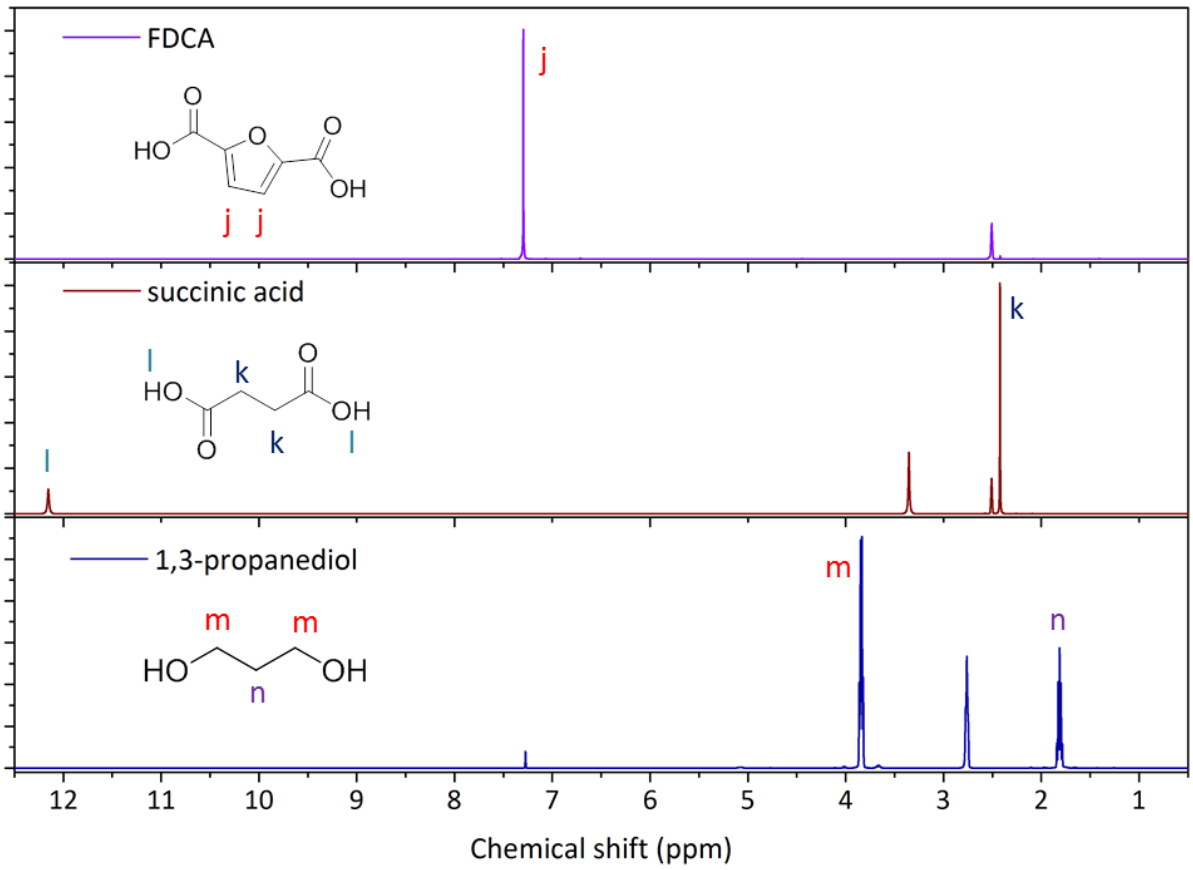

Figure 26. ^{1}H NMR spectra of the biomass-derived monomers used, from top to bottom: FDCA (in DMSO); succinic acid and 1,3-propanediol (in $CDCl_3$).

3.3.2 Molecular weight measurement by GPC

The molecular weights and dispersity of the polyesters were measured by GPC at Becker Industrial Coatings Ltd. The insolubility of polyester **2** in THF prevented measurement of molecular weight. **Table 13** summarises the results of M_n, M_w and dispersities (Đ) of the biomass-derived polyesters and copolyesters as a function of processing temperature whereas **Table 14** focuses on the diacid ratio. **Figure 27** shows the M_w as a function of the process temperature for clarity.

After the acquired experience however, it was suggested that potentially, polyesters **3a** and **3b** could be processable with molar ratios of 1.1:1. The molar ratio was kept at 1.5 though for all the polyesters in family **3** to enable a proper comparison in terms of the kinetic modelling and estimation of kinetic parameters, which is described later in **Chapter 5**.

Table 13. M_n, M_w and Đ as a function of the process temperature, via azeotropic distillation

Polyester	Name	T, °C	M_n, Da	M_w, Da	Đ
1	PPS	210	2100	4300	2.08
		220	2400	5000	2.13
		230	2700	5700	2.17
3a	$PPF_{15}PS_{85}$	210	800	1100	1.45
		220	820	1200	1.46
		230	830	1300	1.47
3b	$PPF_{30}PS_{70}$	210	800	1100	1.44
		220	840	1200	1.47
		230	900	1300	1.50
3c	$PPF_{70}PS_{30}$	210	1200	1500	1.27
		220	1400	1700	1.27
		230	1300	1800	1.35
3d	$PPF_{85}PS_{15}$	210	1200	1500	1.24
		220	1100	1400	1.23
		230	1100	1400	1.28

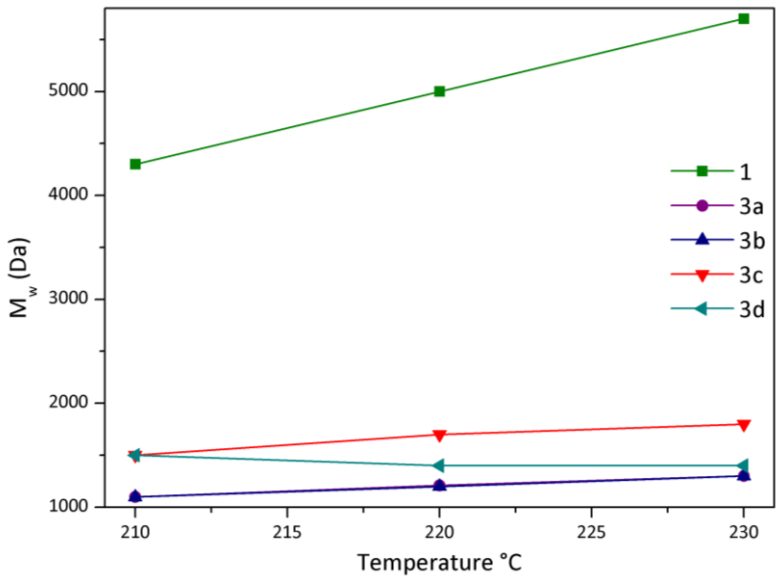

Figure 27. M_w as a function of the process temperature for polyesters **1** (PPS) and **3** (PPFPS).

The GPC chromatogram for polyester **3c** synthesised at different process temperatures is depicted in **Figure 28**. It is observed how the curve corresponding to the synthesis at 230 °C is slightly shifted toward lower retention times. As the process temperature is decreased to 220 °C and 210 °C, the curves tend to shift to the higher detection times, and are

characterised by the presence of different peaks instead of a Gaussian-type curve which suggests the presence of oligomers.

Table 14. M_n, M_w and Đ as a function of the diacids molar ratio, via azeotropic distillation

Polyester	Name	FDCA/SA	M_n, Da	M_w, Da	Đ
		210 °C			
1	PPS	-	2100	4300	2.08
3a	$PPF_{15}PS_{85}$	15/85	800	1100	1.45
3b	$PPF_{30}PS_{70}$	30/70	800	1100	1.44
3c	$PPF_{70}PS_{30}$	70/30	1200	1500	1.27
3d	$PPF_{85}PS_{15}$	85/15	1200	1500	1.24
		220 °C			
1	PPS	-	2400	5000	2.13
3a	$PPF_{15}PS_{85}$	15/85	820	1200	1.46
3b	$PPF_{30}PS_{70}$	30/70	840	1200	1.47
3c	$PPF_{70}PS_{30}$	70/30	1400	1700	1.27
3d	$PPF_{85}PS_{15}$	85/15	1100	1400	1.23
		230 °C			
1	PPS	-	2700	5700	2.17
3a	$PPF_{15}PS_{85}$	15/85	830	1300	1.47
3b	$PPF_{30}PS_{70}$	30/70	900	1300	1.50
3c	$PPF_{70}PS_{30}$	70/30	1400	1700	1.35
3d	$PPF_{85}PS_{15}$	85/15	1100	1400	1.28

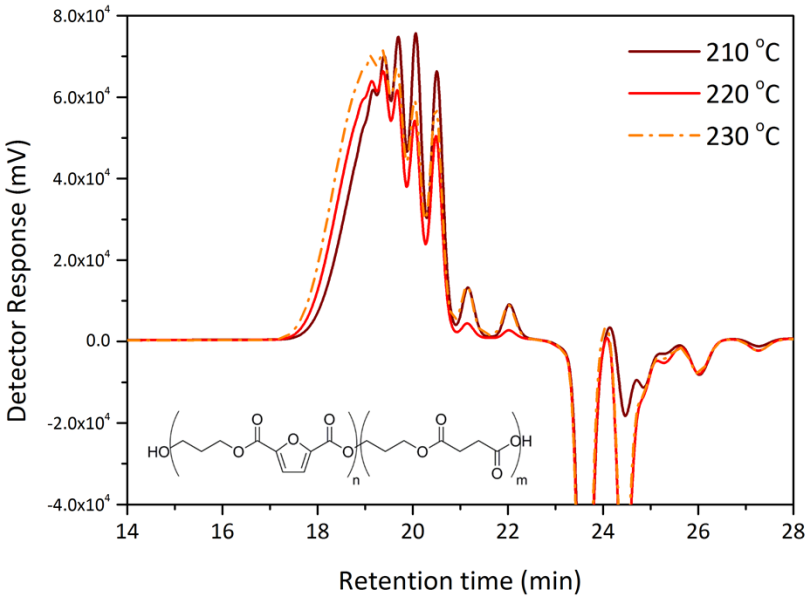

Figure 28. GPC chromatograms of polyester $PPF_{70}PS_{30}$ (**3c**), synthesised by azeotropic distillation in the second stage.

Figure 29 shows the GPC chromatograms for the syntheses at 220 °C. The multiple narrow peaks at high retention times are indicative of the mainly oligomeric nature of the polymer. The presence of cyclic oligomers is a possibility as well, as polymers synthesised by polycondensation could contain some cyclic species.[261] The M_n and M_w of the copolyesters **3** are low and depend on the FDCA/SA composition with higher molecular weights as the FDCA content increases for **3a-3c**. A similar trend was described by Jacquel, et al.[92] as the M_n of PBSF polyesters increased for those bearing FDCA concentrations from 5 to 20 mol%, although it decreased dramatically when the concentration was 60 mol%.

The chromatogram for **1** presents a broad curve with lower retention times corresponding to higher molecular weight. The GPC chromatograms for the syntheses at 210 °C and 230 °C are available in **Appendix B**.

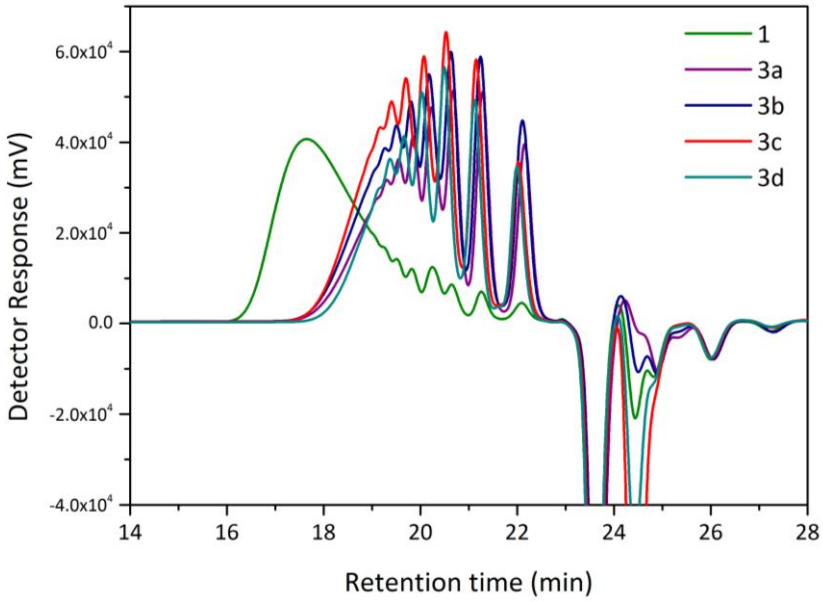

Figure 29. GPC chromatograms for polyesters **1** (PPS) and **3a-3d** (PPFPS).

The results obtained show that the molecular weights of polyesters **3a-3d** are in the lower range of the molecular weights suitable for coatings.[170, 252, 257] The data suggests that the molecular weights are limited by the excess of diol. This excess is necessary in coil coatings formulations to maintain an hydroxyl functionality that would enable further crosslinking of the polyester resins.[175] The results however prompted to compare the polymerisations from a processing perspective, by applying vacuum during the polycondensation (second) stage, which is expected to be more efficient than the azeotropic

distillation and enhance the molecular weights, so they might fall in the upper suitable range for the intended application.

As a proof of concept, the synthesis of **3a** and **3b** were performed as well by applying vacuum in the polycondensation stage. **Table 15** compares the results obtained via azeotropic distillation and application of vacuum. It is clear how the vacuum increased the final molecular weight of the polyesters, as expected. The M_w increased from 1200 Da to 7200 Da and 5300 Da for **3a** and **3b**, respectively; whereas the dispersity increased to 2, which is the expected for polyesters.[177] Furthermore, it is worth noting that the vacuum strips off the diol, which affects the final hydroxyl value and therefore the molecular weight. This loss of diol is normally quantified by refractive index, as suggested by Becker Industrial Coatings Ltd, although they do not do vacuum processing on site. The diol loss quantification remains as part of the future work with the vacuum process. **Figure 30** shows the comparison of **3a** and **3b** between both processing methodologies. It is observed that the presence of oligomeric, narrow peaks is significantly lower for the vacuum-driven process.

Table 15. Comparison of M_n, M_w and Đ synthesised by azeotropic distillation or vacuum in the second stage

		Vacuum			Azeotropic distillation		
Polyester	**Name**	**M_n, Da**	**M_w, Da**	**Đ**	**M_n, Da**	**M_w, Da**	**Đ**
3a	$PPF_{15}PS_{85}$	3400	7200	2.12	800	1200	1.46
3b	$PPF_{30}PS_{70}$	2600	5300	2.03	800	1200	1.47

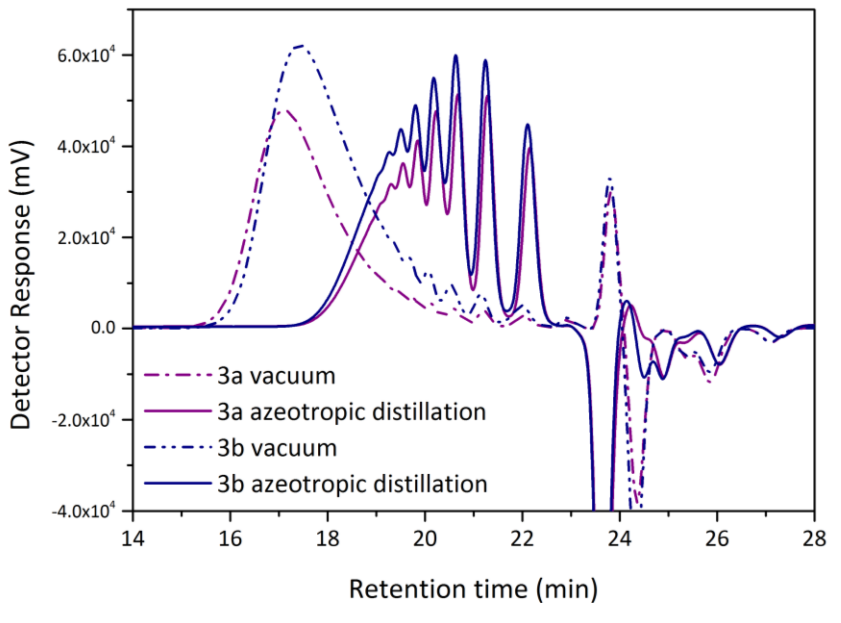

Figure 30. GPC chromatograms for polyesters **3a** and **3b** synthesised by azeotropic distillation or vacuum.

3.3.3 Differential Scanning Calorimetry (DSC)

The thermal transitions of the polyesters were assessed by DSC. **Table 16** summarises the glass transition temperatures (T_g), the melting temperature (T_m) and cold crystallisation (T_{cc}) if it was the case for polyesters **1-3**. The first and second heating scans are shown in **Figure 31** and **Figure 32**, respectively for the syntheses performed at 230 °C. The corresponding thermograms for the other process temperatures are available in **Appendix B**.

Table 16. Thermal transitions of polyesters **1-3** measured by DSC

			First heating scan	Second heating scan		
Polyester	**M_w, Da**	**$T_{process}$, °C**	**T_m, °C**	**T_g, °C**	**T_{cc}, °C**	**T_m, °C**
1 PPS	4300	210	42.9	-37.8	-	-
	5000	220	46.8	-37.7	-	-
	5700	230	44.6	-37.8	-	-
3a $PPF_{15}PS_{85}$	1100	210	Liquid	-43.9	-	-
	1200	220		-45.1	-	-
	1300	230		-45.3	-	-
3b $PPF_{30}PS_{70}$	1100	210	56.3	-39.3	-	-
	1200	220	56.4	-39.7	-	-
	1300	230	47.7	-38.5	-	-
3c $PPF_{70}PS_{30}$	1500	210	110.6	2.5	76.1	109.2
	1700	220	113.0	6.5	95.0	111.7
	1800	230	118.3	2.1	81.1	118.3
3d[a] $PPF_{85}PS_{15}$	1500	210	141.3	17.4	94.5	139.5
	1400	230	133.7	10.1	94.3	131.9
2 PPF	-	210	136.3	12.9	118.7	113.8
	-	220	140.5	11.1	119.4	134.4
	-	230	133.6	10.9	118.2	133.2

[a]: The data corresponding to 220 °C is not available.

The range of T_g of the polyesters was between -45.3 °C and 17.4 °C. The results for pure furan polyester **2** and copolyesters **3c** and **3d** suggest they have a semicrystalline nature, accordingly displaying a glass transition (T_g) and a melting endotherm (T_m) at 133 °C -141 °C. None of the polyesters exhibit observable melt crystallisation, given by the cooling scan. The cold crystallisation temperature (T_{cc}), visible in the second heating scan for polyesters **2**, **3c** and **3d** occur from 76.1 °C to 119.4 °C, suggesting good cold crystallisation ability along

with reasonable melting points (**Figure 33**). The semicrystalline structures of the furan-rich polyesters were confirmed by the X-Ray Diffraction (XRD) results, as described in Section **3.3.5**.

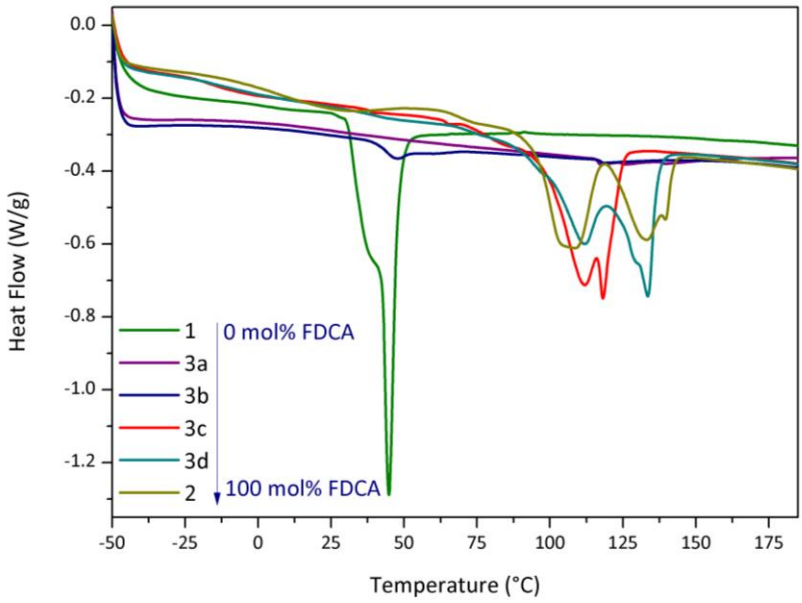

Figure 31. First heating scan at 10 °C/min for polyesters **1** (PPS) and **3** (PPFPS).

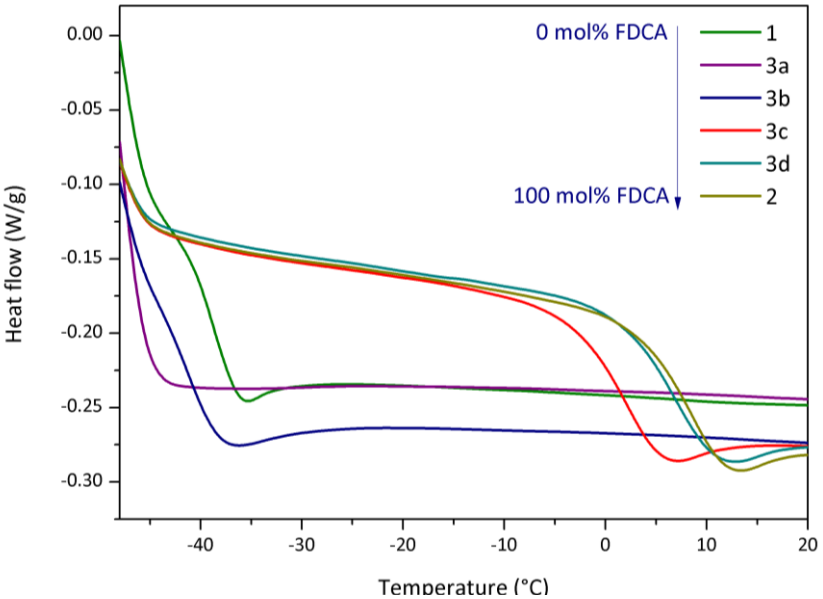

Figure 32. T_g measured during the second heating scan at 10 °C/min for polyesters **1** (PPS) and **3** (PPFPS).

In the case of polyesters **1** and **3a-3b**, neither melt crystallisation in the cooling scan nor cold crystallisation or melting in the second heating scan were observed because of a very

poor crystallisation ability of the copolyesters. These same polyesters however can still crystallise slowly at the condition of natural cooling and therefore exhibit melting peaks at 43-44 °C or **1** and 56 °C for **3b**, respectively.

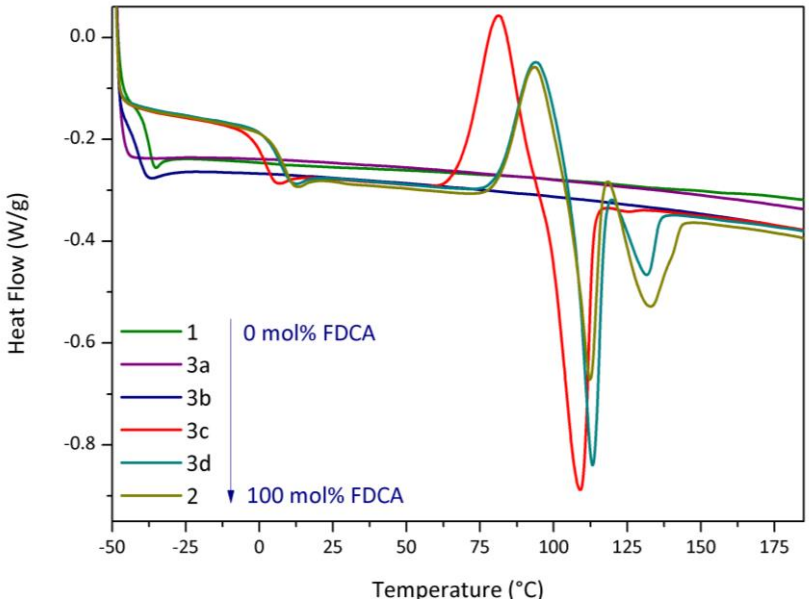

Figure 33. Second heating scan showing T_{cc} for polyesters **2** (PPF), **3c** ($PPF_{70}PS_{30}$) and **3d** ($PPF_{85}PS_{15}$).

The pure succinic acid polymer **1** showed a T_g at -37 °C and T_m at 43-44 °C. The thermal transitions are in accordance with the literature, as it was previously reported that PPS displayed a T_g at -36 °C and T_m at 44 °C.[226]

Polyester **2**, which contains furanic moieties only, exhibited an opposite behaviour to polyester **1**, as it had a T_g at 11-12.9 °C and a T_m at 113-134 °C. Previous research reported T_g for this polyester at 50-53 °C and T_m at 174-180 °C.[227, 262] It is believed that the great difference on T_g is a result of the high M_n values reported, ranging from 13,900 to 21,600 Da.

The dependence of the glass-transition temperature on the composition of copolyesters **3** was evaluated in terms of comonomer unit incorporation. From inspection of **Table 16**, it is observed how the T_g raises as the molar content of FDCA is increased. Polyester **3a** presented the lowest T_g among all the samples (T_g= -45 °C). Besides, the melting behaviour of the semi-crystalline polyesters also showed some sort of trend. Polyesters **2** and **3d** showed the highest melting points (112.2 -139.8 °C), while the lowest corresponded to **1** (43-44 °C).

Previous research on FDCA copolyesters described the T_g as a function of the monomers composition. Wu, et al.[84] reported the thermal transitions for copolyesters of

FDCA and succinic acid with 1,4-butanediol (PBSF) and the results were similar: T_g at -40 °C for the succinic acid polyesters and -25 °C to -3.5 °C for copolyesters with FDCA compositions within 10 and 50 mol% FDCA.

For the same PBSF copolyesters, Jacquel, et al.[92] determined that for compositions bearing from 5 to 60 mol% FDCA, the glass transition temperature varied from -31 °C to -21 °C, although the polymer with 20 mol% FDCA had a slightly higher T_g (-17 °C) than the one with 60 mol% FDCA (-21 °C). In terms of the melting temperatures, the authors reported an inverse trend as a function of the furanic content, with T_m varying from 111 °C to 54 °C as the mol% FDCA increased.

According to other work[84, 86] and our own (**Table 16**), it seems however that T_m increases upon further increasing the furanic content above 30% mol FDCA. In this vein, Wu, et al.[84] showed that PBSF polymers containing 50 mol% up to 100 mol% (PBF) had T_m from 75 to 170 °C. The same behaviour was observed for copolyesters of FDCA, SA and ethylene glycol (PEFS), where the T_m increased from 32.4 °C to 172.9 °C when the mol% FDCA was varied from 50 to 90%.[86] Likewise, Zhou et al.[263] reported copolyesters synthesised from FDCA, 1,4-butanediol and adipic acid (PBF-*co*-PBA) whose crystallisation and melting temperature decreased with FDCA contents from 0 to 50 mol%, but raised again when the concentration was above 75 mol%. These polyesters exhibited T_g from -53 °C to 23 °C and T_m in the range of 27 °C to 156 °C, which are close the to the results obtained in the present work.

The composition range between 100% SA and 100% FDCA therefore enables the synthesis of polyesters with tuneable properties as a function of the monomer content. **Figure 34** displays the FDCA composition dependence of the glass transition temperature of the polyesters **2** and **3**, as well as the relationship between the cold crystallisation T_{cc} and mol% FDCA. In general higher FDCA concentration promotes higher T_g and T_{cc}.

The glass transition temperatures were also compared in terms of processing method. **Table 17** shows the DSC results for **3a** and **3b** synthesised by azeotropic distillation and application of vacuum during the second stage. As the molecular weight increased, the T_g, increased about 20 °C for both polyesters, going from -45.1 °C to -26.7 °C for $PPF_{15}PS_{85}$ (**3a**) and from -39.7 °C to -19.5 °C for $PPF_{30}PS_{70}$ **(3b)**. It is therefore assumed that in order to get a certain range of molecular weight, vacuum-driven processing should be chosen over

azeotropic distillation. **Figure 35** shows the comparison of both processing methods during the second heating scan.

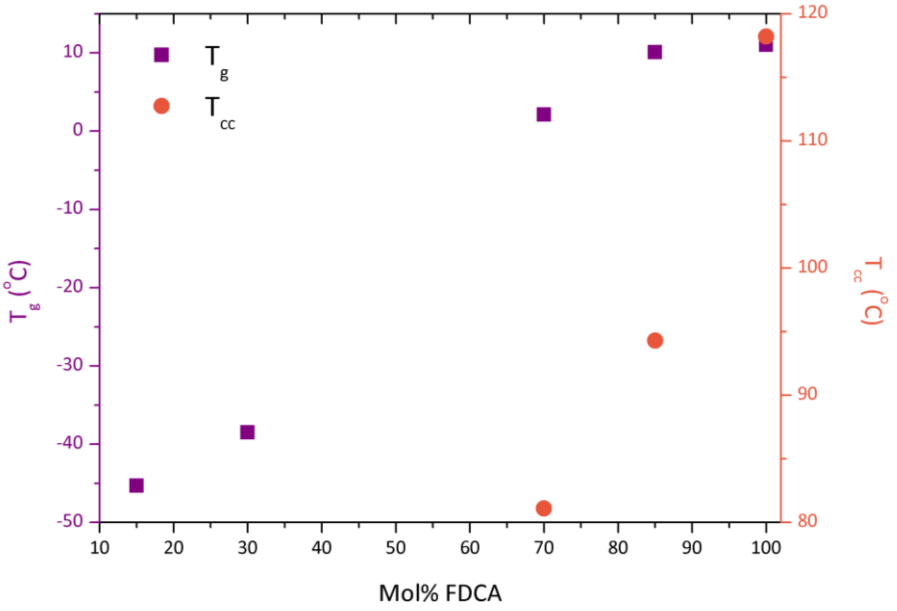

Figure 34. Composition dependence of the glass transition temperature (T_g) and cold crystallisation temperature (T_{cc}).

This process development analysis enables choosing the best configuration according to the final requirements and customers' specifications. The processing methodology will have a big impact in the final properties of the resin. Industrially, vacuum is preferred as it is a faster procedure.

Table 17. Comparison of T_g of **3a** and **3b** synthesised by azeotropic distillation or vacuum in the second stage

		Vacuum			Azeotropic distillation		
Polyester	**Name**	**M_w, Da**	**T_g, °C**	**T_m, °C**	**M_w, Da**	**T_g, °C**	**T_m, °C**
3a	$PPF_{15}PS_{85}$	7200	-26.7	-	1200	-45.1	-
3b	$PPF_{30}PS_{70}$	5300	-19.5	-	1200	-39.7	-

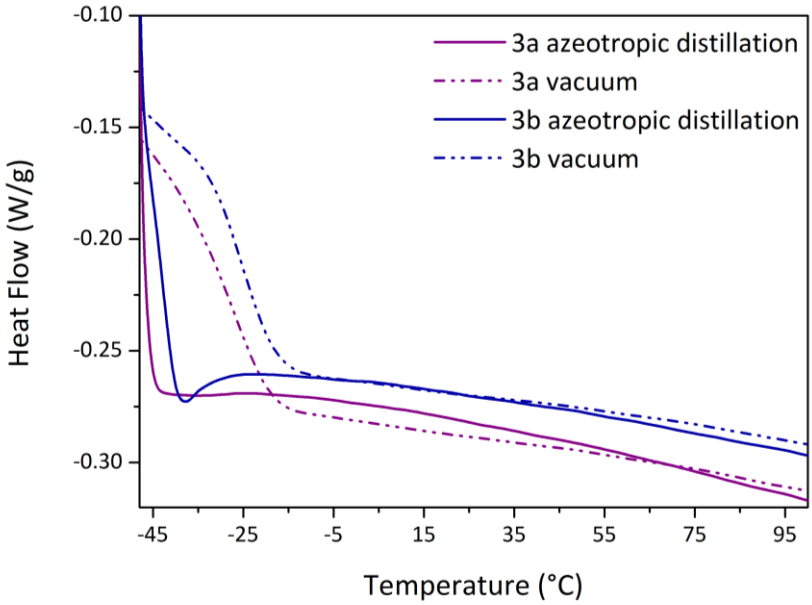

Figure 35. Second heating scan at 10 °C/min for polyesters **3a** ($PPF_{15}PS_{85}$) and **3b** ($PPF_{30}PS_{70}$) synthesised by vacuum and azeotropic distillation.

3.3.4 Thermal Gravimetric Analysis (TGA)

The thermal stability of the resins was assessed by TGA analysis. The decomposition temperature of the polyesters is between 380 °C and 400 °C. **Table 18** summarises the results for each polymer and **Figure 36** and **Figure 37** exhibit the comparison of all the copolyesters along with PPF and PPS synthesised at 220 °C. The thermograms corresponding to the syntheses at 210 °C and 230 °C are available in **Appendix B**. The copolyesters showed two thermal transitions, tentatively corresponding to water or small volatile molecules and the actual polymer. In general, weight loss does not occur below 250 °C, which resembles the results presented by Wu, et al.[84] for PBSF copolyesters.

The process temperature did not play a fundamental role in the decomposition temperature, except in two particular cases. For the copolyester **3a**, with 15 mol% FDCA, the variation goes from 360 °C to 400 °C when it is synthesised at 210 °C and 220 °C, respectively. The synthesis at 210 °C for polyester **2** seemed to be detrimental as well in terms of thermal stability, as the T_d is 380-385 °C when the process temperature is kept between 220 and 230 °C, but it drops to 358.9 °C when the polyester is synthesised at 210 °C. Despite the fact that M_n and M_w were not measured for this polymer, it is believed that the lowest process temperature and excess of diol could have contributed to achieving a low molecular weight or shorter chains in the polymer and thereby affected the thermal stability.

Table 18. Characteristic decomposition temperatures T_{d1}, T_{dmax} and weight loss % of polyesters **1-3**

Polyester	Mol% FDCA	T process, °C	Thermal Transition 1 T_{d1}, °C	Thermal Transition T_{dmax}, °C	Weight loss % (T_{dmax})
1 PPS	-	210	275.3	388.1	95.0
		220	279.7	388.1	94.0
		230	-	387.9	94.0
3a $PPF_{15}PS_{85}$	15	210	302.4	360.4	98.6
		220	298.6	401.0	99.2
		230	295.5	396.4	99.2
3b $PPF_{30}PS_{70}$	30	210	283.5	395.2	98.4
		220	299.5	395.9	98.5
		230	288.9	393.3	96.5
3c $PPF_{70}PS_{30}$	70	210	279.1	382.8	92.4
		220	299.0	394.0	95.7
		230	302.4	386.1	92.0
3d $PPF_{85}PS_{15}$	85	210	280.7	391.3	94.4
		220	291.8	393.8	95.0
		230	280.8	390.5	95.6
2 PPF	100	210	254.2	358.9	98.4
		220	278.6	385.8	94.6
		230	278.5	380.1	94.4

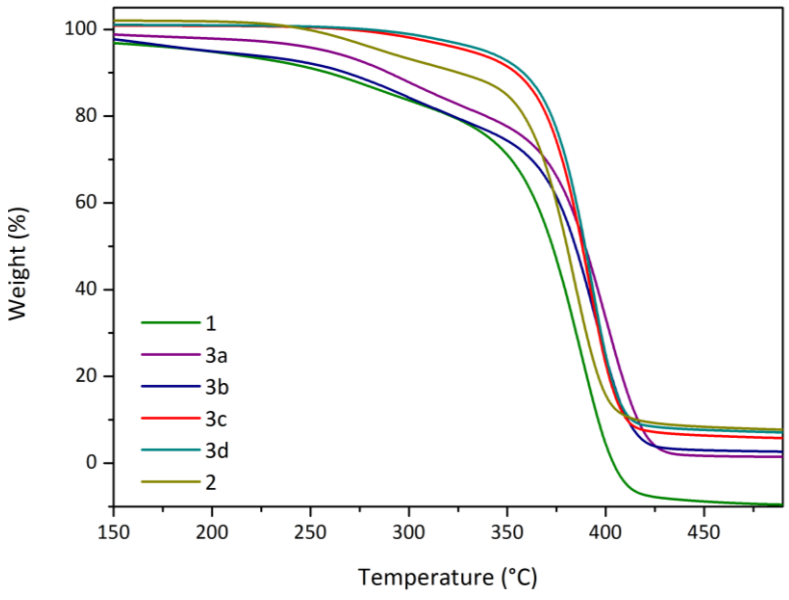

Figure 36. TGA thermogram for polyesters **1** (PPS), **2** (PPF) and **3a-3d** (PPFPS).

The decomposition temperatures of the polyesters **1-3** resemble closely those presented in the literature. For polyester **1**, Chrissafis, et al.[226] reported a T_d at 366 °C while in the

present work a value at 388 °C was obtained. Papageorgiou, et al.[227] recorded a T_d at 396 °C for PPF (polyester **2**), while in the present work the targeted value was 380 °C -385 °C. For the same polymer **2**, another work stated a T_d at 375.3 °C.[75] Comparatively, PET exhibits slightly higher thermal stability (T_d=413 °C) than PEF (T_d=389 °C), which is noteworthy as PEF has a higher chain rigidity than PEF.[71] Similarly, copolyesters of PET-PEF had higher thermal stabilities when the ratio of PET:PEF was 4:1 (408.2 °C) than 1:4 (385.7 °C).[264]

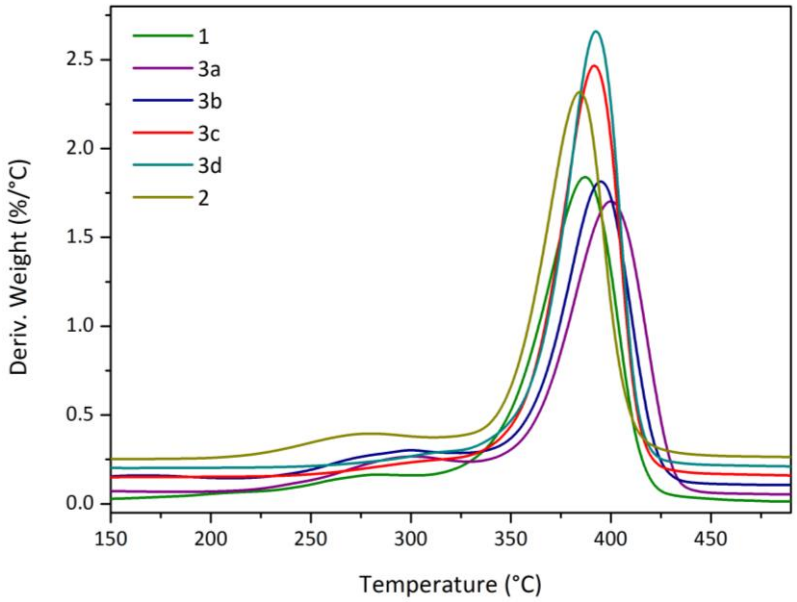

Figure 37. Derivative weight thermogram for polyesters **1** (PPS), **2** (PPF) and **3a-3d** (PPFPS).

There was no evidence of a clear trend in terms of composition and the thermal stability. This lack of direct relationship was mentioned by previous researchers, such as in the case of copolyesters of EG, FDCA and SA, where they exhibited no significant differences or trends dependent on the size or crystallinity of the specimens. The T_d of these polyesters with 10-90 mol% FDCA randomly varied from 378-348 °C.[86] Ma, et al.[77] on the other hand, reported decomposition temperatures from 326 to 341 °C for furan copolyesters with ethylene glycol and 1,4-butanediol (BDO), where no relationship was found either. Moreover, Wu, et al.[265] stated that polyesters of BDO with varying ratios of FDCA and adipic acid displayed a higher T_d range than the furanoates previously mentioned (404-430 °C), although no clear composition dependence was claimed.

The recorded initial decomposition temperature might be a result of degradation reactions. Thermal decomposition of polyesters usually starts with the scission of the polymer chain through a six-membered-ring transition stage.[266] The evolution of light volatile

products, and the formation of vinyl ester chains are a result of secondary reactions.[266] Pyrolysis studies of FDCA polyesters with 1,8-octanediol and 1,10-decanediol carried out at 350 °C recorded the formation of several degradation products, including gases such as CO, CO_2 and aldehyde, as well as alkyl, vinyl or hydroxyl terminated esters of FDCA.[95]

It is concluded that polyesters **1-3** have a good thermal stability, making them suitable for different markets as they align with previous work in the area, and of course, in coating applications. Specifically in the area of coatings, Gubbels, et al.[257] compiled a work where polyesters of FDCA and 2,3-butanediol had thermal stabilities between 304 and 343 °C. The polyester synthesised with ZrBO as catalyst targeted the highest value at 343 °C among different catalysts tested.

3.3.5 XRD

Characteristic peaks at 6.76°2θ, 16.62°2θ, 15.47°2θ, 24.19°2θ and 26.88°2θ were distinguished for **1**, which has been already reported in the literature.[75, 227] Copolyesters **3c** and **3d** displayed the same XRD diffractrograms, with diffraction peaks at 9.82 °2θ, 16.46 °2θ, 18.80 °2θ, 23.26 °2θ, 25.07 °2θ and 28.78 °2θ. The sharp diffraction peaks were indicative of the presence of crystallites in the copolyesters. According to **Figure 38**, it could be found that similar characteristic diffractions were observed for **3c** and **3d**, suggesting that the prepared copolyesters keep a close crystal structure to that of PPF, polyester **1**.

Similar behaviour has been previously observed in other systems; for instance, in the case of copolyesters of EG, SA and FDCA (PEFS), when the number of furanic units was higher (70-90 mol%), well-defined sets of crystalline diffraction peaks similar to those reported for PEF appeared.[86] Moreover, Luo, et al.[267] showed that copolyesters of terephthalic acid, succinic acid and 1,4-butanediol (PBST) with terephthalic content above 50 mol% resembled the crystal structure of the parent polyester, poly(butylene terephthalate) (PBT).

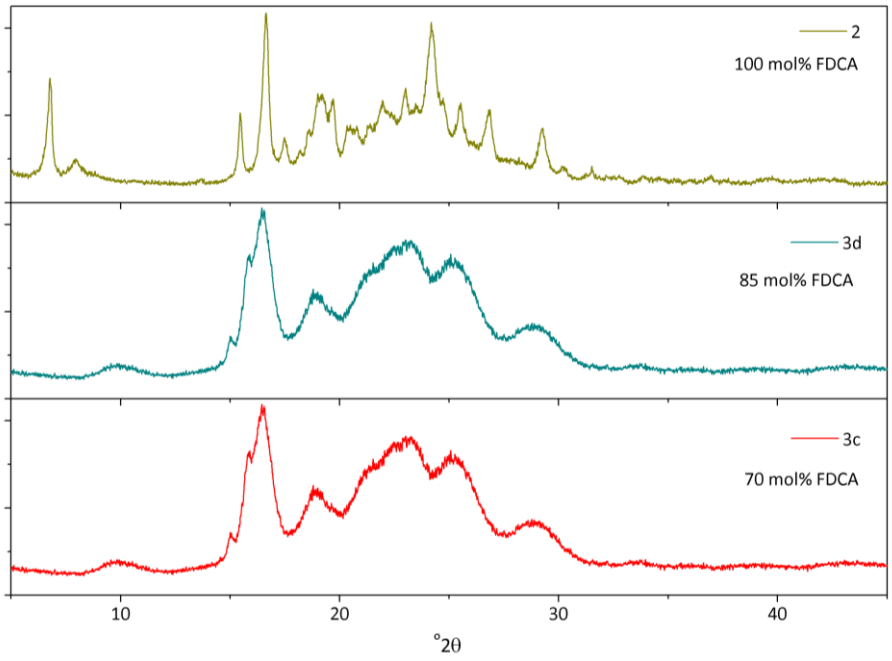

Figure 38. XRD diffractograms for polyester **2** and copolyesters with 85% mol FDCA (**3d**) and 70% mol FDCA (**3c**).

3.3.6 Paint testing

Copolyesters **3a** and **3b** were formulated into the white polyester protocol formulation used at Becker Indsutrial Coatings Ltd. Their performance was compared against that of a reference resin, which will be stated from now on as **R**, whose properties are summarised in **Table 19**. The copolyesters considered were synthesised at 220 °C by the conventional azeotropic distillation during the second stage.

3a and **3b** were the only resins compatible with the solvent blend used at Becker Coatings Ltd. Copolyesters **3c** and **3d** oppositely, remained solid as they would break up a little bit and then revert back to being solid. It was then impossible to make finished paints from these resins. **Table 19** summarises the results from the physical testing performed in the resins.

The data suggests that an increase from 15 to 30 mol% FDCA from copolyester **3a** to **3b** translated into better physical properties that are closer to those of the reference resin, particularly in the microhardness and T_g. It is however observed that although the panels of the finished paints are passing the T-bend and MEK rubs, the microhardness and T_g values are not as high as when using the reference resin, which are 216 $N \cdot m^{-2}$ and 35 °C, whereas for

the bioderived resins, the microhardness ranged from 36 to 45 $N \cdot m^{-2}$ and T_g from 0.6 to 12 °C.

T-Bend no cracking is the number of bends carried out before cracking is observed on the analysed specimen. Our result (3T) indicates no cracking was observed until the sample had been bended three times. The resistance to cracking is an indication of the flexibility of the coating.

Table 19. Physical test results on white paints based on copolyesters **3a** and **3b** and the reference resin **R.**

Test	Specification	R	3a ($PPF_{15}PS_{85}$)	3b ($PPF_{30}PS_{70}$)
Colour	White	White	White	White
Pencil Hardness	H	H	F	H
Gloss Top Coat	30-40 at 60	35	35	34
Reverse Impact 80'' lb	No cracking	Moderate cracking	Slight cracking	Slight cracking
Erichsen 7.5 mm	No cracking	Moderate cracking	Moderate cracking	Moderate cracking
T-Bend NTPO	2T	0.5T	1T	0.5T
T-Bend no cracking[a]	No cracking	3T	3T	3T
MEK[b] rubs primer	100	110	110	110
T_g, °C	-	35	0.6	12
Microhardness, $N \cdot m^{-2}$	-	216	36	45

[a]: Cracking is detected by removal of a pressure-sensitive tape placed on the bend edges and observing the degree of removed coating particles. [b]: Methyl ethyl ketone

T-Bend NTPO is the number of bends carried out before paint pick off is not observed when tape is placed over the bend and pulled off. 0.5T means at 0.5T bend if tape is placed over the bend and pulled away there is no paint stuck on the tape. The greater the number of thicknesses around which the coated metal is bent, the less severe the test and more brittle the residence.[225]

The microhardness and T_g being below the specifications might relate to the molecular weights of the resins, which fall in the lower range of the suitable values for coil coatings. It was already proved that the vacuum-driven polymerisation overcame this problem, so future work relies on the paint testing characterisation of the newly synthesised polymers by this method.

Regarding the furanic content, it appears to be a threshold where the mol% FDCA cannot be as high as 70% mol, which apparently leads to incompatibility of the resin with the solvent system to produce paints. There is thus some window in terms of composition to produce polyesters that would tackle the desired specifications.

3.4 Conclusions

The synthesis of biomass-derived polyesters and copolyesters based on 2,5-furan dicarboxylic acid (FDCA), succinic acid (SA) and 1,3-propanediol (PDO) was successfully performed via a two-step process: polyesterification and polycondensation. The obtained polyesters were characterised by ^{1}H NMR, GPC, DSC, TGA, XRD and paint testing.

^{1}H NMR confirmed the structure of the polyesters with, chemical shifts resembling those at the literature[85, 226, 227] for FDCA (7.2 ppm) , SA (2.64 ppm) and the protons next to the FDCA ester (4.50 ppm) and SA ester (4.26 ppm) bonds. GPC analysis showed that the range of M_w of the polyesters was between 1100 Da to 5700 Da, which is within the suitable molecular weight range for coatings. M_w seemed to increase with the processing temperature, and in the case of copolyesters of FDCA and SA, the M_w kept a strong dependence with the furanic content, as it increased with the mol% FDCA. The GPC data corresponding to polyesters of FDCA and PDO were not available because of the insolubility of the polyesters in THF.

When the syntheses of copolyesters with 15% (Polyester **3a**) and 30 mol% FDCA (**3b**) were performed with application of vacuum during the polycondensation stage, the M_w increased from 1200 Da to 7200 and 5300 Da, respectively, which suggests that vacuum drove the reaction further than azeotropic distillation as diol and water were efficiently released. Future work includes therefore the synthesis of the remaining compositions to complete the vacuum-synthesised library of biomass-derived polyesters.

Thermal analysis showed that the glass transition temperature of the polyesters was found between -45.3 °C and 17.4 °C. The results for the polyfuranoate **2** and copolyesters

with 70 mol% FDCA (**3c)** and 85 mol% (**3d)** suggest they have a semicrystalline nature, displaying melting endotherms (T_m) between 133 °C and 141 °C. None of these polyesters exhibited observable melt crystallisation but they showed cold crystallisation temperature (T_{cc}) from 76.1 °C to 119.4 °C, suggesting good cold crystallisation ability.

The dependence of the glass-transition temperature on the composition of copolyesters **3** was evaluated in terms of comonomer unit incorporation, and it was observed how the T_g rose as the molar content of FDCA increased. For example, Polyester **3a,** with 15 mol% FDCA displayed a T_g at -45 °C whereas **3d**, with 85 mol% FDCA had a T_g at 17.4 °C.

TGA analysis provided that the decomposition temperature (T_d) of the polyesters was found between 360 and 401 °C. The copolyesters showed two thermal transitions, most likely the first one corresponding to water or small volatile molecules and the second and main one to the actual polymer. In general, weight loss did not occur below 250 °C. The process temperature did not play a fundamental role in the decomposition temperature, except for the polyester **3a** (15 mol% FDCA) where the variation went from 360 to 400 °C when synthesised at 210 °C and 220 °C, respectively. The synthesis at 210 °C for polyester **2** seemed to be detrimental as well in terms of thermal stability, as the T_d decreases 20 °C (358.9 °C) when compared to that at 220 and 230 °C (380-385 C)

The paint testing data suggests that an increase from 15 to 30 mol% FDCA from copolyester **3a** to **3b** translated into better physical properties of the coating, that are closer to those of the reference resin, particularly the microhardness and T_g. It is however observed that although the panels of the finished paints are passing the T-bend and MEK rubs, the microhardness and T_g values are not as high as when using the reference resin, which are 216 $N \cdot m^{-2}$ and 35 °C, whereas for the bioderived resins, the microhardness ranged from 36 to 45 $N \cdot m^{-2}$ and T_g from 0.6 to 12 °C. There is seemingly a limit in terms of composition, as the FDCA content cannot exceed 70 mol%, which apparently leads to incompatibility of the resin with the solvent system to produce paints.

The microhardness and T_g below specification might relate to the molecular weights of the resins, which fall in the lower range of the suitable values for coil coatings. As vacuum-driven polymerisation increased the molecular weight of the resins, future work relies on the paint testing characterisation of the newly synthesised polymers by this method.

This chapter provided the fundamentals towards the synthesis of biomass-derived polyesters with tuneable properties, which can be chosen by means of different process variables: Processing methodology –azeotropic distillation or vacuum, depending on the desired range of molecular weight-; diacids ratio and process temperature.

CHAPTER 4

Properties of biomass-derived polyesters with 1,5-pentanediol: PPeS, PPeF and PPeFS

4. Properties of biomass-derived polyesters with 1,5-pentanediol: PPeS, PPeF and PPeFS

This chapter presents the properties' characterisation of biomass-derived polyesters based on 1,5-pentanediol (PTO), 2,5-furandicarboxylic acid (FDCA) and succinic acid (SA): PPeS (Polyester **4**, **Scheme 35**), PPeF (**5**, **Scheme 35**) and PPeFS (**6**, **Scheme 35**).

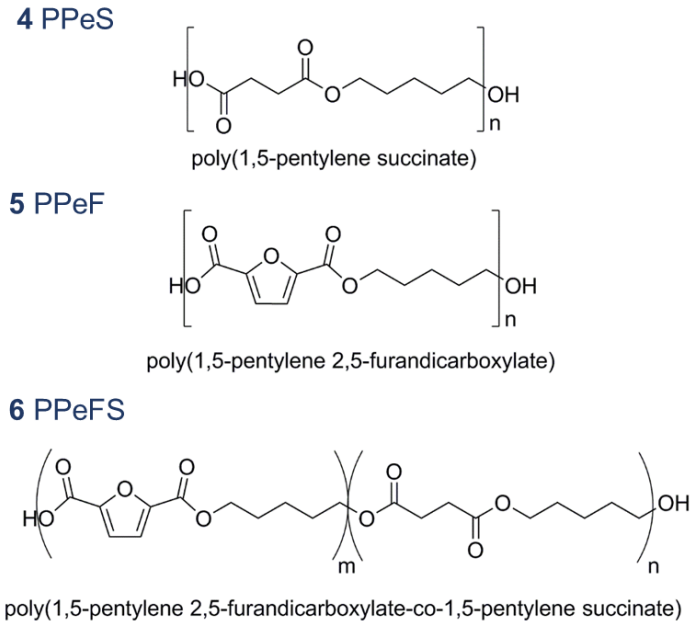

Scheme 35. Chemical structures of polyesters **4-6** derived from succinic acid, FDCA and 1,5-pentanediol.

4.1 Introduction

Biomass transformations toward alcohols and diols of short alkyl chain, particularly C5 diols, are of increasing importance due to their use as monomers in polyesters and their potential use as gasoline additives, fuels or solvents.[148] The current world capacity of 1,5-pentanediol is around 3000 ton per year, due to the limited readily accessible C5 petroleum feedstocks.[268] However, as described in **Chapter 1**, bio-based furfural and its derivatives, such as furfuryl alcohol (FA) and tetrahydrofurfuryl alcohol (THFA), could be transformed into 1,5-pentanediol; for instance, 1,5-pentanediol can be obtained from the hydrolysis of furfural[131] whereas 1,2- and 1,5-pentanediols can be generated from THFA by hydrogenolysis of C–O bonds of the five-member ring heterocycle.[148] **Scheme 36** and **Scheme 37** show the furfural hydrogenation and the hydrogenolysis of THFA toward 1,5-pentanediol, respectively.

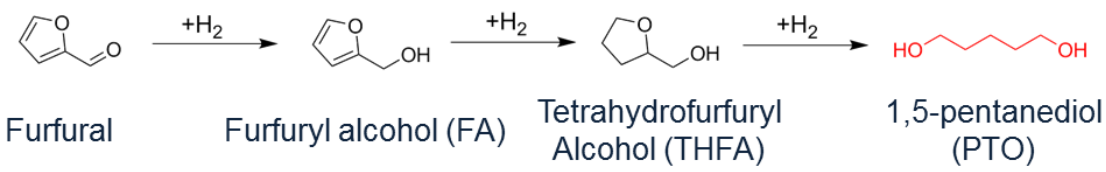

Scheme 36. Furfural hydrogenation into 1,5-pentanediol adapted and modified from Sun, et al.[148]

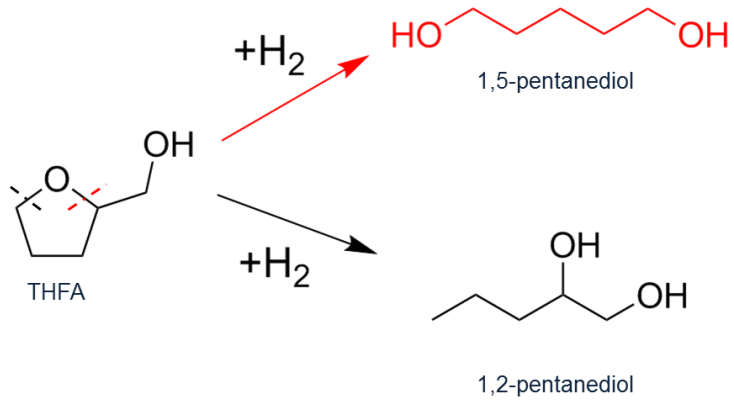

Scheme 37. 1,5-pentanediol and 1,2-pentanediol derived from THFA hydrogenation, adapted and modified from Sun, et al.[148]

Recently, the use of THFA as a starting material for the synthesis of PTO has been reviewed[130] along with several meaningful publications where it has been shown that silica- or carbon-supported rhodium catalysts modified with Re, Mo or W displayed high activity and selectivity, while commercial hydrogenation catalysts such as Ru/C, copper chromite and Raney Ni showed much lower activity and selectivity.[130, 132, 133, 135, 139] Early studies reported a two-step process where the intermediate ω-hydroxyvaleraldehyde was synthesised from THFA followed by the hydrogenation to PTO using copper chromite as catalyst, with a PTO selectivity of 70% a 150 °C.[143] Still, the implications of these catalysts must be assessed in terms of toxicity, availability and recovery in order to be widely adopted by industry.

As previously stated, the role of the metal catalyst is fundamental in the selectivity toward 1,5-pentanediol. Among the aforementioned catalysts, Ir–ReO_x/SiO_2 was the most active material for THFA conversion,[133, 135] whereas Rh–ReO_x/SiO_2 showed a selectivity of 93.7% but was less stable than Rh–MoO_x/SiO_2.[133] The presence of MoO_x at a low Mo/Rh ratio of 0.13 was found to increase selectivity towards 1,5-pentanediol. In the absence of Mo, Rh/SiO_2 gives 1,5-pentanediol in a low 18% selectivity. Guan and co-workers[137] explained in detail the role of Mo in a binary catalyst consisting on MoO_3 and supported Rh nanoparticles

in the ring-opening process of THFA. They claimed that THFA first undergoes acid-catalysed ring-opening process to form the key intermediate 5-hydroxypentanal, which is then quickly hydrogenated into 1,5-pentanediol under the heterogeneous Rh catalysis.

Chatterjee, et al.[269] performed the hydrogenation of THFA over Rh supported on mesoporous silica (MCM-41) under supercritical carbon dioxide. The conversion of THFA was found to increase with increasing CO_2 pressure due to the enhanced solubility of THFA in CO_2. The maximum selectivity to 1,5-pentanediol was 91.2% at 80 °C. Furthermore, Pholjaroen, et al.[138] reported the use of Ir-VOx/SiO_2 catalysts at 80 °C achieving PTO selectivity above 80%.

The direct transformation of furfural and furfuryl alcohol to 1,5-pentanediol without THFA as intermediate has gained attention. Xu, et al.[145] studied the hydrogenolysis of furfural using a Li–Pt/Co_2AlO_4 catalyst at 140 °C, obtaining 34.9% selectivity to 1,5-pentanediol. The selectivity was largely improved by using a modified Ir–ReOx/SiO_2 catalyst with either Pd[139] or Rh,[146] as in the first case the achieved selectivity was 71.4 % and 78.2% in the latter. In the case of having furfuryl alcohol as the substrate, a maximum selectivity to 1,5-pentanediol of 30.5 % was obtained using $Mg_3AlO_{4.5}$ with 10 wt% Cu at 140 °C.[147] The production of 1,2-pentanediol from furfuryl alcohol has been explored as well by using Ru catalysts supported on either Al_2O_3 or carbon at 140 °C, reporting selectivities from 20 to 32%.[270]

Very recently, a pioneer plant analysis for the bio-derived production of 1,5-pentanediol from furfural was presented, providing insightful and promising data for its large scale implementation.[268] The study estimated a yield above 80% and a minimum sale price of $1973 per ton of 1,5-pentanediol. Moreover, the furfural feedstock and plant size were identified as the most important economic parameters to be considered. Comparatively, 1,4-butanediol and 1, 6-hexanediol have projected market prices of $1600−2800 and $2500−4500 per ton, respectively.[268] The technoeconomic feasibility analysis of the process was assessed considering two reaction systems (hydrogenation of furfural to THFA and three-step conversion of THFA into 1,5-pentanediol), as well as subsystems for the separation of: hydrogen; to be recycled back to the hydrogenation reactors; THFA from byproducts and produced water; and 1,5-pentanediol, from water and byproducts.[268] The process flowsheet for the proposed strategy is presented in **Figure 39**.

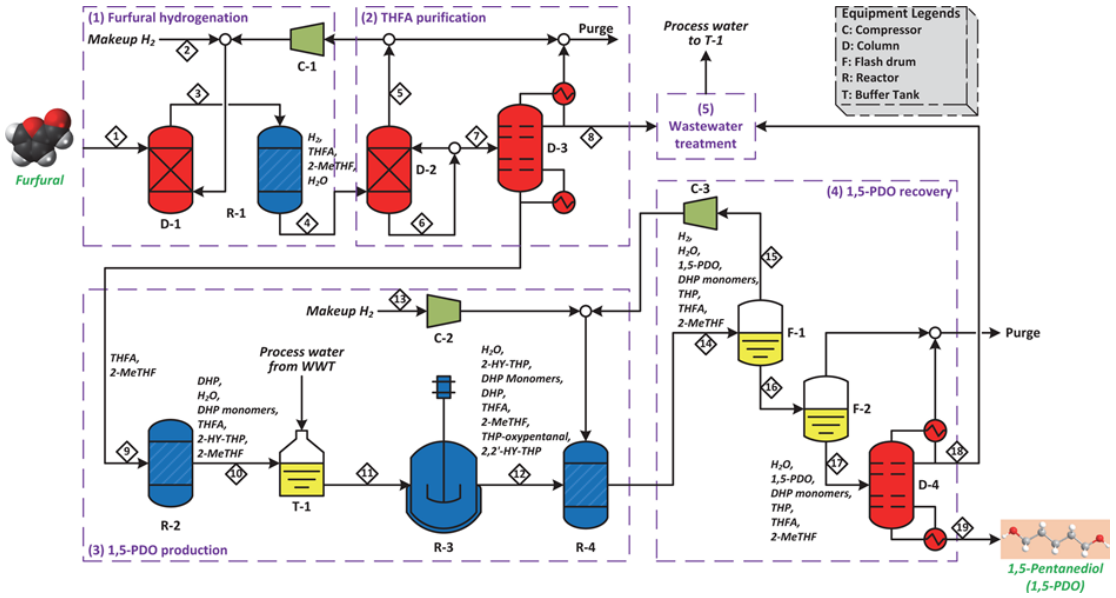

Figure 39. Process flowsheet for the production of 1,5-pentanediol from furfural. Reprinted with permission from (Huang K, et al. DOI: 10.1021/acssuschemeng.7b00059).[268] Copyright (2017) American Chemical Society.

The suitability of 1,5-pentanediol as a monomer for polyester synthesis from a green chemistry perspective is steadily growing as it is derived from second generation-biomass feedstocks, such as furfural, which has been considered a key platform chemical within the biorefinery concept.[29] In terms of final properties of the polyesters, it will be expected that PTO is good for obtaining flexible coatings but with better hardness than 1,6-hexanediol (currently used as a monomer for coatings) as it is known that hardness drops very rapidly with increasing chain length of the glycol: the greater the increase in flexibility, the lower the hardness.[175] The effect of PTO as a chain extender on hydroxyl-terminated polybutadiene-based polyurethanes has been studied in terms of adhesion and mechanical properties. The authors found that the inclusion of PTO led to increased adhesion strength of the polyurethane to aluminium panels, increased cross-linking density and better general final properties compared to an aromatic chain extender, N, N-Bis (hydroxyethyl) aniline.[271]

As briefly described in the introduction in **Chapter 1**, there are few works that consider 1,5-pentanediol as a main building block of polymers, compared to conventional, broadly-used diols such as 1,4-butanediol. Chen, at al.[272] described the synthesis of polyester-based polyurethanes from 1,5-pentanediol and pimelic acid in a diol:diacid molar ratio of 1.21:1. The polyester-based polyurethane presented the following properties: M_n = 2770 Da, T_g = -44 °C and T_m= 22 °C. In another work based on polyurethanes, a polyurethane elastomer was

synthesised using 2,4-diethyl-1,5-pentanediol. This polyurethane showed the best hydrolysis resistance compared with commercial polyurethanes derived from 1,6-hexanediol or 1,9-nonanediol, which are known as hydrolysis-resistant diols.[273]

1,5-pentanediol has been used as well in the field of polyesteramides and poly(ester–carbonate)s. Guang and Gaymans[274] synthesised polyesteramides from N,N'-bis(p-carbomethoxybenzoy)butanediamine as crystalline segments and mixtures of poly(tetramethylene oxide) and 1,5-pentanediol as soft segments. Regarding poly(ester–carbonate)s, the synthesis of oligo(ester–carbonate) diols based on propylene carbonate, dimethyl adipate or succinate and 1,5-pentanediol was reported.[275] The carbonates obtained were oligo(pentamethylene adipate-co-carbonate) with a molar mass of 2385 $g \cdot mol^{-1}$ and T_g at -54.1 °C and oligo(pentamethylene succinate-co-carbonate) of M_n between 1515 and 2385 $g \cdot mol^{-1}$ and T_g in the range of -55 to -51.9 °C, depending on the mol% of carbonate units.

Tang, et al.[112] studied the synthesis of polyester gels from 3-methyl-1,5-pentanediol and itaconic anhydride. The polyesters were synthesised at 60 °C for 24 h using hydroquinone as radical inhibitor to avoid excessive crosslinking, and molar masses of 1400-1600 Da were obtained. The molecular weight increased to 3400-8100 Da when maleic anhydride was added in molar ratios of itaconic anhydride:maleic anhydride from 1:2 to 1:8, getting the highest molecular weight with the ratio of 1:8.

More recently, Tsanaktsis, et al.[81] reported for the first time the synthesis of poly(pentylene furonoate) (PPeF) along with poly(heptylene furonoate) (PHepF). PPeF was identified as a semicrystalline polyester with a melting point at 94 °C, T_g at 19 °C and a maximum decomposition temperature at 394 °C. The same research group studied the thermal decomposition mechanism of PPeF.[276] They found that the decomposition of PPeF released gases, such as CO and CO_2, along other degradation products such as dienes, vinyl- and carboxyl-terminated molecules.

4.2 Experimental

The experimental procedure has been described in **Chapter 2, Section 2.3.3.4** and **2.3.3.5** and resembles the methodology presented in **Chapter 3**, **Section 3.2** by considering FDCA, succinic acid and 1,5-pentanediol, the latter instead of 1,3-propanediol as the diol.

Table 20 lists the polyesters considered in this chapter and their structures are depicted in **Scheme 35**. Polyesters **6a** and **6b** were also synthesised by applying vacuum in the polycondensation stage.

Table 20. Biomass-derived polyesters with PTO, FDCA and SA

No.	Acronym	Mol% FDCA	Mol% SA	r	T, °C
4	PPeS	-	100	1.05	
5	PPeF	100	-	1.3	
6a	$PPeF_{15}S_{85}$	15	85		210-230
6b	$PPeF_{30}S_{70}$	30	70	1.3	
6c	$PPeF_{70}S_{30}$	70	30		
6d	$PPeF_{85}S_{15}$	85	15		

4.3 Characterisation results

4.3.1 ^{1}H NMR

The chemical structures of the polyesters **4-6** were analysed by ^{1}H NMR. The chemical shifts assignments are specified in **Scheme 38.** The ^{1}H NMR spectra for 1,5-pentanediol is shown in **Figure 40** whereas the ones corresponding to **4**, **6a**, **6d** and **5** are depicted in **Figure 41**. The enlarged area from chemical shifts 1.3 ppm to 2 ppm is shown in **Figure 42** for clarity. FPeS refers to the repeating unit of copolyesters **6**. The assignments for terminal 1,5-pentanediol are also considered. The structure of terminal 1,5-pentanediol has been included in **Figure 41** and **Figure 42** along with the corresponding main polymers structures.

Table 21 shows the corresponding assignments and chemical shifts of the resulting polyesters. The ^{1}H NMR spectra of **6b** and **6c** are available in **Appendix C**.

The ^{1}H NMR data show six main signals: the furan ring proton (*a*) at 7.2 ppm, succinic acid methylene protons (*b*) at 2.62 ppm, the pentylene protons at 1.4-1.8 ppm, the protons of the methylene groups adjacent to the furan (*i*) and succinic acid (*f*) esters at 4.35 ppm and 4.09 ppm, respectively and terminal PTO (*c*) at 3.65 ppm. The presence of the peaks at 4.35

(*i*) and 4.09 ppm (*f*) confirms the esterification reactions of both FDCA and SA have taken place. The other methylene protons from the reacted 1,5-pentanediol units appear at 1.84 ppm (*j*) and 1.55 (*k*) for FPeF units (repeating unit polyester **5**) and 1.6 ppm (*g*) and 1.4 ppm (*h*) for SPeS (repeating unit polyester **4**). In the copolyester **6d** with 85 mol% FDCA, three peaks (*h*, *k* and *l*) are visible between 1.3 and 1.55 ppm corresponding to SPeS, FPeF and FPeS repeat units, respectively. The presence of the chemical shift *l* at 1.48 ppm confirms the formation of copolyesters. There is some 1,5-pentanediol left in the system, which corresponds to the assignments from 1.58 to 1.65 ppm (*d*,*e*). Both FDCA and SA are completely incorporated and a single peak is observed for each one, *a* and *b*, respectively. The compositions of the copolyesters **6** were confirmed by the integration of the corresponding peaks, which are summarised in

Table 22. The mol% FDCA was calculated by dividing the integration of the FDCA ester (i) by the sum of FDCA ester and SA ester (*f*). The terminal OH refers to the integration of *c* whereas 1,5-pentanediol refers to all the integrations from 1.40 to 1.55 ppm.

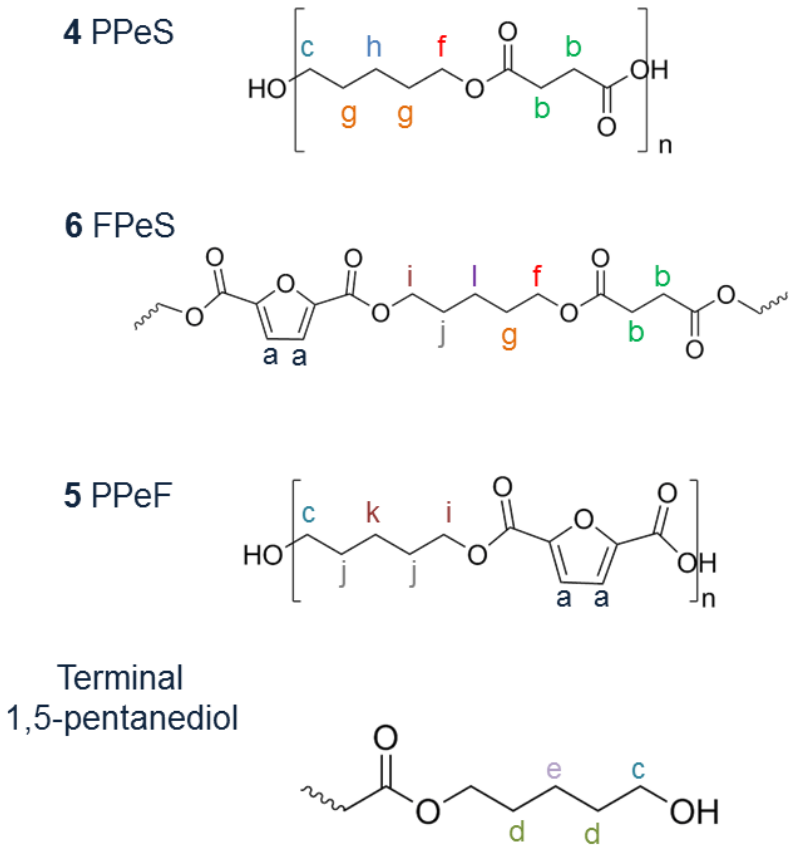

Scheme 38. [1]H NMR assignments (FPeS represents the repeating unit of PPeFS).

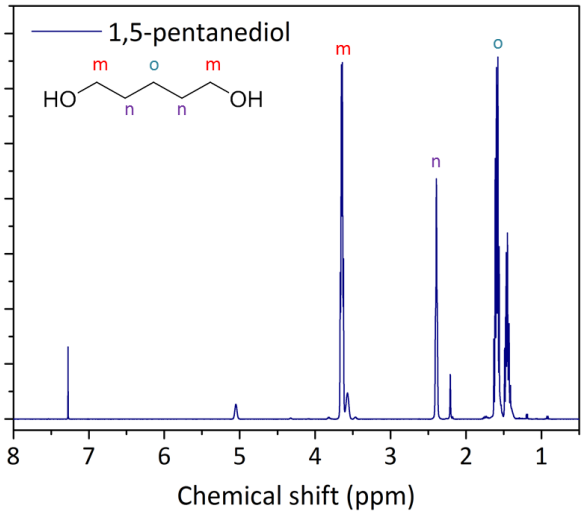

Figure 40. ^{1}H NMR of 1,5-pentanediol in CDCl3.

Table 21. Assignment of chemical shifts of polyesters PPeS, PPeFS, PPeF

Polyester	Assignment of chemical shifts ($CDCl_3$, δ/ppm)											
	a	**b**	**c**	**d**	**e**	**f**	**g**	**h**	**i**	**j**	**k**	**l**
PPeS (4)	-	2.62	3.65	1.65	1.58	4.09	1.66	1.44	-	-	-	-
PPeFS (6)	7.20	2.62	3.68	1.65	1.58	4.11	1.68	1.40	4.36	1.84	1.55	1.48
PPeF (5)	7.20	-	3.68	1.65	1.58	-	-	-	4.35	1.84	1.55	-

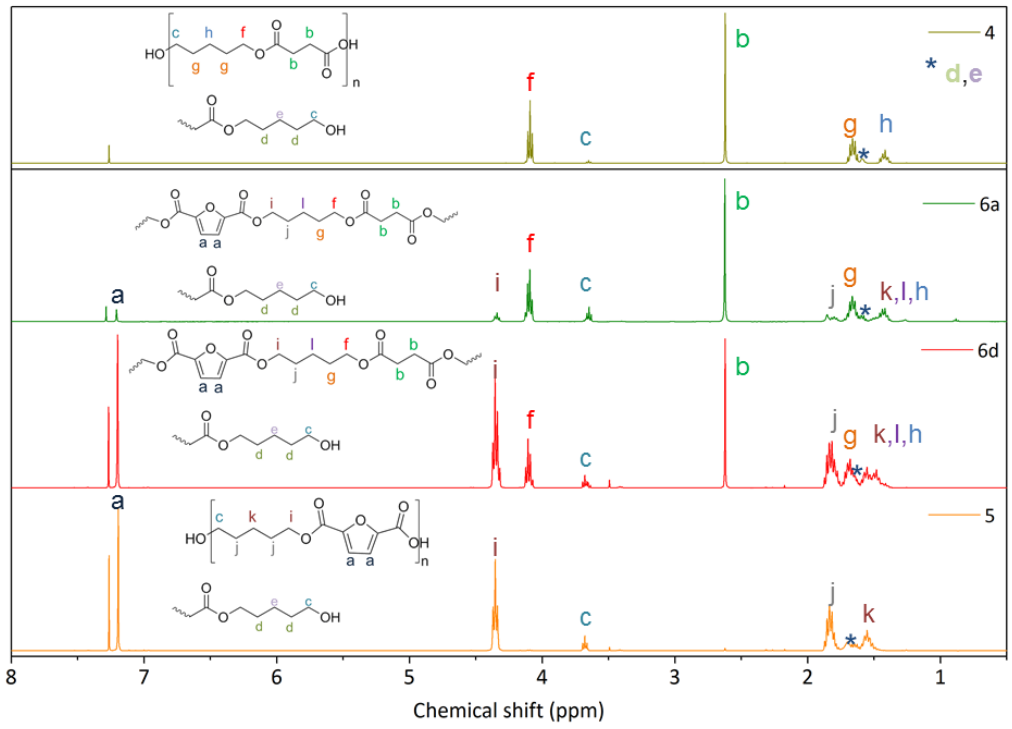

Figure 41. ^{1}H NMR spectra of PPeS (**4**), $PPeF_{15}S_{85}$ (**6a**), $PPeF_{70}S_{30}$ (**6d**) and PPeF (**5**).

Table 22. Integration values of the chemical shifts of polyesters **6** and calculated diacid ratio

Copolyester	FDCA	SA	FDCA ester	SA ester	Terminal OH	1,5-pentanediol	Mol% FDCA[a]	Mol% SA
6a	0.18	1	0.37	2	0.43	1.56	0.16	0.84
6b	0.40	1	0.82	2	0.39	1.65	0.29	0.71
6c	2.34	1	4.68	2	0.87	11.85	0.70	0.30
6d	6.10	1	12.05	2	0.65	8.16	0.86	0.14

[a]Determined from dividing the integration value of FDCA ester by the sum of the integrations of the FDCA and SA esters.

The chemical assignments reported herein align with those in the literature.[81] In the case of PPeF (**5**), chemical shifts appeared at 7.4 ppm (*a*), 4.46 ppm (*f*) 1.92 ppm (*j*) and 1.69 ppm (*k*) in deuterated trifluoroacetic acid.[81] As far as it is known, no copolyesters of 1,5-pentanediol, FDCA and SA have been reported, however, the shifts resemble the behaviour to those of copolyesters of FDCA, SA and 1,4-butanediol,[84] and FDCA, ethylene glycol and SA.[86]

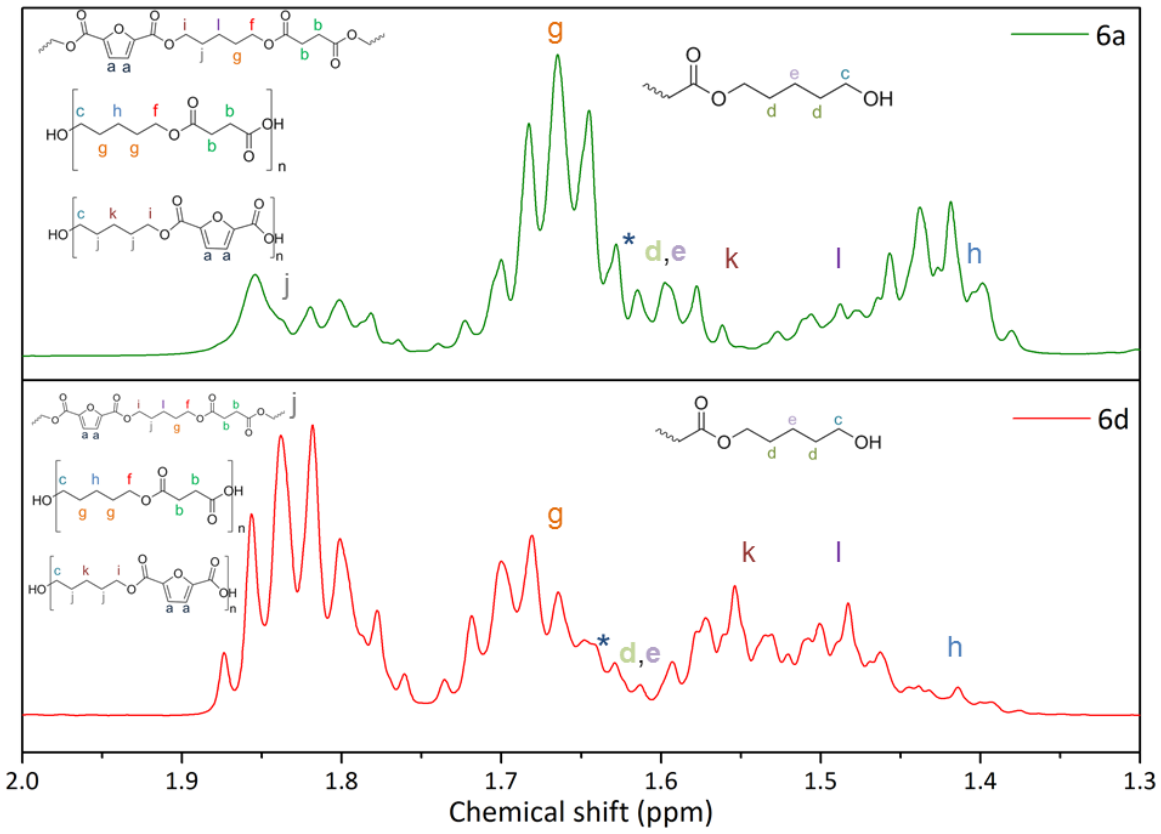

Figure 42. ^{1}H NMR spectra of **6a** and **6d** from 1.3 to 2 ppm.

4.3.2 Molecular weight measurement by GPC

The molecular weights and dispersity of the polyesters were measured by GPC at Becker Industrial Coatings Ltd. **Table 23** summarises the results of M_n, M_w and dispersities (Đ) of the biomass-derived polyesters as a function of processing temperature. **Figure 43** displays M_w as a function of the process temperature.

Table 23. M_n, M_w and Đ as a function of the process temperature, via azeotropic distillation

Polyester	Name	Mol% FDCA	T, °C	M_n, Da	M_w, Da	Đ
4	PPeS	0	210	3000	7500	2.5
			220	3100	8300	2.7
			230	4100	10700	2.6
6a	$PPeF_{15}S_{85}$	15	210	1200	2200	1.8
			220	1400	2700	1.9
			230	1500	3000	2.0
6b	$PPeF_{30}S_{70}$	30	210	1400	2600	1.9
			220	1400	2800	1.9
			230	1800	3800	2.1
6c	$PPeF_{70}S_{30}$	70	210	2400	4500	1.9
			220	3200	5900	1.8
			230	3200	6100	1.9
6d	$PPeF_{85}S_{15}$	85	210	2000	4400	2.1
			220	2100	4100	2.0
			230	3200	7000	2.2
5	PPF	100	210	3100	8300	2.7
			220	3300	8200	2.5
			230	2400	6200	2.6

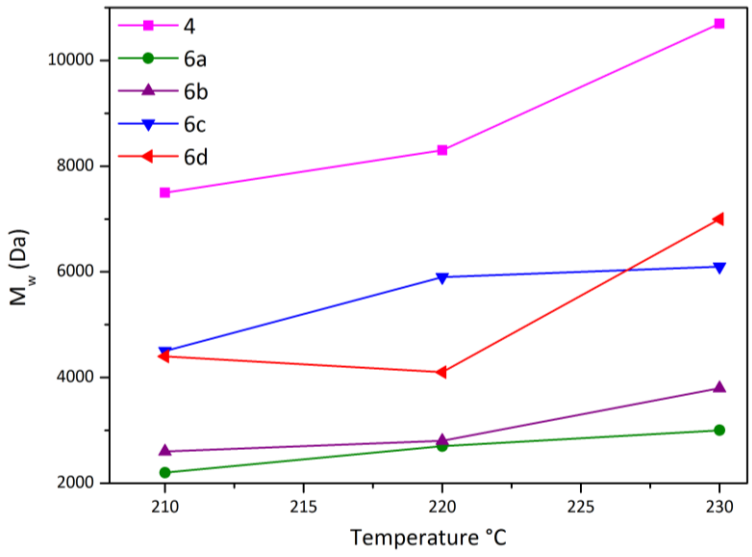

Figure 43. M_w as a function of process temperature for polyesters **4** (PPeS) and **6** (PPeFS).

The M_w measured fall within the range of 2200 to 10700 Da, which are higher than the M_w corresponding to the polyesters prepared from 1,3-propanediol, **1-3**. PPeS (**4**) was the only polyester to be synthesised with a diol:diacid ratio of 1.05:1 as no processability issues such as early gelation points or poor dispersion of the monomers were encountered, which is associated with rich furan mixtures. The lower diol:diacid ratio results in higher final molecular weights with values as high as 10000 Da obtained at a processing temperature of 230 °C.

As studied in **Chapter 3**, process temperature plays a fundamental role in the final molecular weight, as it increases as the temperature is raised. The temperature effect is more evident for **6c** and **6d** where M_w is increased by 60% between 210 °C and 230 °C, going from 4500 Da to 6100 Da and 4100 Da to 7000 Da, respectively, compared to only 25% increase for **6a** over the same temperature range. In this case, the molecular weight was 2000 Da at 210 °C and 3000 Da at 230 °C. It is believed that this behaviour is related to the rate of temperature rather than some chemical explanation.

In the case of furan polyester **5**, it is believed that some issues with the temperature controller might have happened as the lowest molecular weight (6200 Da) was obtained at 230 °C, while a M_w of 8300 Da was achieved at 210 °C. A possible cause might be that the temperature controller could have struggled to reach the set point and keep it throughout the reaction time when processing furan polyesters, **2** and **5**, as the system was highly viscous and would take considerable time to reach clear point, i.e. a homogeneous reaction mixture.

The effect of temperature on the molecular weight is shown for **6b** and **6c** in **Figure 44** and **Figure 45**, respectively. As in the case of polyesters **1** and **3** with 1,3-propanediol, the presence of narrow oligomeric peaks is clear, and they are more pronounced as the reaction temperature is decreased. It can be noted as well that the oligomeric nature is not a characteristic of rich FDCA polyesters, as the case of **6c**, which does not present as may narrow peaks as **6b**. The effect is corroborated by the other compositions, whose chromatographs are available in **Appendix C**. This fact suggests that one should carefully consider the final application so a proper process temperature is chosen and extra energy expenditures and costs are avoided.

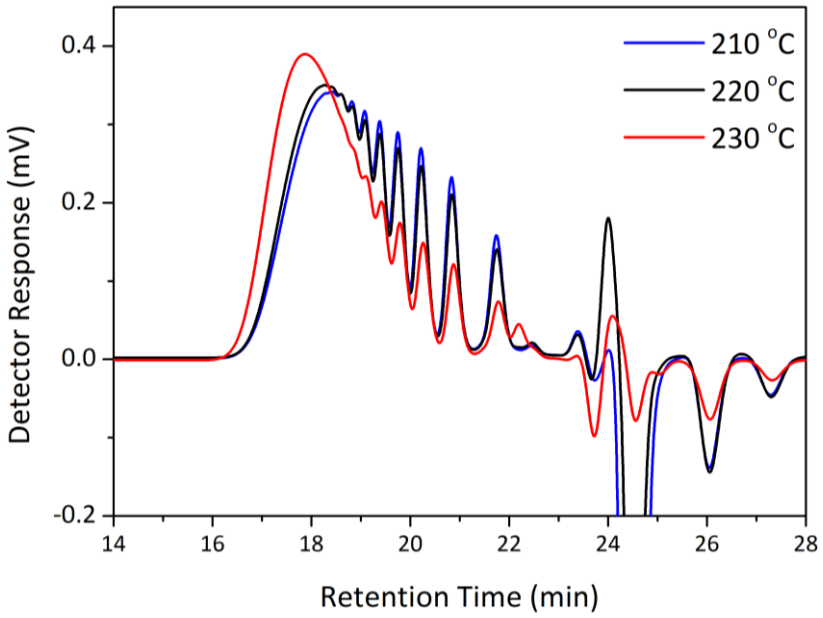

Figure 44. GPC chromatogram for polyester **6b** ($PPeF_{30}S_{70}$) synthesised at 210 °C, 220 °C and 230 °C.

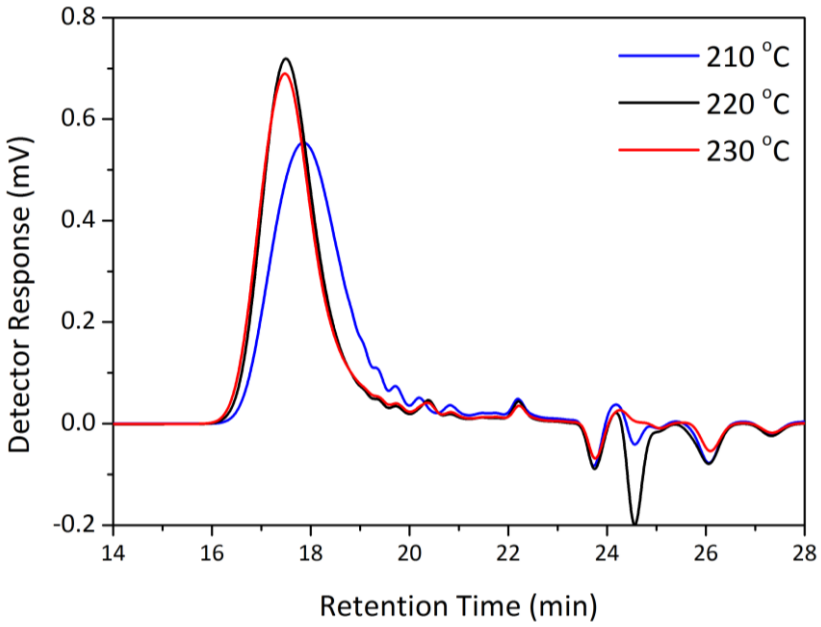

Figure 45. GPC chromatogram for polyester **6c** ($PPeF_{70}S_{30}$) synthesised at 210 °C, 220 °C and 230 °C.

Regarding the diacid composition effect, the same behaviour as in the case of copolyesters **3** with 1,3-propanediol is observed in most cases, where the M_w increases as the FDCA content increases. The trend is shown in the chromatogram in **Figure 46**, corresponding to the syntheses performed at 230 °C. The exception is polyester **6c**, with 70

mol% FDCA at 210 °C (4500 Da) and at 220 °C (5900 Da), whose M_w were higher than those of **6d** with 85 mol% FDCA, 4400 Da and 4100 Da, respectively.

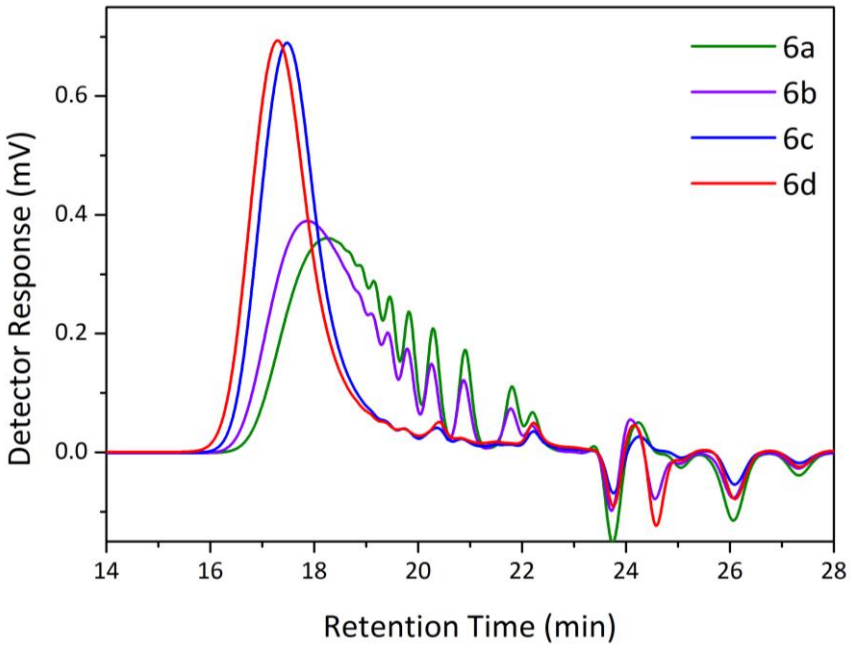

Figure 46. GPC chromatograph for copolyesters **6** synthesised at 230 °C.

The polyesters with 1,5-pentanediol have a more "polymeric" nature when compared with the polyesters from 1,3-propanediol presented in **Chapter 3**, as the oligomer species are less, which is pointed out in the chromatograms in **Figure 47** and **Figure 48** which respectively compare the 15 mol% FDCA (**3a, 6a**) and 85 mol% FDCA (**3d, 6d**) compositions with the two diols considered.

The molecular weights obtained are higher than those for polyesters for coating applications reported in the literature. Gubbels, et al.[252, 257] reported M_w in the range of 2100 to 3100 Da for polyesters prepared from 2,5-dimethyl-furandicarboxylate, 2,3-butanediol, glycerol and trimethylolpropane. Coatings prepared from succinic acid and isosorbide presented M_w between 2000-3100 Da[170] and slightly increased when they were modified with citric acid, falling within 2200 Da and 3800 Da.[166]

In another study, coatings based on cycloaliphatic polyesters of 1,4-cyclohexanedimethanol with 1,4 and 1,3-cyclohexanedicarboxylic acid had M_n between 829 and 900 Da.[277] Finally, polyester-based polyurethanes synthesised from pimelic acid and 1,5-pentanediol had M_w 2770 Da.[272]

The molecular weight of PPeF (**5**) synthesised in the present work cannot be directly compared to the first publication about it since no GPC data was provided.[81] Reported M_w however for a polyester of FDCA and 1,6-hexanediol was 3800 Da (Equimolar diol:diacid molar ratio, 80 °C, 74 h),[278] lower than the one obtained for our PPeF (8200 Da-8300 Da).

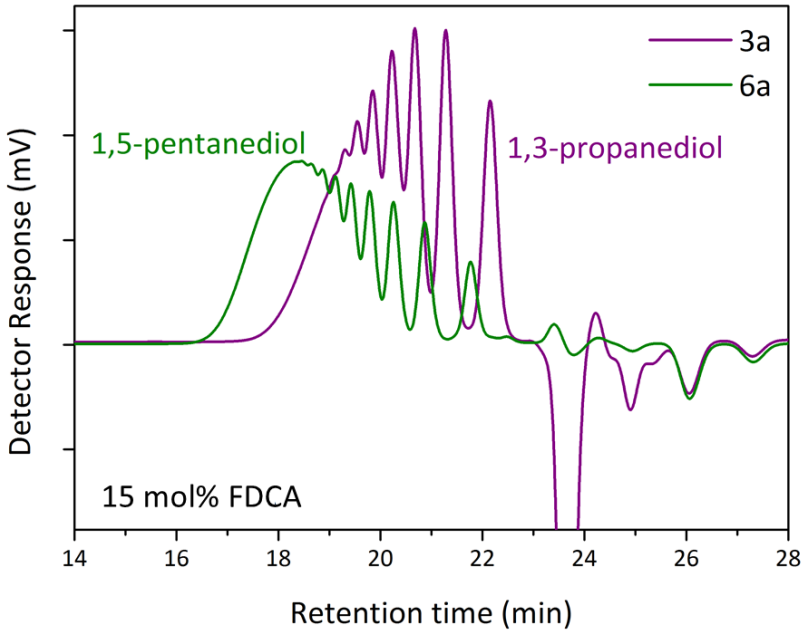

Figure 47. GPC chromatogram comparing polyesters bearing a 15/85 FDCA/SA composition with 1,3-propanediol (**3a**) and 1,5-pentanediol (**6a**).

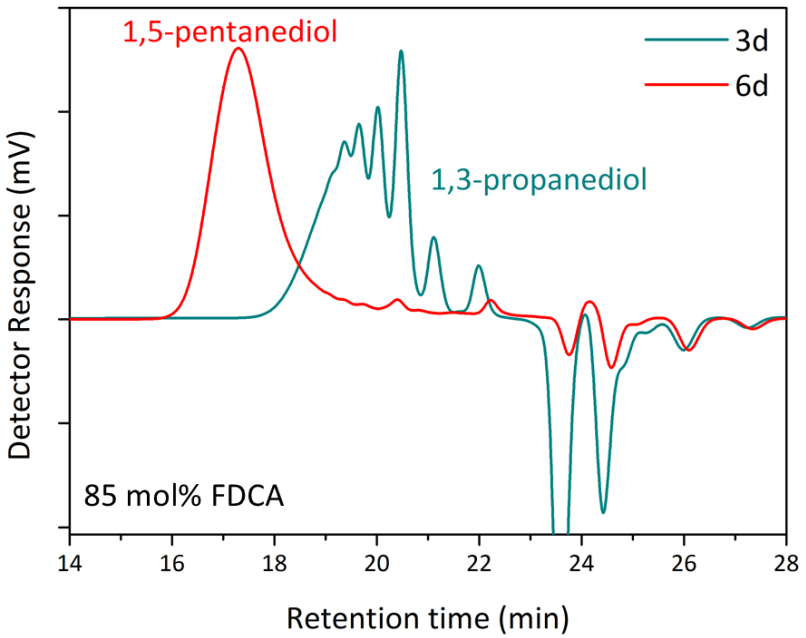

Figure 48. GPC chromatogram comparing polyesters bearing a 85/15 FDCA/SA composition with 1,3-propanediol (**3d**) and 1,5-pentanediol (**6d**).

As a proof of concept, the syntheses of **6a** and **6b** were performed as well by applying vacuum in the polycondensation stage. **Table 24** compares the GPC results of the two processes.

Table 24. Comparison of M_n, M_w and Đ synthesised by vacuum or azeotropic distillation in the second stage

		Vacuum			Azeotropic distillation		
Polyester	**Name**	**M_n, Da**	**M_w, Da**	**Đ**	**M_n, Da**	**M_w, Da**	**Đ**
6a	$PPeF_{15}S_{85}$	4100	8200	2.04	1400	2700	1.90
6b	$PPeF_{30}S_{70}$	4000	7800	1.96	1400	2800	1.90

It is clear how the vacuum increased the final molecular weight of the polyesters, as expected. The M_w increased from 2700 Da to 8200 Da and from 2800 Da to 7800 Da for **6a** and **6b**, respectively and the dispersities were slightly higher. As concluded in **Chapter 3** for the 1,3-propanediol resins, future work will include the completion of the other polyester compositions by applying vacuum, although extra caution during processing should be assured as furan rich polyesters **6d** and **5** would potentially have considerably higher viscosity and molecular weight that would lead to processing limitations.

Figure 49 shows the comparison of **6a** and **6b** between both processing methodologies. The presence of oligomeric, narrow peaks disappears during the vacuum-driven polycondensation.

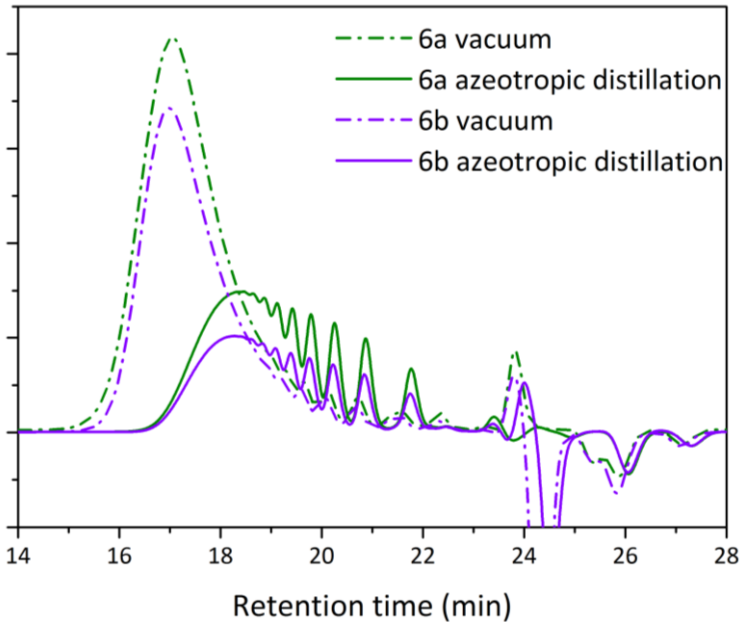

Figure 49. GPC chromatogram of **6a** ($PPeF_{15}S_{85}$) and **6b** ($PPeF_{30}S_{70}$) synthesised by azeotropic distillation and application of vacuum.

4.3.3 Differential Scanning Calorimetry (DSC)

The thermal transitions of the biomass-derived polyesters with 1,5-pentanediol were determined by differential scanning calorimetry. The glass transition temperatures (T_g) and melting temperatures (T_m) are listed in **Table 25** and the first and second heating scans for the syntheses at 220 °C are shown in **Figure 50** and **Figure 51**, respectively. The DSC scans corresponding to the other process temperatures are available in **Appendix C**.

The glass transition temperatures of the polyesters with 1,5-pentanediol are in the range of -48 °C to 18.1 °C, which is below the T_g range found for 1,3-propanediol polyesters **1** and **3** (-45 °C to 17.4 °C, **Chapter 3**), suggesting an enhanced chain flexibility provided by the longer aliphatic chain. It is then suggested that the T_g of the furanic–aliphatic polyesters showed a continuous decrease with increasing chain length of the alkane-α,ω-aliphatic linear diol units. This agreed well with the previous results reported in the literature, where furan polyesters synthesised with 1,4-butanediol, 1,6-hexanediol, 1,8-octanediol and 1,10-decanediol showed glass transitions from 25 °C and below as the diol length increased.[278] The synthesis of **5** at 230 °C did give however a T_g higher than its counterpart with 1,3-propanediol (**2**) at the same conditions (T_g= 10.9 °C, **Table 16**) which might have possibly been caused by a considerable higher molecular weight of **5** or an inconsistent temperature control throughout the reaction time. In fact, the M_w of this particular synthesis was below the range obtained at other process temperature (6200 Da vs. 8300 Da) which strengthens the assumption of a poor process control. The results of **5** synthesised at 210 °C are thereby considered as not satisfactory and are not significant for the analysis.

The composition of the polyesters had a great influence on the thermal transitions. Both T_g and T_m increase with the FDCA content, as the furan ring provides strength and impact resistance, seemingly a more plastic behaviour. Polyesters with low (**6a**, **6b**) or no FDCA (**4**) content are soft, elastomer-like materials. The succinic acid and 1,5-pentanediol polyester **4** had the lowest T_g, -49 °C, whereas the polyester of FDCA and 1,5-pentanediol (**5**) presented a T_g at 18 °C, which closely matched a recently reported result of T_g =19 °C.[81] In the case of other FDCA polyesters with odd numbered methylene groups from a previous study, the T_g was found at 5 °C for a polyester of FDCA with 1,7-heptanediol, and -5 °C with 1,9-nonanediol, although no molecular weights were reported.[81]

Table 25. Thermal transitions of polyesters **4-6** measured by DSC

					First heating scan	Second heating scan
Polyester	**Name**	**Mol% FDCA**	**M_w, Da**	**$T_{process}$, °C**	**T_m, °C**	**T_g, °C**
4	PPeS	-	7500	210	36.8	-48.5
			8300	220	36.0	-48.9
			10700	230	36.8	-48.7
6a	$PPeF_{15}S_{85}$	15	2200	210		-48.8
			2700	220	-	-46.3
			3000	230		-49.2
6b	$PPeF_{30}S_{70}$	30	2600	210		-41.0
			2800	220	-	-41.0
			3800	230		-41.5
6c	$PPeF_{70}S_{30}$	70	4500	210		-12.6
			5900	220	-	-9.9
			6100	230		-9.9
6d	$PPeF_{85}S_{15}$	85	4400	210	50.3	-9.5
			4100	220	48.8	-8.2
			7000	230	49.6	0.6
5	PPeF	100	8300	210	69.2	5.7
			8200	220	76.3	9.1
			6200	230	71.1	18.1

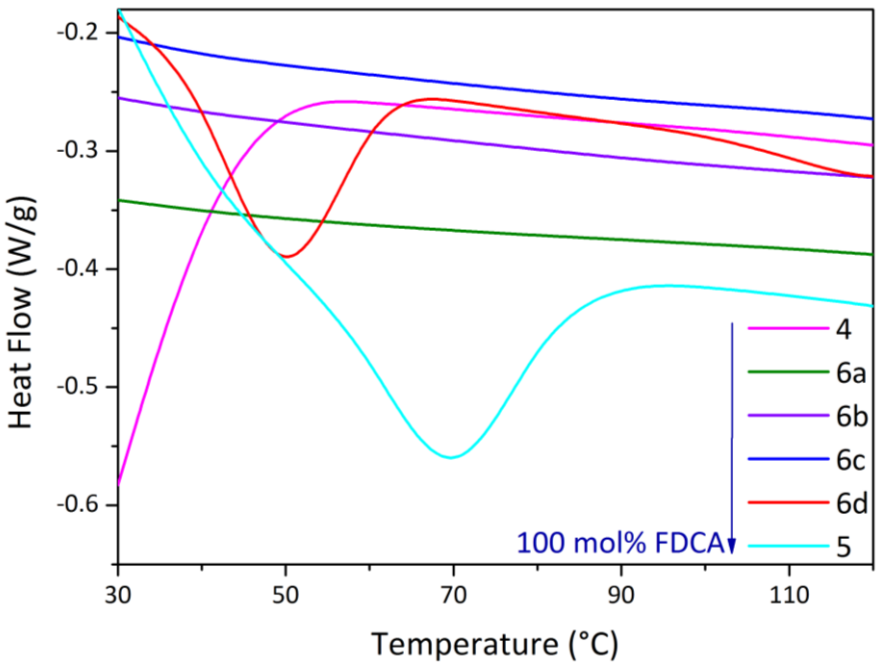

Figure 50. First heating scan at 10 °C/min for polyesters **4-6**.

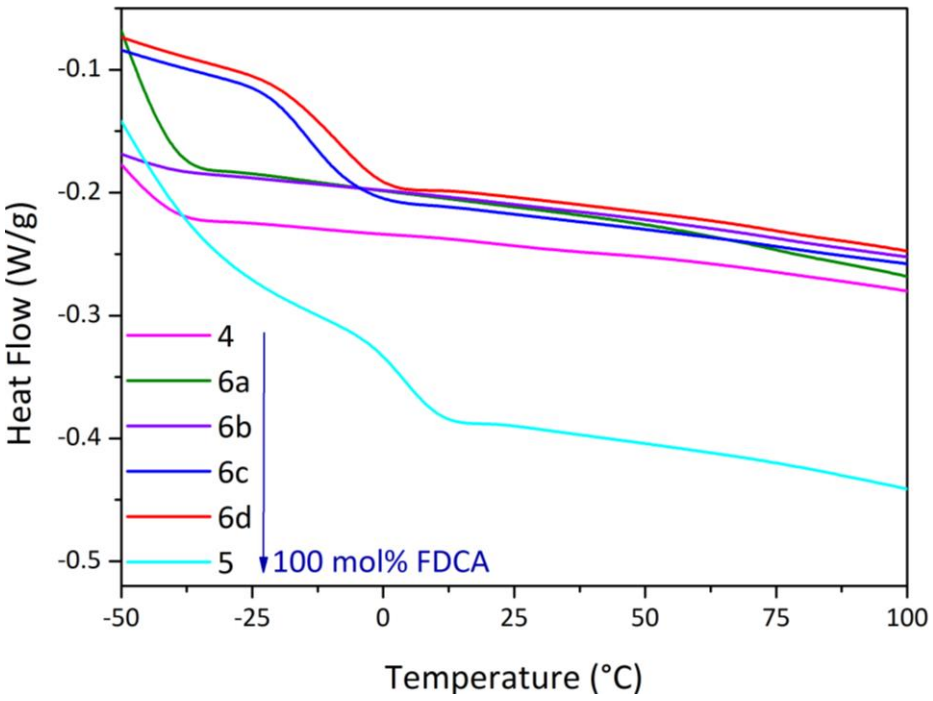

Figure 51. Second heating scan at 10 °C/min for polyesters **4-6**.

Previous works of polyesters with 1,5-pentanediol showed a stronger plasticiser effect and lower glass transitions than those reported herein: T_g=-44 °C with pimelic acid[272] and -55 to -51.9 °C for polyester carbonates with either dimethyl succinate or dimethyl adipate.[275]

The T_m range of the 1,5-pentanediol polyesters was found between 36 °C to 76 °C whereas in the case of 1,3-propanediol the T_m varied from 42.9 °C to 140.5 °C (**Chapter 3**). As in the analysis for T_g, this suggests the T_m of the tested furanic–aliphatic polyesters with similar high molecular weights decreased with increasing chain length of the alkane-α,ω-aliphatic linear diol units. This agreed well with the previous study reported by Jiang, et al.[278] **Figure 52** shows the structure–T_g relationship of the obtained furan polyesters containing 1,3-propanediol (Polyester **2**) and 1,5-pentanediol (Polyester **5**). The values reported by Jiang, et al.[278] for 1,6-hexanediol, 1,8-octanediol and 1,10-decanediol are included to compare the proposed trend, considering polyesters in the same range of molecular weight. 1,7-heptanediol and 1,9-nonanediol are included as well, but the molecular weights were not measured.[81]

The library of polyesters exhibited different degrees of crystallinity. The semicrystalline polyesters were those with 85 mol% (**6d**) and 100 mol% FDCA (**5**) with melting temperatures from 48 to 76 °C. Additionally, polyester **4** presented a semicrystalline

structure as well (T_m=36 °C), whereas the polyesters with succinic acid compositions of 85 mol% (**6a**), 70 mol% (**6b**) and 30 mol% (**6c**) potentially have an amorphous structure. It is then suggested that the presence of a particular range of FDCA content, most likely from 15 to 70 mol%, leads to polyesters with a randomly ordered molecular structure which does not have a sharp melt point. This random incorporation of furanic units into the polymer backbone which altered the semi-crystalline was observed as well for PET-PEF copolyesters.[264]

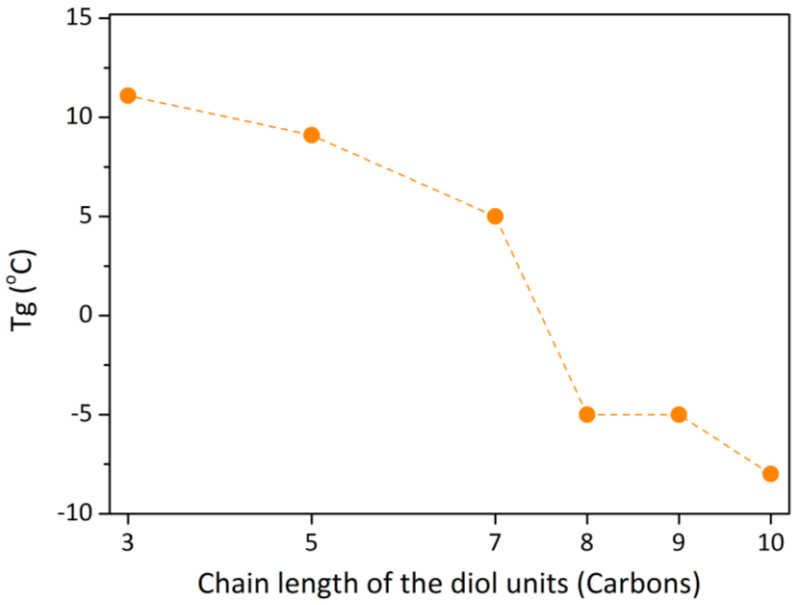

Figure 52. Structure–T_g relationship of the synthesised polyesters **2** and **5** and **C_7-C_{10}** polyesters containing aliphatic linear diol units. Values for $C_{8,}C_{10}$ were obtained from the literature for polyesters with M_w=5800 Da-7600 Da[81, 278]

Wu, et al.[84] reported the thermal transitions for copolyesters of FDCA, SA and BDO, obtaining similar results: T_g at -40 °C for succinic acid polyesters and from -25 °C to -3.5 °C for copolyesters with a range from 10% to 50% molar portion of FDCA. In another study of copolyesters synthesised from FDCA, 1,4-butanediol and adipic acid, the T_g increased with the FDCA content from -62 °C for the polyadipate to 35.6 °C for the polyfuronoate.[265] In this case, the ratio of diol to diacids was 2:1.

In general, it is observed that glass transition temperatures of the resulting polyesters can be adjusted by varying the diacid ratio and consequently, the molecular weight.[279] To examine variations between polyesters, a plot showing M_n, T_g and T_m as a function of FDCA content is presented in **Figure 53**. The effect of the diacid ratio and choice of diol would

allow for some tuning of thermal behaviour. This broad polyester family therefore provides polymer engineers and chemists an interesting library to choose feasible polyesters for potential end uses.

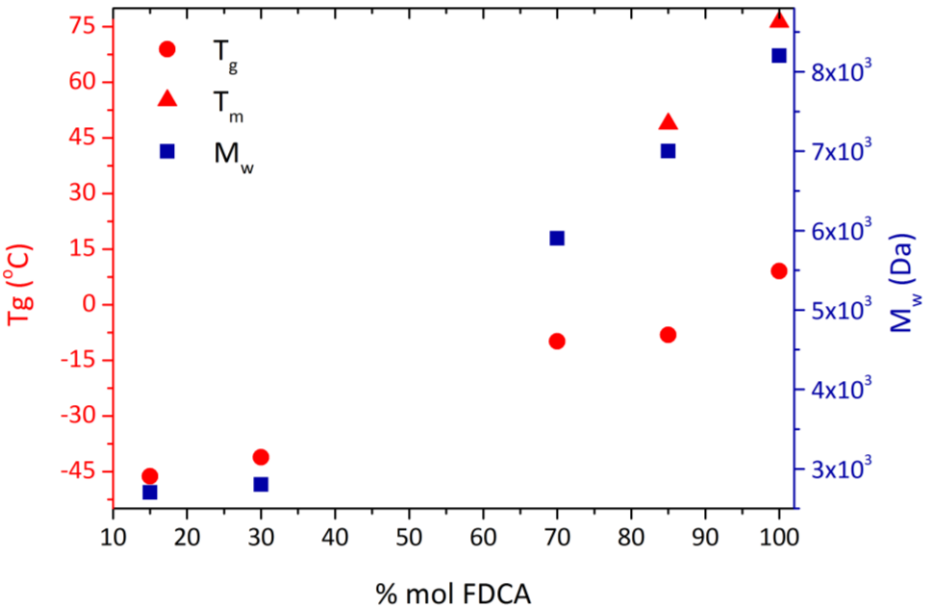

Figure 53. T_g, T_m and M_w as a function of mol% FDCA content.

The glass transition temperatures were also compared in terms of processing method. **Table 26** shows the DSC results for **6a** and **6b** synthesised by azeotropic distillation and application of vacuum during the second stage. As the molecular weight increased, the T_g, slightly increased for both polyesters, going from -46.3 °C to -42.4 °C for $PPeF_{15}S_{85}$ (**6a**) and from -41.0 °C to -34.3 °C for $PPeF_{30}S_{70}$ (**6b**). It is evident that the great chain flexibility of 1,5-pentanediol along with its strong plasticising effect represent a more significant influence on T_g than the molecular weight itself. It is therefore assumed that in order to get certain range of molecular weight, vacuum-driven processing should be chosen over azeotropic distillation, along with enhanced process efficiency. **Figure 54** shows the comparison of both processing methods during the second heating scan.

Table 26. Comparison of T_g of **6a** and **6b** synthesised by vacuum or azeotropic distillation in the second stage

		Vacuum			Azeotropic distillation		
Polyester	**Name**	**M_w, Da**	**T_g, °C**	**T_m, °C**	**M_w, Da**	**T_g, °C**	**T_m, °C**
6a	$PPeF_{15}S_{85}$	8200	-42.4	-	2700	-46.3	-
6b	$PPeF_{30}S_{70}$	7800	-34.3	-	2800	-41.0	-

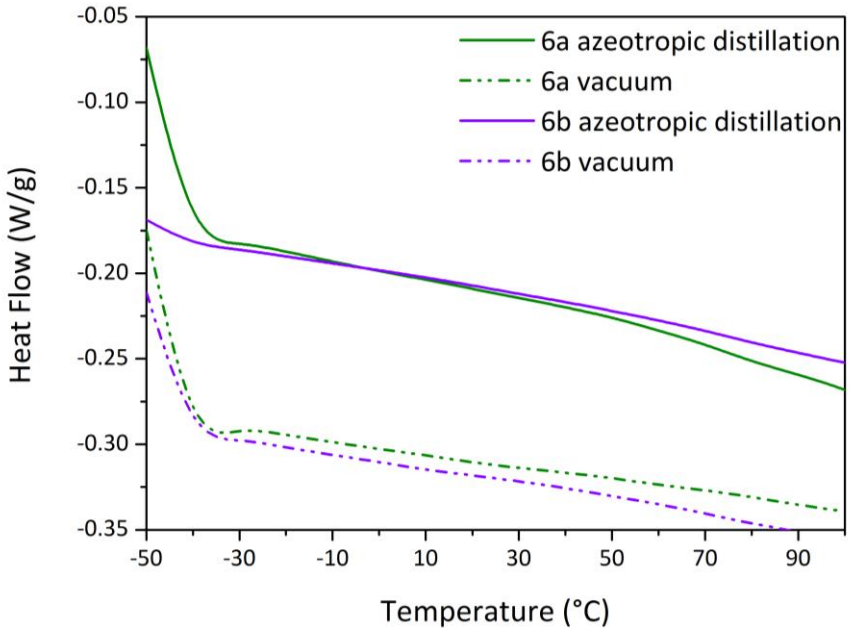

Figure 54. Second heating scan at 10 °C/min for polyesters **6a** ($PPeF_{15}S_{85}$) and **6b** ($PPeF_{30}S_{70}$) synthesised by vacuum and azeotropic distillation.

4.3.4 Thermal gravimetric analysis (TGA)

The thermal stability of the polyesters **4-6** was assessed by TGA. The decomposition temperatures (T_d) of the biomass-derived polyesters are in the range of 360 °C and 403 °C, as summarised in **Table 27**. The thermal stability range is similar to that of the resins with 1,3-propanediol (**Section 3.3.4**) which was found between 380 °C and 400 °C. The weight% and derivative weight% thermograms are shown in **Figure 55** and **Figure 56**, respectively. The remaining thermograms are shown in **Appendix C**.

Neither the molar composition nor the process temperature had a major influence on the decomposition temperature of the polyesters, as they vary randomly throughout the composition range. Among the copolyesters, **6a** presented the highest decomposition temperature -411 °C - while the lowest thermal stability was exhibited by **6c** (378 °C) and the furan polyester **5** (360 °C and 362 °C when synthesised at 210 °C and 220 °C, respectively). The synthesis of **5** at 230 °C gave a T_d at 385 °C which differs by 25 °C to the other processing temperatures. As in the other characterisations methods, this particular synthesis did not align with the other conditions, as it is believed some control issue was encountered during the process.

Table 27. Characteristic decomposition temperatures T_{d1}, T_{dmax} and weight loss % of polyesters **4-6**

Polyester	Mol% FDCA	T process, °C	Thermal Transition 1 T_{d1}, °C	Thermal Transition T_{dmax}, °C	Weight loss % (T_{dmax})
4	-	210	-	402.2	95.6
		220	-	401.4	97.5
		230	-	403.2	97.7
6a	15	210	320.6	411.2	99.7
		220	298.1	399.6	99.9
		230	127.7	398.8	91.1
6b	30	210	293.4	398.5	99.9
		220	140.9	403.4	99.8
		230	-	401.4	90.6
6c	70	210	-	382.7	92.8
		220	-	389.1	97.4
		230	-	378.4	97.4
6d	85	210	316.2	390.1	99.9
		220	104.4	385.3	91.1
		230	129.8	389.6	94.2
5	100	210	-	360.3	99.4
		220	-	362.2	99.9
		230	-	384.6	97.0

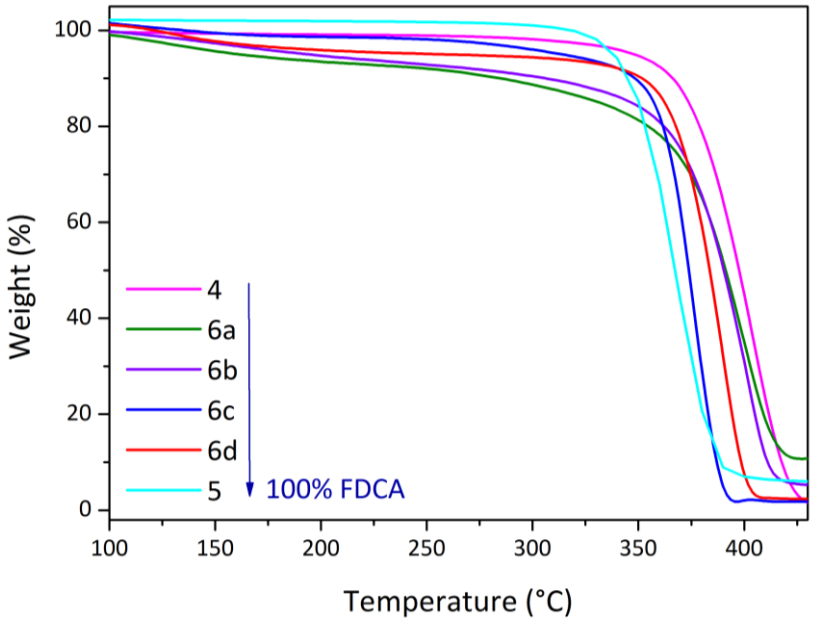

Figure 55. Weight % thermogram of polyesters **4-6** synthesised at 230 °C (N_2 flow, 10 °C/min). The curves have an offset of 0.05.

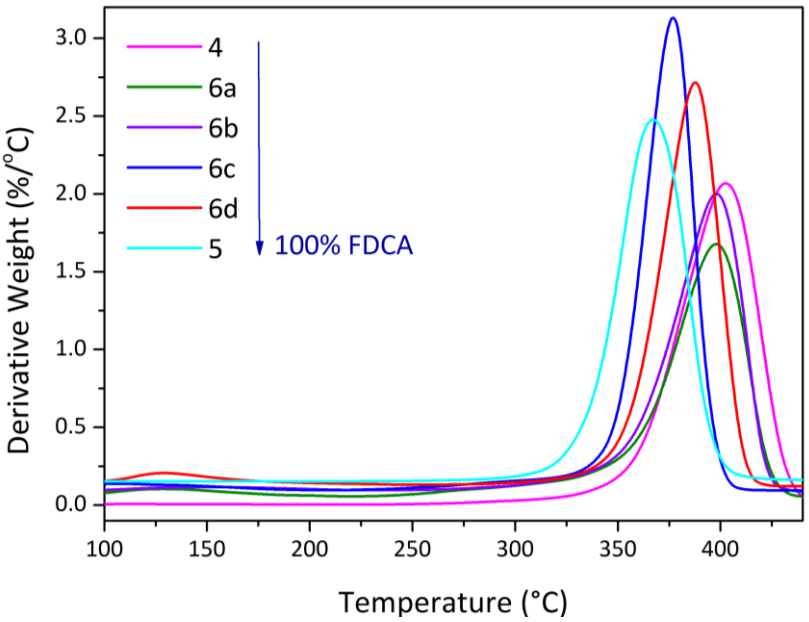

Figure 56. Derivative weight % thermogram of polyesters **4-6** synthesised at 230 °C (N_2 flow, 10 °C/min). The curves have an offset of 0.03.

The polyesters **4**, **5** and **6c** (synthesised at 230 °C) presented only one stage of weight loss between 92.8 and 99.9%, corresponding to the degradation of the ester linkages within the polymeric chain, as defined elsewhere.[78] Polyesters **6a**, **6b** and **6d** on the other hand, show an initial weight loss tentatively ascribed to the degradation of low molecular weight segments that might start to degrade first.

Similar T_d results have been reported for other furanic-aliphatic polyesters and polyfuranoates. The maximum rates of decomposition of polyfuranoates with odd methylene numbers: 5,7 and 9 were reported at 394 °C, 401.12 °C and 396.98 °C, respectively.[81] Jiang, et al.[75] reported thermal decomposition temperatures between 399-407 °C for polyfuranoates prepared from a variety of diols: ethylene glycol, propylene glycol, 1,4-butanediol, 1,6-hexanediol and 1,8-octanediol More recently, the thermal stabilities with several other diols were reported: 1,10-decanediol (402-406 °C), diethylene glycol (413-421 °C) and 2,3-butanediol (360 °C).[278]

In the case of copolyesters of FDCA, Ma, et al.[77] reported thermal stabilities for the copolyesters of FDCA, 1,4-butanediol and ethylene glycol between 326 °C and 341 °C. The copolyesters of FDCA, SA and 1,4-butanediol with different molar ratios presented maximum decomposition temperatures between 394 and 402 °C,[84] whereas FDCA, lactic acid and ethylene glycol copolyesters showed maximum degradation temperatures from 384 °C to

391 °C.[280] Copolyesters of PET and PEF (PET-ran-PEF) in different compositions showed thermal stabilities in the range of 388.8 up to 408.2 °C.[264] Recently, the thermal stability of copolyesters of FDCA, 1,3-propanediol and a fatty acid dimer diol (Pripol) was reported between 383 °C and 390 °C, and the stability increased as the furan content decreased.[281]

4.3.5 Paint testing

Copolyesters **6a**-**6d** and polyester **5** were formulated into the white polyester protocol formulation used at Becker Industrial Coatings Ltd. Their performance was compared against that of a reference resin, which will be stated from now on as **R**. The copolyesters considered were synthesised at 220 °C by the conventional azeotropic distillation during the second stage.

All samples were compatible with the solvent blend used at Becker Industrial Coatings Ltd. **Table 28** summarises the results from the physical testing performed in the resins.

From the physical test results in **Table 28** it is observed that although panels of the finished paints based on the resins are passing MEK rubs, the microhardness and T_g values are not as high as when using the reference resin. In terms of pencil hardness, **6a** and **6b** resulted in very soft paints (2B) whereas **6c** and **6d** (F) are harder although not reaching the specification of H. The pencil hardness is better though than other reported coating systems, where it is in the order of 3H to 4H.[277, 282]

All the coatings show high gloss, which can be clearly seen from the obtained gloss data at 60°.

The data suggests that paints with increased FDCA content lead to better physical properties that are closer to those of the reference resin, particularly in the microhardness and T_g. Still, the effect of FDCA solely did not allow reaching the required specifications. We believe that the inclusion of a trifunctional biobased monomer would increase the hardness and the T_g. This effect is explored in **Chapter 8**.

Comparing directly the effect of the diol between resins **3a** and **3b** with 1,3-propanediol and **6a** and **6b** with 1,5-pentanediol, the former showed enhanced microhardness (36-45 $N \cdot m^{-2}$), T-bend within specification and higher T_g (0.6-12 °C). Rich FDCA compositions however are not possible when using 1,3-propanediol-based resins due to their insolubility in the

solvent system, which limits the threshold of targetable physical properties and prompts us to add another monomer to the system.

Table 28. Physical test results on white paints based on polyesters **5-6** and the reference resin **R**

Test	Specification	R	6a	6b	6c	6d	5
Colour	White	White	White	White	White	White	White
Pencil Hardness	H	H	2B	2B	F	F	B
Gloss Top Coat	30-40 at 60°	35	35	34	33	34	40
Reverse Impact 80'' lb	No cracking	Moderate cracking	No cracking	No cracking	No cracking	No cracking	No cracking
Erichsen 7.5 mm	No cracking	Moderate cracking	No cracking	No cracking	No cracking	No cracking	No cracking
T-Bend NTPO	2T	0.5T	0.5T	0.5T	0T	0T	0T
T-Bend no cracking[a]	3T	3T	1T	1.5T	1.5T	1.5T	1.5T
MEK[b] rubs primer	100	110	110	110	110	110	110
T_g, °C	-	35	-28	-17	6	15	11
Microhardness, $N \cdot m^{-2}$	-	216	11	12	20	21	17

[a]: Cracking is detected by removal of a pressure-sensitive tape placed on the bend edges and observing the degree of removed coating particles. [b]: Methyl ethyl ketone

Despite the fact that copolyesters **6** had higher molecular weights than the resins prepared with 1,3-propanediol, their physical properties below the specifications might relate to the known plasticiser effect inherent to 1,5-pentanediol.[283, 284] Future work relies then on combining 1,5-pentanediol with a short-chain diol along with a trifunctional polyol as mentioned above to tackle the desired mechanical properties.

4.4 Conclusions

The synthesis of biomass-derived polyesters and copolyesters based on 2,5-furan dicarboxylic acid (FDCA), succinic acid (SA) and 1,5-pentanediol (PTO) was successfully

performed via a two-step process: polyesterification and polycondensation. For the first time, these three bioderived monomers have been polyesterified to produce polyesters with tuneable properties depending on the monomer ratio, processing temperature and processing methodology, providing a library of potential biomass-derived coating formulations.

The obtained polyesters were characterised by ^{1}H NMR, GPC, DSC, TGA, and paint testing.

^{1}H NMR confirmed the structure of the polyesters with chemical shifts resembling those at the literature for FDCA (7.20 ppm), SA (2.64 ppm) and the protons next to the FDCA ester (4.35 ppm) and SA ester (4.09 ppm) bonds. GPC analysis showed that the range of M_w of the polyesters was between 2200 to 10700 Da, with M_n within 1200 and 4100 Da, which are in the suitable molecular weight range for coatings. M_w seemed to increase with the processing temperature, and in the case of copolyesters of FDCA and SA, the molecular weight kept a strong dependence with the furanic content, since it increased as the mol% FDCA increased.

When the syntheses of copolyesters with 15% (Polyester **6a**) and 30 mol% FDCA (**6b**) were performed with application of vacuum during the polycondensation stage, the M_w increased from 2700 to 8200 Da and 2800 to 7800 Da, respectively, which represents an increase of more than 100% in the molecular weight. M_n increased from 1400 Da to 4100 and 4000 for **6a** and **6b**, respectively, with dispersities between 1.96 and 2.04, which are expected for polyesters. The data suggests that vacuum satisfactorily drove the reaction further than azeotropic distillation as diol and water were efficiently released. Future work includes therefore the synthesis of the remaining compositions to complete the vacuum-synthesised library of biomass-derived polyesters.

Thermal analysis showed that the glass transition temperature of the polyesters was found between –48 °C to 9 °C, and it varied as a function of the effect of the FDCA content, which directly influenced the molecular weight of the polyesters. The results for the polysuccinate (**4**) pure furan polyester **5** and the copolyester with 85 mol% (**6d)** suggest they have a semicrystalline nature, displaying melting endotherms (T_m) at 36.0 °C-76.3 °C. None of these polyesters exhibited either melt crystallisation or cold crystallisation temperature (T_{cc}).

The dependence of the glass-transition temperature on the composition of copolyesters **6** was evaluated in terms of comonomer unit incorporation, and it was observed how the T_g raised as the molar content of FDCA increased. For example, the succinic acid-rich polyesters, **6a (**15 mol% FDCA) and **6b** (30% mol FDCA) displayed T_g at -49 °C and -41 °C, respectively; whereas the furan rich-resins **6c** and **6d**, with 70 and 85 mol% FDCA showed a T_g in the range of 12.6 °C to -9.9 °C and -9.5 °C to 0.6 °C, respectively. It was then expected that the furan polyester **5** had the highest T_g among all the polyesters, found in the range of 5.7 and 9 °C.

TGA analysis proved that the decomposition temperature (T_d) of the polyesters was found between 360 °C and 403 °C. The polyesters **4** (100 mol% SA), **5** (100 mol% FDCA), and **6c** (70 mol% FDCA) decomposed in a single step corresponding to the ester linkages, whereas **6a** (15 mol% FDCA), **6b** (30 mol% FDCA), and **6d** (85 mol% FDCA) showed two thermal transitions, most likely corresponding to water or small volatile molecules and the actual polymer. Surprisingly, when the syntheses of **6a** and **6b** were performed at 230 °C, the first decomposition step was found around 127 and 129 °C, while the polyesters synthesised at 210 and 220 °C were thermally stable above 300 °C. The process temperature thus had some influence in the first decomposition temperature of these polyesters. Nevertheless, it did not play a fundamental role in the main decomposition temperature throughout all the polyesters' composition range.

The paint testing demonstrated that although panels of the finished paints based on the resins are passing MEK rubs, the microhardness and T_g values are not as high as when using the reference resin. In terms of pencil hardness, **6a** and **6b** resulted in very soft paints (2B) whereas **6c** and **6d** (F) are harder although not reaching the specification (H). The data suggests that paints with increased FDCA content lead to better physical properties that are closer to those of the reference resin, particularly in the microhardness and T_g. Still, the effect of FDCA solely did not allow reaching the required specifications. The inclusion of a trifunctional biobased monomer would increase the hardness and the T_g and therefore the overall performance of the coating.

This chapter highlighted the use of 1,5-pentanediol as one of the main building blocks in the synthesis of polyesters. The research on biomass pathways to obtain 1,5-pentanediol is expanding very quickly and its use in polymers is steadily taking importance. Still, the

industrial implementation and competitiveness of these pathways relies on achieving biomass conversion with high efficiency, along with minimisation of the waste generated.

It could be interesting to investigate the differences between 1,5-pentanediol, 1,4-butanediol and 1,6-hexanediol to produce polyester coatings with tuneable properties in combination with other biomass-derived monomers. Recent, promising research has shown that the biomass-derived production of 1,5-pentanediol has the economic and technical potential to become a key oxygenated chemical within the biorefinery.

CHAPTER 5

Kinetic Modelling of the Polyesterification of Biomass-derived Renewable Polyesters

5. Kinetic Modelling of the Polyesterification of Biomass-derived Renewable Polyesters

In this chapter, the kinetic modelling and estimation of kinetic parameters are presented for the 1,3-propanediol (Polyesters **1-3**) and 1,5-pentanediol (**4-6**) resins by fitting different polyesterification models to the experimental data generated from the batch polymerisation reactors described in **Chapter 2**. The analysis is focused on the effect of temperature and the molar ratio of the diacids. Each model enables the estimation of different parameters, some of which will be used in the process simulation and multiobjective optimisation presented in **Chapters 6** and **7**. The work presented herein corresponding to 1,3-propanediol-based polyesters has already been published.[87]

5.1 Introduction

Despite the continuous growth of polyesters derived from biomass, the kinetic data and modelling for the polyesterification of biomass-derived polyesters are still scarce. In the 1930s, Flory[188] established the foundations of polyesterification or step-growth polymerisation kinetics through the study of a system of ethylene glycol and adipic acid. More than 30 years later, Szabó-Réthy[285] corrected Flory's theory by proposing kinetic rate equations that considered the water released during the polycondensation. The author found that the rate constant calculated by Flory's equations is actually constant only for second order reactions; at higher orders, it depends on the degree of polycondensation. In fact, neglecting the condensation water led to an error between 15-20% for second order reactions; in third order reactions, it rises up to 25–35 % as the reaction proceeds.[285]

Throughout the years, several authors have proposed different reactor and kinetic models for a variety of systems, such as the widely used PET,[286-289] maleic anhydride and 1,2-propanediol,[290-292] or using phthalic anhydride instead of the diacid.[293, 294] Work in the field includes as well the polyesterification of adipic acid with either 1,3-butanediol[295] or propylene glycol;[296] 1,3-propanediol and terephthalic acid[222, 297] and 2-methyl 1,3-propanediol with maleic and phthalic anhydrides and isophthalic acid.[294] The kinetics of a succinic acid-derivative, cinnamyl succinic acid with 1,4-tetramethylene glycol in both equimolar and non-equimolar ratios were investigated with and without catalyst.[298] Fradet and Maréchal[299] compiled a comprehensive review of general polyesterification models, which includes a great compendium of solvents, monomers and reaction conditions, as well

as the main methodologies found in polyesterification kinetic studies. The foundations of the kinetic modelling of the step-growth polymerisation of multifunctional monomers were stablished since the 1960s, with the statistic theory of branching processes based on cascade substitution proposed by Gordon,[300] although the technique is complex and difficult to apply to real systems. Later on, several authors extended the simulation of polymer networks, by using Monte Carlo methods[301] or developing models for intramolecular reactions.[302, 303]

The simulation and modelling of the synthesis of PET has been the subject of substantial and meaningful research, leading to well-defined kinetic schemes and reactor design.[287] Ravindranath, et al.[304] reviewed the thermodynamic and transport data, and the mechanisms in PET synthesis, which include main and side reactions. Modelling side reactions is fundamental as product quality is governed by the formation of certain by-products, such as acetaldehyde and diethylene glycol (DEG).[304] Undesired flavour in PET bottles could be produced by acetaldehyde,[305] while DEG decreases the melting point[306] and thermal stability.[307] Discolouration is also a major problem for white polyester goods which is a result of the formation of polyvinyl esters.[307] Careful modelling should therefore minimise their rate of production. Moreover, studies on reactor design for the production of PET includes simulation in semibatch,[287, 288] continuous[308-310] and wiped film reactors,[220] the latter used in the final polymerisation stages to increase the surface area and reduce the resistance to diffusion.[181]

Little work however has been recently done for full biomass-derived polyesterifications. Bikiaris, et al.[311, 312] reported the mathematical modelling of succinic acid-based polyesters, by treating separately the polyesterification and polycondensation reaction stages. Other kinetic works have specifically focused on modelling poly(1,4-butylene succinate) (PBS), either catalysed by monobutyl tin oxide[313] or titanium butoxide.[314] Hu, et al.[315] developed a kinetic model for the synthesis of copolyesters of 1,4-butanediol, succinic acid and terephthalic acid.

Regarding FDCA-based polyesters, the pseudo first-order reaction polymerisation of ethylene glycol and 1,4-butanediol with FDCA was studied by Ma, et al.[77] Wilsens, et al.[316] reported the kinetic coefficient *k* for the polymerisation of FDCA-based bis(2-oxazoline) and sebacic acid. Finally, our group reported the kinetic modelling of fully biomass-derived polyesters based on 1,3-propanediol, succinic acid and FDCA.[87] To the best of our knowledge, no further work has been published in the field.

An excellent source on the integration of modelling step-growth polymerisation and product design toward an optimised polymer manufacturing process was published by Seavey and Liu.[192] This reference provides an insightful study of the step-grow polymerisation process, and represents a cornerstone in the area towards an integrated work of the fundamentals of polymerisation processes: Reaction kinetics, transport phenomena, phase behaviour and polymer end-properties.

5.2 Kinetic Models for Polyesterification Reactions

5.2.1 Model 1: Flory-derived Model

Starting from Flory's fundamental theory,[188] the overall kinetic rate of the uncatalysed polyesterification reaction can be estimated through the calculation of the concentration of the carboxylic acid groups present. The main assumption is that the overall rate coefficient *k* is independent of molecular size and change length.[177] The reaction rate is thus defined as the decay of COOH groups' concentration *C* with respect to time:

$$r = -\frac{d[C]}{dt} \tag{25}$$

Flory established that the self-catalysed polyesterification rate is second order in respect to the acid and first order for the diol.[188] The model assumes as well that the water produced is immediately removed and that the reverse hydrolysis reaction is negligible. Equation 25 then becomes

$$-\frac{d[C]}{dt} = k[C]^2[OH] \tag{26}$$

Where *[OH]* is the hydroxyl group concentration.

Assuming stoichiometric amounts of diol and diacid ([COOH]=[OH]) and also equal rate of consumption of hydroxyl groups, the rate expression becomes

$$-\frac{d[C]}{dt} = k[C]^3 \tag{27}$$

Integration of the differential equation leads to the mathematical expression below

$$\frac{1}{[C]^2} = \frac{1}{[C_o]^2} + 2kt \tag{28}$$

Equation 28 particularly refers to a third-order reaction. Post-Flory studies however showed that the order of a catalysed or self-catalysed reaction varies during the polymerisation with changes in the reaction medium.[285] Thus, a general equation from the literature was chosen for a two monomer system, equal reactivity of the reactants and the n^{th} reaction order[285]

$$(n-1)k_n t = \frac{1}{[C]^{n-1}} - \frac{1}{[C_o]^{n-1}} \tag{29}$$

Where C_o is the concentration of carboxylic acid groups at time t=0; C is the concentration of carboxylic acid groups at time t and k_n is the kinetic coefficient of the n^{th} order reaction. This equation can be expressed in terms of the degree of reaction (p) or the degree of polycondensation ($1/1-p$), which were defined by Flory[188] and Szabó-Réthy,[285] respectively, as equations 30 and 31

$$p = \frac{[C_o] - [C]}{[C_o]} \tag{30}$$

$$\frac{1}{1-p} = \frac{[C_o]}{[C]} \tag{31}$$

By substituting equation 30 into equation 29, the final expression is derived

$$(n-1)k_n t = \frac{1}{([C_o] \cdot (1-p))^{n-1}} - \frac{1}{[C_o]^{n-1}} = \frac{1}{(C)^{n-1}} - \frac{1}{[C_o]^{n-1}} \tag{32}$$

5.2.2 Model 2: Non-Stoichiometric Model

Model 2 is a modification of the power-law type Model 1 as it takes into account the deviations from a stoichiometric diol:diacid ratio and changes in the reaction mixture because of the loss of water. The importance of considering the water released has been previously pinpointed by other authors, as it is fundamental to obtain reliable and robust kinetic data.[317] Model 2 therefore should represent a closer representation of the actual systems considered, providing model parameters that can better predict the behaviour of polyesterification processes.

Most of the initial reaction mixtures contain an excess of diol. The elimination of the condensate varies the concentration of the diol in the course of the reaction and consequently

decreases the mass of the reaction mixture. Szabó-Réthy[285] modified Flory's kinetic equations so that the water released during the process was considered. The author started by establishing a relationship between the carboxylic acid concentration *C* and the average molecular weight of the polycondensate *M* assuming a non-solvent polycondensation

$$\frac{1}{C} = \frac{M}{1000} \tag{33}$$

C is expressed in terms of mole of carboxylic acid per 1000 g. Hence, C_o is determined by the molecular weights of the dicarboxylic acid and the diol (M_a and M_d)

$$\frac{1}{C_o} = \frac{M_a + M_d}{2 \times 1000} \tag{34}$$

The degree of polycondensation is calculated from the following equation

$$\frac{1}{1-p} = \frac{(M-18)}{M_{segment}} \tag{35}$$

Where $M_{segment}$ is the mean molecular weight of the repeating segment, calculated as

$$M_{segment} = \frac{M_a + M_d}{2} - 18 \tag{36}$$

Plugging equation 36 into equation 35

$$\frac{1}{1-p} = \frac{(M-18)}{\frac{M_a + M_d}{2} - 18} \tag{37}$$

Recalling equations 33 and 34 for 1/C and $1/C_o$, equation 37 is rewritten as

$$\frac{1}{1-p} = \frac{\frac{1}{C} - 0.018}{\frac{1}{C_o} - 0.018} \tag{38}$$

Equation 38 is rewritten for 1/C

$$\frac{1}{C} = \left[\frac{1}{C_o} - 0.018\right]\frac{1}{1-p} + 0.018 \tag{39}$$

Substituting the value of 1/C from equation 39 into the general kinetic equation 32 gives the corrected kinetic equation for the n^{th} order reaction[285]

$$(n-1)C_o^{n-1}k_n t = \left[\frac{1}{1-p}\cdot(1-0.018\cdot C_o)+0.018\cdot C_o\right]^{n-1}-1 \quad (40)$$

The process was non-stoichiometric since an excess of diol concentration is needed in order to achieve solubilisation of the monomers and further processability. The model follows the kinetic equation originally reported by Fradet and Maréchal[299] for self-catalysed, non-equimolar polyesterifications, which is based upon Szabó-Réthy's correction.

The development of this rate expression starts by defining the hydroxyl concentration of diol throughout the reaction

$$[OH] = [C] + b_0 \quad (41)$$

Where b_0 is the initial excess of the hydroxyl group concentration at the beginning of the reaction. Let m_o and m be the weight of the reaction mixture at times 0 and t, respectively and m_{H2O} the weight of water released at time t

$$m = m_o - m_{H_2O} \quad (42)$$

Since the number of moles (N_o and N), concentration (C_o and C) and mass (m and m_o) at times 0 and t are related by equations 43 and 44

$$N_o = C_o \cdot m_o \quad (43)$$

$$N = C \cdot m \quad (44)$$

The following equations can be derived

$$m_{H_2O} = 0.018(N_o - N) \quad (45)$$

$$m_{H_2O} = 0.018(C_o \cdot m_o - C \cdot m) \quad (46)$$

$$m = m_o - 0.018(C_o \cdot m_o - C \cdot m) \quad (47)$$

$$m = m_o - 0.018(C_o \cdot m_o - C \cdot m) \quad (48)$$

Rearranging for the mass m, equation 49 is derived

$$m = m_o\left[\frac{1-0.018C_o}{1-0.018C}\right] \quad (49)$$

When water is released, the weight of the reaction medium decreases, and the excess of the hydroxyl group concentration increases since the number of excess hydroxyl groups does not change[299]

$$b_o \cdot m_o = b \cdot m \tag{50}$$

where *b* is the excess of hydroxyl group concentration at time *t*. Plugging 49 into 50 in terms of *b* leads to the following expression[299]

$$b = b_o \cdot \left[\frac{1 - 0.018C}{1 - 0.018C_o}\right] \tag{51}$$

This definition is then plugged into the power-law equation 26, so the non-stoichiometric reaction rate becomes[299]

$$-\frac{d[C]}{dt} = -k[C]^m \cdot \left[C + b_0\left(\frac{1 - 0.018C}{1 - 0.018C_o}\right)\right]^n \tag{52}$$

Where *k* is the reaction rate coefficient, *m* is the reaction order with respect to the acid, and *n* is the reaction order with respect to the diol. The factor of 0.018 accounts for the water released, as previously described in the Szabó-Réthy correction.

The parameter *k* estimated with this model is used in **Chapters 6** and **7** for the simulation and optimisation of the polyesterification reaction.

5.2.3 Model 3: Chen and Wu Model

The model relies on the assumption that changes in the dielectric constant of the polymerisation medium during polymerisation influenced the probability of ion-pair formation, which the authors defined as the first-step of self-catalysed polyesterification mechanism. This probability of ion-pair formation goes up with decreasing dielectric constant of the medium. The model also assumes that all the water is not removed from the reaction mixture and therefore the hydrolysis of the ester should be taken into account. The reaction mechanism proposed by the authors is shown in **Scheme 39**.

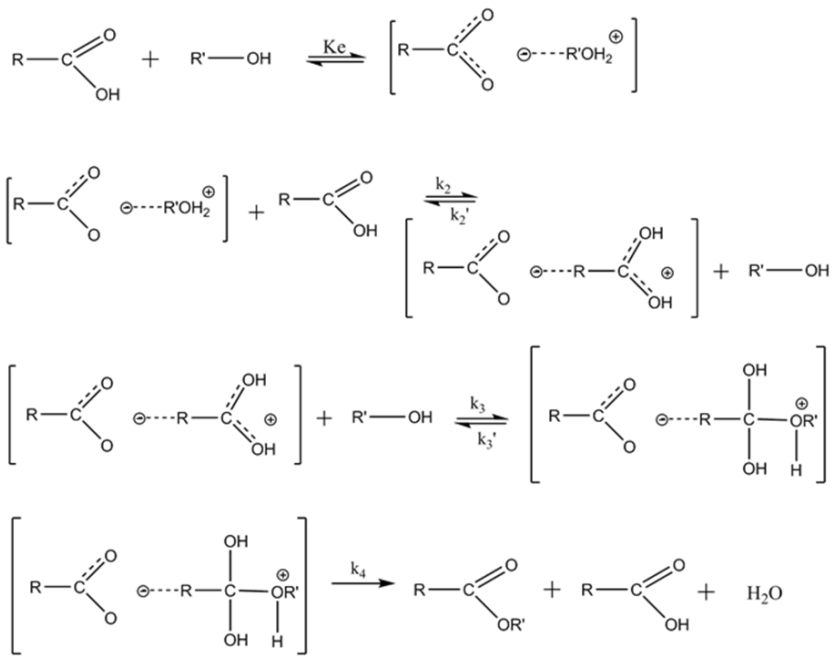

Scheme 39. Mechanism of self-catalysed reactions, adapted from Chen and Wu.[318]

Nalampang and Johnson[294] reported a modified ordinary differential equation upon the original model published by Chen and Wu[318] for the modelling of the uncatalysed reaction between maleic anhydride, phthalic anhydride and 2-methyl-1,3-propanediol, which is defined as equation 53

$$-\frac{dP}{dt} = kK_{e0}e^{\alpha P}C_0^2(1-P)^2(r-P) - k_h[H_2O]P \tag{53}$$

Where k is the polyesterification rate coefficient (kg·mol^{-1}·min^{-1}); k_h is the rate constant hydrolysis of ester bonds (kg·mol^{-1}·min^{-1}); r is the initial diol:diacid molar ratio ([OH]$_o$/[COOH]$_o$; K_{e0} is the equilibrium ionisation constant at zero conversion (P) (kg·mol^{-1}) and the term $exp(\alpha P)$ accounts for the increase in K_{e0} with the decrease of the electric constant with increasing P. In the original work, the authors gave a value for α of 0.61 for self-catalysed polymerisations based on Chen and Wu's work with fitted parameter α ranging from 0.23 to 0.61 depending on the reaction conditions. In the present case, this term will be fitted along with the rate and equilibrium ionisation coefficients.

5.3 Modelling and Parameter Estimation

The adjustable parameters of Models 1-3 in **Section 5.2** were estimated by fitting the kinetic models to experimental acid conversion-time data over the entire conversion range

under the different reaction conditions specified in **Chapters 3** and **4** for polyesters **1-3** and **4-6**, respectively. Samples were taken every half an hour throughout the entire reaction time and titrated according to the methodology for the determination of the acid value described in **Section 2.8.1**. The acid-conversion data for the different syntheses are available in **Appendix D**.

Figure 57 depicts the algorithm used to solve the ordinary differential equations (ODE) referred to each of the reaction rate laws, whereas **Figure 58** describes the estimation of the kinetic parameters of Model 2 by fitting the data through a non –linear square minimisation of the objective function *Z.* Matlab was used for the modelling and parameter estimation. The minimisation and fitting of data was done with the *fminunc* routine, which is a nonlinear programming solver which attempts to find a local minimum of a described function.[319] The ODE system is solved via the Runge-Kutta or any multistep method with either the *ode45* or *ode15s* Matlab functions, respectively. A general Matlab code for the fitting and solution of the ODE using Model 2 is available in **Appendix D.**

The objective function is expressed as equation 54:

$$\min_{yp} Z = \sum_{i=1}^{Np} \left(C_i - C_{i(p)}\right)^2 \tag{54}$$

$$Z = (Z, t, y, y_p, u) \tag{55}$$

$$y = \left[C_j\right]; j = PPS, PPeS, PPFS, PPeFS, PPF, PPeF \tag{56}$$

$$y_p = [k, m, n, kK_{eo}, k_h[H_2O], \alpha, k_o, K, E_a] \tag{57}$$

Where Z is the sum over all N_p data points of the squared difference between the model predictions $C_{i(p)}$ and the measurement C_i; being i each carboxylic acid concentration point throughout the reaction time for every polyester analysed. Moreover, y refers to the state variables (carboxylic acid concentration during polyesterification); u is the vector of manipulated variables (Temperature and molar ratio) and y_p is the set of kinetic parameters to be estimated, corresponding to Models 1-3. The parameters for the considered models are defined as follows: k, kinetic coefficient; m, reaction order in respect to the acid; n, reaction order in respect to the diol; kK_{eo}, equilibrium ionisation constant at zero fractional conversion; $k_h[H_2O]$, rate coefficient for the hydrolysis of ester bond; α, empirical exponent;

k_o, preexponential factor; K, equilibrium constant and E_a, activation energy. The fitting for each polyester was done separately.

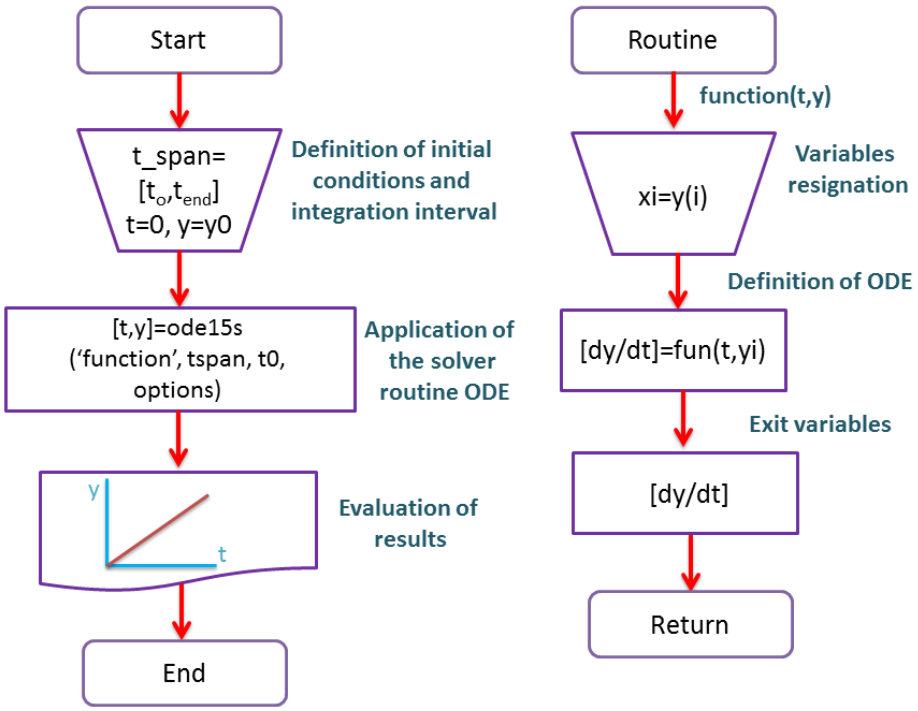

Figure 57. Algorithm for the solution of an ordinary differential equation (ODE) with the *ode15s* solver in Matlab.

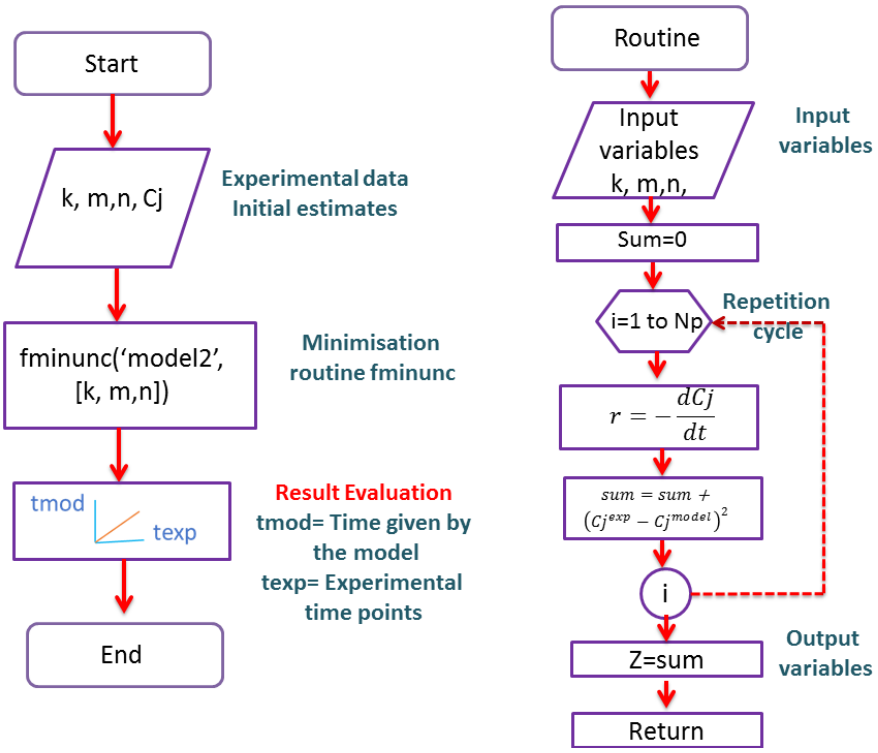

Figure 58. Algorithm for the implementation of a non-linear square minimisation in Matlab using the *fminunc* routine.

5.4 Results and discussion

The following sections describe the effect of the temperature and diacid ratio during the kinetics of polyesterification, as described by Models 2 and 3. Model 1 was only used as a baseline towards Model 2 because of its simplicity and therefore is not included in the results. The applicability of each model was assessed by the numerical value of the Z function in equation 52, with the lowest Z value resulting in the most satisfactory fitting.

5.4.1 Influence of temperature

The influence of the temperature and composition is analysed by using Models 2-3. The polyesters bearing one acid only were first studied. **Figure 59** shows Model 2 fitted to the conversion of carboxylic acid groups (COOH) during the polymerisation of PPS (**1**) and PPF (**2**). In the case of PPF, both higher conversion (P) and higher initial rates were achieved as the process temperature was increased. At 230 °C, the conversion of PPF reached approximately 80% after the first hour of reaction, while it took 3 hours to achieve the same conversion at lower temperatures. After 330 minutes of reaction, the conversion reached 96% at 230 °C and 94% at 210 °C. Interestingly, the PPS polyesters exhibited an almost opposite response to temperature compared to their furan counterparts. The highest conversions of 98 and 97% were achieved at 210 °C and 220 °C, respectively, with no significant difference in the kinetic plots between the two process temperatures. At 230 °C, the rate of reaction was significantly lower and the final conversion was only 94%.

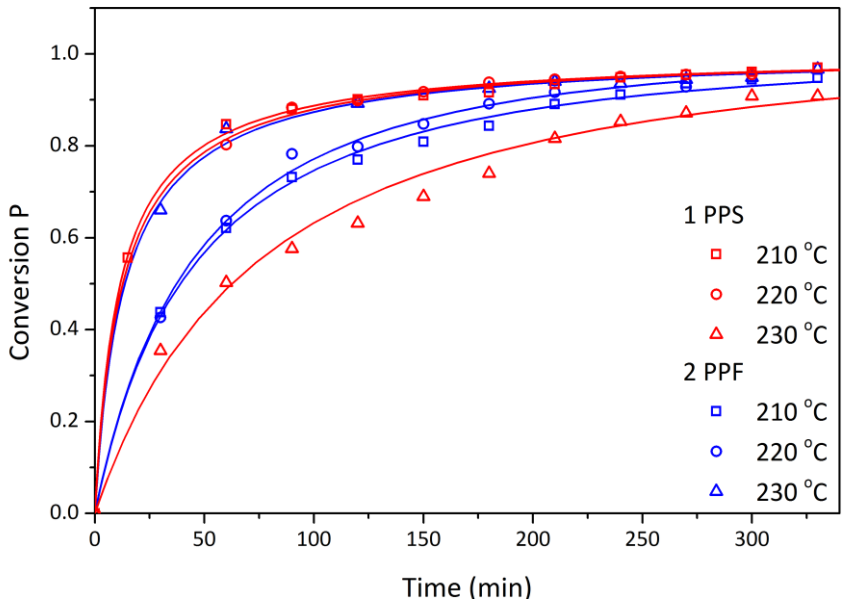

Figure 59. Conversion of COOH groups versus time during the polymerisation of PPS (**1**) and PPF (**2**) at different temperatures fitted to Model 2. Symbols: experimental data.

It is believed that these drops in the kinetic rate and conversion observed at 230 °C could be attributed to the proximity of the boiling point of succinic acid at 235 °C, creating a competition between esterification and evaporation/refluxing. Indeed, some crystallisation of succinic acid was observed on the glass walls of the reactor during the first trials, which supports this hypothesis.

In the case of 1,5-pentanediol polyesters, PPeS (**4**) and PPeF (**5**), **Figure 60** shows the conversion-time plot for polyester **4**. The model was satisfactorily fitted throughout the entire reaction time, with some outlier points between 120 and 150 minutes, possibly being due to the change in equipment during the configuration setup to azeotropic distillation, when the addition of xylene translates into a temperature drop for few minutes until the system reaches the set point again. As with polyester PPF (**2**), the conversion increases with temperature.

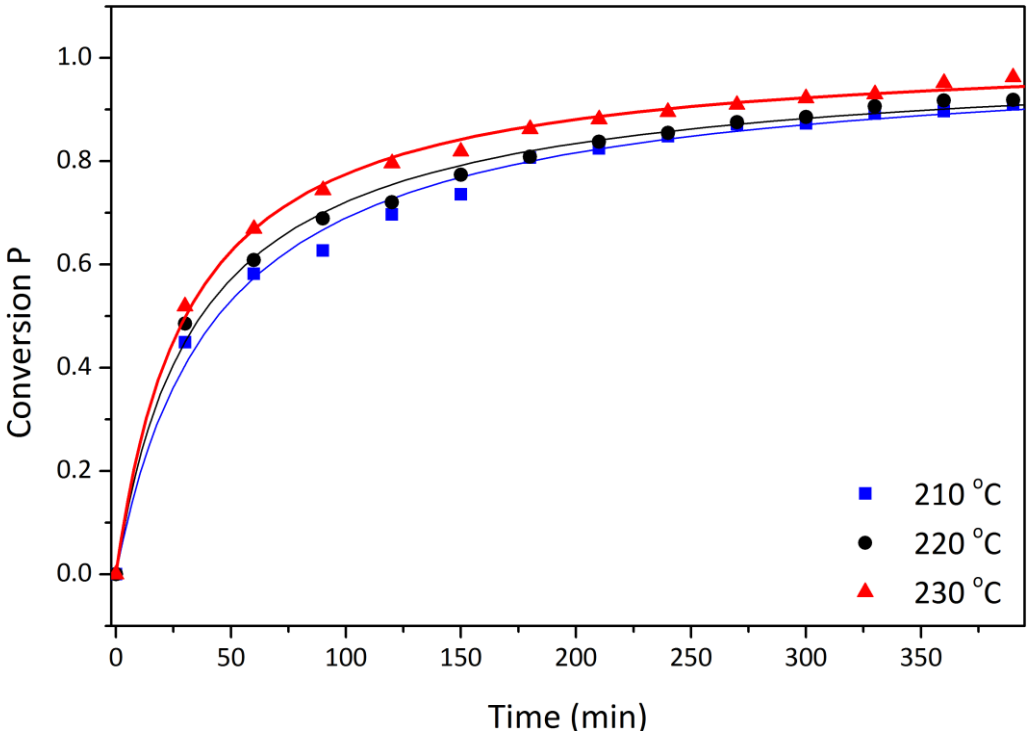

Figure 60. Conversion of COOH groups versus time during the polymerisation of PPeS (**4**) at different temperatures fitted to Model 2. Symbols: experimental data, lines, model estimations.

Regarding PPeF (**5**), a set of experimental data is temperature-off trend, as it is observed in **Figure 61**. At 210 °C, the expected effect of temperature is kept up to 80% conversion as the conversion is lower than those at 220 and 230 °C but actually goes higher by the final stages of the reaction. Besides, the model is not fitted well to the data, as it can be seen that the experimental curve does not follow the same trend as the other syntheses. This

inaccuracy is thought to be merely experimental error, probably given by differences on reaching the clear point, resulting in variations while taking samples. Temperature control issues could also be a possibility as the high viscosity of the furan systems led to considerable delays in reaching the clear point, probably enhanced by the low processing temperature at 210 °C. Another possible phenomena leading to this result could be molecular diffusion in melt polycondensation. The volatile products which diffuse out of the polymer are the diol and water. However, when many simultaneous reversible reactions result due to the interaction of the diffusing species, it becomes very difficult to take any reliable and meaningful measurements. This implies that a total analysis of the reaction-diffusion problem is needed for deducing the diffusivity values [304] which fell out of the scope of the study.

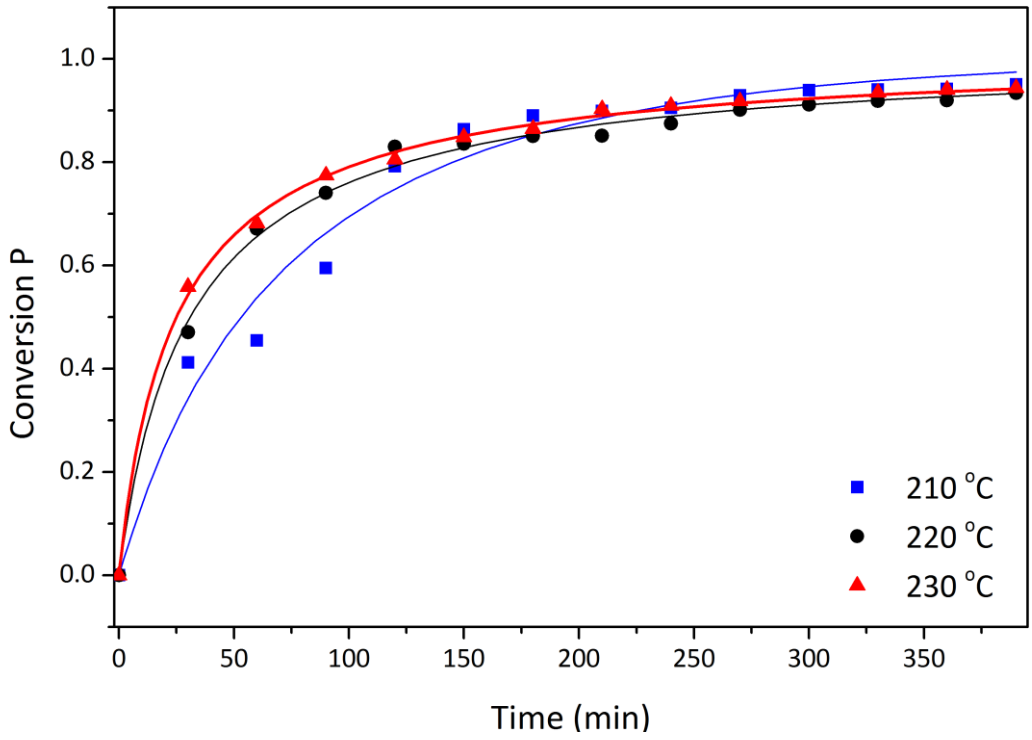

Figure 61. Conversion of COOH groups versus time during the polymerisation of PPeF (**5**) at different temperatures fitted to Model 2. Symbols: experimental data, lines, model estimations.

When comparing the polymerisations of both succinic acid and FDCA (**Figure 59**), it was found that the polymerisation of PPF at 230 °C had a similar rate to succinic acid polymerised at 210 or 220 °C. This demonstrates that FDCA requires more energy than succinic acid to achieve similar results, which is confirmed by the estimation of activation energies and the results of the multiobjective optimisation in **Chapters 6** and **7**. An important outcome of the modelling study is therefore in terms of the optimum polyesterification

temperatures; for polyesters containing both FDCA and succinic acid, the temperatures are between 10-20 °C higher than for polyesters bearing succinic acid and diol units.

While increasing temperature is beneficial for the polymerisations containing FDCA it can promote side reactions leading to colouring and appears detrimental to polysuccinates polymerisations In the present study, no side reactions were considered because the only experimental data acquired referred to the carboxylic acid, diol and water concentration throughout the reaction time. The inclusion of side products formation in modelling leads to more accurate systems, as their rate of formation depends on the operation conditions and therefore could be minimised to promote a better product quality. [304]

Polymerisations with compositions containing both bioderived acids were also studied. **Figure 62** and **Figure 63** show the influence of temperature by fitting Model 2 to the data of $PPF_{15}PS_{85}$ (**3a**) and $PPF_{30}PS_{70}$ (**3b**), respectively.

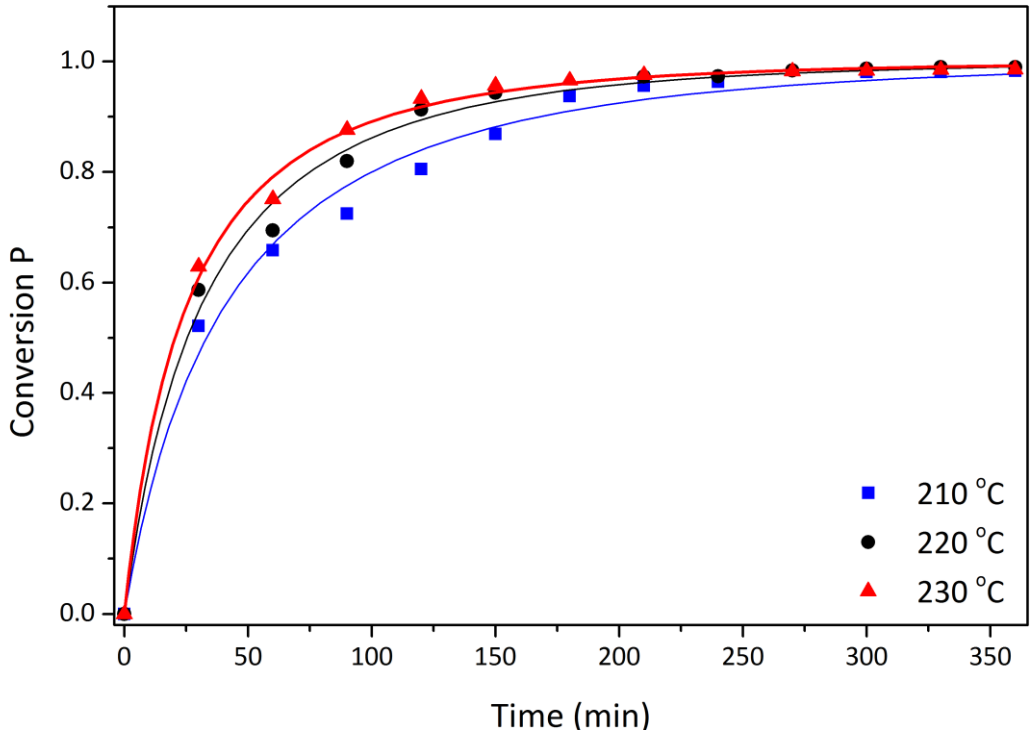

Figure 62. Conversion of COOH groups versus time during the polymerisation of $PPF_{15}PS_{85}$ (**3a**) at different temperatures fitted to Model 2. Symbols: experimental data; lines, model estimations.

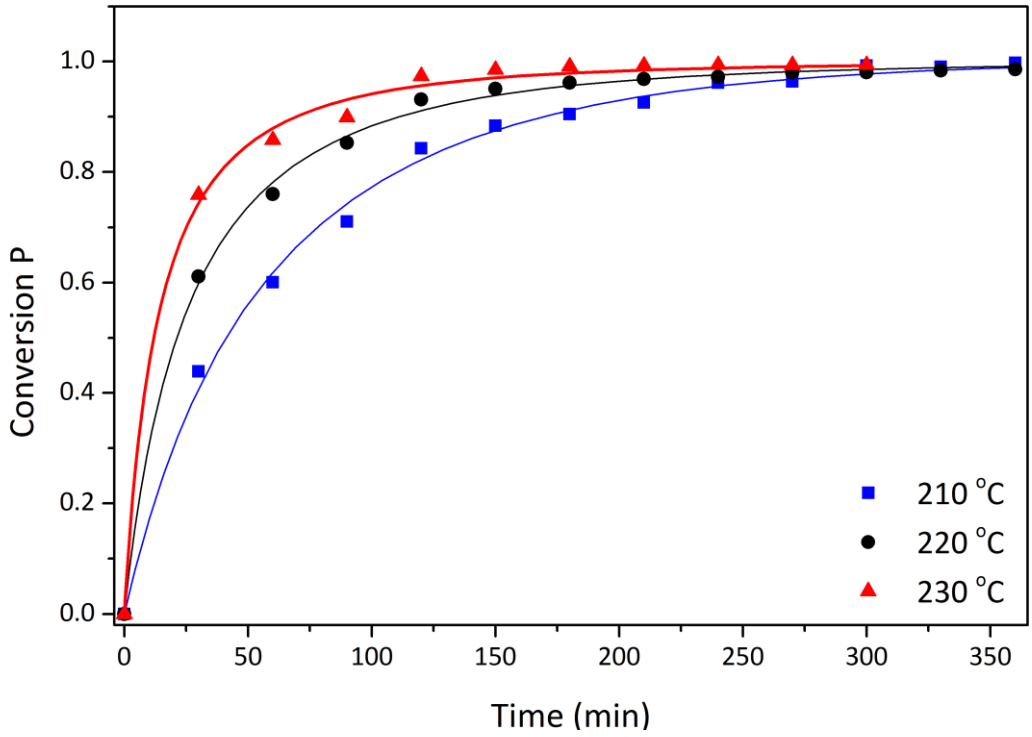

Figure 63. Conversion of COOH groups versus time during the polymerisation of $PPF_{30}PS_{70}$ (**3b**) at different temperatures fitted to Model 2. Symbols: experimental data; lines, model estimations.

The conversion plots with Model 3 are shown in **Figure 64** and **Figure 65** for $PPF_{70}PS_{30}$ (**3c**) and $PPF_{85}PS_{15}$ (**3d**), respectively. The conversion plots of Model 2 with **3c** and **3d** and Model 3 with **3a** and **3b** are available in **Appendix D**.

It was found that for all copolyesters increasing process temperature resulted in both an increase in the rate of polymerisation and in the final conversion. The extent to which the change in temperature affected these variables was not consistent through all compositions. **Figure 62** shows that the rate and final conversions of $PPF_{15}PS_{85}$ at 220 and 230 °C are close while for $PPF_{70}PS_{30}$ the polymerisations at 210 and 220 °C have similar rates and the largest change occurs between 220 and 230 °C, as shown in **Figure 64.** The largest influence of temperature happens during the first 2.5 hours (150 minutes) of reaction, as the conversion is already 95% at 230 °C but is slightly above 80% at 210 °C, as observed in **Figure 63**.

The data suggests that Model 3 is better fitted at higher temperatures. Considering **Figure 64** and **Figure 65**, the model does not perfectly fit the data at 210 °C from 150 minutes of reaction time and onwards. It considerably improves however for the synthesis at 220 °C, finally giving an overall satisfactory fitting at 230 °C.

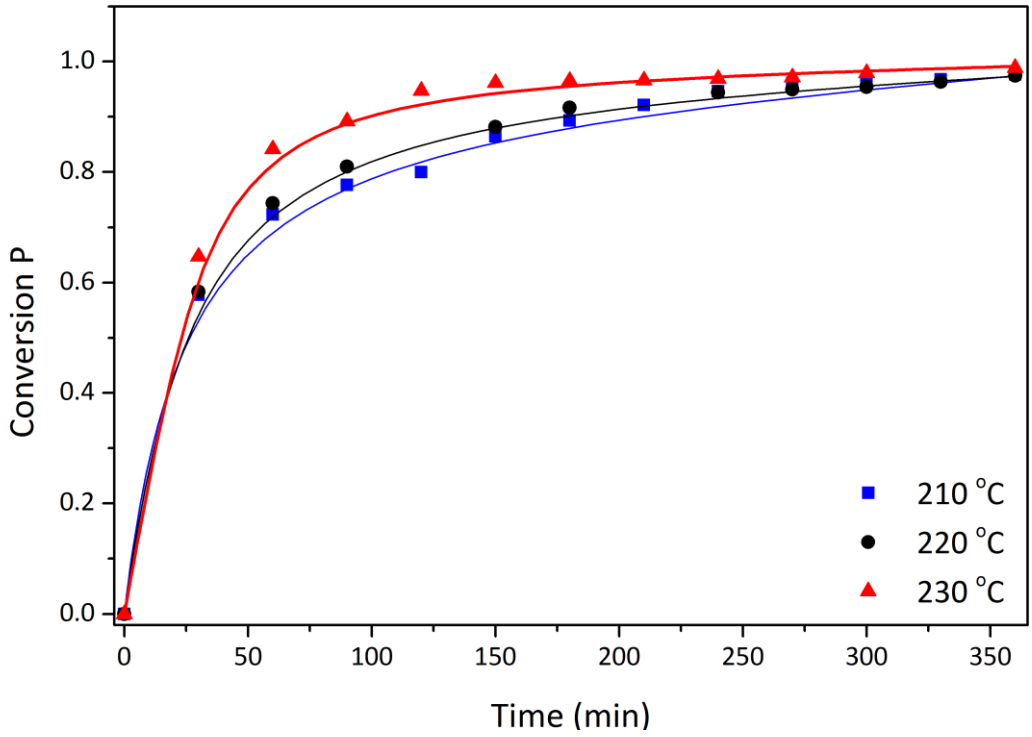

Figure 64. Conversion of COOH groups versus time during the polymerisation of $PPF_{70}PS_{30}$ (**3c**) at different temperatures fitted to Model 3. Symbols: experimental data; lines, model estimations.

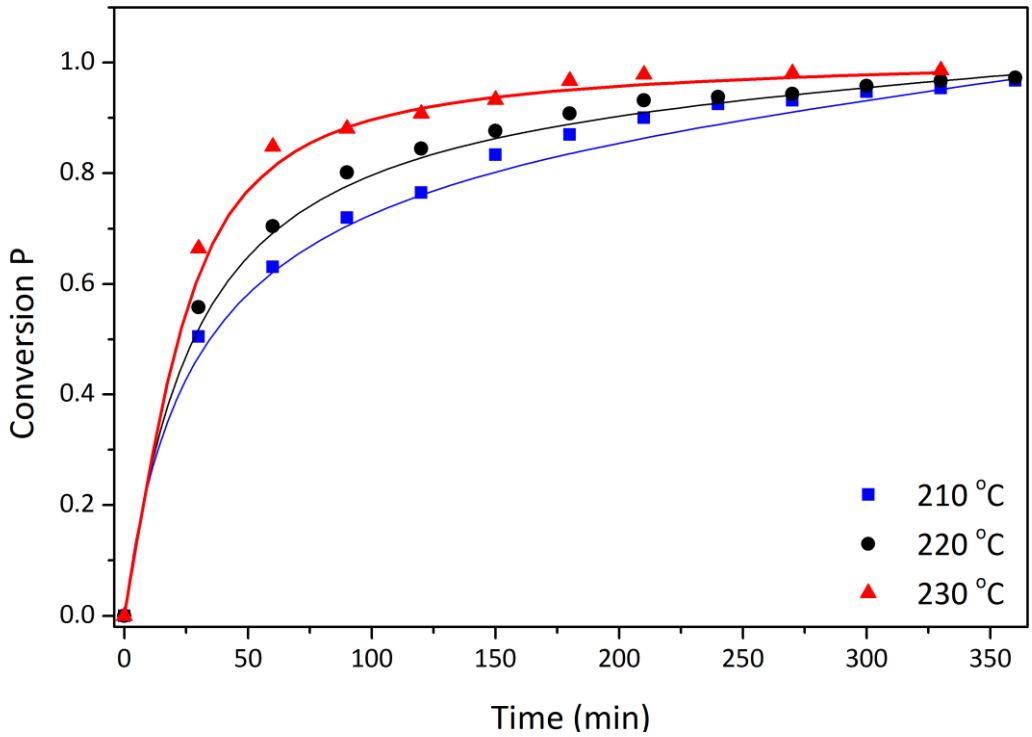

Figure 65. Conversion of COOH groups versus time during the polymerisation of $PPF_{85}PS_{15}$ (**3d**) at different temperatures fitted to Model 3. Symbols: experimental data; lines, model estimations.

The effect of temperature was also observable in the copolyesters **6** with 1,5-pentanediol, where the greatest carboxylic acid conversion was achieved at 230 °C. **Figure 66** and **Figure 67** provide the conversion plots showing Model 2 and Model 3 fitted to the experimental data of $PPeF_{15}S_{85}$ (**6a**) and $PPeF_{85}S_{15}$ (**6d**), respectively. The plots of the remaining compositions are available in **Appendix D**.

In the case of $PPeF_{85}S_{15}$ **6d** (**Figure 67**), there is practically no difference in the reaction rate when performing the reaction either at 220 °C or 230 °C. From the very beginning, the reaction rate and conversion at both process temperatures increase almost equally, with the experimental data points overlaying each other. This type of knowledge is useful when performing process optimisation and scale up, as the modelling suggests that it would be an unnecessary use of energy to increase the process temperature from a kinetic perspective. It is still fundamental to bear in mind the final application, as the temperature increase might be necessary to reach certain M_w (7000 Da at 230 °C and 4100 Da at 220 °C), as described in **Chapter 4**, **Section 4.3.2**.

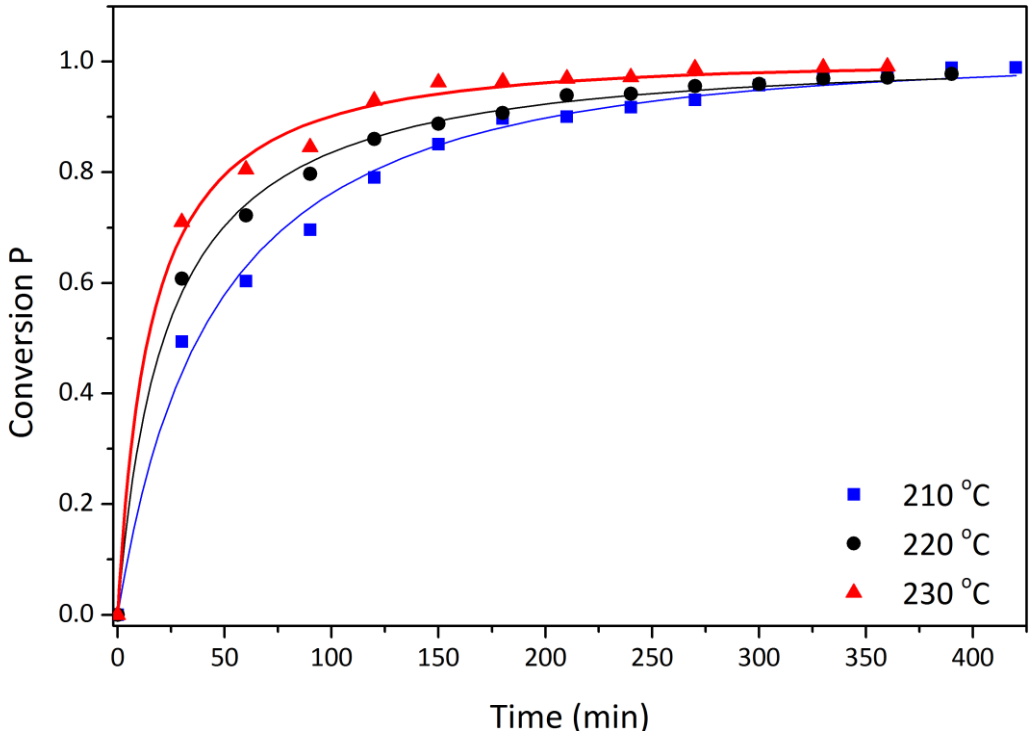

Figure 66. Conversion of COOH groups versus time during the polymerisation of $PPeF_{15}S_{85}$ (**6a**) at different temperatures fitted to Model 2. Symbols: experimental data; lines, model estimations.

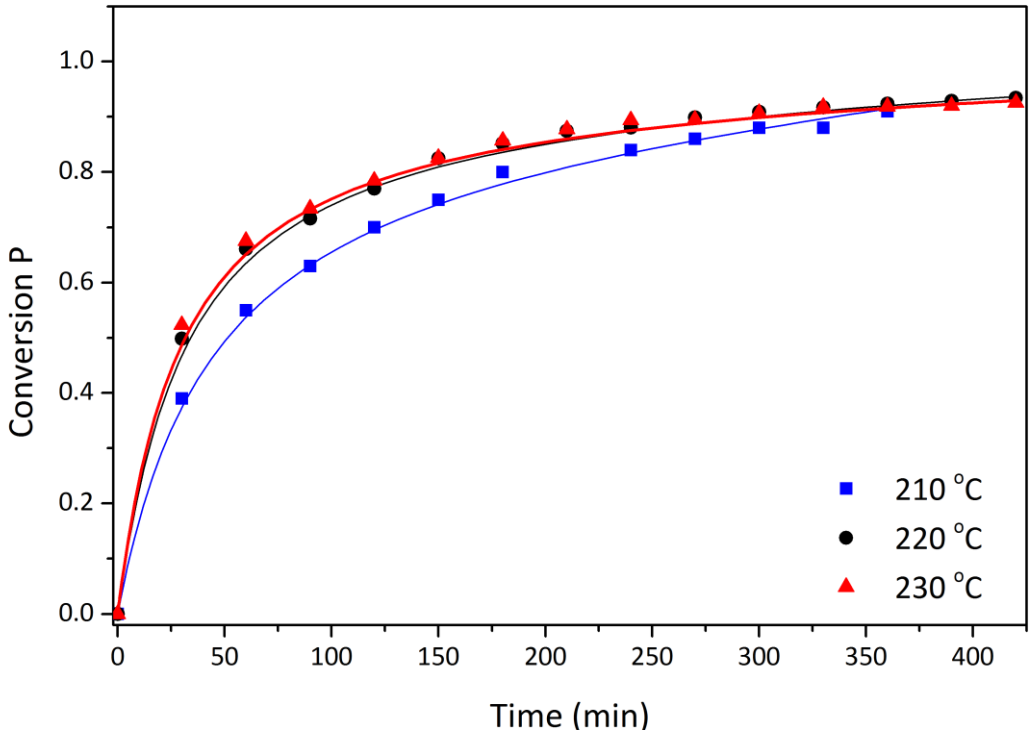

Figure 67. Conversion of COOH groups versus time during the polymerisation of $PPeF_{85}S_{15}$ (**6d**) at different temperatures fitted to Model 3. Symbols: experimental data; lines, model estimations.

5.4.2 Influence of diacid composition

In terms of diacid composition, at 210 °C, the final conversions of all the copolyesters PPFPS (**3**) are above 95% after 350 minutes; however, it is expected that higher conversions could be achieved if the reactions were allowed to proceed for longer times as the trend suggests in **Figure 68**. Although the conversion flattens after 200 min, the reaction needs to proceed to increase the molecular weight of the polymer, most importantly at 210 °C, temperature at which the lowest M_w and M_n were obtained, as shown in **Chapters 3** and **4**. At 210 °C, the final conversion was generally lower for polyesters containing the highest ratios of FDCA.

Figure 69 shows the carboxylic acid conversion at 220 °C. It is observed that the FDCA rich systems (**3c** and **3d**) had the lowest initial rate and succinic acid rich ones had the highest. The difference in final conversion is less significant at 220 °C than at 210 °C and at 230 °C (**Figure 70**), as all copolyesters reached a conversion of around 99% before 350 minutes of reaction time.

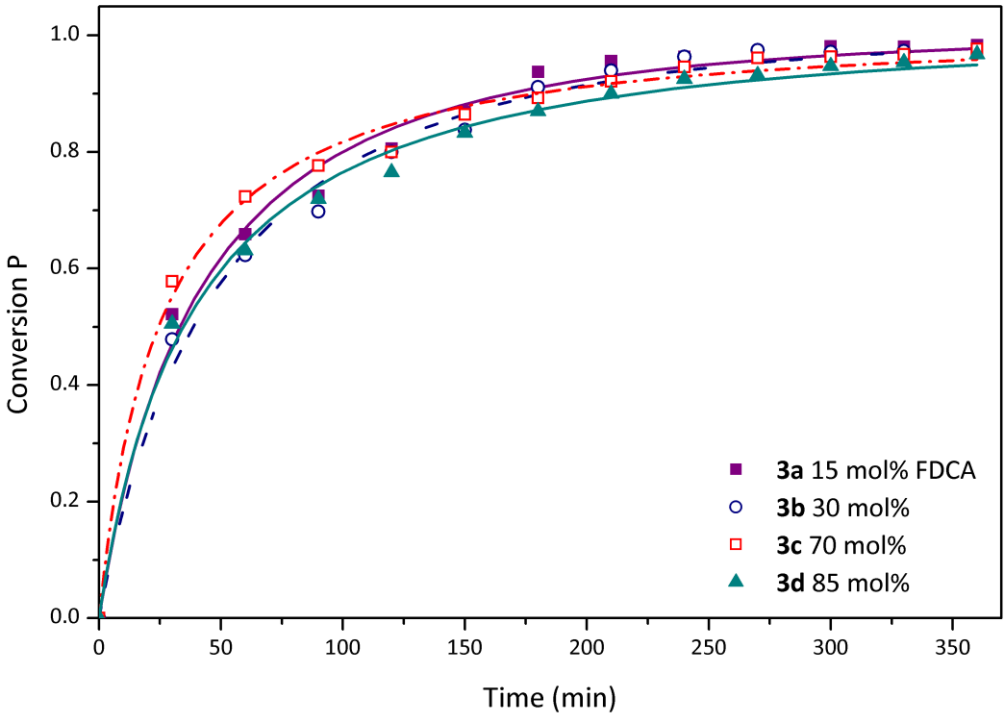

Figure 68. Conversion of COOH groups versus time for all monomer compositions of polyesters **3** fitted to Model 2 at 210 °C. Symbols: experimental data, lines, model estimations.

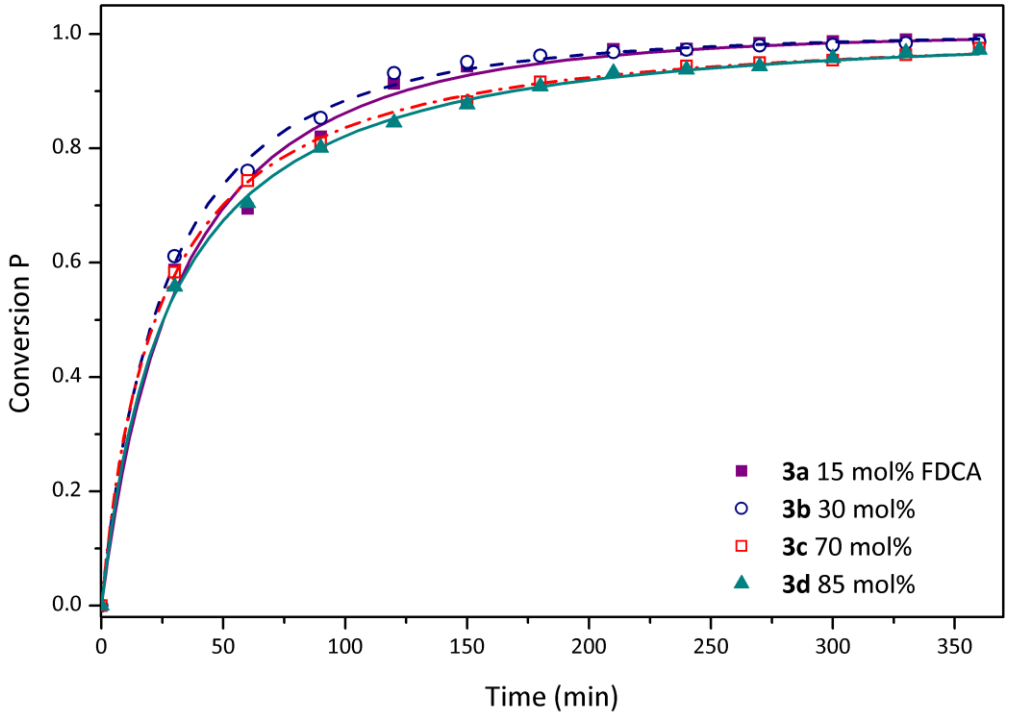

Figure 69. Conversion of COOH groups versus time for all monomer compositions of polyesters **3** fitted to Model 2 at 220 °C. Symbols: experimental data, lines, model estimations.

At 230 °C, $PPF_{15}PS_{85}$ (**3a**) showed the slowest initial rate of the PPFPS copolyesters, **Figure 70**. This is an agreement with the prior observations in the synthesis of PPS (**1**), whereby temperatures higher than 220 °C reduced the reaction rate. The same effect seems apparent for the copolyester containing the highest relative ratio of succinic acid.

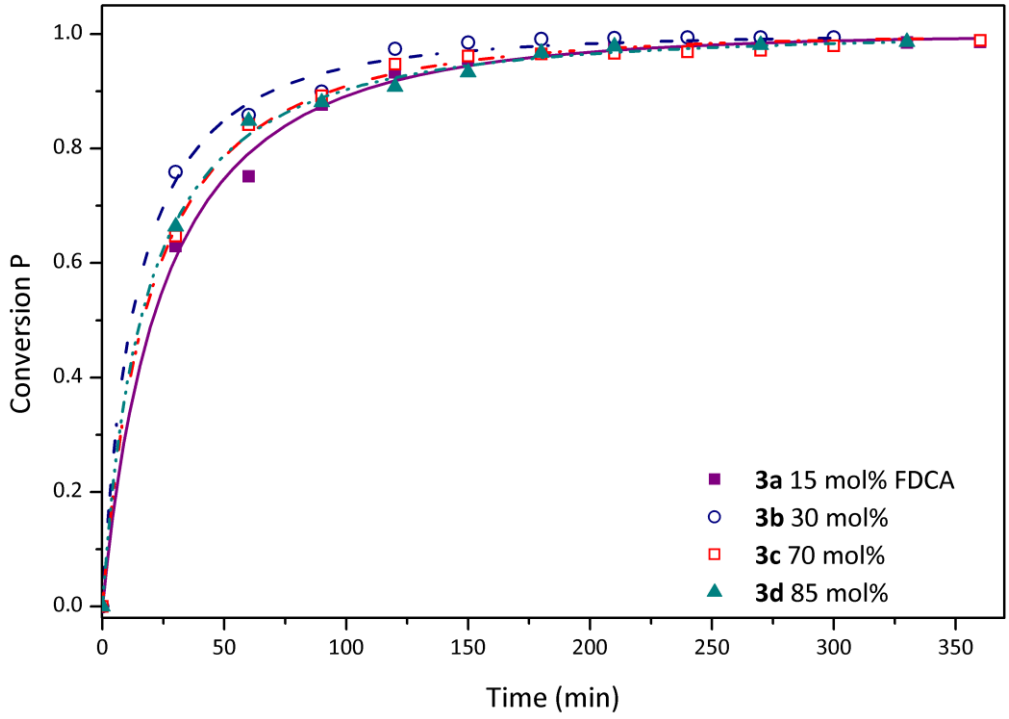

Figure 70. Conversion of COOH groups versus time for all monomer compositions of polyesters **3** fitted to Model 2 at 230 °C. Symbols: experimental data, lines, model estimations.

Regarding the 1,5-pentanediol copolyesters (**6**) , an increase in succinic content resulted in an increase in the reaction rate which is in agreement with the previous findings corresponding to 1,3-propanediol. **Figure 71** shows Model 2 fitted to the experimental conversion at 230 °C. The kinetic plots at 210 °C and 220 °C are shown in **Appendix D**.

In general, all monomer compositions could be successfully synthesised via the two-step polyesterification process at temperatures of 210 to 230 °C with final conversions for PPFPS polymers between 95% and 99% and PPeFS polymers between 92% and 99%.

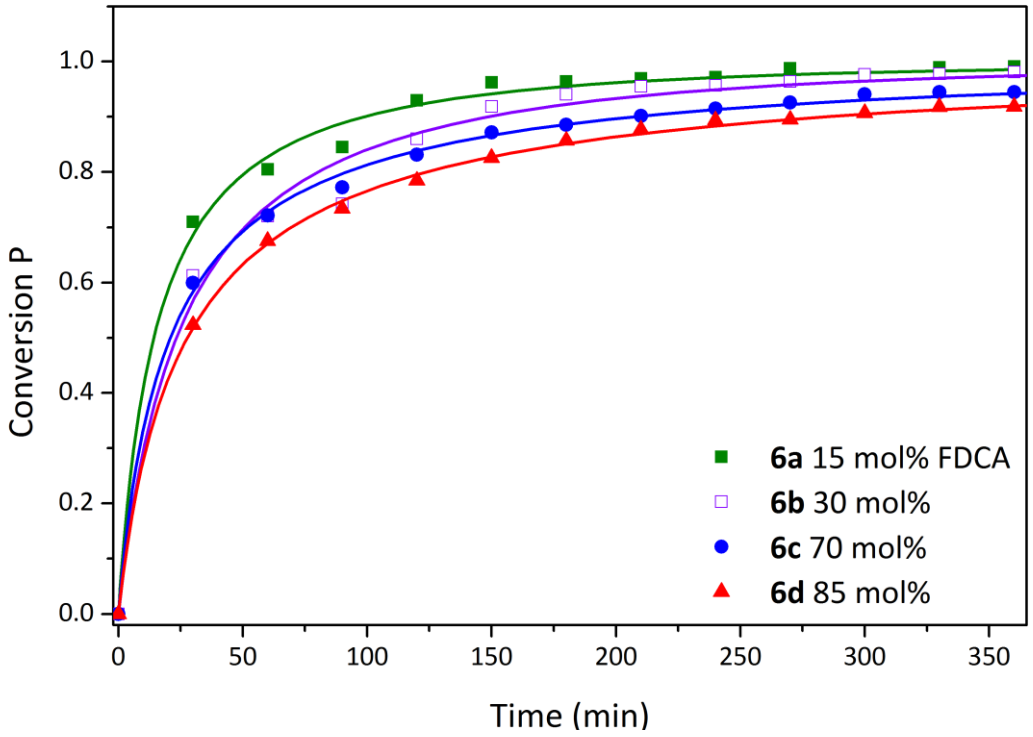

Figure 71. Conversion of COOH groups versus time for all monomer compositions of polyesters **6** fitted to Model 2 at 230 °C. Symbols: experimental data, lines, model estimations.

5.4.3 Polyesterification reaction modelling

Three models were fitted to the acid value data for the polymerisations of 1,3-propanediol or 1,5-pentanediol with FDCA, succinic acid, and mixtures of both diacids. These models were chosen as they represent a progression in the number of parameters taken into account in the rate equations. Each model's application is limited because of assumptions made when defining variables and key parameters. The main assumption made in Model 1, stoichiometric amounts of diol to diacid, differ from our own experimental conditions of 1.1:1 for PPS (**1**), 1.6:1 for PPF (**2**), 1.5:1 for PPFPS (**3**), and 1.05:1 for PPeS (**4**), 1.3:1 for PPeF (**5**) and PPeFS (**6**).

In Model 2, all water is considered to be removed from the polymerisation medium which is not guaranteed in the system. Model 3 takes into account variations in the properties of the reaction medium and potential ester hydrolysis due to leftover water.

The best results of the kinetic parameter optimisation with the proposed models for polyesters **1-3** are summarised in **Table 29** and **Table 30**. *Z* factor accounts for the numerical value of the least squares minimisation objective function. A lower Z value suggests that the objective function has been better minimised. The models are satisfactorily fitted throughout

all the reaction time for all the molar ratios, up to high conversions. In general, the simulation results show that the polyesterification models satisfactorily reproduce the experimental data in the temperature range between 210-230 °C, giving an indication of a feasible operation range, which is later optimised in **Chapter 6**. Fitting issues were observed around 80% of conversion in a number of polymerisations. This was particularly visible at 210 °C, **Figure 68** and is thought to be due to the experimental set-up change from stage 1 to stage 2 which resulted in a drop in the temperature of the system. Recovery to the desired process temperature was much quicker at 220 °C and 230 °C resulting in less obvious deviations of conversion data points, as seen in **Figure 69** and **Figure 70.** Although the deviation appears more pronounced at 210 °C, Z values are not systematically higher at this temperature and the fitting is still considered satisfactory.

Table 29. Optimisation of kinetic parameters with proposed Models 1 and 2 for polyesters **1-3**

		Model 1			Model 2			
Polyester	**T, °C**	**$k \cdot 10^2$, $(kg/mol)^{n-1} min^{-1}$**	**n**	**$Z \cdot 10^3$**	**$k \cdot 10^2$, $(kg/mol)^{n-1} min^{-1}$**	**m**	**n**	**$Z \cdot 10^3$**
	210	2.6	2.0	43.0	2.1	1.2	2.0	12.0
1	220	1.8	1.8	9.7	1.8	1.0	2.0	5.9
	230	1.8	1.5	2.2	2.0	0.9	2.0	1.8
	210	3.0	1.4	0.5	2.5	1.1	2.0	0.3
3a	220	4.0	1.4	1.6	4.0	1.2	2.0	1.3
	230	4.8	1.4	0.6	4.5	1.2	2.0	0.8
	210	3.0	1.2	20.0	2.5	0.9	2.0	1.4
3b	220	4.0	1.6	0.3	3.5	1.3	2.0	2.0
	230	7.9	1.7	1.7	7.5	1.5	2.0	1.5
	210	4.4	1.8	4.1	3.6	1.5	2.0	3.3
3c	220	4.9	1.7	0.4	4.1	1.47	2.0	0.2
	230	7.3	1.0	0.3	6.6	1.4	2.0	2.7
	210	3.0	1.7	3.7	2.4	1.3	2.0	2.7
3d	220	4.3	1.7	0.6	3.6	1.4	2.0	0.3
	230	6.1	1.6	1.9	5.3	1.3	2.0	1.8
	210	3.1	1.6	0.8	2.5	1.3	2.0	0.6
2	220	3.4	1.5	0.3	3.0	1.3	2.0	0.3
	230	10.0	1.9	0.6	8.0	1.7	2.0	0.7

It was found that Model 1 and Model 2 were similarly fitted with slightly lower Z values overall for Model 2, **Table 29**. Model 3 represented an improved fit in particular at higher conversions for FDCA-rich systems. A comparison of the three models is shown in **Figure 72** for $PPF_{70}PS_{30}$ (**3c**) at 220 °C.

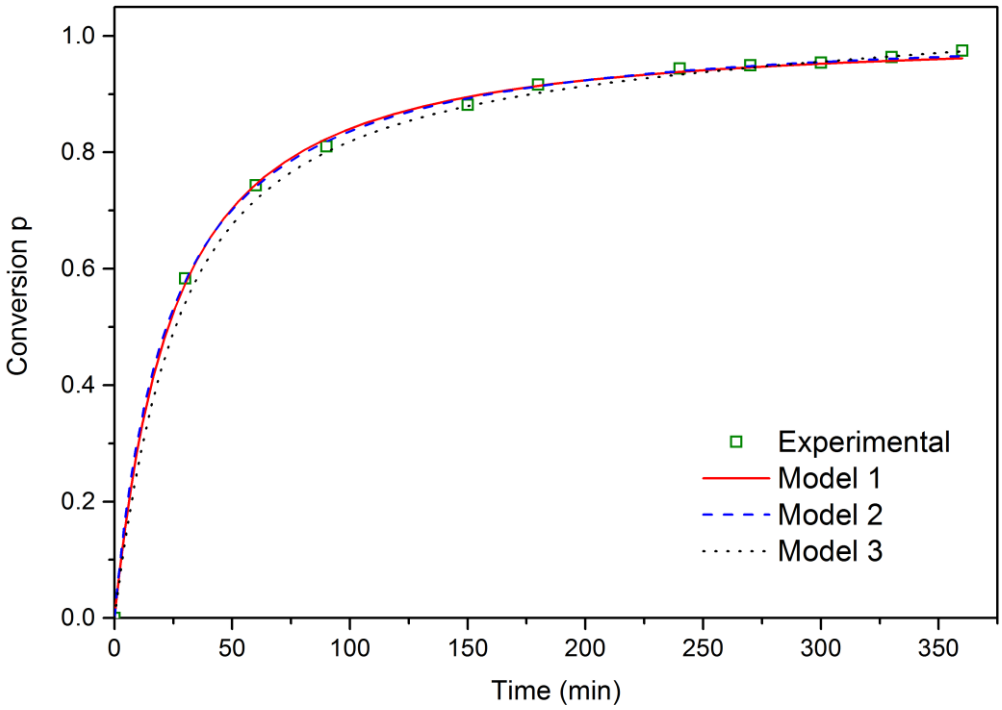

Figure 72. Conversion of COOH groups versus time for $PPF_{70}PS_{30}$ (**3c**) at 220 °C fitted with all three models.

The kinetic rate coefficients *k* depend on several process variables, such as temperature, concentration and catalyst, if any.[286, 311] The estimated values of *k* with Model 2 are between 1.8 and $8 \cdot 10^{-2}$ kg·mol^{-1}·min^{-1}, and increase upon the process temperature. Previous studies on the catalysed polyesterification of PPS (**1**) by titanium butoxide (TBT) reported *k* values of $1.5 \cdot 10^{-3}$ and $2.2 \cdot 10^{-3}$ L·mol^{-1}·min^{-1} with catalyst concentrations of 1.5 and $3 \cdot 10^{-4}$ mol TBT per mol SA, respectively. Garin, et al.[314] looked at the kinetics of PBS at 200 °C with and without catalyst (1mmol TBT/mol SA) and estimated *k* values of $1.2 \cdot 10^{-2}$ kg·mol^{-1}·min^{-1} and $8.4 \cdot 10^{-3}$ kg·mol^{-1}·min^{-1}, respectively. In another study on the kinetics of PBS, the product of the kinetic coefficient and the initial succinic acid concentration, the apparent coefficient K_{app}, was found between 0.33 and 1.90 L^{2}·mol^{-2}·min^{-1} at 170–190 °C [313], although the concentration value was not provided so it could be compared to other systems. As far as it is known, no more data on the uncatalysed polyesterification of succinic acid with either 1,3-propanediol or 1,5-pentanediol are available in the literature.

Table 30. Optimisation of kinetic parameters with Model 3 for polyesters **1-3**

Polyester	T °C	kK_{e0}, $kg^2 \cdot mol^{-2} \cdot min^{-1} \cdot 10^2$	$k_h[H_2O]$, $kg \cdot mol^{-1} \cdot min^{-1} \cdot 10^4$	α
1	210	0.5	1.2	1.70
	220	4.8	11.4	0.60
	230	5.9	11.0	0.23
3a	210	5.8	7.0	0.42
	220	10.6	5.9	0.75
	230	14.6	2.0	1.43
3b	210	3.3	7.4	1.25
	220	6.4	63.0	0.72
	230	9.6	33.0	0.35
3c	210	4.1	4.0	0.69
	220	3.8	2.5	1.40
	230	8.7	2.7	2.80
3d	210	4.1	6.5	0.12
	220	4.2	3.7	1.10
	230	4.6	0.3	2.60
2	210	4.0	4.0	1.20
	220	6.4	2.2	2.00
	230	3.9	2.2	2.40

The lumped parameters estimated with Model 3 had values between $0.5 \cdot 10^{-2}$ and $10.6 \cdot 10^{-2}$ $kg^2 \cdot mol^{-2} \cdot min^{-1}$ for kK_{e0} and between $0.3 \cdot 10^{-4}$ and $63 \cdot 10^{-4}$ $kg \cdot mol^{-1} \cdot min^{-1}$ for $k_h[H_2O]$. The values reported by Nalampang and Johnson[294] were kK_{e0} in the range of $1.45 \cdot 10^{-3}$ $kg^2 \cdot mol^{-2} \cdot min^{-1}$ and $1.89 \cdot 10^{-3}$ $kg^2 \cdot mol^{-2} \cdot min^{-1}$ while $k_h[H_2O]$ was within $1.31 \cdot 10^{-5}$

$kg \cdot mol^{-1} \cdot min^{-1}$ and $1.43 \cdot 10^{-5}$ $kg \cdot mol^{-1} \cdot min^{-1}$ for the polyesterification of 2-methyl-1,3-propanediol and either phthalic anhydride or isophthalic acid at 210 °C. Likewise, for the uncatalysed polyesterification reaction between adipic acid and ethylene glycol at 180 °C the estimated parameters were $kK_{e0} = 4 \cdot 10^{-4}$ $kg^2 \cdot mol^{-2} \cdot min^{-1}$ and $k_h[H_2O]=2.47 \cdot 10^{-5}$ $kg \cdot mol^{-1} \cdot min^{-1}$.[318]

The kinetics of 1,5-pentanediol resins had a close resemblance to the kinetic behaviour of 1,3-propanediol resins. **Table 31** and **Table 32** summarise the estimated kinetic parameters with Models 1-3. A proper distribution is observed, as experimental points fall both above and below the curves of the models. The experimental data is generally adequately fitted along the entire conversion range. The estimated *k* values with Model 2 fell within $1.8 \cdot 10^{-2}$ $kg \cdot mol^{-1} \cdot min^{-1}$ and $9.9 \cdot 10^{-2}$ $kg \cdot mol^{-1} \cdot min^{-1}$. The relatively high variation in the reaction orders, as in the case of polyester **5** in **Table 31**, is suggested to be a function of the changing properties of the medium, intermolecular interactions and the influence of the water removal.[320] It is believed FDCA plays a fundamental role in the properties of the medium, and therefore in the whole kinetic response, as proposed later in **Section 5.4.4**.

A deviation of the fitting was observed at values around 80% of conversion for many of the polymerisations due to the experimental set-up change from stage 1 to stage 2, in which xylene is added to achieve an efficient separation and removal of water and excess diol. A drop of temperature of around 15 °C is observed, recovering a few minutes after. This is observable in **Figure 71**, but given that *Z* values do not increase significantly, the fitting can be considered satisfactory.

Model 3 significantly underestimates the conversion for **6a and 6b** between 70-90% conversion, as shown in **Figure 73** and **Figure 74**. Model 3 generally provides a better fit for systems containing higher levels of FDCA, which is depicted as well in **Figure 73** and **Figure 74** as the kinetic model is better fitted to the data of **6c** and **6d**.

Table 31. Optimisation of kinetic parameters with proposed Models 1 and 2 for polyesters **4-6**

Polyester	T, °C	Model 1			Model 2			
		$k \cdot 10^2$, $(kg/mol)^{n-1}min^{-1}$	n	$Z \cdot 10^3$	$k \cdot 10^2$, $(kg/mol)^{n-1}min^{-1}$	m	n	$Z \cdot 10^3$
4	210	2.7	2.1	5.0	2.7	1.1	2.0	4.4
	220	3.6	1.9	3.1	3.6	1.0	2.0	1.9
	230	6.3	1.8	2.4	6.6	1.0	2.0	1.9
6a	210	2.6	1.5	4.1	2.6	1.1	2.0	2.0
	220	2.1	1.2	3.8	5.2	1.4	2.0	0.9
	230	8.0	1.7	1.5	9.9	1.4	2.0	1.0
6b	210	2.7	1.5	1.5	2.7	1.2	2.0	1.0
	220	3.7	1.4	1.1	5.4	1.6	2.0	0.3
	230	5.0	1.6	3.7	5.7	1.3	2.0	3.0
6c	210	3.1	1.8	1.1	3.0	1.4	2.0	0.9
	220	3.8	1.8	2.1	3.6	1.4	2.0	1.0
	230	7.0	2.1	0.8	6.9	1.7	2.0	0.5
6d	210	2.0	1.4	3.5	2.8	1.5	2.0	0.5
	220	4.7	2.0	0.6	4.6	1.6	2.0	0.3
	230	7.0	2.1	0.3	7.3	1.7	2.0	0.2
5	210	1.6	1.2	5.8	1.8	0.9	2.0	6.0
	220	5.9	2.0	0.6	6.4	1.6	2.0	0.7
	230	6.3	2.0	0.6	6.4	1.6	2.0	0.3

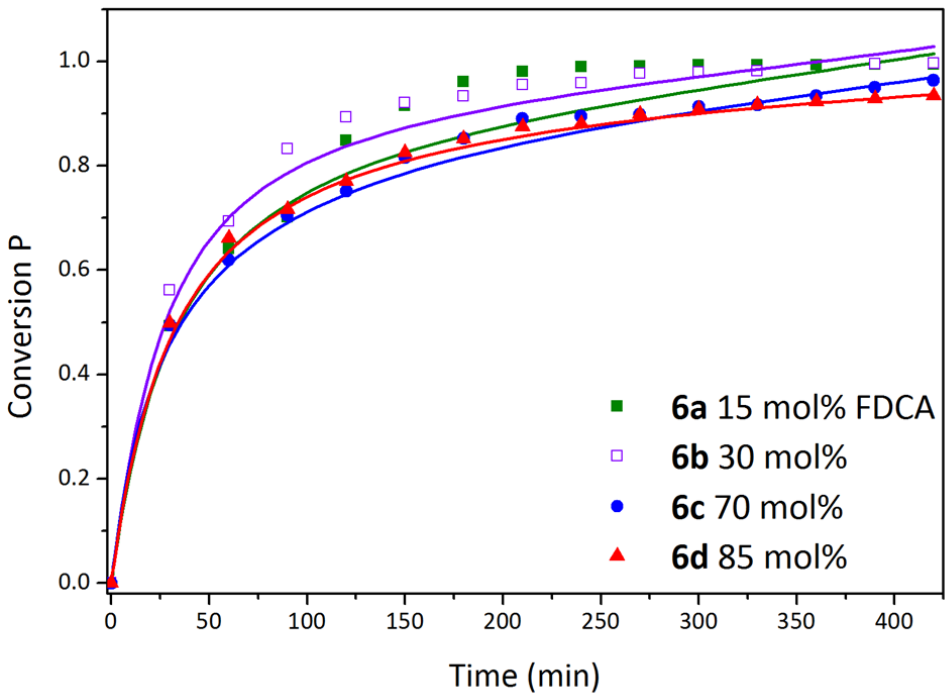

Figure 73. Conversion of COOH groups versus time for all monomer compositions of polyesters **6** fitted to Model 3 at 220 °C. Symbols: experimental data, lines, model estimations.

Table 32. Optimisation of kinetic parameters with Model 3 for polyesters **4-6**

Polyester	T °C	kK_{e0}, $kg^2 \cdot mol^{-2} \cdot min^{-1} \cdot 10^2$	$k_h[H_2O]$, $kg \cdot mol^{-1} \cdot min^{-1} \cdot 10^4$	α
4	210	4.2	5.1	0.21
	220	2.9	2.4	2.74
	230	3.8	3.8	1.46
6a	210	6.1	6.7	0.18
	220	6.3	4.0	0.87
	230	12.5	4.2	1.17
6b	210	5.9	5.0	0.85
	220	6.1	3.3	0.77
	230	12.9	5.1	0.28
6c	210	4.3	4.7	0.67
	220	5.1	1.8	1.00
	230	7.8	1.0	0.98
6d	210	4.2	5.5	0.65
	220	6.4	0.6	1.89
	230	7.7	1.0	0.98
5	210[a]	-	-	-
	220	6.4	0.5	1.90
	230	7.3	2.9	0.74

[a] Model was not satisfactorily fitted to the experimental data

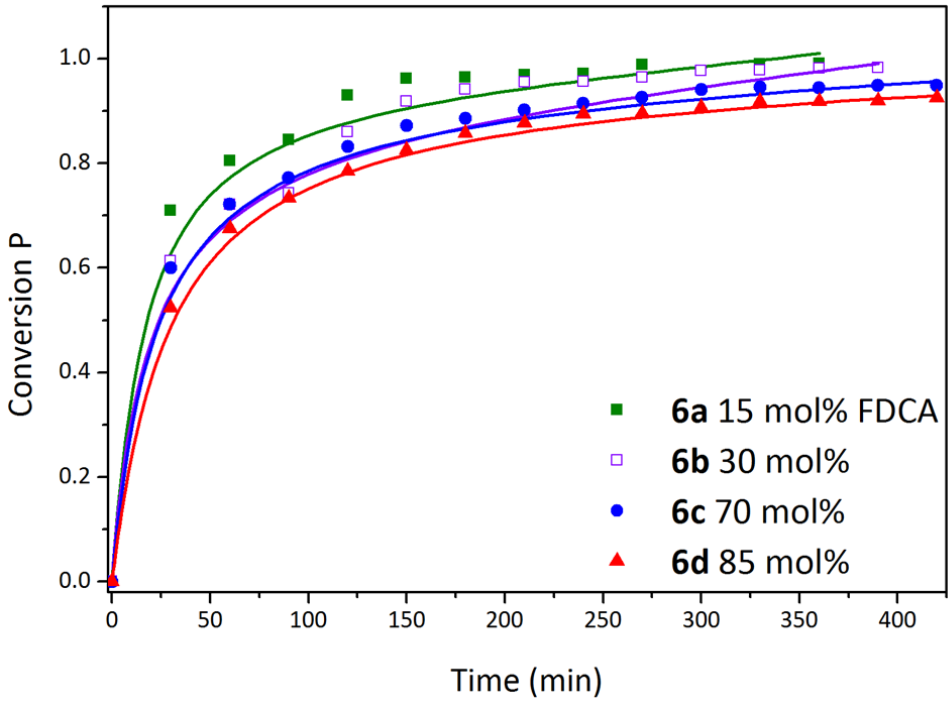

Figure 74. Conversion of COOH groups versus time for all monomer compositions of polyesters PPeFS (**6**) fitted to Model 3 at 230 °C. Symbols: experimental data, lines, model estimations.

Figure 75 shows the kinetic plot of Models 1-3 fitted to the experimental data of PPeF **5** at 220 °C. The three models satisfactorily predict the carboxylic acid conversion of **5**, suggesting that the three models are adequate for systems with 1,5-pentanediol and FDCA.

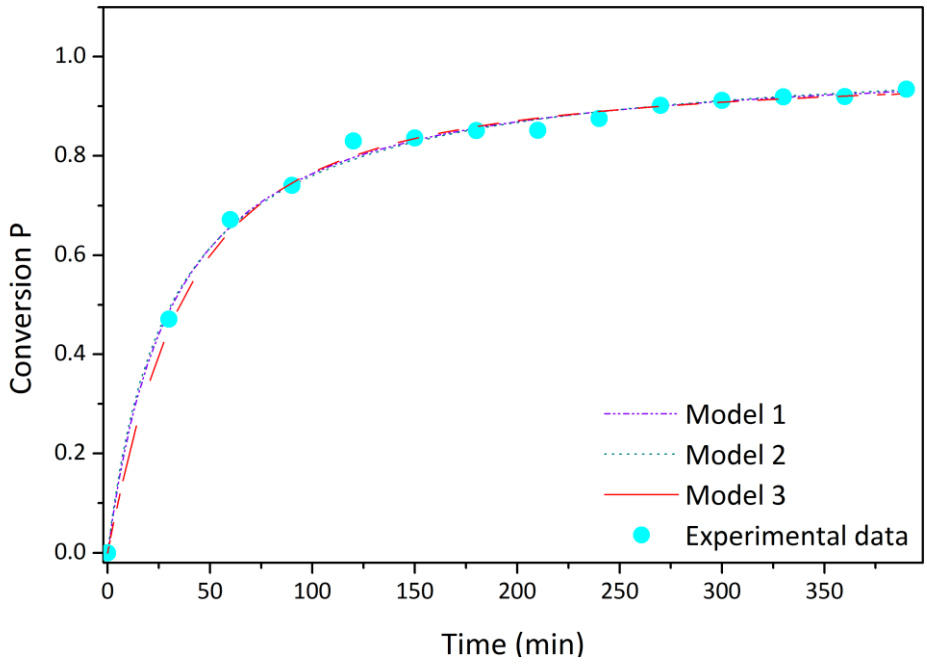

Figure 75. Conversion of COOH groups versus time for PPeF (**5**) at 220 °C fitted with all three models.

Comparison of *Z* values for Models 1 and 2 (**Table 29** and **Table 31**) shows that in general, these are lower for Model 2 making it the best fitting model tested for our dataset. The selection of a model is dependent on the specific parameters needed or the process requirements.

For most 1,5-pentanediol polymerisations, the kinetic parameters are higher than those of their 1,3-propanediol counterparts, meaning that 1,5-pentanediol leads to slightly higher conversions, as observed in **Figure 76**, which shows the conversion plot for polyesters PPS (**1**) and PPeS (**4**). The initial conversion is considerably higher for PTO, as after 2 hours of reaction time the conversion is already 80% while it is below 60% with PDO. By the end of the reaction, the final conversion is 97% for **4** and 93% for **1**.

These results agree with the literature, where it was observed that the rate constants increased with the chain-length of the diol during the reactions of the same dicarboxylic acid with various glycols.[321] The authors assumed that the inverse reaction, i.e. the hydrolysis rather than the direct esterification, was influenced by the chain-length of the glycol.

The diol effect was also observed by Bikaris, et al.[311] who described the effect of EG, PDO and BDO on the kinetic rate of the polyesterification with succinic acid. The authors found that *k* increased in the order BDO>PDO>EG.

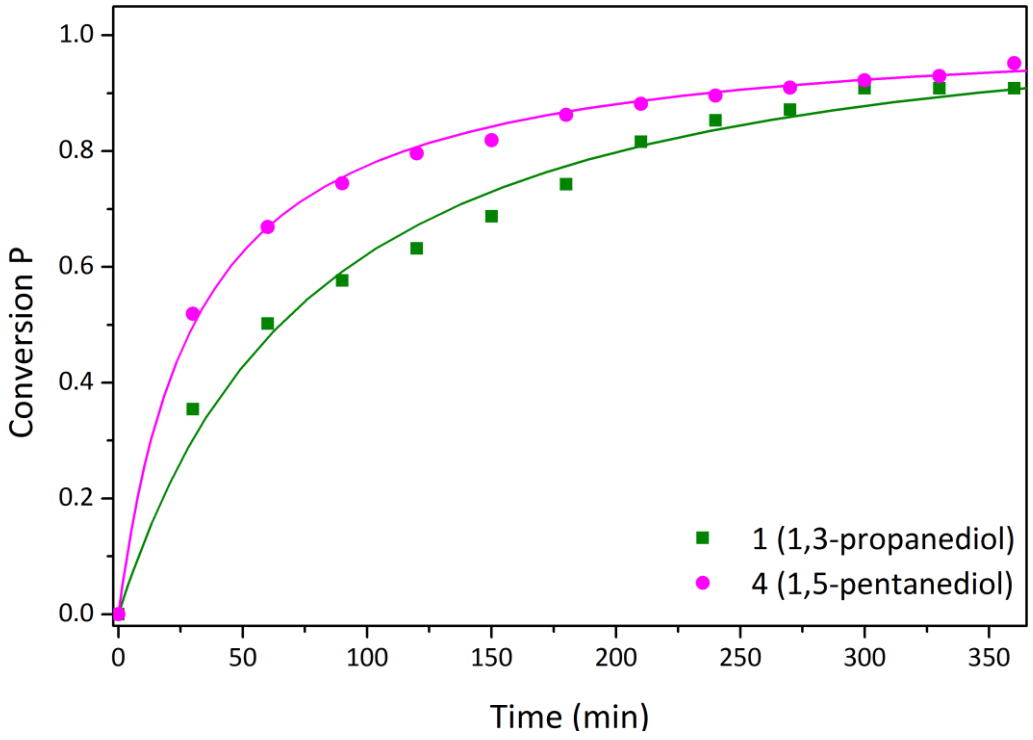

Figure 76. Conversion of COOH groups versus time for PPS (**1**) and PPeS (**4**) fitted with Model 2.

The estimation of kinetic parameters with 1,5-pentanediol is scarce, and few data have been reported. Davies, et al.[322] studied the reaction of adipic acid with 1,5-pentanediol under different conditions. The kinetic coefficient *k* was between $6.12 \cdot 10^{-3}$ kg·eq^{-1}·min^{-1} and $4.0 \cdot 10^{-2}$ kg·eq^{-1}·s^{-1} when the reaction was performed in diphenyl oxide in a temperature range of 166.5 °C to 233. 5 °C whereas in diethylaniline was between $8.5 \cdot 10^{-3}$ kg·eq^{-1}·s^{-1} and $1.96 \cdot 10^{-2}$ kg·eq^{-1}·s^{-1} for process temperatures within 178.5 °C and 208.5 °C.[299, 322]

Generally the reaction order in acid was found to be between 1 and 2 which corresponds to other reported studies.[293, 299, 320, 323] Several studies suggested that the reaction order for the diacid changes during polymerisation and that the overall order of reaction can be fractional as it is a composite of multiple processes.[295, 320] This phenomena could lead to the fractional reaction orders shown in **Table 29** and **Table 31**. Flory[324] determined that the overall reaction order relative to different polyesterifications is 3, which resemble the overall orders obtained for our systems (**Table 29** and **Table 31**). Similarly, Lin, et al.[325] found a third order (first with respect to the acid and second with respect to the diol) for the reaction of succinic acid and ethylene glycol at 195 °C in the presence of an excess of diol.

The apparent orders of reaction estimated with Models 1 and 2 were determined by the best fit between the given rate equation and the experimental data and differ from the theoretical or true values. In fact, it has been proposed that the variable reaction order is an inherent characteristic of uncatalysed polyesterifications.[322] Fang, et al[326] showed that the reaction order increases throughout the polyesterification as a result of changes in the dielectric constant and the viscosity of the medium. More recently, Salmi, et al.[320] developed an empirical, straight-forward model which predicts the increase of the reaction order, and was satisfactorily fitted to the experimental data from the polyesterification of adipic acid with ethylene glycol.

Experimental reaction order and stoichiometry do not represent the same concept. Molecularity refers to the reaction mechanism whereas reaction order pertains to an experimental specific rate equation. The reaction order only coincides with the molecularity for elementary reactions that occur in the standard form, $aA+bB \rightarrow cC+dD$. Reaction orders of 1–3 are only found for elementary reactions. With Models 1 and 2, the fractional orders are an indication of a series of molecules interacting with active species in the reaction media giving place to the formation of a system with multiple reactions: esterification,

polycondensation and ester interchange reactions with the polymer but also with end and bound segments.[327, 328] Tang and Yao[329] proposed a 2.5 order for the uncatalysed, non-equimolar reaction of succinic acid or adipic acid with ethylene glycol. Meanwhile, other fractional orders of 2.5 have been reported for the polyesterification of maleic acid[330] and 1,6-hexanedioic acid with ethylene glycol.[331] Approaches such as the transition state theory allow the theoretical determination of true kinetic parameters of a series of elementary steps in particular reaction schemes through the formation of activated complexes. However, the use of this computational chemistry tool is beyond the scope of this work.

Parameter α takes into account the variation of the dielectric constant of the reaction medium during polymerisation. In general, in polyesterification reactions the dielectric constant of the reaction mixture decreases as conversion increases. Chen and Wu[318] reported values of a of 0.61, 0.40 and 0.23 for the uncatalysed adipic acid-ethylene glycol system at 180, 160 and 140 °C, respectively. Accordingly, parameter α was also found to increase with increasing temperature but the range of values observed was much greater in our case. As the monomers, which provide the dielectric constant of the medium, are consumed faster at higher temperatures, it is expected α should follow a similar trend. Interestingly, the highest value for α for **1** was achieved at 210 °C (α=1.7), whereas for **3** a higher value for α (2.4) was estimated for the process at 230 °C.

5.4.4 Estimation of Activation Energy (E_a)

The activation energy (E_a) was estimated for all the polyesters synthesised at different process temperatures. The logarithmic values of the kinetic rate coefficients were plotted against 1/T (Absolute temperature, K) to prepare an Arrhenius plot. The activation energy was computed from the values of a gradient obtained by least-square method and an intercept. The Arrhenius equation explains the reaction rate coefficient as a function of temperature, and it is defined as in equation 58

$$k(T) = k_o e^{\frac{-E_a}{RT}} \tag{58}$$

Where k_o is the preexponential factor, R is the universal gas constant (8.314 J·mol^{-1}K^{-1}) and T is the absolute temperature (K). The Arrhenius plots of the polyesterification rate constants of the different systems analysed are displayed in **Figure 77** for **1-3** and in **Figure**

78 for **4-6**. **Table 33** presents the comparison between the activation energies obtained for the various copolymer compositions, along with the regression coefficient R^2. The kinetic coefficients *k* considered where those estimated with Model 2, previously listed in **Table 29** and **Table 31**.

Table 33. Estimated Activation Energies (E_a) by Arrhenius Plots

Polyester	Name	Mol% FDCA	Activation Energy, kJ·mol^{-1}	R^2
			1,3-propanediol	
1	PPS	0	44.7	0.91
3a	$PPF_{15}PS_{85}$	15	59.6	0.95
3b	$PPF_{30}PS_{70}$	30	172.2	0.99
3c	$PPF_{70}PS_{30}$	70	63.9	0.92
3d	$PPF_{85}PS_{15}$	85	80.0	1.00
2	PPF	100	183.4	0.99
			1,5-pentanediol	
4	PPeS	0	91.3	0.96
6a	$PPeF_{15}S_{85}$	15	136.3	0.99
6b	$PPeF_{30}S_{70}$	30	74.3	0.99
6c	$PPeF_{70}S_{30}$	70	83.2	0.90
6d	$PPeF_{85}S_{15}$	85	95.1	0.97
5	PPeF	100	127.9	0.77

In the case of PPF (**2**), the estimated E_a is 183.4 kJ·mol^{-1}, which is in good agreement with the estimated value previously reported, 184.3 kJ·mol^{-1} for the esterification of PEF synthesis.[332] The activation energy for PPS (**1**) was estimated to be 44.7 kJ·mol^{-1}. Bikiaris, et al.[312] reported the activation energies of transesterification and esterification for **1** to be 68.3 kJ·mol^{-1} and 52.0 3 kJ·mol^{-1}, respectively, with a diol:diacid molar ratio of 1.2 and

tetrabutoxytitanium as catalyst. The value is again close to that of the esterification step but the difference in E_a is somewhat surprising considering that no catalyst was used. The activation energies for the polyesterification of 2-methyl-1,3-propanediol with maleic anhydride and phthalic anhydride were 65.25 and 82.34 kJ·mol^{-1}, respectively.[294] Comparatively, other E_a values include those reported for the reaction between propylene glycol and maleic anhydride with 0.05 mol% catalyst (58.2 kJ·mol^{-1});[333] for the uncatalysed synthesis of poly(butylene succinate) at 170-190 °C (149 kJ·mol^{-1})[313] as well as the E_a for the esterification (82.2 kJ·mol^{-1}) and polycondensation (104 kJ·mol^{-1}) reactions of terephthalic acid and 1,4-butanediol at 195-215 °C.[315] Similarly, the calculated E_a for the polyesterification of PET was 82.21 kJ·mol^{-1} [334] and 75.35 kJ·mol^{-1}.[288]

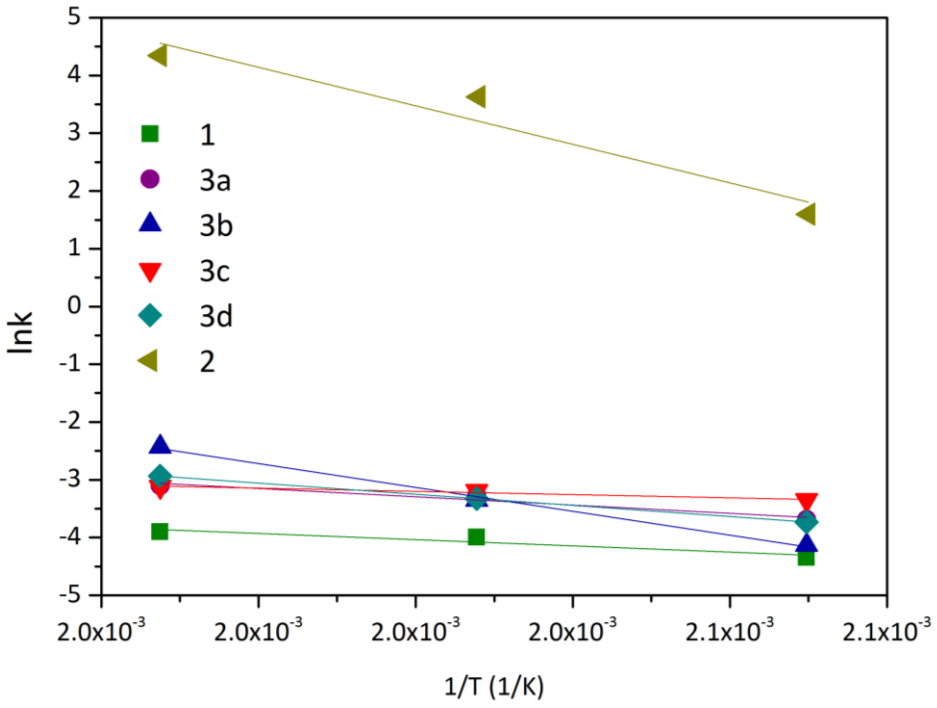

Figure 77. Arrhenius plot for polyesters **1-3**.

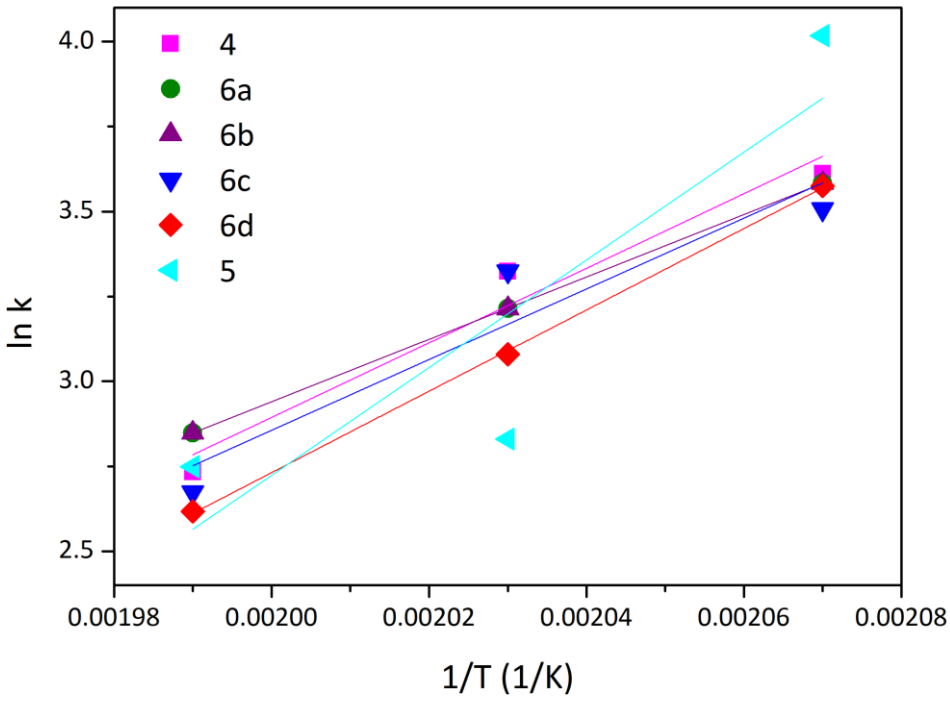

Figure 78. Arrhenius plot for polyesters **4-6**.

There are several parameters which could explain or contribute to the high activation energy observed for the furan polyesters PPF **2** and PPeF **5** compared to PPS **1** and PPeS **4**. It should be noted that if the rate limiting step of the polyesterification was only dependent on the amount of protons in solution then FDCA should have a faster polymerisation than SA as pK_a1 for FDCA is 2.6 while pK_a1 for SA is 4.21. **Scheme 40** depicts this proposed mechanism. Under acidic conditions, nucleophilic acyl substitution takes place through the protonation of the carbonyl group, activating it for the substitution.[335] In the case of FDCA, there are two potential processes that could lower the reactivity of the carbonyl carbon. First electron donation of the oxygen of the furan ring to the carbonyl carbon makes it less δ+ which could lead to reduced reactivity.[336] In the second donation, the positive charge of the protonated carbonyl group is delocalised through mesomeric structures which make the carbonyl less δ+. The proposed mechanism is based upon the competition between the formation of these mesomeric structures and the nucleophilic attack from the alcohol on the carbonyl carbon, slowing down what is already the rate limiting step in the process. For succinic acid, there are no mechanisms by which the carbonyl carbon is made less reactive by reduction of the δ+.[87]

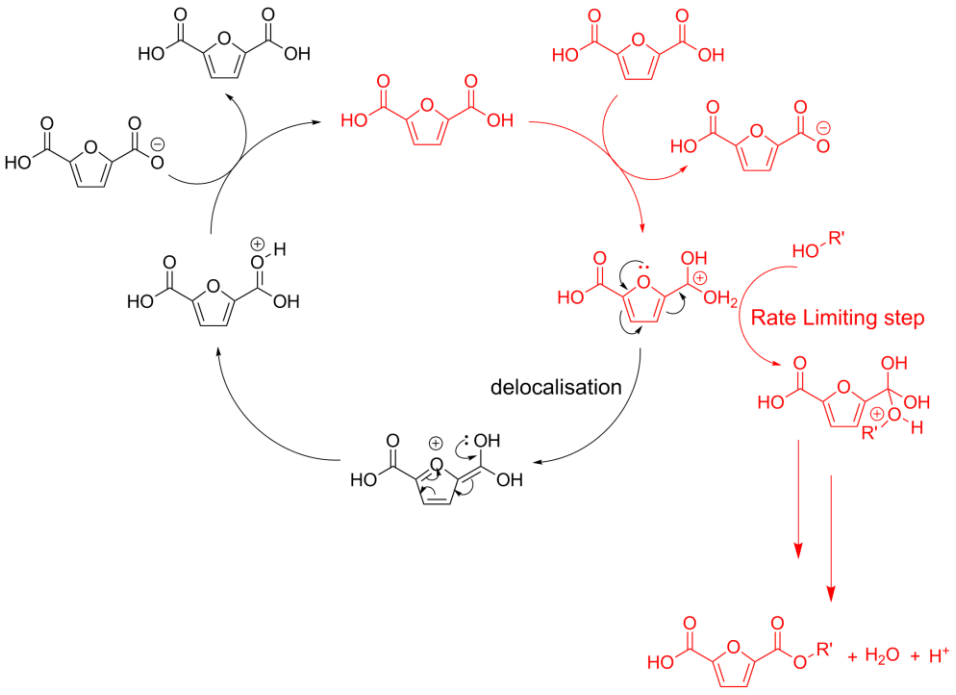

Scheme 40. Proposed mechanism for reduced reactivity of FDCA.

It should be noted that other factors may contribute to the high activation energy for **2**. FDCA has a high dielectric constant which can limit its solubility in the reaction medium.[337] As FDCA is only just solubilised in the reaction medium under polymerisation conditions, polymerisation mixtures containing FDCA have higher viscosities than those with succinic acid only. Reduced diffusion of end groups could lead to a reduction in rate. Finally, although a small contributing factor, reverse polyesterification is greater for stronger acids which would make the ester products from FDCA more prone to hydrolysis than those of succinic acid.[330] Interestingly, Rolfe and Hinshelwood[338] suggested that quantum mechanical restrictions could be responsible of making the transition probability in activated systems very small, leading to a high activation energy and low rates in their early study of the esterification of acetic acid with methanol. Molecular simulations were out of the scope of our work, but open the possibility of an in-depth kinetic study of polyesterification reactions.

5.5 Conclusions

The kinetic modelling of the uncatalysed polyesterification of biomass derived polyesters based on 2,5-furandicarboxylic acid (FDCA), succinic acid (SA) and either 1,3-propanediol (PDO) or 1,5-pentanediol (PTO) was satisfactorily performed by fitting three different kinetic models from the literature to the experimental carboxylic acid concentration

data. To the best of our knowledge, this is the first time that these kinetic models and the data obtained have been presented for FDCA, succinic acid and either 1,3-propanediol or 1,5-pentanediol biobased polyesters. Although succinic acid has been subject of kinetic modelling, the present results are novel for the combination of biomonomers, selection of models and reaction conditions.

The kinetic parameters calculated with Models 1 and 2 were the reaction orders for the diacid (*m*) and the diols (*n*), and the kinetic coefficient *k*. Model 3 allowed the calculation of the rate constant for the hydrolysis of ester bonds k_h and the equilibrium ionisation constant at zero fractional conversion, kKe_0.

As expected, the polymerisation rate of FDCA polyesters and copolyesters increased with temperature for most compositions. However, it was found the rate of polymerisation of PPS (**1**) decreased at 230 °C, which is attributed to competition of monomer evaporation and polymerisation. This was not the case for the polymerisation of its 1,5-pentanediol homologue, PPeS (**5**).

The diacid composition also influenced the kinetics, as the final conversion decreased as the FDCA content increased. It is believed that this behaviour could be prompted by two probable processes taking place in FDCA systems: the first electron donation of the oxygen of the furan ring to the carbonyl carbon makes it less δ+ which could lead to reduced reactivity. On the other hand, during the second donation, the positive charge of the protonated carbonyl group is delocalised through mesomeric structures which make the carbonyl less δ+. This effect is observed in the large activation energies (E_a) obtained for furan polyesters PPF (**2**) and PPeF (**5**) compared to their succinic acid counterparts PPS (**1**) and PPeS (**4**): 183.4 kJ·mol^{-1} and 127.9 kJ·mol^{-1} l against 44.7 kJ·mol^{-1} and 29.9 kJ·mol^{-1} , respectively. The E_a for the copolyesters PPFPS (**3**) and PPeFS (**6**) were found between 59.6 and 172.2 kJ·mol^{-1}, with regression coefficients R^2 from 0.90 and 0.99, except for **5**, whose estimation is recommended to be carried out again.

All monomer compositions could be successfully polymerised via the two-step polyesterification process at temperatures from 210 °C to 230 °C with final conversions for PPFPS (**3**) polymers between 95% and 99%. The final conversions of PPeFS (**6**) polyesters were in the range of 92 and 99%. All polymerisations were modelled using three models with increasing complexity. Model 3, which accounts for the changes in the dielectric constant of

the medium throughout the reaction, was found to provide better fit for polymerisations with high FDCA contents, which is suggested to be related to the strong effect of the high dielectric constant of FDCA. Calculated kinetic parameters were in agreement with reported values. Models 1-3 serve as a general screening and particularly, the results from Model 2 are used for the simulation work in **Chapter 6**.

This work represents a valuable industrial reference for a variety of biomass-based polyesterifications since it is a compendium of reaction conditions, choice of monomers, activation energies and kinetic coefficients of more than 10 different polyesters, providing comprehensive yet accessible and useful data in the area of polymerisation processing. It should also be noted that the approach followed in the chapter could be further expanded toward different bio-derived monomers and the needs of particular industries.

Future work would be focused in the modelling of catalysed polyesterification reactions with appropriate models which consider the effect of the catalyst, as well as the study of the influence of other process variables in the systems, such as agitation speed and geometry of the stirrer. The kinetic modelling presented herein could also be expanded by measuring the formation of side products during polyesterification and implementing their rates of formation in a main model.

The kinetic coefficients *k* estimated herein with Model 2 are used in the definition of the step-growth kinetic model for the process simulation of the polycondensation reactions in **Chapters 6** and **7**.

CHAPTER 6

Optimum Batch-Reactor Operation: Process Simulation and Multiobjective Optimisation

6. Optimum Batch-Reactor Operation: Process Simulation and Multiobjective Optimisation

This chapter describes the process simulation and multiobjective optimisation of the batch-reactor polyesterification of the biomass-derived polyesters **1** and **3** with 1,3-propanediol and **4-6** with 1,5-pentanediol. Our optimisation work on the production of 1,5-pentanediol polyesters has been published recently;[88] therefore, the chapter is mostly focused in these results.

6.1 Introduction

As continuous research and progress have been pursued in the synthesis of novel renewable biomass-derived polyesters and their potential applications, it is imperative to properly scale up the production processes so that these are feasible from a sustainable and economical perspective and can eventually replace the petrochemical-based processes. Therefore, the implementation of a range of process engineering tools, such as modelling, sensitivity analysis, and optimisation would allow the determination of the best configurations and operation conditions for the production of these polymers. Proper modelling provides thorough information about the process, ensuring improved safety, cleanliness, profitable operations, and a smooth introduction of new products into markets. [339]

With the proliferation of computing power, chemical process simulation has quickly advanced as complex, fundamental models are easily accessible and commercially available. These models integrate knowledge of physical properties, unit operations, and reaction kinetics in order to understand how unit operations work.[340]

Process simulation must be accompanied by mathematical optimisation to make sure the final products specifications are met, along with compliance of environmental, sustainability and economic criteria of a certain process. Process optimisation then represents a powerful and necessary tool for effectively designing efficient industrial processes.[214]

The solutions of problems with only one objective function present a single solution. Multiobjective optimisation (MOO) problems however, feature more than one objective function and there is no single optimal solution that simultaneously optimises all the objective functions.[341] The problems exhibiting a multiobjective nature thus bring along the concept of Pareto optimality. The Pareto optimal or efficient solutions are the solutions that

cannot be improved in one objective function without deteriorating their performance in another one.[341]

The non-linear MOO methods can be divided into three major categories: Methods with *a priori* articulation of preferences, methods with *a posteriori* articulation of preferences and methods with no articulation of preferences.[216] The selection of method depends on the type of information that is provided in the problem, the solution requirements and the availability of software.[216]

Regarding polyesterification process simulations, previous research has focused on different polyester systems such as the reaction of maleic anhydride with 1,2-propanediol, where the authors proposed a dynamic model in a system containing a batch-wise operating reaction vessel connected to a flash separation unit.[205, 292] Moreover, the reaction of glycerol and adipic acid was evaluated from both technical and economical perspectives for the production of polyesters integrated within biodiesel production facilities.[206] Within the area of FDCA-derived polyesters, Eerhart, et al.[208, 342] performed an energy and greenhouse gas (GHG) balance study on the production of poly(ethylene furandicarboxylate) (PEF) starting from corn based fructose[208] and lignocellulosic biomass.[342] The authors claimed that the production of PEF can reduce the non-renewable energy use approximately 40% to 50% while GHG emissions can be reduced approximately 45% to 55%, compared to PET.[208] In the area of sustainability, a life-cycle assessment comparing the impacts of using ethylene glycol from biomass against petrochemical sources for the production of PET showed reductions of 3.6%-28% in greenhouse-gas emissions and a 16% reduction of fossil-fuel consumption for the use of biomass-derived ethanol.[343] Finally, Seavey[340] analysed the simulation of commercial nylon-6 manufacturing process and compiled a valuable and comprehensive textbook that has set a cornerstone in the field of step-growth kinetics simulation coupled with product design.[192]

Some work has been done in the MOO field for step-growth polymerisations, i.e. synthesis of polyesters and polyamides. Mitra, et al.[219] studied the semi-batch production of nylon-6 by setting the total reaction time and the concentration of an undesirable cyclic dimer in the product as two individual objectives for minimisation, while simultaneously requiring the attainment of design values of the number-average chain length. Regarding the manufacture of PET, either from dimethyl terephthalate (DMT)[218] or terephthalic acid,[220] it was optimised by minimising the formation of side products as well as attaining a high

conversion of the methyl ester groups. Moreover, the MOO of the batch reactor for the synthesis of copoly(ethylene-polyoxyethylene terephthalate) was applied to the minimisation of the reaction time along with the formation of undesirable side products such as acid end group, vinyl ester end group, and diethylene glycol.[223] Another multiobjective optimisation study focused on poly(propylene terephthalate) (PTT), where the objective was to maximise the population of desired functional groups while minimising the time required for the process.[222]

In this chapter, an integrative process engineering study for the batch synthesis of the biomass derived polyesters in **Chapters 3** and **4** is described in detail. First, the reaction modelling is performed, including estimating kinetic parameters by fitting a predetermined polyesterification model to the experimental data, following the mathematical algorithm presented in **Chapter 5**. Next, the batch process simulation and multiobjective optimisation were carried out for all of the systems in Aspen Plus, concluding with the assessment of sustainability indicators for each case. The analysis of PET was included as a comparative petroleum-derived polyester reference. The simulation and optimisation problems are focused solely on the chemical reactor because it is considered to be the heart of any process; however, a complete chemical manufacturing process simulation would need to consider other stages such as separation and purification and, specifically for polymers, compounding, blending, and polymer reinforcement.[177]

Although the analysis of the full manufacturing process is beyond the scope of the present work, this study does set the basis for future research in this area. Note that the sustainability indicators refer exclusively to the optimised reactor operating conditions and a similar assessment should be completed for the next production stages, as well as the production of monomers from carbohydrate sources, which will enable the performance of a complete life-cycle assessment (LCA). To the best of our knowledge, this is the first time that a comprehensive process modelling, simulation, and optimisation work for a batch polymerisation reactor has been presented for potential fully biomass-derived renewable polyesters.

6.2 Development of the Kinetic Model

6.2.1 Initial Definition of the Problem

The polyesters were synthesised by the experimental procedures explained in **Chapter 2**. The kinetic modelling presented herein is therefore validated against our own acquired experimental data.

To perform an accurate simulation and allow for further optimisation, a robust kinetic model must be implemented. Therefore, the general kinetic approach for Model 2, which was considered in **Chapter 5**, needs to be complemented with a modelling framework that accounts for varying chain lengths, commonly found in kinetics of step-growth polymerisation.[288] This particular framework also allows simulating the polyesterification process in Aspen Plus, as described in detail later on. The functional-group approach has been considered to establish the overall reaction network, which has been commonly used for step-growth polymerisations, as in the cases of the kinetics of PET,[192, 288] PTT[222, 297] and nylon-6.[340]

First, the main species present were identified and the segments defined. We then proceeded with the definition of the reactions in the system and the species mass balance, to derive a particular reaction rate for each of the polyesterifications. The conventional species considered were water, 1,5-pentanediol or 1,3-propanediol, succinic acid, and FDCA. The diol and diacids polymerise to form the corresponding polyesters, which are composed of terminal (T-) and bound (B-) segments for both the diacids and the diol. **Scheme 41** shows the structures of the different segments involved in the mechanism. As in the case of PET,[192] two main reactions were considered: esterification or water formation and ester interchange (transesterification). Side reactions such as degradation of the diester group or dehydration of the diol and its end segments, however, were not included in the kinetic model because experimental data were not available to validate the estimation of the kinetic parameters. The general schemes of the esterification and ester interchange reactions are depicted in **Scheme 42** and **Scheme 43**, respectively.

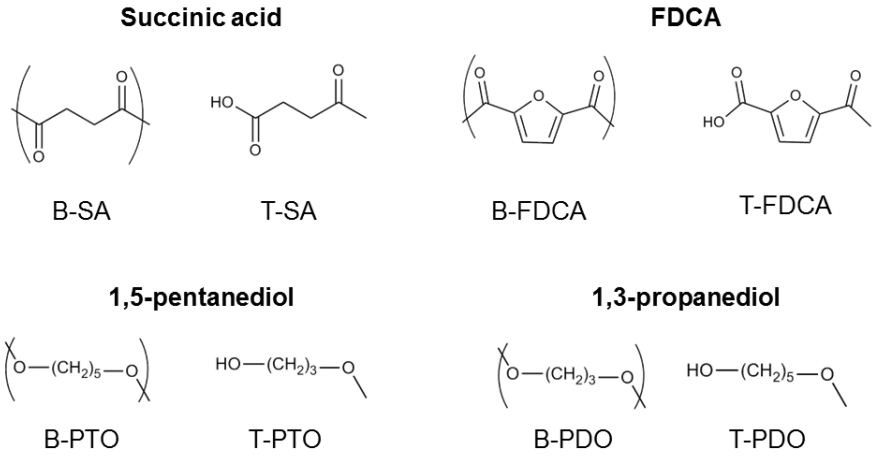

Scheme 41. Chemical structures of the repeat (B-) and terminal (T-) segments.

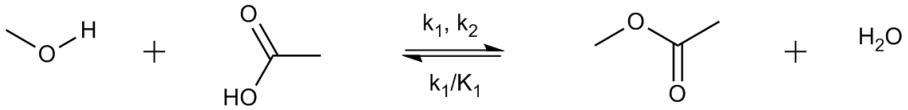

Scheme 42. General water formation or esterification reaction between a hydroxyl group and a carboxyl group to form an ester group and water.

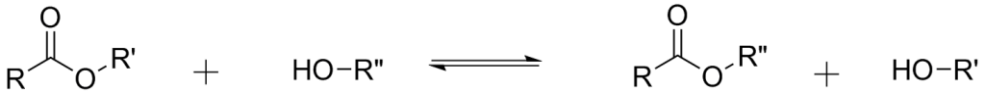

Scheme 43. General ester interchange reaction between an ester and alcohol.

The following assumptions are also considered in the group contribution method:

1. The reactivity of the molecules is not a function of the size of the molecule (known as the equal reactivity hypothesis).[184]
2. The rate coefficients k_i of the conventional species are equal to those of the segments.
3. The reversible reactions do not govern the kinetics; they govern only the equilibrium and are disregarded.
4. No mass-transfer limitations are encountered.

6.2.2 Definition of the step-growth model in Aspen Plus

The first step in the development of the structure of the step-growth model in Aspen Plus is to define segments corresponding to the monomers which are used to produce the polymer (**Scheme 41**). Aspen Plus uses the monomer as a reference point for molecular size,

as the reaction kinetics involve adding monomer to the end of the growing polymer chains.[344] **Figure 79** shows the definition of the main components and segments in Aspen Plus.

The step-growth model implemented in Aspen Plus calculates the component reaction rates and the rate of change of the zeroth and first polymer moments (λ_0,λ_1') of the polymer chain length distribution. These moments allow the calculation of polymer attributes that are used to calculate polymer properties such as viscosity, melt flow index, melting point, etc.[344]

Aspen Plus generates the reactions based on the functional groups involved, which the simulator classifies as nucleophilic or electrophilic functional groups,[344] as depicted in **Figure 80**. Nucleophilic groups are electron-strong groups (diol and water) whereas electrophilic groups are electron-weak groups (acids and esters). The reactions follow second order kinetics: one order with respect to the nucleophilic reactant and one order with respect to the electrophilic reactant.

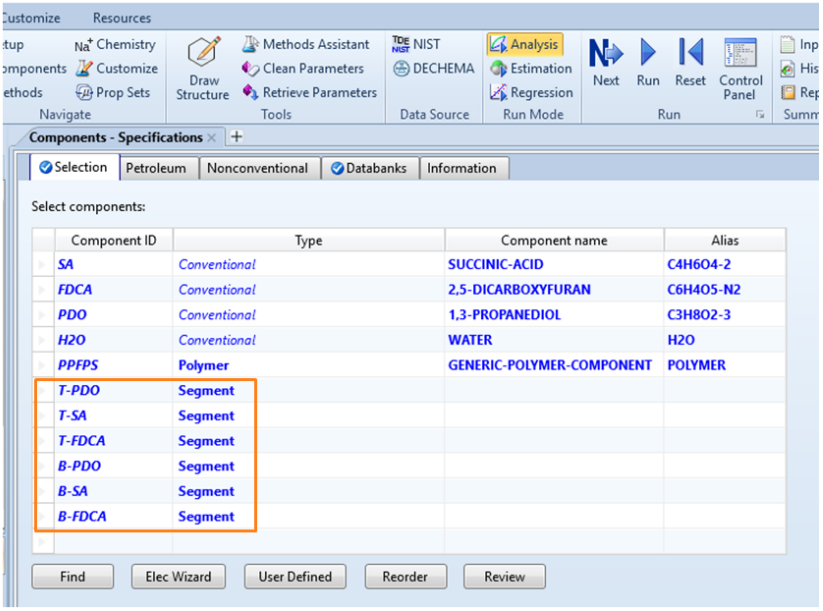

Figure 79. Definition of main components and segments for the implementation of the step-growth model in Aspen Plus.

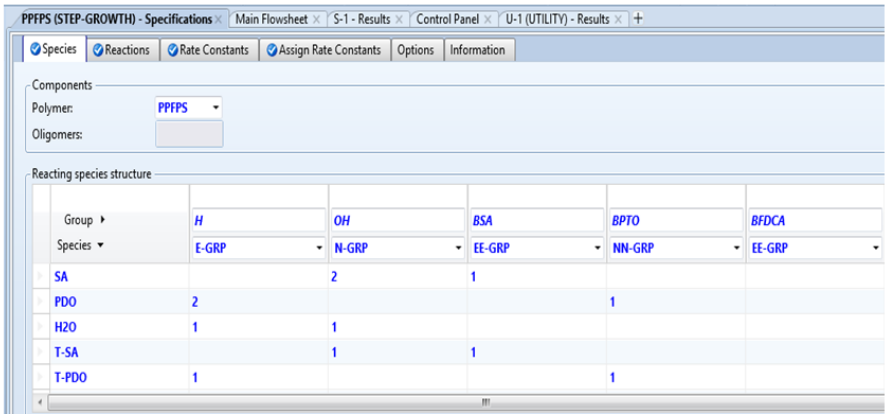

Figure 80. Definition of nucleophilic (N-GRP, NN-GRP) and electrophilic (E-GRP, EE-GRP) functional groups in Aspen Plus.

With the assumptions and species defined, Aspen Plus automatically[192, 344] generated a set of 12 reactions for each of the polyesters PPeF (**5**), PPeS (**4**) and PPS (**1**) and 24 for the PPeFS (**6**) and PPFPS (**3**) copolyesters (**Figure 81** and **Figure 82**), which were classified into the following five sets of rate constants (k_i, i = 1, ..., 5). The sets listed below correspond to the reactions with 1,5-pentanediol (PTO). The ones referring to 1,3-propanediol (PDO) are equivalent just by changing the species PTO, T-PTO and B-PTO for PDO, T-PDO and B-PDO, respectively.

1. **Forward water formation considering the diol (1,5-pentanediol) (k_1)**

$$PTO + FDCA \rightarrow H_2O + (T-PTO) + (T-FDCA) \quad (59)$$

$$PTO + (T-FDCA) \rightarrow H_2O + (T-PTO) + (B-FDCA) \quad (60)$$

$$PTO + SA \rightarrow H_2O + (T-PTO) + (T-SA) \quad (61)$$

$$PTO + (T-SA) \rightarrow H_2O + (T-PTO) + (B-SA) \quad (62)$$

2. **Forward water formation considering the diol terminal segment (T-PTO) (k_2; $k_2 = k_1$)**

$$(T-PTO) + FDCA \rightarrow H_2O + (B-PTO) + (T-FDCA) \quad (63)$$

$$(T-PTO) + (T-FDCA) \rightarrow H_2O + (B-PTO) + (B-FDCA) \quad (64)$$

$$(T-PTO) + SA \rightarrow H_2O + (B-PTO) + (T-SA) \quad (65)$$

$$(T-PTO) + (T-SA) \rightarrow H_2O + (B-PTO) + (B-SA) \quad (66)$$

3. Backward water formation (k_1'; k_1'= 0)

$$H_2O + (T - PTO) + (T - FDCA) \rightarrow PTO + FDCA \quad (67)$$

$$H_2O + (T - PTO) + (B - FDCA) \rightarrow PTO + (T - FDCA) \quad (68)$$

$$H_2O + (T - PTO) + (T - SA) \rightarrow PTO + SA \quad (69)$$

$$H_2O + (T - PTO) + (B - SA) \rightarrow PTO + (T - SA) \quad (70)$$

$$H_2O + (B - PTO) + (T - FDCA) \rightarrow (T - PTO) + FDCA \quad (71)$$

$$H_2O + (B - PTO) + (B - FDCA) \rightarrow (T - PTO) + (T - FDCA) \quad (72)$$

$$H_2O + (B - PTO) + (T - SA) \rightarrow (T - PTO) + SA \quad (73)$$

$$H_2O + (B - PTO) + (B - SA)(T - PTO) + (T - SA) \quad (74)$$

4. Forward ester interchange (k_3)

$$PTO + (T - FDCA) + (B - PTO) \rightarrow (T - PTO) + (T - PTO) + (T - FDCA) \quad (75)$$

$$PTO + (B - FDCA) + (B - PTO) \rightarrow (T - PTO) + (T - PTO) + (B - FDCA) \quad (76)$$

$$PTO + (T - SA) + (B - PTO) \rightarrow (T - PTO) + (T - PTO) + (T - SA) \quad (77)$$

$$PTO + (B - SA) + (B - PTO) \rightarrow (T - PTO) + (T - PTO) + (B - SA) \quad (78)$$

5. Reverse ester interchange (k_3'; k_3'=*0*)

$$(T - PTO) + (T - PTO) + (T - FDCA) \rightarrow PTO + (T - FDCA) + (B - PTO) \quad (79)$$

$$(T - PTO) + (T - PTO) + (B - FDCA) \rightarrow PTO + (B - FDCA) + (B - PTO) \quad (80)$$

$$(T - PTO) + (T - PTO) + (T - SA) \rightarrow PTO + (T - SA) + (B - PTO) \quad (81)$$

$$(T - PTO) + (T - PTO) + (B - SA) \rightarrow PTO + (B - SA) + (B - PTO) \quad (82)$$

The complete set of reaction stoichiometry and associated reaction rates of the esterification and ester interchange reactions for 1,5-pentanediol polyesters are summarised in **Table 34** and **Table 35,** while the corresponding mass balances of all species are listed in **Table 36**. The equivalent data for 1,3-propanediol are available in **Appendix E.**

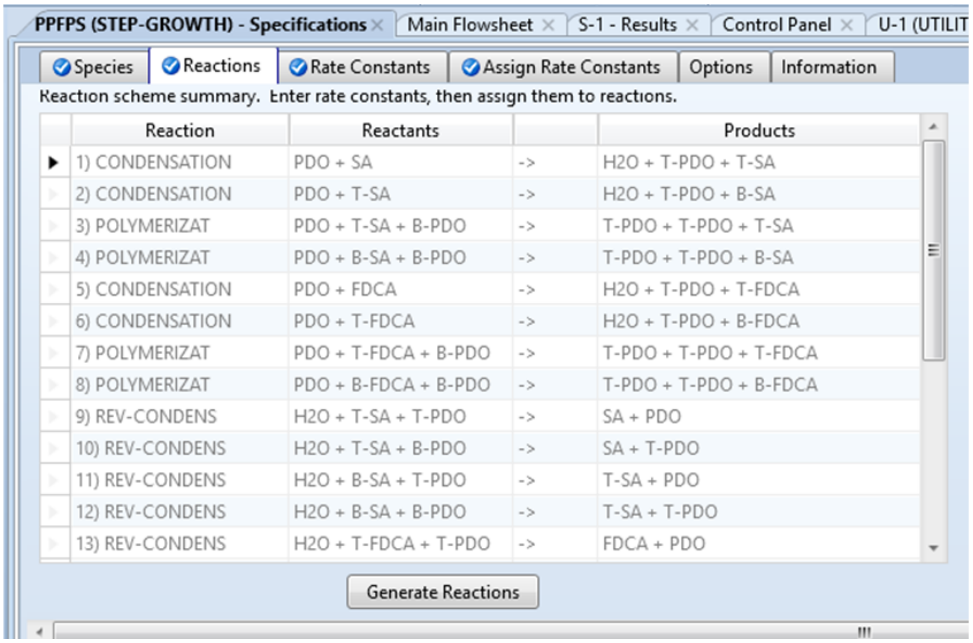

Figure 81. Step-growth reaction scheme summary in Aspen Plus for PPFPS (**3**) (Reactions 1-13).

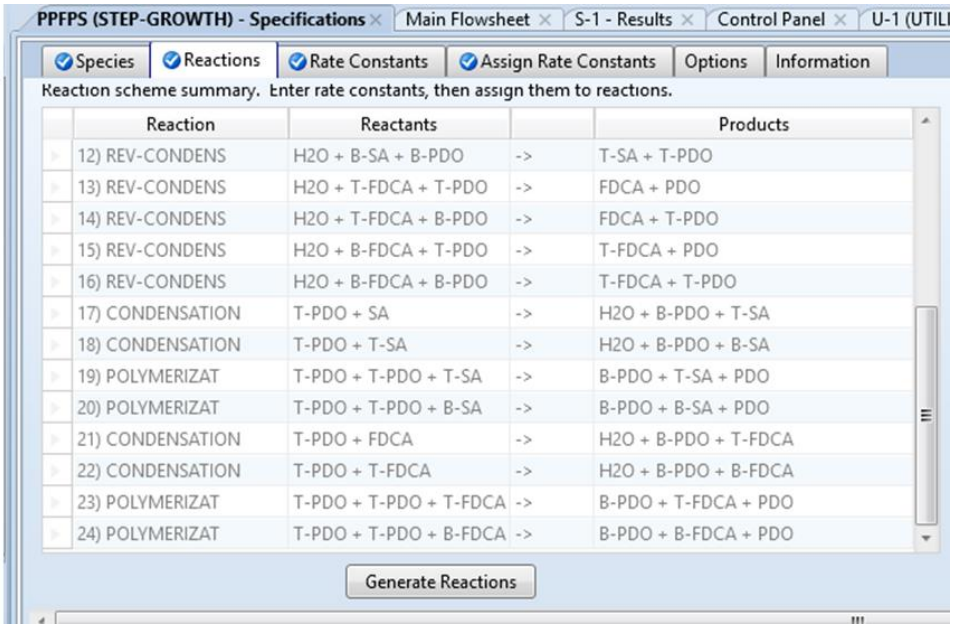

Figure 82. Step-growth reaction scheme summary in Aspen Plus for PPFPS (**3**) (Reactions 14-24).

Table 34. Esterification Reactions

Stoichiometry	Reaction Rate[a]
$PTO + FDCA \Leftrightarrow (T - PTO) + (T - FDCA) + W$	$R_1 = 4k_1[PTO][FDCA] - \frac{k_i}{K_1}[T - PTO] \times \frac{[T - FDCA][W]}{[T - FDCA] + [B - FDCA]}$
$PTO + SA \Leftrightarrow (T - PTO) + (T - SA) + W$	$R_{1SA} = 4k_1[PTO][SA] - \frac{k_i}{K_1}[T - PTO] \times \frac{[T - SA][W]}{[T - SA] + [B - SA]}$
$PTO + (T - FDCA) \Leftrightarrow (T - PTO) + (B - FDCA) + W$	$R_2 = 2k_1[PTO][T - FDCA] - \frac{k_1}{K_1}[T - PTO] \times \frac{[B - FDCA][W]}{[T - FDCA] + [B - FDCA]}$
$PTO + (T - SA) \Leftrightarrow (T - PTO) + (B - SA) + W$	$R_{2SA} = 2k_1[PTO][T - SA] - \frac{k_1}{K_1}[T - PTO] \times \frac{[B - SA][W]}{[T - SA] + [B - SA]}$
$(T - PTO) + FDCA \Leftrightarrow (B - PTO) + (T - FDCA) + W$	$R_3 = 2k_2[T - PTO][FDCA] - \frac{k_1}{K_1}[B - PTO] \times \frac{[T - FDCA][W]}{[T - FDCA] + [B - FDCA]}$
$(T - PTO) + SA \Leftrightarrow (B - PTO) + (T - SA) + W$	$R_{3SA} = 2k_2[T - PTO][SA] - \frac{k_1}{K_1}[B - PTO] \times \frac{[T - SA][W]}{[T - SA] + [B - SA]}$
$(T - PTO) + (T - FDCA) \Leftrightarrow (B - PTO) + (B - FDCA) + W$	$R_4 = k_2[T - PTO][T - PTO] - \frac{k_1}{K_1}[B - PTO] \times \frac{[B - FDCA][W]}{[T - FDCA] + [B - FDCA]}$
$(T - PTO) + (T - SA) \Leftrightarrow (B - PTO) + (B - SA) + W$	$R_{4SA} = k_2[T - PTO][T - PTO] - \frac{k_1}{K_1}[B - PTO] \times \frac{[B - SA][W]}{[T - SA] + [B - SA]}$

[a] R_{iSA} refers to the corresponding reaction rates of the reactions with succinic acid.

Table 35. Ester interchange reactions

Stoichiometry	Reaction Rate
$PTO + (T-FDCA) + (B-PTO) \Leftrightarrow (T-PTO) + (T-FDCA) + (T-PTO)$	$R_5 = 2k_3[PTO][B-PTO] \times \frac{[T-FDCA]}{[T-FDCA]+[B-FDCA]} - \frac{k_3}{K_3}[T-PTO][T-PTO] \times \frac{[T-FDCA]}{[T-FDCA]+[B-FDCA]}$
$PTO + (T-SA) + (B-PTO) \Leftrightarrow (T-PTO) + (T-SA) + (T-PTO)$	$R_{5SA} = 2[PTO][B-PTO] \times \frac{[T-SA]}{[T-SA]+[B-SA]} - \frac{k_3}{K_3}[T-PTO][T-PTO] \times \frac{[T-SA]}{[T-SA]+[B-SA]}$
$PTO + (B-FDCA) + (B-PTO) \Leftrightarrow (T-PTO) + (B-FDCA) + (T-PTO)$	$R_6 = 2k_3[PTO][B-PTO] \times \frac{[B-FDCA]}{[T-FDCA]+[B-FDCA]} - \frac{k_3}{K_3}[T-PTO][T-PTO] \times \frac{[B-FDCA]}{[T-FDCA]+[B-FDCA]}$
$PTO + (B-SA) + (B-PTO) \Leftrightarrow (T-PTO) + (B-SA) + (T-PTO)$	$R_{6SA} = 2k_3[PTO][B-PTO] \times \frac{[B-SA]}{[T-SA]+[B-SA]} - \frac{k_3}{K_3}[T-PTO][T-PTO] \times \frac{[B-SA]}{[T-SA]+[B-SA]}$

To estimate the reaction coefficients k_i, the models proposed in the literature were fitted to the experimental carboxylic acid data.[299, 333] The predictions of the models were obtained on ordinary differential equations (ODEs) defined by the reaction rate equations implemented in the MATLAB interface. The experimental data were regressed using the weighted-sum-of squares method stated in equation 54 in **Chapter 5**. The state and control variables were defined as well in **Chapter 5**. The algorithms for the simultaneous solution of the corresponding ODE and the non-linear square minimisation for the estimation of the kinetic parameters were introduced in **Figure 57** and **Figure 58**.

Table 36. Mass balances of species present.

Species	Mass Balance
1,5-pentanediol (PTO)	$\frac{d[PTO]}{dt} = -R_1 - R_2 - R_5 - R_6 - R_{1SA} - R_{2SA} - R_{5SA} - R_{6SA}$
2,5-furandicarboxylic acid (FDCA)	$\frac{d[FDCA]}{dt} = -R_1 - R_3$
Succinic acid (SA)	$\frac{d[SA]}{dt} = -R_{1SA} - R_{3SA}$
Water (W)	$\frac{d[W]}{dt} = R_1 + R_2 + R_3 + R_6 + R_{1SA} + R_{2SA} + R_{3SA} + R_{6SA}$
PTO end segment (T-PTO)	$\frac{d[T-PTO]}{dt} = R_1 + R_2 - R_3 - R_4 + 2R_5 + 2R_6 + R_{1SA} + R_{2SA} - R_{3SA} - R_{4SA} + 2R_{5SA} + 2R_{6SA}$
PTO bound segment (B-PTO)	$\frac{d[B-PTO]}{dt} = R_1 - R_2 + R_3 - R_4 + R_{1SA} - R_{2SA} + R_{3SA} - R_{4SA}$
FDCA end segment (T-FDCA)	$\frac{d[T-FDCA]}{dt} = -R_1 - R_5 + R_3 - R_4$
FDCA bound segment (B-FDCA)	$\frac{d[B-FDCA]}{dt} = R_2 + R_4$
SA end segment (T-SA)	$\frac{d[T-SA]}{dt} = -R_{1SA} - R_{5SA} + R_{3SA} - R_{4SA}$
SA bound segment (B-SA)	$\frac{d[B-SA]}{dt} = R_{2SA} + R_{4SA}$

For the esterification reactions, the model developed by Lehtonen, et al.[333] was chosen. This polyesterification model is defined not only in terms of the concentration of carboxylic acid groups, but also considers the presence of more species in the reaction mixture, which are water (C_{H2O}), ester (C_{COOR}), and hydroxyl groups (C_{OH}), allowing to model the evolution of water during the first stage of the reaction (polyesterification). Equation 83 describes the proposed rate equation[333]

$$r = k_o e^{\frac{-E_a}{RT}} \left(C_{COOH} C_{OH} - \frac{C_{COOR} \cdot C_{H_2O}}{K} \right) \quad (83)$$

The concentration of carboxylic acid, water, diol and ester are calculated with equations 84, 85, 86 and 87, respectively

$$\frac{dC_{COOH}}{dt} = r_{COOH} \tag{84}$$

$$\frac{dC_{H_2O}}{dt} = r_{H_2O}; \quad r_{H_2O} = -r_{COOH} \tag{85}$$

$$\frac{dC_{OH}}{dt} = r_{OH}; \quad r_{OH} = r_{COOH} \tag{86}$$

$$\frac{dC_{COOR}}{dt} = r_{COOR}; \quad r_{COOR} = -r_{COOH} \tag{87}$$

With initial values at *t=0*

$$C_{COOH} = C_{COOHo} \tag{88}$$

$$C_{H_2O} = 0 \tag{89}$$

$$C_{OH} = C_{COOHo} + b_0 \tag{90}$$

$$C_{COOR} = 0 \tag{91}$$

Where k_o is the pre-exponential factor in kg·mol^{-1}min^{-1}; E_a is the activation energy in J·mol^{-1}; R is the universal gas constant in J·mol^{-1}K^{-1}; $C_{COOH,}$ C_{OH}, C_{H2O} and C_{COOR} are the concentrations of carboxylic acid, hydroxyl, water and ester, respectively, in mol·kg^{-1}; K is the dimensionless equilibrium constant, and b_0 is the initial excess of hydroxyl group concentration. The parameters estimated were k_o, E_a and K, and implemented in Aspen Plus for the definition of the kinetic network presented in **Table 34** and **Table 35**.

Note that Aspen Plus defines ester interchange reactions as polymerisation reactions. Thus, the overall rate equation considered is the one proposed in Model 2, already presented in **Chapter 5**. This general step-growth polymerisation model reported by Fradet and Marechal[299] incorporates the deviation from stoichiometry of the diol/diacid molar ratio and the change in volume of the reaction mixture due to the loss of water and was proposed for uncatalysed reactions. The model was selected upon the fact that our reaction conditions fall within these specifications and also because it was validated against our experimental data throughout the entire reaction time, as described in **Chapter 5**.

The flowchart in **Figure 83** depicts the procedure followed for the whole reaction kinetics procedure, linking the different aspects involved from the synthesis of the polyesters, the kinetic fitting and parameter estimation in Matlab, and the implementation of the step-growth kinetic mechanism (Equations 59-82) in Aspen Plus.

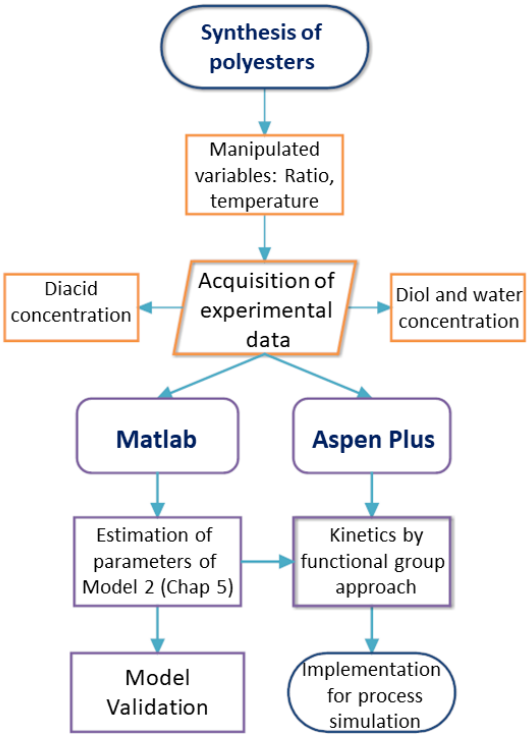

Figure 83. Flowchart of the implementation of the different kinetic mechanisms involved during the polyesterification modelling in Matlab and Aspen Plus.

6.3 Process Simulation and Multiobjective optimisation

The general multiobjective optimisation problem is defined as

$$\min_{x,u} \Psi(x,u) = [\psi_1(x,u), \psi_2(x,u), \dots, \psi_k(x,u)]^T \tag{92}$$

Subject to the mass balance and energy balance given by

$$\frac{dx}{dt} = f(x,u), \tag{93}$$

With the initial conditions: $t = t_0$, $x = x_0$ and the following equality $h(x,u)$ and inequality $g(x,u)$ constraints

$$h(x,u) = 0 \tag{94}$$

$$g(x,u) \leq 0 \tag{95}$$

$$x_{lb} \leq x \leq x_{ub} \tag{96}$$

$$u_{lb} \leq u \leq u_{ub} \tag{97}$$

As stated elsewhere,[217] x is the vector of decision variables $x \in R^n$, u corresponds to the vector of manipulated variables (Temperature and monomer ratio) $u \in R^m$, $\Psi \in E^k$ is a vector of objective functions $\Psi_i(x)$: $\Psi^n \rightarrow \Psi^1$ where n, m, k refer to the number of states or decision variables x, manipulated variables and objective functions, respectively while the equality and inequality constraints are given by $h(x,u)$ and $g(x,u)$ with its corresponding lower (*lb*) and upper (*ub*) bounds. The equality constraints are defined by the thermodynamic equilibrium models that allow the computation of physical and thermodynamic properties, whereas the inequality constrains are bounded by the operation range of the decision variables. The time spam was discretized by a multi-step, predictor/corrector method implemented in Aspen Plus (Runge-Kutta), so a system of algebraic equations is generated from differential equations.

Because of the multiobjective nature of the optimisation, there is no single solution to the problem, and a set of feasible points must be determined.[216] This is accomplished through the Pareto solution. The Pareto optimality states that any feasible point x^* is said to be Pareto optimal if and only if there exists no other feasible point (x) such that $\Psi_k(x) \leq \Psi_k(x^*)$ and $\psi_i(x) < \psi_i(x^*)$ for at least one function. All the Pareto points lie on a feasible performance space for the objective function, defined as the Pareto frontier. Another important definition is the *utopia point*, which is the interjection of the optimum solutions of certain equation set. The solution of the utopia point (x_i^{up}) is obtained from min $\Psi_k(x)$ subject to $h(x)=0$, $g(x)\leq 0$ and their boundary conditions.[215] The utopia point is unattainable as it lies outside the Pareto frontier, but it is used as a reference point. Within the Pareto frontier, the efficient or compromise solution x^s of the objective function $\Psi_n(x^s)$ is defined as

$$\Psi_n(x^s) = \min_{x,u} \left\{ \sum_{k \in R^n} [\psi_k(x,u) - \psi_k(x^{up},u)]^2 \right\}^{1/2} \tag{98}$$

Recently, Dowling, et al.[345] proposed a variant of a multiobjective optimisation problem by presenting a conditional-value-at-risk (CVaR) framework when dealing with multiple-stakeholder decision making. To assess the stakeholders' satisfaction with a decision and how the stakeholders reflect the overall population's opinions, the authors proposed a

method that weighs each of the stakeholder's preferences and, from them, formulates dissatisfaction functions that account for the deviations from the ideal solution. Following this framework allows situations in which a single stakeholder dictates the solution to be avoided, enabling a solution to be obtained that complies with economic, sustainability, and safety targets. Such an approach would be very convenient when the multiobjective optimisation of the full production process of biomass derivatives is undertaken.

To solve the MOO problem, the ε-constraint method was used, an *a posteriori* MOO method in which one of the objective functions is optimised while the other is considered as a constraint.[341] The decision was made upon the facile implementation of the ε-constraint method in Aspen Plus, whereas other methods, such as NBI (Normal Boundary Intersection) require more evaluations to find the optimum solutions during the construction of the Pareto frontier.

The problem is then defined as

$$\min_x \psi_1 \tag{99}$$

Subject to

$$g \leq 0; h = 0 \tag{100}$$

$$\psi_2 \leq \varepsilon \tag{101}$$

Where ε defines the values along the Pareto frontier in the range

$$\min \psi_2 \leq \varepsilon \leq \max \psi_2 \tag{102}$$

The two objective functions considered for the biomass derived polyesterification in a batch process refer to both the polymer quality and the costs of production, as defined by the expressions

$$\max(DP_n) \tag{103}$$

$$\min(Q) \tag{104}$$

Where DP_n is the number-average degree of polymerisation and Q is the heat duty in kBTU·h^{-1}. DP_n is calculated from the ratio of the first and zeroth moments of the chain length distribution

$$DP_n = \frac{\lambda_1}{\lambda_0} \tag{105}$$

whereas Q accounts for the contribution of the heat (ΔH_r) of every chemical reaction j with their corresponding reaction rate r_k

$$Q = \Delta H_r \sum r_{j,k} \tag{106}$$

The heat duty was considered as an objective function because energy needs to be managed carefully and intelligently in every process. The heat duty is a direct consequence of the operating temperature, which is manipulated to ensure the required quality of the final polymer. Energy losses could occur by dissipation or leaks, and such losses might translate into higher residence times, which could lead to hot spots, gelation, degradation, or undesired side reactions. The total energy of the process can be defined by the simple equation

$$\mathrm{Q}_T = Q_{net} + Q_{losses} \tag{107}$$

In practice, this minimisation of energy losses could be achieved through optimisation strategies applied to the energy use, such as ensuring that the equipment is in good condition, that the pipes are correctly insulated, and that the return of condensates when using direct steam is efficient. The net heat of the process cannot be minimised, however, as it is the energy needed by the reaction to achieve completion. The objective function was not defined in terms of gross profit because of the lack of complete information regarding the costs of the biomass transformation processes for all of the biomonomers considered and of the current commercial production of these types of polyesters. Currently, only succinic acid is commercially produced from biomass, and its synthesis reduces greenhouse-gas emissions by 94% compared to those of petroleum-derived succinic acid.[346] Although carbohydrate based FDCA is not yet produced industrially, plans for an FDCA production facility with an annual capacity of 50000 t·year^{-1} were recently announced.[68]

Even though sustainability indicators were not explicitly used in the objective functions, the parameters of these indicators, such as the CO_2 emission rates, amount of polymer produced, and heat duty, are contained within the objective functions, as they are the monitored response during the optimisation. The diagram in **Figure 84** shows the relationship between these response variables, whose values are used for the calculation of the indicators along with the solution of the optimisation functions.

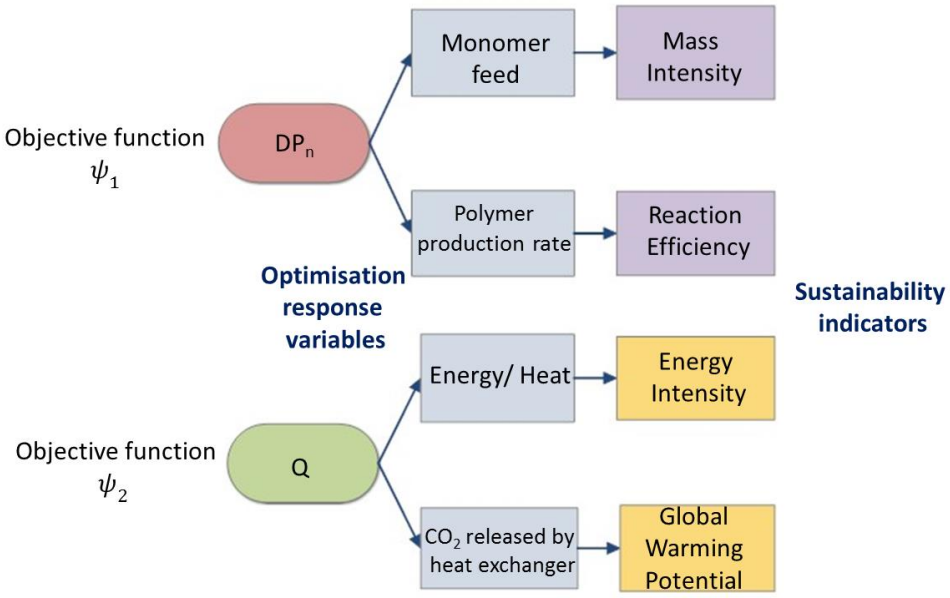

Figure 84. Flowchart depicting the calculation of the sustainability indicator from the optimisation response variables and the objective functions DP_n and Q.

These indicators were calculated during the simulations, enabling an initial evaluation of the degree of sustainability achieved by means of the synthesis stage while ensuring the fulfilment of the required product quality.

6.4 Results and Discussion

6.4.1 Kinetic Modelling

A functional group-approach was developed for the design and simulation of an optimum and sustainable process to produce polyesters from biomass in Aspen Plus, considering a step-growth kinetic model. This model relies on the end-group analysis presented in **6.2**, providing information in terms of the number-average molecular weight, M_n, and the number-average degree of polymerisation, DP_n. Aspen Plus is unable to calculate weight-average molecular weight (M_w) and, thus, the dispersities of the studied systems. Therefore, the results solely refer to the number-average polymer attributes. We considered a production rate of 40 t·day^{-1} as the base case of the batch process. Low-capacity plants are convenient in terms of minimisation of risk, safety hazards and waste generated, and would be preferred as the biomass-polyesters presented herein are in an industrial introduction stage. The monomers, namely, PTO/PDO, FDCA, and SA, were fed at 25 °C at the molar ratios specified in **Chapters 3** and **4**. The initial estimates for the operating conditions were a processing temperature of 220 °C and a residence time of 8 h.

The differential equations in Aspen Plus were solved by a Runge-Kutta multi-step method, whereas the solutions of the algebraic equations were obtained using Quasi-Newton methods such as the secant or Broyden methods. Regarding the optimisation, algorithms based on the interior point method (Sequential quadratic programming, SQP) were implemented. For the estimation of the physical and thermodynamic properties, we used the polymer nonrandom two-liquid (PolyNRTL) activity-coefficient method because the system was operating at low pressure with varying copolymer compositions and sizes. This method was coupled with the Van Krevelen[347] and Joback[348] group-contribution methods. The PolyNRTL model was also chosen over other thermodynamic methods because it has been satisfactorily implemented for the modelling of segment-based step-growth polymerisations.[349, 350] The Aspen Plus flowsheet for the batch reactor is shown in **Figure 85**.

The estimation of the kinetic parameters for esterification reactions was carried out using the standard methods embedded in MATLAB (Broyden-Fletcher-Goldfarb-Shannon or DFP, Davidson-Fletcher-Powell) using the model proposed by Lehtonen, et al.,[333] and the values obtained are summarised in **Appendix E**. The sensitivity analysis for these parameters and a general MATLAB code are included in **Appendix E** as well.

As observed in **Figure 86**, the experimental conversion of copolyesters was satisfactorily fitted to the esterification model throughout the entire reaction time, with some outlier points between about 120 and 150 min possibly being due to the change in the configuration setup to azeotropic distillation, as already discussed in **Chapter 5**. Systems rich in FDCA were found to present the lowest initial rates, whereas SA-rich systems had the highest rates; however, all the polyesters reached a carboxylic acid conversion of 90% or above. This trend was also observed for the kinetic modelling presented in **Chapter 5**. Representative simulated concentration profiles of water and diol using the model proposed by Lehtonen et al.[333] are depicted in **Figure 87**. The kinetic fitting and estimated parameters of the nonstoichiometric model (Model 2) were given in **Chapter 5**.

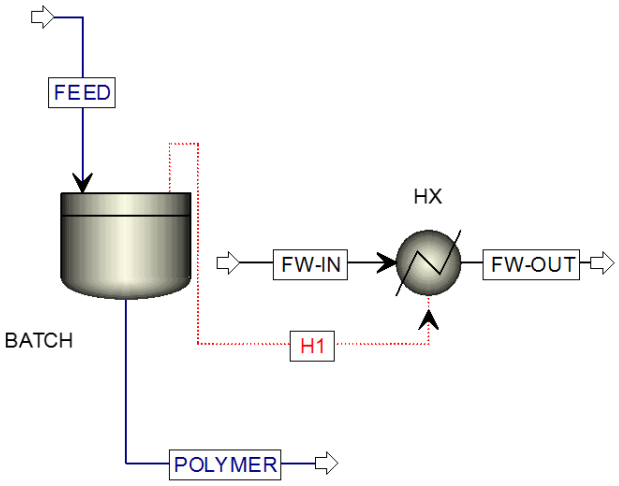

Figure 85. Aspen Plus flowsheet for the batch polyesterification process showing the batch reactor and heat exchanger (HX).

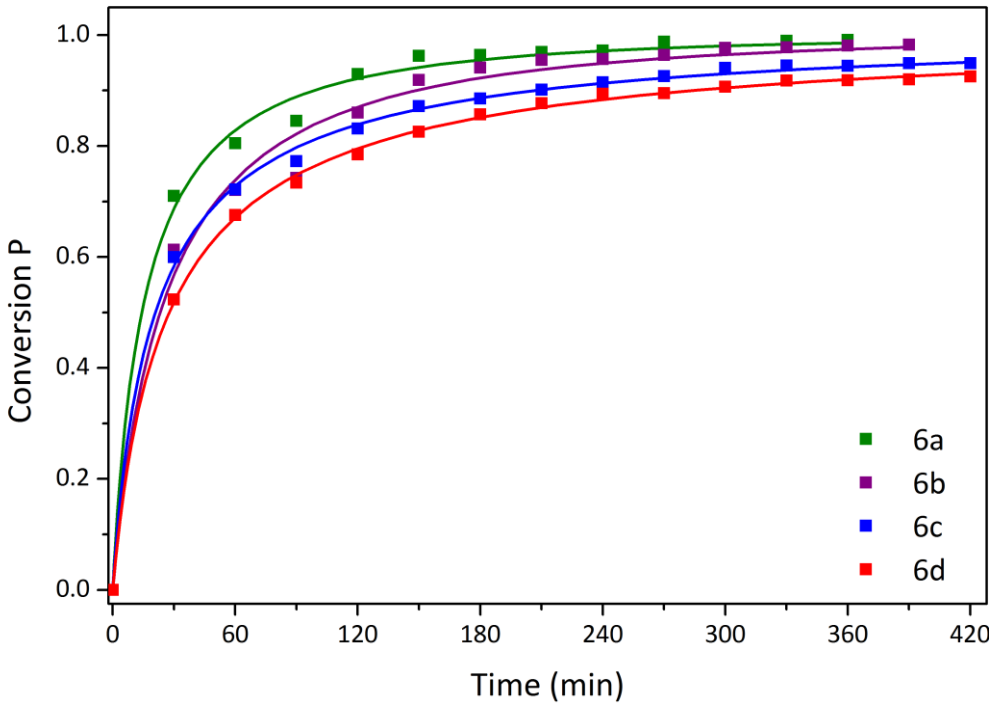

Figure 86. Conversion of COOH groups versus time for the PPeFS copolyesters (**6**), fitted to the polyesterification model. Symbols, experimental data; lines, model estimations.

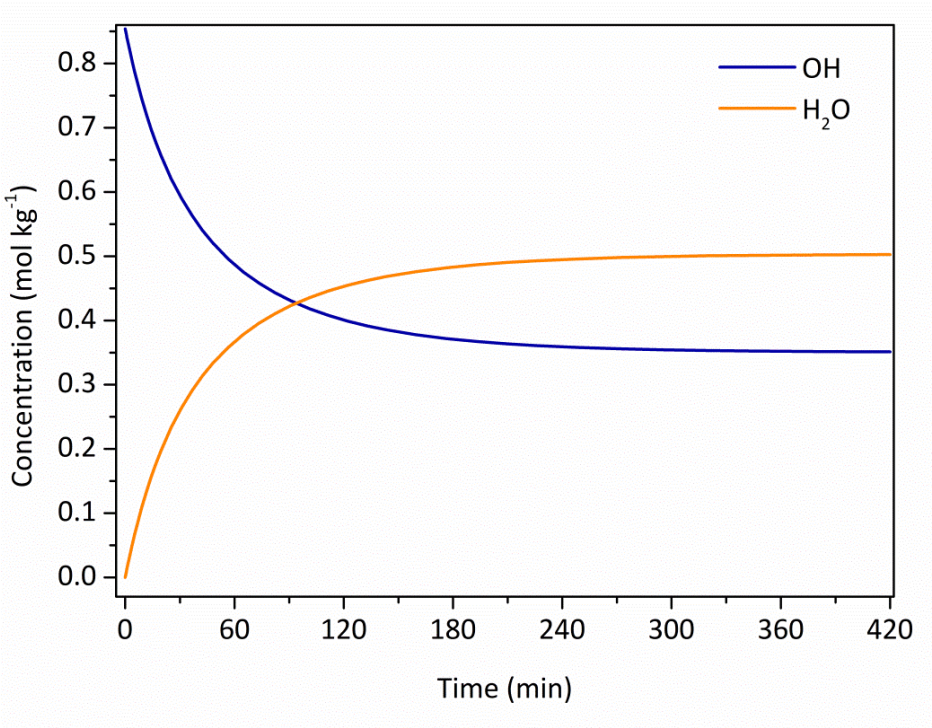

Figure 87. Simulated concentration profiles of hydroxyl groups (OH) and water for $PPeF_{85}S_{15}$ (**6d**).

6.4.2 Simulation and Optimisation

The batch simulations and ε-constraint optimisations performed in Aspen Plus for the different polyesters provided the optimum operating conditions and the results of the mass balances for each of the monomers, segment concentration profiles, energy balances, and polymer attributes such as number-average molecular weight M_n and DP_n. These attributes were chosen because of the strong relationship between polymer structure and final polymer properties. Many of these properties increase with molecular weight, before reaching an asymptotic value. If the molecular weight and degree of polymerisation were too low, the material would have oligomeric nature, and therefore, the final properties would probably not be suitable for the intended application. However, if the M_n and DP_n values were above the upper limits, this would lead to a situation in which processability issues would be inevitable and the safety of the process would be put at risk.[177] The intended application for the polyesters synthesised in this work is coil coatings. The molecular weights of most polyesters used in coatings range between 2 and 6 kDa.[175, 257]

In the case of PPF (**2**), the simulation was not successful and therefore the optimisation could not be performed. The simulation overestimated the molecular weight of the polyester

and predicted a fast reaction rate, which our experimental experience proved wrong. PPF is a highly viscous system where the probability of effective collisions between reactants is diminished and the reaction takes longer. The results are therefore not included because they lacked physical meaning, and detailed modelling is needed in order to correct the simulation. It is believed that this problem could be overcome by adding a mass transfer subroutine within the Aspen Plus environment that would enable modelling mass-transfer-limited reactors.[192] In order to determine if the polymerisation process is either reaction or diffusion limited, dimensionless numbers need to be calculated, such as the Damköhler number, which relate the reaction rate to the mass transport phenomena rate. The Damköhler number (Da) is defined as[209]

$$Da = \frac{kR}{D_i} \tag{108}$$

Where k is the reaction rate constant, R is the outside ratio of a solid particle and D is the diffusivity of species i in the polymer, evaluated in the interphase. This analysis however is part of the future work of the project, after the validation of the experimental data and operation conditions. **Table 37** summarises the results of the optimisation of polyesters with 1,5-pentanediol, indicating the efficient or compromise solutions. The Pareto frontiers for PPeS, $PPeF_{15}S_{85}$, $PPeF_{85}S_{15}$, and PET are depicted in **Figure 88**. The efficient solution refers to the balance achieved between the opposing objective functions. It is defined as the minimisation of the distance (2-norm) between the potential optimal point and a utopia point.[216] All of the optimum process temperatures of the polyesters were in the range of 190−220°C, which corresponds to our previous experimental experience.

The optimisation suggests that the lowest processing temperature of 191 °C is sufficient for PPeS and PPS, which is expected because SA does not lead to gelation or poor solubility as in the case of FDCA. All of the process temperatures for the furan polyesters were found to be above 210 °C, whereas PET was found to be processed well above that range, at 269 °C, which falls within the operating conditions found in the literature.[192, 288]

Table 37. ε-Constraint Optimisation Results for the Batch Syntheses of **4-6** and PET

Polyester	Temperature, °C	M_n, Da	DP_n	Polymer produced,[a] kg·hr^{-1}	Heat Duty, [a] kBTU·hr^{-1}
PPeS (4)	191	4200	45	1401	2114
PPeF$_{15}$S$_{85}$ (6a)	213	4100	43	1407	2082
PPeF$_{30}$S$_{70}$ (6b)	217	4200	43	1414	1217
PPeF$_{70}$S$_{30}$ (6c)	216	4500	42	1429	2098
PPeF$_{85}$S$_{15}$ (6d)	217	4200	42	1401	2114
PPeF (5)	210	4700	42	1305	1012
PET	269	3600	38	1276	2267

[a] Refers to the flow during the residence time of 8 h, by considering the amount of polymer and the initial monomer load per batch.

The simulated final production of polymer in each case was between 1300 and 1430 kg·h^{-1}, with M_n and DP_n values of about 4000 Da and 40, respectively. The polymeric attributes for PET were lower, with a final M_n value of 3600 Da and a degree of polymerisation of 38. In terms of heat duty, PET exhibited a slightly higher energy consumption (2.2 kBTU·h^{-1}) than our biomass-derived polyesters with 1,5-pentanediol shown in **Table 37** (1.0−2.1 kBTU·h^{-1}), which was further analysed in terms of sustainability indicators, as reported in the next section.

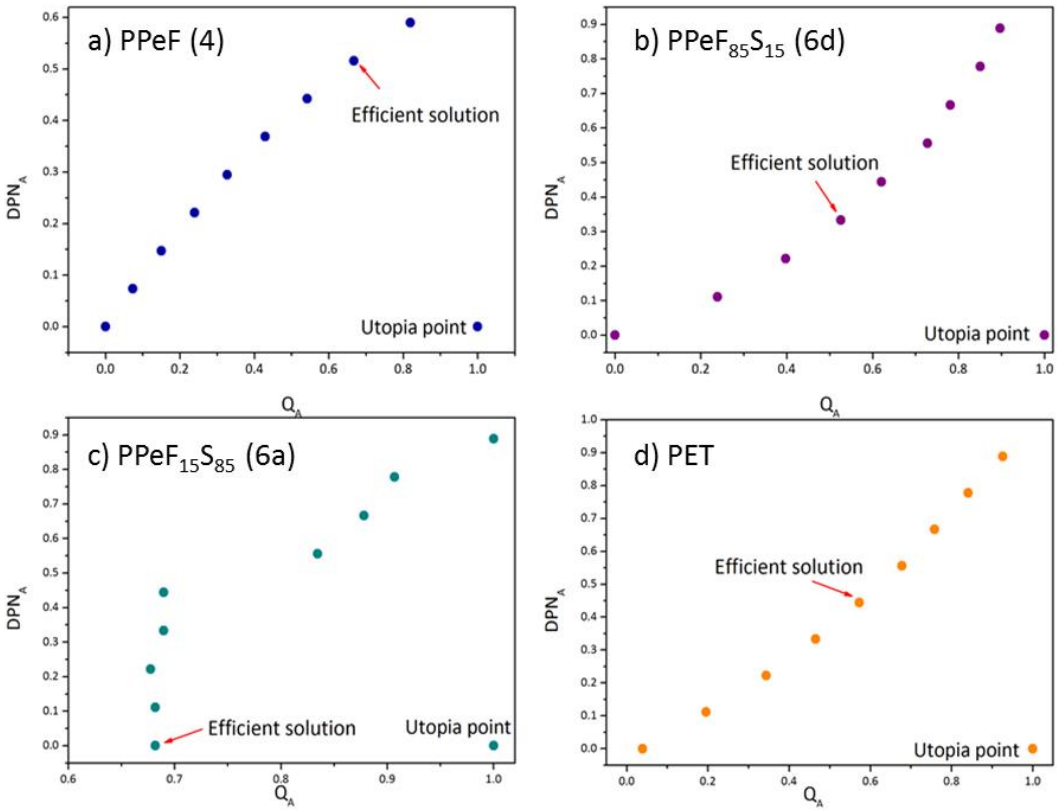

Figure 88. Pareto frontiers and utopia points of a) PPeS, b) $PPeF_{85}S_{15}$, c) $PPeF_{15}S_{85}$ and d) PET. The objective functions are in dimensionless form (DP_{nA} and Q_A).

It is noted that multiplicity behaviour could be found in the polymerisation reactors, because of the high nonlinearity of the system, which represents the different dynamic trajectories during the system operation, and results in a succession of stationary states. In the present case, the temperature, as the manipulated variable, enables these different trajectories, transforming the stationary optimisation problem into a dynamic problem as a function of temperature. Multiplicity behaviour is evident in the Pareto plot for $PPeF_{15}S_{85}$ (**6a**) in **Figure 88c**. In the interval between 0.70 and 0.85 the operation points are unstable (i.e., positive real integers of the Jacobian matrix) and are therefore not found by the process simulator. These solutions could be found by using bifurcation analysis via continuation methods.[351] The efficient solution was found to be a local solution because it fulfilled optimality requirements in a multisteady-state system. If the aim was finding other solutions, the initial estimates should be different from the original ones. Moreover, no global optimum solutions were determined as no global optimisation algorithms were implemented during the optimisation.

Unfortunately, regarding 1,3-propanediol-based polyesters, only bio-derived $PPF_{30}PS_{70}$ (**3b**) and $PPF_{85}PS_{15}$ (**3d**) had lower heat duties than petro-derived PET, as summarised in **Table 38**. The simulation suggested than processing the remaining polyesters would consume between 2302 and 2385 $kBTU \cdot h^{-1}$, that represents an increase of 1.5%-5% in energy consumption, compared to PET. In this case, however, it is very convenient to do an extended simulation including more process equipment than the reactor itself, as bio-derived 1,3-propanediol is currently commercially available, and therefore, the energy savings and sustainability advantages might be evident by performing a thorough supply-processing-usage life cycle analysis. **Figure 89** shows the Pareto frontier for PPS (**1**) and $PPF_{30}PS_{70}$ (**3b**) is depicted in **Figure 90**.

Table 38. ε-Constraint Optimisation Results for the Batch Syntheses of **1, 3** and PET

Polyester	Temperature, °C	M_n, Da	DPN	Polymer produced, $kg \cdot hr^{-1}$	Heat Duty, $kBTU \cdot hr^{-1}$
PPS (1)	191	4184	43	1363	2333
$PPF_{15}PS_{85}$ (3a)	212	4177	43	1401	2113
$PPF_{30}PS_{70}$ (3b)	218.5	3609	43	1378	2385
$PPF_{70}PS_{30}$ (3c)	220	3943	43	1398	2302
$PPF_{85}PS_{15}$ (3d)	215	4022	42	1405	2248
PET	269	3600	38	1276	2267

Further analysis of this matter would be required to establish the effects of the operating conditions in multiplicity regions, but such an analysis falls out the scope of the present work. Research on multiplicity regions has been carried out for a continuous reactor for the polymerisation of methyl methacrylate.[352]

The Pareto frontiers presented herein report the trajectories of Q and DP_n in terms of the process temperature and the monomers ratio. The response variables Q and DP_n are presented in dimensionless form so they are comparable as their magnitudes are different. The dimensionalisation was done by identifying the maximum and minimum values of each variable within the operation domain, as defined in equation 109 for dimensionless DP_n, DP_{nA}

$$DP_{nA} = \frac{DP_{nmax} - DP_{ni}}{DP_{nmax} - DP_{nmin}} \tag{109}$$

Where DP_{nmax} and DP_{nmin} are the maximum and minimum values, respectively and DP_{ni} refers to the value at any point *i* along the Pareto frontier.

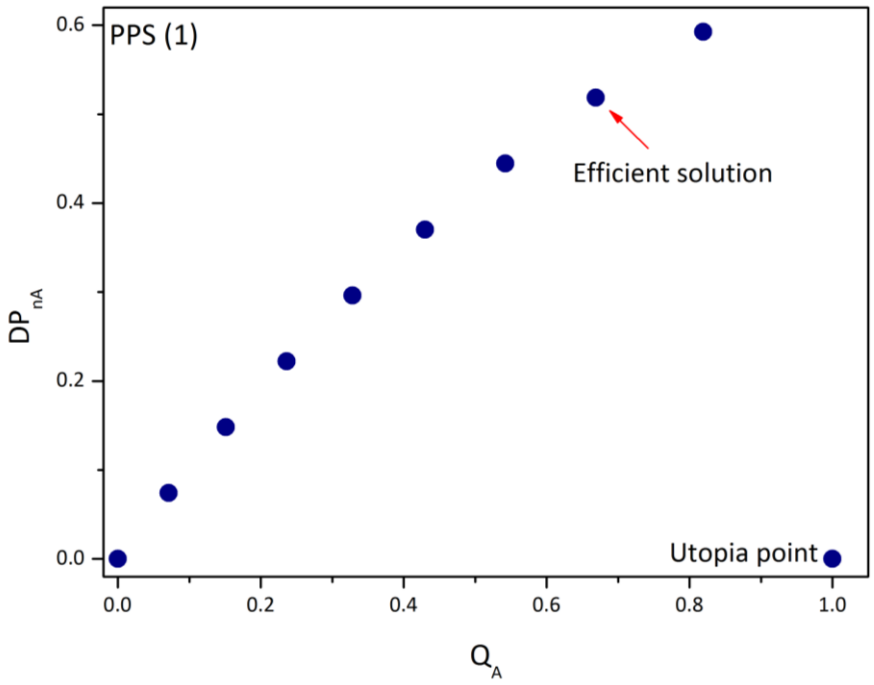

Figure 89. Pareto frontier and utopia point of PPS. The objective functions are in dimensionless form (DP_{nA} and Q_A).

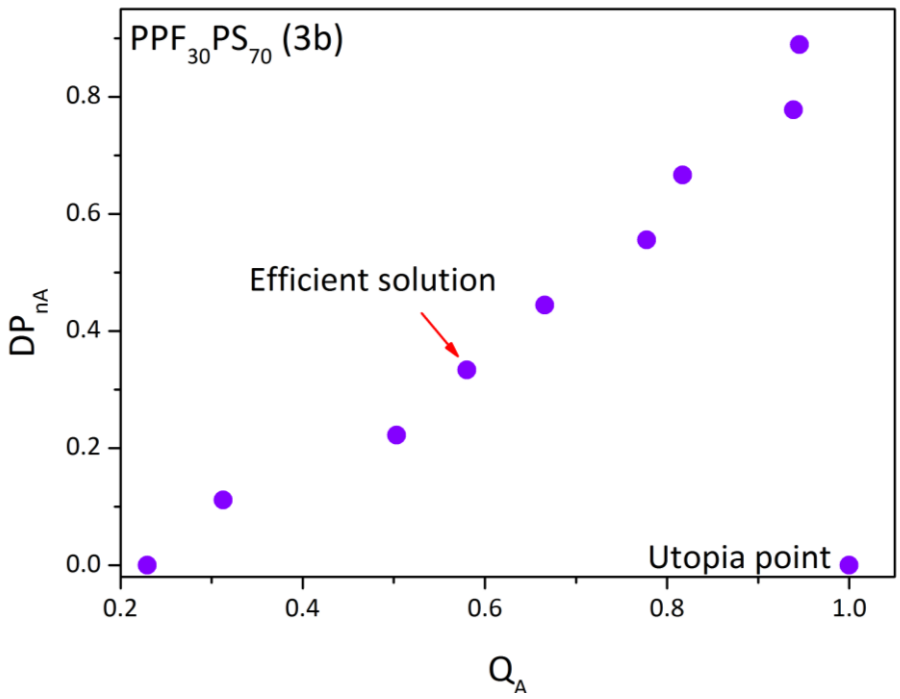

Figure 90. Pareto frontier and utopia point of $PPF_{30}PS_{70}$. The objective functions are in dimensionless form (DP_{nA} and Q_A).

The simulation provided the molar flows of the bound and end segments of the polymers. These flows refer to the rate of production within each batch operation. The profiles for each segment, for $PPeF_{70}S_{30}$ (**6c**) and $PPF_{15}PS_{85}$ (**3a**) are shown in **Figure 91** and **Figure 92**. The profiles of the degree of polymerisation DP_n and number molecular weight M_n for $PPeF_{30}S_{70}$ (**6b**) and $PPeF_{85}S_{15}$ **6d**) are depicted in **Figure 93** and **Figure 94**.

The concentrations of all oligomeric segments increased rapidly, but after 1 hour, the concentration decreased for the terminal segments. This led to a considerably greater amount of bound segments and, therefore, chain growth, to finally reach a constant profile. Similar profiles were obtained for the segment-based kinetic approach used in the polyesterification of succinic acid with propylene glycol.[311] The higher concentrations of segments of both FDCA and SA align with the particular concentration of diacids in each copolyester, as expected. The complete set of Pareto curves and profiles of the segments of the remaining polyesters is available in **Appendix E**.

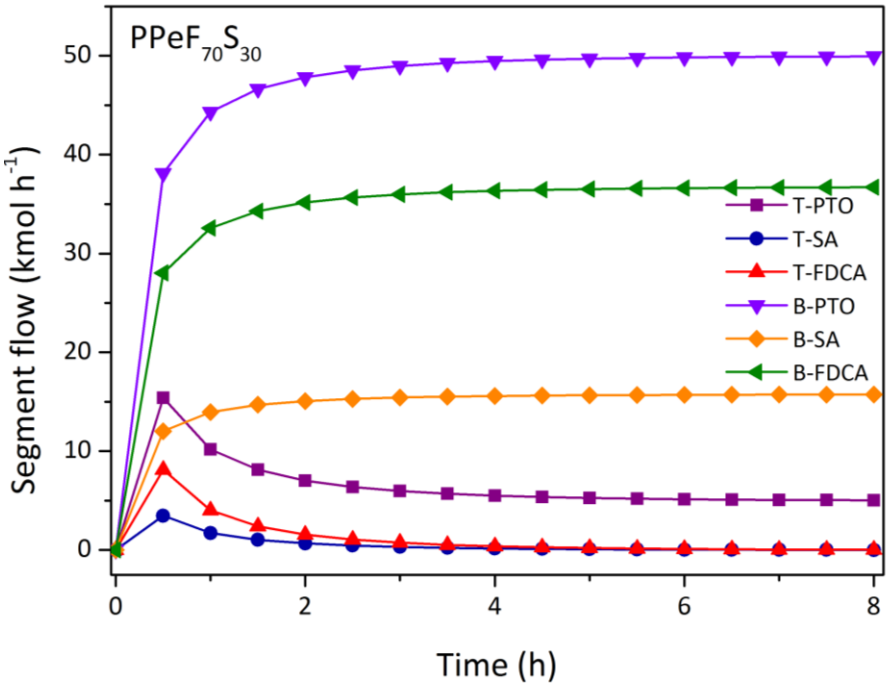

Figure 91. Segment flow for $PPeF_{70}S_{30}$ (**6c**).

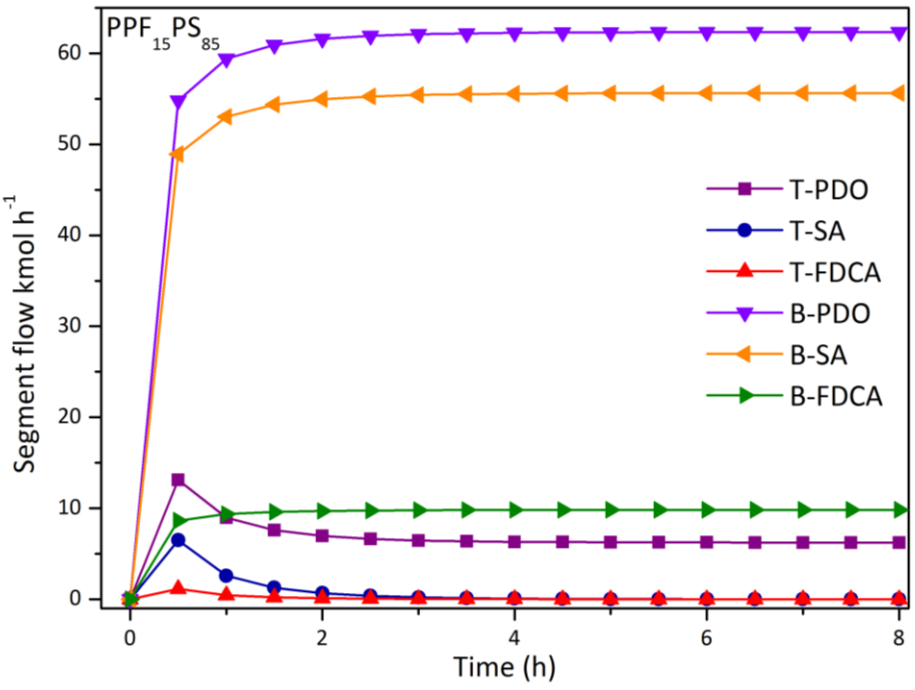

Figure 92. Segment flow for $PPF_{15}PS_{85}$ (**3a**).

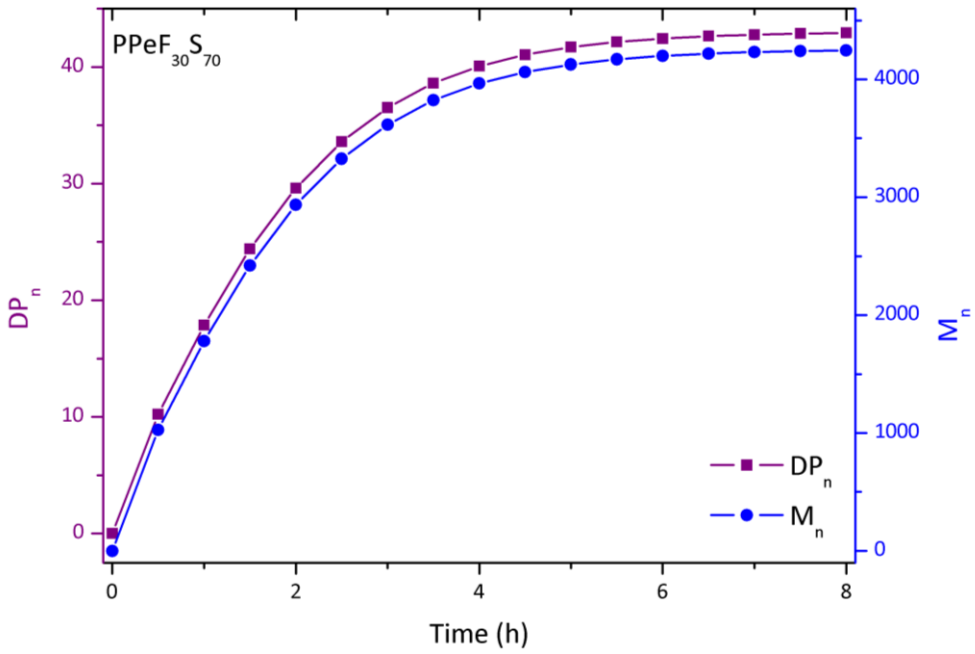

Figure 93. DP_n and M_n profiles for $PPeF_{30}S_{70}$ (**6b**).

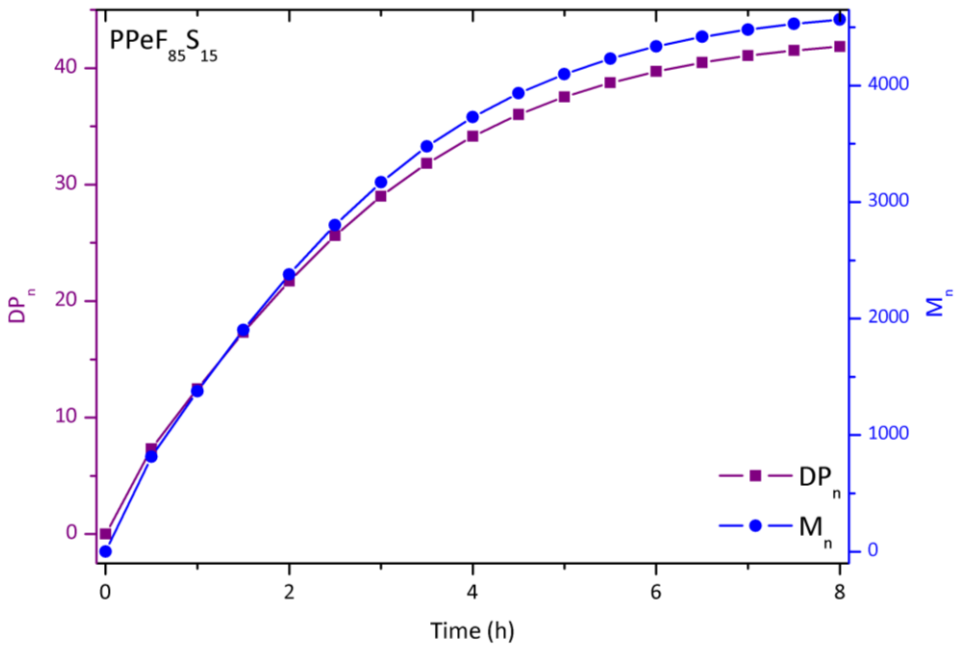

Figure 94. DP_n and M_n profiles for $PPeF_{85}S_{15}$ (**6d**).

6.4.3 Sustainability Indicators

Today, process simulations must include a sustainability approach intended to minimise the mass and energy demands and environmental impacts.[353] Biomass-derived process

assessments must include sustainability metrics along with techno-economic measures, useful for decision making in biorefinery planning and design.[354]

The simulations were thus assessed according to environmental, energy, and economic quantities in terms of common sustainability indicators for chemical processes.[353] The four indicators considered for each batch polyesterifications are gathered in **Table 39**. The global warming potential (GWP) refers to the CO_2 equivalents released by the auxiliary services used by the heat exchanger in **Figure 85**. The energy intensity is expressed as kBTU per unit output. It is a measure of the net fuel-energy consumed to provide the heat and power requirements for the process. Energy inputs to the process include natural gas, fuel oil, steam and electricity.[355] The reaction mass efficiency (RME) is defined as the ratio of mass of targeted product to the sum of masses of all reactants.[356] These quantities are listed in **Appendix E**.

Table 39. Sustainability Indicators Considered for the Batch Polyesterification Process[353]

Indicator	Formula	Units	Best target	Worst case
Global warming potential (GWP)[355, 357]	$GWP = \frac{Total\ mass\ of\ CO_2\ equivalents}{Mass\ of\ product}$	kg·kg^{-1}	0	All GWP is released.
Specific energy intensity (R_{SEI})[355, 357]	$R_{SEI} = \frac{Net\ energy\ used\ as\ primary\ fuel\ equivalent}{Mass\ of\ product}$	kBTU·kg^{-1}	0	1.847×10^3 kBTU·kg^{-1}
Reaction mass efficiency[356]	$RME = \frac{Mass\ of\ product}{Total\ mass\ reagents}$	kg·kg^{-1}	1	0
Mass intensity[355, 357]	$MI = \frac{1}{RME}$	kg·kg^{-1}	1	40[358]

The estimation of the sustainability indicators after the optimisation was done considering natural gas and lignite coal as base fuels under the U.S. Environmental Protection Agency (EPA) rule E9-5711. The results for polyesters based on 1,5-pentanediol are summarised in **Table 40**, including the normalised results, so the quantities are easily

comparable. The results for 1,3-propanediol can be found in **Appendix E**. The normalisation was done within each indicator following the expression below

$$z_i = \frac{x_i - \min(x)}{\max(x) - \min(x)} \tag{110}$$

Where $x=(x_i,\ldots,x_n)$ and z_i is the normalised data.

Table 40. Sustainability Indicators Estimated for the Different Polyesters based on 1,5-pentanediol

						Normalised Results				
Polyester	$GWP_{natural\ gas}$ $kg \cdot kg^{-1}$	GWP_{coal} $kg \cdot kg^{-1}$	R_{SEI} $kBTU \cdot kg^{-1}$	RME $kg \cdot kg^{-1}$	MI $kg \cdot kg^{-1}$	$GWP_{natural\ gas}$	GWP_{coal}	R_{SEI}	RME	MI
PPeS	0.10	0.19	1.51	0.84	1.19	0.73	0.19	0.73	0	1.00
$PPeF_{15}S_{85}$	0.09	0.20	1.48	0.84	1.18	0.48	0.21	0.70	0.16	0.84
$PPeF_{30}S_{70}$	0.06	0.11	0.86	0.85	1.18	0.08	0.02	0.08	0.32	0.67
$PPeF_{70}S_{30}$	0.10	0.56	1.47	0.86	1.17	0.69	1.00	0.69	0.72	0.27
$PPeF_{85}S_{15}$	0.09	0.18	1.45	0.86	1.16	0.68	0.18	0.68	0.86	0.13
PPeF	0.05	0.09	0.78	0.86	1.16	0	0	0	1.00	0
PET	0.12	0.22	1.78	0.84	1.18	1.00	0.27	1.00	0.14	0.85

The results in **Table 40** suggest that the productions of PPeF and $PPeF_{30}S_{70}$ release less CO_2, as their GWPs are 0.05 and 0.06 kg $CO_2 \cdot kg_{polymer}^{-1}$, respectively, as well as the lowest specific energy intensities (0.78 and 0.86 $kBTU \cdot kg^{-1}$). The value of the GWP indicator for PPeF represents a reduction of 60% with respect to PET. Also, the efficiency of the polyesterification processes, evaluated in terms of the RME and MI indicators, was found to be satisfactory, because the relationship between the raw materials and the amount of polymer produced was close to the best target of 1 for all of the systems. In comparison, the continuous production of the common ester ethyl acetate was reported to have MI and R_{SEI} values of 1.58 $kg_{input} \cdot kg_{polymer}^{-1}$ and 2.17 $kJ \cdot kg_{polymer}^{-1}$, respectively, although the residence time was 200 min at 80 °C.[359] The production of PET presented the highest energy consumption and CO_2 release among all of the polymers studied, suggesting that our polyesters would provide sustainable and efficient alternatives to conventional PET for the intended applications. Also, comparing the two fossil fuels, there is a considerable difference

between natural gas and coal in terms of CO_2 equivalents, especially in the syntheses of $PPeF_{15}S_{85}$ and $PPeF_{70}S_{30}$.

Since the present comparison refers to production only, a complete life-cycle analysis (LCA) should be performed to obtain a complete cradle-to-grave assessment of the polymerisations.[360] Ideally, an LCA analysis should be complemented with other set of sustainability metrics, for instance, the evaluation of the E factor, which is defined as the actual amount of waste produced in a process.[361] E factors, along with atom economy, are useful tools for assessing the environmental footprint of complete manufacturing processes.[361] The atom economy is calculated by dividing the molecular weight of the desired product by the total of the molecular weights of the reagents used in the stoichiometric reaction, and provides a rough estimate of the efficiency of the studied process.[362] If no by-product is formed, the atom economy is 100%.[362] More complementary information could be included to promote a thorough decision making toward de design and operation of a polymerisation system. These additional data could be, but is not limited to, waste streams, land use, health hazard potential, carcinogens, waste management effect and sources of emissions (Vent, storage and fugitive emissions).[363] The inclusion of life cycle inventories of waste or left monomer, along with these different sources of emissions would certainly shift the results presented in **Table 40**.

Additionally, economic criteria should be considered so the process is competitive against petrochemical counterparts. For example, Martínez-Hernández, et al[354] developed a biorefinery systems analysis tool that combines the concepts of economic value and environmental impact analysis, which determine whether a bioderived-process is more sustainable than a fossil-based one. The authors validated the model by considering a biorefinery which produced bioethanol as case study, in order to determine the sustainability associated with the production of this biofuel. It was found that GHG emissions savings for bioethanol with respect to gasoline was 31%.[354]

Our results however provide interesting insight into a potential opportunity for these biomass-derived polyesters to be used at the industrial scale. In general, all of the polyesterifications hit the best target of each indicator. The combination of such indicators provides an initial evaluation of the design of sustainable processes and also the improvement of existing ones as assessments can be performed to determine the influence of green engineering principles for initial implementation stages or varying process configurations.

6.4 Conclusions

Kinetic modelling, process simulation, and optimisation were successfully implemented in Aspen Plus and Matlab for the polyesterifications of the biomass-derived monomers 2,5-furandicarboxylic acid, succinic acid, and either 1,5-pentanediol or 1,3-propanediol. The kinetic parameters were estimated for each polyester system by fitting the experimental batch data to a polyesterification model proposed in the literature and regressing the data using the weighted-sum-of-squares method. The kinetic model proposed was based on the functional-group approach by defining the main species involved in the polyesterification along with bound and terminal segments of each monomer. Aspen Plus generated 12 reactions for the polyesters and 24 for the polyesters with both FDCA and SA, which were classified either in esterification or ester interchange-type reactions.

The a posteriori optimisation ε-constraint method was applied to determine the utopia points and compromise solutions of all the systems. The model was chosen because its implementation in Aspen Plus is straightforward and does not require many evaluations as other optimisation methods.

The optimum process temperatures were found to be in the range of 190−220 °C, whereas the processing temperature for PET was found to be 269 °C. The values of the number-average molecular weight (M_n) and degree of polymerisation (DP_n) for the polyesters were in the ranges of 4.1−4.7 kDa and 42−45, respectively, with a final production of about 1400 $kg_{polymer} \cdot h^{-1}$. The best bioderived polyesters in terms of molecular weight and low heat duty are PPeF and PPFPS with Mn of 4700 and 4177 Da and heat duty of 1012 and 2113 $kBTU \cdot h^{-1}$, respectively.

The sustainability impact of the processes was addressed by means of sustainability performance indicators, providing information on energy consumption, CO_2 equivalents released, and efficiency in terms of the relationship between the mass input and the final product. The productions of the polyfuranoates and succinates achieved better targets and slightly higher final polymer attributes when compared to the production of PET, which had a M_n value of 3.6 kDa and a DP_n of 38. It is important to observe that the range obtained for the polyesters is within the desired range for application as coil coatings, without resulting in practical problems because of an excessive system viscosity. The inclusion of other material and energy streams in the system, along with a breakdown of the different emissions released

during the process could switch the sustainability indicators presented; therefore, a thorough life cycle analysis is recommended as the next stage of the simulation work.

The present process engineering study of this biomass-derived family of polyfuranoates and polysuccinates provides an insightful and useful resource for further polymerisation process design and implementation stages. Multiobjective optimisations of the different production stages, including separation, purification, and compounding, are required to develop a full optimisation of the manufacturing process of biomass-derived polyesters. The evaluation of different reactor configurations is analysed in **Chapter 7**.

CHAPTER 7

Process Intensification of the Synthesis of Biomass-Derived Renewable Polyesters: Reactive Distillation and Divided Wall Column Polyesterification

7. Process Intensification of the Synthesis of Biomass-Derived Renewable Polyesters: Reactive Distillation and Divided Wall Column Polyesterification

This chapter describes the process simulation and multiobjective optimisation of a plug flow reactor (PFR), followed by the implementation of process intensification principles by performing the polyesterification in reactive distillation (RD) and a divided wall column (DW) configuration.

We have recently published the process intensification of 1,5-pentanediol polyesters;[151] hereby, the results and discussion presented in this chapter refer to that publication. The general results on 1,3-propanediol polyesters are available in **Appendix F**.

7.1 Introduction

The use of biomass as a potential feedstock for fine chemicals, pharmaceuticals, and polymers continues to grow as both industry and academia strive to tackle the effects of pollution on climate change as a result of the continued use of non-renewable petrochemical sources. Recent research in the field of bioderived monomers for polymers has resulted in significant developments. To date, several polyesters based on biomass-derived monomers have been synthesised intended for a wide variety of applications such as coatings, binders, plasticizers, films, and engineering thermoplastics.[21, 23]

Ideally, the valorisation of biomass should be performed in a sustainable manner under mild conditions using benign solvents while minimising energy consumption and the use of auxiliary services.[364] As a consequence of the chemical industry's continuous development of more energy and cost efficient processes, the concept of process intensification and its application has emerged as an entire discipline across process engineering. Key competitive factors such as process flexibility, energy reduction, end product quality, and operations' safety are enhanced by this methodology.[365, 366] In particular, energy efficiency is fundamental to tackling the climate change and carbon-dependency problems by the implementation of strategies that accelerate transport phenomena in processing fluids in common unit operations.[366]

Within these operations, a perfect example of successful process intensification is the simultaneous physical separation of components with a chemical reaction, which is achieved

through reactive distillation (RD). Reactive distillation is a process where fractional distillation is accompanied by a chemical reaction on some or all of the trays in a column[367] and is therefore considered a single operation vessel.[365] The main objective is thus to remove the products from the reactants by distillation, where the products can be considered either the light or heavy components.[365, 368] By using RD, conversion limitations are diminished in equilibrium-controlled reactions by continuous removal of products from the reaction zone.[369] It is also an interesting alternative not only for equilibrium-limited reactions but also exothermic reactions and poor raw-materials usage.[370] The most important applications of the RD column include: polyesterification, etherification, esterification, hydrolysis, alkylation, isomerisation, and condensation.[365]

Harmsen[371] reviewed the current commercial applications and industrial scale up and operation of RD. These include: the synthesis of ethyl, butyl and methyl acetate; the hydrogenation of aromatics and light sulphur; isobutylene and ethylbenzene production and the fatty acid esters production, as well as a number of other licensed commercial RD scale processes amounting to approximately 200 such processes. Other recognized advantages of RD are reduction of capital cost, as the separation and synthesis stages are embedded in a single one; improved conversion and selectivity as impurities and undesired species are removed; reduced energy requirements and hotspots, removal of azeotropes and efficient heat integration.[366]

As in any process, reactive distillation presents however some limitations and trade-offs. Processing constraints include suitable volatility of reagents and products ($\alpha < 1.06$)[367] to maintain high and low concentrations in the reaction zone, respectively; difficulty to scale up to large flow rates because of liquid distribution problems; residence time requirement, and assuring a common operation range, since the optimum conditions for distillation may differ from the ones needed for reaction.[372, 373]

Hiwale et al.[374] listed some cases where the success of reactive distillation is either selectivity-limited or cost-effective-limited. In the case of selectivity issues, the side-formation of n-butyl ether was observed in the bottom of the column during the esterification of acetic acid with n-butanol, where the expected main product is n-butyl acetate. Nicol[375] compared the synthesis of diacetone alcohol via the aldol condensation of acetone in a conventional multistep process and using reactive distillation. It was highlighted that the main disadvantage of reactive distillation was the high external catalyst-liquid mass transfer

resistance and the dependency of reaction temperature on operating pressure. Moreover, it was found not ideal for catalysts that present fast deactivation, which favours undesired secondary reactions.

In terms of cost limitations, the economic potential of reactive distillation was evaluated in the disproportionation of toluene for the synthesis of xylenes.[376] The author reported a thorough cost analysis of the conventional process over a fixed-bed catalyst against the reactive distillation process. Surprisingly, reactive distillation did not offer substantial benefits, namely because of the high design pressure (30 bar) which translated into a high cost of the reactive distillation column. Considering green chemical engineering principles, such as minimisation of material diversity, durability, and commercial afterlife, Malone, et al.[377] concluded that reactive distillation might not align with some of them as different materials of construction might be needed in certain reactive systems as well as the installation of an active control system.

The main difference between conventional and reactive distillation is that the latter requires specifications for both product compositions and conversions, resulting in a greater number of degrees of freedom: pressure, reactive trays, tray holdup, reflux ratio, location of reactant feed streams, and reboiler heat input, among others. The ideal reactive distillation column is depicted in **Figure 95**.

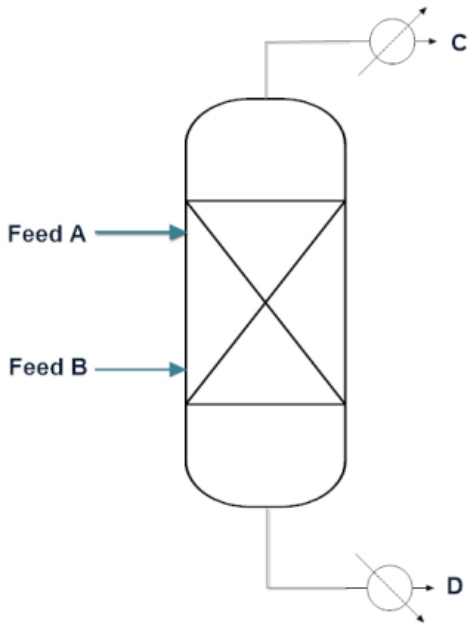

Figure 95. General diagram for a reactive distillation column.

The operational benefits of RD have promoted the development of diverse simulation, design, and modelling work of the process. Pérez-Cisneros and co-workers[378] proposed a systematic method for the design and operation of reactive distillation processes, showing that the existence of multiple solutions is explained by the presence of azeotropes, so the operation will be highly related to the phase diagrams of the system. The simplification of the phase diagrams could be accomplished by the introduction of a new set of composition variables for treating phase equilibria when dealing with multicomponent systems.[379]

Recently, Huang, et al.[380] proposed a classification of reactive distillation columns in terms of the ratio between the heat released by the reaction and the latent heat of the mixture: reactive distillation columns with high thermal effect, where the ratio is below 1; moderate thermal effect ($0.05 < \Delta H_R/\Delta H_V < 1$); and no thermal effect (<0.05). This classification enables specific integrations of internal energy and/or internal mass accordingly, which leads to simplified process design and hence, reduction of capital investment and operation cost.[380] RD columns with high thermal effect could be used for the production of ethylene glycol, which can be produced by the hydration of ethylene oxide in a highly exothermic reaction, with the polymerisation to polyethylene glycol as side reaction. The heat evolved during this type of reactions can be used for distillation, saving the energy required by the reboiler.[381]

Comprehensive reviews on the design and development of models for reactive distillation covering equilibrium and non-equilibrium stage modeling,[372, 382] and also dynamic modeling[373] are available for further reference. Step-growth polymerisation reactions which specifically include polyesterification, have been subject to considerable process analysis and simulation. In this regard, Doherty and Malone[367] developed a model for the synthesis of polyamides by RD, particularly nylon-6,6 where the removal of water and stoichiometric ratio of reactants must be assured to build up the molecular weight of the final product.

Shah and co-workers[383] developed a reactive distillation model in Aspen Custom Modeler which was applied to the polyesterification of maleic anhydride and propylene glycol. The authors reported the operating conditions and final product specifications and later validated the model against pilot scale data with two different configurations: A single RD column and a column coupled with a prereactor, achieving conversions of 37% and 90%, respectively.[384] Moreover, the modelling of the production of poly(ethylene adipate) was carried out considering two bubbling reactive distillation towers.[385] The effect of operating

conditions such as residence time, reaction pressure, feed ratio, and temperature were analysed.

Several more simulation works have been reported for esterification problems. For instance, the process simulation of the esterification of acetic acid using RD has been extensively studied with several alcohols such as methanol,[386, 387] ethanol,[382, 388] and butanol.[389-391] Peng, et al.[392] studied the design and full plant control for the reactive distillation production of n-butyl levulinate. The steady and dynamic states simulation of the esterification of acetic acid with ethylene glycol to produce ethylene glycol diacetate was recently explored.[393] In another design and control coupled work, the synthesis of methyl valerate, a product of the esterification of valeric acid and methanol, was studied using conventional and thermally coupled RD analysing both the steady state and the control structure.[142] The simulation of the esterification of fatty acid and oleic acid with methanol has been considered as well.[394] In this work, a reactive distillation column with a top recycle was chosen since 90% of oleic acid conversion was achieved, higher than other setups. The recycle is done by replacing a total condenser with a partial one, so water is recovered in the bottom instead of being recovered as a top distillate. Furthermore, another interesting RD work highlighted the importance of succinic acid as a biomass-derived high value chemical and its commercial availability as a bioproduct by analysing the esterification of mixtures of succinic acid and acetic acid with ethanol.[395] The authors performed the simulation considering an activity phase model in order to determine the effects of the reflux ratio, column pressure, ethanol, and acid feed location toward optimum operating conditions. Following this study, the same group proposed a similar experimental and simulation approach of the RD esterification solely of succinic acid with ethanol, where it was found that a prereactor is needed in the proposed configuration along with an ethanol stream below the reactive zone of the column to enhance conversion.[396]

As process intensification continues to expand across the chemical industry as a result of the imperative need to diminish energy consumption, another example of thermal efficiency is the divided wall configuration (DW). This configuration is based on the original design of two columns for the separation of multicomponent mixtures proposed by Petlyuk[397] where the vapour and liquid streams leaving the first column are connected to the second one. There are only one main condenser and a reboiler since there is a prefractionator that is thermally coupled to the main column.[397]

A DW column is a reconfiguration of the Petlyuk column as it is designed as a single shell column with a partition that separates the middle section of the column into a feed section and a side draw section which produces a high purity product, hence delivering three high purity products in a single column.[397, 398] **Figure 96** shows the Petlyuk column in an Aspen Plus flowsheet which resembles a DW column as they are thermodynamically equivalent, making the DW setup advantageous due to its single shell design.[397, 398] BASF established the first industrial DW column in 1985,[399] and since then, more than 100 commercial applications have been implemented, with studies reporting both capital cost and energy reductions of 10−30%.[400]

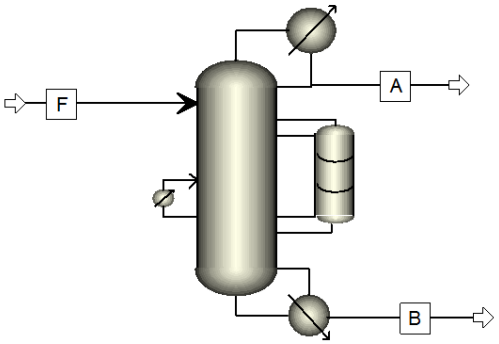

Figure 96. Aspen Plus flowsheet for a Petlyuk column.

Within divided wall column configurations, different designs have been proposed. For instance, the more common variety is where both the feed stream and side draw are located in the middle of the column,[401] and this was originally patented years before the commercialisation of the BASF divided wall column application.[402] Another widely used configuration is the so-called split shell column which can be designed either with a common overhead section and divided bottoms or the other way around.[401] Reviews and illustrations on the design[397-399, 401, 403] and control of DW[397, 398, 403-406] are recommended as excellent references. Moreover, integrative works such as the design procedure and sensitivity analysis based on parameters such as the number of stages, vertical position, and height of the wall with further experimental validation for the separation of a multicomponent alcohol mixture have also been recently reported.[407]

The integration of reactive distillation and divided wall has emerged as a new concept known as reactive divided wall column (R-DWC), representing a combination of a reactor

and a separation unit in one column[401] useful for the separation of components in systems where consecutive and side reactions are observed or excessive reagents are required.[397, 408] The common integrated configuration then includes a condenser, a reboiler, reactive zones, prefractionator, and the main column, all embedded in a single shell.[409, 410]

Theoretical and experimental studies on the design and simulation of reactive divided wall columns have been applied to esterification problems; however, they have not been applied yet to polyesterification reactions. The design and operation of a reactive divided wall column for the esterification of acetic acid with ethanol was reported, being an integrative experimental and theoretical study of R-DWC.[411] The same group further performed the steady and dynamic states simulation for the same reaction system, by using two control loops of temperature.[412] Studying the same esterification reaction, Santaella, et al.[359] reported a sustainability oriented work focused on the performance of several configurations, including reactive distillation and divided wall, in terms of sustainability indicators such as the ones considered in the present chapter. The production of methyl acetate in a R-DWC system, its steady simulation, and dynamic responses along with a parameter sensitivity analysis and economic optimisation have also been recently published, highlighting the expansion reactive divided wall setups have had over the past decade.[413] Similarly, another brand new design and control-oriented study implemented in R-DWC dealt with a widely industrially used ester, n-propyl propionate.[414]

At the current point, despite the varied experimental and theoretical studies of reactive-divided wall columns, no industrial application is available yet.[401]

The other variety of chemical reactor considered in this chapter as the base reactor case is the plug flow reactor (PFR) or tubular reactor, which has been extensively used and its introduction for the development of polyester synthesis occurred between 1950 and 1980,[415] leading to several patented tubular reactor based processes.[416-418] The PFR is generally considered as a cylindrical pipe with turbulent flow, so the concentration does not vary in the radial direction, but only axially.[196] The general mole balance equation for component *i* for a PFR model is given by equation 111

$$\frac{\partial C_i}{\partial t} = -\frac{\partial F_i}{\partial V} + \nu_i(-r_A) \qquad i = A, B, C \ldots Components \tag{111}$$

In our case, the reactants are FDCA, succinic acid, and 1,5-pentanediol and the products are polyester and water.

Considering an operation in steady state, the balance equation is given by the following expression

$$\frac{dF_i}{dV} = \nu_i(-r_A) \tag{112}$$

Where F_i is the molar flow rate of component *i*, *V* is the reactor volume, ν_i is the stoichiometric coefficient of component *i* (positive for products and negative for reactants), and r_A is the reaction rate for limiting reactant *A*.

The modelling and design of plug flow reactors for step-growth polymerisation reactions have been applied for varied configurations: wiped-film reactors[192, 220] and rotating disk finishers[192] where a liquid phase and a well-mixed vapour phase are considered; the lower sections of the industrial Vereinfacht Kontinuierliches Rohr (VK) columns for a single liquid phase[192, 220] and even microwave induced PFR for the esterification of benzoic acid with ethanol.[419] Gupta[220] developed a model for the last vacuum stage of a PET reactor as a wiped film reactor which considers main and side reactions and is validated against industrial data which is also used to tune parameters such as the Flory−Huggins' interaction parameter and equilibrium constants.

The objective of the present chapter is to perform the process simulation, sensitivity analysis, and multiobjective optimisation in Aspen Plus for the step-growth polymerisation of the biomass-derived polyesters described in previous chapters using three different configurations: plug flow reactor (PFR), reactive distillation (RD), and reactive divided wall column (DW). First, the process simulation was carried out after the definition of the kinetic model, which was previously analysed for the batch case in **Chapter 6**.[88] Next, the multiobjective optimisation was performed for the plug flow reactor case whereas a sensitivity analysis was done in the case of RD and DW for the determination of the intermediate temperatures and split fraction that maximised polymer production and promoted a high final product quality. The polymer attributes such as number molecular weight (M_n), degree of polymerisation (DP_n), and species concentration profiles are reported, as well as energy requirements of each reactor and their performance in terms of the sustainability indicators considered in **Chapter 6**.[353] The production of PET is included as the

petrochemical-derived polyester case. The simulation and optimisation proposed are specifically focused on the chemical reactor. A plant simulation of the complete polyesterification should include more process equipment and further stages such as purification and compounding; however, this falls outside the scope of the present work. To the best of our knowledge, this is the first time that a reactive distillation and divided wall process intensification study is reported for a similar library of potentially fully biomass-derived polyesters for coil coating applications.

7.2 Development of the Kinetic Model

The development of the segment approach kinetic model for step-growth polymerisation as proposed by Seavey[192] and the estimation of kinetic parameters using a polyesterification model from the literature[333] have been discussed in our previous batch simulation work[88] presented in **Chapter 6** along with the reaction stoichiometry. This segment approach has been used before for common polyesters such as PET[192, 288, 344] and poly(propylene succinate).[311] The conventional species considered are water, PTO or PDO, SA, and FDCA. The resulting polyesters are made up by different segments terminal (T-) and bound (B-) segments for both diacids and diol.

The structures of the segments involved in the polyesterification are shown in **Scheme 41** in **Chapter 6**. The main reactions considered by the model are thus esterification or water formation and ester interchange with all the species involved. As stated previously[88] and in **Chapter 6**, the following assumptions are made:

1. Equal reactivity hypothesis.[184]
2. The rate coefficients k_i of the conventional species and segments are the same.
3. Reversible reactions are negligible.
4. No mass transfer limitations.

As described in **Chapter 6**, Aspen Plus automatically generates the complete set of reactions which encompasses 12 reactions for PPeF and PPeS polyesters and 24 reactions in the case of PPeFS copolyesters.

The reactions are classified into five groups: (1) Forward water formation with PTO; (2) Forward water formation with the diol terminal segment (T-PTO); (3) Backward water formation; (4) Forward ester interchange; and (5) Reverse ester interchange. **Chapter 6**

includes the complete defined set of reactions as well as the associated stoichiometry rate equations and mass balances.

7.3 Process Simulation, Sensitivity Analysis and Multiobjective Optimisation

The problem analysed considered a daily production of 40 tons, as done with the base batch case in **Chapter 6**.[88] The monomers 1,5-pentanediol, FDCA, and succinic acid are fed at 25 °C. The initial estimates are a processing temperature of 220 °C and a residence time of 8 h, according to our experimental experience. For the estimation of the physical and thermodynamic properties, the polymer non-random liquid (PolyNRTL) activity coefficient method was chosen because the system was operating at low pressure with varying copolymer compositions and sizes.[420] The activity coefficients of this model account for the NRTL contribution and the Flory−Huggins contribution.[192] The PolyNRTL method was coupled with the Van Krevelen[347] and Joback[348] group contribution methods and was selected over other thermodynamic methods because it has been already implemented for the modelling of segment-based step-growth polymerisations.[349, 350]

Table 41 indicates the specification of each unit operation used during the process simulations. **Figures 97-99** show the Aspen Plus flowsheets for the PFR, reactive distillation, and divided wall configurations, respectively. In the case of reactive distillation and divided wall, the top stage is the first stage where the feed stream is located. The last stage is the bottom stage, where the polymer is recovered.

Common distillation modules in Aspen, such as the Petlyuk or RadFrac columns were not used as they were limited to reaction schemes of the power law type, and did not allow the implementation of the step-growth kinetic scheme presented in **Chapter 6**. The multi-reactor, multi-flash approach in **Figure 98** and **Figure 99** represents the thermodynamic equivalent of reactive distillation.[421] During the simulation of reactive distillation and divided wall, no tear streams were specified as the simulator has the required convergence specifications implemented. Methods such as Weigstein, Broyden and Newton were used throughout the different simulation cases.

Table 41. Model palette of the unit operations for the PFR, reactive distillation and divided wall simulations

Unit Operation	Aspen Plus Module
PFR	
CSTR	
Flash Unit	
Condenser	
Heat exchanger	
Mixer	
Splitter	

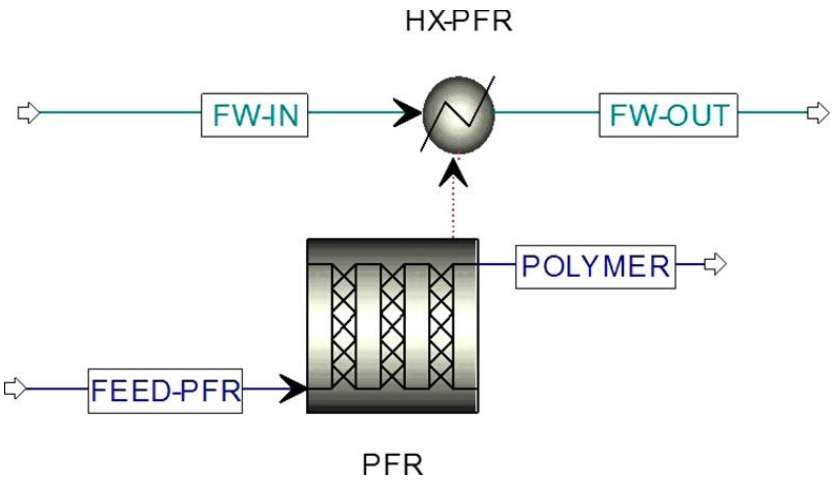

Figure 97. Aspen Plus flowsheet for the plug flow reactor (PFR) polyesterification process, showing the PFR reactor and heat exchanger (HX-PFR).

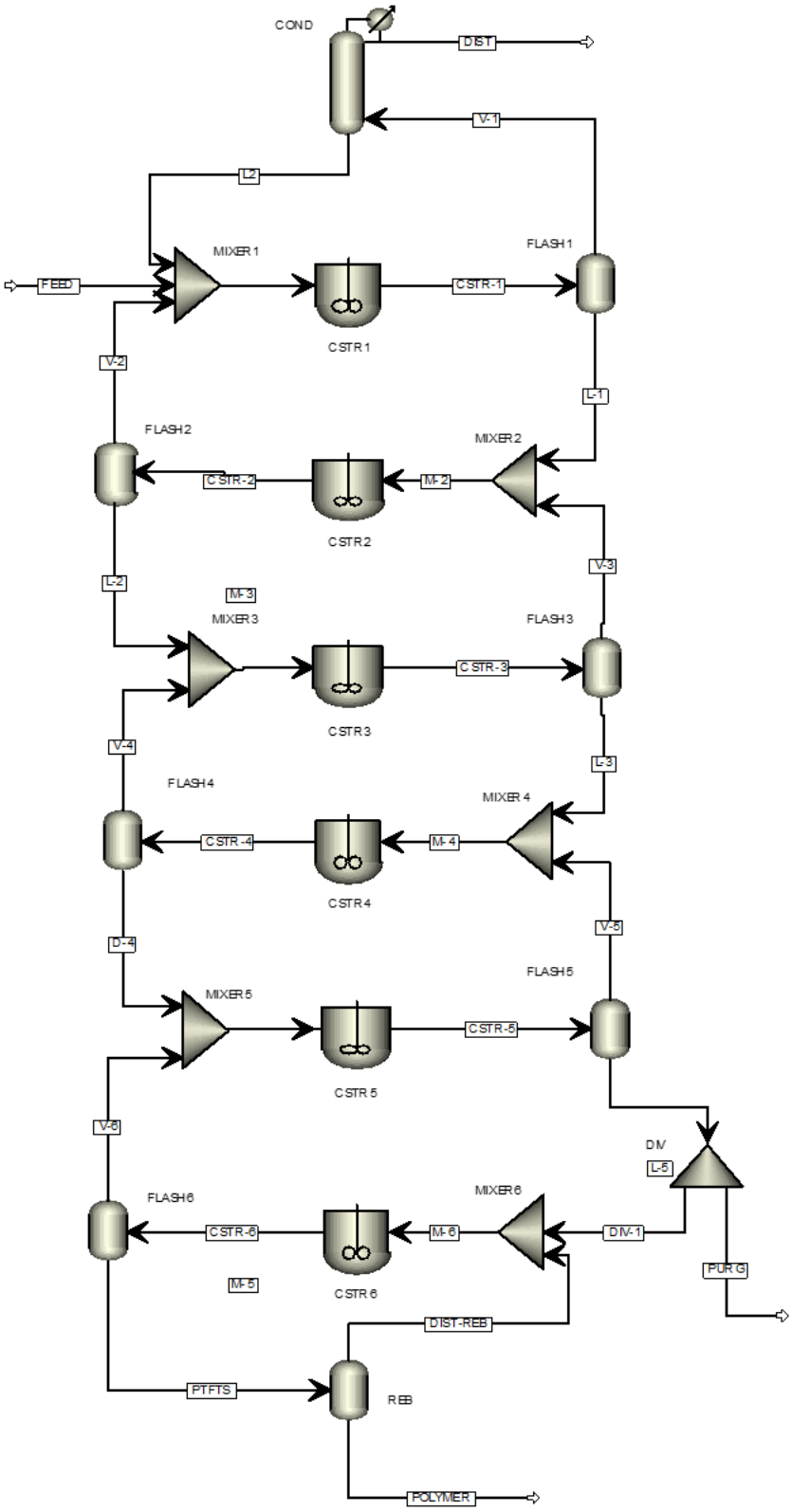

Figure 98. Aspen Plus flowsheet for the reactive distillation (RD) polyesterification process.

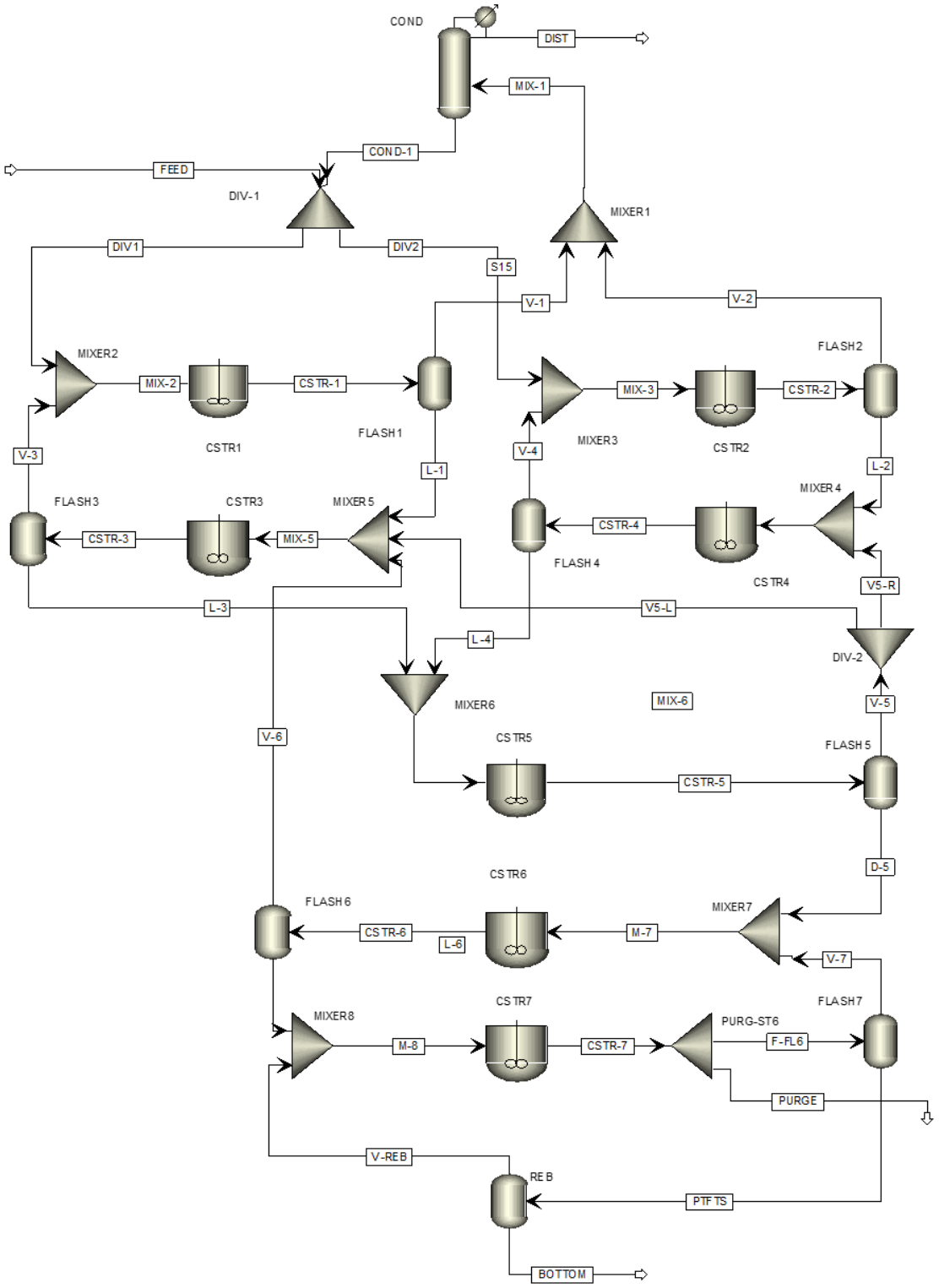

Figure 99. Aspen Plus flowsheet for the divided wall (DW) polyesterification process.

7.3.1 Definition of the Multiobjective Optimisation Problem

The general multiobjective optimisation problem is defined equally as presented in **Section 6.3**.

7.3.2 Sensitivity Analysis

The objective of sensitivity analysis is to estimate the change in the optimal solution given an estimated error in the parameters of a defined model.[422] This analysis could be employed to establish the effect of different manipulated variables over response variables and final product specifications. The information provided hence is important to determine the most efficient point of operation of a given process.[210] The sensitivity problem is widely encountered in chemical processes, due to the repeated computation of the sensitivity response of output variables to input variables in further process optimisation.[423] Sensitivity analysis is therefore a great method of checking the robustness and reliability of a given model.[424]

As defined elsewhere,[425] when performing a simulation flowsheet, the magnitude of the sensitivity coefficients of the flowsheet are matrices of dimensionless, normalised partial derivatives in terms of the solution x_i and the parameter α_j and take the form of equation 113

$$\frac{\partial ln x_i}{\partial ln \alpha_j} = \frac{\alpha_j}{x_i}\frac{\partial x_i}{\partial \alpha_j} \tag{113}$$

The sensitivity analysis was performed in Aspen Plus for the reactive distillation and divided wall configurations. In the simulator interphase, the model analysis tool is selected to access the sensitivity analysis, where the variables are defined. A detailed step by step methodology for the application of the sensitivity analysis in Aspen Plus is found elsewhere.[210] The manipulated variables were the split fraction of the splitter in the final stage and the intermediate temperatures of the trays of stirred tanks 3-5.

7.4 Results and Discussion

The process simulation was implemented in Aspen Plus for the three configurations considered: PFR, reactive distillation and divided wall. Multiobjective optimisation was done for the PFR problem whereas the optimum RD and DW operation conditions were obtained through sensitivity analysis. This methodology provided the optimum operation conditions, species and segments profiles and the polymeric attributes M_n and DPN of each case.

In the case of reactive distillation and divided wall, it was not possible to implement the commonly used operations equipment for their simulation in Aspen Plus due to the complexity of the step-growth polymerisation mechanism, with all the reactions, species and terminal and bound segments involved.[88, 192, 344]

Previous RD and DW simulation work in Aspen Plus considered arrangements for divided wall and reactive distillation with RADFRAC modules such as the separation of benzene, toluene, and xylene,[426] the RD esterification of succinic acid with ethanol,[395] or the synthesis of methyl acetate.[380] Likewise, the esterification of acetic acid with different alcohols using reactive distillation was simulated through flowsheets with combinations of stripper, rectifier, and decanter,[387] and the simulation of a plant scale reactive distillation column for the esterification of acetic acid with ethanol was also carried out using a column model available in Aspen Plus coupled with a decanter.[388]

In our case, we propose the simulation of reactive distillation and divided wall using a cascade of continuously stirred tank reactors (CSTRs) with a total condenser and a reboiler, resembling the Cavett problem,[210] which also allowed us to reach convergence in the algorithm implemented. The Cavett problem is defined as four interlinked flash tanks with different operating temperatures and pressures,[427] as shown in **Figure 100**. This configuration consists of three nested loops of mixers and flashes where the solution of the process is achieved through the selection of only two streams that will lead to the evaluation of all the existent recycles.[210, 428] Our proposed RD model and consequently DW model are inspired by the simulation methodology presented by Doherty and Malone[421] and their model assumptions: adiabatic conditions; the heat of reaction is negligible if compared to the heat of vaporisation; the reaction takes place in the liquid phase only; total condenser and each stage is considered a perfectly mixed stirred tank reactor (CSTR). The required number of stages resulted from an iterative process to reach similar product specifications with the operation conditions stablished in **Chapter 6**.

Similar reactive distillation simulation models to our work include the mathematical model proposed by Chen, et al.[385] where the authors consider each column tray as a perfectly mixed reactor due to the backmixing and bubbling effect of the water and the diol present. Reactive distillation and divided wall are used for liquid phase, reversible reactions, favouring products in terms of the Le Chatelier principle while decreasing heating and cooling utility services.

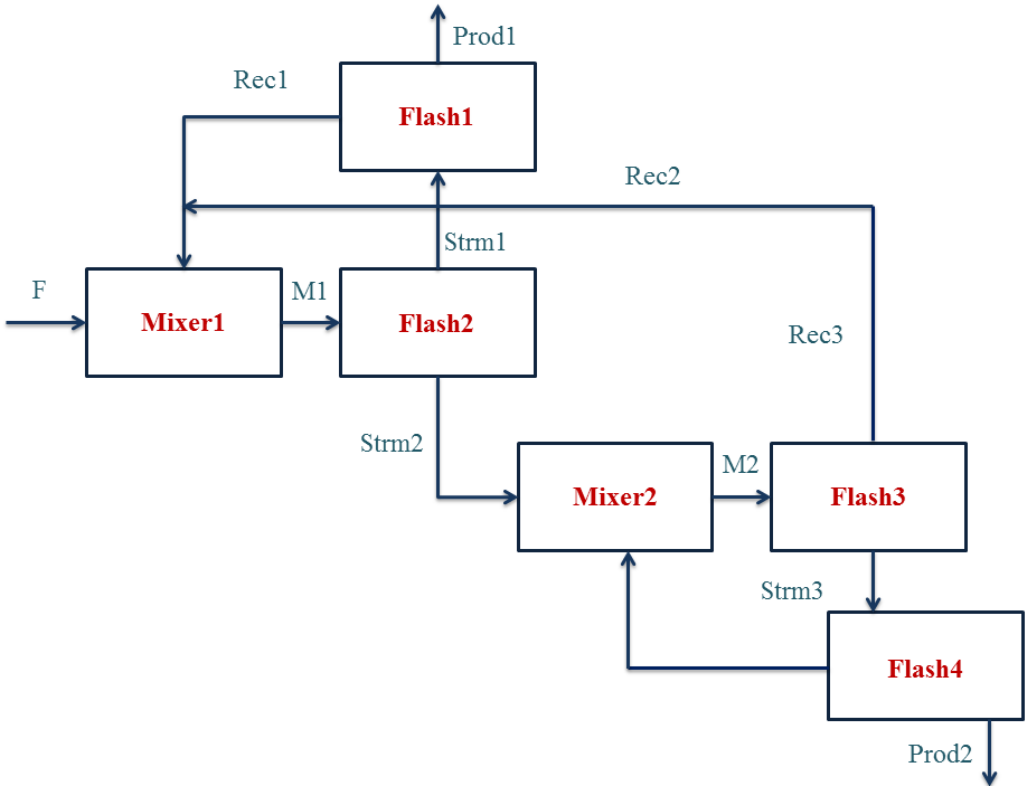

Figure 100. Cavett nested recycle configuration adapted and modified from the work of Chaves, et al[210] (F: feed; Rec: recycle stream; Prod: product stream; Strm, M1, M2: internal streams).

7.4.1 PFR optimisation

Table 42 presents the multiobjective optimisation PFR results for the different polyesters and copolyesters. The dimensionless Pareto frontier for $PPeF_{85}S_{15}$ (**6d**) and $PPeF_{15}S_{85}$ (**6a**) are presented in **Figure 101** and **Figure 102** while the concentration profiles of all the segments along with the M_n and DPN profiles are depicted in **Figure 103** for **6d** and in **Figure 104** for $PPeF_{30}S_{70}$ (**6b**). The Pareto frontiers and segment flow profiles for all the polyesters are available in **Appendix F**.

The optimum process temperature for the biomass-derived polyesters is between 207 and 224 °C, whereas the PET operation temperature was 270 °C, which correlates with the processing conditions for PET found in the literature.[192, 308, 309] The molecular weights of the biopolyesters range from 4100 to 4800 Da, and the final polymer production is around 1400 $kg \cdot h^{-1}$.

Table 42. ε-Constraint Optimisation Results for the PFR Synthesis

Polyester	Temperature, °C	M_n, Da	DPN	Polymer produced, kg·hr^{-1}	Heat Duty, kBTU·hr^{-1}
PPeS	207	4700	49	1401	2145
PPeF$_{15}$S$_{85}$	213	4100	43	1407	2184
PPeF$_{30}$S$_{70}$	224	4300	43	1414	1248
PPeF$_{70}$S$_{30}$	224	4600	43	1429	2137
PPeF$_{85}$S$_{15}$	224	4400	41	1434	2114
PPeF	223	4800	43	1512	1065
PET	270	3700	40	1276	2273

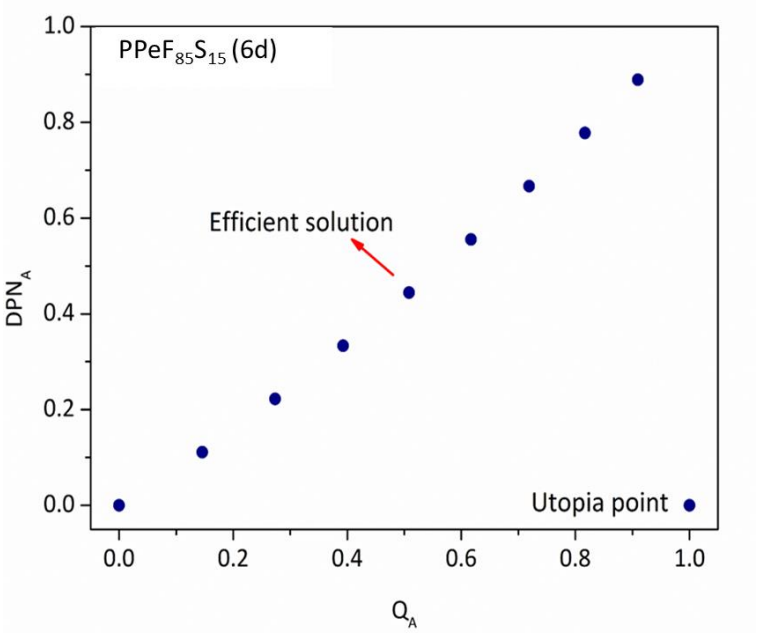

Figure 101. Pareto frontier for the PFR polyesterification of PPeF$_{85}$S$_{15}$ (**6d**). The objective functions are in dimensionless form (DP_{nA} and Q_A).

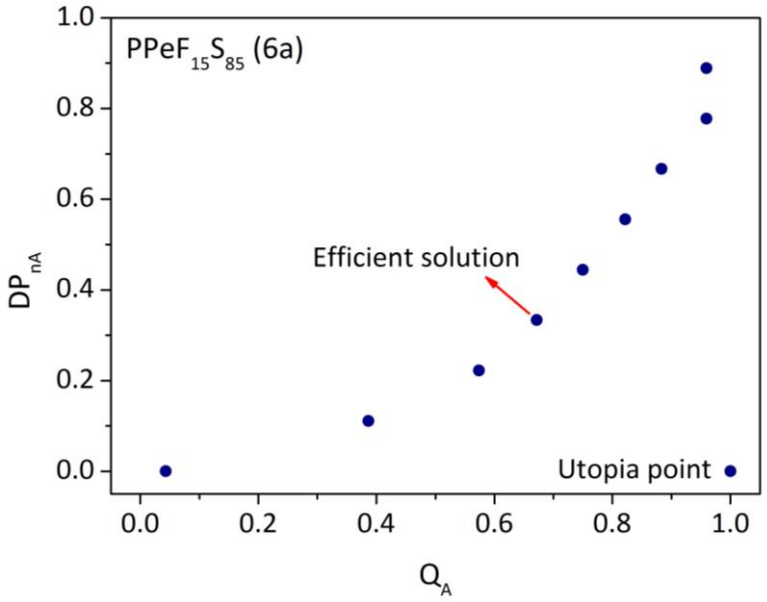

Figure 102. Pareto frontier for the PFR polyesterification of $PPeF_{15}S_{85}$ (**6a**). The objective functions are in dimensionless form (DP_{nA} and Q_A).

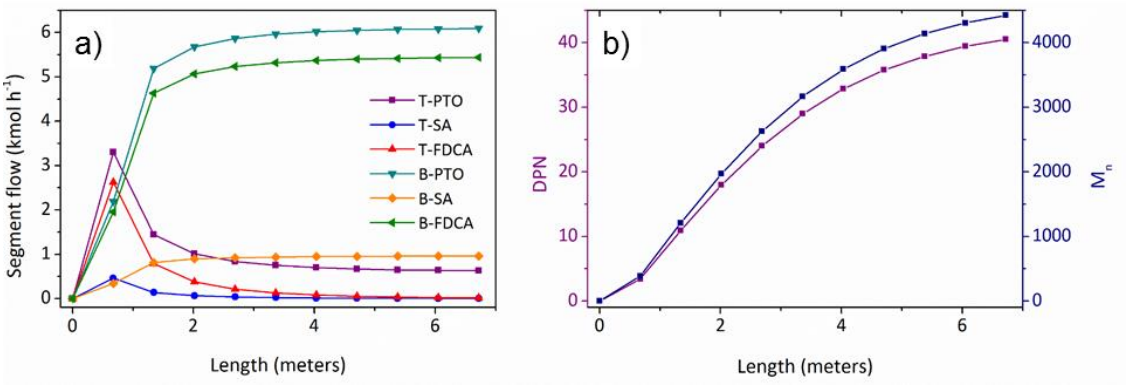

Figure 103. a) Segment concentration profiles. b) DP_n and M_n for the PFR polyesterification of $PPeF_{85}S_{15}$ (**6d**).

The polymer properties obtained in the batch simulation were in the same range[88] as described in **Chapter 6**. The segment concentration profiles along the reactor's length show how the bound-segments (B-PTO and B-FDCA) increase rapidly as a result of the molecular weight building up, reaching a steady flow afterward. These type of molar flow profiles were similar to those reported by Bikiaris, et al.[311] for the polyesterification of PPS at 190 °C. The B-SA concentration profile is lower than the FDCA and PTO bound segments due to the initial diacid FDCA:SA ratio of 85:15. When the polyester is rich in succinic acid, as in $PPeF_{15}S_{85}$ (**6a**) or $PPeF_{30}S_{70}$ (**6b**), the B-SA segment molar flow increases up to 6 $kmol \cdot h^{-1}$,

as shown in **Figure 104**. The process conditions and the final polymer quality are very homogeneous throughout all the library of polymers, leading to a versatile operation in the same plug flow reactor. The final polymer quality achieved for PET is lower than our biomass-derived polymers, with a DP_n of 40 and M_n of 3700 Da.

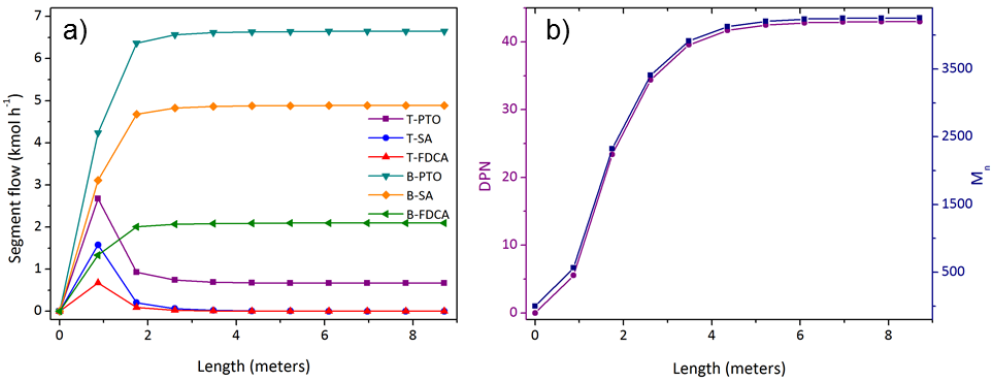

Figure 104. a) Segment concentration profiles. b) DP_n and M_n for the PFR polyesterification of $PPeF_{30}S_{70}$ (**6b**).

7.4.2 Sensitivity Analysis for RD and DW Columns

As previously stated, a sensitivity analysis was performed in order to determine the best intermediate temperatures of trays 3-5 (CSTR3-CSTR5) as well as the split fraction of the splitter in the last stage, to maximise the polymer flow, diminish the formation of oligomers, and promote the release of water and diol. The sensitivity results are presented in **Table 43** for the reactive distillation column and **Table 45** for the divided wall configuration. The results refer to the last stage of each configuration. The complete sets of temperatures and split fractions for the different systems are summarised in **Table 44** and **Table 46**.

In comparison with the results from the PFR configuration, the molecular weight M_n and DPN with both reactive distillation and divided wall column decreased, ranging from 2300 to 4200 Da and 21 to 27, respectively. These molecular weights are however in the suitable M_n range for coatings, 2000−6000 Da.[252] This information would be useful for decision-making processes of equipment implementation for the synthesis of polyesters with certain final properties and specifications. As shown in **Figure 105** for $PPeF_{70}S_{30}$, the segment concentration profiles are different from the ones for the plug flow reactor, since the bound segments do not reach a plateau but decrease in the last stages, leading to a lower degree of polymerisation and consequently, lower M_n. This suggests that the equilibrium is limiting the reaction, so a different arrangement should be tested, with only 5 stages as the simulation shows it would be enough. **Figure 106** depicts the M_n and DP_n profiles during the

reactive distillation process for $PPeF_{30}S_{70}$ and $PPeF_{70}S_{30}$. The M_n and DP_n obtained were nevertheless in the same range of those reported for other polyesterification systems in reactive distillation, such as maleic anhydride and propylene glycol -2800 Da-[383] and poly(ethylene adipate) -1500−2500 Da.[385] All the segments' profiles are available in **Appendix F**.

Table 43. Sensitivity Analysis for the Reactive Distillation Configuration

Polyester	Temperature (T_3-T_5), °C	M_n	DPN	Polymer produced, kg·hr^{-1}	Heat Duty, kBTU·hr^{-1}
PPeS	210,210,205	2700	28	1401	1184
$PPeF_{15}S_{85}$	230,230,229.5	3800	39	1408	2032
$PPeF_{30}S_{70}$	215,230,230	3400	34	1415	1051
$PPeF_{70}S_{30}$	230,230,225	2800	26	1430	1929
$PPeF_{85}S_{15}$	230,230,229.5	2300	21	1005	1936
PPeF	230,230,220	4200	37	1583	1142
PET	270,265,280	2200	23	1278	2030

Table 44. Temperature Distribution for Reactive Distillation

	Polyester						
CSTR	**PPeS**	**$PPeF_{15}S_{85}$**	**$PPeF_{30}S_{70}$**	**$PPeF_{70}S_{30}$**	**$PPeF_{85}S_{15}$**	**PPeF**	**PET**
$T_{condenser}$, °C	121	121	121	121	121	121	121
T_1, °C	215	230	230	230	230	220	277
T_2, °C	215	230	230	230	230	220	277
T_3, °C	210	230	215	230	230	230	270
T_4, °C	210	230	230	230	230	230	265
T_5, °C	205	229.5	230	225	229.5	220	280
T_6, °C	225	225	220.3	225	225	210	260
$T_{reboiler}$, °C	230	230	230	230	230	230	230
Split fraction	0.30	0.30	0.30	0.30	0.30	0.35	0.25

Table 45. Sensitivity Analysis for the Divided Wall Configuration

Polyester	Temperature (T_3-T_5), °C	M_n	DPN	Polymer produced, kg·hr^{-1}	Heat Duty, kBTU·hr^{-1}
PPeS	210,215,205	2600	28	2157	2213
PPeF$_{15}$S$_{85}$	210,220,230	3200	33	1409	2175
PPeF$_{30}$S$_{70}$	230,230,230	3900	39	1414	2164
PPeF$_{70}$S$_{30}$	230,230,230	3600	34	1430	2100
PPeF$_{85}$S$_{15}$	230,230,230	2800	25	1435	2089
PPeF	230,230,230	4100	37	1440	2041
PET	280,275,260	1800	18	1407	2266

Table 46. Temperature Distribution for Divided Wall

	Polyester						
CSTR	**PPeS**	**PPeF$_{15}$S$_{85}$**	**PPeF$_{30}$S$_{70}$**	**PPeF$_{70}$S$_{30}$**	**PPeF$_{85}$S$_{15}$**	**PPeF**	**PET**
$T_{condenser}$, °C	121	121	121	121	121	121	121
T_1, °C	215	230	230	230	230	220	277
T_2, °C	215	230	230	230	230	220	277
T_3, °C	210	210	230	230	230	230	280
T_4, °C	215	220	230	230	230	230	275
T_5, °C	205	230	230	230	230	230	260
T_6, °C	215	225	220	230	225	220	280
T_7, °C	215	210	220	220	225	210	260
$T_{reboiler}$, °C	230	230	230	230	230	230	230
Split fraction	0.35	0.30	0.40	0.35	0.35	0.35	0.35

The sudden change in the divided wall bound segment profiles between stage 4 and 5 in **Figure 105b** is an indication of the column section where most of the M_n increase takes place. This is potentially because the high temperature was maintained through these stages.

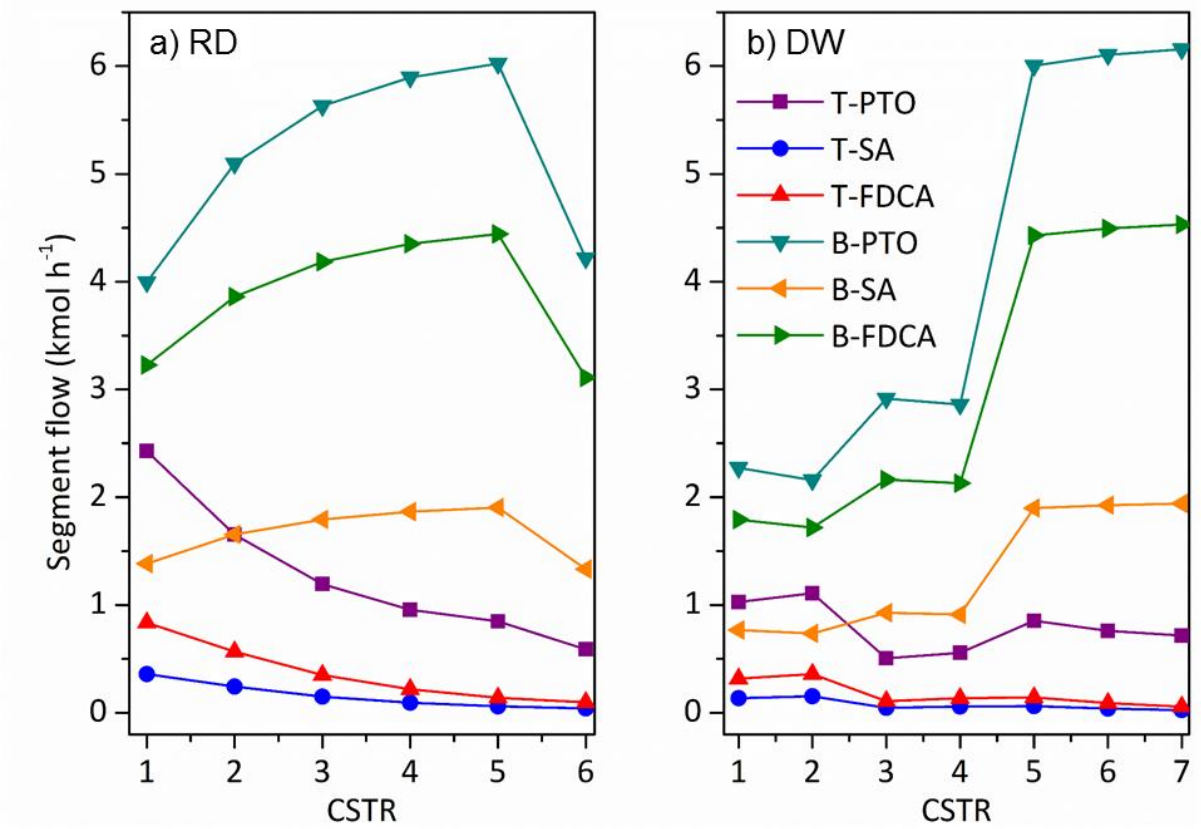

Figure 105. Segment flow profiles for $PPeF_{70}S_{30}$ (**6c**) for a) reactive distillation and b) divided wall.

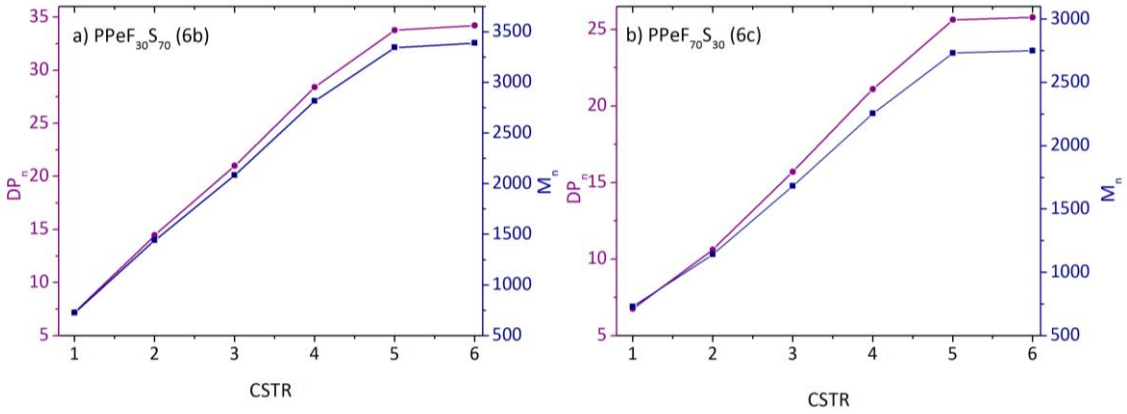

Figure 106. M_n and DP_n reactive distillation profiles for a) $PPeF_{30}S_{70}$ (**6b**) and b) $PPeF_{70}S_{30}$ (**6c**).

7.4.3 Sustainability Indicators

The four indicators considered for all the polyesterifications are the same indicators considered in **Chapter 6**, **Section 6.4.3.** The results are summarised in **Table 47** for each case. All indicators, except GWP, are the same regardless the type of fuel considered as they depend on the final polymer produced.

The normalised values for the indicators from 0% (worst case) to 100% sustainability (best target) are available in **Table 48**. It is observed that in the case of global warming potential GWP, the values are in the range of 0.06−0.43 $kg_{CO2}·kg_{polymer}^{-1}$ for all the configurations studied.

Within PFR, the lowest release of CO_2 corresponds to the synthesis of PPeF and $PPeF_{30}S_{70}$, with a GWP of 0.05 and 0.06 $kg_{CO2}·kg_{polymer}^{-1}$, respectively, when using natural gas as fuel. Notably, the production of petrochemical derived PET is the largest CO_2 releasing process, with GWP values of 0.12 with natural gas and 0.22 $kg_{CO2}·kg_{polymer}^{-1}$ with coal.

Table 47. Sustainability Indicators Estimated for the Different Biomass-Derived Polyesters

Polyester	**R_{SEI}**[a] kBTU·kg^{-1}	**RME**[b] kg·kg^{-1}	**MI**[c] kg·kg^{-1}	**$GWP_{natural\ gas}$**[d] kg·kg^{-1}	**GWP_{coal}** kg·kg^{-1}
		PFR			
PPeS	1.56	0.84	1.19	0.11	0.20
$PPeF_{15}S_{85}$	1.55	0.84	1.18	0.11	0.20
$PPeF_{30}S_{70}$	0.88	0.85	1.18	0.06	0.11
$PPeF_{70}S_{30}$	1.50	0.86	1.17	0.10	0.19
$PPeF_{85}S_{15}$	1.47	0.86	1.16	0.09	0.16
PPeF	0.70	1.00	1.00	0.05	0.09
PET	1.78	0.84	1.18	0.12	0.22
Polyester	**R_{SEI}**	**RME**	**MI**	**GWP**	**GWP**
		Reactive Distillation			
PPeS	0.84	0.84	1.18	0.23	0.43
$PPeF_{15}S_{85}$	1.44	0.84	1.18	0.18	0.32
$PPeF_{30}S_{70}$	0.74	0.85	1.18	0.14	0.25
$PPeF_{70}S_{30}$	1.35	0.86	1.17	0.16	0.30
$PPeF_{85}S_{15}$	1.35	0.86	1.16	0.14	0.25
PPeF	0.72	0.95	1.05	0.20	0.37
PET	1.59	0.85	1.18	0.23	0.41
Polyester	**R_{SEI}**	**RME**	**MI**	**GWP**	**GWP**
		Divided Wall			
PPeS	1.03	0.84	1.19	0.20	0.36
$PPeF_{15}S_{85}$	0.49	0.84	1.18	0.21	0.39
$PPeF_{30}S_{70}$	1.30	0.85	1.18	0.21	0.38
$PPeF_{70}S_{30}$	1.47	0.86	1.16	0.20	0.37
$PPeF_{85}S_{15}$	1.45	0.86	1.16	0.20	0.37
PPeF	1.22	0.86	1.58	0.19	0.34
PET	1.61	0.84	1.18	0.25	0.46

[a]Specific energy intensity; [b]Reaction mass efficiency; [c]Mass intensity; [d]Global warming potential

In terms of specific energy, the same polyesters PPeF and $PPeF_{30}S_{70}$ scored the best values, 0.70 and 0.88 kBTU·kg^{-1} since the best target is 0. PET again proved to be the least

sustainable option among all the polymers analysed, since the energy consumption per mass of polymer produced is high, 1.78 kBTU·kg^{-1}.

Table 48. Normalised Sustainability Indicators (0-100% Sustainability)

	Natural gas				Lignite coal
Polyester	**GWP**	**R_{SEI}**	**RME**	**MI**	**GWP**
		PFR			
PPeS	89.0	99.92	84.0	97.02	80.0
$PPeF_{15}S_{85}$	89.0	99.92	84.0	97.05	80.0
$PPeF_{30}S_{70}$	94.0	99.95	85.0	97.05	89.0
$PPeF_{70}S_{30}$	90.0	99.92	86.0	97.07	81.0
$PPeF_{85}S_{15}$	91.0	99.92	86.0	97.10	84.0
PPeF	95.0	99.96	100	97.50	91.0
PET	88.0	99.90	84.0	97.05	78.0
Polyester	**GWP**	**R_{SEI}**	**RME**	**MI**	**GWP**
		Reactive Distillation			
PPeS	77.0	99.95	84.0	97.05	57.0
$PPeF_{15}S_{85}$	82.0	99.92	84.0	97.05	68.0
$PPeF_{30}S_{70}$	86.0	99.96	85.0	97.05	75.0
$PPeF_{70}S_{30}$	84.0	99.93	86.0	97.08	70.0
$PPeF_{85}S_{15}$	86.0	99.96	86.0	97.10	76.0
PPeF	80.0	99.96	95.0	97.38	63.0
PET	77.0	99.91	85.0	97.05	59.0
Polyester	**GWP**	**R_{SEI}**	**RME**	**MI**	**GWP**
		Divided Wall			
PPeS	80.0	99.94	84.0	97.02	64.0
$PPeF_{15}S_{85}$	79.0	99.91	84.0	97.05	61.0
$PPeF_{30}S_{70}$	79.0	99.93	85.0	97.05	62.0
$PPeF_{70}S_{30}$	80.0	99.92	86.0	97.10	63.0
$PPeF_{85}S_{15}$	80.0	99.92	86.0	97.10	63.0
PPeF	81.0	99.93	86.0	96.05	66.0
PET	75.0	99.91	84.0	97.05	54.0

Moreover, it is worth mentioning that for all the systems, the evaluation in terms of the relation of raw materials and final products is close to the unity, with the synthesis of PPeF

reaching a perfect 1.0 in both mass intensity (MI) and reaction mass efficiency (RME) indicators, meaning that all the mass input was transformed into the final polymer, reaching 100% conversion. This is particularly interesting since it could represent an efficient, direct replacement for PET, expanding the real possibilities of the inclusion of biomass-derived materials.

Regarding the intensification of the process, the reactive distillation is the most energy-efficient configuration, as expected, since the specific energy indicators R_{SEI} are lower than PFR or even divided wall. For example, the synthesis of PPeS, $PPeF_{70}S_{30}$, and PET in a PFR reactor showed R_{SEI} values of 1.56, 1.50 and 1.78 $kBTU \cdot kg^{-1}$, respectively, whereas in reactive distillation, the indicators were 0.84, 1.35 and 1.59 $kBTU \cdot kg^{-1}$. These values are also below the indicators estimated for the batch case, where we reported 1.51, 1.47 and 1.78 $kBTU \cdot kg^{-1}$, respectively.[88]

In terms of mass efficiency, there is no considerable difference between the three setups. GWP is higher though for both reactive distillation and divided wall compared to PFR, mainly due to the inclusion of new operation units: the reboiler, the condenser and with the latter, the necessary reflux ratio to drive the reaction far from equilibrium. The divided wall configuration also had higher energy release due to addition of an extra stage or CSTR with its corresponding flash tank. It would be highly desirable to perform the reactive distillation and divided wall simulations using rigorous distillation column modules once the step-growth kinetic mechanism implementation is enabled in the simulator.

The synthesis of PET in both reactive distillation and divided wall presented the largest CO_2 release -0.23 and 0.25 $kg_{CO2} \cdot kg_{polymer}^{-1}$-and higher energy use -1.59 and 1.61 $kBTU \cdot kg^{-1}$ - among all the polymers analysed. The data suggests as well that is preferred as expected to use natural gas as primary fuel instead of coal to diminish the generation of greenhouse gases.

Our proposed biomass-derived polyesters represent potential new materials whose simulated production proves to be more environmental, energy and cost efficient than current commercial petrochemical PET. The definite assessment should be completed though with a thorough life cycle analysis (LCA), which would ideally include inventory analysis and the consideration of other indicators such as non-renewable source depletion, ecotoxicity, acidification, ozone depletion, smog formation, and human health, among others.[198]

7.5 Conclusions

The process simulation, multiobjective optimisation, and sensitivity analysis were performed in Aspen Plus for a library of biomass-derived renewable polyesters. Initially, a plug flow reactor was considered, followed by the process intensification by the implementation of reactive distillation and divided wall columns. These configurations were compared in terms of the sustainable indicators considered: global warming potential, specific energy intensity, mass intensity, and reaction mass efficiency, so the processes are analysed from environmental and economic efficiency perspectives. The multiobjective optimisation suggested that the process temperature needs to be kept between 207 and 224 °C in order to obtain polyesters with M_n of 4100 to 4800 Da and degrees of polymerisation above 40. This molecular weight range is desirable for coil coating applications, since higher molecular weights are not necessary and could lead to poor processability. The evolution of the segments was presented as well, enabling the determination of the most convenient reactor length in the PFR and number of stages in the process. The simulation suggested that the strategy proposed for the process intensification was successful since the reactive distillation is the most energy-efficient and therefore preferred option, as the specific energy indicators are lower than the PFR and divided wall configurations ones. All the biomass-derived polyesterifications ranked satisfactorily in the sustainability indicators considered, being close to unity for the mass efficiency and 0 for the CO_2 release and specific energy, which are the defined best targets.

In the case of reactive distillation and divided wall the M_n range was 2300−4200 Da, which is in the range of previously reported results for other polyesters synthesised by reactive distillation. This molecular weight range is appropriate as well for the end application of the polyester as coil coatings. It would be highly convenient however that Aspen Plus would enable the implementation of step-growth polymerisation kinetics in rigorous column modules such as RADFRAC to compare the results with the ones obtained by using the Cavett configuration. The simulation of the petrochemical derived PET resulted in the highest CO_2 release and energy consumption, along with the lowest mass efficiencies across all the polyesters. This comprehensive simulation and optimisation work then provides a preliminary work for the process design, process intensification and industrialisation of fundamental unit operations within the biorefinery concept. **Table 49** provides a ranking of the different configurations evaluated in respect to each indicator, where the notation

PFR<RD<DW would indicate that the PFR has a lower and therefore better performance in terms of GWP and R_{SEI}.

Table 49. Ranking of Reactor Configurations in respect to Sustainability Indicators

Polyester	**R_{SEI}** kBTU·kg^{-1}	**RME** kg·kg^{-1}	**MI** kg·kg^{-1}	**$GWP_{natural\ gas}$** kg·kg^{-1}
PPeS	RD<DW<PFR	RD=DW=PFR	RD<DW=PFR	PFR<DW<RD
$PPeF_{15}S_{85}$	DW<RD<PFR	RD=DW=PFR	RD=DW=PFR	PFR<RD<DW
$PPeF_{30}S_{70}$	RD<PFR<DW	RD=DW=PFR	RD=DW=PFR	PFR<RD<DW
$PPeF_{70}S_{30}$	RD<DW<PFR	RD=DW=PFR	DW<RD=PFR	PFR<RD<DW
$PPeF_{85}S_{15}$	RD<DW<PFR	RD=DW=PFR	RD=DW=PFR	PFR<RD<DW
PPeF	PFR<RD<DW	DW<RD<PFR	PFR<RD<DW	PFR<DW<RD
PET	RD<DW<PFR	PFR=DW<RD	RD=DW=PFR	PFR<RD<DW

CHAPTER 8

Property diversification through the introduction of isosorbide and itaconic acid

8. Property diversification through the introduction of isosorbide and itaconic acid

Chapter 8 presents the synthesis and characterisation of the polyesters studied in **Chapters 3** and **4** with the incorporation of isosorbide (IS), another biomass-derived monomer. A brief screening of itaconic acid as a polyester building block is also studied. The purpose of **Chapter 8** is to synthesise polyesters with improved mechanical properties than the ones previously reported by substituting the linear diol with the cyclic, rigid structure of IS in different concentrations.

8.1 Introduction

8.1.1 Isosorbide polyesters

Carbohydrates are a source of sugar-derived diols like byciclic ethers D-hexitols or 1,4:3,6-dianhydrohexitols.[429] Dianhydrohexitols are a by-product of the starch industry obtained by reduction of hexose sugars followed by dehydration. 1,4:3,6-dianhydro-D-glucitol (isosorbide), 1,4:3,6-dianhydrohexitol-D-mannitol (isomannide), and 1,4:3,6-dianhydro-L-iditol (isoidide) are known as its three main diastereoisomers derived from D-glucose, D-mannose, and L-fructose, respectively.[430] The 1,4:3,6-dianhydrohexitols are composed of two cis-fused tetrahydrofuran rings, nearly planar and V-shaped with a 120◦ angle between rings. The hydroxyl groups are situated at C_2 and C_5 and positioned on either inside or outside the V-shaped molecule.[153] **Scheme 44** shows the structures of isosorbide, isomannide and isoidide.

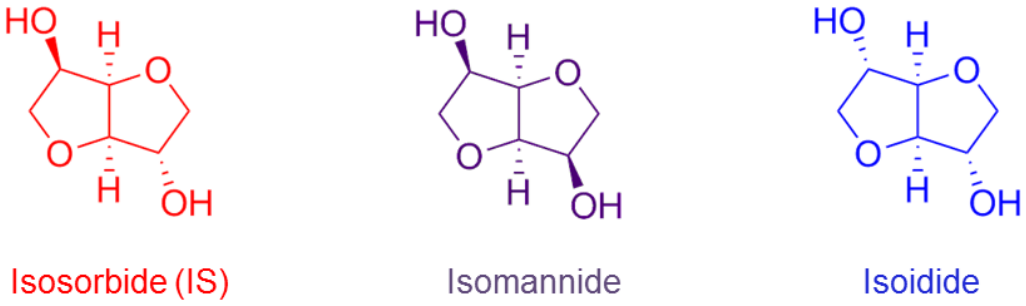

Scheme 44. Molecular structures of isosorbide, isomannide and isoidide.

Among the three isomers, isosorbide is the only one produced at an industrial scale, as it has potential applications in sectors such as energy and fuels, base chemicals and

materials.[431] Isosorbide is commonly synthesised from the double hydrogenation of glucose,[110] whereas isoidide is not found naturally in biomass.[153] Isomannide on the other hand, is the least reactive compound compared with the other two isomers because of the steric effects and hydrogen bonding.[430] Despite its availability, isosorbide is still not produced in a high purity because of the presence of isomers, less dehydrated products such as sorbitan and degradation products and residues.[153] Nevertheless, isosorbide is an outstanding example of a biomass-derived product with a combination of enzymatical and chemical technologies and for which, in fact, no comparison can be made with the classical petrochemistry.[432]

Isosorbide has a considerable potential for the production of versatile new chemicals and other products from renewable resources as its hydroxyl groups allow for further functionalisation or direct processing.[154] The use of 1,4:3,6-dianhydrohexitols in polyesters can be motivated by several features: rigidity, chirality, non-toxicity,[153] and recently, its use as a monomer for the preparation of UV-cured coatings has been highlighted.[433] An efficient strategy to improve the performance of aliphatic polyesters is to introduce some rigid molecular structure into the polymeric backbone. Isosorbide has thus gained attention due to the two tetrahydrofuran rings. However, the hydroxyl group in *endo* position easily forms intra-molecular hydrogen bond with the oxygen in the other ring, which leads to the poor reactivity of the secondary hydroxyl group and the low number average molecular weights of copolyesters.[434] However, isosorbide has a relatively high thermostability and low segmental mobility, and can be used to improve the glass transition temperatures of polyesters.[435]

A considerable amount of work on isosorbide-based polyesters has been reported. Goerz, et al.[110] studied the synthesis of polyesters from isosorbide, itaconic acid and succinic acid. The obtained polyesters had T_g from 57 °C to 65 °C and molecular weights from 1200 Da up to 3500 Da depending on the molar ratio of the monomers. Also with succinic acid, the biocompatibility of these polyesters was reported along with their homologue polymers from isosorbide coupled with adipic acid and sebacic acid, concluding that the polymer from sebacic acid and isosorbide has good potential for biomedical applications.[169] In the field of coatings, Noordover, et al.[166, 170, 253] reported the synthesis of terpolyesters for powder coatings based on isosorbide, succinic acid, citric acid and aliphatic diols such as 1,3-propanediol, 1,4-butanediol and neopentyl glycol, showing M_n from 2700 up to 4600 Da and highlighting the effect of isosorbide content on the glass transition temperature.[170]

Jacquel, et al.[92] prepared bioderived copolyesters of succinic acid and isosorbide by varying the mol% isosorbide from 5 to 20 mol%. The polyesters had T_g from -28 °C to -11 °C, which increased with increasing mol% of IS, although the esterification yield decreased with the incorporation of isosorbide.

Zhou, et al.[171, 434, 435] studied the properties and crystallisation kinetics of copolyesters based on isosorbide, sebacic acid and either 1,10-decanediol[171], or 1,3-propanediol.[435] The authors varied the mol% isosorbide from 5.3 mol% to 66.2%, reporting glass transition temperatures ranging from -26 °C to -5 °C, although no glass transition was observed when the mol% isosorbide was below 30%. The M_n range was broad, with the polyester of isosorbide and sebacic acid showing the lowest M_n (2800 Da) whereas the copolyester with 25.4 mol% isosorbide had the highest M_n, 17000 Da. No relationship was found between the molecular weight and the amount of incorporated isosorbide.[171]

Polyesters bearing isosorbide and a cyclic aliphatic diacid, cis–trans-1,4-cyclohexane dicarboxylic acid (CHDA), have been prepared by using the free acid, the dichloride and the dimethyl ester derivatives of CHDA. No product was obtained with either the free acid or the dimethyl ester, although 95% yield was obtained with the dichloride at 140 °C and using chlorobenzene as the reaction medium.[168]

Isosorbide has been largely incorporated into aromatic polyesters, either as the main diol component or by being included in limited proportions. Thiem and Lüders[436] were the first to synthesise polyterephthalates with isosorbide and its isomers as the diol monomer. The molecular weights for poly(isosorbide terephthalate) and poly(isoidide terephthalate) were 3000 and 3800 Da, respectively, with glass transition temperatures at 155 °C for the former and at 153 °C for the latter.

Other works regarding terephthalates with isosorbide include the screening of catalysts for the synthesis of poly(ethylene terephthalate-co-isosorbide terephthalate) (PEIT). The authors found that combinations of antimony oxide with lithium, magnesium or aluminium based salts successfully increased the efficiency of the transesterification step.[161] Moreover, Yoon, et al.[163] studied the synthesis of a partially biobased terephthalate with a very high thermal resistance consisting of three different reactive diols: isosorbide, cyclohexane dimethanol and ethylene glycol.

Isophthalic acid-based polyesters have been synthesised with isosorbide as well. Kricheldorf, et al.[167] studied the oligomerisation of L-lactide in bulk with isosorbide as initiator. The molar ratio isosorbide/lactide was varied from 8/2 to 2/8. The oligomers were then polycondensed with isophthaloyl chloride in various aromatic solvents. The obtained average molecular weights were around 4000 Da.

The properties of polyesters from isosorbide and FDCA derivatives were studied by Storbeck and Ballauf[90] through the polycondensation of 2,5-furandicarbonyl dichloride with either isosorbide, isomannide or isoidide. The polyester with the lowest M_n was obtained with isosorbide (9000 Da) whereas the incorporation of isoidide resulted in the polyester with greatest M_n (21500 Da). Other furan derivatives, such as 1,1-bis[5-(methoxycarbonyl)-2-furyl]ethane and 1,1-bis[5-(methoxycarbonyl)-2-furyl]methane were polymerised with isosorbide to obtain amorphous polymers with the T_g ranging from -13 66 °C to 66 °C depending on the molar ratios and length of the dialkanoate.[437] Sousa, et al.[438] reported the synthesis of a poly((ether) ester) of FDCA, poly(ethylene glycol) and 25 mol% isosorbide with a T_g at -26.4 °C and M_w= 13200 Da.

Alternative polymerisation syntheses were analysed by Sablong, et al.[164] who reported the incorporation of isosorbide into poly(butylene terephthalate) (PBT) by solid-state polymerisation (SSP), whereas Gioia, et al.[162] combined the chemical recycling of PET with the use of isosorbide and succinic acid.

8.1.2 Itaconic acid polyesters

Itaconic acid has been the subject of extended research within the field of polyesters not only because it is a biomass-derived monomer, but also because of its particular structural features, bearing a vinyl double bond and two carboxylic groups, which allow its use as AA-type monomer for polycondensation reactions and curing or crosslinking.[117]

Full bioderived polyesters of itaconic acid with other monomers have been reported; for instance, isosorbide and succinic acid,[110] 1,3-propanediol,[114] 1,4-butanediol,[108, 111, 114] glycerol,[111] sorbitol and succinic acid,[109] soybean oil,[439] and very recently, FDCA and succinic acid.[440]

Specifically, the coatings industry has been benefited by the incorporation of IA into the market, as its similarity with acrylic and methacrylic acids makes it a feasible candidate for radiation curing binders for coating applications.[101] Dai, et al.[441] synthesised coatings

using itaconic acid as the crosslinking group with either ethylene glycol, 1,4-butanediol or 1,6-hexanediol in the presence of p-toluenesulfonic acid at 160 °C. The polyesters were UV-cured and the resulting coatings exhibited a high hardness and good water and solvent resistance.[441] Later on, the same authors added glycerol to these systems, which improved the adhesion and flexibility of the final coatings.[442] Likewise, the development of polyester resins from itaconic acid, 1,6-hexanediol, 13-propanediol and neopentyl glycol for wood coating applications has been reported, using methanesulfonic acid as the catalyst and temperature between 120 and 180 °C for 8 hours.[101, 443]

An interesting field of application of itaconic acid polyesters is the post-polymerisation modification of the *exo*-chain double bond.[101] Itaconic acid polyesters are susceptible to undergo Michael additions, which is a practical bond forming strategy for carbon-carbon and carbon-heteroatom bonds.[444] In this vein, it has been demonstrated that itaconic acid polyesters are susceptible to Michael additions, such as thiol-ene reactions.[115, 116, 445]

8.2 Experimental Procedure

The experimental procedure to synthesise isosorbide-based polyesters has been highlighted in **Chapter 2**, **Section 2.3.3.7** for 1,3-propanediol and **2.3.3.8** and **2.3.3.9** for 1,5-pentanediol. **Table 50** summarises the polyesters synthesised along with the reaction conditions. **Scheme 45**, **Scheme 46**, and **Scheme 47** show the synthesis of PPFIS, PPeIS and PPeFIS, respectively. The analogue polyesters of PPeIS (**11**) with 1,3-propanediol instead were not synthesised as the series of polyesters **11** served as an initial screening of the effect of isosorbide, moving toward to more complex systems containing FDCA. The synthesis of itaconic acid polyesters was described in **Section 2.3.3.10**, and is depicted in **Scheme 48** for PPeSIa (**16**).

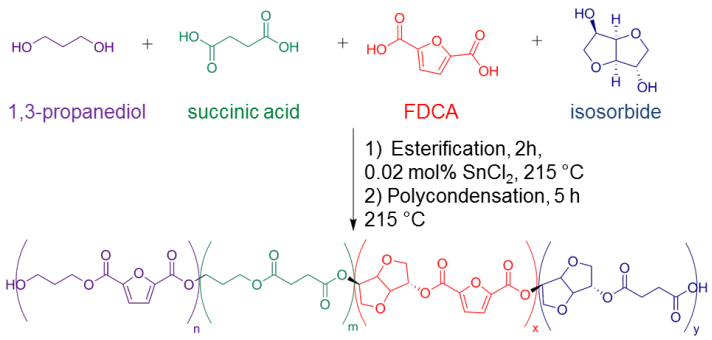

7-10 PPFIS

Scheme 45. Synthesis of isosorbide-based polyesters with 1,3-propanediol and FDCA, PPFIS (**7-10**).

Table 50. Synthesised biomass-derived polyesters with 1,3-propanediol and isosorbide

No.	Acronym	Catalyst[a]	T[b], °C	Mol% FDCA	Mol% IS[c]	r[d]
			Isosorbide			
			1,3-propanediol			
7a	$PPF_{15}I_{30}S_{85}$				30	
7b	$PPF_{15}I_{60}S_{85}$	$SnCl_2$	215	15	60	1.5
7c	$PPF_{15}I_{70}S_{85}$				70	
8a	$PPF_{30}I_{30}S_{70}$				30	
8b	$PPF_{30}I_{60}S_{70}$	$SnCl_2$	215	30	60	1.5
8c	$PPF_{30}I_{70}S_{70}$				70	
9a	$PPF_{70}I_{10}S_{30}$				10	
9b	$PPF_{70}I_{30}S_{30}$	$SnCl_2$	215	70	30	1.5
9c	$PPF_{70}I_{50}S_{30}$				50	
10a	$PPF_{85}I_{10}S_{15}$				10	
10b	$PPF_{85}I_{30}S_{15}$	$SnCl_2$	215	85	30	1.5
10c	$PPF_{85}I_{50}S_{15}$				50	

[a] 0.02 mol%$SnCl_2$/mol diacid [b] Reaction temperature, [c] Isosorbide, [d]Molar ratio diols:diacids.

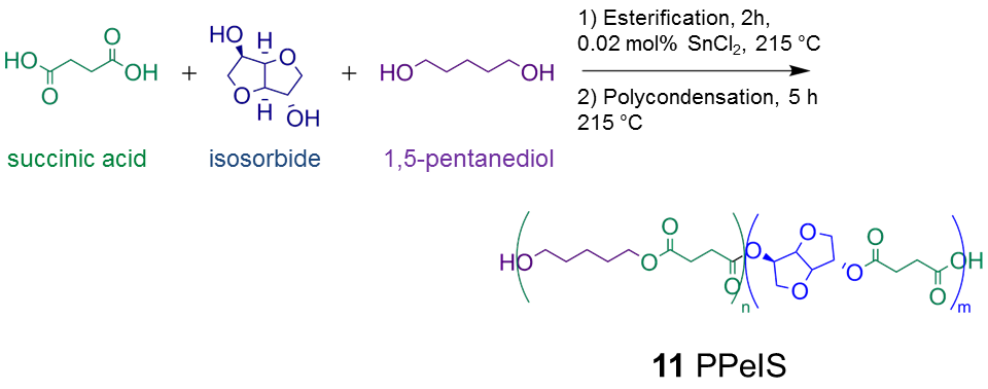

Scheme 46. Synthesis of isosorbide-based polyesters with 1,5-pentanediol, PPeIS (**11**).

Table 51. Synthesised biomass-derived polyesters with 1,5-pentanediol and isosorbide

No.	Acronym	Catalyst[a]	T[b], °C	Mol% FDCA	Mol% IS[c]	r[d]
			1,5-pentanediol			
11a	$PPeI_{10}S$				10	
11b	$PPeI_{30}S$				30	
		$SnCl_2$	215	-		1.3
11c	$PPeI_{50}S$				50	
11d	$PPeI_{60}S$				60	
12a	$PPeF_{15}I_{10}S_{85}$				10	
12b	$PPeF_{15}I_{30}S_{85}$				30	
12c	$PPeF_{15}I_{50}S_{85}$	$SnCl_2$	215	15	50	1.3
12d	$PPeF_{15}I_{60}S_{85}$				60	
12e	$PPeF_{15}I_{70}S_{85}$				70	
13a	$PPeF_{30}I_{10}S_{70}$				10	
13b	$PPeF_{30}I_{30}S_{70}$				30	
13c	$PPeF_{30}I_{50}S_{70}$	$SnCl_2$	215	30	50	1.3
13d	$PPeF_{30}I_{60}S_{70}$				60	
13e	$PPeF_{30}I_{70}S_{70}$				70	
14a	$PPeF_{70}I_{10}S_{30}$				10	
14b	$PPeF_{70}I_{30}S_{30}$	$SnCl_2$	215	70	30	1.3
14c	$PPeF_{70}I_{50}S_{30}$				50	
15a	$PPeF_{85}I_{10}S_{15}$				10	
15b	$PPeF_{85}I_{30}S_{15}$	$SnCl_2$	215	85	30	1.3
15c	$PPeF_{85}I_{50}S_{15}$				50	

[a] 0.02 mol%$SnCl_2$/mol diacid [b] Reaction temperature, [c] Isosorbide, [d]Molar ratio diols:diacids

Table 52. Synthesised biomass-derived polyesters with itaconic acid, succinic acid and 1,5-pentanediol

No.	Acronym	Catalyst	T,[c] °C	Mol% IA	r[d]
16a	$PPeSIa_5$			5	
16b	$PPeSIa_{10}$	$Ti(OBu)_4$[a]	190	10	1
16c	$PPeSIa_{15}$			15	
17	PPeIa	$SnCl_2$[b]	160	100	1

[a] 0.05 weight% $Ti(OBu)_4$/total charge, [b] 0.5 mol% $SnCl_2$/mol_{IA} [c]Reaction temperature, [d] Molar ratio diols:diacids

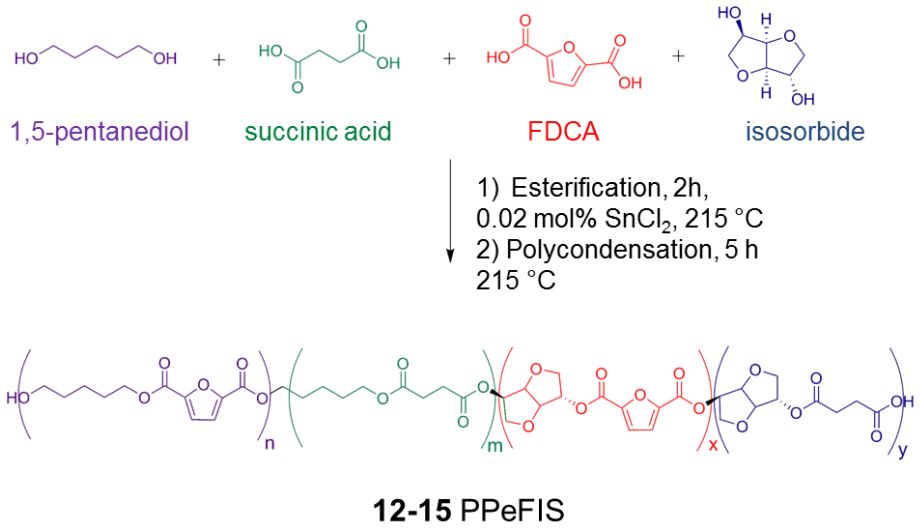

Scheme 47. Synthesis of isosorbide-based polyesters with 1,5-pentanediol and FDCA, PPeFIS (**12-15**).

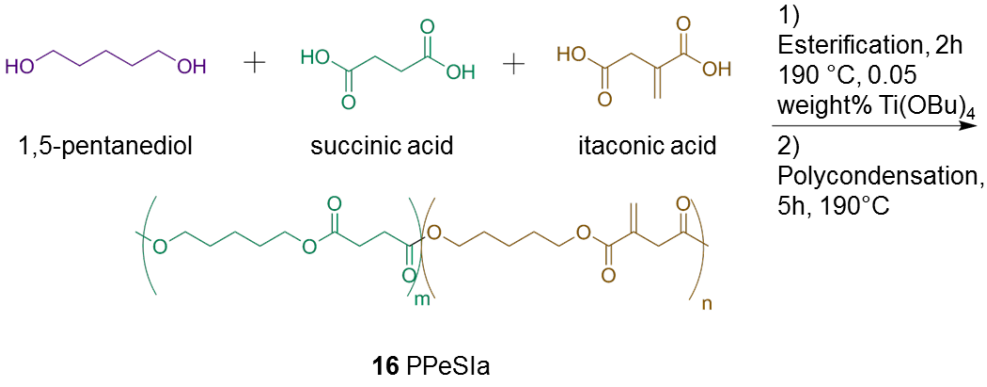

Scheme 48. Synthesis of itaconic acid-based polyesters with 1,5-pentanediol and succinic acid PPeSIa (**16**).

8.3 Characterisation Results of Isosorbide Polyesters

8.3.1 ^{1}H NMR

The chemical structure of the polyesters was determined by ^{1}H NMR. The NMR spectra of the isosorbide monomer is shown in **Figure 107**. The chemical shifts and assignments are summarised in **Table 53** and **Figure 108** shows the NMR spectra for 1,5-pentanediol copolyesters $PPeF_{85}I_{10}S_{15}$ (**15a**), **12b** and **13c**, which contain 10, 30 and 50 mol% IS, respectively. The identification of single peaks was a complex process since the incorporation of isosorbide could possibly facilitate the formation of cyclic structures and short chain oligomers, along with the probable presence of unreacted isosorbide within the polymer sample, due to isosorbide's limited reactivity. The presence of impurities in the isosorbide monomer is a possibility as well (>98% purity), as it was mentioned in the chapter's introduction as one of the limitations of industrially-sourced isosorbide. With this said, the intention of the present ^{1}H NMR analysis is to provide solely a general idea of the regions that identify these carbohydrate-derived polyesters. Furthermore, no quantitative analysis or precise definition of every signal is undertaken. The analysis by ^{13}C NMR and 2D NMR could facilitate the study, and remains as part of the future work regarding the isosorbide polyesters.

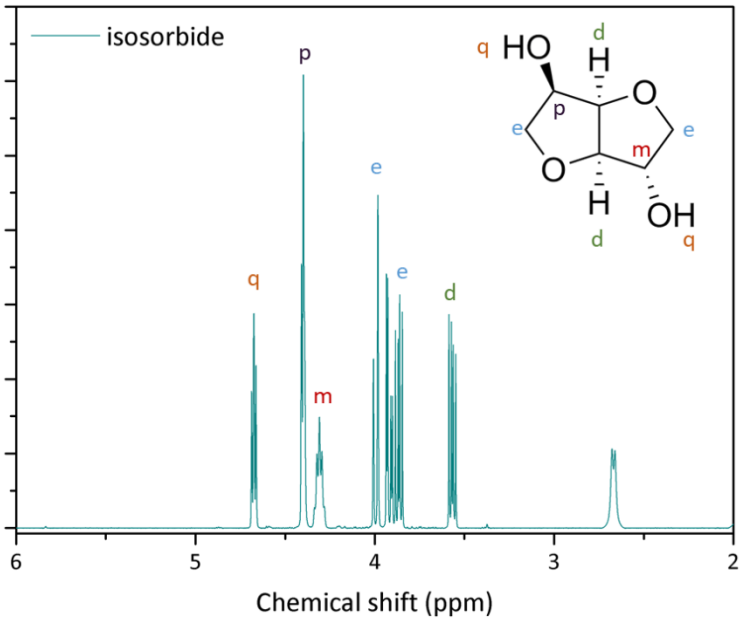

Figure 107. ^{1}H NMR spectra of isosorbide monomer.

The formation of the FDCA and SA esters is confirmed by the shifts at 4.34 (*i*) and 4.09 (*f*), respectively, as the protons of the FDCA esters tend to shift to higher ppm values,[78, 84, 85] in a similar fashion as described in **Chapters 3** and **4**. The assignment *a* (7.2 ppm) corresponds to the protons of the furan ring of FDCA. The signals between 3.8 ppm and 5.4 ppm (*e,d,m,n,o,p*) are attributed to the protons of isosorbide, which is in good agreement with previous literature of different isosorbide-based polyesters: 3.9-5.6 ppm,[162] 3.7-5.2 ppm,[169] 3.8-5.4 ppm[171] and 3.8-5.15 ppm.[170] The differences in shifts between peaks *p* (5.40-5.46 ppm) and *m* (5.21-5.25ppm) are suggested result of the *endo* (*p*) and *exo* (*m*) stereochemistry of the two hydroxyl groups of isosorbide, as well as between peaks *d* (4.62-4.67 ppm) and *n* (4.84-4.97 ppm).[170] Gioia, et al.[162] identified the *endo* and *exo* OH groups at 5.2 ppm and 5.5 ppm, respectively. The broadening of the CH_2-signal of succinic acid (*b* and *b'*, 2.62 and 2.69 ppm) is derived from the presence of two diols, 1,5-pentanediol and isosorbide, coupled with the *endo* and *exo* stereochemistry of isosorbide. A similar behaviour was reported for polyesters conformed by 1,3-propanediol and isosorbide with succinic acid, where the succinic acid shifts were observable between 2.6 and 2.8 ppm.[170] Apparently, from **15a** up to **13c** with 50 mol% IS, the characteristic peaks of 1,5-pentanediol (1.42-1.80 ppm) decrease as the isosorbide concentration increases,[171] although a quantitative analysis should be performed to confirm the assumption. Representative ^{1}H NMR, ^{13}C NMR and 2D NMR of 1,3-propanediol polyesters with isosorbide is available in **Appendix G**, along with a representative PPeFIS polyester.

Table 53. Assignment of chemical shifts of isosorbide polyesters **12-15** and integrations for $PPeF_{85}I_{10}S_{15}$ (**15a**)

Polyester	**Assignment of chemical shifts ($CDCl_3$, δ/ppm)**						
12-15 PPeFIS	**a**	**b,b'**	**c**	**d**	**e**	**f**	**g,j**
	7.20	2.62, 2.69	3.68	4.62-4.67	3.80-3.97	4.09	1.80
	h,k	**i**	**l**	**m**	**n**	**o**	**p**
	1.66	4.34	1.42-1.48	5.21-5.25	4.84-4.97	4.48	5.40-5.46
	Integrations for $PPeF_{85}I_{10}S_{15}$ (15a)						
	a	**b,b'**	**c**	**d**	**e**	**f**	**g,j**
	2.03	2.00, 1.13	0.47	0.53	1.17	2.24	4.05
	h,k	**i**	**l**	**m**	**n**	**o**	**p**
	1.97	4.57	2.95	0.14	0.21	0.21	0.47

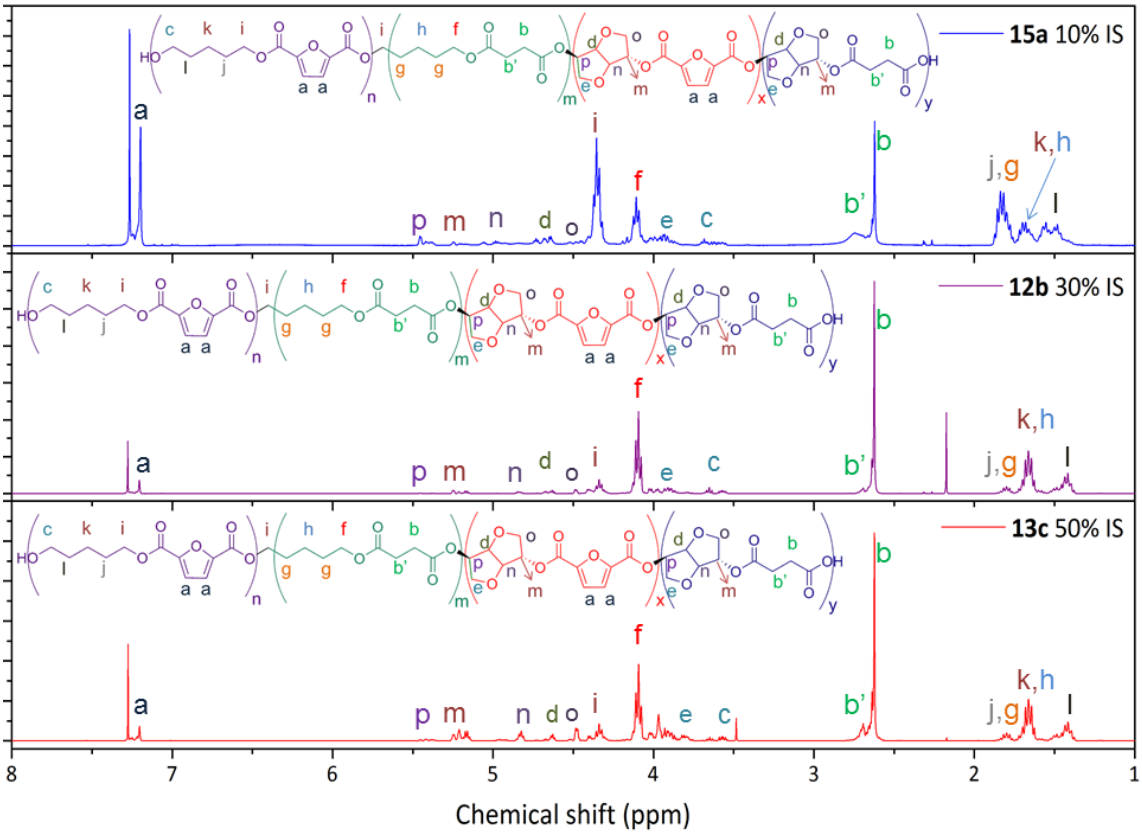

Figure 108. ^{1}H NMR spectra of $PPeF_{85}I_{10}S_{15}$ (**15a**), $PPeF_{30}I_{30}S_{70}$ (**12b**) and $PPeF_{70}I_{50}S_{30}$ (**13c**).

8.3.2 Molecular weight measurement by GPC

M_n, M_w and dispersity Đ were measured by gel permeation chromatography. **Table 54** and **Table 55** show the results obtained for the isosorbide based polyesters and **Figures 109-113** show the corresponding chromatographs. The parent polyesters with 1,5-pentanediol (**6**) and 1,3-propanediol (**3**) have been included in the aforementioned tables as comparison. Note however that the parent polyesters had no catalyst added, which would lead them to having higher acid values than the isosorbide-based polyesters. The acid values of the isosorbide polyesters are available in **Appendix H.** The range of M_w for the polyesters is between 700 and 10200 Da, whereas M_n falls within 500 and 3100 Da, indicating the great influence that the addition of isosorbide imparts, which allows a great versatility within the properties of these biomass-derived polyesters. The results obtained suggest that in general, M_n and M_w decrease as the isosorbide content increases.

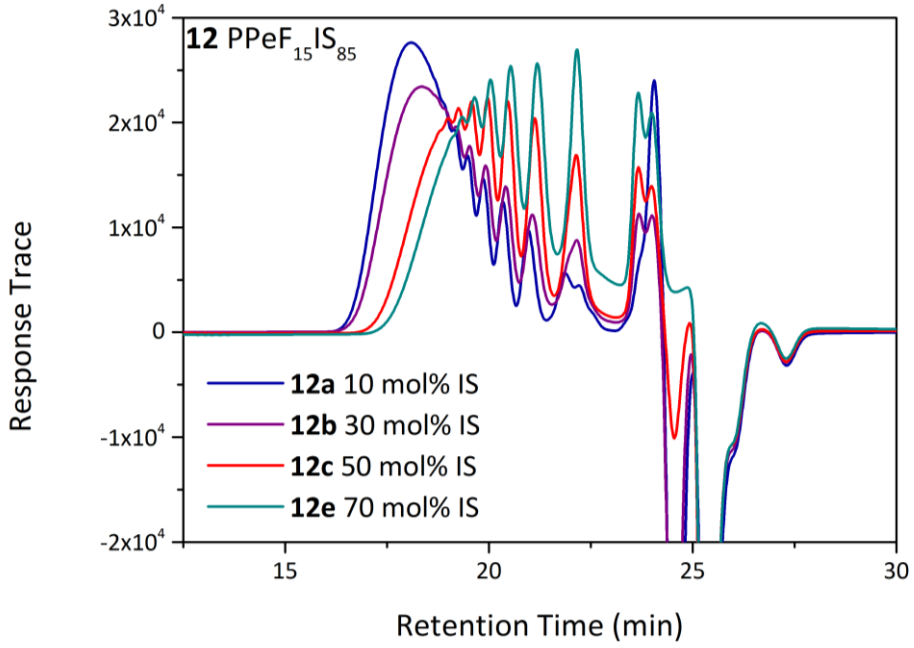

Figure 109. GPC chromatograph of polyester $PPeF1_5IS_{85}$ **12**, synthesised by azeotropic distillation in the second stage.

As we found previously with copolyesters of FDCA and SA (**Chapters 3** and **4**), the highest M_n and M_w were achieved with the furan rich polyesters $PPeF_{85}IS_{15}$ (**15**) and $PPeF_{70}IS_{30}$ (**14**) and the trend is followed as the FDCA content is decreased, although **14** had slightly higher molecular weight when the mol% IS was between 30 and 50%. The incorporation of isosorbide was limited to 50 mol% for **14** and **15**, as the mixture becomes extremely viscous and highly unprocessable above that concentration.

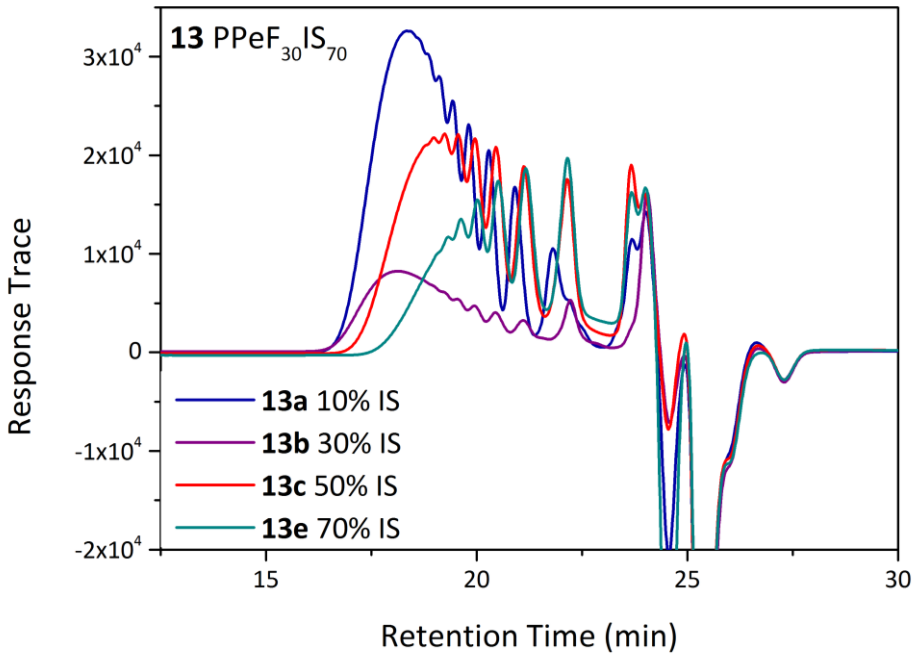

Figure 110. GPC chromatograms of polyesters $PPeF_{30}IS_{70}$ **13**, synthesised by azeotropic distillation in the second stage.

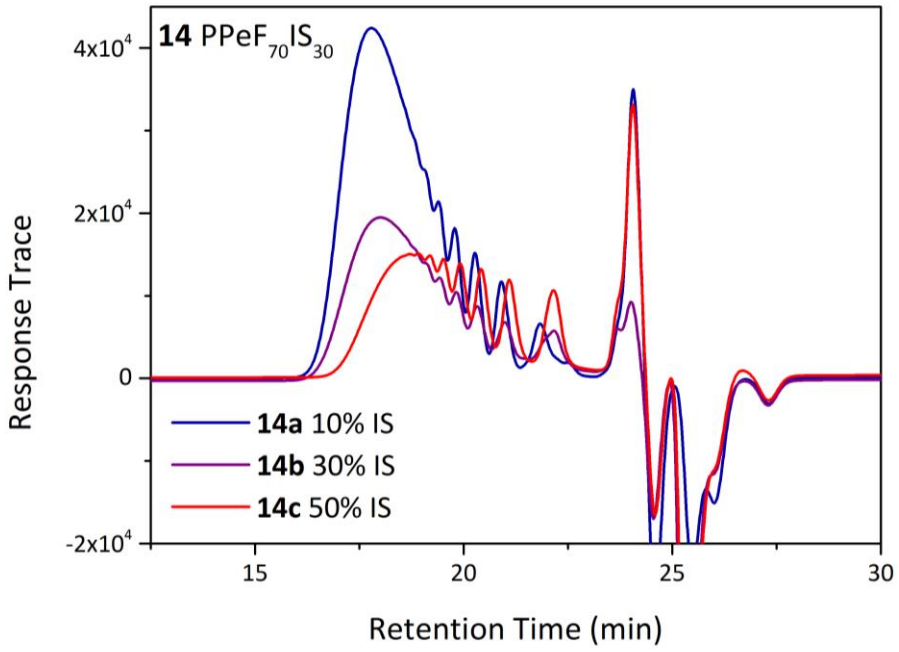

Figure 111. GPC chromatograms of polyesters $PPeF_{70}IS_{30}$ **14**, synthesised by azeotropic distillation in the second stage.

Table 54. M_n, M_w and Đ for isosorbide-based polyesters with 1,5-pentanediol, via azeotropic distillation

Polyester	Mol% Isosorbide	M_n, Da	M_w, Da	Đ
		PPeIS		
4	0	3100	8300	2.70
11a	10	3100	10200	3.29
11b	30	1000	2100	2.00
11c	50	1200	2400	1.10
11d	60	900	1700	1.87
		$PPeF_{15}IS_{85}$		
6a	0	1400	2700	1.90
12a	10	1500	3100	2.11
12b	30	1200	2500	2.15
12c	50	800	1500	1.81
12d	60	500	1100	2.08
12e	70	700	1100	1.70
		$PPeF_{30}IS_{70}$		
6b	0	1400	2800	1.90
13a	10	1300	2600	1.99
13b	30	1100	2800	2.50
13c	50	900	1600	1.87
13d	60	500	700	1.50
13e	70	600	1000	1.61
		$PPeF_{70}IS_{30}$		
6c	0	3200	5900	1.80
14a	10	1800	3800	2.11
14b	30	1300	3200	2.42

14c	50	1000	1900	2.02
		$PPeF_{85}IS_{15}$		
6d	0	2100	4100	2.00
15a	10	2300	5400	2.29
15b	30	1300	2800	2.10
15c	50	1000	1800	1.83

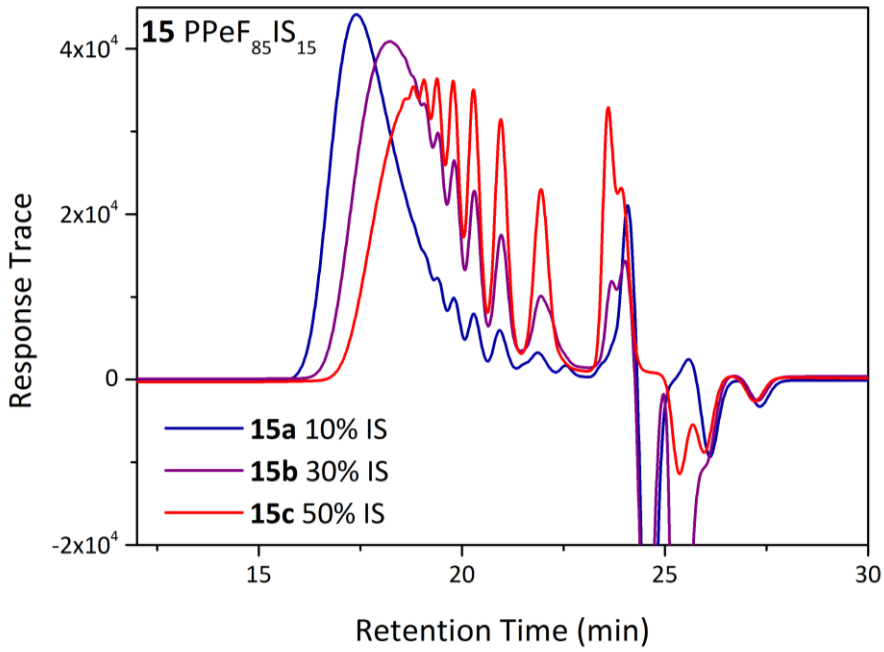

Figure 112. GPC chromatograms of polyesters $PPeF_{85}IS_{15}$ **15**, synthesised by azeotropic distillation in the second stage.

The molecular weight as a function of FDCA/SA composition is depicted in **Figure 113** for copolyesters bearing 10 mol% IS. The chromatograms for 30 and 50 mol% IS are available in **Appendix G**. The copolyesters $PPeF_{70}I_{10}S_{30}$ (**14a**) and $PPeF_{85}I_{10}S_{15}$ (**15a**) with 10% IS presented M_w of 3800 Da and 5400 Da, respectively and the dispersities of both compositions with different mol% IS were above 2. These values represent the highest molecular weights among the copolyesters of FDCA and succinic acid with isosorbide, whereas the lowest M_w figures correspond to $PPeF_{15}IS_{85}$ (**12**) and $PPeF_{30}IS_{70}$ (**13**) with either

60 or 70 mol% IS (1000 Da). In the case of $PPeF_{15}IS_{85}$ (**12**) and $PPeF_{30}IS_{70}$ (**13**), dispersities of 2 and M_w above 2000 Da were obtained when the isosorbide content was limited to 30%.

Table 55. M_n, M_w and Đ for isosorbide-based polyesters with 1,3-propanediol, via azeotropic distillation

Polyester	Mol% Isosorbide	M_n, Da	M_w, Da	Đ
		$PPF_{15}IS_{85}$		
3a	0	820	1200	1.46
7a	30	700	1100	1.60
7b	60	650	1000	1.53
7c	70	600	1000	1.50
		$PPF_{30}IS_{70}$		
3b	0	840	1200	1.47
8a	30	900	1500	1.68
8b	60	600	1000	1.61
8c	70	500	700	1.32

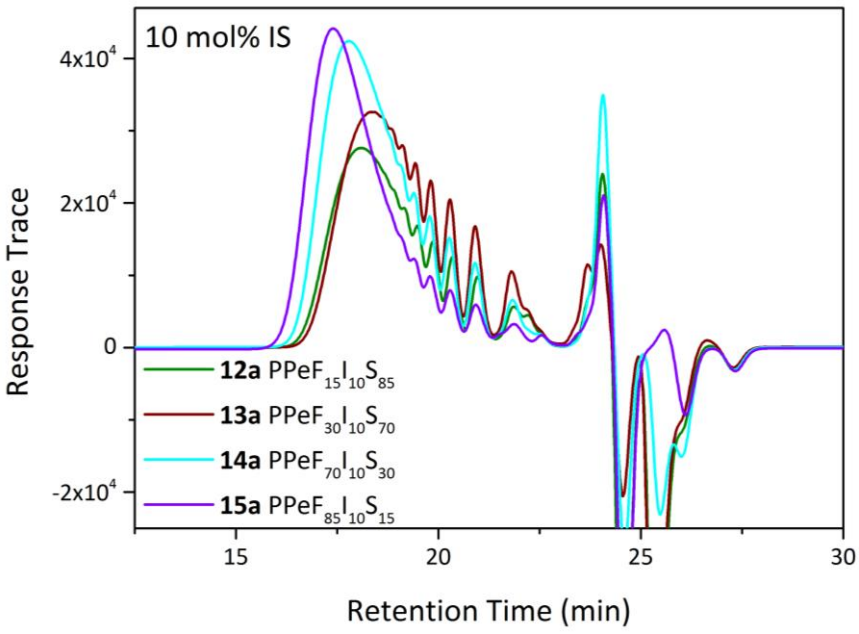

Figure 113. GPC chromatograms of polyesters PPeFIS **12a-15a** with 10 mol% isosorbide, synthesised by azeotropic distillation in the second stage.

The polyester composed by succinic acid moieties only, PPeIS (**11**), was greatly influenced by the addition of isosorbide. Polyester **11a**, with 10 mol% IS, had a M_w of 10200 Da, while polyester **11b**, bearing 30 mol% IS, had a dramatic decrease in the molecular weight, going down to 2100 Da. The last member of the polysuccinates, polyester **11d**, with 70 mol% had a M_w of 1700 Da. The chromatogram of **11** is included in **Appendix G**.

The results for PPFIS (**7-8**) resemble our findings with PPeFIS copolyesters. It was observed that M_n decreases as isosorbide content increases, for all compositions. **Figure 114** illustrates the chromatogram for $PPF_{15}IS_{85}$ (**7**). The one corresponding to $PPF_{30}IS_{70}$ (**8**) is shown in **Appendix G**.

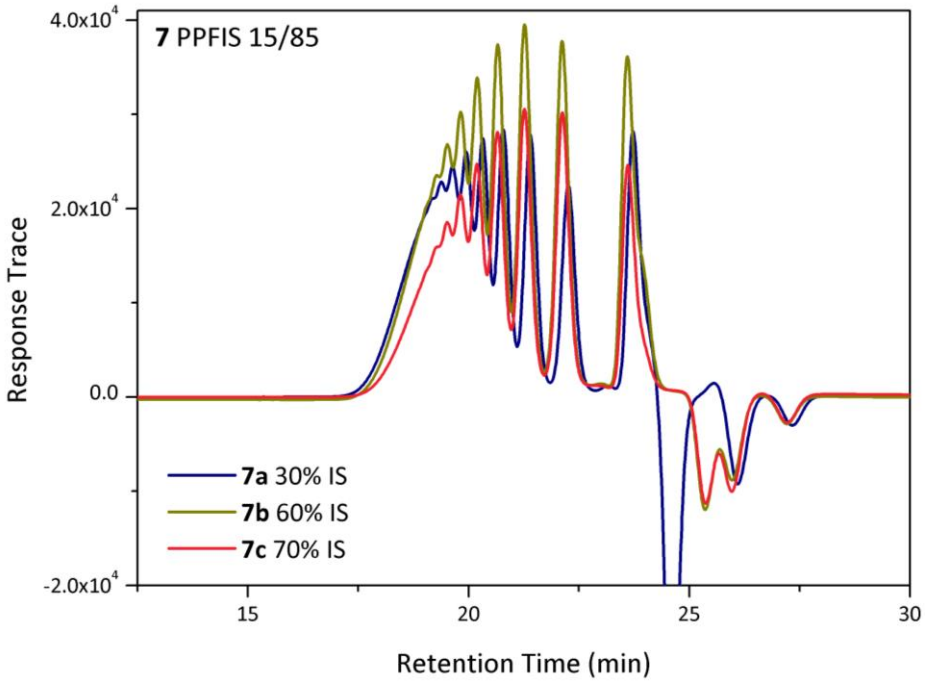

Figure 114. GPC chromatograms of polyesters **7**, synthesised by azeotropic distillation in the second stage.

Furthermore, the recorded M_n, M_w and Đ were lower than the ones obtained with 1,5-pentanediol. It was previously shown that copolyesters $PPeF_{15}IS_{85}$ (**12**) and $PPeF_{30}IS_{70}$ (**13**) presented M_w values in the ranges of 1100 to 3100 and 900 to 2500 Da, respectively whereas for $PPF_{15}IS_{85}$ and $PPF_{30}IS_{70}$were 900 to 1200 Da and 600 to 1300 Da, respectively. **Figure 115** illustrates this comparison between diols for $PPeF_{15}IS_{85}$ (**12**). Unfortunately, the results for $PPF_{70}IS_{30}$ (**9**) and $PPF_{85}IS_{15}$ (**10**) are not available since the samples were insoluble in THF. Although the results are incomplete, when comparing $PPF_{15}IS_{85}$ (**7**) and $PPF_{30}IS_{70}$ (**8**), the latter had higher M_n and M_w, suggesting the previous trend of increased M_n with FDCA

content is kept. This behaviour is depicted in **Figure 116** for $PPF_{15}I_{30}S_{85}$ (**7a**) and $PPF_{30}I_{30}S_{70}$ (**8a**) with 30 mol% IS.

The decrease in M_n as the isosorbide content increases was also reported in the literature.[167, 170, 171, 435, 446] One of the possible explanations was the decreased reactivity of the secondary OH groups when compared with the primary OH groups present in aliphatic linear diols, possibly corresponding to a lower acidic character.[162] Also, another contribution could be the difference in reactivity of the OH groups present in isosorbide, due to their stereochemical nature –*endo* and *exo*- and the steric hindrance of the *endo* hydroxyl group which is known to decrease the whole reactivity of the system.[162] The OH in *endo* position is more likely to form intra-molecular hydrogen bonding with the oxygen in main chains while the other in *exo* position is more reactive in polycondensation reactions.[447] In addition, the *endo* hydroxyl is protected by the steric bulk of the rest of the molecule.[448] It has been reported as well that cyclic structures could be formed, leading to a reduction of available functional groups.[170] It might be worthwhile to do a kinetic study to explore different catalysts and reaction times and their influence on the final molecular weight of the polyesters.

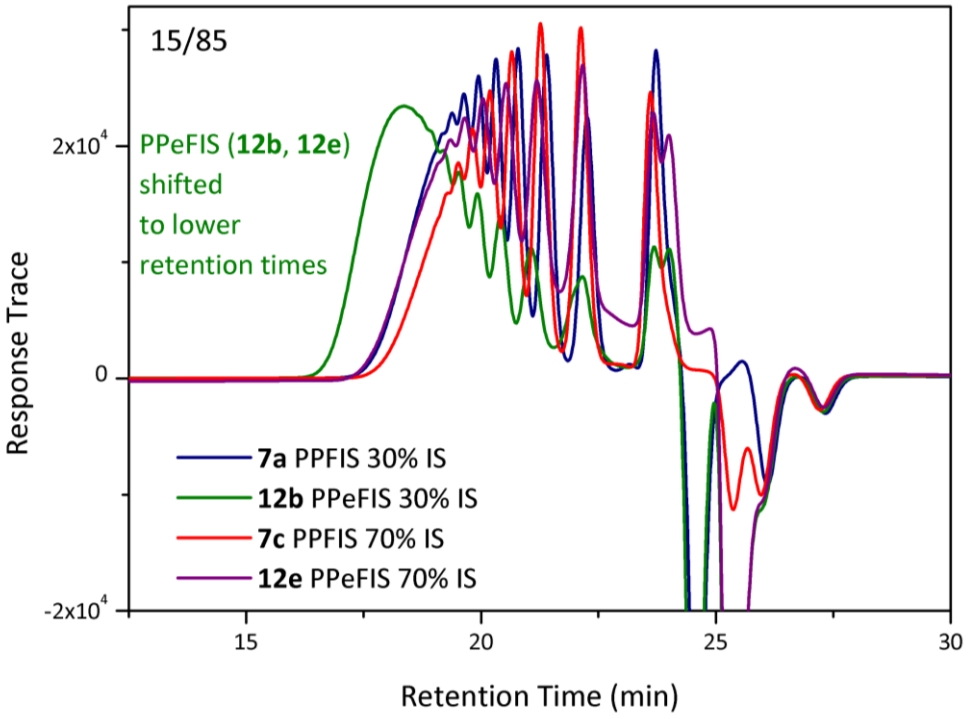

Figure 115. GPC chromatogram comparing $PPF_{15}IS_{85}$ with 1,3-propanediol (**7**) and $PPe_{15}FIS_{85}$ with 1,5-pentanediol (**12**) synthesised by azeotropic distillation in the second stage.

Wei, et al.[171] showed that in the copolyester poly(decamethylene sebacate-co-isosorbide sebacate), increasing the isosorbide content above 30%, resulted in a significant decrease in the number average molecular weights of the polyesters. In fact, the M_n of the homopolymer poly(isosorbide sebacate) was lower than 3000 Da. Sadler, et al.[446] synthesised unsaturated polyesters of phthalic anhydride, maleic anhydride, ethylene glycol and isosorbide. The polyesters had isosorbide contents from 10 to 25 mol%, and the molecular weight decreased accordingly from 7000 to 3500 Da. In the same vein, Noordover, et al.[170] reported M_n from 2000 to 3100 Da for polyesters of succinic acid and isosorbide, and M_n from 2700 to 4600 Da with the addition of 1,4-butanediol or neopentyl glycol as the second diol monomer. Moreover, Jasinska and Koning[256] synthesised unsaturated polyester resins via radical polymerisation of isosorbide, maleic anhydride and succinic acid with M_n in the range of 830 to 1770 Da.

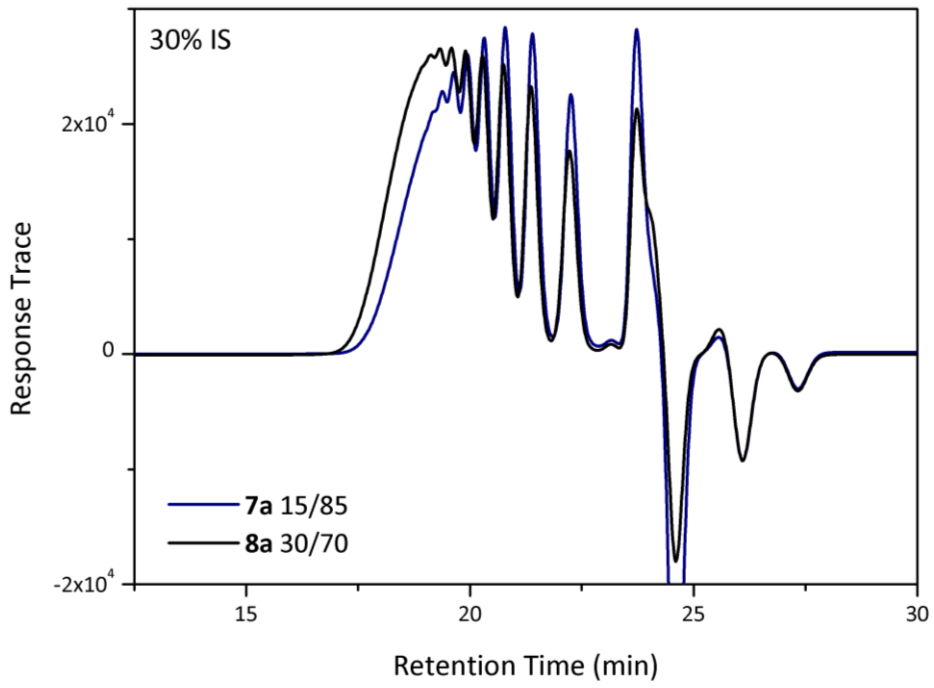

Figure 116. GPC chromatograms of PPFIS polyesters with 30 mol% IS: **7a** ($PPF_{15}I_{30}S_{85}$) and **8a** ($PPF_30I_{30}S_{70}$), synthesised by azeotropic distillation in the second stage.

The results suggest that the incorporation of more than 50 mol% IS when processing via azeotropic distillation is considerably detrimental to the molecular weight of the polyesters, even though a catalyst is added to the reaction mixture. If the isosorbide content is kept between 10 and 30 mol%, the molecular weights are in the desirable range for coatings, 2000 to 6000 Da.[170, 252] The following sections describe how the incorporation of isosorbide

leads to an improvement to the thermal and paint properties, compared to the parent polyesters in **Chapters 3** and **4**.

Some of the isosorbide-based polyesters were synthesised by applying vacuum in the second stage. **Table 56** summarises the results measured by GPC. It is evident how the application of vacuum increased the final molecular weight of the polyesters, as expected. In the case of isosorbide polyesters with 1,3-propanediol, there was no considerable difference in the M_w compared to the synthesis with azeotropic distillation. For instance, polyester **7a** has an increase of only 1100 Da when using vacuum. The difference is even less when the isosorbide content is increased from 30 to 50 mol% (Polyester **7b**) where the difference was only 250 Da in M_w and 90 Da in M_n. This suggests how the low reactivity and steric limitations of isosorbide are still detrimental to the synthesis, and could not be overcome despite the combined effect of vacuum and 0.02 mol% $SnCl_2$ as catalyst. Additionally, isosorbide is not volatile, property that could have prevented its release from the system.

Table 56. Comparison of M_n, M_w and Đ synthesised by azeotropic distillation or vacuum in the second stage

		Vacuum			Azeotropic distillation		
Polyester	**Mol% IS**	**M_n, Da**	**M_w, Da**	**Đ**	**M_n, Da**	**M_w, Da**	**Đ**
1,3-propanediol							
$PPF_{15}I_{30}S_{85}$ 7a	30	1200	2300	1.91	700	1100	1.60
$PPF_{15}I_{60}S_{85}$ 7b	60	770	1250	1.62	600	1000	1.53
1,5-pentanediol							
$PPeF_{15}I_{30}S_{85}$ 12b	30	3800	8800	2.31	1200	2500	2.15
$PPeF_{15}I_{50}S_{85}$ 12c	50	1850	4400	2.37	800	1500	1.81
$PPeF_{30}I_{30}S_{70}$ 13b	30	3400	7800	2.31	1100	2800	2.50

It is worth mentioning however than the vacuum did considerably push the reaction forward with isosorbide when the second diol was 1,5-pentanediol (**12b, 12c, 13b**). In the case of polyesters with 15 mol% FDCA, **12b** (30 mol% IS) and **12c** (50 mol% IS), the M_w greatly increased from 2500 to 8800 Da and 1500 to 4400 Da, respectively. It is observed that the M_w is higher as the isosorbide content decreases from 50 to 30 mol%, which resembles the previous results obtained with the azeotropic distillation. Finally, polyester **13b**, having 30 mol% isosorbide, showed a significant increase of 5000 Da in the final M_w. It is clear then that polyesters with 1,5-pentanediol and isosorbide are preferred in terms of macromolecular structure as the known plasticiser effect of 1,5-pentanediol seems to overcome the low reactivity of isosorbide. **Figure 117** shows the comparison between azeotropic distillation

and vacuum processing for polyesters **7a** and **7b**, respectively. The GPC chromatogram for polyesters **12b** and **12c** with 1,5-pentanediol and isosorbide are shown in **Figure 118**.

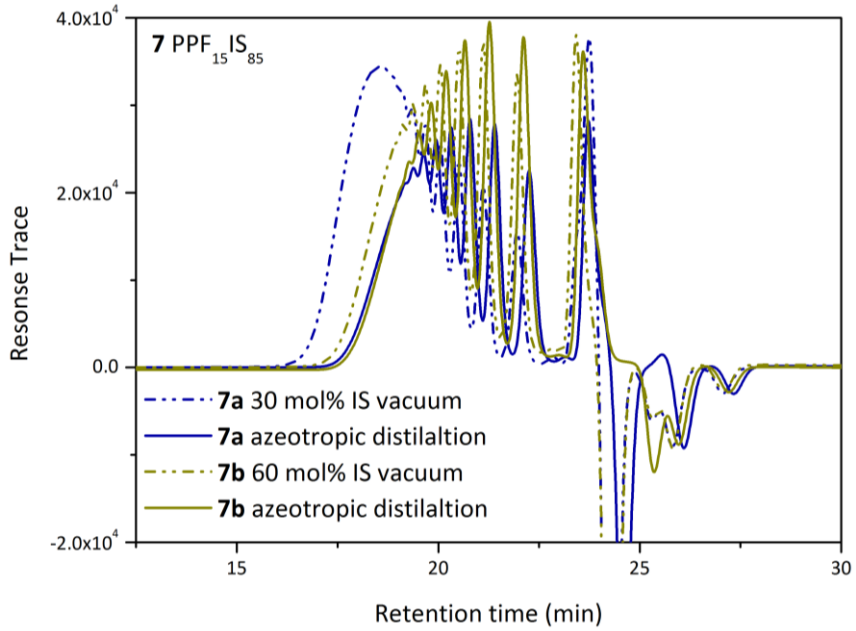

Figure 117. GPC chromatogram of **7b and 7c** synthesised by azeotropic distillation and application of vacuum.

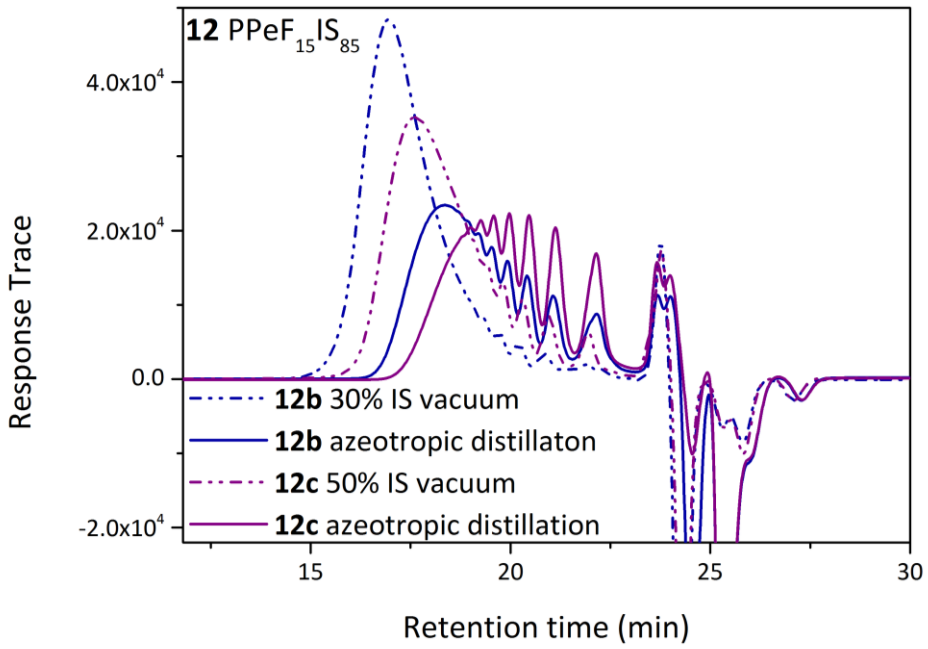

Figure 118. GPC chromatogram of **12b** and **12c** synthesised by azeotropic distillation and application of vacuum.

8.3.3 Differential Scanning Calorimetry (DSC)

The DSC scans for the copolyesters with 1,5-pentanediol, **12-15** are shown in **Figures 119-122** and the glass transition temperatures (T_g), melting temperatures (T_m) are summarised in **Table 57**. The T_g of the parent resins with no isosorbide is included as reference. The DSC thermogram for **11** is available in **Appendix G**.

The isosorbide content and glass transition temperature keep a linear relationship as expected. In all the different compositions, the T_g increases as a function of the mol% isosorbide. Sadler, et al.[446] demonstrated that adding as little as 10 mol % IS to the reaction mixture in place of an equivalent amount of a linear diol resulted in a significant increase in T_g.[446] Moreover, Noodover, et al.[170] demonstrated that by adding 60 and 80 mol% isosorbide to resins based on succinic acid and neopentyl glycol, the final achieved glass transition temperatures were 30.5 °C and 47.1 °C, respectively.

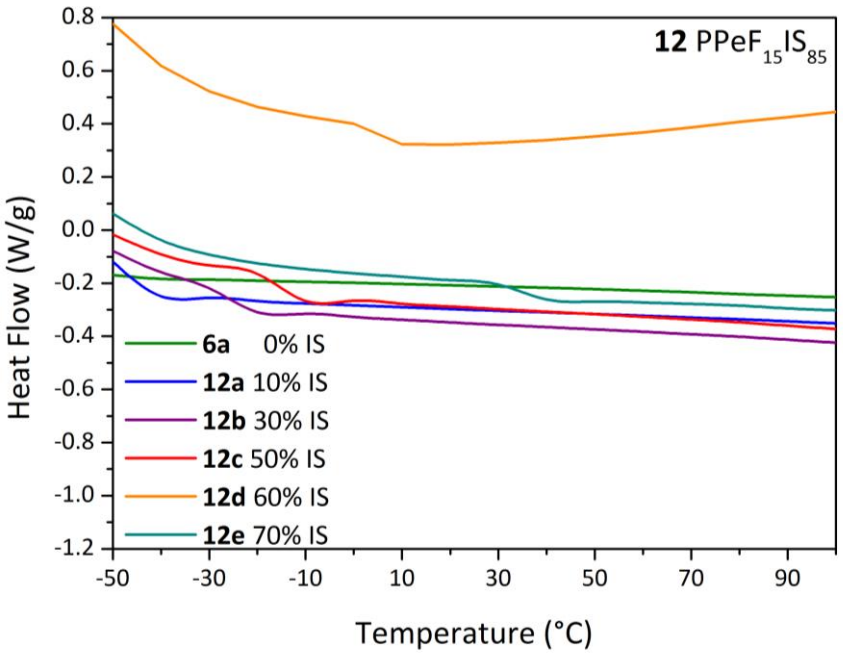

Figure 119. Second heating scan at 10 °C/min for polyesters $PPeF_{15}IS_{85}$ (**12a-12e**) including **6a** ($PPe_{15}FS_{85}$) as reference.

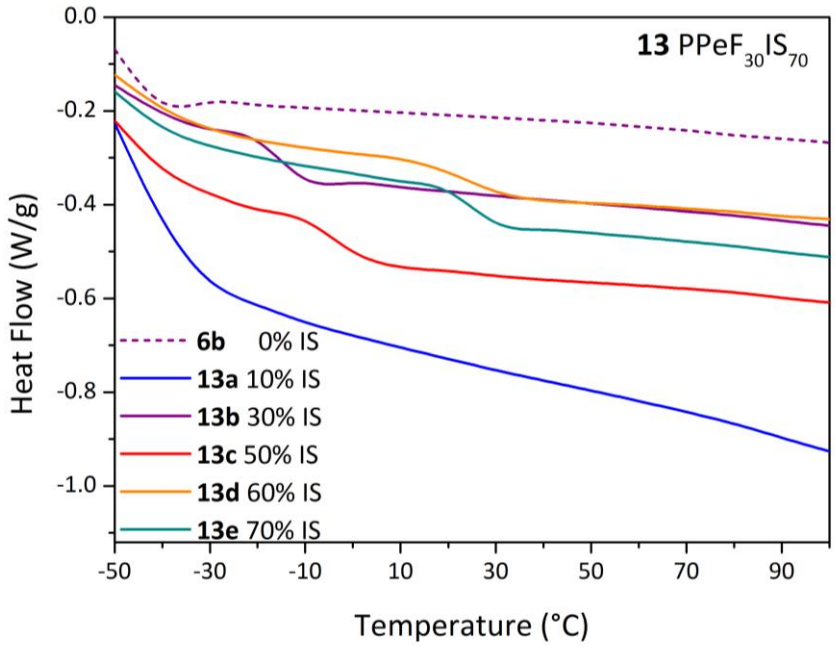

Figure 120. Second heating scan at 10 °C/min for polyesters $PPeF_{30}IS_{70}$ (**13a-13e**) including **6b** ($PPeF_{30}S_{70}$) as reference.

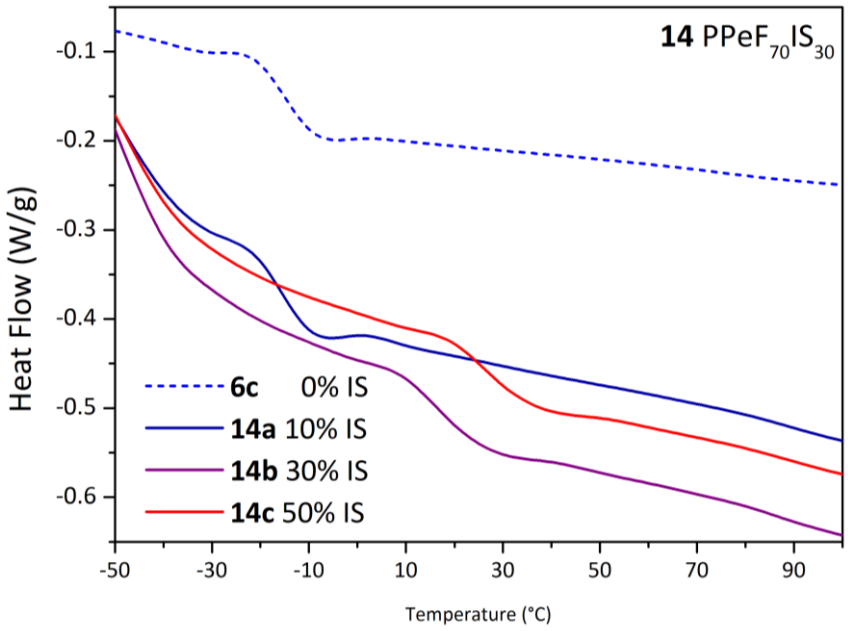

Figure 121. Second heating scan at 10 °C/min for polyesters $PPeF_{70}IS_{30}$ (**14a-14c**) including **6c** ($PPeF_{70}S_{30}$) as reference.

Table 57. Thermal transitions of isosorbide polyesters **11-15** measured by DSC

Code	Mol% Isosorbide	M_w, Da	T_g, °C	T_m, °C
		PPeIS		
4	0	8300	-48.7	36.8
11a	10	10200	-39.7	-
11b	30	2100	-36.0	-
11c	50	2400	-14.0	-
11d	60	1700	-0.5	-
		$PPeF_{15}IS_{85}$		
6a	0	2700	-46.0	-
12a	10	3100	-42.8	-
12b	30	2500	-26.5	-
12c	50	1500	-12.0	-
12d	60	1100	7.3	-
12e	70	1100	35.4	116.8
		$PPeF_{30}IS_{70}$		
6b	0	2800	-38.6	-
13a	10	2600	-38.6	-
13b	30	2800	-11.6	154.7
13c	50	1600	0.7	139.5
13d	60	700	22.7	105.1
13e	70	1000	24.3	77.3
		$PPeF_{70}IS_{30}$		
6c	0	5900	-10	-
14a	10	3800	-11.4	-
14b	30	3200	19.0	93.6
14c	50	1900	30.6	105.5
		$PPeF_{85}IS_{15}$		
6d	0	4100	0.6	49.6
15a	10	5400	3.6	119.2
15b	30	2800	20.2	101.5
15c	50	1800	22.3	138.7

Within the range of molecular weights of the resins, and taking into account the FDCA:SA composition of the base polyester, a minimum content of 50 mol% isosorbide is needed in order to achieve glass transition temperatures above 0 °C and above room temperature. This fact has been previously reported for the synthesis of polyesters based on succinic acid, neopentyl glycol and isosorbide.[170] The pure succinic acid polyester **11** presents low T_g values regardless the isosorbide content, therefore, a resin containing FDCA is preferred. The copolyesters $PPeF_{70}IS_{30}$ (**14**) and $PPeF_{85}IS_{15}$ (**15**) exhibited the highest T_g among the 1,5-pentanediol polyesters, achieving values of 30.6 °C and 22.3 °C, respectively.

Surprisingly, $PPeF_{70}I_{50}S_{30}$ (**14c**) had higher T_g (30.6 °C) than $PPeF_{85}I_{50}S_{15}$ (22.3 °C) with 50% mol isosorbide, but when only 10% mol isosorbide was added, the difference in respect to the base polyester is either negligible (-11°C for $PPeF_{70}I_{10}S_{30}$, **14a** and -10 °C for $PPeF_{70}S_{30}$, **6c**) or very little as per 85 mol% FDCA (3.6 °C, $PPeF_{85}I_{10}S_{15}$, **15a** and 0.6 °C, $PPeF_{85}S_{15}$, **6d**). Nonetheless, the slight difference might not be significant, and could come down to the acid value that was processed, which has a great influence on the final performance, as discussed with Becker Industrial Coatings Ltd. For the succinic acid rich polyesters $PPeF_{15}IS_{85}$ (**12**) and $PPeF_{30}IS_{70}$ (**13**), there is an abrupt increase in the glass transition temperature when the isosorbide content is 60% or above, going from values of approximately -40 °C up to 30 °C. This suggests that our library of polymers, based in three main monomers, would have different end properties just by tuning the desired content of isosorbide, expanding the potential applications of our renewable polyesters. **Figure 123** shows T_g and M_n as a function of isosorbide content for $PPeF_{70}IS_{30}$ (**14**) and $PPeF_{85}IS_{15}$ (**15**). It is observed how M_n decreases as the isosorbide content increases, as explained in the GPC section. The T_g-M_n-IS relationships for the remaining FDCA/SA compositions are included in **Appendix G**.

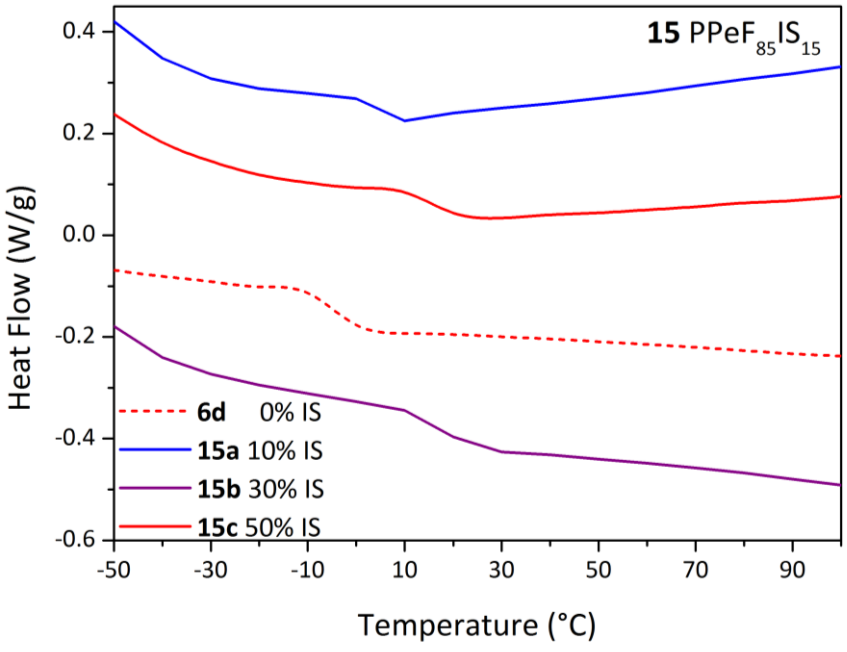

Figure 122. Second heating scan at 10 °C/min for polyesters $PPeF_{85}IS_{15}$ (**15a-15c**) including **6d** ($PPeF_{85}S_{15}$) as reference.

.

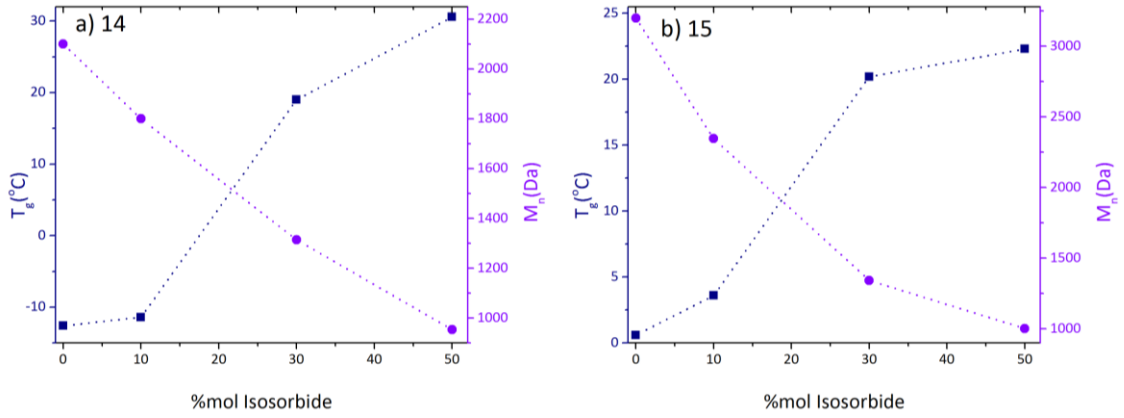

Figure 123. T_g and M_n as a function of mol% Isosorbide for a) $PPeF_{70}IS_{30}$ (**14**) and b) $PPeF_{85}IS_{15}$ (**15**).

Regarding the polyesters prepared with 1,3-propanediol, the results are presented in **Table 58**. The glass transition temperatures are slightly higher since they present lower chain flexibility than their 1,5-pentanediol counterparts**.** **Figure 124** shows the second heating scan for $PPF_{15}IS_{85}$ (**7**). The inclusion of 30 mol% isosorbide leads to an increase of T_g of about 30 °C (-45 °C to -14 °C) achieving a T_g at 6.2 °C with 70% mol IS.

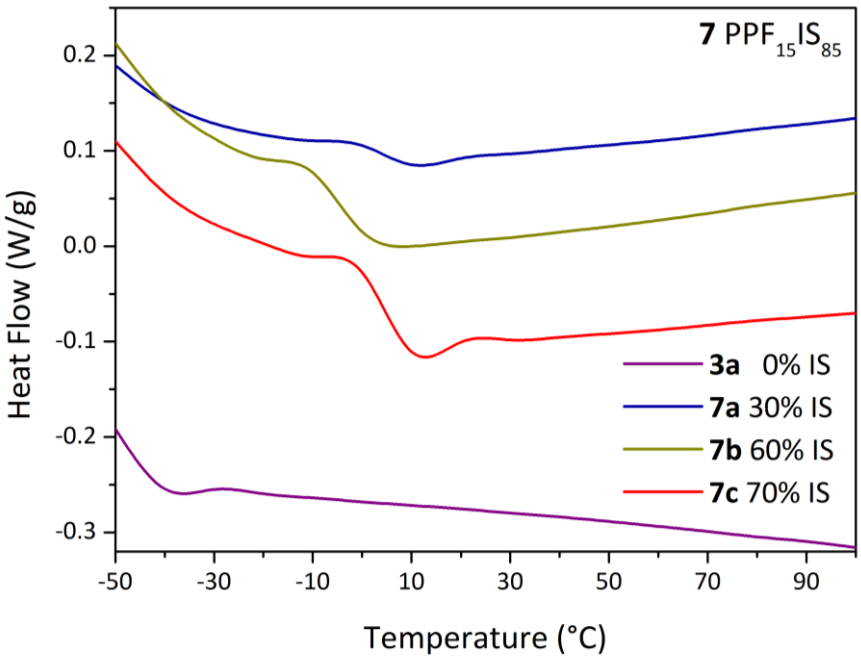

Figure 124. Second heating scan at 10 °C/min for polyesters $PPF_{15}IS_{85}$ (**7a-7c**) including **3a** ($PPF_{15}PS_{85}$) as reference.

Table 58. Thermal transitions of isosorbide polyesters **7**-**10** measured by DSC

Code	Mol% Isosorbide	M_w, Da	T_g, °C	T_m, °C
		$PPF_{15}IS_{85}$		
3a	0	1200	-45.0	-
7a	30	1100	-14.1	-
7b	60	1000	0.1	-
7c	70	1000	6.2	-
		$PPF_{30}IS_{70}$		
3b	0	1200	-39.0	-
8a	30	1500	4.0	-
8b	60	1000	10.2	-
8c	70	700	-36	-
		$PPF_{70}IS_{30}$		
3c	0	1700	2.1	111.7
9a	10	-	-6.4	97.0
9b	30	-	8.3	98.0
9c	50	-	29.2	113.7
		$PPF_{85}IS_{15}$		
3d	0	1400	10.1	133.6
10a	10	-	1.6	131.6
10b	30	-	19.8	114.6
10c	50	-	53.2	97.1

In the case of $PPF_{30}I_{70}S_{70}$ (**8c**) with 70% it is observed that the T_g of -36 °C is below those of the resins with 30 and 60% isosorbide (4 °C and 10.2 °C, respectively) when it should be higher according to the isosorbide effect. The M_n and M_w of the resin are very low - 500 and 700 Da, respectively- which could be the explanation for the observed phenomenon. The DSC scan of **8** is included in **Appendix G**.

The copolyesters $PPF_{70}I_{50}S_{30}$ with 50% IS (**9c, Figure 125**) and $PPF_{85}I_{50}S_{15}$ with 50% (**10c**) exhibited the highest T_g among all the polyesters, achieving values of 29.2 and 53.2 °C, respectively. The first and second heating scans for **9** and **10**, respectively, are available in **Appendix G**.

For the succinic acid rich polyesters $PPF_{15}IS_{85}$ (**7**) and $PPF_{30}IS_{70}$ (**8**), there is an abrupt increase in the glass transition temperature from an isosorbide content of 60%, going from approximately -40 °C up to 10 °C. **Figure 126** shows T_g and M_n as a function of isosorbide content for **7** and **8** since GPC data is unavailable for 70 mol% and 85 mol% FDCA compositions. It is observed how in all cases M_n decreases as the isosorbide content increases, as explained in the GPC section. No crystallisation peaks were observed for any of

the isosorbide-based polyesters. This type of transition is normally found in long chain aliphatic polyesters with a high tendency to crystallise into perfect and stable crystals.[311]

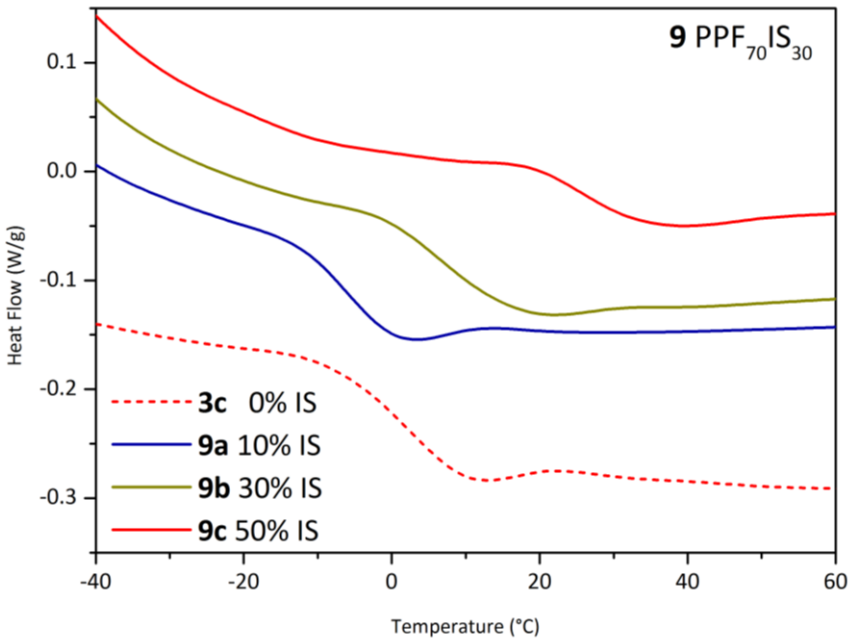

Figure 125. Second heating scan at 10 °C/min for polyesters $PPF_{70}IS_{30}$ (**9a-9c**).

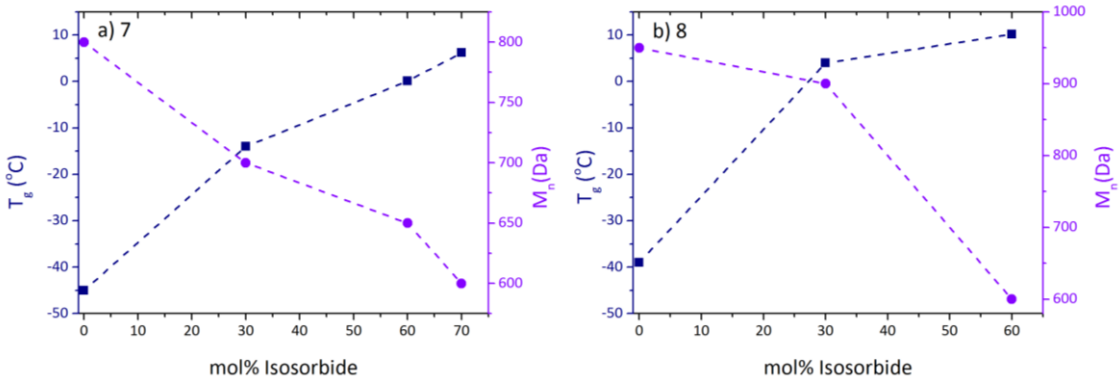

Figure 126. T_g and M_n as a function of mol% Isosorbide for a) $PPF_{15}IS_{85}$ (**7**) and b) $PPF_{30}IS_{70}$ (**8**).

Regarding melting temperatures (T_m) 1,5-pentanediol polyesters with FDCA contents of 30% and above (**13-15**) showed melting endotherms from 77.3 °C to 154.7 °C, whereas for 1,3-propanediol the only observable T_m's (97-131 °C) correspond to those of 70 (**9**) and 85 (**10**) mol% FDCA. In the case of **10** and **13**, T_m decrease with an increase of IS content, a

phenomenon that was previously observed in copolyesters of sebacic acid, 1,3-propanediol and varying isosorbide content,[435] whereas the other compositions exhibit the opposite trend.

Particularly, polyesters **9** and **10** did not show a single melting peak in the DSC heating scan, as observed in **Figure 127** for **10**. This behaviour has been reported in the literature[435, 449-451] for different copolyesters, and it is thought to be potentially the result of the existence of different crystal types in the same polymer sample,[449] melting–recrystallisation–remelting processes,[451-453] or the presence of different molecular weight species.[435] It is necessary to confirm the assumptions regarding crystallinity features by performing a XRD analysis of the polyesters, which remains as future work. There is a strong possibility that the polyesters are conformed by different oligomers with varying molecular weights, as the presence of isosorbide tends to form cyclic oligomeric structures.[170, 454] Again, the confirmation of these structures requires further analysis, such as MALDI-TOF-MS, and is part of the future work regarding these polyesters.

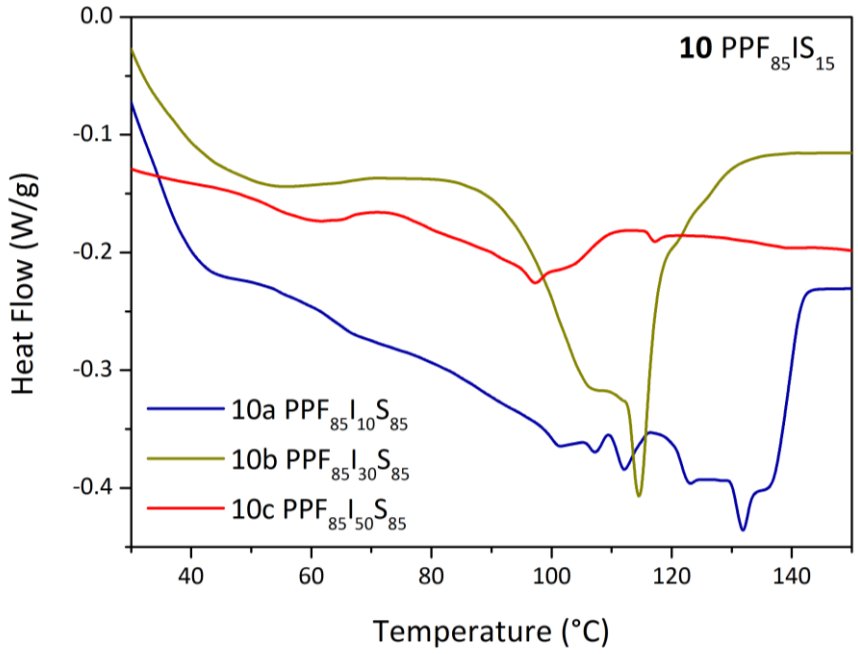

Figure 127. First heating scan at 10 °C/min for polyesters $PPF_{85}IS_{15}$ (**10**).

Previous syntheses of IS-derived polyesters have reported glass transition temperatures in the range presented herein or below. For instance, the T_g's of PIS poly(isosorbide sebacate) and PIA poly(isosorbide itaconate) were 6.4 °C (M_n=19200 Da) and 34.5 °C (M_n= 8700 Da), respectively.[169] Wei, et al.[171] synthesised polyesters of 1,10-decanediol, sebacic acid and

isosorbide with different mol% isosorbide, namely, 43.9, 66.2 % and 100 %. The polyesters showed T_g's at -26 °C, -18 °C and -5 °C, with M_w= 8900, 8699 and 2800 Da, respectively. The authors did not observe glass transitions for 5.3 or 16.7 mol %, IS, which they attribute to the fact that long chain aliphatic polyesters have a strong crystallisation capacity and crystallize very fast.[171] Likewise, Okada, et al.[174] synthesised polyesters from isosorbide and different diacid chlorides, such as succinyl dichloride, glutaryl dichloride, adipoyl dichloride, and sebacoyl dichloride. The polyesters had T_g's between 36 °C (adipoyl dichloride. M_n=8000 Da) and -10 °C (sebacoyl dichloride, M_n= 34000 Da).

As analysed in **Section 8.3.2**, polyesters **7a-7b** and **12a-12b** were alternatively synthesised by applying vacuum during the second stage of the polymerisation. The DSC results are summarised in **Table 59**, along with the results obtained with azeotropic distillation. In the case of **7a**, the T_g did not change when processed under reduced pressure, probably because of the small difference in molecular weight obtained with both processing methods. Interestingly, **7b** synthesised by azeotropic distillation displayed a T_g at 0.1 °C, whereas the polyester synthesised via vacuum had a T_g at 8.7 °C.

PPeFIS (**12**) had increased T_g for the polyesters with higher M_w obtained via the application of vacuum, as expected. The largest effect is observed for **12c**, which bears 50 mol% IS, for whose T_g varied from -3.1 °C to 12.0 °C**.** The DSC scan comparing the processing methods for **12** is illustrated in **Figure 128.**

Table 59. Comparison of T_g for **7** and **8** synthesised by azeotropic distillation or vacuum in the second stage.

	Vacuum			Azeotropic distillation		
Polyester	**Mol% IS**	**M_w, Da**	**T_g, °C**	**Mol% IS**	**M_w, Da**	**T_g, °C**
$PPF_{15}IS_{85}$						
7a $PPF_{15}I_{30}S_{85}$	30	2300	-15.3	30	1100	-14.1
7b $PPF_{15}I_{60}S_{85}$	60	1250	-8.7	60	1000	0.1
$PPeF_{15}IS_{85}$						
12b $PPeF_{15}I_{30}S_{85}$	30	8800	-21.7	30	2500	-26.5
12c $PPeF_{15}I_{50}S_{85}$	50	4400	-3.1	50	1500	-12.0

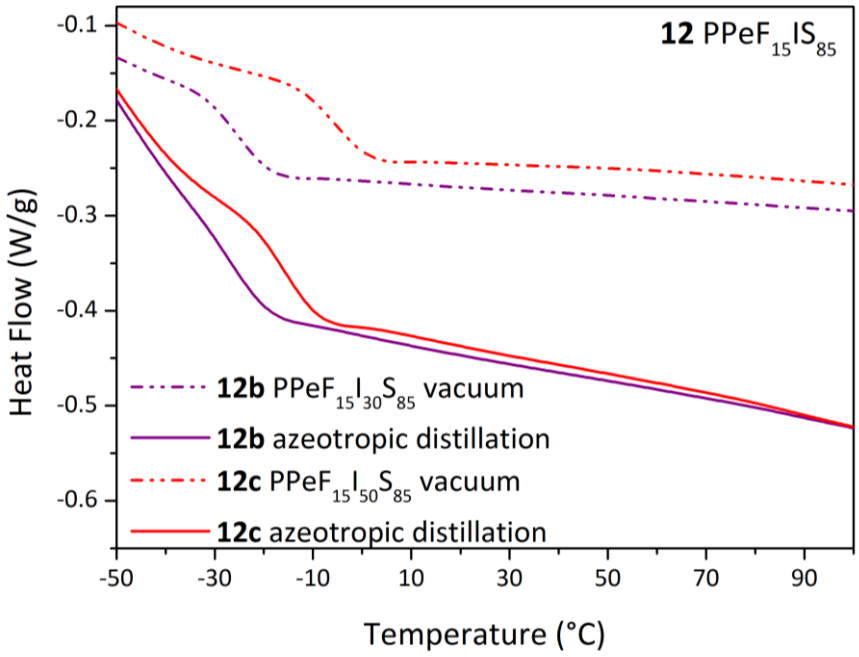

Figure 128. DSC scan of $PPeF_{15}I_{30}S_{85}$ (**12b**) and $PPeF_{15}I_{50}S_{85}$ (**12c**) synthesised by azeotropic distillation and application of vacuum.

8.3.4 Thermal Gravimetric Analysis (TGA)

The thermal stability of the isosorbide polyesters was measured by TGA. **Table 60** shows the thermal decomposition temperatures (T_d) for 1,5-pentanediol resins (**11-15**) whereas **Table 61** summarises the results using 1,3-propanediol (**7-10**). TGA indicates that the thermal stability ranges from 308 °C to 371 °C for **11-15**. Interestingly, **7-10** showed a slightly higher and narrower T_d range between 362 and 372 °C for **7-10**. **Figure 129** shows the thermograms for the polyesters $PPeF_{15}IS_{85}$ (**12**) and $PPeF_{30}IS_{70}$ (**13**); $PPeF_{70}IS_{30}$ (**14**) and $PPeF_{85}IS_{15}$ (**15**) are depicted in **Figure 130**. The thermograms for 1,3-propanediol resins are illustrated in **Figure 131** and **Figure 132**.

Table 60. Characteristic decomposition temperatures T_{d1}, T_{dmax} and weight loss % of polyesters **11-15**

Code	Mol% Isosorbide	T_{d1}, °C	T_{dmax}, °C	Weight loss % (T_{dmax})
		PPeIS		
4[a]	0	-	401.4	97.5
11a	10	-	371.6	98.8
11b	30	287.9	371.0	98.3
11c	50	258.9	367.7	96.9
11d	60	291.9	376.3	99.2
		$PPeF_{15}IS_{85}$		
6a[a]	0	298.1	399.6	99.9
12a	10	277.3	365.8	98.2
12b	30	-	370.2	97.9
12c	50	228.5	368.3	98.4
12d	60	273.8	373.8	98.8
12e	70	214.3	371.2	96.8
		$PPeF_{30}IS_{70}$		
6b[a]	0	140.9	403.4	99.8
13a	10	284.0	361.6	97.3
13b	30	125.4	362.4	97.2
13c	50	127.4	366.7	97.6
13d	60	207.0	368.8	93.9
13e	70	237.7	369.8	96.9
		$PPeF_{70}IS_{30}$		
6c[a]	0	-	389.1	97.4
14a	10	252.9	357.7	97.8
14b	30	89.9	348.1	96.6
14c	50	110.4	340.9	97.1
		$PPeF_{85}IS_{15}$		
6d[a]	0	104.4	385.3	91.1
15a	10	-	364.3	99.8
15b	30	114.9	340.9	96.4
15c	50	158.7	366.1	99.8

[a] Synthesised at 220 °C.

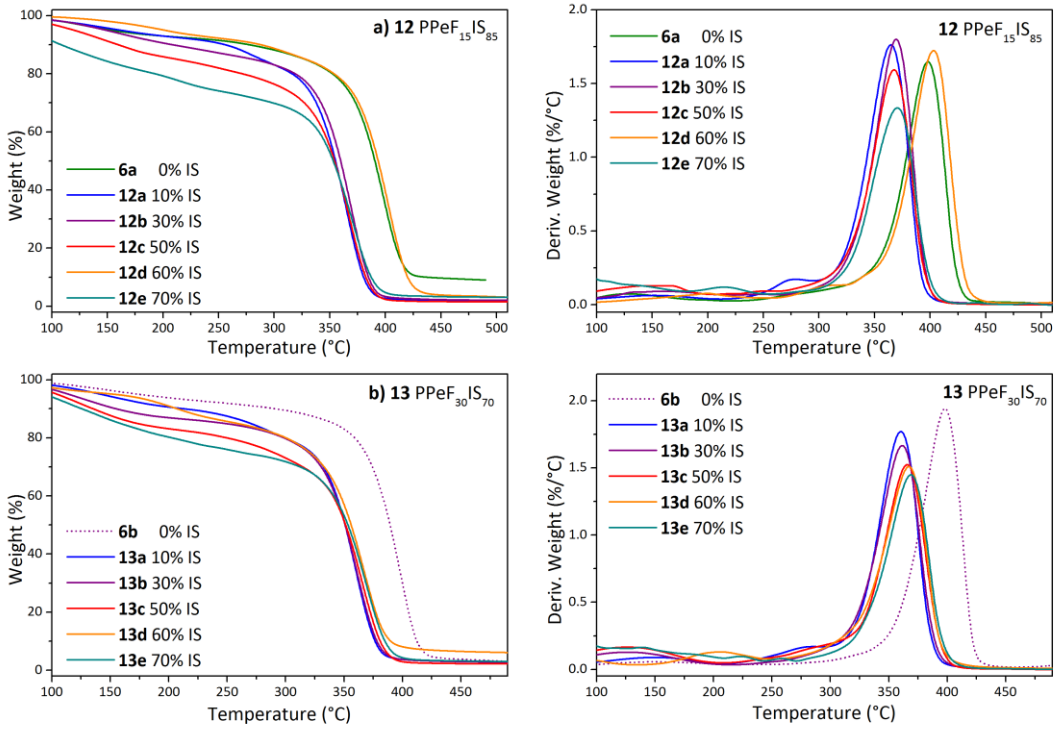

Figure 129. Weight % and derivative weight thermograms of polyesters a) $PPeF_{15}IS_{85}$ (**12**) and b) $PPeF_{30}IS_{70}$ (**13**) (N_2 flow, 10 °C/min).

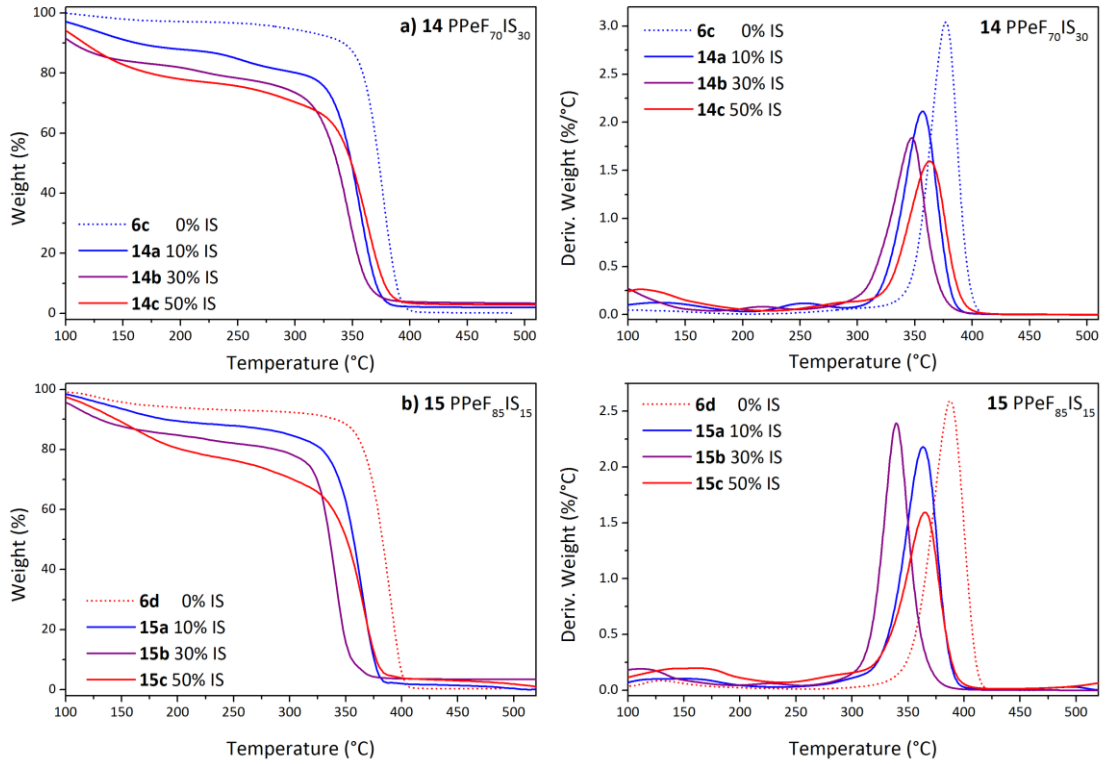

Figure 130. Weight % and derivative weight thermograms of polyesters a) $PPeF_{70}IS_{30}$ (**14**) and b) $PPeF_{85}IS_{15}$ (**15**) (N_2 flow, 10 °C/min).

Table 61. Characteristic decomposition temperatures T_{d1}, T_{dmax} and weight loss % of polyesters **7-10**

Code	Mol% Isosorbide	T_{d1}, °C	T_{d2}, °C	T_{dmax}, °C	Weight loss % (T_{dmax})
		$PPF_{15}IS_{85}$			
3a[a]	0	298.6	-	401.0	99.2
7a	30	181.9	281.1	370.5	98.3
7b	60	176.9	290.9	371.1	97.1
7c	70	174.1	278.2	368.7	98.3
		$PPF_{30}IS_{70}$			
3b[a]	0	299.5	-	395.9	98.5
8a	30	163.5	288.6	367.2	97.1
8b	60	122.5	180.3	372.0	97.7
8c	70	194.0	253.7	368.8	98.7
		$PPF_{70}IS_{30}$			
3c[a]	0	299.0	-	394.0	95.7
9a	10	280.3	-	368.0	99.7
9b	30	266.1	-	371.3	98.9
9c	50	98.7	277.4	371.4	99.8
		$PPF_{85}IS_{15}$			
3d[a]	0	291.8	-	393.8	95.0
10a	10	273.8	-	371.5	97.5
10b	30	143.4	277.4	363.0	99.4
10c	50	113.8	290.0	361.8	93.1

[a] Synthesised at 220 °C

For both linear aliphatic diols, it is observed that in general, the incorporation of isosorbide to the main polymers resulted in a decrease of approximately 30-40 °C in the maximum T_d of the resins, which were close (~385 °C) or above 400 °C. Within each FDCA/SA composition, the results suggest that the PPeFIS polyesters with highest mol% isosorbide present the highest decomposition temperature. However, the same trend was not observed for PPFIS, where all the polyesters had similar T_d values.

As previously reported by Noordover, et. al,[170] the 1,5-pentanediol polyesters are thermally stable up to 230 °C, except for **14** and **15** with more than 30 mol% isosorbide, where the first decomposition temperature is around 90-115 °C. This low decomposition temperature appears as well for $PPeF_{30}IS_{70}$ (**13**) with either 30 or 50 mol%, where the T_d is between 125 and 127 °C.

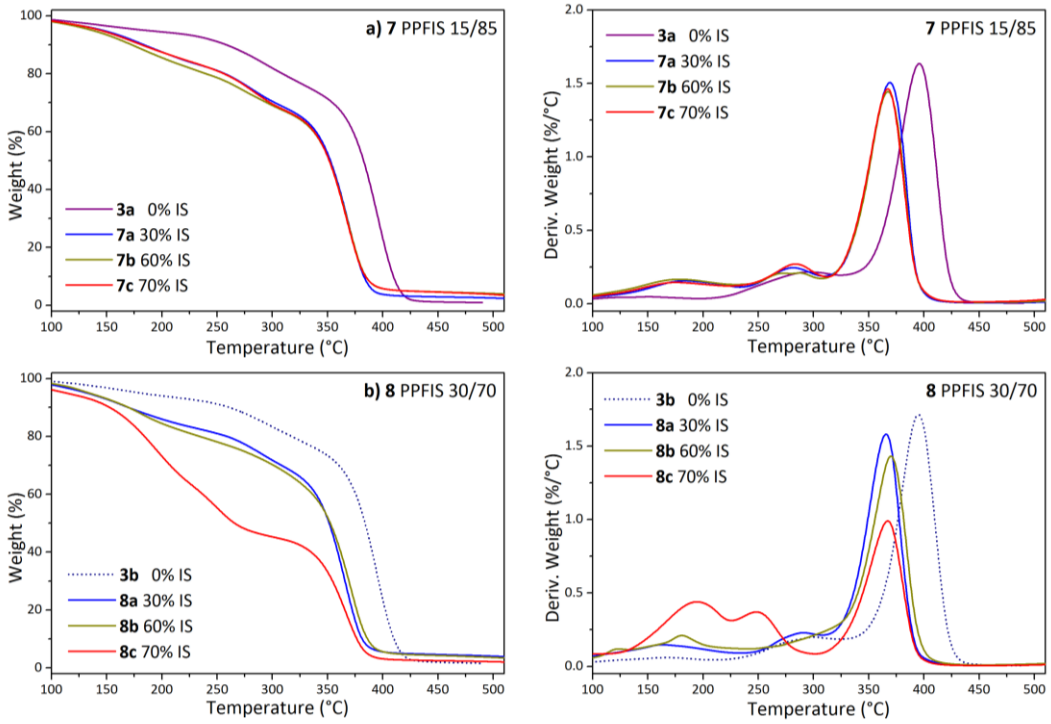

Figure 131. Weight % and derivative weight thermograms of polyesters a) $PPF_{15}IS_{85}$ (**7**) and b) $PPF_{30}IS_{70}$ (**8**) (N_2 flow, 10 °C/min).

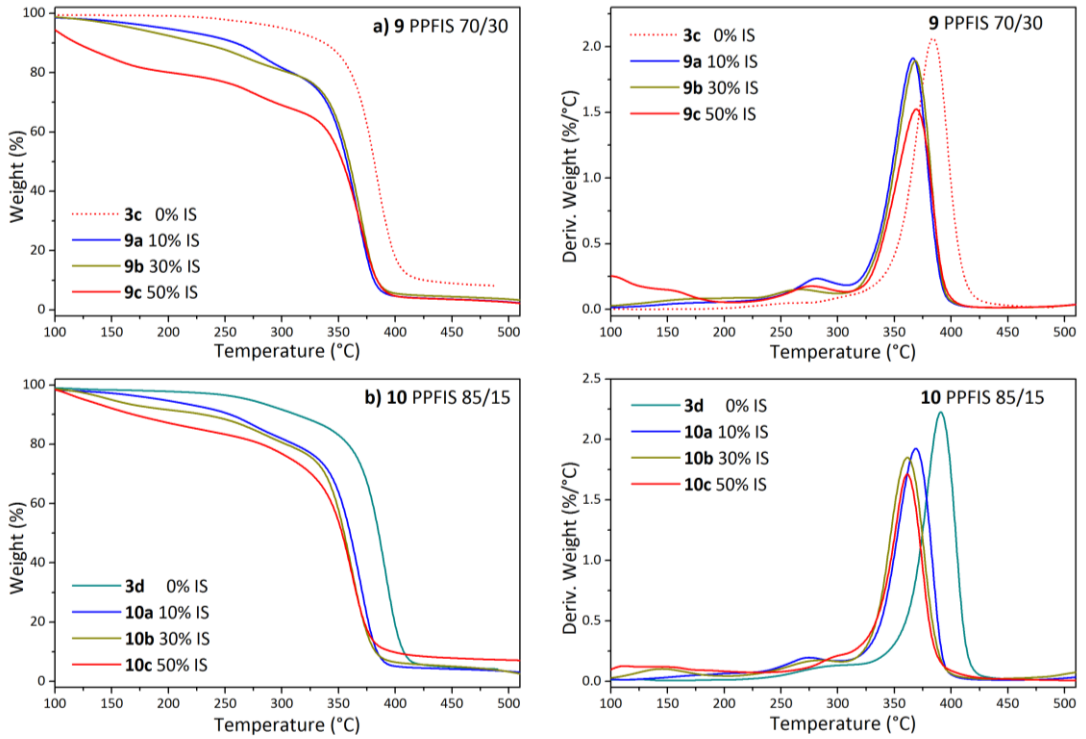

Figure 132. Weight % and derivative weight thermograms of polyesters a) $PPF_{70}IS_{30}$ (**9**) and b) $PPF_{85}IS_{15}$ (**10**) (N_2 flow, 10 °C/min).

Storbeck and Ballauff[90] reported T_d values of 320 °C to 350 °C for polyesters prepared with the acid chloride of FDCA and different 1,4:3,6-dianhydrohexitols. Other T_d ranges include those for isosorbide-isophthalate and lactide copolyesters (346-397 °C)[167] and 400-419 °C for unsaturated polyester resins of isosorbide, maleic anhydride and phthalic anhydride.[446] For these resins, the authors reported initial decomposition temperatures from 208 to 299 °C, and concluded that despite that the incorporation of isosorbide did not have a clear effect on the maximum decomposition temperature; it did seem to increase the initial T_d. The authors attributed the phenomena to the molecular weight of the oligomers, being the ones with higher molecular weights capable of withstanding higher temperatures before beginning to decompose.[446]

It is worth mentioning that within some diacid compositions, higher isosorbide content did promote the formation of more oligomeric, low molecular weights species which decompose at lower temperatures, as analysed in **Section 8.3.2**. Nevertheless, the contrary effect was reported by Zhou and co-workers,[435] where it was concluded that the incorporation of IS improved the thermal stability of the copolymers of sebacic acid and 1,3-propanediol, going from a T_d of 414 °C for the polyester of sebacic acid and 1,3-propanediol, although the mol% IS was kept between 11 and 53%, with a molar diacid:diols ratio of 1.05:1 Few of our biomass-derived resins follow this trend, namely polyesters **8, 9, 11** and **13**.

Specifically for 1,3-propanediol, the thermogravimetric data (**Figure 131**, **Figure 132**) suggests the presence of diverse species within the polymer matrix, as three different decomposition temperatures (T_{d1}, T_{d2} and T_{dmax}) are observed. All the diacid compositions present the first decomposition temperature between 98.7 °C and 194 °C, followed by a second transition at 180-290 °C. The lowest T_d's appear to be prompted by isosorbide concentrations of above 50 mol%. The nature of these species has not been determined; however, previous research has shown that polyesters like PET and PBT undergo decomposition mechanisms initiated by scission of an alkyl-oxygen bond, suggesting a random-chain scission.[455] Also, the decomposition of these polyesters is suggested to be dominated by cyclic or open chain oligomers with carboxylic-end groups. The formation of these cyclic oligomers is done through an intramolecular exchange reaction which happens below 300 °C[456] which could be the same process that took place in our polyesters. Cyclisation of isosorbide-based polyesters has indeed been reported by other authors.[167, 170] **Scheme 49** shows the formation of cyclic oligomers for generic poly(terephthalate)s. A

detailed MS analysis is needed to determine the exact species formed, along with a study on decomposition kinetics. In the case of polyesters with low FDCA and rich isosorbide contents, data suggests the formation of more volatile products, which some authors have determined to arise from the secondary breakdown of end-groups, which follows the primary step of cyclic concerted decomposition.[457]

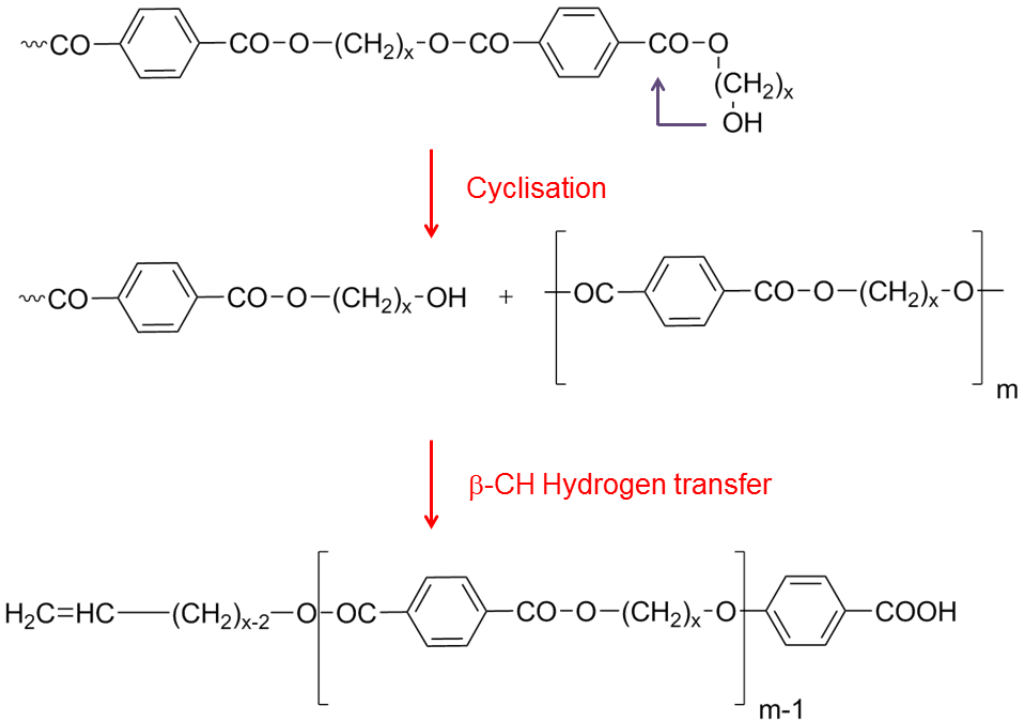

Scheme 49. Formation of cyclic oligomers for poly(terephthalate)s, adapted and modified from Montaudo, et al.[456]

8.3.5 Paint testing

Representative samples of the isosorbide polyesters synthesised via azeotropic distillation were formulated into the white polyester protocol formulation described in previous chapters.

Table 62 and **Table 63** summarise the results obtained. For succinic acid-rich polyesters, the chosen samples were those with higher isosorbide concentrations. Specifically in the case of 1,3-propanediol resins however, it was not possible to make paints with $PPF_{15}I_{70}S_{85}$ (**7c**) and $PPF_{30}I_{70}S_{70}$ (**8c**) (70 mol% isosorbide) as they were immiscible with the paint system. In the case of **9c** (50% mol isosorbide) the resin was a brittle solid, which prevented to dissolve it in the paint solvents required for characterisation.

Table 62. Physical test results on white paints based on polyesters **12-14** and the reference resin **R**

Test	Specification	R	12e	13e	14b	14c
Colour	White	White	White	White	White	White
Pencil Hardness	H	H	2H	3H	H	H
Gloss Top Coat	30-40 at 60°	35	39	35	40	39
Reverse Impact 80" lb	No cracking	Moderate cracking	Moderate cracking	Moderate cracking	Slight cracking	Moderate cracking
Erichsen 7.5 mm	No cracking	Moderate cracking	Severe cracking	Severe cracking	Slight cracking	No cracking
T-Bend NTPO	2T	0.5T	1T	1.5T	0	1T
T-Bend no cracking[a]	3T	3T	5T	6T	2.5T	5T
MEK[b] rubs primer	100	110	110	110	110	110
T_g, °C	-	35	66	53	34	67
Microhardness, $N{\cdot}m^{-2}$	-	216	237	287	190	270

[a]: Cracking is detected by removal of a pressure-sensitive tape placed on the bend edges and observing the degree of removed coating particles. [b]: Methyl ethyl ketone

As previously reported for coating applications,[162, 170, 259, 446] the introduction of isosorbide into the synthesis of the polyester resins improved the thermomechanical properties of the resulting paints, compared to the parent polyesters **3** and **6** presented in **Chapters 3** and **4**, respectively. $PPeF_{15}S_{85}$ (**6a**) and $PPeF_{30}S_{70}$ (**6b**) had very low microhardness (11 $N{\cdot}m^{-2}$ and 12 $N{\cdot}m^{-2}$, respectively) and low T_g (-28 °C and -17 °C, respectively), but when 70 mol% isorbide was added ($PPeF_{15}I_{70}S_{85}$ **12e**, $PPeF_{30}I_{70}S_{70}$ **13e**) the microhardness was 237 $N{\cdot}m^{-2}$ and 287 $N{\cdot}m^{-2}$, with T_g at 66 °C and 53 °C. The resins were not very flexible as T-Bend was 5T and 6T and both presented severe cracking after the Erichsen testing, which suggested that the concentration of FDCA should be increased. $PPeF_{70}I_{30}S_{30}$ with an isosorbide concentration of 30 mol% (**14b**) showed an improvement in flexibility

(2.5T) respect to the reference resin (3T), T_g on specification at 34 °C and better impact resistance as it presented a slight cracking. Moreover, $PPeF_{70}I_{50}S_{30}$ (**14c**) had above-specification Erichsen (No cracking), T_g (67°C) and microhardness (270 $N{\cdot}m^{-2}$) than the reference resin **R**. Similarly, comparing **14** with the parent resin **6c**, the properties are considerably improved (T_g= 6 °C, Microhardness= 20 $N{\cdot}m^{-2}$ and T-Bend no cracking of 1.5T).

$PPeF_{85}IS_{15}$ resins (**15**) again showed better microhardness and higher T_g than $PPeF_{85}S_{15}$ (**6d**), as the results were 21 $N{\cdot}m^{-2}$ and 15 °C. **15c** (50 mol% IS), despite having the highest T_g (69 °C) and enhanced microhardness (299 $N{\cdot}m^{-2}$) is slightly harder (Pencil Hardness 2H) and presents poor flexibility measured by T-Bend no cracking (5.5T). **15b** therefore, with 30 mol% isosorbide, presents the best overall properties.

Table 63. Physical test results on white paints based on polyesters **10** and **15** and the reference resin **R**

Test	Specification	R	15a	15b	15c	10b
Colour	White	White	White	White	White	White
Pencil Hardness	H	H	H	F	2H	H
Gloss Top Coat	30-40 at 60°	35	40	43	38	39
Reverse Impact	80'' lb	Moderate cracking	No cracking	Moderate cracking	Severe cracking	Slight cracking
Erichsen	7.5 mm	Moderate cracking	No cracking	No cracking	Severe cracking	Slight cracking
T-Bend NTPO	2T	0.5T	0	1.5	1T	1.5T
T-Bend no cracking[a]	3T	3T	1T	2T	5.5T	2.5T
MEK[b] rubs primer	100	110	110	110	110	110
T_g, °C	-	35	32	42	69	34
Microhardness, $N{\cdot}m^{-2}$	-	216	174	194	299	169

Regarding 1,3-propanediol, the only possible resin analysed was **10b** (30 mol% isosorbide), although it cannot be compared to the parent resin **6d** because it was impossible to make a paint out of it as it remained solid and would break up when adding solvent. The reverse impact and Erichsen of **10b** were although better than the reference resin, had the same pencil hardness, close flexibility and T_g (2.5T, 34 °C), but presented microhardness below specification (169 $N \cdot m^{-2}$).

The results show that resins rich in FDCA but lower in isosorbide content could target or even improve the specification, for example 70/30 with 10 or 30 mol% isosorbide. All the other properties' specifications were targeted; although our results for microhardness were slightly lower (169 and 190 $N \cdot m^{-2}$ vs. specification of 216 $N \cdot m^{-2}$). A small addition of isosorbide (35-40% IS) however could help to reach this specification as well. The inclusion of little amounts of branched alcohols could also lead to improved hardness and impact resistance, if necessary. Furthermore, more $PPF_{15}IS_{85}$ and $PPF_{30}IS_{70}$ resins with intermediate isosorbide contents, namely 30-50%, should be tested, so a complete performance of 1,3-propanediol resins is completed. Out of the outcome of our industrial partner, the overall performance of these bioderived resins makes them a suitable replacement for current fossil-derived coatings.

8.4 Characterisation Results of Itaconic Acid Polyesters

8.4.1 ^{1}H NMR

The chemical structure of **16** was confirmed by ^{1}H NMR. **Figure 133** shows the ^{1}H NMR for $PPeSIa_{15}$ (**16c**). The assignment of the chemical shifts is listed in **Table 64**. The two peaks around 5.71 ppm (*a*) and 6.32 ppm (*b*) are characteristic of the double bond of itaconic acid,[108, 110, 114, 115, 118] whereas the peaks at 4.09 ppm (*d*) and 4.16 ppm (*d'*) confirm the formation of the succinic acid ester and IA ester, respectively.[108, 109] The presence of succinic acid is confirmed by the shift at 2.62 ppm (*h*), as seen in previous chapters, and the methylene groups of 1,5-pentanediol correspond to the attributions *e, f,* and *g*. The two extra pair of signals around 2.1 ppm and 5.9 ppm along with 2.2 ppm and 6.7 ppm could suggest some degree of isomerisation of the double bond, probably due to the formation of citraconate and mesaconate structures, respectively, which was previously found for the polycondensation of itaconic acid with 1,4-butanediol,[108, 118] and succinic acid with 1,3-propanediol.[118] It has been suggested that the isomerisation may result from using IA instead of itaconic anhydride and the relatively short reaction time.[108]

A general scheme of the isomerisation of itaconate to mesaconate and citraconate is shown in **Scheme 50**.

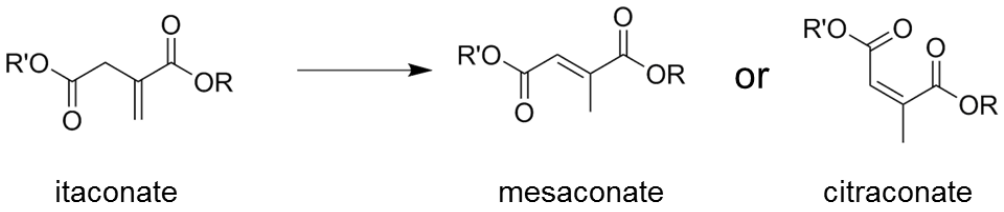

Scheme 50. Isomerisation of itaconate to mesaconate or citraconate, adapted from Farmer, et al.[118]

Table 64. Attribution of chemical shifts and integrations of itaconic acid polyester $PPeSIa_{15}$ (**16c**)

Polyester	**Attribution of chemical shifts ($CDCl_3$, δ/ppm)**								
16c	**a**	**b**	**c**	**d**	**d'**	**e**	**f**	**g**	**h**
$PPeSIa_{15}$	5.71	6.32	3.33	4.09	4.16	1.66	1.42	3.67	2.62
Integrations	0.10	0.10	0.23	2.24	0.36	2.72	1.33	0.10	2.00

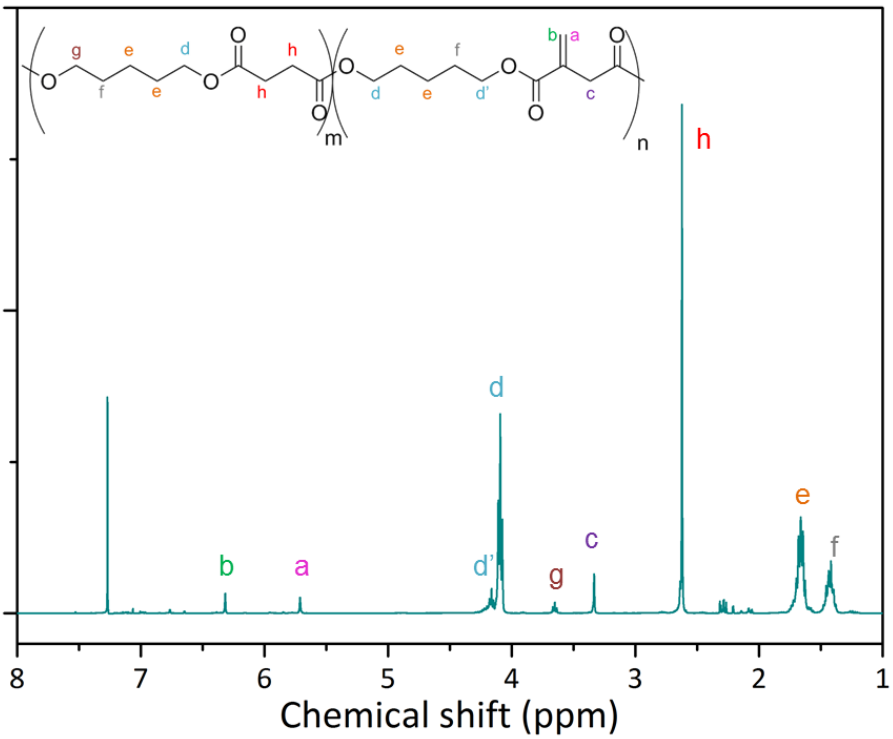

Figure 133. ^1H NMR spectra of $PPeSIa_{15}$ (**16c**).

8.4.2 Gel Permeation Chromatography (GPC)

The GPC results for polyesters **16** and **17** are shown in **Table 65** along with the chromatogram of **16** in **Figure 134**. The GPC chromatogram of **17** is shown in **Appendix G**. For the polyitaconates **16**, the molecular weights increased with the itaconic acid content, starting with M_w=4500 Da for **16a** with 5 mol% IA and finally reaching 11400 Da and a dispersity of 4.57 for **16c.** This high dispersity suggests a broad range of molecular weight, or alternatively, many short polymeric chain. The relatively high molecular weights possibly suggest slight crosslinking. In the case of **17**, the molecular weight was very low, as M_n is 800 Da and M_w is 1400 Da. Dai, et al.[111] reported M_n values of 900 to 1000 for itaconic acid polyesters with ethylene glycol, 1,4-butanediol and 1,6-hexanediol which is consistent with our findings. Likewise, the same research group reported molecular weights between 900 and 1100 Da for itaconic acid polyesters with 1,3-propanediol and different FDCA compositions.[440] Moreover, the synthesis of polyesters of itaconic acid with trimethylolpropane and adipic acid produced M_n between 940 and 2200 Da.[109] Farmer, et al,[118] reported M_n of 500, 600 and 2400 for poly(propylene itaconate) (PPI), poly(butylene itaconate) (PBI) and poly(butylene itaconate-co-butylene succinate) (PBIBS), respectively.

The results suggest that in order to achieve high molecular weights, the molar ratio of diol:diacids should be kept equimolar and the content of itaconic acid should be kept around 5-15% mol. Teramoto, et al.[108] reported M_w of 10000 Da for PBIBS with 5% IA, which increased to 11000 with 10 and 15 mol% IA. Higher molecular weights could be achieved by increasing the reaction time and the temperature of **17** should be at least 190 °C, as in the case of **16**. Additionally, the vacuum-driven synthesis is another alternative to increase the molecular weight.

Table 65. M_n, M_w and dispersity Đ of itaconic acid polyesters **16** and **17**

Polyester	Mol% IA	M_n, Da	M_w, Da	Đ
16a	0	1800	4500	2.45
16b	10	2300	6900	2.95
16c	30	2500	11400	4.57
17	100	800	1400	1.9

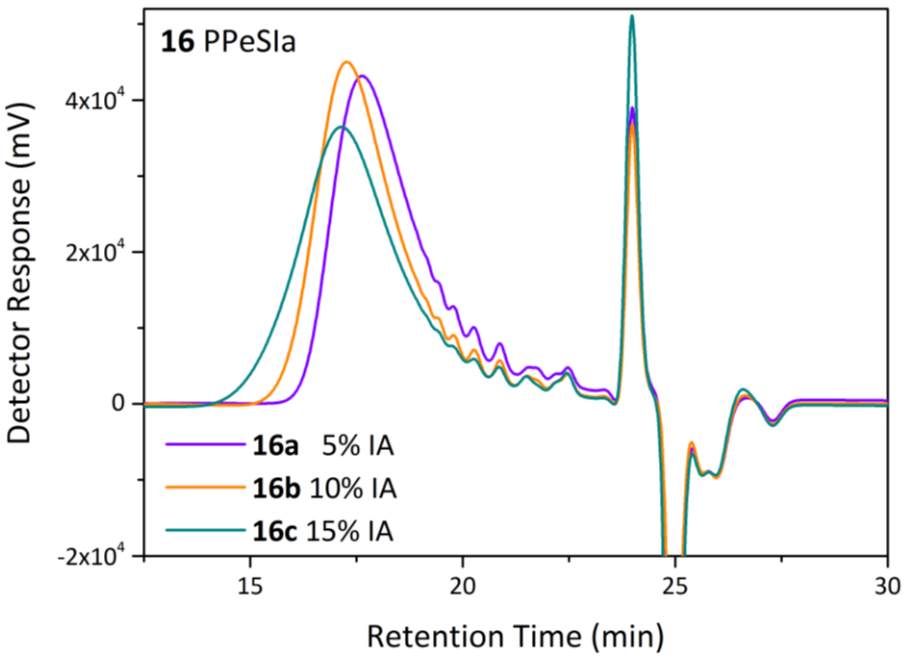

Figure 134. GPC chromatogram of PPeSIa (**16**).

8.4.3 Differential Scanning Calorimetry (DSC)

The glass transition temperatures of the IA polyesters were measured by DSC, and the results are shown in **Table 66** and **Figure 135**. Polyester **17** is shown in **Appendix G**. It is observed that as the itaconic acid content increases, so does the T_g, which is in accordance with the increasing molecular weight described in the previous section. No melting or crystallisation transitions were observed for polyesters **16** and **17**.

Table 66. Thermal transitions of itaconic acid polyesters **16** and **17** measured by DSC

Polyester	Mol% IA	T_g, °C	M_w, Da
16a	0	-47.4	4500
16b	10	-46.6	6900
16c	30	-43.9	11400
17	100	-36.0	1400

Previous T_g values of itaconic acid polyesters go from -57.6 °C to -7.4 °C using adipic acid and trimethylol propane as comonomers, and specifically -57.6 °C when using 3-methyl-

1,5-pentanediol.[109] For PBIBS polyesters with 5, 10 and 15 mol% IA the T_g's were found at -29 °C, -29 °C and -36.5 °C, respectively.[108] Similarly, PPI, PBI and PBIBS showed glass transition temperatures at -51.5 °C, -41.7 °C and -41.3 °C, respectively.[118]

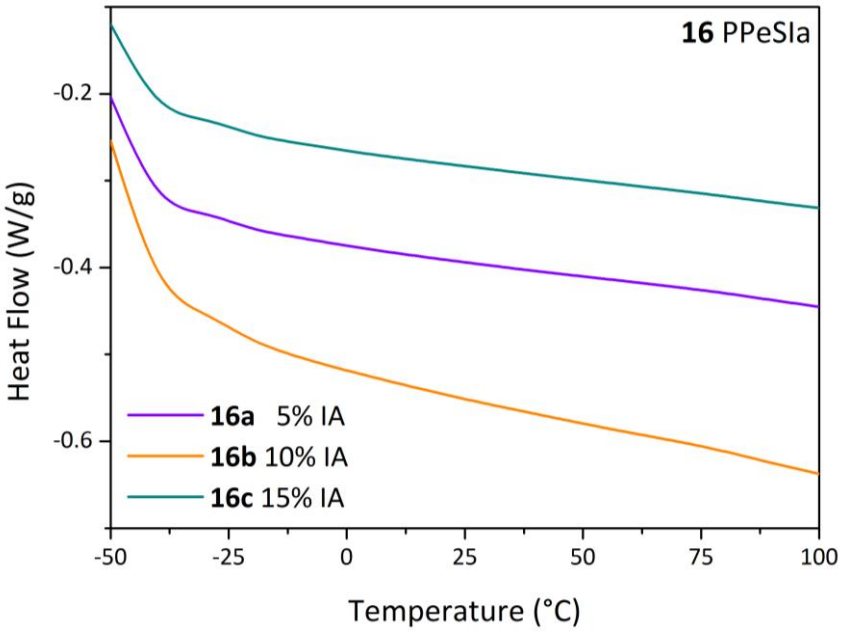

Figure 135. Second heating scan at 10 °C/min for polyester PPeSIa (**16**).

8.4.4 Thermal gravimetric analysis (TGA)

Table 67 lists the TGA results of polyesters **16** and the TGA thermogram is depicted in **Figure 136.** The maximum decomposition temperature T_{dmax} is around 374 °C, which suggests the little influence that the amount of itaconic acid has in the thermal stability. The thermal stability is slightly below other polyitaconates, such as PBIBS (377 to 385 °C),[108] PPI (406 °C)[118] and PBI (396 °C).[118] Farmer, et al,[114] reported the first decomposition T_{d1} from 258.7 °C to 345.1 °C for the same polyesters, along with poly(butylene fumarate).

Table 67. Characteristic decomposition temperatures T_{d1}, T_{dmax} and weight loss % of polyesters **16**

Polyester	Mol% IA	T_{d1}, °C	T_{dmax}, °C	Weight loss %
16a	0	294.1	374.4	99.4
16b	10	295.1	373.9	98.8
16c	30	293.2	373.9	98.2

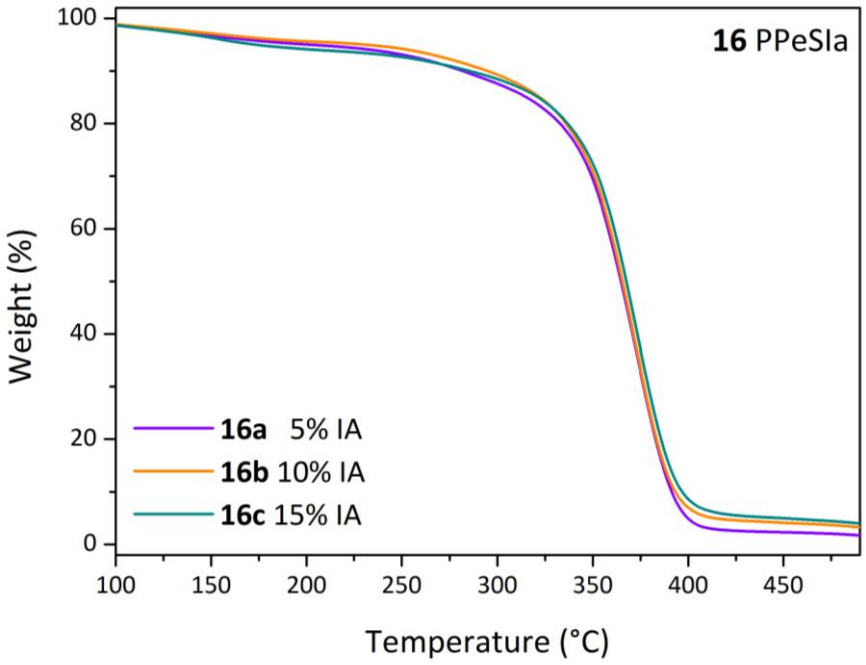

Figure 136. Weight % thermogram of polyesters PPeSIa (**16**).

8.5 Conclusions

Chapter 8 presented the diversification of properties of the biomass-derived polyesters presented in **Chapters 3** and **4** based on FDCA, succinic acid (SA) and either 1,3-propanediol or 1,5-pentanediol by incorporating isosorbide into the polyesters' backbone. A brief insight into the properties of itaconic acid-based polyesters was also included as a general overview of the potential behind this industrial-available, biomass-derived monomer.

As it was expected, the incorporation of isosorbide led to improved mechanical and thermal properties of the original polyesters. The isosorbide concentration was varied from 10 to 70 mol% for 15 and 30 mol% FDCA, whereas it was kept up to 50 mol% when synthesising polyesters with 70 and 85 mol% FDCA, as the mixture becomes highly viscous and prompts processability issues.

The inclusion of isosorbide was also translated into a good application versatility of the polyesters, as the molecular weight and glass transition temperature were functions of the isosorbide content. Depending on the concentration of isosorbide, the molecular weight of the polyesters could be tuned from 700 to 10200 Da. In general, the molecular weight decreased

as the isosorbide content increased. This behaviour could be attributed to the difference in reactivity of the e*xo* and *endo* OH groups present in isosorbide, and the steric hindrance of the latter.

The highest M_w were obtained for the copolyesters with 1,5-pentanediol, $PPeF_{70}I_{10}S_{30}$ (**14a**) and $PPeF_{85}I_{10}S_{15}$ (1**5a**) with 10 mol% IS: 3800 Da and 5400 Da, respectively and the dispersities within both compositions with different mol% isosorbide were above 2. On the other hand, the lowest M_w corresponded to $PPeF_{15}IS_{85}$ (**12**) and $PPeF_{30}IS_{70}$ (**13**) with either 60 or 70 mol% IS (1000 Da). For the same copolyesters, dispersities of 2 and above were obtained when the isosorbide content was limited to 30%.

The vacuum-driven polyesterifications of isosorbide polyesters with 1,5-pentanediol did greatly increase the molecular weights, compared to the conventional synthesis by azeotropic distillation. In the case of polyesters with 15 mol% FDCA, **12b** (30 mol% IS) and **12c** (50 mol% IS), the M_w greatly increased from 2500 to 8800 Da and 1500 to 4400 Da, respectively.

In terms of the thermal properties, the data suggested the T_g increased as a function of the mol% isosorbide, in all the different compositions. The results indicated that a minimum content of 50% mol isosorbide is needed in order to achieve glass transition temperatures above 0 $^{\circ}$C and above room temperature. The copolyesters $PPeF_{70}IS_{30}$ (**14**) and $PPeF_{85}IS_{15}$ (**15**) exhibited the highest T_g among the 1,5-pentanediol polyesters, achieving values of 30.6 °C and 22.3 °C, respectively, whereas 1,3-propanediol resins showed T_g's at 29.2 °C (**9c** $PPF_{70}I_{50}S_{30}$, 50 mol %IS) and 53.2 °C (**10c** $PPF_{85}I_{50}S_{15}$, 50 mol% IS). The polyesters with succinic acid as the only diacid monomer had the lowest T_g, from -48.7 °C to -0.5 °C. When processing under reduced pressure, PPeFIS (**12c**) had increased T_g from -3.1 °C to 12.0 °C, being the polymer that exhibited the largest increase in T_g among those synthesised under vacuum.

Regarding melting temperatures T_m, polyesters with 1,5-pentanediol and 30 mol% FDCA and above (PPeFIS **13-15**), showed T_m's from 77.3 to 154.7 °C, while $PPF_{70}IS_{30}$ (**9**) and $PPF_{70}IS_{30}$ (**10**) exhibited T_m's from 97 to 131 °C.

The TGA analysis suggested that the polyesters PPeFIS and PPFIS are stable from 348 to 372 °C, which is a lower range than the parent polyesters without isosorbide. Moreover, the results indicated that higher isosorbide content did promote the formation of more

oligomeric, low molecular weights species which decompose at lower temperatures, as some polymers had initial decomposition temperatures between 98 and 194 °C.

The results from the paint testing were considerably improved compared to the initial polyesters **3** and **4**. For instance, $PPeF_{70}I_{30}S_{30}$ (**14b**) showed an improvement in flexibility (2.5T) respect to the reference resin (3T), T_g on specification at 34 °C and better impact resistance as it presented a slight cracking. Moreover, $PPeF_{70}I_{50}S_{30}$ (**14c**) had above-specification Erichsen (No cracking), T_g (67°C) and microhardness (270 $N{\cdot}m^{-2}$). $PPeF_{85}IS_{15}$ resins (**15**) again showed better microhardness and higher T_g than $PPeF_{85}S_{15}$ (**6d**), as the results were 21 $N{\cdot}m^{-2}$ and 15 °C. $PPeF_{85}I_{50}S_{15}$ (**15c**), despite having the highest T_g (69 °C) and enhanced microhardness is slightly harder (Pencil Hardness 2H) and presents poor flexibility (5.5T). Overall, $PPeF_{85}I_{30}S_{15}$ (**15b**) therefore, with 30 mol% isosorbide, presented the best properties.

Chapter 8 additionally included a brief overview of itaconic acid (IA) polyesters with succinic acid and 1,5-pentanediol. These polyesters had M_w between 4500 and 11400 Da, and T_g from -47 to -44 °C, which increased with varying mol% IS from 5 to 15 %. The future work intended with itaconic acid, besides the vacuum-driven syntheses, is mainly related to the post-polymerisation functionalisation of these polyesters, namely thiol-ene reactions, as well as their possible use for catalysis applications.

The inclusion of the carbohydrate-derived diol isosorbide to our polyesters did promote better thermomechanical properties of the final coatings and allowed to tune fully biomass-derived resins that could easily replace the current petrochemical-derived ones in different applications, with controlled molecular weights and glass transition temperatures. Future work however needs to be done in terms of the identification of the nature of the different oligomers or cyclic structures formed during the polymerisation, as well as a kinetic study to determine the best reaction conditions to overcome the low reactivity inherent to isosorbide. The paint testing characterisation remains to be done with vacuum-synthesised polyesters with higher molecular weight than their azeotropic distillation counterparts.

CHAPTER 9

Conclusions and Future Work

9. Conclusions and Future Work

The present PhD project aims to become a substantial and comprehensive literature source to the fields of polymer science and process engineering. The main highlight of this research study is the systematic framework proposed, as it is comprised of aspects from different disciplines, such as polymer science, process engineering and reactor design, to develop a novel and substantial contribution to the ever growing area of sustainable engineering and biomass-derived polymers. This framework was achieved by linking aspects of polymer chemistry, such as monomers, materials characterisation and polyester processing, with chemical engineering knowledge; for example, modelling, sensitivity analysis and process simulation and optimisation. The result is a thorough, versatile work which could be applied to any type of step-growth or free radical polymerisation polymer. Additionally, the study provides a reliable foundation and motivation towards the use of biomass-derived polymers, as the polyesters presented herein possess interesting properties, suitable for a real –industry application, coil coatings. Furthermore, their production release less greenhouse-gas and consume less energy than petrochemical-derived polyesters, such as PET.

This PhD also represents my personal goal of fighting for our environment and it is an effort to raise consciousness regarding sustainability, pollution and climate change. I desire to provide a meaningful and substantial study on different aspects of polymers and plastics, accessible to industry, academia, and the general public. In the end, if the research is not shared and exploited, it would not be aligned with the objectives of the policy makers and therefore its full implementation will not become a reality.

The polyesters were successfully synthesised at two different laboratory scales, 250 and 500 mL at three different process temperatures: 210, 220 and 230 °C. The temperatures were chosen mainly for kinetic purposes. Remarkably, in terms of processing, it was found that a preliminary step of mechanical mixing of either diol and FDCA followed by heating up to 150 °C before the addition of succinic acid overcame the diffusion limitation provoked by the poor solubility of FDCA which leads to gelation and hot spots. This step was particularly important for the syntheses of polyesters with 70 and 85 mol% FDCA.

In **Chapter 3**, synthesised polyesters had M_w between 1100 and 5700 Da. The M_w seemed to increase with the processing temperature, and interestingly, in the case of

copolyesters with FDCA and SA, the M_w kept a strong dependence with the furanic content, as it increased as the mol% FDCA increased as well. The use of vacuum for the last 5 hours of reaction time led to increased molecular weights, for example, going from an original M_w of 1200 Da up to 7200 Da. The effect on M_w seen for 1,3-propanediol polyesters was analysed as well in **Chapter 4** for the 1,5-pentanediol polyesters. These polyesters had higher M_w than 1,3-propanediol polyesters, between 2200 to 10700 Da.

The thermal analysis suggested that the glass transition temperature (T_g) of the polyesters with 1,3-propanediol was found between -45 °C and 17 °C, whereas for the 1,5-pentanediol counterparts fell within –48 °C to 9 °C. The use of 1,5-pentanediol leads to enhanced flexibility of the polymer backbone due to the longer aliphatic chain of the diol, and it is the reason behind the T_g's being lower in general.

The application of vacuum satisfactorily drove the reaction further than azeotropic distillation as diol and water were efficiently released. The process comparison between azeotropic distillation and vacuum extended the analysis presented herein, providing the necessary information and data to choose the best processing methodology according to the economic, capability, properties or sustainability constraints that might be in place for certain customer and/or application.

The dependence of the glass-transition temperature on the composition of copolyesters was evaluated in terms of comonomer unit incorporation, and it was observed how the T_g raised as the molar content of FDCA increased. The two libraries of polyesters were comprised of amorphous and semicrystalline polyesters.

The paint testing characterisation for these resins showed that an increase on FDCA content led to better mechanical properties, although FDCA concentrations above 70 mol% with 1,3-propanediol do not allow the preparation of paints due to the insolubility of the system in the solvents used.

The chemical process engineering part of the research study provided very interesting results. Firstly, in **Chapter 5** it was shown that different kinetic models, namely Models 1-3, which varied in complexity, satisfactorily fitted the experimental carboxylic acid data of the different polyesterifications. Important kinetic parameters were estimated, such as reaction orders, kinetic coefficients, equilibrium constants and activation energies (E_a). It was confirmed that the conversion rate increased not only with temperature but it was also

influenced by the diacid composition as the conversion decreased as the FDCA content increased. Model 3 in particular was better fitted to those polymerisations rich in FDCA.

Chapters 6 and **7** presented an innovative work on the process simulation of biomass-derived polyesters, describing a thorough and comprehensive kinetic model for the step-growth kinetics of the polyesters based on a functional group approach method that considered terminal (T-) and bound (B-) segments of the monomers involved, which had been used previously for PET. As far it is known, no previous work has been done with FDCA polyesters using this particular step-growth functional group methodology. The model was comprised by 12 reactions for the polyesters with either FDCA or SA and 24 for the polyesters bearing both diacids. The model implementation in Aspen Plus was successful as it allowed the process simulation of the polyesterification in a batch reactor and a plug-flow reactor considering a production of 40 tons per day and it was validated against our own experimental data.

The multiobjective optimisation made through the ε-constraint *a posteriori* optimisation method simultaneously considered two objectives functions, the minimisation of the heat duty Q of the reactor and the maximisation of the degree of polymerisation, DP_n. For the batch case, the operation temperatures were between 190−220 °C, whereas for PFR, the process temperature needs to be kept between 207 and 224 °C in order to obtain polyesters with M_n suitable for coatings. The production of PET required higher temperature and energy than the biomass-derived polyesters.

The sustainability impact of the processes was addressed by means of sustainability performance indicators, providing information on energy consumption, CO_2 equivalents released, and efficiency in terms of the relationship between the mass input and the final product. When compared to the production of PET, the production of our biomass-derived polyesters achieved better targets and higher final polymer attributes, regardless the reactor configuration, which is encouraging and enhances the potential of biomass-derived products in industry.

Regarding the process intensification analysis, the reactive distillation was successful as it was the most energy-efficient configuration and therefore preferred option, as the specific energy indicators are lower than for the batch, PFR and divided wall configurations. This simulation was a great example of how polyesterification could and should be performed

always considering green chemical engineering principles, which is translated into energy and cost savings.

In order to extend the properties of the polyesters synthesised in **Chapters 3** and **4**, **Chapter 8** describes the use of isosorbide as an additional rigid monomer for the improvement of thermal properties of renewable polyesters. Although the performance is enhanced with the incorporation of FDCA, the final properties, such as microhardness and T_g were not good enough for coil coatings. As it was expected, the incorporation of isosorbide led to improved mechanical and thermal properties of the original polyesters. The isosorbide content was directly related to the molecular weight and glass transition temperature. Depending of the concentration of isosorbide, the molecular weight of the polyesters could be tuned from 700 to 10200 Da. In general, the molecular weight decreased as the isosorbide content increased. This behaviour could be attributed to the difference in reactivity of the OH groups present in isosorbide, due to their stereochemical nature –*endo* and *exo*- and the steric hindrance of the *endo* hydroxyl.

DSC analysis indicated that T_g increased as a function of the isosorbide concentration. The results suggested that a minimum content of 50 mol% IS is needed in order to achieve glass transition temperatures above 0 $^{\circ}$C and above room temperature, and it was also observed there is a strong relationship between mol% IS and T_g. For instance, the difference in T_g could vary approximately 40 degrees by adjusting the IS concentration.

Paint testing results showed that the isosorbide led to better overall performance, making the resins suitable for coil coating applications, mainly, $PPeF_{85}I_{30}S_{85}$ and $PPeF_{70}I_{30}S_{30}$ (**15b a**nd **14b**), along with $PPF_{85}I_{30}S_{15}$ (**10b**).

There is some suggested future work within this PhD project. In terms of synthesis and characterisation, all the different compositions with 1,3-propanediol and 1,5-pentanediol should be processed by applying vacuum, so a complete comparison in terms of structural, thermal and paint properties is achieved.

In the case of the kinetic modelling, catalysed polyesterifications could be analysed, as well as the effect of other process variables in the systems, such as agitation speed and geometry of the stirrer. Moreover, the evaluation of E_a and k_o since the beginning of the parameter fitting could be subject to study in terms of any potential differences with the methodology followed. The process simulation could be enhanced by performing a chemical

manufacturing simulation that included other stages such as separation, purification, compounding, and blending, embedded in an integrated biorefinery simulation. Besides, a complete cradle-to-grave life cycle analysis would provide a thorough sustainability analysis. Moreover, the process dynamic simulation in Aspen HYSYS, along with the implementation of mass transfer subroutines, particularly for PPF, would extend the process engineering knowledge presented herein.

Finally, the future work within the isosorbide polyesters includes the identification of the different oligomers and/or cyclic structures present in the final polymer, along with more method development and kinetic studies that would enable the optimisation of the reaction conditions to tackle the low reactivity of isosorbide. Additionally, the post-polymerisation functionalisation of the itaconic-acid polyesters would extend the applications of our biomass-derived polyesters.

REFERENCES

1. Mohr, A.; Raman, S., Lessons from first generation biofuels and implications for the sustainability appraisal of second generation biofuels. *Energy policy* **2013,** 63, 114-122.
2. Meier, M. A.; Metzger, J. O.; Schubert, U. S., Plant oil renewable resources as green alternatives in polymer science. *Chemical Society Reviews* **2007,** 36, (11), 1788-1802.
3. Agriculture and renewable: energy biomass potential. http://ec.europa.eu/agriculture/bioenergy/potential_en (23 January 2017),
4. Serrano-Ruiz, J. C.; Luque, R.; Sepulveda-Escribano, A., Transformations of biomass-derived platform molecules: from high added-value chemicals to fuels via aqueous-phase processing. *Chemical Society Reviews* **2011,** 40, (11), 5266-5281.
5. Fiorentino, G.; Ripa, M.; Ulgiati, S., Chemicals from biomass: technological versus environmental feasibility. A review. *Biofuels, Bioproducts and Biorefining* **2016**.
6. United States Environmental Protection Agency Basics of Green Chemistry. https://www.epa.gov/greenchemistry/basics-green-chemistry#twelve (25 January),
7. How much bioenergy can Europe produce without harming the environment? . http://www.eea.europa.eu/publications/eea_report_2006_7 (23 January),
8. Biomass as Feedstock for a Bioenergy and Bioproducts Industry: The Technical Feasibility of a Billion-Ton Annual Supply. https://www1.eere.energy.gov/bioenergy/pdfs/final_billionton_vision_report2.pdf (23 January),
9. Nanda, S.; Mohanty, P.; Pant, K. K.; Naik, S.; Kozinski, J. A.; Dalai, A. K., Characterization of North American lignocellulosic biomass and biochars in terms of their candidacy for alternate renewable fuels. *Bioenergy Research* **2013,** 6, (2), 663-677.
10. Coma, M.; Martinez Hernandez, E.; Abeln, F.; Raikova, S.; Donnelly, J.; Arnot, T. C.; Allen, M.; Hong, D. D.; Chuck, C. J., Organic waste as a sustainable feedstock for platform chemicals. *Faraday Discussions* **2017**.
11. Sun, Y.; Cheng, J., Hydrolysis of lignocellulosic materials for ethanol production: a review. *Bioresource technology* **2002,** 83, (1), 1-11.
12. Gírio, F. M.; Fonseca, C.; Carvalheiro, F.; Duarte, L. C.; Marques, S.; Bogel-Łukasik, R., Hemicelluloses for fuel ethanol: a review. *Bioresource technology* **2010,** 101, (13), 4775-4800.
13. Azadi, P.; Inderwildi, O. R.; Farnood, R.; King, D. A., Liquid fuels, hydrogen and chemicals from lignin: A critical review. *Renewable and Sustainable Energy Reviews* **2013,** 21, 506-523.
14. Kubicek, C. P., Lignocellulose biorefinery. *Fungi and Lignocellulosic Biomass* **2013**, 201-227.
15. Ragauskas, A. J.; Williams, C. K.; Davison, B. H.; Britovsek, G.; Cairney, J.; Eckert, C. A.; Frederick, W. J.; Hallett, J. P.; Leak, D. J.; Liotta, C. L., The path forward for biofuels and biomaterials. *science* **2006,** 311, (5760), 484-489.
16. Gallezot, P., Catalytic routes from renewables to fine chemicals. *Catalysis today* **2007,** 121, (1), 76-91.
17. Naik, S. N.; Goud, V. V.; Rout, P. K.; Dalai, A. K., Production of first and second generation biofuels: a comprehensive review. *Renewable and Sustainable Energy Reviews* **2010,** 14, (2), 578-597.
18. Fernando, S.; Adhikari, S.; Chandrapal, C.; Murali, N., Biorefineries: current status, challenges, and future direction. *Energy & Fuels* **2006,** 20, (4), 1727-1737.
19. Kamm, B.; Kamm, M., Biorefineries–multi product processes. In *White Biotechnology*, Springer: 2007; pp 175-204.
20. Van Dyne, D. L.; Blase, M. G.; Clements, L. D., A strategy for returning agriculture and rural America to long-term full employment using biomass refineries. *Perspectives on new crops and new uses. ASHS Press, Alexandria, Va* **1999**, 114-123.
21. Isikgor, F. H.; Becer, C. R., Lignocellulosic biomass: a sustainable platform for the production of bio-based chemicals and polymers. *Polymer Chemistry* **2015,** 6, (25), 4497-4559.

22. Martinez-Hernandez, E.; Martinez-Herrera, J.; Campbell, G. M.; Sadhukhan, J., Process integration, energy and GHG emission analyses of Jatropha-based biorefinery systems. *Biomass Conversion and Biorefinery* **2014,** 4, (2), 105-124.
23. Vilela, C.; Sousa, A. F.; Fonseca, A. C.; Serra, A. C.; Coelho, J. F.; Freire, C. S.; Silvestre, A. J., The quest for sustainable polyesters–insights into the future. *Polymer Chemistry* **2014,** 5, (9), 3119-3141.
24. Bioplastics market data. http://www.european-bioplastics.org/market/ (Accessed 02 February 2017),
25. Tokiwa, Y.; Calabia, B. P.; Ugwu, C. U.; Aiba, S., Biodegradability of plastics. *International journal of molecular sciences* **2009,** 10, (9), 3722-3742.
26. Robertson, G. L., *Food packaging: principles and practice*. CRC press: 2016.
27. European Technology Platform for Sustainable Chemistry. http://www.suschem.org/ (23 January),
28. Werpy, T.; Petersen, G.; Aden, A.; Bozell, J.; Holladay, J.; White, J.; Manheim, A.; Eliot, D.; Lasure, L.; Jones, S. *Top value added chemicals from biomass. Volume 1-Results of screening for potential candidates from sugars and synthesis gas*; DTIC Document: 2004.
29. Bozell, J. J.; Petersen, G. R., Technology development for the production of biobased products from biorefinery carbohydrates—the US Department of Energy's "Top 10" revisited. *Green Chemistry* **2010,** 12, (4), 539-554.
30. Yao, K.; Tang, C., Controlled polymerization of next-generation renewable monomers and beyond. *Macromolecules* **2013,** 46, (5), 1689-1712.
31. Pellis, A.; Herrero Acero, E.; Gardossi, L.; Ferrario, V.; Guebitz, G. M., Renewable building blocks for sustainable polyesters: new biotechnological routes for greener plastics. *Polymer International* **2016**.
32. Delidovich, I.; Hausoul, P. J.; Deng, L.; Pfützenreuter, R.; Rose, M.; Palkovits, R., Alternative monomers based on lignocellulose and their use for polymer production. *Chemical reviews* **2015,** 116, (3), 1540-1599.
33. Bechthold, I.; Bretz, K.; Kabasci, S.; Kopitzky, R.; Springer, A., Succinic acid: a new platform chemical for biobased polymers from renewable resources. *Chemical engineering & technology* **2008,** 31, (5), 647-654.
34. Delhomme, C.; Weuster-Botz, D.; Kühn, F. E., Succinic acid from renewable resources as a C 4 building-block chemical—a review of the catalytic possibilities in aqueous media. *Green Chemistry* **2009,** 11, (1), 13-26.
35. Bio-based succinic acid. https://www.ihs.com/pdf/RW2010-14_220240110917062932.pdf (23 January),
36. Xu, J.; Guo, B.-H., Microbial succinic acid, its polymer poly (butylene succinate), and applications. In *Plastics from Bacteria*, Springer: 2010; pp 347-388.
37. Cukalovic, A.; Stevens, C. V., Feasibility of production methods for succinic acid derivatives: a marriage of renewable resources and chemical technology. *Biofuels, Bioproducts and Biorefining* **2008,** 2, (6), 505-529.
38. Pinazo, J. M.; Domine, M. E.; Parvulescu, V.; Petru, F., Sustainability metrics for succinic acid production: a comparison between biomass-based and petrochemical routes. *Catalysis Today* **2015,** 239, 17-24.
39. Morales, M.; Ataman, M.; Badr, S.; Linster, S.; Kourlimpinis, I.; Papadokonstantakis, S.; Hatzimanikatis, V.; Hungerbühler, K., Sustainability assessment of succinic acid production technologies from biomass using metabolic engineering. *Energy & Environmental Science* **2016,** 9, (9), 2794-2805.
40. Dutta, S.; Wu, L.; Mascal, M., Efficient, metal-free production of succinic acid by oxidation of biomass-derived levulinic acid with hydrogen peroxide. *Green Chemistry* **2015,** 17, (4), 2335-2338.
41. Chen, Y.; Nielsen, J., Biobased organic acids production by metabolically engineered microorganisms. *Current opinion in biotechnology* **2016,** 37, 165-172.
42. Biosuccinium™ Technology. http://www.reverdia.com/technology/technology-overview/ (6 January),

43. Babu, R. P.; O'connor, K.; Seeram, R., Current progress on bio-based polymers and their future trends. *Progress in Biomaterials* **2013,** 2, (1), 8.
44. Bionolle™. http://www.sds.com.sg/products/functional-polymers/bionolle/ (11 January),
45. BioPBS. http://www.mcpp-global.com/en/asia/products/brand/biopbstm/ (11 January),
46. Adkins, J.; Pugh, S.; McKenna, R.; Nielsen, D. R., Engineering microbial chemical factories to produce renewable "biomonomers". *Synthetic biology applications in industrial microbiology* **2014**, 31.
47. Bionolle, biodegradable aliphatic polyester. http://www.showa-denko.com/wp-content/uploads/2015/03/Bionolle_2015.pdf (Accessed 14 February 2017),
48. BioPBS. http://www.mcpp-global.com/en/america/products/brand/biopbstm/ (Accessed 14 February 2017),
49. van Putten, R.-J.; van der Waal, J. C.; De Jong, E.; Rasrendra, C. B.; Heeres, H. J.; de Vries, J. G., Hydroxymethylfurfural, a versatile platform chemical made from renewable resources. *Chemical reviews* **2013,** 113, (3), 1499-1597.
50. Rosatella, A. A.; Simeonov, S. P.; Frade, R. F.; Afonso, C. A., 5-Hydroxymethylfurfural (HMF) as a building block platform: Biological properties, synthesis and synthetic applications. *Green Chemistry* **2011,** 13, (4), 754-793.
51. Mukherjee, A.; Dumont, M.-J.; Raghavan, V., Review: sustainable production of hydroxymethylfurfural and levulinic acid: challenges and opportunities. *Biomass and Bioenergy* **2015,** 72, 143-183.
52. Casanova, O.; Iborra, S.; Corma, A., Biomass into Chemicals: Aerobic Oxidation of 5-Hydroxymethyl-2-furfural into 2, 5-Furandicarboxylic Acid with Gold Nanoparticle Catalysts. *ChemSusChem* **2009,** 2, (12), 1138-1144.
53. Pasini, T.; Piccinini, M.; Blosi, M.; Bonelli, R.; Albonetti, S.; Dimitratos, N.; Lopez-Sanchez, J. A.; Sankar, M.; He, Q.; Kiely, C. J., Selective oxidation of 5-hydroxymethyl-2-furfural using supported gold–copper nanoparticles. *Green Chemistry* **2011,** 13, (8), 2091-2099.
54. Albonetti, S.; Pasini, T.; Lolli, A.; Blosi, M.; Piccinini, M.; Dimitratos, N.; Lopez-Sanchez, J. A.; Morgan, D. J.; Carley, A. F.; Hutchings, G. J., Selective oxidation of 5-hydroxymethyl-2-furfural over TiO 2-supported gold–copper catalysts prepared from preformed nanoparticles: Effect of Au/Cu ratio. *Catalysis today* **2012,** 195, (1), 120-126.
55. Yi, G.; Teong, S. P.; Zhang, Y., Base-free conversion of 5-hydroxymethylfurfural to 2, 5-furandicarboxylic acid over a Ru/C catalyst. *Green Chemistry* **2016,** 18, (4), 979-983.
56. Hayashi, E.; Komanoya, T.; Kamata, K.; Hara, M., Heterogeneously-Catalyzed Aerobic Oxidation of 5-Hydroxymethylfurfural to 2, 5-Furandicarboxylic Acid with MnO2. *ChemSusChem* **2017**.
57. Ait Rass, H.; Essayem, N.; Besson, M., Selective Aerobic Oxidation of 5-HMF into 2, 5-Furandicarboxylic Acid with Pt Catalysts Supported on TiO2-and ZrO2-Based Supports. *ChemSusChem* **2015,** 8, (7), 1206-1217.
58. Davis, S. E.; Houk, L. R.; Tamargo, E. C.; Datye, A. K.; Davis, R. J., Oxidation of 5-hydroxymethylfurfural over supported Pt, Pd and Au catalysts. *Catalysis Today* **2011,** 160, (1), 55-60.
59. Van Nguyen, C.; Liao, Y.-T.; Kang, T.-C.; Chen, J. E.; Yoshikawa, T.; Nakasaka, Y.; Masuda, T.; Wu, K. C.-W., A metal-free, high nitrogen-doped nanoporous graphitic carbon catalyst for an effective aerobic HMF-to-FDCA conversion. *Green Chemistry* **2016,** 18, (22), 5957-5961.
60. Tong, X.; Ma, Y.; Li, Y., Biomass into chemicals: conversion of sugars to furan derivatives by catalytic processes. *Applied Catalysis A: General* **2010,** 385, (1), 1-13.
61. Sousa, A. F.; Vilela, C.; Fonseca, A. C.; Matos, M.; Freire, C. S.; Gruter, G.-J. M.; Coelho, J. F.; Silvestre, A. J., Biobased polyesters and other polymers from 2, 5-furandicarboxylic acid: a tribute to furan excellency. *Polymer Chemistry* **2015,** 6, (33), 5961-5983.
62. Pan, T.; Deng, J.; Xu, Q.; Zuo, Y.; Guo, Q. X.; Fu, Y., Catalytic Conversion of Furfural into a 2, 5-Furandicarboxylic Acid-Based Polyester with Total Carbon Utilization. *ChemSusChem* **2013,** 6, (1), 47-50.
63. Kang, E. S.; Hong, Y. W.; Chae, D. W.; Kim, B.; Kim, B.; Kim, Y. J.; Cho, J. K.; Kim, Y. G., From Lignocellulosic Biomass to Furans via 5-Acetoxymethylfurfural as an Alternative to 5-Hydroxymethylfurfural. *ChemSusChem* **2015,** 8, (7), 1179-1188.

64. Grushin, V.; Manzer, L. E.; Partenheimer, W. Processes for preparing diacids, dialdehydes and polymers. 2013.
65. Sanborn, A. Oxidation of furfural compounds. 2010.
66. MUÑOZ, D. E. D. C.; Dam, M. A.; Gruter, G. J. M. Method for the preparation of 2,5-furandicarboxylic acid and for the preparation of the dialkyl ester of 2,5-furandicarboxylic acid. 2011.
67. Sustainability Towards second-generation feedstocks. https://www.avantium.com/yxy/yxy-technology/ (9 January),
68. Synvina: Joint venture of BASF and Avantium established. https://www.avantium.com/press-releases/synvina-joint-venture-basf-avantium-established/ (9 January),
69. Chheda, J. N.; Román-Leshkov, Y.; Dumesic, J. A., Production of 5-hydroxymethylfurfural and furfural by dehydration of biomass-derived mono-and poly-saccharides. *Green Chemistry* **2007,** 9, (4), 342-350.
70. Ghosh, T.; Mahajan, K.; Narayan-Sarathy, S.; Balgacem, M. N.; Gopalakrishnan, P. 2,5-furan dicarboxylic acid-based polyesters prepared from biomass. 2013.
71. Burgess, S. K.; Leisen, J. E.; Kraftschik, B. E.; Mubarak, C. R.; Kriegel, R. M.; Koros, W. J., Chain mobility, thermal, and mechanical properties of poly (ethylene furanoate) compared to poly (ethylene terephthalate). *Macromolecules* **2014,** 47, (4), 1383-1391.
72. Moore, J.; Kelly, J., Polyesters derived from furan and tetrahydrofuran nuclei. *Macromolecules* **1978,** 11, (3), 568-573.
73. Gandini, A.; Silvestre, A. J.; Neto, C. P.; Sousa, A. F.; Gomes, M., The furan counterpart of poly (ethylene terephthalate): An alternative material based on renewable resources. *Journal of Polymer Science Part A: Polymer Chemistry* **2009,** 47, (1), 295-298.
74. Gopalakrishnan, P.; Narayan-Sarathy, S.; Ghosh, T.; Mahajan, K.; Belgacem, M. N., Synthesis and characterization of bio-based furanic polyesters. *Journal of Polymer Research* **2014,** 21, (1), 340.
75. Jiang, M.; Liu, Q.; Zhang, Q.; Ye, C.; Zhou, G., A series of furan-aromatic polyesters synthesized via direct esterification method based on renewable resources. *Journal of Polymer Science Part A: Polymer Chemistry* **2012,** 50, (5), 1026-1036.
76. Papageorgiou, G. Z.; Tsanaktsis, V.; Papageorgiou, D. G.; Exarhopoulos, S.; Papageorgiou, M.; Bikiaris, D. N., Evaluation of polyesters from renewable resources as alternatives to the current fossil-based polymers. Phase transitions of poly (butylene 2, 5-furan-dicarboxylate). *Polymer* **2014,** 55, (16), 3846-3858.
77. Ma, J.; Pang, Y.; Wang, M.; Xu, J.; Ma, H.; Nie, X., The copolymerization reactivity of diols with 2, 5-furandicarboxylic acid for furan-based copolyester materials. *Journal of Materials Chemistry* **2012,** 22, (8), 3457-3461.
78. Sousa, A.; Fonseca, A.; Serra, A.; Freire, C.; Silvestre, A.; Coelho, J., New unsaturated copolyesters based on 2, 5-furandicarboxylic acid and their crosslinked derivatives. *Polymer Chemistry* **2016,** 7, (5), 1049-1058.
79. Vannini, M.; Marchese, P.; Celli, A.; Lorenzetti, C., Fully biobased poly (propylene 2, 5-furandicarboxylate) for packaging applications: excellent barrier properties as a function of crystallinity. *Green Chemistry* **2015,** 17, (8), 4162-4166.
80. Knoop, R. J.; Vogelzang, W.; Haveren, J.; Es, D. S., High molecular weight poly (ethylene-2, 5-furanoate); critical aspects in synthesis and mechanical property determination. *Journal of Polymer Science Part A: Polymer Chemistry* **2013,** 51, (19), 4191-4199.
81. Tsanaktsis, V.; Terzopoulou, Z.; Nerantzaki, M.; Papageorgiou, G. Z.; Bikiaris, D. N., New poly (pentylene furanoate) and poly (heptylene furanoate) sustainable polyesters from diols with odd methylene groups. *Materials Letters* **2016,** 178, 64-67.
82. Zhu, J.; Cai, J.; Xie, W.; Chen, P.-H.; Gazzano, M.; Scandola, M.; Gross, R. A., Poly (butylene 2, 5-furan dicarboxylate), a biobased alternative to PBT: synthesis, physical properties, and crystal structure. *Macromolecules* **2013,** 46, (3), 796-804.
83. Terzopoulou, Z.; Tsanaktsis, V.; Bikiaris, D. N.; Exarhopoulos, S.; Papageorgiou, D. G.; Papageorgiou, G. Z., Biobased poly (ethylene furanoate-co-ethylene succinate) copolyesters: solid state structure, melting point depression and biodegradability. *RSC Advances* **2016,** 6, (87), 84003-84015.

84. Wu, L.; Mincheva, R.; Xu, Y.; Raquez, J.-M.; Dubois, P., High molecular weight poly (butylene succinate-co-butylene furandicarboxylate) copolyesters: from catalyzed polycondensation reaction to thermomechanical properties. *Biomacromolecules* **2012,** 13, (9), 2973-2981.
85. Hbaieb, S.; Kammoun, W.; Delaite, C.; Abid, M.; Abid, S.; El Gharbi, R., New copolyesters containing aliphatic and bio-based furanic units by bulk copolycondensation. *Journal of Macromolecular Science, Part A* **2015,** 52, (5), 365-373.
86. Yu, Z.; Zhou, J.; Cao, F.; Wen, B.; Zhu, X.; Wei, P., Chemosynthesis and characterization of fully biomass-based copolymers of ethylene glycol, 2, 5-furandicarboxylic acid, and succinic acid. *Journal of Applied Polymer Science* **2013,** 130, (2), 1415-1420.
87. Lomelí-Rodríguez, M.; Martín-Molina, M.; Jiménez-Pardo, M.; Nasim-Afzal, Z.; Cauët, S. I.; Davies, T. E.; Rivera-Toledo, M.; Lopez-Sanchez, J. A., Synthesis and kinetic modeling of biomass-derived renewable polyesters. *Journal of Polymer Science Part A: Polymer Chemistry* **2016,** 54, (18), 2876-2887.
88. Lomelí-Rodríguez, M.; Rivera-Toledo, M.; López-Sánchez, J. A., Optimum Batch-Reactor Operation for the Synthesis of Biomass-Derived Renewable Polyesters. *Industrial & Engineering Chemistry Research* **2017,** 56, (2), 549-559.
89. Matos, M.; Sousa, A. F.; Fonseca, A. C.; Freire, C. S.; Coelho, J. F.; Silvestre, A. J., A New Generation of Furanic Copolyesters with Enhanced Degradability: Poly (ethylene 2, 5-furandicarboxylate)-co-poly (lactic acid) Copolyesters. *Macromolecular Chemistry and Physics* **2014,** 215, (22), 2175-2184.
90. Storbeck, R.; Ballauff, M., Synthesis and properties of polyesters based on 2, 5-furandicarboxylic acid and 1, 4: 3, 6-dianhydrohexitols. *Polymer* **1993,** 34, (23), 5003-5006.
91. Wu, J.; Eduard, P.; Thiyagarajan, S.; Noordover, B. A.; van Es, D. S.; Koning, C. E., Semi-Aromatic Polyesters Based on a Carbohydrate-Derived Rigid Diol for Engineering Plastics. *ChemSusChem* **2015,** 8, (1), 67-72.
92. Jacquel, N.; Saint-Loup, R.; Pascault, J.-P.; Rousseau, A.; Fenouillot, F., Bio-based alternatives in the synthesis of aliphatic–aromatic polyesters dedicated to biodegradable film applications. *Polymer* **2015,** 59, 234-242.
93. Papageorgiou, G. Z.; Guigo, N.; Tsanaktsis, V.; Papageorgiou, D. G.; Exarhopoulos, S.; Sbirrazzuoli, N.; Bikiaris, D. N., On the bio-based furanic polyesters: Synthesis and thermal behavior study of Poly (octylene furanoate) using Fast and Temperature Modulated Scanning Calorimetry. *European Polymer Journal* **2015,** 68, 115-127.
94. Tsanaktsis, V.; Vouvoudi, E.; Papageorgiou, G. Z.; Papageorgiou, D. G.; Chrissafis, K.; Bikiaris, D. N., Thermal degradation kinetics and decomposition mechanism of polyesters based on 2, 5-furandicarboxylic acid and low molecular weight aliphatic diols. *Journal of Analytical and Applied Pyrolysis* **2015,** 112, 369-378.
95. Terzopoulou, Z.; Tsanaktsis, V.; Nerantzaki, M.; Achilias, D. S.; Vaimakis, T.; Papageorgiou, G. Z.; Bikiaris, D. N., Thermal degradation of biobased polyesters: Kinetics and decomposition mechanism of polyesters from 2, 5-furandicarboxylic acid and long-chain aliphatic diols. *Journal of Analytical and Applied Pyrolysis* **2016,** 117, 162-175.
96. Thiyagarajan, S.; Vogelzang, W.; Knoop, R. J.; Frissen, A. E.; van Haveren, J.; van Es, D. S., Biobased furandicarboxylic acids (FDCAs): effects of isomeric substitution on polyester synthesis and properties. *Green Chemistry* **2014,** 16, (4), 1957-1966.
97. Pfister, D.; Storti, G.; Tancini, F.; Costa, L. I.; Morbidelli, M., Synthesis and Ring-Opening Polymerization of Cyclic Butylene 2, 5-Furandicarboxylate. *Macromolecular Chemistry and Physics* **2015,** 216, (21), 2141-2146.
98. Morales-Huerta, J. C.; Ciulik, C. B.; de Ilarduya, A. M.; Muñoz-Guerra, S., Fully bio-based aromatic–aliphatic copolyesters: poly (butylene furandicarboxylate-co-succinate) s obtained by ring opening polymerization. *Polymer Chemistry* **2017**.
99. Papageorgiou, G. Z.; Papageorgiou, D. G.; Terzopoulou, Z.; Bikiaris, D. N., Production of bio-based 2, 5-furan dicarboxylate polyesters: Recent progress and critical aspects in their synthesis and thermal properties. *European Polymer Journal* **2016,** 83, 202-229.

100. Determination of market potentials for selected platform chemicals http://www.bioconsept.eu/wp-content/uploads/BioConSepT_Market-potential-for-selected-platform-chemicals_ppt1.pdf (26 January 2017),
101. Robert, T.; Friebel, S., Itaconic acid–a versatile building block for renewable polyesters with enhanced functionality. *Green Chemistry* **2016,** 18, (10), 2922-2934.
102. Geiser, E.; Przybilla, S. K.; Friedrich, A.; Buckel, W.; Wierckx, N.; Blank, L. M.; Bölker, M., Ustilago maydis produces itaconic acid via the unusual intermediate trans-aconitate. *Microbial biotechnology* **2016,** 9, (1), 116-126.
103. Rose, M.; Palkovits, R., Cellulose-Based Sustainable Polymers: State of the Art and Future Trends. *Macromolecular rapid communications* **2011,** 32, (17), 1299-1311.
104. Corma, A.; Iborra, S.; Velty, A., Chemical routes for the transformation of biomass into chemicals. *Chemical reviews* **2007,** 107, (6), 2411-2502.
105. Ramos, J. L.; Udaondo, Z.; Fernández, B.; Molina, C.; Daddaoua, A.; Segura, A.; Duque, E., First-and second-generation biochemicals from sugars: biosynthesis of itaconic acid. *Microbial biotechnology* **2016,** 9, (1), 8-10.
106. Hull, E. H.; Leach, J. M.; Tate, B. E. Preparation of polyitaconic acid. 1962.
107. Retuert, J.; Pedram, M. Y.-.; Martinez, F.; Jeria, M., Soluble Itaconic Acid–Ethylene Glycol Polyesters. *Bulletin of the Chemical Society of Japan* **1993,** 66, (6), 1707-1708.
108. Teramoto, N.; Ozeki, M.; Fujiwara, I.; Shibata, M., Crosslinking and biodegradation of poly (butylene succinate) prepolymers containing itaconic or maleic acid units in the main chain. *Journal of applied polymer science* **2005,** 95, (6), 1473-1480.
109. Barrett, D. G.; Merkel, T. J.; Luft, J. C.; Yousaf, M. N., One-step syntheses of photocurable polyesters based on a renewable resource. *Macromolecules* **2010,** 43, (23), 9660-9667.
110. Goerz, O.; Ritter, H., Polymers with shape memory effect from renewable resources: crosslinking of polyesters based on isosorbide, itaconic acid and succinic acid. *Polymer International* **2013,** 62, (5), 709-712.
111. Dai, J.; Ma, S.; Wu, Y.; Han, L.; Zhang, L.; Zhu, J.; Liu, X., Polyesters derived from itaconic acid for the properties and bio-based content enhancement of soybean oil-based thermosets. *Green Chemistry* **2015,** 17, (4), 2383-2392.
112. Tang, T.; Moyori, T.; Takasu, A., Isomerization-free polycondensations of cyclic anhydrides with diols and preparation of polyester gels containing cis or trans carbon double bonds via photo-cross-linking and isomerization in the gels. *Macromolecules* **2013,** 46, (14), 5464-5472.
113. Okuda, T.; Ishimoto, K.; Ohara, H.; Kobayashi, S., Renewable biobased polymeric materials: facile synthesis of itaconic anhydride-based copolymers with poly (L-lactic acid) grafts. *Macromolecules* **2012,** 45, (10), 4166-4174.
114. Farmer, T. J.; Castle, R. L.; Clark, J. H.; Macquarrie, D. J., Synthesis of unsaturated polyester resins from various bio-derived platform molecules. *International journal of molecular sciences* **2015,** 16, (7), 14912-14932.
115. Chanda, S.; Ramakrishnan, S., Poly (alkylene itaconate) s–an interesting class of polyesters with periodically located exo-chain double bonds susceptible to Michael addition. *Polymer Chemistry* **2015,** 6, (11), 2108-2114.
116. Lv, A.; Li, Z.-L.; Du, F.-S.; Li, Z.-C., Synthesis, functionalization, and controlled degradation of high molecular weight polyester from itaconic acid via ADMET polymerization. *Macromolecules* **2014,** 47, (22), 7707-7716.
117. Winkler, M.; Lacerda, T. M.; Mack, F.; Meier, M. A., Renewable polymers from itaconic acid by polycondensation and ring-opening-metathesis polymerization. *Macromolecules* **2015,** 48, (5), 1398-1403.
118. Farmer, T.; Clark, J.; Macquarrie, D.; Ogunjobi, J.; Castle, R., Post-polymerisation modification of bio-derived unsaturated polyester resins via Michael additions of 1, 3-dicarbonyls. *Polymer Chemistry* **2016,** 7, (8), 1650-1658.
119. Lee, C.; Aroua, M.; Daud, W.; Cognet, P.; Pérès-Lucchese, Y.; Fabre, P.; Reynes, O.; Latapie, L., A review: Conversion of bioglycerol into 1, 3-propanediol via biological and chemical method. *Renewable and Sustainable Energy Reviews* **2015,** 42, 963-972.

120. Da Silva, G. P.; Mack, M.; Contiero, J., Glycerol: a promising and abundant carbon source for industrial microbiology. *Biotechnology advances* **2009,** 27, (1), 30-39.
121. Anand, P.; Saxena, R. K., A comparative study of solvent-assisted pretreatment of biodiesel derived crude glycerol on growth and 1, 3-propanediol production from Citrobacter freundii. *New Biotechnology* **2012,** 29, (2), 199-205.
122. Zhang, G.; Ma, B.; Xu, X.; Li, C.; Wang, L., Fast conversion of glycerol to 1, 3-propanediol by a new strain of Klebsiella pneumoniae. *Biochemical Engineering Journal* **2007,** 37, (3), 256-260.
123. Liu, H.-J.; Zhang, D.-J.; Xu, Y.-H.; Mu, Y.; Sun, Y.-Q.; Xiu, Z.-L., Microbial production of 1, 3-propanediol from glycerol by Klebsiella pneumoniae under micro-aerobic conditions up to a pilot scale. *Biotechnology letters* **2007,** 29, (8), 1281-1285.
124. Wilkens, E.; Ringel, A. K.; Hortig, D.; Willke, T.; Vorlop, K.-D., High-level production of 1, 3-propanediol from crude glycerol by Clostridium butyricum AKR102a. *Applied microbiology and biotechnology* **2012,** 93, (3), 1057-1063.
125. Forsberg, C. W., Production of 1, 3-propanediol from glycerol by Clostridium acetobutylicum and other Clostridium species. *Applied and Environmental Microbiology* **1987,** 53, (4), 639-643.
126. Biebl, H.; Spröer, C., Taxonomy of the glycerol fermenting clostridia and description of Clostridium diolis sp. nov. *Systematic and applied microbiology* **2002,** 25, (4), 491-497.
127. Yazdani, S. S.; Gonzalez, R., Anaerobic fermentation of glycerol: a path to economic viability for the biofuels industry. *Current opinion in biotechnology* **2007,** 18, (3), 213-219.
128. Willke, T.; Vorlop, K., Biotransformation of glycerol into 1, 3-propanediol. *European Journal of Lipid Science and Technology* **2008,** 110, (9), 831-840.
129. Kurian, J. V., A new polymer platform for the future—Sorona® from corn derived 1, 3-propanediol. *Journal of Polymers and the Environment* **2005,** 13, (2), 159-167.
130. Nakagawa, Y.; Tomishige, K., Production of 1, 5-pentanediol from biomass via furfural and tetrahydrofurfuryl alcohol. *Catalysis today* **2012,** 195, (1), 136-143.
131. Yan, K.; Wu, G.; Lafleur, T.; Jarvis, C., Production, properties and catalytic hydrogenation of furfural to fuel additives and value-added chemicals. *Renewable and Sustainable Energy Reviews* **2014,** 38, 663-676.
132. Koso, S.; Furikado, I.; Shimao, A.; Miyazawa, T.; Kunimori, K.; Tomishige, K., Chemoselective hydrogenolysis of tetrahydrofurfuryl alcohol to 1, 5-pentanediol. *Chemical Communications* **2009**, (15), 2035-2037.
133. Koso, S.; Ueda, N.; Shinmi, Y.; Okumura, K.; Kizuka, T.; Tomishige, K., Promoting effect of Mo on the hydrogenolysis of tetrahydrofurfuryl alcohol to 1, 5-pentanediol over Rh/SiO 2. *Journal of Catalysis* **2009,** 267, (1), 89-92.
134. Chia, M.; Pagan-Torres, Y. J.; Hibbitts, D.; Tan, Q.; Pham, H. N.; Datye, A. K.; Neurock, M.; Davis, R. J.; Dumesic, J. A., Selective hydrogenolysis of polyols and cyclic ethers over bifunctional surface sites on rhodium–rhenium catalysts. *Journal of the American Chemical Society* **2011,** 133, (32), 12675-12689.
135. Chen, K.; Mori, K.; Watanabe, H.; Nakagawa, Y.; Tomishige, K., C–O bond hydrogenolysis of cyclic ethers with OH groups over rhenium-modified supported iridium catalysts. *Journal of catalysis* **2012,** 294, 171-183.
136. Lee, J.; Xu, Y.; Huber, G. W., High-throughput screening of monometallic catalysts for aqueous-phase hydrogenation of biomass-derived oxygenates. *Applied Catalysis B: Environmental* **2013,** 140, 98-107.
137. Guan, J.; Peng, G.; Cao, Q.; Mu, X., Role of MoO3 on a rhodium catalyst in the selective hydrogenolysis of biomass-derived tetrahydrofurfuryl alcohol into 1, 5-pentanediol. *The Journal of Physical Chemistry C* **2014,** 118, (44), 25555-25566.
138. Pholjaroen, B.; Li, N.; Huang, Y.; Li, L.; Wang, A.; Zhang, T., Selective hydrogenolysis of tetrahydrofurfuryl alcohol to 1, 5-pentanediol over vanadium modified Ir/SiO 2 catalyst. *Catalysis Today* **2015,** 245, 93-99.
139. Liu, S.; Amada, Y.; Tamura, M.; Nakagawa, Y.; Tomishige, K., One-pot selective conversion of furfural into 1, 5-pentanediol over a Pd-added Ir–ReO x/SiO 2 bifunctional catalyst. *Green Chemistry* **2014,** 16, (2), 617-626.

140. Xing, R.; Qi, W.; Huber, G. W., Production of furfural and carboxylic acids from waste aqueous hemicellulose solutions from the pulp and paper and cellulosic ethanol industries. *Energy & Environmental Science* **2011,** 4, (6), 2193-2205.
141. Brentzel, Z. J.; Barnett, K. J.; Huang, K.; Maravelias, C. T.; Dumesic, J. A.; Huber, G. W., Chemicals from Biomass: Combining Ring-Opening Tautomerization and Hydrogenation Reactions to Produce 1,5-Pentanediol from Furfural. *ChemSusChem* **2017,** 10, (7), 1351-1355.
142. Chen, C.-L.; Chung, Y.-H.; Lee, H.-Y., Design and Control of Reactive Distillation Process for the Production of Methyl Valerate. *Industrial & Engineering Chemistry Research* **2016,** 55, (5), 1347-1360.
143. Schniepp, L.; Geller, H., Preparation of dihydropyran, δ-hydroxyvaleraldehyde and 1, 5-pentanediol from tetrahydrofurfuryl alcohol. *Journal of the American Chemical Society* **1946,** 68, (8), 1646-1648.
144. Nakagawa, Y.; Tamura, M.; Tomishige, K., New Reaction Schemes for the Production of Biomass-Based Chemicals Created by Selective Catalytic Hydrogenolysis: Catalysts with Noble Metal and Tungsten. In *Reaction Pathways and Mechanisms in Thermocatalytic Biomass Conversion I*, Springer: 2016; pp 203-225.
145. Xu, W.; Wang, H.; Liu, X.; Ren, J.; Wang, Y.; Lu, G., Direct catalytic conversion of furfural to 1, 5-pentanediol by hydrogenolysis of the furan ring under mild conditions over Pt/Co 2 AlO 4 catalyst. *Chemical Communications* **2011,** 47, (13), 3924-3926.
146. Liu, S.; Amada, Y.; Tamura, M.; Nakagawa, Y.; Tomishige, K., Performance and characterization of rhenium-modified Rh–Ir alloy catalyst for one-pot conversion of furfural into 1, 5-pentanediol. *Catalysis Science & Technology* **2014,** 4, (8), 2535-2549.
147. Liu, H.; Huang, Z.; Zhao, F.; Cui, F.; Li, X.; Xia, C.; Chen, J., Efficient hydrogenolysis of biomass-derived furfuryl alcohol to 1, 2-and 1, 5-pentanediols over a non-precious Cu–Mg 3 AlO 4.5 bifunctional catalyst. *Catalysis Science & Technology* **2016,** 6, (3), 668-671.
148. Sun, D.; Sato, S.; Ueda, W.; Primo, A.; Garcia, H.; Corma, A., Production of C4 and C5 alcohols from biomass-derived materials. *Green Chemistry* **2016,** 18, (9), 2579-2597.
149. Buchholz, V.; Agarwal, S.; Greiner, A., Synthesis and Enzymatic Degradation of Soft Aliphatic Polyesters. *Macromolecular Bioscience* **2016,** 16, (2), 207-213.
150. Wang, Z.; Kastern, B.; Randazzo, K.; Ugrinov, A.; Butz, J.; Seals, D. W.; Sibi, M. P.; Chu, Q. R., Linear polyester synthesized from furfural-based monomer by photoreaction in sunlight. *Green Chemistry* **2015,** 17, (10), 4720-4724.
151. Lomelí-Rodríguez, M.; Rivera-Toledo, M.; López-Sánchez, J. A., Process Intensification of the Synthesis of Biomass-Derived Renewable Polyesters: Reactive Distillation and Divided Wall Column Polyesterification. *Industrial & Engineering Chemistry Research* **2017,** 56, (11), 3017-3032.
152. Kim, S.; Mayeda, M. K.; Sasmaz, E.; Lauterbach, J., One-Step Process for the Production of BTEX and LPG-like fuel from Pentanediol. *ACS Sustainable Chemistry & Engineering* **2015,** 3, (3), 381-385.
153. Fenouillot, F.; Rousseau, A.; Colomines, G.; Saint-Loup, R.; Pascault, J.-P., Polymers from renewable 1, 4: 3, 6-dianhydrohexitols (isosorbide, isomannide and isoidide): A review. *Progress in Polymer Science* **2010,** 35, (5), 578-622.
154. Rose, M.; Palkovits, R., Isosorbide as a renewable platform chemical for versatile applications—Quo Vadis? *ChemSusChem* **2012,** 5, (1), 167-176.
155. Roquette. www.roquette.com (13 January 2017),
156. Feng, X.; Saini, P.; Busto, G.; East, A. J.; Hammond, W. B.; Jaffe, M. In *Isosorbide Containing Polyesters: Homopolymers and Copolymers*, ABSTRACTS OF PAPERS OF THE AMERICAN CHEMICAL SOCIETY, 2012; AMER CHEMICAL SOC 1155 16TH ST, NW, WASHINGTON, DC 20036 USA: 2012.
157. Charbonneau, L. F.; Johnson, R. E.; Witteler, H. B.; Khanarian, G. Isosorbide containing polyesters and methods for making same. 2000.
158. Lee, R.; Kim, J. R.; Lim, J.; Yoon, W.; Kim, D.; Park, J. T.; Lee, Y. J. Polyester resin and method for preparing the same. 2012.
159. Germroth, T. C. METHOD FOR MAKING ISOSORBIDE CONTAINING POLYESTERS. 2005.

160. Abid, M.; Abid, S.; El Gharbi, R., Polyterephthalates bearing bio-based moieties. *Journal of Macromolecular Science, Part A* **2012,** 49, (9), 758-763.
161. Bersot, J. C.; Jacquel, N.; Saint-Loup, R.; Fuertes, P.; Rousseau, A.; Pascault, J. P.; Spitz, R.; Fenouillot, F.; Monteil, V., Efficiency Increase of Poly (ethylene terephthalate-co-isosorbide terephthalate) Synthesis using Bimetallic Catalytic Systems. *Macromolecular Chemistry and Physics* **2011,** 212, (19), 2114-2120.
162. Gioia, C.; Vannini, M.; Marchese, P.; Minesso, A.; Cavalieri, R.; Colonna, M.; Celli, A., Sustainable polyesters for powder coating applications from recycled PET, isosorbide and succinic acid. *Green Chemistry* **2014,** 16, (4), 1807-1815.
163. Yoon, W. J.; Hwang, S. Y.; Koo, J. M.; Lee, Y. J.; Lee, S. U.; Im, S. S., Synthesis and characteristics of a biobased high-T g terpolyester of isosorbide, ethylene glycol, and 1, 4-cyclohexane dimethanol: effect of ethylene glycol as a chain linker on polymerization. *Macromolecules* **2013,** 46, (18), 7219-7231.
164. Sablong, R.; Duchateau, R.; Koning, C. E.; Wit, G. d.; Es, D. v.; Koelewijn, R.; Haveren, J. v., Incorporation of isosorbide into poly (butylene terephthalate) via solid-state polymerization. *Biomacromolecules* **2008,** 9, (11), 3090-3097.
165. Lavilla, C.; Muñoz-Guerra, S., Sugar-based aromatic copolyesters: a comparative study regarding isosorbide and diacetalized alditols as sustainable comonomers. *Green Chemistry* **2013,** 15, (1), 144-151.
166. Noordover, B. A.; Duchateau, R.; van Benthem, R. A.; Ming, W.; Koning, C. E., Enhancing the functionality of biobased polyester coating resins through modification with citric acid. *Biomacromolecules* **2007,** 8, (12), 3860-3870.
167. Kricheldorf, H. R.; Weidner, S. M., High T g copolyesters of lactide, isosorbide and isophthalic acid. *European Polymer Journal* **2013,** 49, (8), 2293-2302.
168. Garaleh, M.; Yashiro, T.; Kricheldorf, H. R.; Simon, P.; Chatti, S., (Co-) Polyesters Derived from Isosorbide and 1, 4-Cyclohexane Dicarboxylic Acid and Succinic Acid. *Macromolecular Chemistry and Physics* **2010,** 211, (11), 1206-1214.
169. Park, H.-S.; Gong, M.-S.; Knowles, J. C., Synthesis and biocompatibility properties of polyester containing various diacid based on isosorbide. *Journal of biomaterials applications* **2012,** 27, (1), 99-109.
170. Noordover, B. A.; van Staalduinen, V. G.; Duchateau, R.; Koning, C. E.; van Benthem, R. A.; Mak, M.; Heise, A.; Frissen, A. E.; van Haveren, J., Co-and terpolyesters based on isosorbide and succinic acid for coating applications: synthesis and characterization. *Biomacromolecules* **2006,** 7, (12), 3406-3416.
171. Wei, Z.; Zhou, C.; Yu, Y.; Li, Y., Biobased copolyesters from renewable resources: synthesis and crystallization behavior of poly (decamethylene sebacate-co-isosorbide sebacate). *RSC Advances* **2015,** 5, (53), 42777-42788.
172. Wu, J.; Eduard, P.; Thiyagarajan, S.; Jasinska-Walc, L.; Rozanski, A.; Guerra, C. l. F.; Noordover, B. A.; van Haveren, J.; van Es, D. S.; Koning, C. E., Semicrystalline polyesters based on a novel renewable building block. *Macromolecules* **2012,** 45, (12), 5069-5080.
173. Okada, M.; Okada, Y.; Aoi, K., Synthesis and degradabilities of polyesters from 1, 4: 3, 6-dianhydrohexitols and aliphatic dicarboxylic acids. *Journal of Polymer Science Part A: Polymer Chemistry* **1995,** 33, (16), 2813-2820.
174. Okada, M.; Okada, Y.; Tao, A.; Aoi, K., Biodegradable polymers based on renewable resources: Polyesters composed of 1, 4: 3, 6-dianhydrohexitol and aliphatic dicarboxylic acid units. *Journal of applied polymer science* **1996,** 62, (13), 2257-2265.
175. Oldring, P. K.; Tuck, N., *Resins for Surface Coatings, Alkyds & Polyesters*. John Wiley & Sons: 2000; Vol. 2.
176. Carraher Jr, C. E., *Carraher's polymer chemistry*. CRC Press: 2010.
177. Allcock, H. R.; Lampe, F. W.; Mark, J. E.; Allcock, H., *Contemporary polymer chemistry*. Pearson/Prentice Hall Upper Saddle River, N. J: 2003.
178. Ravve, A., *Principles of polymer chemistry*. Springer Science & Business Media: 2013.
179. Bakare, I.; Pavithran, C.; Okieimen, F.; Pillai, C., Polyesters from renewable resources: preparation and characterization. *Journal of applied polymer science* **2006,** 100, (5), 3748-3755.

180. Braun, D.; Cherdron, H.; Rehahn, M.; Ritter, H.; Voit, B., *Polymer synthesis: theory and practice: fundamentals, methods, experiments*. Springer Science & Business Media: 2012.
181. Kumar, A.; Gupta, R. K., *Fundamentals of polymer engineering, revised and expanded*. CRC Press: 2003.
182. Asua, J., *Polymer Reaction Engineering*. John Wiley & Sons, Incorporated: Chichester, 2008.
183. Rudin, A.; Choi, P., *The elements of polymer science and engineering*. Academic press: 2012.
184. Gupta, S. K.; Kumar, A., *Reaction engineering of step growth polymerization*. Springer Science & Business Media: 2012.
185. Kuchanov, S. I.; Keshtov, M. L.; Halatur, P. G.; Vasnev, V. A.; Vinogradova, S. V.; Korshak, V. V., On the principle of equal reactivity in solution polycondensation. *Die Makromolekulare Chemie* **1983,** 184, (1), 105-111.
186. Park, O. O., Molecular weight distribution and moments for condensation polymerization with variant reaction rate constant depending on chain lengths. *Macromolecules* **1988,** 21, (3), 732-735.
187. Kronstadt, M.; Dubin, P. L.; Tyburczy, J. A., Molecular weight distribution of a novel condensation polymerization. Comparison with theory. *Macromolecules* **1978,** 11, (1), 37-40.
188. Flory, P. J., Kinetics of polyesterification: a study of the effects of molecular weight and viscosity on reaction rate. *Journal of the American chemical society* **1939,** 61, (12), 3334-3340.
189. Stockmayer, W. H., Theory of Molecular Size Distribution and Gel Formation in Branched-Chain Polymers. *The Journal of Chemical Physics* **1943,** 11, (2), 45-55.
190. Mueller, P. A.; Richards, J. R.; Congalidis, J. P., Polymerization reactor modeling in industry. *Macromolecular Reaction Engineering* **2011,** 5, (7-8), 261-277.
191. Boyd, R. H.; Phillips, P. J., *The science of polymer molecules. [electronic book]*. Cambridge : Cambridge University Press, 1993.: 1993.
192. Seavey, K.; Liu, Y. A., *Step-growth polymerization process modeling and product design*. John Wiley & Sons: 2009.
193. Polymerization. http://www.umich.edu/~elements/07chap/html/polymerization.pdf (Accessed 19 February 2017),
194. Thomas, D.; Hagan, R., The influence of molecular weight distribution on melt viscosity, melt elasticity, processing behavior and properties of polystyrene. *Polymer Engineering & Science* **1969,** 9, (3), 164-171.
195. Rodriguez, F., *Principles of polymer systems*. New York: McGraw-Hill, 1970.: 1970.
196. Fogler, H. S., *Elements of chemical reaction engineering*. Upper Saddle River, NJ : Prentice Hall PTR ; 2006.

4th ed.: 2006.
197. Rootsaert, W.; Van de Vusse, J., Kinetics of an infinite series of consecutive reactions. Studies on the preparation of epoxy esters. *Chemical Engineering Science* **1966,** 21, (11), 1067-1078.
198. Mochizuki, S.; Itoh, N., Optimal polymerization temperature profile for nylon-6 with low cyclic oligomers content. *Chemical Engineering Science* **1978,** 33, (10), 1401-1403.
199. Tai, K.; Tagawa, T., Simulation of hydrolytic polymerization of. epsilon.-caprolactam in various reactors. A review on recent advances in reaction engineering of polymerization. *Industrial & Engineering Chemistry Product Research and Development* **1983,** 22, (2), 192-206.
200. Wenhua, X.; Huang, N.; Tang, Z.; Filippini-Fantoni, R., Simulation of Nylon 6 Polymerization in an Industrial Two-Step VK Tubular Reactor. *Macromolecular Materials and Engineering* **2003,** 288, (3), 235-244.
201. Agrawal, A. K.; Devika, K.; Manabe, T., Simulation of hydrolytic polymerization of nylon-6 in industrial reactors: Part I. mono-acid-stabilized systems in VK tube reactors. *Industrial & engineering chemistry research* **2001,** 40, (12), 2563-2572.
202. Penlidis, A.; Ponnuswamy, S.; Kiparissides, C.; O'Driscoll, K., Polymer reaction engineering: modelling considerations for control studies. *The chemical engineering journal* **1992,** 50, (2), 95-107.
203. Seider, W. D.; Seader, J. D.; Lewin, D. R., *PRODUCT & PROCESS DESIGN PRINCIPLES: SYNTHESIS, ANALYSIS AND EVALUATION, (With CD)*. John Wiley & Sons: 2009.

204. Towler, G.; Sinnott Ray, K., *Chemical Engineering Design - Principles, Practice and Economics of Plant and Process Design (2nd Edition)*. Elsevier: 2013.
205. Shah, M.; Zondervan, E.; de Haan, A., Modelling and simulation of an unsaturated polyester process. *Journal of Applied Sciences(Faisalabad)* **2010,** 10, (21), 2551-2557.
206. Bueno, L.; Toro, C.; Martín, M., Techno-economic evaluation of the production of polyesters from glycerol and adipic acid. *Chemical Engineering Research and Design* **2015,** 93, 432-440.
207. Choi, J.-i.; Lee, S. Y., Process analysis and economic evaluation for poly (3-hydroxybutyrate) production by fermentation. *Bioprocess and Biosystems Engineering* **1997,** 17, (6), 335-342.
208. Eerhart, A.; Faaij, A.; Patel, M. K., Replacing fossil based PET with biobased PEF; process analysis, energy and GHG balance. *Energy & Environmental Science* **2012,** 5, (4), 6407-6422.
209. Perry, R. H.; Green, D. W.; Maloney, J. O., *Perry's Chemical engineer's handbook*. New York: McGraw-Hill, 1984.

6th ed.; prepared by a staff of specialists under the direction of [the] late editor: Robert H. Perry; editor: Don W. Green; assistant editor: James O. Maloney.: 1984.
210. Chaves, I. D. G.; López, J. R. G.; Zapata, J. L. G.; Robayo, A. L.; Niño, G. R., Process Simulation in Chemical Engineering. *Process Analysis & Simulation in Chemical Engineering* **2016**, 1.
211. Rangaiah, G. P.; Bonilla-Petriciolet, A., *Multi-objective optimization in chemical engineering. [electronic book] : developments and applications*. Chichester [England] : Wiley, 2013.: 2013.
212. Kiparissides, C., Polymerization reactor modeling: a review of recent developments and future directions. *Chemical Engineering Science* **1996,** 51, (10), 1637-1659.
213. Garg, S.; Gupta, S. K., Multiobjective optimization of a free radical bulk polymerization reactor using genetic algorithm. *Macromolecular Theory and Simulations* **1999,** 8, (1), 46-53.
214. Curteanu, S.; Leon, F.; Gâlea, D., Alternatives for multiobjective optimization of a polymerization process. *Journal of applied polymer science* **2006,** 100, (5), 3680-3695.
215. Rivera-Toledo, M.; Flores-Tlacuahuac, A., A Multiobjective Dynamic Optimization Approach for a Methyl-Methacrylate Plastic Sheet Reactor. *Macromolecular Reaction Engineering* **2014,** 8, (4), 358-373.
216. Marler, R. T.; Arora, J. S., Survey of multi-objective optimization methods for engineering. *Structural and multidisciplinary optimization* **2004,** 26, (6), 369-395.
217. Rivera-Toledo, M.; Del Río-Chanona, E. A.; Flores-Tlacuahuac, A., Multiobjective dynamic optimization of the cell-cast process for poly (methyl methacrylate). *Industrial & Engineering Chemistry Research* **2014,** 53, (37), 14351-14365.
218. Kumar, A.; Sukthankar, V.; Vaz, C.; Gupta, S. K., Optimization of the transesterification stage of polyethylene terephthalate reactors. *Polymer Engineering & Science* **1984,** 24, (3), 185-193.
219. Mitra, K.; Deb, K.; Gupta, S. K., Multiobjective dynamic optimization of an industrial nylon 6 semibatch reactor using genetic algorithm. *Journal of Applied Polymer Science* **1998,** 69, (1), 69-87.
220. Bhaskar, V.; Gupta, S. K.; Ray, A. K., Multiobjective optimization of an industrial wiped-film pet reactor. *AIChE journal* **2000,** 46, (5), 1046-1058.
221. Xi, Z.; Chen, L.; Sun, W.; Zhao, L.; Yuan, W., Optimization of the Continuous Polycondensation Process for Polyethylene Adipate. *Chemical Engineering & Technology* **2014,** 37, (7), 1163-1169.
222. Majumdar, S.; Mitra, K.; Sardar, G., Kinetic analysis and optimization for the catalytic esterification step of PPT polymerization. *Macromolecular theory and simulations* **2005,** 14, (1), 49-59.
223. Kachhap, R.; Guria, C., Multi-Objective Optimization of a Batch Copoly (ethylene-polyoxyethylene terephthalate) Reactor Using Different Adaptations of Nondominated Sorting Genetic Algorithm. *Macromolecular theory and simulations* **2005,** 14, (6), 358-373.
224. Mitra, K., Genetic algorithms in polymeric material production, design, processing and other applications: a review. *International Materials Reviews* **2008,** 53, (5), 275-297.
225. Koleske, J. V., Paint and Coating Testing Manual - Fifteenth Edition of the Gardner-Sward Handbook: (MNL 17-2nd). In ASTM International.

226. Chrissafis, K.; Paraskevopoulos, K.; Bikiaris, D., Thermal degradation kinetics of the biodegradable aliphatic polyester, poly (propylene succinate). *Polymer degradation and stability* **2006,** 91, (1), 60-68.
227. Papageorgiou, G. Z.; Papageorgiou, D. G.; Tsanaktsis, V.; Bikiaris, D. N., Synthesis of the bio-based polyester poly (propylene 2, 5-furan dicarboxylate). Comparison of thermal behavior and solid state structure with its terephthalate and naphthalate homologues. *Polymer* **2015,** 62, 28-38.
228. Wade, L. G., *Organic chemistry*. Harlow : Pearson Education, 2013.

8th ed, New International Edition.: 2013.
229. Determination of polymer structure by GPC. http://www.malvern.com/en/support/resource-center/application-notes/AN091001polymerStructByGPC.aspx (Accessed 09 February 2017),
230. Investigation of Polymers with Differential Scanning Calorimetry. https://polymerscience.physik.hu-berlin.de/docs/manuals/DSC.pdf (Accessed 09 February 2017),
231. Glass transition temperature for epoxies. http://www.epotek.com/site/files/Techtips/pdfs/tip23.pdf (Accessed 09 February 2017),
232. Polymer properties database. http://polymerdatabase.com/polymer%20physics/GlassTransition.html (Accessed 09 February 2017),
233. Polymer chemistry. http://faculty.uscupstate.edu/llever/Polymer%20Resources/GlassTrans.htm (Accessed 09 February 2017),
234. Differential Scanning Calorimetry. http://nptel.ac.in/courses/115103030/module4/lec22/2.html (Accessed 12 February 2017),
235. TGA A Beginner's Guide. http://www.perkinelmer.co.uk/CMSResources/Images/44-74556GDE_TGABeginnersGuide.pdf (Accessed 09 February 2017),
236. Standard Test Method for Resistance of Organic Coatings to the Effects of Rapid Deformation (Impact). https://compass.astm.org/EDIT/html_annot.cgi?D2794+93(2010) (Accessed 14 February 2017),
237. Standard Test Methods for Indentation Hardness of Organic Coatings. https://compass.astm.org/download/D1474D1474M.4895.pdf (Accessed 15 February 2017),
238. Coil coated metals. Test methods. Pencil hardness. http://shop.bsigroup.com/ProductDetail/?pid=000000000030268977 (Accessed 14 February 2017),
239. Standard Test Method for Specular Gloss. https://compass.astm.org/Standards/HISTORICAL/D523-89R99.htm (Accessed 14 February 2017),
240. EN 13523-1:2001 Coil Coated Metals - Test Methods - Part 1: Coating Thickness. http://infostore.saiglobal.com/emea/Details.aspx?ProductID=268219&refs=1#refs (Accessed 15 February 2017),
241. Standard Practice for Assessing the Solvent Resistance of Organic Coatings Using Solvent Rubs. https://compass.astm.org/download/D5402-93R99.15287.pdf (Accessed 15 February 2015),
242. ISO 14577-1:2015 Metallic materials — Instrumented indentation test for hardness and materials parameters — Part 1: Test method. https://www.iso.org/obp/ui/#iso:std:iso:14577:-1:ed-2:v1:en (Accessed 15 February 2017),
243. Standard Test Method for Assignment of the Glass Transition Temperatures by Differential Scanning Calorimetry or Differential Thermal Analysis. https://compass.astm.org/download/E1356-98.33431.pdf (Accessed 15 February 2017),
244. Standard Test Method for Coating Flexibility of Prepainted Sheet. https://compass.astm.org/download/D4145.28079.pdf (Accessed 15 February 2017),
245. World's top ten paints companies 2013 annual report. http://en.topbm.com/News-news_detail-id-2903.shtml.2014.02.08 (Accessed 13 February 2017),
246. Siyab, N.; Tenbusch, S.; Willis, S.; Lowe, C.; Maxted, J., Going Green: making reality match ambition for sustainable coil coatings. *Journal of Coatings Technology and Research* **2016,** 13, (4), 629-643.
247. Giannakopoulos, I.; Taylor, A., A modelling study of the visco-elastic behaviour of polyester-based coil coatings. *Progress in Organic Coatings* **2013,** 76, (11), 1556-1566.

248. Sander, J. Coil coating eBook European coatings tech files. https://leseprobe.buch.de/images-adb/00/92/00929bc5-f953-4cab-9f29-b40d80e5dd58.pdf (Accessed 24 May 2017),
249. Coil coatings. http://www.beckers-group.com/our-business/coil-coatings/ (Accessed 13 February 2017),
250. Coil Coating: Sustainable Process, Sustainable Products. http://prepaintedmetal.eu/repository/Publications%20-%20Press/sustainability%20report%20051112.pdf (Accessed 15 February 2017),
251. Schmitthenner, M., Basic resins for coil coatings. *European coatings journal* **1998**, 618-625.
252. Gubbels, E.; Drijfhout, J. P.; Posthuma-van Tent, C.; Jasinska-Walc, L.; Noordover, B. A. J.; Koning, C. E., Bio-based semi-aromatic polyesters for coating applications. *Progress in Organic Coatings* **2014,** 77, (1), 277-284.
253. Van Haveren, J.; Oostveen, E. A.; Micciché, F.; Noordover, B. A. J.; Koning, C. E.; Van Benthem, R.; Frissen, A. E.; Weijnen, J. G. J., Resins and additives for powder coatings and alkyd paints, based on renewable resources. *Journal of Coatings Technology and Research* **2007,** 4, (2), 177-186.
254. Noordover, B. A. J.; van Staalduinen, V. G.; Duchateau, R.; Koning, C. E.; van Benthem, R. A. T. M.; Mak, M.; Heise, A.; Frissen, A. E.; van Haveren, J., Co-and terpolyesters based on isosorbide and succinic acid for coating applications: synthesis and characterization. *Biomacromolecules* **2006,** 7, (12), 3406-3416.
255. Noordover, B. A. J.; Heise, A.; Malanowksi, P.; Senatore, D.; Mak, M.; Molhoek, L.; Duchateau, R.; Koning, C. E.; van Benthem, R. A. T. M., Biobased step-growth polymers in powder coating applications. *Progress in Organic Coatings* **2009,** 65, (2), 187-196.
256. Jasinska, L.; Koning, C. E., Unsaturated, biobased polyesters and their cross-linking via radical copolymerization. *Journal of Polymer Science Part A: Polymer Chemistry* **2010,** 48, (13), 2885-2895.
257. Gubbels, E.; Jasinska-Walc, L.; Noordover, B. A. J.; Koning, C. E., Linear and branched polyester resins based on dimethyl-2, 5-furandicarboxylate for coating applications. *European Polymer Journal* **2013,** 49, (10), 3188-3198.
258. Argyropoulos, J.; Popa, P.; Spilman, G.; Bhattacharjee, D.; Koonce, W.; Argyropoulos, J.; Popa, P.; Spilman, G.; Bhattacharjee, D.; Koonce, W.; Argyropoulos, J.; Popa, P.; Spilman, G.; Bhattacharjee, D.; Koonce, W., Seed oil based polyester polyols for coatings. *Journal of Coatings Technology and Research* **2009,** 6, (4), 501.
259. Noordover, B. A. J.; Duchateau, R.; van Benthem, R. A. T. M.; Ming, W.; Koning, C. E., Enhancing the functionality of biobased polyester coating resins through modification with citric acid. *Biomacromolecules* **2007,** 8, (12), 3860-3870.
260. Plackett, D. V., *Biopolymers [electronic book] : new materials for sustainable films and coatings / editor, David Plackett*. Chichester, West Sussex, UK : Hoboken, NJ : Wiley, c2011.

1st ed.: 2011.
261. Olewnik, E.; Czerwiński, W.; Nowaczyk, J.; Sepulchre, M.-O.; Tessier, M.; Salhi, S.; Fradet, A., Synthesis and structural study of copolymers of l-lactic acid and bis(2-hydroxyethyl terephthalate). *European Polymer Journal* **2007,** 43, (3), 1009-1019.
262. Gomes, M.; Gandini, A.; Silvestre, A. J.; Reis, B., Synthesis and characterization of poly (2, 5-furan dicarboxylate) s based on a variety of diols. *Journal of Polymer Science Part A: Polymer Chemistry* **2011,** 49, (17), 3759-3768.
263. Zhou, W.; Wang, X.; Yang, B.; Xu, Y.; Zhang, W.; Zhang, Y.; Ji, J., Synthesis, physical properties and enzymatic degradation of bio-based poly (butylene adipate-co-butylene furandicarboxylate) copolyesters. *Polymer degradation and stability* **2013,** 98, (11), 2177-2183.
264. Sousa, A. F.; Matos, M.; Freire, C. S. R.; Silvestre, A. J. D.; Coelho, J. F. J., New copolyesters derived from terephthalic and 2,5-furandicarboxylic acids: A step forward in the development of biobased polyesters. *Polymer* **2013,** 54, (2), 513-519.
265. Wu, B.; Xu, Y.; Bu, Z.; Wu, L.; Li, B.-G.; Dubois, P., Biobased poly (butylene 2, 5-furandicarboxylate) and poly (butylene adipate-co-butylene 2, 5-furandicarboxylate) s: From

synthesis using highly purified 2, 5-furandicarboxylic acid to thermo-mechanical properties. *Polymer* **2014,** 55, (16), 3648-3655.
266. Levchik, S. V.; Weil, E. D., A review on thermal decomposition and combustion of thermoplastic polyesters. *Polymers for Advanced Technologies* **2004,** 15, (12), 691-700.
267. Luo, S.; Li, F.; Yu, J., The thermal, mechanical and viscoelastic properties of poly(butylene succinate- co-terephthalate) (PBST) copolyesters with high content of BT units. *Journal of Polymer Research* **2011,** 18, (3), 393-400.
268. Huang, K.; Brentzel, Z. J.; Barnett, K. J.; Dumesic, J. A.; Huber, G. W.; Maravelias, C. T., Conversion of Furfural to 1,5-Pentanediol: Process Synthesis and Analysis. *ACS Sustainable Chemistry & Engineering* **2017**.
269. Chatterjee, M.; Ishizaka, T.; Kawanami, H., Hydrogenation of 5-hydroxymethylfurfural in supercritical carbon dioxide–water: a tunable approach to dimethylfuran selectivity. *Green Chemistry* **2014,** 16, (3), 1543-1551.
270. Götz, D.; Lucas, M.; Claus, P., C–O bond hydrogenolysis vs. C [double bond, length as m-dash] C group hydrogenation of furfuryl alcohol: towards sustainable synthesis of 1, 2-pentanediol. *Reaction Chemistry & Engineering* **2016,** 1, (2), 161-164.
271. Sheikhy, H.; Shahidzadeh, M.; Ramezanzadeh, B., An evaluation of the mechanical and adhesion properties of a hydroxyl-terminated polybutadiene (HTPB)-based adhesive including different kinds of chain extenders. *Polymer Bulletin* **2015,** 72, (4), 755-777.
272. Chen, K.-S.; Leon Yu, T.; Chen, Y.-S.; Lin, T.-L.; Liu, W.-J., Soft-and hard-segment phase segregation of polyester-based polyurethane. *Journal of Polymer Research* **2001,** 8, (2), 99-109.
273. Murata, S.; Nakajima, T.; Tsuzaki, N.; Yasuda, M.; Kato, T., Synthesis and hydrolysis resistance of polyurethane derived from 2,4-diethyl-1,5-pentanediol. *Polymer Degradation and Stability* **1998,** 61, (3), 527-534.
274. Guang, L.; Gaymans, R. J., Polyesteramides with mixtures of poly(tetramethylene oxide) and 1,5-pentanediol. *Polymer* **1997,** 38, (19), 4891-4896.
275. Mazurek, M. M.; Parzuchowski, P. G.; Rokicki, G., Propylene carbonate as a source of carbonate units in the synthesis of elastomeric poly(carbonate–urethane)s and poly(ester–carbonate–urethane)s. *Journal of Applied Polymer Science* **2014,** 131, (5), n/a-n/a.
276. Terzopoulou, Z.; Tsanaktsis, V.; Nerantzaki, M.; Papageorgiou, G. Z.; Bikiaris, D. N., Decomposition mechanism of polyesters based on 2,5-furandicarboxylic acid and aliphatic diols with medium and long chain methylene groups. *Polymer Degradation and Stability* **2016,** 132, 127-136.
277. Ni, H.; Daum, J. L.; Thiltgen, P. R.; Soucek, M. D.; Simonsick Jr, W. J.; Zhong, W.; Skaja, A. D., Cycloaliphatic polyester-based high-solids polyurethane coatings: II. The effect of difunctional acid. *Progress in Organic Coatings* **2002,** 45, (1), 49-58.
278. Jiang, Y.; Woortman, A. J. J.; Alberda van Ekenstein, G. O. R.; Loos, K., A biocatalytic approach towards sustainable furanic-aliphatic polyesters. *Polymer Chemistry* **2015,** 6, (29), 5198-5211.
279. Fox, T. G.; Flory, P. J., Second-Order Transition Temperatures and Related Properties of Polystyrene. I. Influence of Molecular Weight. *Journal of Applied Physics* **1950,** 21, (6), 581-591.
280. Wu, H.; Wen, B.; Zhou, H.; Zhou, J.; Yu, Z.; Cui, L.; Huang, T.; Cao, F., Synthesis and degradability of copolyesters of 2, 5-furandicarboxylic acid, lactic acid, and ethylene glycol. *Polymer Degradation and Stability* **2015,** 121, 100-104.
281. Kwiatkowska, M.; Kowalczyk, I.; Kwiatkowski, K.; Szymczyk, A.; Rosłaniec, Z., Fully biobased multiblock copolymers of furan-aromatic polyester and dimerized fatty acid: Synthesis and characterization. *Polymer* **2016,** 99, 503-512.
282. Velayutham, T. S.; Majid, W. H. A.; Ahmad, A. B.; Kang, G. Y.; Gan, S. N., Synthesis and characterization of polyurethane coatings derived from polyols synthesized with glycerol, phthalic anhydride and oleic acid. *Progress in Organic Coatings* **2009,** 66, (4), 367-371.
283. Gooch, J. W., Polymeric Plasticizer. *Encyclopedic Dictionary of Polymers* **2011**, 564-564.
284. Cuirassier, F.; Baradji, C. H.; Riess, G., Preparation of Microlatex with Functionalized Polyesters as Surfactants. In *Polymer Association Structures*, American Chemical Society: 1989; Vol. 384, pp 100-115.

285. Szabó-Réthy, E., Comments on the calculation methods of kinetics of polyesterification reactions. *European Polymer Journal* **1971,** 7, (10), 1485-1499.
286. Yamada, T.; Imamura, Y.; Makimura, O., A mathematical model for computer simulation of a direct continuous esterification process between terephthalic acid and ethylene glycol: Part 1. Model development. *Polymer Engineering & Science* **1985,** 25, (12), 788-795.
287. Ravindranath, K.; Mashelkar, R. A., Polyethylene terephthalate—II. Engineering analysis. *Chemical Engineering Science* **1986,** 41, (12), 2969-2987.
288. Kang, C. K.; Lee, B. C.; Ihm, D. W., Modeling of semibatch direct esterification reactor for poly (ethylene terephthalate) synthesis. *Journal of applied polymer science* **1996,** 60, (11), 2007-2015.
289. Patel, H.; Feix, G.; Schomäcker, R., Modeling of Semibatch Esterification Process for Poly(ethylene terephthalate) Synthesis. *Macromolecular Reaction Engineering* **2007,** 1, (4), 502-512.
290. Jedlovčnik, R.; Šebenik, A.; Golob, J.; Korbar, J., Step-growth polymerization of maleic anhydride and 1,2-propylene glycol. *Polymer Engineering & Science* **1995,** 35, (17), 1413-1417.
291. Zetterlund, P. B.; Weaver, W.; Johnson, A. F., KINETICS OF POLYESTERIFICATION: MODELLING OF THE CONDENSATION OF MALEIC ANHYDRIDE, PHTHALIC ANHYDRIDE, AND 1,2-PROPYLENE GLYCOL. *Polymer Reaction Engineering* **2002,** 10, (1-2), 41-57.
292. Shah, M.; Zondervan, E.; de Haan, A. B., Process modeling for the synthesis of unsaturated polyester. *Polymer Engineering & Science* **2011,** 51, (12), 2495-2504.
293. Salmi, T.; Paatero, E.; Nyholm, P.; Still, M.; Na¨rhi, K., Kinetics of melt polymerization of maleic acid phthalic acids with propylene glycol. *Chemical Engineering Science* **1994,** 49, (24), 5053-5070.
294. Nalampang, K.; Johnson, A. F., Kinetics of polyesterification: modelling and simulation of unsaturated polyester synthesis involving 2-methyl-1,3-propanediol. *Polymer* **2003,** 44, (19), 6103-6109.
295. Bacaloglu, R.; Fisch, M.; Biesiada, K., Kinetics of polyesterification of adipic acid with 1, 3-butanediol. *Polymer engineering and science* **1998,** 38, (6), 1014.
296. Simitzis, J., A mathematical model for computer simulation of the production of unsaturated polyesters with catalysts. *European Polymer Journal* **1988,** 24, (10), 999-1003.
297. Karayannidis, G. P.; Roupakias, C. P.; Bikiaris, D. N.; Achilias, D. S., Study of various catalysts in the synthesis of poly(propylene terephthalate) and mathematical modeling of the esterification reaction. *Polymer* **2003,** 44, (4), 931-942.
298. Shaaban, A. F.; Salem, M. A.; Messiha, N. N., Unsaturated polyesters—IV. Kinetics of polyesterification of cinnamylsuccinic acid with 1,4-tetramethylene glycol. *European Polymer Journal* **1987,** 23, (2), 153-158.
299. Fradet, A.; Maréchal, E., Kinetics and mechanisms of polyesterifications. In *Polymerizations and Polymer Properties*, Springer Berlin Heidelberg: Berlin, Heidelberg, 1982; pp 51-142.
300. Gordon, M., Good's Theory of Cascade Processes Applied to the Statistics of Polymer Distributions. *Proceedings of the Royal Society of London. Series A. Mathematical and Physical Sciences* **1962,** 268, (1333), 240-256.
301. Mikes, J.; Dusek, K., Simulation of polymer network formation by the Monte Carlo method. *Macromolecules* **1982,** 15, (1), 93-99.
302. Kumar, A.; Wahal, S.; Sastri, S.; Gupta, S. K., Modelling of intramolecular reactions in the step-growth polymerization of multifunctional monomers. *Polymer* **1986,** 27, (4), 583-591.
303. Stepto, R. F. T., Theoretical and experimental studies of network formation and properties. *Polymer* **1979,** 20, (11), 1324-1326.
304. Ravindranath, K.; Mashelkar, R. A., Polyethylene terephthalate—I. Chemistry, thermodynamics and transport properties. *Chemical Engineering Science* **1986,** 41, (9), 2197-2214.
305. Schaul, J. S., Drying and Injection Molding Pet for Beverage Bottle Preforms. *Polymer-Plastics Technology and Engineering* **1981,** 16, (2), 209-230.
306. Fakirov, S.; Seganov, I.; Kurdowa, E., Effect of chain composition of poly(ethylene terephthalate) structure and properties. *Die Makromolekulare Chemie* **1981,** 182, (1), 185-197.
307. Buxbaum, L. H., The Degradation of Poly(ethylene terephthalate). *Angewandte Chemie International Edition in English* **1968,** 7, (3), 182-190.

308. Kang, C. K.; Lee, B. C.; Ihm, D. W.; Tremblay, D. A., A simulation study on continuous direct esterification process for poly (ethylene terephthalate) synthesis. *Journal of applied polymer science* **1997,** 63, (2), 163-174.
309. Ravindranath, K.; Mashelkar, R. A., Modeling of poly(ethylene terephthalate) reactors: 4. A continuous esterification process. *Polymer Engineering & Science* **1982,** 22, (10), 610-618.
310. Yamada, T., Influence of Reaction Pressure below Atmosphere on Esterification Reaction between Terephthalic Acid and Ethylene Glycol. *Polym J* **1992,** 24, (1), 43-61.
311. Bikiaris, D. N.; Achilias, D. S., Synthesis of poly(alkylene succinate) biodegradable polyesters I. Mathematical modelling of the esterification reaction. *Polymer* **2006,** 47, (13), 4851-4860.
312. Bikiaris, D. N.; Achilias, D. S., Synthesis of poly(alkylene succinate) biodegradable polyesters, Part II: Mathematical modelling of the polycondensation reaction. *Polymer* **2008,** 49, (17), 3677-3685.
313. Park, S. S.; Jun, H. W.; Im, S. S., Kinetics of forming poly(butylene succinate) (PBS) oligomer in the presence of MBTO catalyst. *Polymer Engineering & Science* **1998,** 38, (6), 905-913.
314. Garin, M.; Tighzert, L.; Vroman, I.; Marinkovic, S.; Estrine, B., The kinetics of poly(butylene succinate) synthesis and the influence of molar mass on its thermal properties. *Journal of Applied Polymer Science* **2014,** 131, (16), n/a-n/a.
315. Hu, L.; Wu, L.; Song, F.; Li, B.-G., Kinetics and Modeling of Melt Polycondensation for Synthesis of Poly[(butylene succinate)-co-(butylene terephthalate)], 1 – Esterification. *Macromolecular Reaction Engineering* **2010,** 4, (9-10), 621-632.
316. Wilsens, C. H. R. M.; Wullems, N. J. M.; Gubbels, E.; Yao, Y.; Rastogi, S.; Noordover, B. A. J., Synthesis, kinetics, and characterization of bio-based thermosets obtained through polymerization of a 2,5-furandicarboxylic acid-based bis(2-oxazoline) with sebacic acid. *Polymer Chemistry* **2015,** 6, (14), 2707-2716.
317. Chen, Q.; Chang, H.; Zhang, D., How to Take the Removal of Condensation Water into Account in Polyesterification Kinetics? *Polym J* **1999,** 31, (7), 599-601.
318. Chen, S.-a.; Wu, K. C., Kinetics of polyesterification. II. Foreign acid-catalyzed dibasic acid and glycol systems. *Journal of Polymer Science: Polymer Chemistry Edition* **1982,** 20, (7), 1819-1831.
319. Mathworks Documentation. https://uk.mathworks.com/help/optim/ug/fminunc.html (Accessed 18 July 2017),
320. Salmi, T.; Paatero, E.; Nyholm, P., Kinetic model for the increase of reaction order during polyesterification. *Chemical Engineering and Processing: Process Intensification* **2004,** 43, (12), 1487-1493.
321. Makay-Bödi, E.; Vancsó-Szmercsányi, I., Kinetic studies on the polycondensation effects of chain-lengths of the reagents on the reaction rate. *European Polymer Journal* **1969,** 5, (1), 145-153.
322. Davies, M.; Hill, D. R. J., The kinetics of an uncatalyzed polycondensation reaction. *Transactions of the Faraday Society* **1953,** 49, (0), 395-404.
323. Au-Chin, T.; Kuo-Sui, Y., Mechanism of hydrogen ion catalysis in esterification. II. Studies on the kinetics of polyesterification reactions between dibasic acids and glycols. *Journal of Polymer Science* **1959,** 35, (128), 219-233.
324. Flory, P. J., Fundamental Principles of Condensation Polymerization. *Chemical Reviews* **1946,** 39, (1), 137-197.
325. Lin, C. C.; Yu, P. C., The kinetics of polyesterification. II. Succinic acid and ethylene glycol. *Journal of Polymer Science: Polymer Chemistry Edition* **1978,** 16, (5), 1005-1016.
326. Fang, Y.-R.; Lai, C.-G.; Lu, J.-L.; Chen, M.-K., KINETICS AND MECHANISM OF POLYESTERIFICATION OF BINARY ACID AND BINARY ALCOHOL. *SCIENTIA SINICA* **1975,** 18, (1), 72-87.
327. Carberry, J. J., *Chemical and catalytic reaction engineering. [electronic book]*. Mineola, N.Y. : Dover Publications, 2001.

Dover edition.: 2001.
328. Froment, G. F.; Bischoff, K. B., *Chemical reactor analysis and design*. Wiley: 1979.

329. Au-Chin, T.; Kuo-Sui, Y., Mechanism of hydrogen ion catalysis in esterification. II. Studies on the kinetics of polyesterification reactions between dibasic acids and glycols. *Journal of Polymer Science* **1959,** 35, (128), 219-233.
330. Vancsó-Szmercsányi, I.; Maros-Gréger, K.; Makay-Bödi, E., Investigations on polyesterification reactions. *European Polymer Journal* **1969,** 5, (1), 155-161.
331. Amass, A. J., Comments on the kineticsof uncatalysed polyesterification reactions. *Polymer* **1979,** 20, (4), 515-516.
332. Matsuo, T.; Kamikawa, M.; Kondo, T.; Maeda, N. Polyester production process and apparatus. 2014.
333. Lehtonen, J.; Salmi, T.; Immonen, K.; Paatero, E.; Nyholm, P., Kinetic Model for the Homogeneously Catalyzed Polyesterification of Dicarboxylic Acids with Diols. *Industrial & Engineering Chemistry Research* **1996,** 35, (11), 3951-3963.
334. Yamada, T.; Imamura, Y.; Makimura, O.; Kamatani, H., A mathematical model for computer simulation of the direct continuous esterification process between terephthalic acid and ethylene glycol. Part II: Reaction rate constants. *Polymer Engineering & Science* **1986,** 26, (10), 708-716.
335. Ingold, C. K., *Structure and mechanism in organic chemistry*. Cornell University Press; Ithaca; New York: 1953.
336. Joule, J. A.; Mills, K., *Heterocyclic chemistry*. John Wiley & Sons: 2008.
337. Zhang, Z.; Zhen, J.; Liu, B.; Lv, K.; Deng, K., Selective aerobic oxidation of the biomass-derived precursor 5-hydroxymethylfurfural to 2,5-furandicarboxylic acid under mild conditions over a magnetic palladium nanocatalyst. *Green Chemistry* **2015,** 17, (2), 1308-1317.
338. Rolfe, A. C.; Hinshelwood, C. N., The kinetics of esterification. The reaction between acetic acid and methyl alcohol. *Transactions of the Faraday Society* **1934,** 30, (0), 935-944.
339. Tolsma, J. E.; Clabaugh, J. A.; Barton, P. I., Symbolic incorporation of external procedures into process modeling environments. *Industrial & engineering chemistry research* **2002,** 41, (16), 3867-3876.
340. Seavey, K. C. RESEARCH AND DEVELOPMENT OF SIMULATION AND OPTIMIZATION TECHNOLOGY FOR COMMERCIAL NYLON-6 MANUFACTURING PROCESSES. Virginia Polytechnic Institute, 2003.
341. Mavrotas, G., Effective implementation of the ε-constraint method in multi-objective mathematical programming problems. *Applied mathematics and computation* **2009,** 213, (2), 455-465.
342. Eerhart, A. J. J. E.; Huijgen, W. J. J.; Grisel, R. J. H.; van der Waal, J. C.; de Jong, E.; de Sousa Dias, A.; Faaij, A. P. C.; Patel, M. K., Fuels and plastics from lignocellulosic biomass via the furan pathway; a technical analysis. *RSC Advances* **2014,** 4, (7), 3536-3549.
343. Van Uytvanck, P. P.; Hallmark, B.; Haire, G.; Marshall, P. J.; Dennis, J. S., Impact of Biomass on Industry: Using Ethylene Derived from Bioethanol within the Polyester Value Chain. *ACS Sustainable Chemistry & Engineering* **2014,** 2, (5), 1098-1105.
344. Aspen Polymers: User Guide Volume 1 AspenTech: Cambridge, MA, 2011. http://docs.chejunkie.com/wp-content/uploads/sites/2/2014/11/AspenPolymers-Vol1V7_3-Usr.pdf (Accessed May 2 2016),
345. Dowling, A. W.; Ruiz-Mercado, G.; Zavala, V. M., A framework for multi-stakeholder decision-making and conflict resolution. *Computers & Chemical Engineering* **2016,** 90, 136-150.
346. Bio-Succinic Acid: A High Performing Green Chemical without a "Green Premium" Price. Myriant: Quincy, MA. http://www.myriant.com/media/press-kit-files/Myriant-BioSFactSheet-0613.pdf (Accessed October 2016),
347. Van Krevelen, D., Properties of polymers: their correlation with chemical structure; their numerical estimation and prediction from additive group contributions. *Elsevier Sci. Pub. Co., Amsterdam Netherlands* **1990**.
348. Reid, R. C.; Prausnitz, J. M.; Poling, B. E., The properties of gases and liquids. **1987**.
349. Chen, C.-C., A segment-based local composition model for the Gibbs energy of polymer solutions. *Fluid Phase Equilibria* **1993,** 83, 301-312.
350. Seavey, K. C.; Khare, N. P.; Liu, Y.; Williams, T. N.; Chen, C.-C., A new phase-equilibrium model for simulating industrial nylon-6 production trains. *Industrial & engineering chemistry research* **2003,** 42, (17), 3900-3913.

351. Sendín, J.-O. H.; Otero-Muras, I.; Alonso, A. A.; Banga, J. R., Improved Optimization Methods for the Multiobjective Design of Bioprocesses. *Industrial & Engineering Chemistry Research* **2006,** 45, (25), 8594-8603.
352. Silva-Beard, A.; Flores-Tlacuahuac, A., Effect of process design/operation on the steady-state operability of a methyl methacrylate polymerization reactor. *Industrial & engineering chemistry research* **1999,** 38, (12), 4790-4804.
353. Ruiz-Mercado, G. J.; Smith, R. L.; Gonzalez, M. A., Sustainability indicators for chemical processes: I. Taxonomy. *Industrial & Engineering Chemistry Research* **2012,** 51, (5), 2309-2328.
354. Martinez-Hernandez, E.; Campbell, G.; Sadhukhan, J., Economic value and environmental impact (EVEI) analysis of biorefinery systems. *Chemical Engineering Research and Design* **2013,** 91, (8), 1418-1426.
355. Schwarz, J.; Beloff, B.; Beaver, E., Use sustainability metrics to guide decision-making. *Chemical Engineering Progress* **2002,** 98, (7), 58-63.
356. Andraos, J., Unification of reaction metrics for green chemistry: applications to reaction analysis. *Organic process research & development* **2005,** 9, (2), 149-163.
357. Veleva, V.; Ellenbecker, M., Indicators of sustainable production: framework and methodology. *Journal of cleaner production* **2001,** 9, (6), 519-549.
358. Constable, D. J.; Curzons, A. D.; Cunningham, V. L., Metrics to 'green'chemistry—which are the best? *Green Chemistry* **2002,** 4, (6), 521-527.
359. Santaella, M. A.; Orjuela, A.; Narváez, P. C., Comparison of different reactive distillation schemes for ethyl acetate production using sustainability indicators. *Chemical Engineering and Processing: Process Intensification* **2015,** 96, 1-13.
360. Hottle, T. A.; Bilec, M. M.; Landis, A. E., Sustainability assessments of bio-based polymers. *Polymer Degradation and Stability* **2013,** 98, (9), 1898-1907.
361. Sheldon, R. A., Utilisation of biomass for sustainable fuels and chemicals: Molecules, methods and metrics. *Catalysis Today* **2011,** 167, (1), 3-13.
362. Dusselier, M.; Mascal, M.; Sels, B. F., Top Chemical Opportunities from Carbohydrate Biomass: A Chemist's View of the Biorefinery. In *Selective Catalysis for Renewable Feedstocks and Chemicals*, Nicholas, K. M., Ed. Springer International Publishing: Cham, 2014; pp 1-40.
363. Smith, R. L.; Ruiz-Mercado, G. J.; Meyer, D. E.; Gonzalez, M. A.; Abraham, J. P.; Barrett, W. M.; Randall, P. M., Coupling Computer-Aided Process Simulation and Estimations of Emissions and Land Use for Rapid Life Cycle Inventory Modeling. *ACS Sustainable Chemistry & Engineering* **2017,** 5, (5), 3786-3794.
364. Llevot, A.; Dannecker, P.-K.; von Czapiewski, M.; Over, L. C.; Söyler, Z.; Meier, M. A. R., Renewability is not Enough: Recent Advances in the Sustainable Synthesis of Biomass-Derived Monomers and Polymers. *Chemistry – A European Journal* **2016,** 22, (33), 11510-11521.
365. Aneesh, V.; Antony, R.; Paramasivan, G.; Selvaraju, N., Distillation technology and need of simultaneous design and control: A review. *Chemical Engineering and Processing: Process Intensification* **2016,** 104, 219-242.
366. Reay, D.; Ramshaw, C.; Harvey, A., *Process Intensification: Engineering for efficiency, sustainability and flexibility*. Butterworth-Heinemann: 2013.
367. Grosser, J. H.; Doherty, M. F.; Malone, M. F., Modeling of reactive distillation systems. *Industrial & engineering chemistry research* **1987,** 26, (5), 983-989.
368. Luyben, W. L.; Yu, C.-C., *Reactive distillation design and control*. John Wiley & Sons: 2009.
369. Tuchlenski, A.; Beckmann, A.; Reusch, D.; Düssel, R.; Weidlich, U.; Janowsky, R., Reactive distillation—industrial applications, process design & scale-up. *Chemical Engineering Science* **2001,** 56, (2), 387-394.
370. Chen, F.; Huss, R. S.; Malone, M. F.; Doherty, M. F., Simulation of kinetic effects in reactive distillation. *Computers & Chemical Engineering* **2000,** 24, (11), 2457-2472.
371. Harmsen, G. J., Reactive distillation: the front-runner of industrial process intensification: a full review of commercial applications, research, scale-up, design and operation. *Chemical Engineering and Processing: Process Intensification* **2007,** 46, (9), 774-780.
372. Taylor, R.; Krishna, R., Modelling reactive distillation. *Chemical Engineering Science* **2000,** 55, (22), 5183-5229.

373. Noeres, C.; Kenig, E.; Gorak, A., Modelling of reactive separation processes: reactive absorption and reactive distillation. *Chemical Engineering and Processing: Process Intensification* **2003,** 42, (3), 157-178.
374. Hiwale, R. S.; Bhate, N. V.; Mahajan, Y. S.; Mahajani, S. M., Industrial applications of reactive distillation: recent trends. *International Journal of Chemical Reactor Engineering* **2004,** 2, (1), R1.
375. Nicol, W., Comparing catalytic distillation to separate reaction and distillation for the production of diacetone alcohol. *Chemical Engineering Research and Design* **2003,** 81, (8), 1026-1032.
376. Stitt, E., Reactive distillation for toluene disproportionation: a technical and economic evaluation. *Chemical Engineering Science* **2002,** 57, (9), 1537-1543.
377. Malone, M. F.; Huss, R. S.; Doherty, M. F., Green Chemical Engineering Aspects of Reactive Distillation. *Environmental Science & Technology* **2003,** 37, (23), 5325-5329.
378. Perez-Cisneros, E.; Schenk, M.; Gani, R.; Pilavachi, P., Aspects of simulation, design and analysis of reactive distillation operations. *Computers & chemical engineering* **1996,** 20, S267-S272.
379. Ung, S.; Doherty, M. F., Vapor-liquid phase equilibrium in systems with multiple chemical reactions. *Chemical Engineering Science* **1995,** 50, (1), 23-48.
380. Huang, K.; Lin, Q.; Shao, H.; Wang, C.; Wang, S., A fundamental principle and systematic procedures for process intensification in reactive distillation columns. *Chemical Engineering and Processing: Process Intensification* **2010,** 49, (3), 294-311.
381. Segovia-Hernández, J. G.; Hernández, S.; Petriciolet, A. B., Reactive distillation: A review of optimal design using deterministic and stochastic techniques. *Chemical Engineering and Processing: Process Intensification* **2015,** 97, 134-143.
382. Higler, A.; Taylor, R.; Krishna, R., Modeling of a reactive separation process using a nonequilibrium stage model. *Computers & chemical engineering* **1998,** 22, S111-S118.
383. Shah, M.; Zondervan, E.; Oudshoorn, M.; de Haan, A., A novel process for the synthesis of unsaturated polyester. *Chemical Engineering and Processing: Process Intensification* **2011,** 50, (8), 747-756.
384. Shah, M.; Kiss, A. A.; Zondervan, E.; de Haan, A. B., Pilot-scale experimental validation of unsaturated polyesters synthesis by reactive distillation. *Chemical engineering journal* **2012,** 213, 175-185.
385. Chen, L.; Xi, Z.; Qin, Z.; Zhao, L.; Yuan, W. In *New Reactor for Polyester Polyols Continuous Synthetic Process*, Macromolecular Symposia, 2013; Wiley Online Library: 2013; pp 151-161.
386. Sawistowski, H.; Pilavakis, P., Performance of esterification in a reaction-distillation column. *Chemical engineering science* **1988,** 43, (2), 355-360.
387. Tang, Y. T.; Chen, Y. W.; Huang, H. P.; Yu, C. C.; Hung, S. B.; Lee, M. J., Design of reactive distillations for acetic acid esterification. *AIChE Journal* **2005,** 51, (6), 1683-1699.
388. Singh, D.; Gupta, R. K.; Kumar, V., Simulation of a plant scale reactive distillation column for esterification of acetic acid. *Computers & Chemical Engineering* **2015,** 73, 70-81.
389. Steinigeweg, S.; Gmehling, J., n-Butyl acetate synthesis via reactive distillation: thermodynamic aspects, reaction kinetics, pilot-plant experiments, and simulation studies. *Industrial & engineering chemistry research* **2002,** 41, (22), 5483-5490.
390. Gangadwala, J.; Kienle, A.; Stein, E.; Mahajani, S., Production of butyl acetate by catalytic distillation: process design studies. *Industrial & engineering chemistry research* **2004,** 43, (1), 136-143.
391. Hanika, J.; Kolena, J.; Smejkal, Q., Butylacetate via reactive distillation—modelling and experiment. *Chemical engineering science* **1999,** 54, (21), 5205-5209.
392. Chung, Y.-H.; Peng, T.-H.; Lee, H.-Y.; Chen, C.-L.; Chien, I.-L., Design and Control of Reactive Distillation System for Esterification of Levulinic Acid and n-Butanol. *Industrial & Engineering Chemistry Research* **2015,** 54, (13), 3341-3354.
393. Huang, F.; Xu, S.; Li, T.; Zhu, D., Innovative Ethylene Glycol Diacetate synthesis process in a single reactive distillation column. *Chemical Engineering and Processing: Process Intensification* **2016,** 109, 80-89.

394. Banchero, M.; Kusumaningtyas, R. D.; Gozzelino, G., Reactive distillation in the intensification of oleic acid esterification with methanol–A simulation case-study. *Journal of Industrial and Engineering Chemistry* **2014,** 20, (6), 4242-4249.
395. Orjuela, A.; Kolah, A.; Lira, C. T.; Miller, D. J., Mixed Succinic Acid/Acetic Acid Esterification with Ethanol by Reactive Distillation. *Industrial & Engineering Chemistry Research* **2011,** 50, (15), 9209-9220.
396. Orjuela, A.; Kolah, A.; Hong, X.; Lira, C. T.; Miller, D. J., Diethyl succinate synthesis by reactive distillation. *Separation and purification technology* **2012,** 88, 151-162.
397. Kiss, A. A., *Advanced distillation technologies: design, control and applications*. John Wiley & Sons: 2013.
398. Dejanović, I.; Matijašević, L.; Olujić, Ž., Dividing wall column—a breakthrough towards sustainable distilling. *Chemical Engineering and Processing: Process Intensification* **2010,** 49, (6), 559-580.
399. Asprion, N.; Kaibel, G., Dividing wall columns: fundamentals and recent advances. *Chemical Engineering and Processing: Process Intensification* **2010,** 49, (2), 139-146.
400. Harmsen, J., Process intensification in the petrochemicals industry: drivers and hurdles for commercial implementation. *Chemical Engineering and Processing: Process Intensification* **2010,** 49, (1), 70-73.
401. Yildirim, Ö.; Kiss, A. A.; Kenig, E. Y., Dividing wall columns in chemical process industry: a review on current activities. *Separation and Purification Technology* **2011,** 80, (3), 403-417.
402. Wright, R. O. Fractionation apparatus. 1949.
403. Kiss, A. A.; Bildea, C. S., A control perspective on process intensification in dividing-wall columns. *Chemical Engineering and Processing: Process Intensification* **2011,** 50, (3), 281-292.
404. Mutalib, M. A.; Zeglam, A.; Smith, R., Operation and control of dividing wall distillation columns: Part 2: Simulation and pilot plant studies using temperature control. *Chemical Engineering Research and Design* **1998,** 76, (3), 319-334.
405. Zong, X.; Huang, K.; Yuan, Y.; Chen, H.; Yu, J., Design and operation of dividing-wall distillation columns. 2. Process dynamics and operation. *Chemical Engineering and Processing: Process Intensification* **2015,** 91, 89-103.
406. van Diggelen, R. C.; Kiss, A. A.; Heemink, A. W., Comparison of control strategies for dividing-wall columns. *Industrial & Engineering Chemistry Research* **2009,** 49, (1), 288-307.
407. Nguyen, T. D.; Rouzineau, D.; Meyer, M.; Meyer, X., Design and simulation of divided wall column: Experimental validation and sensitivity analysis. *Chemical Engineering and Processing: Process Intensification* **2016,** 104, 94-111.
408. Mueller, I.; Kenig, E. Y., Reactive distillation in a dividing wall column: rate-based modeling and simulation. *Industrial & engineering chemistry research* **2007,** 46, (11), 3709-3719.
409. Kiss, A. A.; Pragt, J.; van Strien, C., Reactive dividing-wall columns: towards enhanced process integration. *Distillation & Absorption, IChemE, Eindhoven, The Netherlands* **2010**, 253-258.
410. Kiss, A. A.; Pragt, J.; Van Strien, C., Reactive dividing-wall columns—how to get more with less resources? *Chemical Engineering Communications* **2009,** 196, (11), 1366-1374.
411. Barroso-Muñoz, F. O.; Hernandez, S.; Segovia-Hernández, J. G.; Hernández-Escoto, H.; Rico-Ramírez, V.; Chávez, R. H., Implementation and Operation of a Dividing-Wall Distillation Column. *Chemical Engineering & Technology* **2011,** 34, (5), 746-750.
412. Hernández, S.; Sandoval-Vergara, R.; Barroso-Muñoz, F. O.; Murrieta-Dueñas, R.; Hernández-Escoto, H.; Segovia-Hernández, J. G.; Rico-Ramirez, V., Reactive dividing wall distillation columns: simulation and implementation in a pilot plant. *Chemical Engineering and Processing: Process Intensification* **2009,** 48, (1), 250-258.
413. An, D.; Cai, W.; Xia, M.; Zhang, X.; Wang, F., Design and control of reactive dividing-wall column for the production of methyl acetate. *Chemical Engineering and Processing: Process Intensification* **2015,** 92, 45-60.
414. Dai, X.; Ye, Q.; Yu, H.; Suo, X.; Li, R., Design and Control of Dividing-Wall Column for the Synthesis of n-Propyl Propionate by Reactive Distillation. *Industrial & Engineering Chemistry Research* **2015,** 54, (15), 3919-3932.

415. Ray, W. H.; Soares, J. B.; Hutchinson, R. A. In *Polymerization reaction engineering: past, present and future*, Macromolecular Symposia, 2004; Wiley Online Library: 2004; pp 1-14.
416. Yount, T. L.; DeBruin, B. R.; Ekart, M. P.; Windes, L. C.; Sliger, D. A., Multi-level tubular reactor with oppositely extending segments. In Google Patents: 2010.
417. Yount, T. L.; DeBruin, B. R.; Ekart, M. P.; Windes, L. C.; Sliger, D. A., Multi-level tubular reactor with dual headers. In Google Patents: 2010.
418. Debruin, B. R., Polyester process using a pipe reactor. In Google Patents: 2005.
419. Pipus, G.; Plazl, I.; Koloini, T., Esterification of benzoic acid in microwave tubular flow reactor. *Chemical Engineering Journal* **2000,** 76, (3), 239-245.
420. Bokis, C. P.; Orbey, H.; Chen, C.-C., Properly model polymer processes. *Chemical engineering progress* **1999,** 95, (4), 39-52.
421. Huss, R.; Chen, F.; Malone, M.; Doherty, M., Computer-aided tools for the design of reactive distillation systems. *Computers & Chemical Engineering* **1999,** 23, S955-S962.
422. Seferlis, P.; Hrymak, A., Sensitivity analysis for chemical process optimization. *Computers & chemical engineering* **1996,** 20, (10), 1177-1200.
423. Volin, Y. M.; Ostrovskiy, G., Sensitivity calculation methods for complex chemical systems—1: algorithmization. *Computers & Chemical Engineering* **1981,** 5, (1), 21-30.
424. Li, Z.; Ierapetritou, M., Process scheduling under uncertainty: Review and challenges. *Computers & Chemical Engineering* **2008,** 32, (4), 715-727.
425. Leis, J.; Gallagher, A.; Kramer, M., Parametric sensitivity analysis of complex process flowsheets using sequential modular simulation. *Computers & chemical engineering* **1987,** 11, (4), 409-421.
426. Khushalani, K.; Maheshwari, A.; Jain, N., Separation of Mixture by Divided Wall Column using ASPEN PLUS.
427. Gani, R.; Soerensen, E. L.; Perregaard, J., Design and analysis of chemical processes through DYNSIM. *Industrial & engineering chemistry research* **1992,** 31, (1), 244-254.
428. Dimian, A. C.; Bildea, C. S.; Kiss, A. A., *Integrated design and simulation of chemical processes*. Elsevier: 2014; Vol. 13.
429. Naves, A. F.; Fernandes, H. T. C.; Immich, A. P. S.; Catalani, L. H., Enzymatic syntheses of unsaturated polyesters based on isosorbide and isomannide. *Journal of Polymer Science Part A: Polymer Chemistry* **2013,** 51, (18), 3881-3891.
430. Feng, X.; East, A. J.; Hammond, W. B.; Zhang, Y.; Jaffe, M., Overview of advances in sugar-based polymers. *Polymers for Advanced Technologies* **2011,** 22, (1), 139-150.
431. Sanders, J. P. M.; Clark, J. H.; Harmsen, G. J.; Heeres, H. J.; Heijnen, J. J.; Kersten, S. R. A.; van Swaaij, W. P. M.; Moulijn, J. A., Process intensification in the future production of base chemicals from biomass. *Chemical Engineering and Processing: Process Intensification* **2012,** 51, 117-136.
432. Flèche, G.; Huchette, M., Isosorbide. Preparation, Properties and Chemistry. *Starch - Stärke* **1986,** 38, (1), 26-30.
433. Fertier, L.; Ibert, M.; Buffe, C.; Saint-Loup, R.; Joly-Duhamel, C.; Robin, J. J.; Giani, O., New biosourced UV curable coatings based on isosorbide. *Progress in Organic Coatings* **2016,** 99, 393-399.
434. Wang, G.; Jiang, M.; Zhang, Q.; Wang, R.; Zhou, G., Biobased copolyesters: synthesis, crystallization behavior, thermal and mechanical properties of poly(ethylene glycol sebacate-co-ethylene glycol 2,5-furan dicarboxylate). *RSC Advances* **2017,** 7, (23), 13798-13807.
435. Zhou, C.; Wei, Z.; Yu, Y.; Wang, Y.; Li, Y., Biobased copolyesters from renewable resources: synthesis and crystallization kinetics of poly(propylene sebacate-co-isosorbide sebacate). *RSC Advances* **2015,** 5, (84), 68688-68699.
436. Thiem, J.; Lüders, H., Synthesis of polyterephthalates derived from dianhydrohexitols. *Polymer Bulletin* **1984,** 11, (4), 365-369.
437. Okada, M.; Tachikawa, K.; Aoi, K., Biodegradable polymers based on renewable resources. III. copolyesters composed of 1, 4: 3, 6-dianhydro-D-glucitol, 1, 1-bis (5-carboxy-2-furyl) ethane and aliphatic dicarboxylic acid units. *Journal of applied polymer science* **1999,** 74, (14), 3342-3350.

438. Sousa, A. F.; Coelho, J. F. J.; Silvestre, A. J. D., Renewable-based poly((ether)ester)s from 2,5-furandicarboxylic acid. *Polymer* **2016,** 98, 129-135.
439. Li, P.; Ma, S.; Dai, J.; Liu, X.; Jiang, Y.; Wang, S.; Wei, J.; Chen, J.; Zhu, J., Itaconic Acid as a Green Alternative to Acrylic Acid for Producing a Soybean Oil-Based Thermoset: Synthesis and Properties. *ACS Sustainable Chemistry & Engineering* **2017,** 5, (1), 1228-1236.
440. Dai, J.; Ma, S.; Teng, N.; Dai, X.; Shen, X.; Wang, S.; Liu, X.; Zhu, J., 2,5-Furandicarboxylic Acid- and Itaconic Acid-Derived Fully Biobased Unsaturated Polyesters and Their Cross-Linked Networks. *Industrial & Engineering Chemistry Research* **2017,** 56, (10), 2650-2657.
441. Dai, J.; Ma, S.; Liu, X.; Han, L.; Wu, Y.; Dai, X.; Zhu, J., Synthesis of bio-based unsaturated polyester resins and their application in waterborne UV-curable coatings. *Progress in Organic Coatings* **2015,** 78, 49-54.
442. Dai, J.; Ma, S.; Wu, Y.; Zhu, J.; Liu, X., High bio-based content waterborne UV-curable coatings with excellent adhesion and flexibility. *Progress in Organic Coatings* **2015,** 87, 197-203.
443. Wood Plastic Composites. https://international.fnr.de/renewable-resources/biomaterial/woodplasticcomposites/ (Accessed 24 March 2017),
444. Tang, T.; Takasu, A., Facile synthesis of unsaturated polyester-based double-network gels via chemoselective cross-linking using Michael addition and subsequent UV-initiated radical polymerization. *RSC Advances* **2015,** 5, (2), 819-829.
445. Li, H.; Thanneeru, S.; Jin, L.; Guild, C. J.; He, J., Multiblock thermoplastic elastomers via one-pot thiol-ene reaction. *Polymer Chemistry* **2016,** 7, (29), 4824-4832.
446. Sadler, J. M.; Toulan, F. R.; Palmese, G. R.; La Scala, J. J., Unsaturated polyester resins for thermoset applications using renewable isosorbide as a component for property improvement. *Journal of Applied Polymer Science* **2015,** 132, (30), n/a-n/a.
447. Łukaszczyk, J.; Janicki, B.; Kaczmarek, M., Synthesis and properties of isosorbide based epoxy resin. *European Polymer Journal* **2011,** 47, (8), 1601-1606.
448. Zhu, Y.; Molinier, V.; Durand, M.; Lavergne, A.; Aubry, J.-M., Amphiphilic Properties of Hydrotropes Derived from Isosorbide: Endo/Exo Isomeric Effects and Temperature Dependence. *Langmuir* **2009,** 25, (23), 13419-13425.
449. Papageorgiou, G. Z.; Achilias, D. S.; Bikiaris, D. N., Crystallization Kinetics and Melting Behaviour of the Novel Biodegradable Polyesters Poly(propylene azelate) and Poly(propylene sebacate). *Macromolecular Chemistry and Physics* **2009,** 210, (1), 90-107.
450. Wang, X.; Zhou, J.; Li, L., Multiple melting behavior of poly(butylene succinate). *European Polymer Journal* **2007,** 43, (8), 3163-3170.
451. Papageorgiou, G. Z.; Bikiaris, D. N., Crystallization and melting behavior of three biodegradable poly(alkylene succinates). A comparative study. *Polymer* **2005,** 46, (26), 12081-12092.
452. Gunaratne, L. M. W. K.; Shanks, R. A., Multiple melting behaviour of poly(3-hydroxybutyrate-co-hydroxyvalerate) using step-scan DSC. *European Polymer Journal* **2005,** 41, (12), 2980-2988.
453. Song, P.; Chen, G.; Wei, Z.; Zhang, W.; Liang, J., Calorimetric analysis of the multiple melting behavior of melt-crystallized poly(l-lactic acid) with a low optical purity. *Journal of Thermal Analysis and Calorimetry* **2013,** 111, (2), 1507-1514.
454. Chatti, S.; Weidner, S. M.; Fildier, A.; Kricheldorf, H. R., Copolyesters of isosorbide, succinic acid, and isophthalic acid: Biodegradable, high Tg engineering plastics. *Journal of Polymer Science Part A: Polymer Chemistry* **2013,** 51, (11), 2464-2471.
455. Beyler, C. L.; Hirschler, M. M., Thermal decomposition of polymers. *SFPE handbook of fire protection engineering* **2002,** 2, 32.
456. Montaudo, G.; Puglisi, C.; Samperi, F., Primary thermal degradation mechanisms of PET and PBT. *Polymer Degradation and Stability* **1993,** 42, (1), 13-28.
457. Goldfarb, I. J.; McGuchan, R. *THERMAL DEGRADATION OF POLYESTERS. 1. ALIPHATIC POLYMERS*; DTIC Document: 1968.

APPENDIX

Appendix A (Chapter 2)

A.1 Monomer charge for polyesters 3b-3d

Table 68. Monomer charge for polysters **3b-3d**

	Mol%	Mol			Mass, g		
Polyester	**FDCA**	**FDCA**	**SA**	**PDO**	**FDCA**	**SA**	**PDO**
3b	30	0.24	0.56	1.2	37.46	66.13	91.31
3c	70	1.19	0.51	2.55	185.75	60.23	194.03
3d	85	1.275	0.225	2.25	199.01	26.57	171.20

A.2 Monomer charge for polyesters 6b-6d

Table 69. Monomer charge for polysters **6b-6d**

	Mol%	Mol			Mass, g		
Polyester	**FDCA**	**FDCA**	**SA**	**PTO**	**FDCA**	**SA**	**PTO**
6b	30	0.22	0.52	0.97	35.02	61.82	101.24
6c	70	0.77	0.33	1.43	120.19	38.97	148.92
6d	85	1.06	0.19	1.62	165.27	22.06	168.64

A.3 Monomer charge for polyesters 7-10

Table 70. Monomer charge for polysters **7-10**

	Mol%		Mol			Mass, g			
Polyester	**IS**	**IS**	**SA**	**FDCA**	**PDO**	**IS**	**SA**	**FDCA**	**PDO**

7b	30	0.32	0.60	0.11	0.74	46.03	70.26	16.39	55.93
7c	60	0.6	0.57	0.1	0.4	87.68	66.92	15.61	30.44
7d	70	0.69	0.56	0.1	0.3	102	66.92	15.61	22.83
8a	30	0.28	0.44	0.19	0.69	41.65	52.35	29.66	52.55
8b	60	0.6	0.37	0.16	0.40	87.68	44.09	24.97	30.44
8c	70	0.7	0.47	0.2	0.3	102.3	55.11	31.22	22.8
9a	10	0.19	0.38	0.89	1.71	27.76	44.87	138.4	130.11
9b	30	0.42	0.28	0.65	0.98	61.37	33.07	101.98	74.57
9c	50	0.87	0.35	0.82	0.88	127.87	41.33	127.47	66.58
10a	10	0.19	0.19	1.07	1.71	27.76	22.44	168.0	130.11
10b	30	0.55	0.19	1.05	1.3	81.1	21.85	163.63	98.54
10c	50	0.8	0.16	0.91	0.8	116.91	18.89	141.52	60.87

A.4 Monomer charge for polyesters 11-15

Table 71. Monomer charge for polysters **11-15**

	Mol%	**Mol**				**Mass, g**			
Polyester	**IS**	**IS**	**SA**	**FDCA**	**PTO**	**IS**	**SA**	**FDCA**	**PTO**
11b	30	0.25	0.65	-	0.6	37.26	77.21	-	61.96
11c	50	0.42	0.65	-	0.43	62.11	77.21	-	44.26
11d	60	0.541	0.74	-	0.34	74.53	87.28	-	35.41
12a	10	0.08	0.56	0.1	0.77	12.42	65.63	15.31	79.67
12b	30	0.25	0.56	0.1	0.6	37.27	65.63	15.31	61.96
12c	50	0.45	0.59	0.1	0.45	65.76	69.49	16.21	46.86

12d	60	0.15	0.16	0.03	0.10	21.92	19.3	4.5	10.41
12e	70	0.59	0.56	0.1	0.26	86.95	65.63	15.31	26.56
13a	10	0.08	0.46	0.2	0.77	12.42	54.05	30.62	79.67
13b	30	0.25	0.45	0.19	0.59	37.26	54.05	30.62	61.96
13c	50	0.42	0.46	0.2	0.43	62.1	54.05	30.62	44.26
13d	60	0.15	0.13	0.06	0.10	21.92	15.9	9.01	10.41
13e	70	0.59	0.46	0.2	0.26	86.95	54.05	30.62	26.56
14a	10	0.15	0.35	0.81	1.35	21.92	40.88	126.0	140.59
14b	30	0.51	0.39	0.91	1.19	74.53	46.33	142.88	123.93
14c	50	0.75	0.35	0.81	0.75	109.6	40.88	126.0	78.11
15a	10	0.15	0.17	0.98	1.35	21.92	20.44	153.09	140.6
15b	30	0.45	0.17	0.98	1.05	65.73	20.44	153.09	109.35
15c	50	0.75	0.17	0.98	0.75	109.6	20.44	153.09	78.11

A.5 Monomer charge for polyesters 16b and 16c

Table 72. Monomer charge for polysters **16b** and 1**6c**

	Mol%	**Mol**			**Mass, g**		
Polyester	**IA**	**IA**	**SA**	**PTO**	**IA**	**SA**	**PTO**
16b	10	0.17	0.68	0.85	22.12	80.3	88.52
16c	15	0.25	0.59	0.85	33.17	70.3	88.52

Appendix B (Chapter 3)

B.1 ^{1}H NMR of 1,3-propanediol

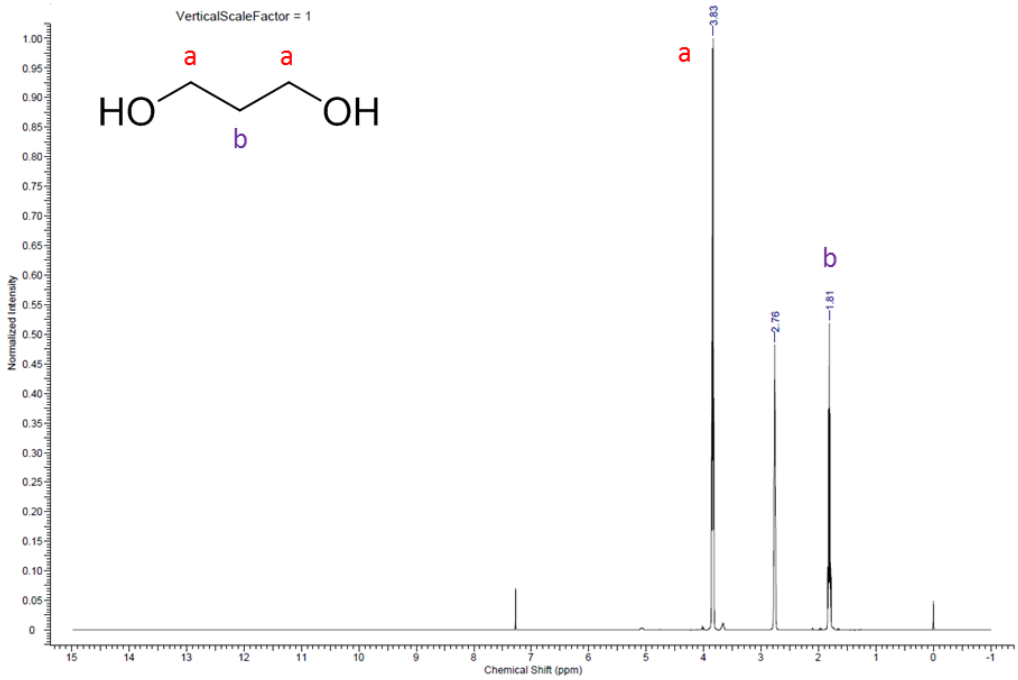

Figure 137. ^{1}H NMR of 1,3-propanediol.

B.2 ^{1}H NMR of succinic acid

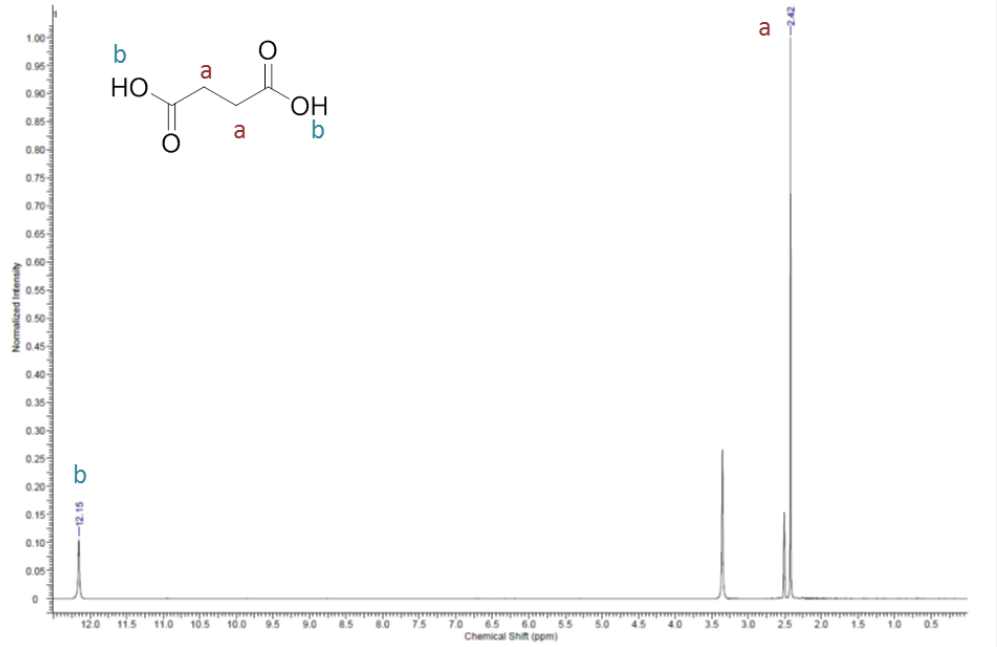

Figure 138. ^{1}H NMR of succinic acid.

B.3 ^{1}H NMR of 2,5-furan dicarboxylic acid

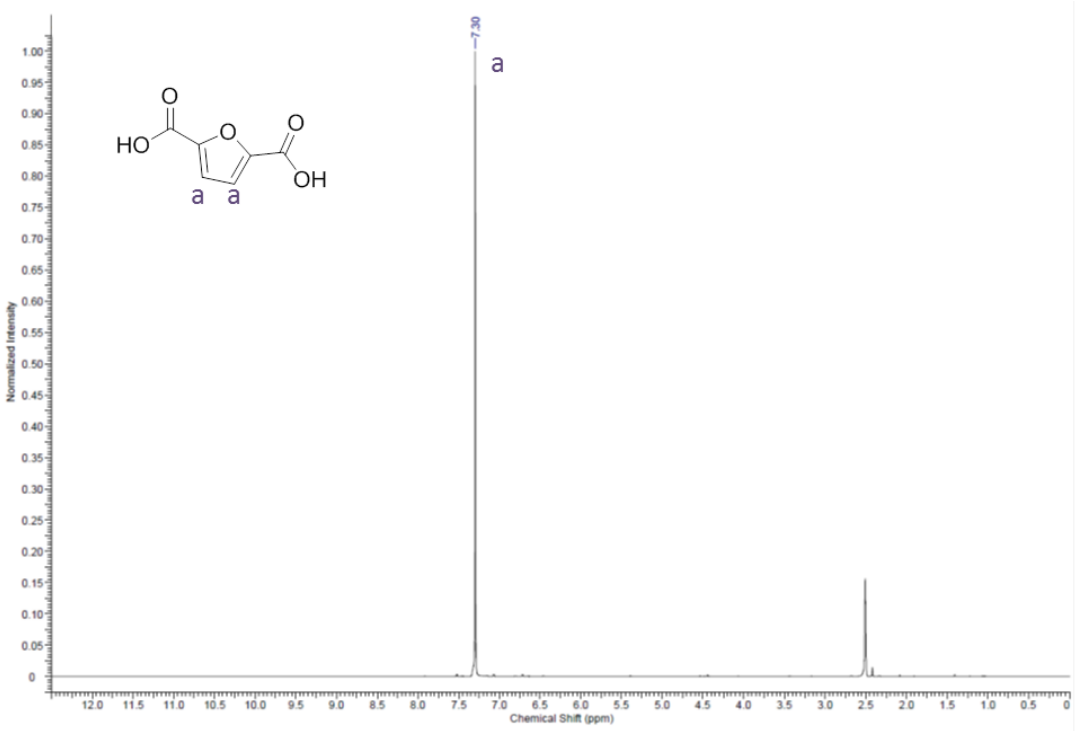

Figure 139. ^{1}H NMR of FDCA.

B.4 GPC chromatogram of polyesters at 210 °C

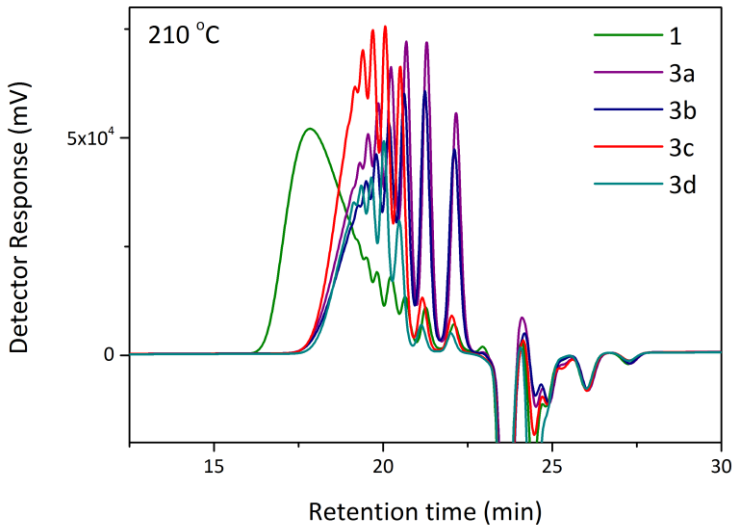

Figure 140. GPC chromatogram of polyesters at 210 °C.

B.5 GPC chromatogram of polyesters at 230 °C

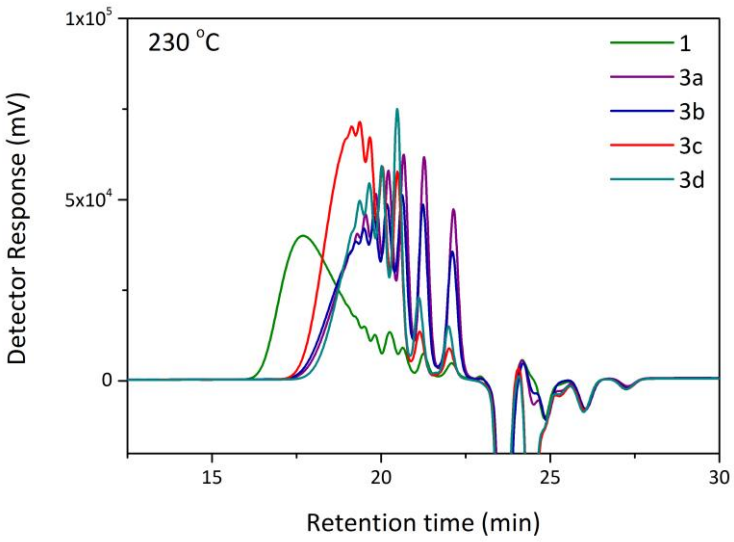

Figure 141. GPC chromatogram of polyesters at 230 °C.

B.6 DSC first heating scan of polyesters at 210 °C

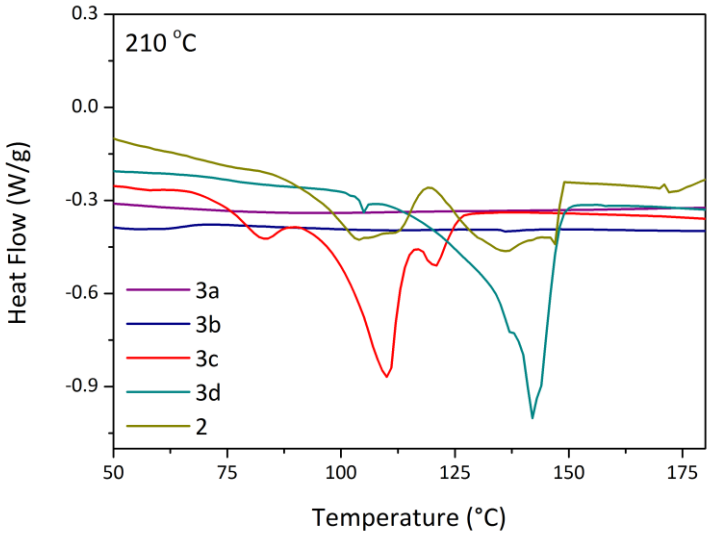

Figure 142. DSC first heating scan of polyesters at 210 °C.

B.7 DSC second heating scan of polyesters at 210 °C

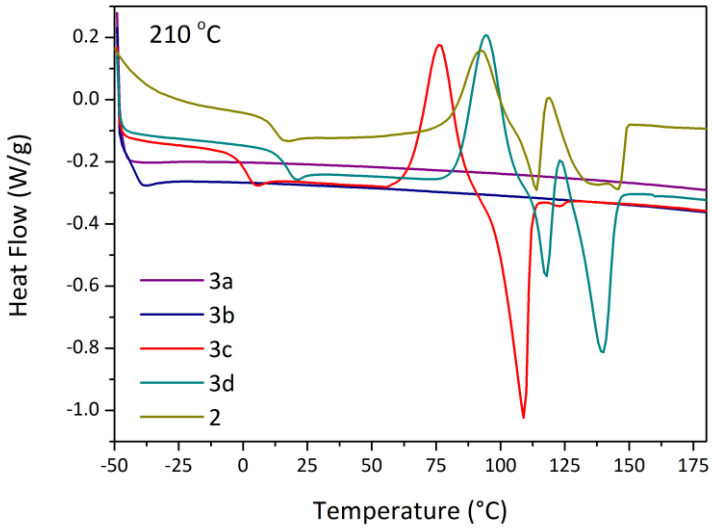

Figure 143. DSC second heating scan of polyesters at 210 °C.

B.8 DSC first heating scan of polyesters at 220 °C

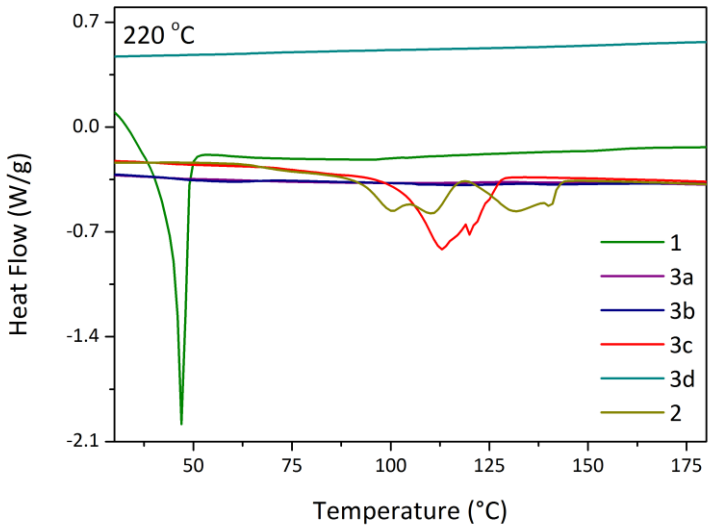

Figure 144. DSC first heating scan of polyesters at 220 °C.

B.9 DSC second heating scan of polyesters at 220 °C

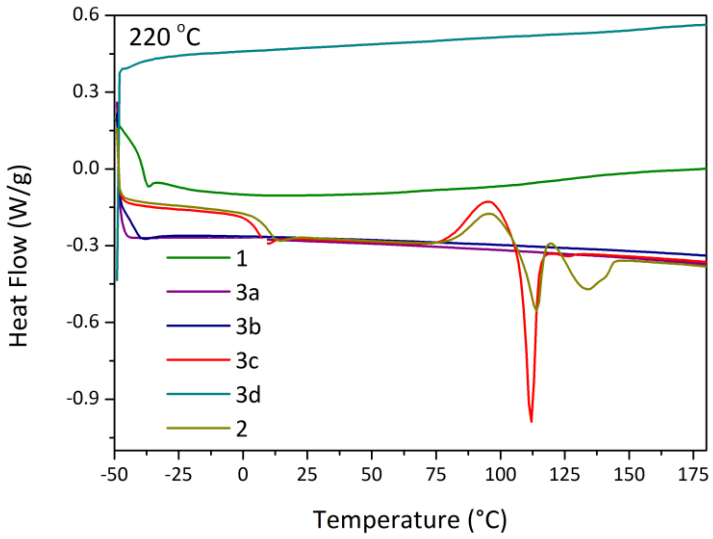

Figure 145. DSC second heating scan of polyesters at 220 °C.

B.10 TGA Weight% thermogram of polyesters at 210 °C

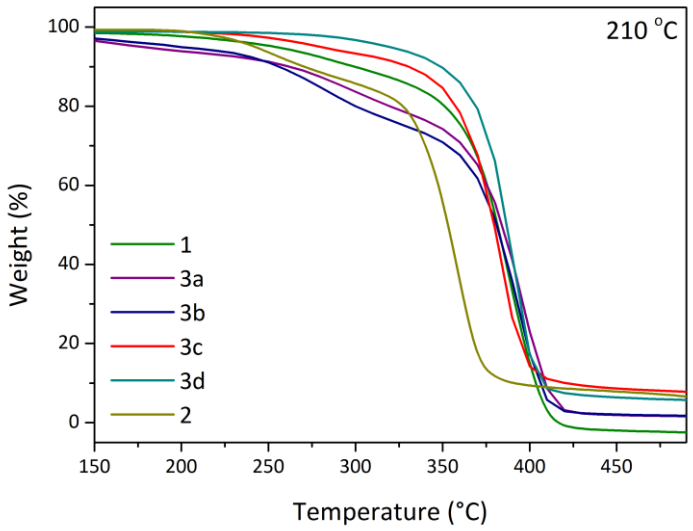

Figure 146. TGA Weight% thermogram of polyesters at 210 °C.

B.11 TGA Derivative Weight% thermogram of polyesters at 210 °C

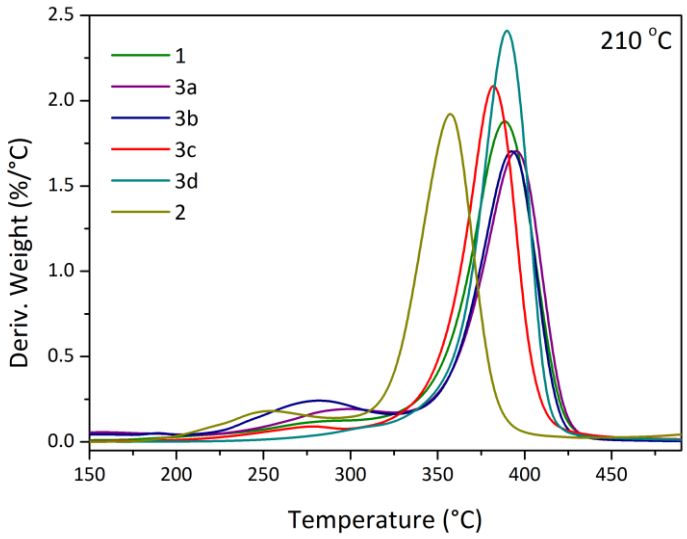

Figure 147. TGA Derivative Weight% thermogram of polyesters at 210 °C.

B.12 TGA Weight% thermogram of polyesters at 230 °C

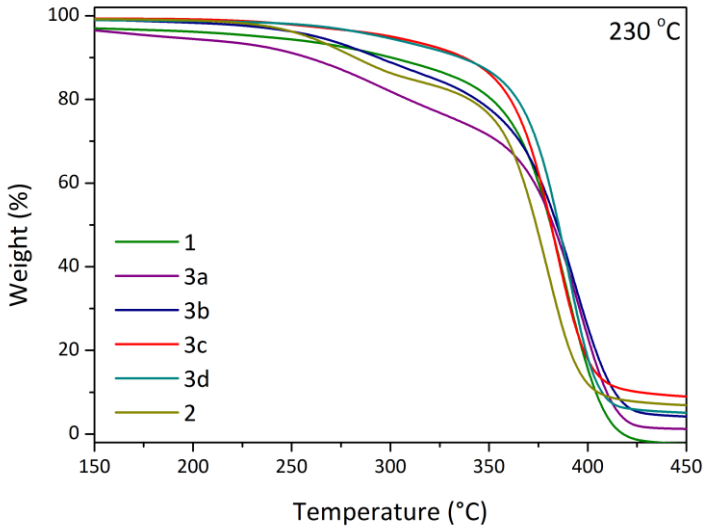

Figure 148. TGA Weight% thermogram of polyesters at 230 °C.

B.13 TGA Derivative Weight% thermogram of polyesters at 230 °C

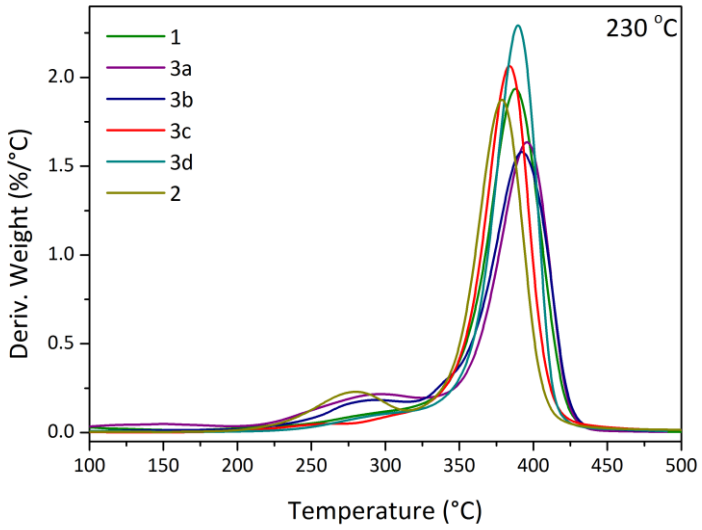

Figure 149. TGA Derivative Weight% thermogram of polyesters at 230 °C.

Appendix C (Chapter 4)

C.1 ^{1}H NMR 1,5-pentanediol

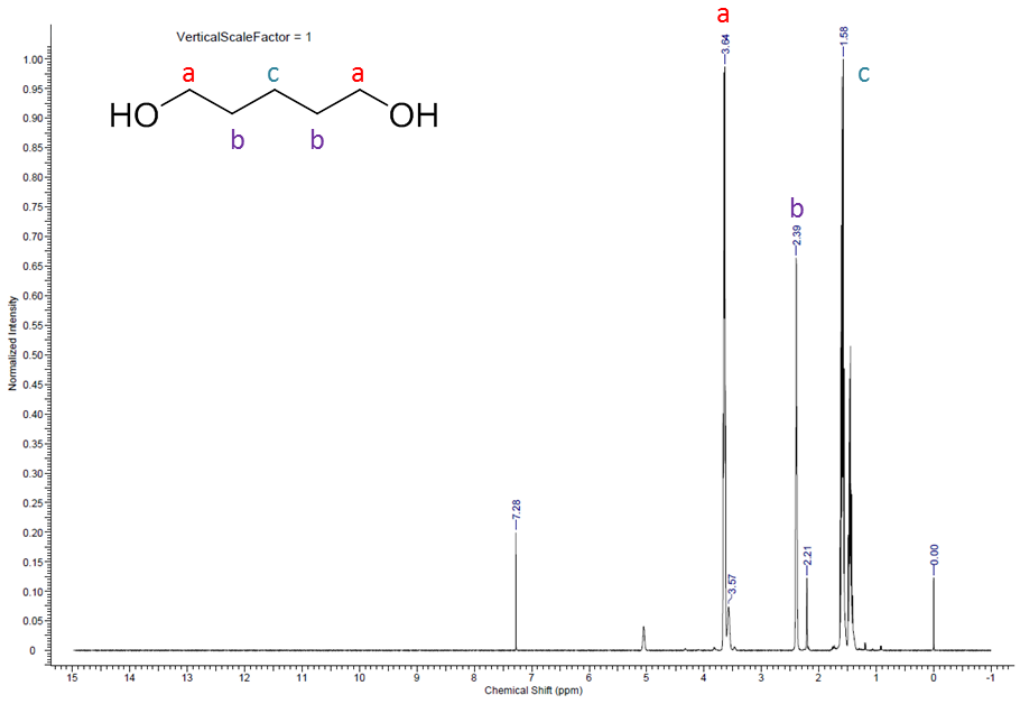

Figure 150. ^{1}H NMR 1,5-pentanediol.

C.2 ^{1}H NMR PPeFS 30/70 (6b)

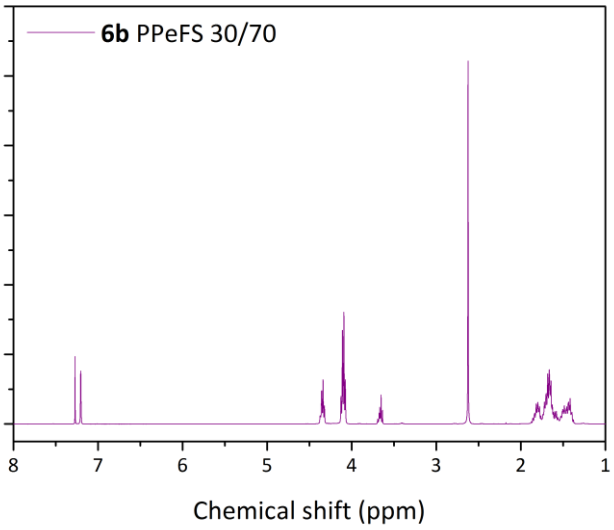

Figure 151. ^{1}H NMR PPeFS 30/70 (**6b**).

C.3 ^{1}H NMR PPeFS 70/30 (6c)

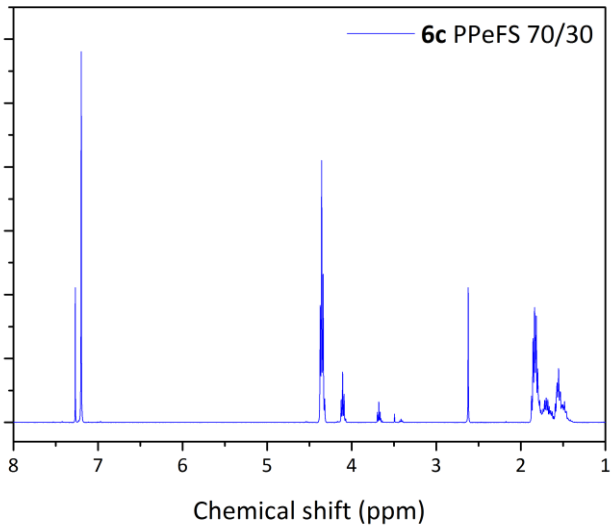

Figure 152. ^{1}H NMR PPeFS 70/30 (**6c**).

C.4 GPC chromatogram of PPeS (4)

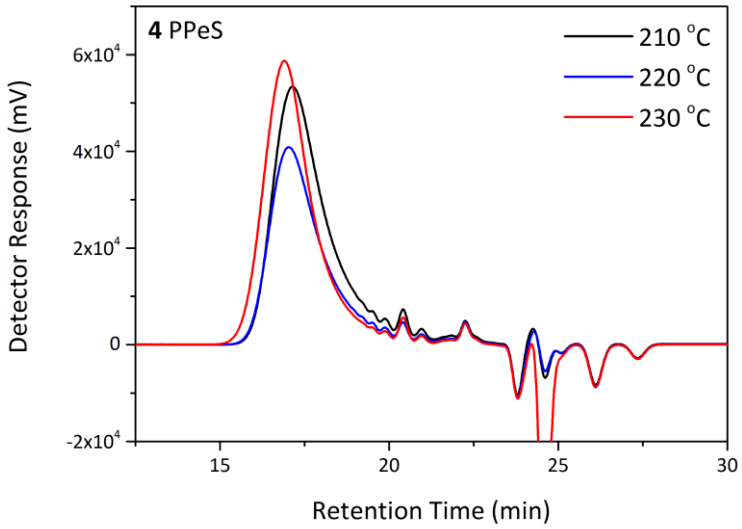

Figure 153. GPC chromatogram of PPeS (**4**).

C.5 GPC chromatogram of PPeF (5)

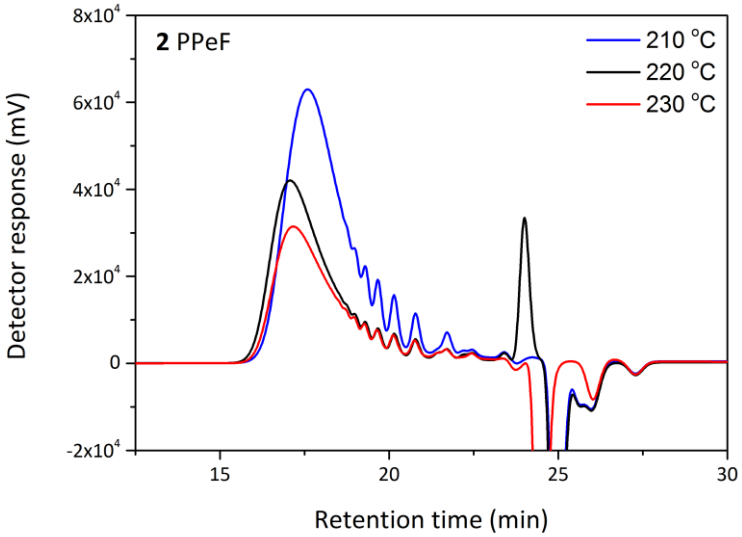

Figure 154. GPC chromatogram of PPeF (**5**).

C.6 GPC chromatogram of PPeFS (6) at 210°C

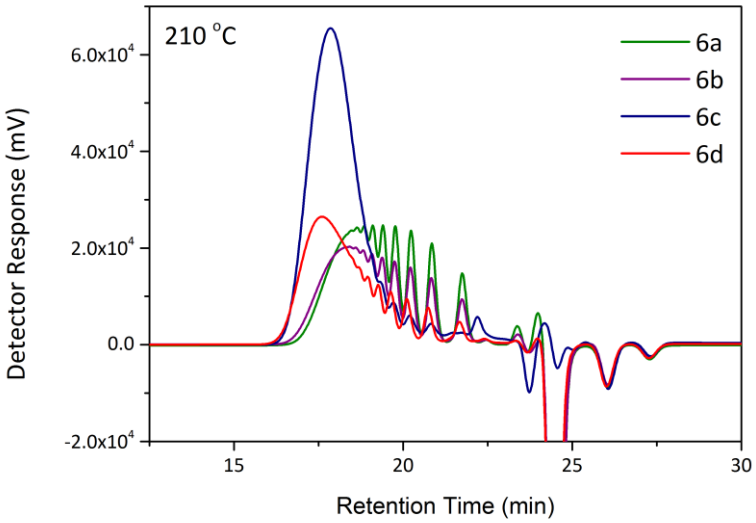

Figure 155. GPC chromatogram of PPeFS (**6**) at 210°C.

C.7 GPC chromatogram of PPeFS (6) at 220°C

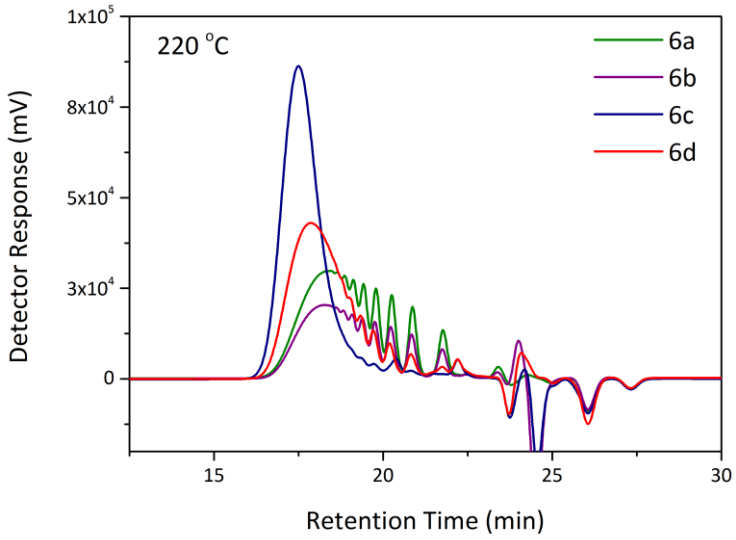

Figure 156. GPC chromatogram of PPeFS (**6**) at 220°C.

C.8 DSC first heating scan of polyesters at 210 °C

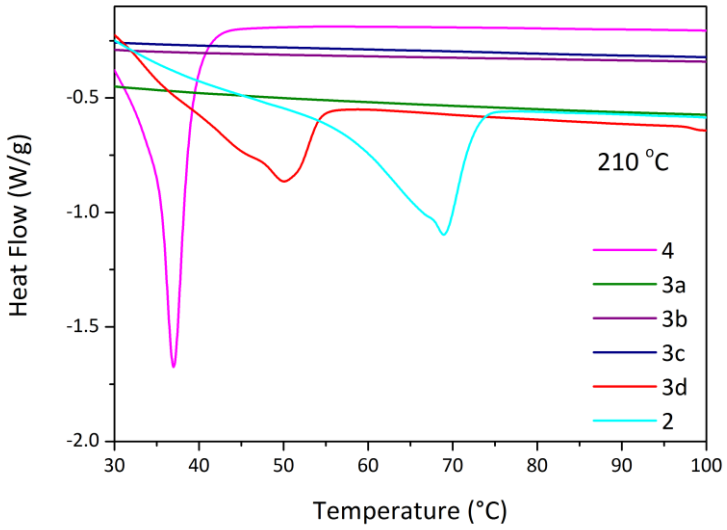

Figure 157. DSC first heating scan of polyesters at 210 °C.

C.9 DSC second heating scan of polyesters at 210 °C

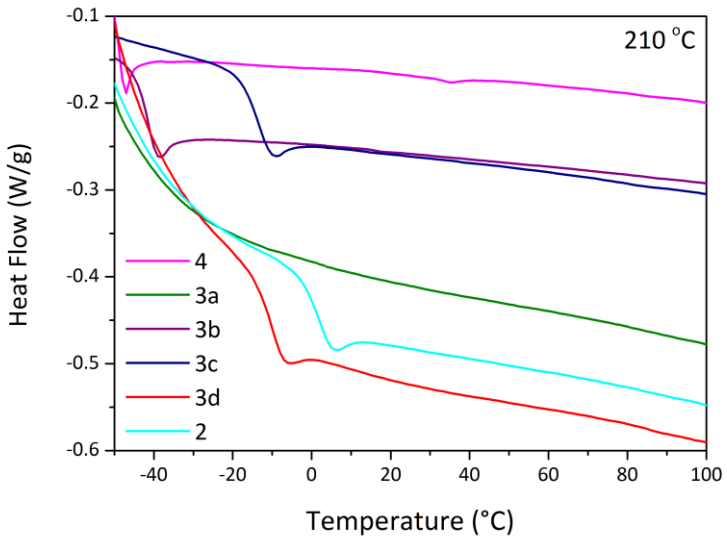

Figure 158. DSC second heating scan of polyesters at 210 °C.

C.10 DSC first heating scan of polyesters at 230 °C

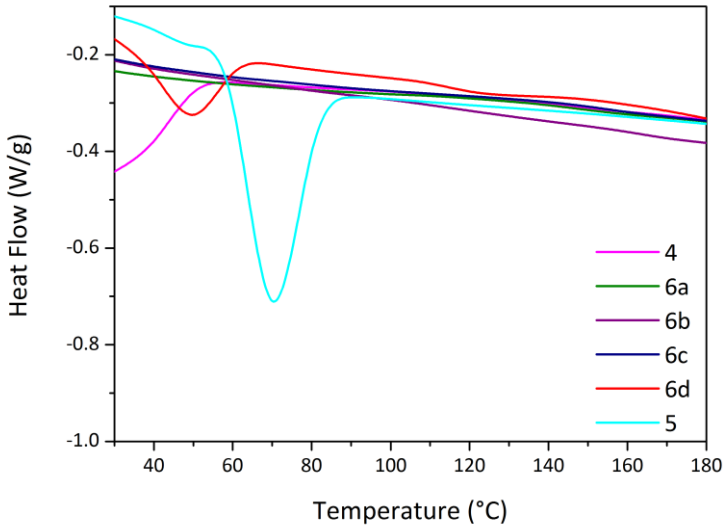

Figure 159. DSC first heating scan of polyesters at 230 °C.

C.11 DSC second heating scan of polyesters at 230 °C

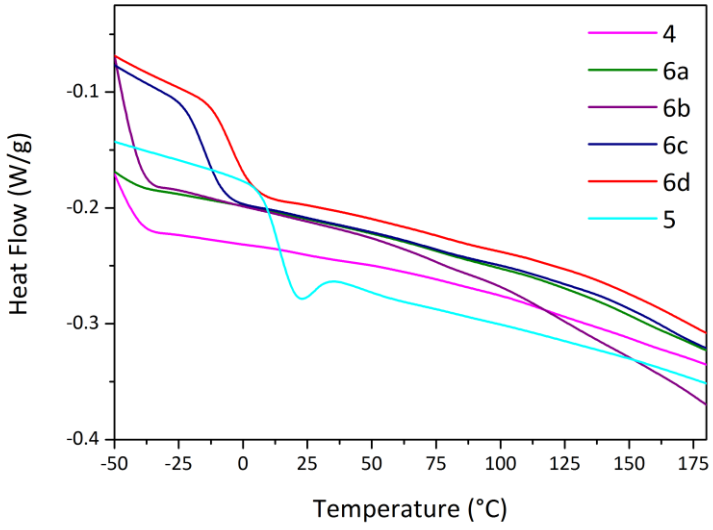

Figure 160. DSC second heating scan of polyesters at 230 °C.

C.12 TGA Weight% thermogram of polyesters at 210 °C

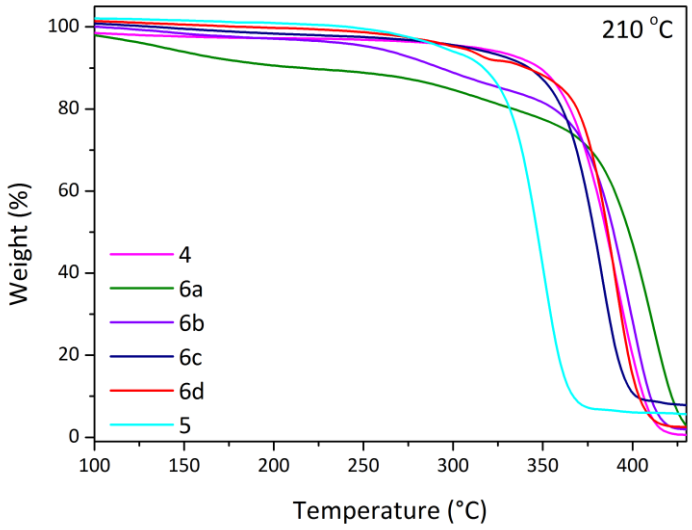

Figure 161. TGA Weight% thermogram of polyesters at 210 °C.

C.13 TGA Derivative Weight% thermogram of polyesters at 210 °C

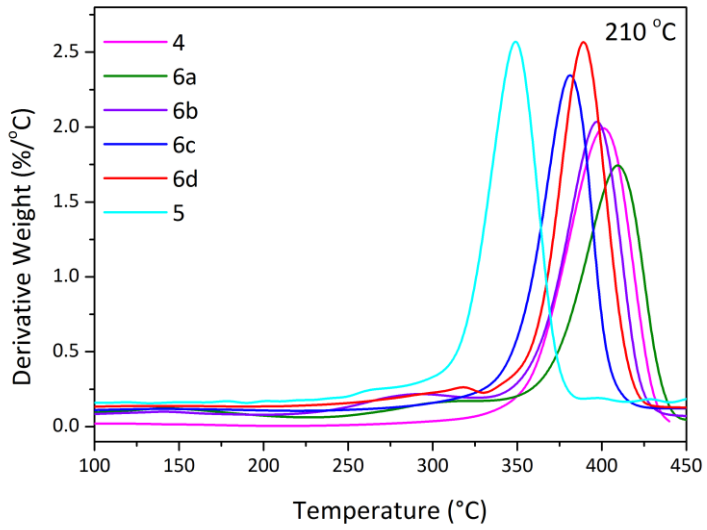

Figure 162. TGA Derivative Weight% thermogram of polyesters at 210 °C.

C.14 TGA Weight% thermogram of polyesters at 220 °C

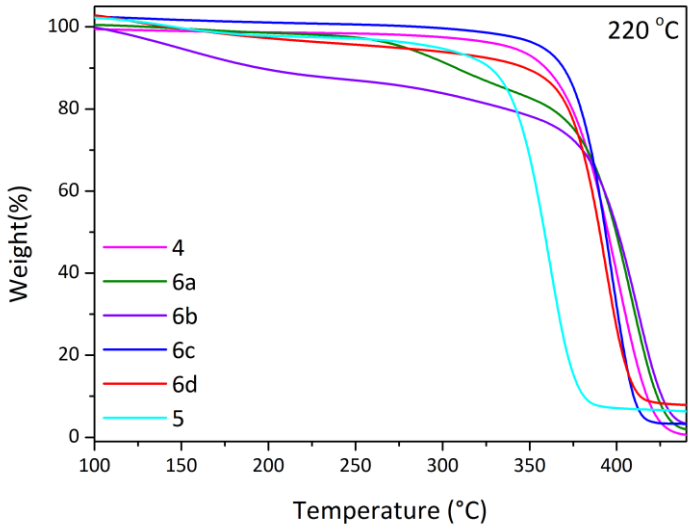

Figure 163. TGA Weight% thermogram of polyesters at 220 °C.

C.15 TGA Derivative Weight% thermogram of polyesters at 220 °C

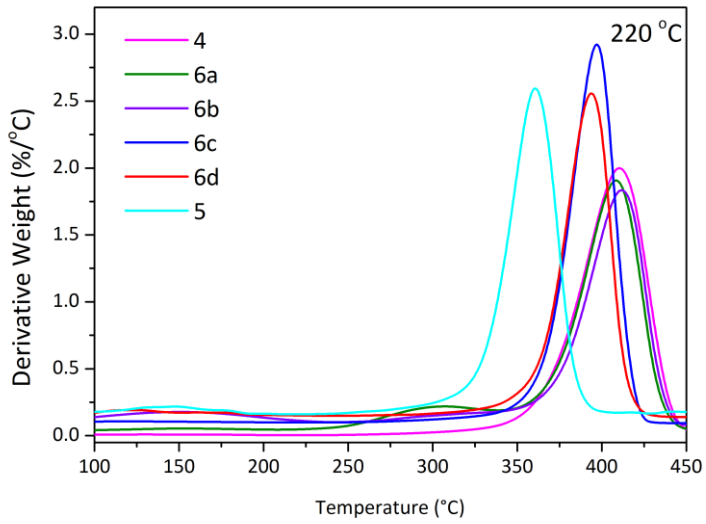

Figure 164. TGA Derivative Weight% thermogram of polyesters at 220 °C.

Appendix D (Chapter 5)

D.1 Acid value-conversion data for the polyesterifications with 1,3-propanediol (Polyesters 1-3)

Table 73. Acid value-conversion data for the polyesterifications with 1,3-propanediol

Concentration: 15% FDCA, 85% SA			
PPFPS 15% FDCA/85% SA 210 °C			
Time	**A. Value**	**A. Concentration**	**p**
(min)	**(g KOH/kg resin)**	**(mol acid/kg resin)**	**-**
0	33.660	0.30000	0.00000
30	24.043	0.21429	0.28682
60	19.388	0.17279	0.42534
90	13.713	0.12222	0.59390
120	9.240	0.08235	0.72657
150	4.415	0.03935	0.86944
180	3.099	0.02762	0.90837
210	2.576	0.02296	0.92385
240	1.829	0.01630	0.94593
270	1.323	0.01179	0.96090
300	1.345	0.01199	0.96025
330	1.181	0.01053	0.96510
360	0.941	0.00839	0.97218
PPFPS 15% FDCA/85% SA 220 °C			
Time	**A. Value**	**A. Concentration**	**p**
(min)	**(g KOH/kg resin)**	**(mol acid/kg resin)**	**-**
0	55.138	0.49143	0.00000
30	22.889	0.20400	0.58704
60	16.953	0.15110	0.69442
90	9.995	0.08908	0.82005
120	4.818	0.04294	0.91332
150	3.148	0.02806	0.94338
180	1.670	0.01488	0.96998
210	1.503	0.01339	0.97298
240	1.476	0.01316	0.97346
270	0.907	0.00809	0.98369
300	0.725	0.00646	0.98697
330	0.557	0.00496	0.98999
360	0.565	0.00503	0.98985
PPFPS 15% FDCA/85% SA 230 °C			
Time	**A. Value**	**A. Concentration**	**p**
(min)	**(g KOH/kg resin)**	**(mol acid/kg resin)**	**-**
0	23.346	0.20807	0.00000
30	15.670	0.13966	0.32960
60	7.792	0.06944	0.66709
90	4.239	0.03778	0.81900
120	2.743	0.02444	0.88291
150	2.167	0.01931	0.90750
180	1.540	0.01373	0.93427

240	1.111	0.00990	0.95259
270	1.045	0.00932	0.95538
300	0.939	0.00837	0.95993
330	0.894	0.00797	0.96184
360	0.866	0.00772	0.96305

Concentration: 30% FDCA, 70% SA			
PPFPS 30% FDCA/70% SA 210 °C			
Time	**A. Value**	**A. Concentration**	**p**
(min)	**(g KOH/kg resin)**	**(mol acid/kg resin)**	**-**
0	69.985	0.62375	0.00000
30	36.694	0.32704	0.47850
60	26.647	0.23750	0.62190
90	21.354	0.19032	0.69726
120	14.147	0.12609	0.79967
150	11.410	0.10169	0.83850
180	6.321	0.05634	0.91060
210	4.208	0.03750	0.94051
240	2.589	0.02308	0.96340
270	1.845	0.01645	0.97392
300	2.072	0.01847	0.97072
330	1.880	0.01676	0.97342
360	1.705	0.01519	0.97591
PPFPS 30% FDCA/70% SA 220 °C			
Time	**A. Value**	**A. Concentration**	**p**
(min)	**(g KOH/kg resin)**	**(mol acid/kg resin)**	**-**
0	69.769	0.62183	0.00000
30	27.308	0.24339	0.61127
60	16.858	0.15025	0.76044
90	10.364	0.09237	0.85287
120	4.820	0.04296	0.93164
150	3.468	0.03091	0.95082
180	2.697	0.02404	0.96176
210	2.237	0.01993	0.96829
240	1.941	0.01730	0.97248
270	1.415	0.01261	0.97994
300	1.365	0.01217	0.98065
330	1.130	0.01007	0.98399
360	0.987	0.00879	0.98601
PPFPS 30% FDCA/70% SA 230 °C			
Time	**A. Value**	**A. Concentration**	**p**
(min)	**(g KOH/kg resin)**	**(mol acid/kg resin)**	**-**
0	62.158	0.55399	0.00000
30	15.104	0.13462	0.75885
60	8.894	0.07927	0.85814
90	6.311	0.05625	0.89937
120	1.636	0.01458	0.97393
150	0.941	0.00839	0.98501
180	0.550	0.00490	0.99124
210	0.449	0.00400	0.99285

Concentration: 30% FDCA, 70% SA			
PPFPS 30% FDCA/70% SA 210 °C			
Time	**A. Value**	**A. Concentration**	**p**
(min)	**(g KOH/kg resin)**	**(mol acid/kg resin)**	**-**
240	0.386	0.00344	0.99385
270	0.391	0.00349	0.99377
300	0.387	0.00345	0.99384

Concentration: 70% FDCA, 30% SA			
PPFPS 70% FDCA/30% SA 210 °C			
Time	**A. Value**	**A. Concentration**	**p**
(min)	**(g KOH/kg resin)**	**(mol acid/kg resin)**	**-**
0	87.932	0.78371	0.00000
30	37.400	0.33333	0.57814
60	24.567	0.21895	0.72347
90	19.856	0.17697	0.77666
120	17.765	0.15833	0.80025
150	12.070	0.10758	0.86441
180	9.523	0.08487	0.89307
210	7.013	0.06250	0.92129
240	4.804	0.04282	0.94609
270	3.435	0.03061	0.96147
300	3.233	0.02882	0.96373
330	2.850	0.02540	0.96803
360	2.069	0.01844	0.97679
PPFPS 70% FDCA/30% SA 220 °C			
Time	**A. Value**	**A. Concentration**	**p**
(min)	**(g KOH/kg resin)**	**(mol acid/kg resin)**	**-**
0	84.032	0.74895	0.00000
30	35.293	0.31455	0.58331
60	21.767	0.19400	0.74357
90	16.133	0.14379	0.81011
150	10.069	0.08974	0.88160
180	7.120	0.06346	0.91631
240	4.746	0.04230	0.94424
270	4.280	0.03815	0.94972
300	3.893	0.03469	0.95427
330	3.108	0.02770	0.96350
360	2.149	0.01916	0.97476
PPFPS 70% FDCA/30% SA 230 °C			
Time	**A. Value**	**A. Concentration**	**p**
(min)	**(g KOH/kg resin)**	**(mol acid/kg resin)**	**-**
0	71.044	0.63319	0.00000
30	22.743	0.20270	0.68236
60	15.037	0.13402	0.79025
90	11.160	0.09947	0.84442
120	10.878	0.09695	0.84836
180	3.929	0.03501	0.94530
210	1.327	0.01182	0.98153

Concentration: 70% FDCA, 30% SA			
PPFPS 70% FDCA/30% SA 210 °C			
Time	**A. Value**	**A. Concentration**	**p**
(min)	**(g KOH/kg resin)**	**(mol acid/kg resin)**	**-**
240	1.177	0.01049	0.98362
270	1.131	0.01008	0.98426
300	0.990	0.00882	0.98622
330	0.920	0.00820	0.98720
360	0.534	0.00476	0.99256

Concentration: 85% FDCA, 15% SA.			
PPFPS 85% FDCA/15% SA 210 °C			
Time	**A. Value**	**A. Concentration**	**p**
(min)	**(g KOH/kg resin)**	**(mol acid/kg resin)**	**-**
0	83.607	0.74516	0.00000
30	41.650	0.37121	0.50521
60	31.103	0.27721	0.63113
90	23.663	0.21090	0.71971
120	19.833	0.17677	0.76521
150	14.086	0.12554	0.83341
180	10.997	0.09801	0.87000
210	8.430	0.07513	0.90039
240	6.303	0.05618	0.92554
270	5.754	0.05128	0.93204
300	4.449	0.03966	0.94746
330	3.875	0.03454	0.95424
360	2.741	0.02443	0.96764
PPFPS 85% FDCA/15% SA 220 °C			
Time	**A. Value**	**A. Concentration**	**p**
(min)	**(g KOH/kg resin)**	**(mol acid/kg resin)**	**-**
0	79.509	0.70863	0.00000
30	35.389	0.31541	0.55807
60	23.735	0.21154	0.70417
90	15.957	0.14222	0.80136
120	12.467	0.11111	0.84489
150	9.889	0.08814	0.87701
180	7.362	0.06562	0.90848
210	5.454	0.04861	0.93222
240	4.997	0.04454	0.93790
270	4.561	0.04065	0.94333
300	3.384	0.03016	0.95796
330	2.609	0.02326	0.96759
360	2.205	0.01965	0.97261
PPFPS 85% FDCA/15% SA 230 °C			
Time	**A. Value**	**A. Concentration**	**p**
(min)	**(g KOH/kg resin)**	**(mol acid/kg resin)**	**-**
0	83.837	0.74721	0.00000
30	28.411	0.25322	0.66414
60	12.871	0.11472	0.84822

Concentration: 85% FDCA, 15% SA.			
PPFPS 85% FDCA/15% SA 210 °C			
Time	**A. Value**	**A. Concentration**	**p**
(min)	**(g KOH/kg resin)**	**(mol acid/kg resin)**	**-**
90	10.110	0.09011	0.88084
120	7.832	0.06981	0.90772
150	5.691	0.05072	0.93297
180	2.797	0.02493	0.96707
210	1.816	0.01619	0.97862
270	1.611	0.01435	0.98104
330	1.162	0.01036	0.98633

D.2 Acid value-conversion data for the polyesterifications with 1,3-propanediol (Polyesters 4-6)

Table 74. Acid value-conversion data for the polyesterifications with 1,5-pentanediol

Succinic Acid Polyesters (PPeS)			
PPeS 210 °C			
Time	**A. Value**	**A. Concentration**	**p**
(min)	**(g KOH/kg resin)**	**(mol acid/kg resin)**	**-**
0	92.66	0.82581	0.00000
30	51.32	0.45739	0.44984
60	39.08	0.34834	0.58183
90	34.87	0.31075	0.62721
120	28.41	0.25316	0.69661
150	24.73	0.22041	0.73602
180	18.11	0.16143	0.80686
210	16.46	0.14674	0.82449
240	14.24	0.12690	0.84827
270	12.04	0.10734	0.87170
300	11.88	0.10588	0.87345
330	10.10	0.09005	0.89240
360	9.66	0.08607	0.89717
390	8.45	0.07527	0.91009
420	7.60	0.06777	0.91905
450	7.19	0.06406	0.92349
PPeS 220 °C			
Time	**A. Value**	**A. Concentration**	**P**
(min)	**(g KOH/kg resin)**	**(mol acid/kg resin)**	**-**
0	88.50	0.78877	0.00000
30	45.82	0.40838	0.48583
60	34.95	0.31148	0.60852
90	27.76	0.24740	0.68942
120	24.97	0.22251	0.72079
150	20.26	0.18056	0.77361
180	17.12	0.15254	0.80883
210	14.53	0.12952	0.83775

240	13.02	0.11603	0.85468
270	11.17	0.09957	0.87534
300	10.27	0.09152	0.88543
330	8.40	0.07485	0.90633
360	7.41	0.06601	0.91741
390	7.27	0.06478	0.91895
420	6.91	0.06162	0.92290
450	5.53	0.04926	0.93838
PPeS 230 °C			
Time	**A. Value**	**A. Concentration**	**P**
(min)	**(g KOH/kg resin)**	**(mol acid/kg resin)**	**-**
0	94.56	0.84277	0.00000
30	45.83	0.40851	0.51909
60	31.61	0.28172	0.66912
90	24.46	0.21802	0.74422
120	19.51	0.17385	0.79621
150	17.34	0.15451	0.81895
180	13.17	0.11737	0.86255
210	11.37	0.10135	0.88135
240	10.00	0.08913	0.89568
270	8.67	0.07729	0.90955
300	7.45	0.06641	0.92231
330	6.73	0.06000	0.92981
360	4.62	0.04118	0.95185
390	3.58	0.03188	0.96273
420	3.16	0.02817	0.96707
450	2.57	0.02290	0.97323

15% FDCA 85% SA			
PPeFS 15% FDCA, 85% SA, 210 °C			
Time	**A. Value**	**A. Concentration**	**p**
(min)	**(g KOH/kg resin)**	**(mol acid/kg resin)**	**-**
0	73.27	0.65301	0.00000
30	37.30	0.33245	0.49385
60	29.27	0.26087	0.60334
90	22.44	0.20000	0.69623
120	15.49	0.13805	0.79056
150	11.02	0.09825	0.85105
180	7.63	0.06796	0.89702
210	7.35	0.06550	0.90076
240	6.11	0.05447	0.91749
270	5.12	0.04566	0.93084
300	3.17	0.02826	0.95721
330	2.31	0.02055	0.96889
360	1.91	0.01703	0.97422
390	0.84	0.00746	0.98870
420	0.78	0.00692	0.98953
PPeFS 15% FDCA, 85% SA, 220 °C			
Time	**A. Value**	**A. Concentration**	**P**

(min)	(g KOH/kg resin)	(mol acid/kg resin)	-
0	80.03	0.71326	0.00000
30	31.66	0.28219	0.60745
60	22.41	0.19971	0.72260
90	16.40	0.14617	0.79716
120	11.34	0.10111	0.85981
150	9.10	0.08108	0.88762
180	7.57	0.06748	0.90649
210	4.89	0.04355	0.93968
240	4.76	0.04240	0.94128
270	3.57	0.03179	0.95597
300	3.25	0.02900	0.95984
330	2.47	0.02200	0.96954
360	2.36	0.02100	0.97092
390	1.80	0.01600	0.97785
PPeFS 15% FDCA, 85% SA, 230 °C			
Time	**A. Value**	**A. Concentration**	**P**
(min)	**(g KOH/kg resin)**	**(mol acid/kg resin)**	**-**
0	62.96	0.56111	0.00000
30	18.39	0.16389	0.71002
60	12.37	0.11026	0.80510
90	9.82	0.08750	0.84539
120	4.46	0.03979	0.92975
150	2.39	0.02128	0.96245
180	2.31	0.02055	0.96374
210	1.95	0.01736	0.96936
240	1.80	0.01601	0.97174
270	0.77	0.00685	0.98792
330	0.57	0.00612	0.98921
360	0.69	0.00498	0.99121
30% FDCA 70% SA			
PPeFS 30% FDCA, 70% SA, 210 °C			
Time	**A. Value**	**A. Concentration**	**p**
(min)	**(g KOH/kg resin)**	**(mol acid/kg resin)**	**-**
0	61.90	0.55172	0.00000
30	35.04	0.31229	0.43642
60	25.93	0.23108	0.58360
90	21.21	0.18900	0.65969
120	14.52	0.12941	0.76723
150	10.81	0.09639	0.82674
180	7.09	0.06318	0.88650
210	6.79	0.06050	0.89132
240	5.61	0.05000	0.91019
270	4.85	0.04325	0.92232
300	4.04	0.03604	0.93529
330	3.92	0.03492	0.93730
360	3.54	0.03153	0.94338
390	3.25	0.02895	0.94803
420	3.17	0.02826	0.94926
PPeFS 30% FDCA, 70% SA, 220 °C			

Time	A. Value	A. Concentration	p
(min)	(g KOH/kg resin)	(mol acid/kg resin)	-
0	75.08	0.66917	0.00000
30	33.66	0.30000	0.55468
60	24.09	0.21471	0.68177
90	18.12	0.16154	0.76081
120	14.11	0.12576	0.81391
150	11.34	0.10111	0.85045
180	9.72	0.08665	0.87188
210	8.74	0.07787	0.88487
240	6.82	0.06081	0.91012
300	4.97	0.04427	0.93459
330	4.40	0.03922	0.94206
360	4.14	0.03693	0.94544
390	3.39	0.03018	0.95541
420	2.86	0.02551	0.96232
PPeFS 30% FDCA, 70% SA, 230 °C			
Time	**A. Value**	**A. Concentration**	**p**
(min)	(g KOH/kg resin)	(mol acid/kg resin)	-
0	61.58	0.54885	0.00000
30	23.99	0.21379	0.61283
60	17.33	0.15445	0.72060
90	15.98	0.14244	0.74238
120	8.70	0.07752	0.85996
150	5.05	0.04500	0.91875
180	3.67	0.03267	0.94103
210	2.79	0.02482	0.95520
240	2.69	0.02397	0.95674
270	2.24	0.02000	0.96391
300	1.45	0.01294	0.97664
330	1.37	0.01224	0.97792
360	1.18	0.01049	0.98107
390	1.10	0.00977	0.98237

70% FDCA 30% SA			
PPeFS 70% FDCA, 30% SA, 210 °C			
Time	**A. Value**	**A. Concentration**	**p**
(min)	(g KOH/kg resin)	(mol acid/kg resin)	-
0	63.64	0.56719	0.00000
30	39.55	0.35253	0.38087
60	27.10	0.24155	0.57663
90	23.35	0.20813	0.63542
120	17.65	0.15730	0.72471
180	14.61	0.13021	0.77224
210	12.82	0.11429	0.80015
240	8.47	0.07547	0.86812
270	8.05	0.07171	0.87471
300	7.93	0.07071	0.87645
330	6.53	0.05818	0.89837

360	6.09	0.05431	0.90514
405	5.22	0.04651	0.91877
PPeFS 70% FDCA, 30% SA, 220 °C			
Time	**A. Value**	**A. Concentration**	**p**
(min)	**(g KOH/kg resin)**	**(mol acid/kg resin)**	**-**
0	72.13	0.64286	0.00000
30	36.70	0.32714	0.49403
60	27.61	0.24609	0.61993
90	21.40	0.19072	0.70574
120	18.08	0.16116	0.75149
150	13.40	0.11940	0.81602
180	10.79	0.09615	0.85190
210	7.99	0.07117	0.89044
240	7.67	0.06839	0.89472
270	7.39	0.06590	0.89855
300	6.33	0.05639	0.91321
330	6.06	0.05405	0.91681
360	4.85	0.04327	0.93342
390	3.64	0.03243	0.95010
420	2.61	0.02326	0.96423
PPeFS 70% FDCA, 30% SA, 230 °C			
Time	**A. Value**	**A. Concentration**	**p**
(min)	**(g KOH/kg resin)**	**(mol acid/kg resin)**	**-**
0	76.42	0.68107	0.00000
30	30.82	0.27470	0.59962
60	21.45	0.19118	0.72178
90	17.55	0.15639	0.77255
120	13.00	0.11583	0.83166
150	9.91	0.08833	0.87170
180	8.86	0.07895	0.88534
210	7.60	0.06777	0.90160
240	6.58	0.05867	0.91482
270	5.74	0.05119	0.92569
300	4.59	0.04088	0.94067
330	4.26	0.03801	0.94483
360	4.29	0.03822	0.94454
390	3.92	0.03497	0.94926
420	3.92	0.03495	0.94927

85% FDCA 15% SA
PPeFS 85% FDCA, 15% SA, 210 °C

Time	A. Value	A. Concentration	p
(min)	(g KOH/kg resin)	(mol acid/kg resin)	-
0	68.48	0.61034	0.00000
30	41.80	0.37258	0.39219
60	31.11	0.27727	0.54845
90	25.19	0.22455	0.63466
120	20.90	0.18625	0.69719
150	17.44	0.15541	0.74747
180	13.66	0.12176	0.80226
240	10.85	0.09667	0.84309
270	9.87	0.08800	0.85718
300	8.45	0.07534	0.87775
330	8.01	0.07143	0.88411
360	6.47	0.05769	0.90642
390	4.99	0.04444	0.92792
420	4.79	0.04270	0.93076
PPeFS 85% FDCA, 15% SA, 220 °C			
Time	**A. Value**	**A. Concentration**	**p**
(min)	(g KOH/kg resin)	(mol acid/kg resin)	-
0	73.63	0.65625	0.00000
30	37.16	0.33122	0.49825
60	25.17	0.22436	0.66079
90	21.09	0.18793	0.71605
120	17.06	0.15207	0.77038
150	13.01	0.11597	0.82501
180	11.01	0.09811	0.85200
210	9.35	0.08333	0.87433
240	8.87	0.07905	0.88079
270	7.52	0.06701	0.89897
300	6.79	0.06053	0.90876
330	6.16	0.05492	0.91721
360	5.70	0.05081	0.92342
390	5.30	0.04722	0.92883
420	4.89	0.04358	0.93433
PPeFS 85% FDCA, 15% SA, 230 °C			
Time	**A. Value**	**A. Concentration**	**p**
(min)	(g KOH/kg resin)	(mol acid/kg resin)	-
0	62.16	0.55405	0.00000
30	29.78	0.26540	0.52349
60	20.30	0.18093	0.67564
90	16.65	0.14837	0.73417
120	13.49	0.12021	0.78474
150	10.93	0.09739	0.82568
180	8.96	0.07986	0.85709
210	7.69	0.06857	0.87732
240	6.64	0.05921	0.89409
270	6.58	0.05869	0.89503
300	5.84	0.05208	0.90685
330	5.15	0.04591	0.91790
360	5.11	0.04556	0.91853

390	5.02	0.04476	0.91995
420	4.67	0.04167	0.92549

PPeF 210 °C			
Time	**A. Value**	**A. Concentration**	**p**
(min)	**(g KOH/kg resin)**	**(mol acid/kg resin)**	**-**
0	55.17	0.49167	0.00000
30	32.54	0.29000	0.41232
60	30.21	0.26923	0.45462
90	22.44	0.20000	0.59536
120	11.55	0.10294	0.79210
150	7.58	0.06757	0.86362
180	6.10	0.05435	0.89033
210	5.61	0.05000	0.89911
240	5.26	0.04687	0.90542
270	3.91	0.03488	0.92963
300	3.37	0.03000	0.93949
330	3.30	0.02941	0.94068
360	3.22	0.02874	0.94204
390	2.74	0.02439	0.95081
PPeF 220 °C			
Time	**A. Value**	**A. Concentration**	**p**
(min)	**(g KOH/kg resin)**	**(mol acid/kg resin)**	**-**
0	56.57	0.50420	0.00000
30	30.05	0.26786	0.47102
60	18.70	0.16667	0.67146
90	14.76	0.13158	0.74079
120	9.67	0.08621	0.83031
150	9.35	0.08333	0.83598
180	8.50	0.07576	0.85091
210	8.47	0.07547	0.85147
240	7.11	0.06338	0.87529
270	5.61	0.05000	0.90164
300	5.02	0.04478	0.91193
330	4.62	0.04118	0.91901
360	4.58	0.04082	0.91972
390	3.74	0.03333	0.93445
PPeF 230 °C			
Time	**A. Value**	**A. Concentration**	**P**
(min)	**(g KOH/kg resin)**	**(mol acid/kg resin)**	**-**
0	69.84	0.62242	0.00000
30	31.00	0.27626	0.55894
60	22.39	0.19954	0.68186
90	15.88	0.14151	0.77462
120	13.71	0.12222	0.80541
150	10.66	0.09500	0.84882
180	9.53	0.08491	0.86491

210	6.84	0.06098	0.90303
240	6.38	0.05688	0.90955
270	5.75	0.05128	0.91846
330	4.60	0.04098	0.93484
360	4.21	0.03750	0.94039
390	3.97	0.03538	0.94375

D.3 Conversion of COOH groups during the polymerisation of 3c at different temperatures fitted to Model 2

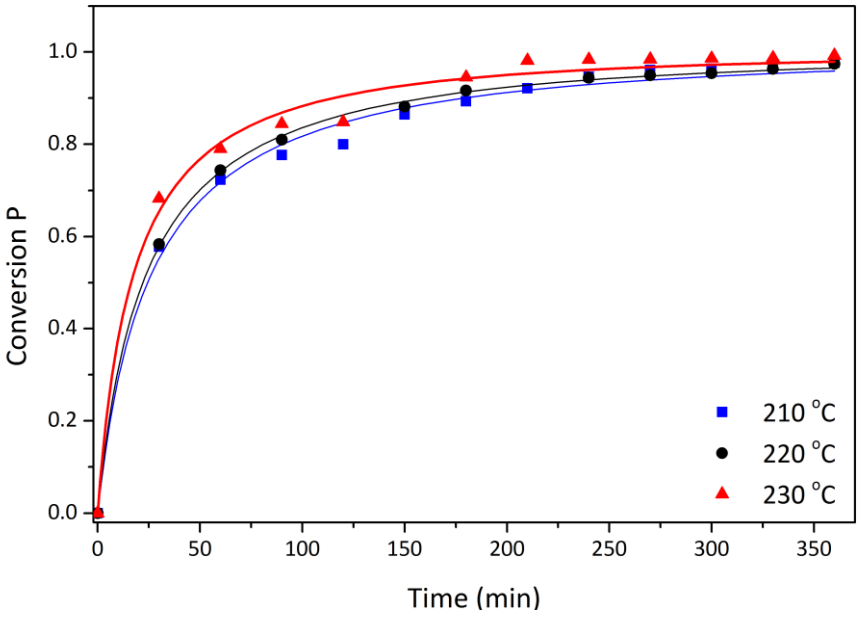

Figure 165. Conversion of COOH groups during the polymerisation of **3c** at different temperatures fitted to Model 2. Symbols: Experimental data; lines: Model.

D.4 Conversion of COOH groups during the polymerisation of 3d at different temperatures fitted to Model 2

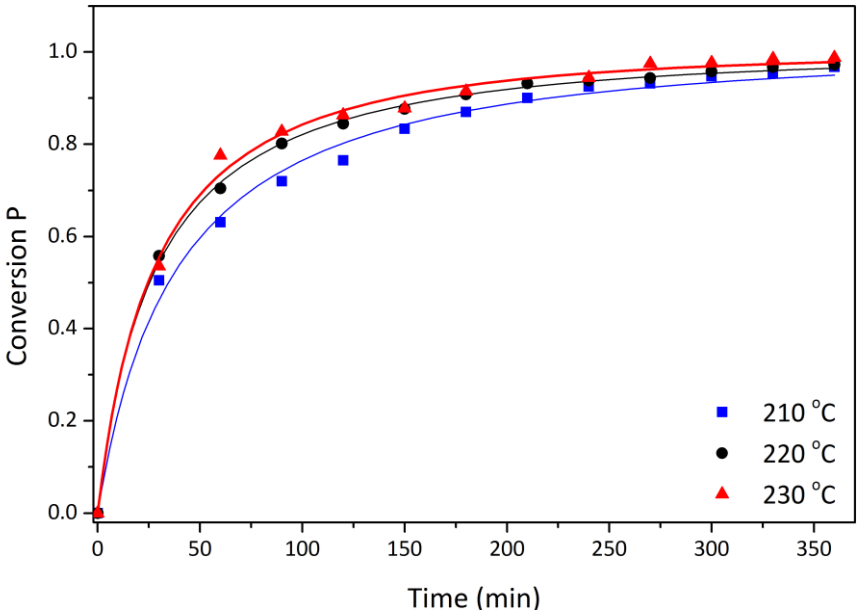

Figure 166. Conversion of COOH groups during the polymerisation of **3d** at different temperatures fitted to Model 2. Symbols: Experimental data; lines: Model.

D.5 Conversion of COOH groups during the polymerisation of 3a at different temperatures fitted to Model 3

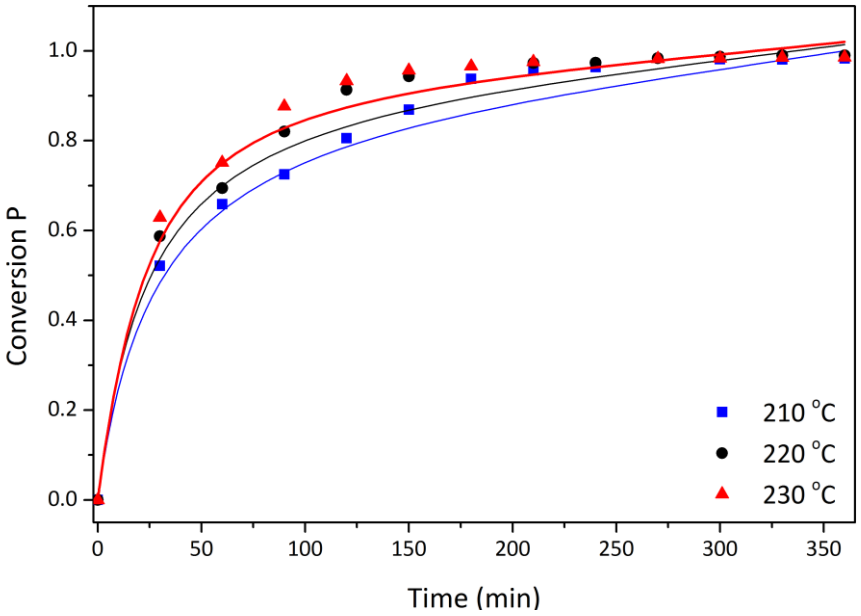

Figure 167. Conversion of COOH groups during the polymerisation of **3a** at different temperatures fitted to Model 3. Symbols: Experimental data; lines: Model.

D.6 Conversion of COOH groups during the polymerisation of 3b at different temperatures fitted to Model 3

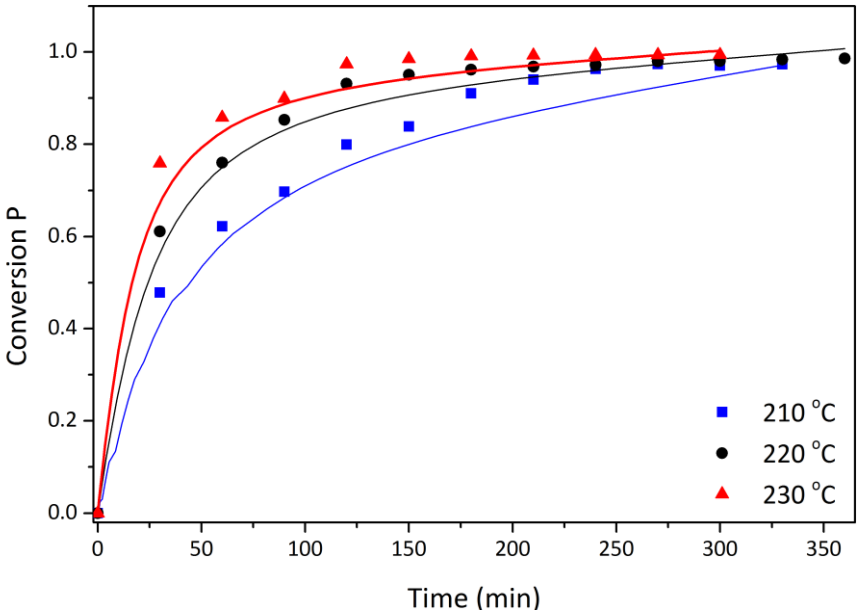

Figure 168. Conversion of COOH groups during the polymerisation of **3b** at different temperatures fitted to Model 3. Symbols: Experimental data; lines: Model.

D.7 Conversion of COOH groups during the polymerisation of 5 at different temperatures fitted to Model 2

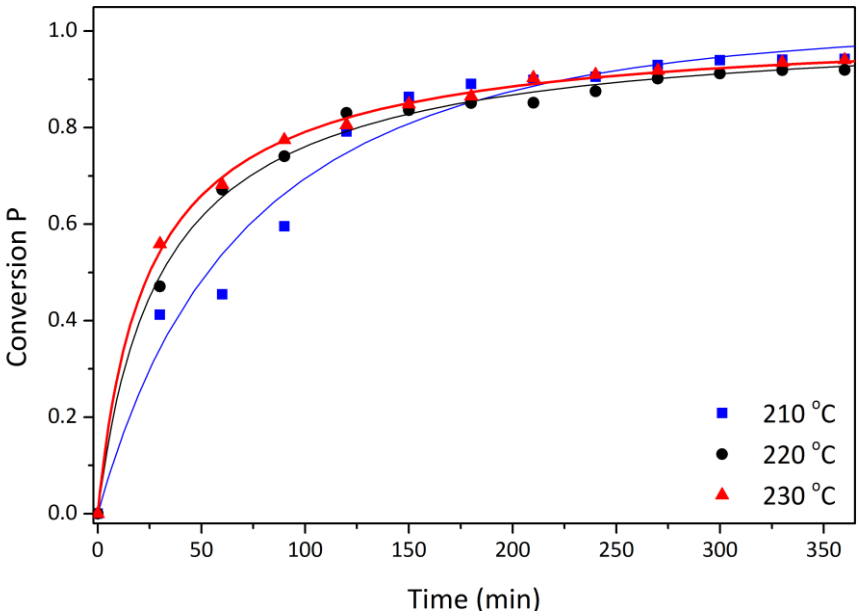

Figure 169. Conversion of COOH groups during the polymerisation of **5** at different temperatures fitted to Model 2. Symbols: Experimental data; lines: Model.

D.8 Conversion of COOH groups during the polymerisation of 4 at different temperatures fitted to Model 3

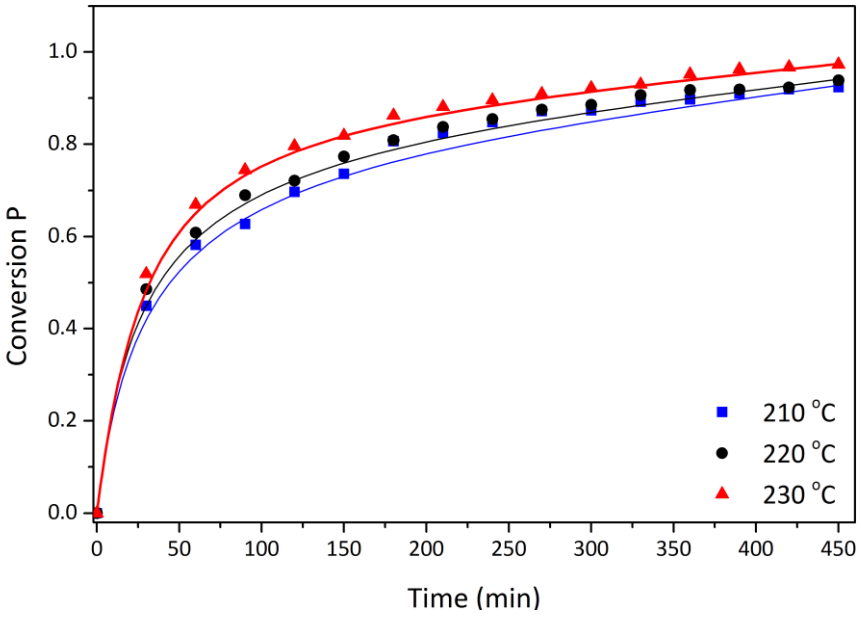

Figure 170. Conversion of COOH groups during the polymerisation of **4** at different temperatures fitted to Model 3. Symbols: Experimental data; lines: Model.

D.9 Conversion of COOH groups during the polymerisation of 6b at different temperatures fitted to Model 2

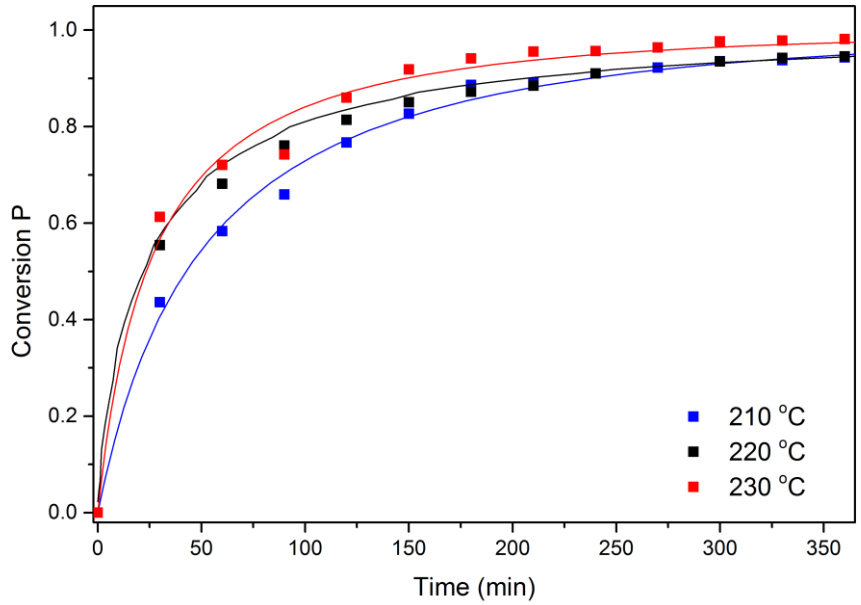

Figure 171. Conversion of COOH groups during the polymerisation of **6b** at different temperatures fitted to Model 2. Symbols: Experimental data; lines: Model.

D.10 Conversion of COOH groups during the polymerisation of 6c at different temperatures fitted to Model 2

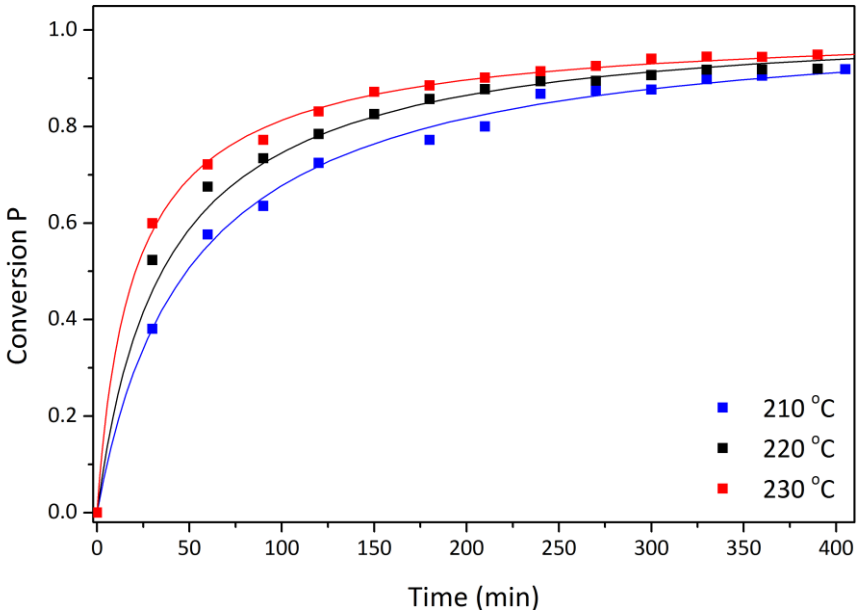

Figure 172. Conversion of COOH groups during the polymerisation of **6c** at different temperatures fitted to Model 2. Symbols: Experimental data; lines: Model.

D.11 Conversion of COOH groups during the polymerisation of 6c at different temperatures fitted to Model 2

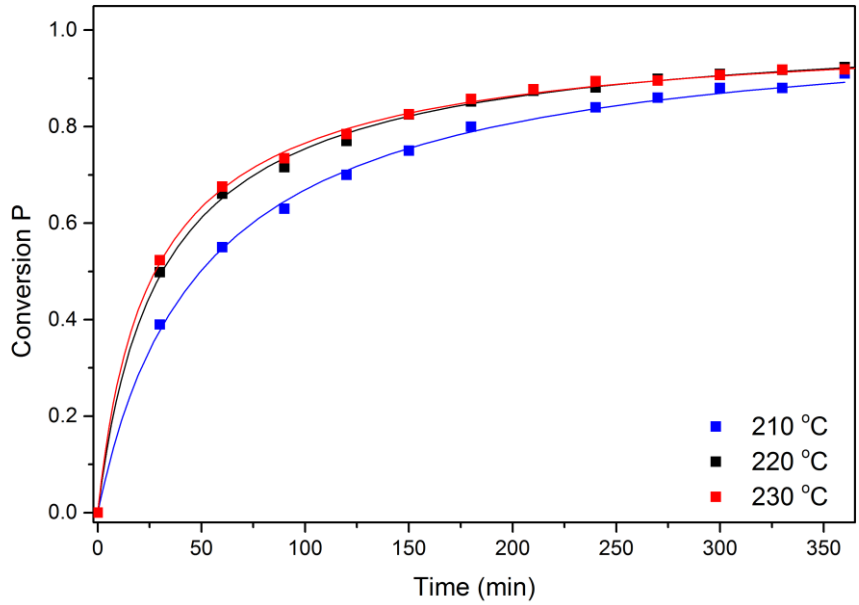

Figure 173. Conversion of COOH groups during the polymerisation of **6c** at different temperatures fitted to Model 2. Symbols: Experimental data; lines: Model.

D.12 Conversion of COOH groups during the polymerisation of 6a at different temperatures fitted to Model 3

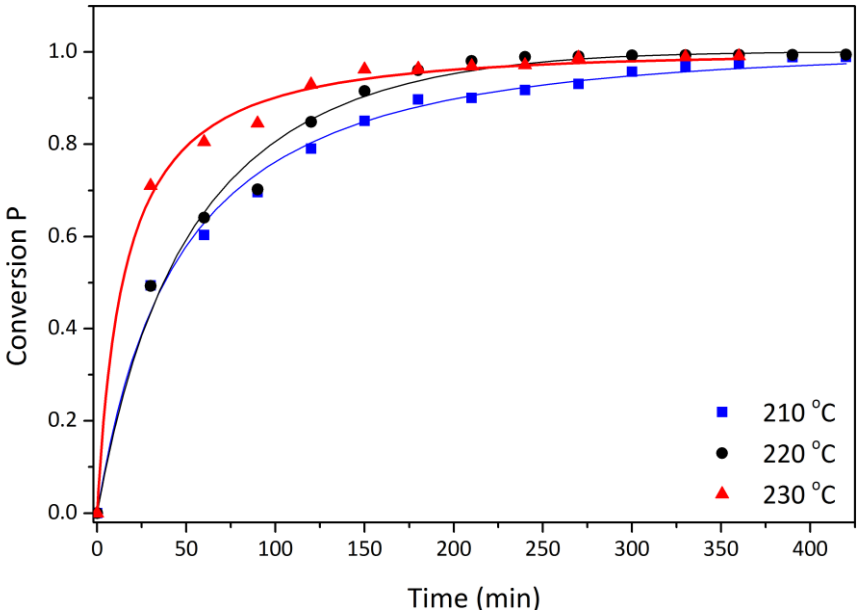

Figure 174. Conversion of COOH groups during the polymerisation of **6a** at different temperatures fitted to Model 3. Symbols: Experimental data; lines: Model.

D.13 Conversion of COOH groups during the polymerisation of 6b at different temperatures fitted to Model 3

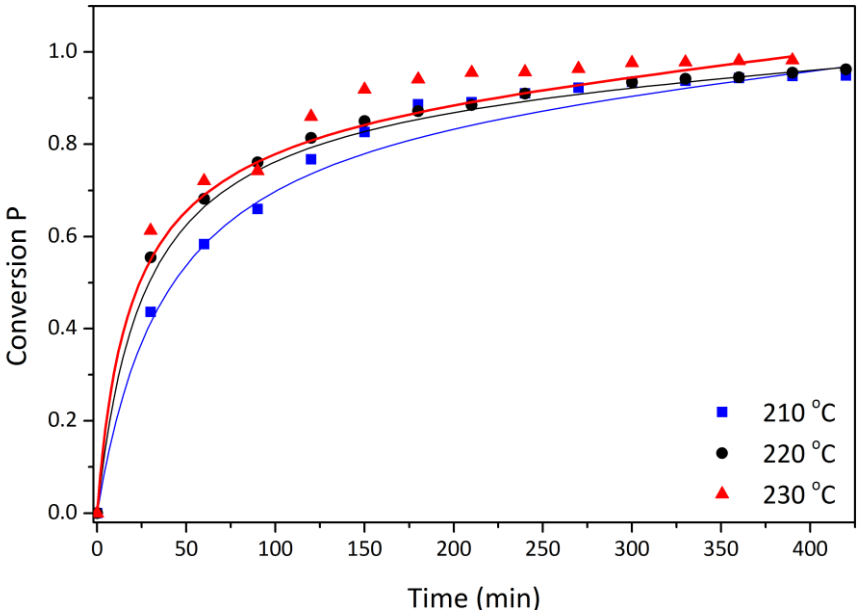

Figure 175. Conversion of COOH groups during the polymerisation of **6b** at different temperatures fitted to Model 3. Symbols: Experimental data; lines: Model.

D.14 Conversion of COOH groups during the polymerisation of 6c at different temperatures fitted to Model 3

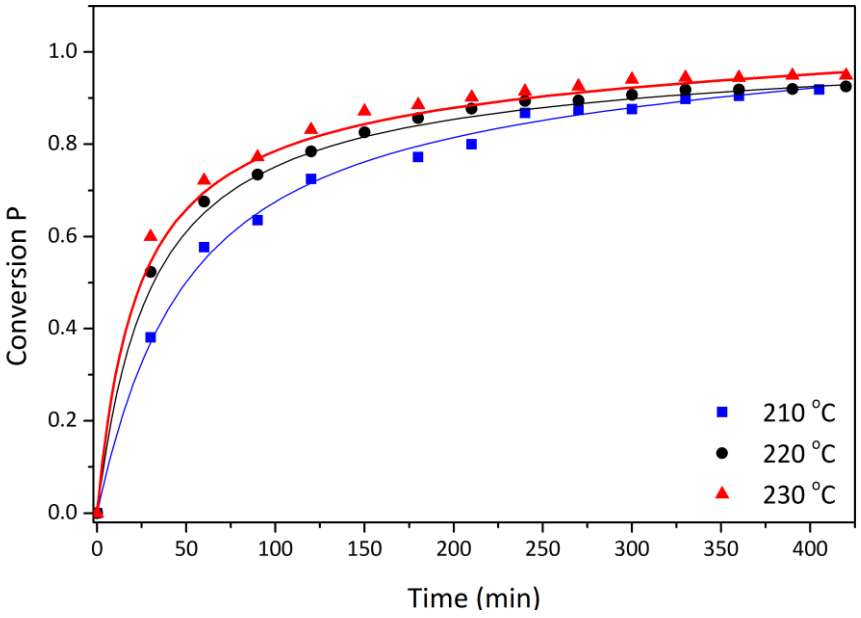

Figure 176. Conversion of COOH groups during the polymerisation of **6c** at different temperatures fitted to Model 3. Symbols: Experimental data; lines: Model.

D.15 Conversion of COOH groups for all monomer compositions of polyesters 6 fitted to Model 2 at 210 °C

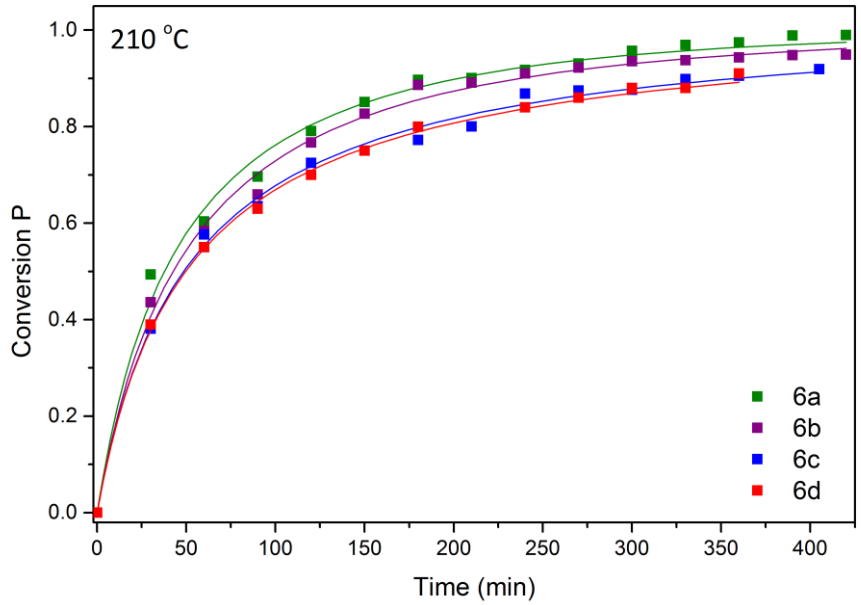

Figure 177. Conversion of COOH groups for all monomer compositions of polyesters **6** fitted to Model 2 at 210 °C. Symbols: Experimental data; lines: Model.

D.16 Conversion of COOH groups for all monomer compositions of polyesters 6 fitted to Model 2 at 220 °C

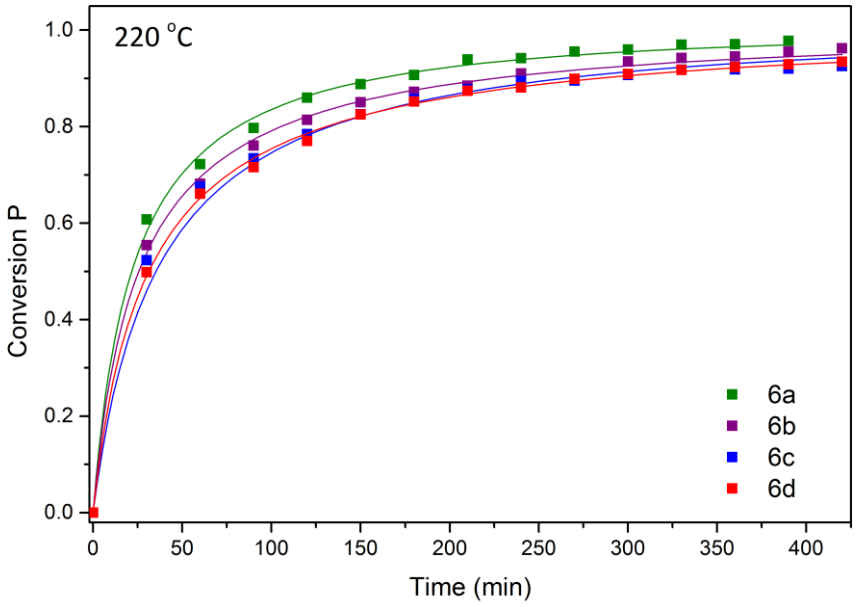

Figure 178. Conversion of COOH groups for all monomer compositions of polyesters **6** fitted to Model 2 at 220 °C. Symbols: Experimental data; lines: Model.

D.17 General Matlab code for the routine using "fminunc" for polyester $PPeF_{85}S_{15}$

```
%Objective function min z=(Ca exp-Camod)^2
clc;clear all; format compact; format long
global t np COOHo COOH b0
%Experimental data
t=[0
30
60
90
120
150
180
210
240
270
300
330
360
390
420]'; %min
COOH= [0.554054054
0.265395894
0.180933852
0.148367953
0.120209059
0.097387173
0.079861111
0.068571429
```

```
0.059210526
0.058685446
0.052083333
0.045905707
0.045555556
0.044761905
0.041666667]'; %g/mol
COOHo=COOH(1);
np=length(t); %calculate number of experimental points
b0=.3;
%Initial estimates
k0=0.070141;  %Rate constant
m0=2.107272; %reaction order for acid
n0=2; %reaction order for alcohol
x0=[k0 m0 n0];
options=optimset('LargeScale','off', 'Display','iter');
[x, Zmin,
flag,output,grad_Z,hessian]=fminunc('kineticsml102nonstoichio',x0,options)
fprintf('Values=%f\n',eig(hessian))
%Data results
k=x(1); m=x(2); n=x(3); %parameter reasignation
fprintf('k=%f\n',k)
fprintf('m=%f\n',m)
fprintf('n=%f\n',n)

[t_mod,COOH_mod]=ode15s(@modelml102nonstoichio,[0,t(np)],COOH(1),[],k,m,n);
figure(3),plot(t,COOH,'o',t_mod,COOH_mod)
xlabel('Time [min]')
ylabel('Concentration')
legend('COOHexp', 'COOHmodel')
title('Model 2 Prediction for ml102 Synthesis')
%%%%%% function file%%%%
function dCOOHdt=modelml102nonstoichio(ti,COOHi,k,m,n)
global t np COOHo COOH b0
dCOOHdt=-(k*COOHi.^m)*(COOHi+b0*((1-0.018*COOHi)./(1-0.018*COOHo)).^n);
%End of routine modelml102.m
%%% ode15s file%%%%
%Start of file kineticsml102nonstoichio
function Z=kineticsml102nonstoichio(x)
global t np COOHo COOH b0
k=x(1);m=x(2);n=x(3);
sum=0;
for i=1:np
    if i==1
        COOH_mod(1)=COOH(1);
    else
        delta_t=[0 t(i)]; %interval integration
        COOH0=COOH(1); %initial concentration
        [ts,COOHs]=ode15s(@modelml102nonstoichio,delta_t,COOH0,[],k,m,n);
        COOH_mod(i)=COOHs(end);
    end
    sum=sum+(COOH(i)-COOH_mod(i))^2;
end
Z=sum;
%end of file kineticsml102nonstoichio.m
```

Appendix E (Chapter 6)

E.1 Stoichiometry and Reaction Rates for Esterification Reactions with 1,3-propanediol

Table 75. Stoichiometry and Reaction Rates for Esterification Reactions with 1,3-propanediol

Stoichiometry	Reaction Rate
$PDO + FDCA \Leftrightarrow T - PDO + \quad T - FDCA + W$	$R_1 = 4k_1[PDO][FDCA] - \frac{k_i}{K_1}[T - PDO] \times \frac{[T - FDCA][W]}{[T - FDCA] + [B - FDCA]}$
$PDO + SA \Leftrightarrow T - PDO + T - SA + W$	$R_{1SA} = 4k_1[PDO][SA] - \frac{k_i}{K_1}[T - PDO] \times \frac{[T - SA][W]}{[T - SA] + [B - SA]}$
$PDO + T - FDCA \Leftrightarrow T - PDO + B - FDCA + W$	$R_2 = 2k_1[PDO][T - FDCA] - \frac{k_1}{K_1}[T - PDO] \times \frac{[B - FDCA][W]}{[T - FDCA] + [B - FDCA]}$
$PDO + T - SA \Leftrightarrow T - PDO + B - SA + W$	$R_{2SA} = 2k_1[PDO][T - SA] - \frac{k_1}{K_1}[T - PDO] \times \frac{[B - SA][W]}{[T - SA] + [B - SA]}$
$T - PDO + FDCA \Leftrightarrow B - PDO + T - FDCA + W$	$R_3 = 2k_2[T - PDO][FDCA] - \frac{k_1}{K_1}[B - PDO] \times \frac{[T - FDCA][W]}{[T - FDCA] + [B - FDCA]}$
$T - PDO + SA \Leftrightarrow B - PDO + T - SA + W$	$R_{3SA} = 2k_2[T - PDO][SA] - \frac{k_1}{K_1}[B - PDO] \times \frac{[T - SA][W]}{[T - SA] + [B - SA]}$
$T - PDO + T - FDCA \Leftrightarrow B - PDO + B - FDCA + W$	$R_4 = k_2[T - PDO][T - PDO] - \frac{k_1}{K_1}[B - PDO] \times \frac{[B - FDCA][W]}{[T - FDCA] + [B - FDCA]}$

$T-PDO+T-SA \Leftrightarrow B-PDO+B-SA+W$	$R_4 = k_2[T-PDO][T-PDO] - \frac{k_1}{K_1}[B-PDO] \times \frac{[B-SA][W]}{[T-SA]+[B-SA]}$

E.2 Stoichiometry and Reaction Rates for Ester Interchange Reactions with 1,3-propanediol

Table 76. Stoichiometry and Reaction Rates for Ester Interchange Reactions with 1,3-propanediol

Stoichiometry	Reaction Rate
$PDO+T-FDCA+B-PDO \Leftrightarrow T-PDO+T-FDCA+T-PDO$	$R_5 = 2k_3[PDO][B-PDO] \times \frac{[T-FDCA]}{[T-FDCA]+[B-FDCA]} - \frac{k_3}{K_3}[T-PDO][T-PDO] \times \frac{[T-FDCA]}{[T-FDCA]+[B-FDCA]}$
$PDO+T-SA+B-PDO \Leftrightarrow T-PDO+T-SA+T-PDO$	$R_{5SA} = 2[PDO][B-PDO] \times \frac{[T-SA]}{[T-SA]+[B-SA]} - \frac{k_3}{K_3}[T-PDO][T-PDO] \times \frac{[T-SA]}{[T-SA]+[B-SA]}$
$PDO+B-FDCA+B-PDO \Leftrightarrow T-PDO+B-FDCA+T-PDO$	$R_6 = 2k_3[PDO][B-PDO] \times \frac{[B-FDCA]}{[T-FDCA]+[B-FDCA]} - \frac{k_3}{K_3}[T-PDO][T-PDO] \times \frac{[B-FDCA]}{[T-FDCA]+[B-FDCA]}$
$PDO+B-SA+B-PDO \Leftrightarrow T-PDO+B-SA+T-PDO$	$R_{6SA} = 2k_3[PDO][B-PDO] \times \frac{[B-SA]}{[T-SA]+[B-SA]} - \frac{k_3}{K_3}[T-PDO][T-PDO] \times \frac{[B-SA]}{[T-SA]+[B-SA]}$

E.3 Mass balances of monomers

Table 77. Mass balances of monomers

Species	Mass Balance
1,3-propanediol (PDO)	$\frac{d[PDO]}{dt} = -R_1 - R_2 - R_5 - R_6 - R_{1SA} - R_{2SA} - R_{5SA} - R_{6SA}$
2,5-furandicarboxylic acid (FDCA)	$\frac{d[FDCA]}{dt} = -R_1 - R_3$
Succinic acid (SA)	$\frac{d[SA]}{dt} = -R_{1SA} - R_{3SA}$
Water (W)	$\frac{d[W]}{dt} = R_1 + R_2 + R_3 + R_6 + R_{1SA} + R_{2SA} + R_{3SA} + R_{6SA}$

PDO end segment (T-PDO)	$\frac{d[T-PDO]}{dt} = R_1 + R_2 - R_3 - R_4 + 2R_5 + 2R_6 + R_{1SA} + R_{2SA} - R_{3SA} - R_{4SA} + 2R_{5SA} + 2R_{6SA}$
PDO bound segment (B-PDO)	$\frac{d[B-PDO]}{dt} = R_1 - R_2 + R_3 - R_4 + R_{1SA} - R_{2SA} + R_{3SA} - R_{4SA}$
FDCA end segment (T-FDCA)	$\frac{d[T-FDCA]}{dt} = -R_1 - R_5 + R_3 - R_4$
FDCA bound segment (B-FDCA)	$\frac{d[B-FDCA]}{dt} = R_2 + R_4$
SA end segment (T-SA)	$\frac{d[T-SA]}{dt} = -R_{1SA} - R_{5SA} + R_{3SA} - R_{4SA}$
SA bound segment (B-SA)	$\frac{d[B-SA]}{dt} = R_{2SA} + R_{4SA}$

E.4 Estimated kinetic parameters using the Lehtonen and Salmi model

Table 78. Estimated kinetic parameters using the Lehtonen and Salmi model

Polyester	k_o x 10^4, kg·mol^{-1} min^{-1}	K	E_a, kJ·mol^{-1}
PPeS	3.45	179.1	57.5
PPeF$_{15}$S$_{85}$	1.02	76.9	50.6
PPeF$_{30}$S$_{70}$	1.59	74.0	54.2
PPeF$_{70}$S$_{30}$	0.59	25.8	50.54
PPeF$_{85}$S$_{15}$	1.39	14.24	54.5
PPeF	0.92	20.32	52.8

E.5 Sensitivity analysis of the kinetic coefficient k, activation energy E_a and equilibrium constant K

Figure 179 below shows the calculated sensitivity, a negative value for these ones indicate that an increase in the mol concentrations led to a decrease in the dependent variable as activation energy, Kinetic coefficient and the equilibrium constant. As it can be seen, if the sensitivities have the same percentage increase or decrease, there will be no change in the final concentrations. In addition, the total change for sensitivities are 0.0349 -0.4580 +

0.0941 -= -0.3290 each ones have been evaluated at 400 minutes. From these results, it is noticed that only the C_{OH} concentration displayed a modest sensitivity, the rest of the concentrations (C_{COOH}, C_{COOR} and C_{H2O}) do not have any significant change.

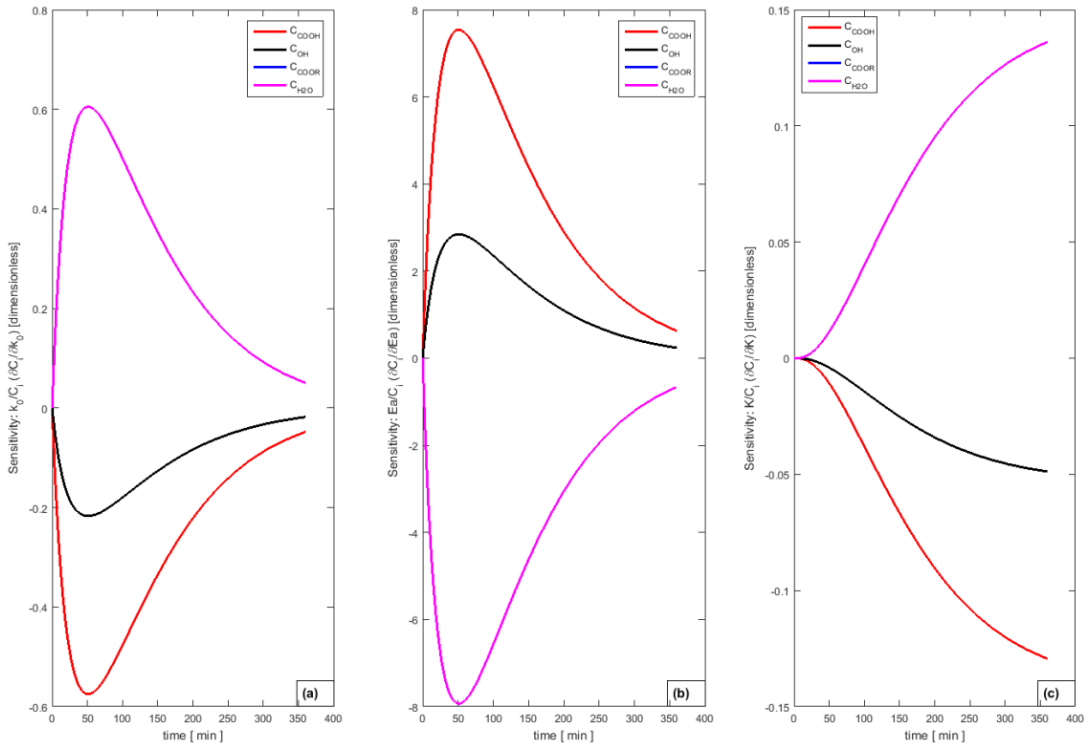

Figure 179. Sensitivity analysis of the kinetic coefficient k, activation energy E_a and equilibrium constant K.

E. 6 General Matlab code for the solution of the objective function and estimation of kinetic parameters

```
%Objective function min z=(Ca exp-Camod)^2
clc;clear all; format compact;

%Problem parameters
COOHo=0.7178423; %Initial Concentration
CH2Oo=0; % water concentration
CCOORo=0; %ester concentration
Vo=0.423240; %initial volume
b0=0.5; %algebraic excess of the hydroxygroup at the beginning of reaction
T= 230+273.15; %K
R= 8.314; %J/mol K
COHo=0.7178423+b0; %Diol concentration, according to Fradet and Marechal
t=[0
30
60
90
120
150
180
240
```

```
270
300
330
360]';
COOH= [0.7178423
0.3355556
0.1623134
0.1250000
0.0991736
0.0883534
0.0617284
0.0403846
0.0180328
0.0169082
0.0106383
0.0087719
]'; %mol/kg

np=length(t); %calculate number of experimental points
tH2O=[0
8
12
19
30
37
41
46
51
55
59
62
68
73
77
82
87
95
99
116
122
]; %min
QH2O=[0
0.000186988
0.000291056
0.000341589
0.000382715
0.000404429
0.000425543
0.000444005
0.000449111
0.000461588
0.00047242
0.000489649
0.000483035
0.000484078
0.000491309
0.000491764
0.000492176
0.000476988
0.00047788
```

```
0.000429374
0.000428729]; % mass flow of water, g/min
mH2O=[0
0.001495904
0.003492674
0.006490198
0.011481453
0.01496389
0.017447257
0.020424224
0.022904657
0.025387324
0.027872801
0.030358207
0.032846365
0.035337672
0.037830756
0.040324682
0.042819283
0.045313875
0.047310089
0.049807435
0.052304977
]; %mass of water , kg
np=length(t); %calculate number of experimental points

%%%%%%%%Estimation of parameters%%%%%%%%%%%%
%Initial estimates k0, Eao, Ko %kinetic coefficient, activation energy,
%equlibrium constant
k0=0.033854;%Rate constant
Ea0=60000; %Activation energy, J/mol
K0=30; %Equilibrium constant
%Vector of initial estimates
x0=[k0 Ea0 K0];
% trust-region-reflective
options=optimset('LargeScale','off', 'Display','iter','tolfun',1e-
9);%,'algorithm','levenberg-marquardt');
lb(1:3) = -inf; ub(1:3) = inf;

[x, Zmin, Zt,
flag,output,grad_Z]=lsqnonlin(@kineticsml80lehtonen,x0,lb,ub,options,t,np,C
OOHo,CH2Oo,CCOORo,COHo,T,R,b0,COOH,Vo,tH2O, mH2O, QH2O)
%Reasignation
k=x(1); Ea=x(2); K=x(3); %parameter reasignation
fprintf('k=%f\n',k)
fprintf('Ea=%f\n',Ea)
fprintf('K=%f\n',K)
[ts,y]=ode15s(@lehtonenmodelml80,[0,t(end)],[COOHo,COHo,CCOORo,CH2Oo,Vo],[]
,k,Ea,K,t,np,COOHo,CH2Oo,CCOORo,COHo,T,R,b0,COOH,Vo,tH2O, mH2O, QH2O);
C_COOH=y(:,1); COH=y(:,2); CCOOR=y(:,3); CH2O=y(:,4); V=y(:,5);
figure(1),subplot(1,2,1),plot(ts,C_COOH,'--',t,COOH,'*')
legend('C_{COOH}^{mod}','C_{COOH}^{exp}')
subplot(1,2,2),
plot(ts,C_COOH,'*r',ts,COH,'-ok',ts,CCOOR,'ob',ts,CH2O,'*m')
xlabel('time, min'), ylabel('Ci, mol/kg')
legend('C_{COOH}','C_{OH}','C_{COOR}','C_{H2O}')
%File for the estimation of kinetic parameters
function Z=kineticsml80lehtonen(x,t,np,COOHo,CH2Oo,CCOORo,COHo,T,R,b0,COOH,
Vo,QH2O,mH2O, tH2O)
%Concentration in mmol/L
```

```
zz1 = [0
 38.04
22.50
11.50
24.36
69.91
92.68
106.96
109.03
96.59
80.93
81.32
65.99
48.44
38.54
33.84
30.09
30.13
26.37
14.79
13.70
];
CH2O = zz1/1000;
k=x(1); Ea=x(2); K=x(3);
sol=ode15s(@lehtonenmodelml80,[0,t(end)],[COOHo,COHo,CCOORo,CH2Oo,Vo],[],k,
Ea,K,t,np,COOHo,CH2Oo,CCOORo,COHo,T,R,b0,COOH,Vo,tH2O, mH2O, QH2O);
stint = deval(sol,t);
COOH_mod = stint(1,:);
stint_H2O = deval(sol,tH2O);
CH2O_mod = stint_H2O(4,:);
Z1 = COOH - COOH_mod; % lsqnonlin
Z = Z1;
% end of file
%Star of the model routine
function dCdt=lehtonenmodelml80(ti,y,
k,Ea,K,t,np,COOHo,CH2Oo,CCOORo,COHo,T,R,b0,COOH,Vo,tH2O, mH2O, QH2O)
C_COOH=y(1); COH=y(2); CCOOR=y(3); CH2O=y(4); V=y(5);
%% reaction rates
rCOOH=-(k*exp(-Ea/(R*T)))*(C_COOH*COH-(CCOOR*CH2O)/K); %reaction rate of
COOH
rOH=rCOOH;
rCCOOR=-rCOOH;
rH2O=-rCOOH;
%%%%With distillate correction
if ( ti<= tH2O(end)  )
    QH2Oi = interp1(tH2O,QH2O,ti);
    mH2Oi = interp1(tH2O,mH2O,ti);
    %With diatillate correction
    dH2Odt= rH2O -QH2Oi/(mH2Oi*V)-(C_COOH*QH2Oi)/V;
    dVdt=-QH2Oi;
else
    QH2Oi = 0;
    mH2Oi = 0;
    %With diatillate correction
    dH2Odt= rH2O;
    dVdt= 0;
end % if
%Mass Balance of all species
dCOOHdt=rCOOH ;
dOHdt=rOH;
```

```
dCCOORdt=rCCOOR;
dH2Odt=rH2O;
dCdt=[dCOOHdt dOHdt dCCOORdt dH2Odt dVdt]';
%end
```

E. 7. Pareto frontiers batch reactor

E.7.1 PPeFS 30/70

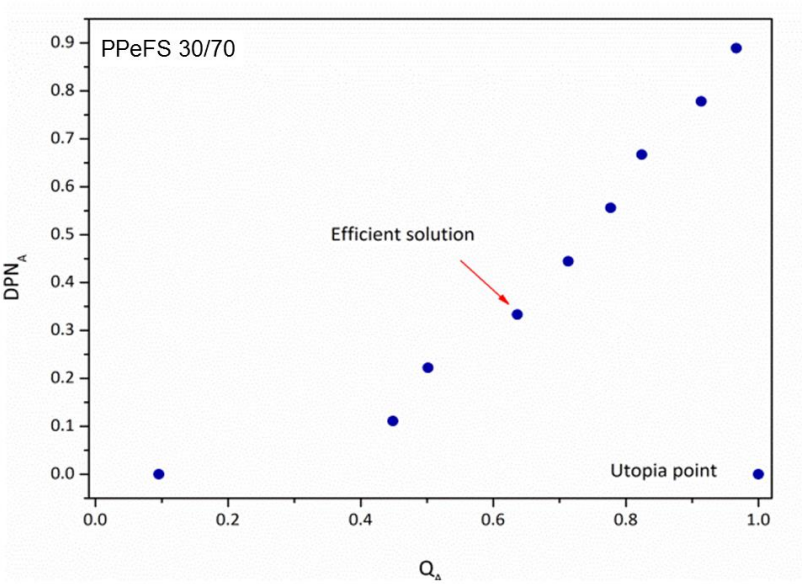

Figure 180. Batch Pareto frontier PPeFS 30/70.

E.7.2 PPeFS 70/30

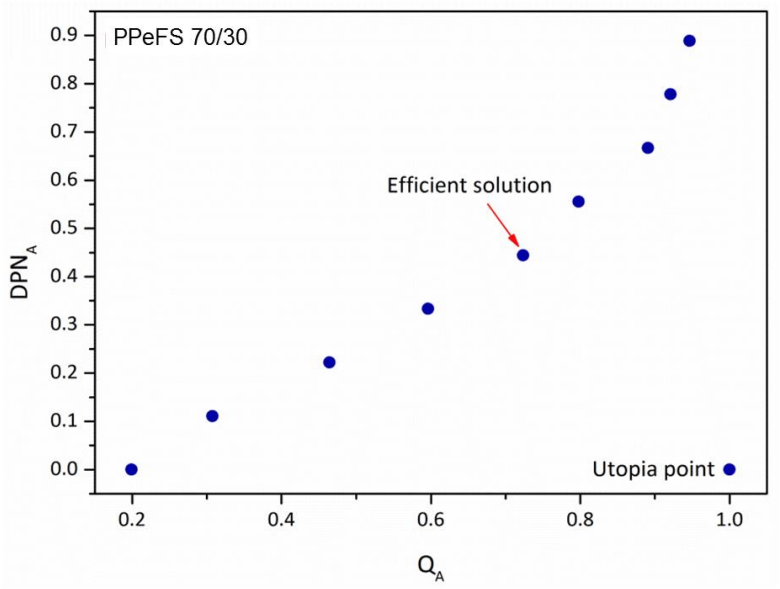

Figure 181. Batch Pareto frontier PPeFS 70/30.

E.7.3 PPeF

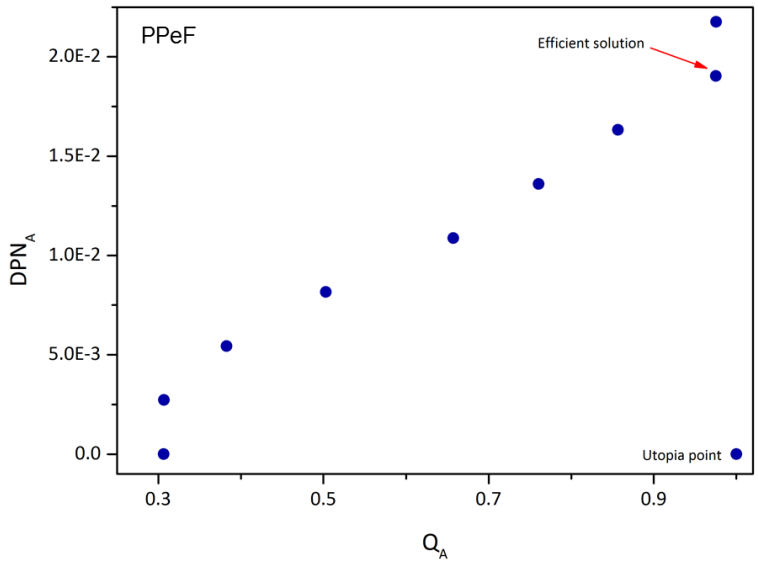

Figure 182. Batch Pareto frontier PPeF.

E.7.4 PPFPS 15/85

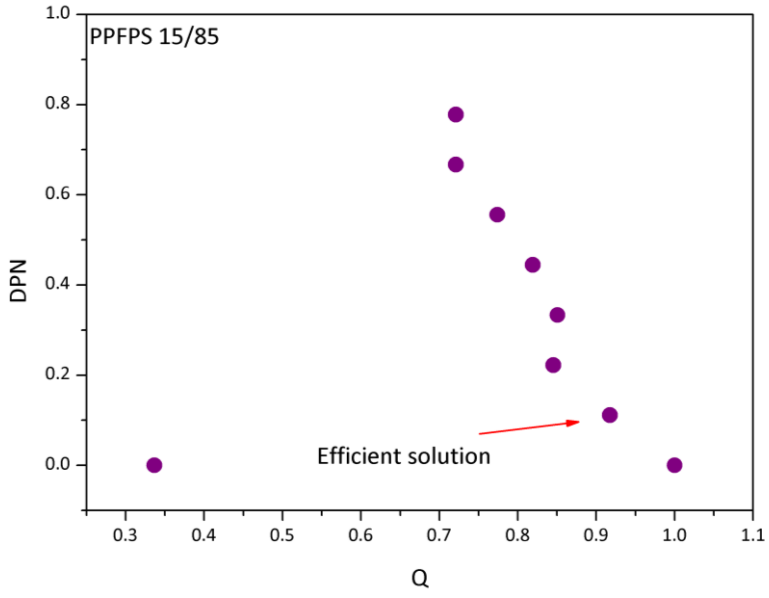

Figure 183. Batch Pareto frontier PPFPS 15/85.

E.7.5 PPFPS 70/30

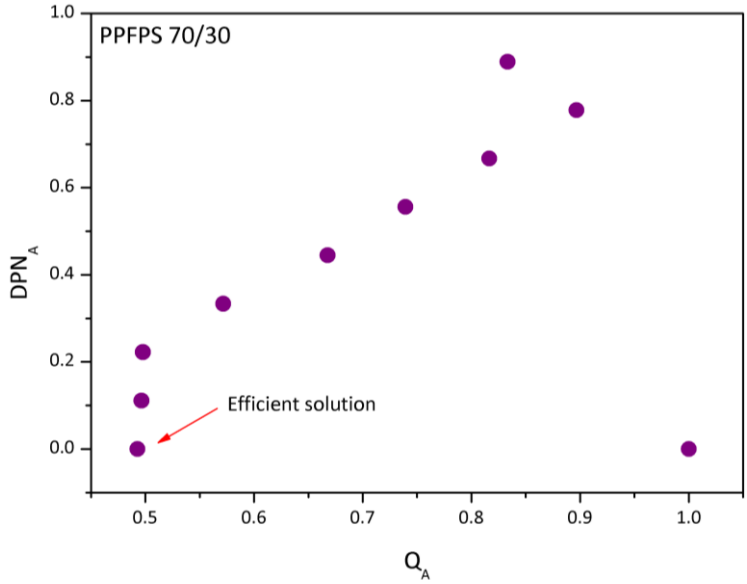

Figure 184. Batch Pareto frontier PPFPS 70/30.

E.7.6 PPFPS 85/15

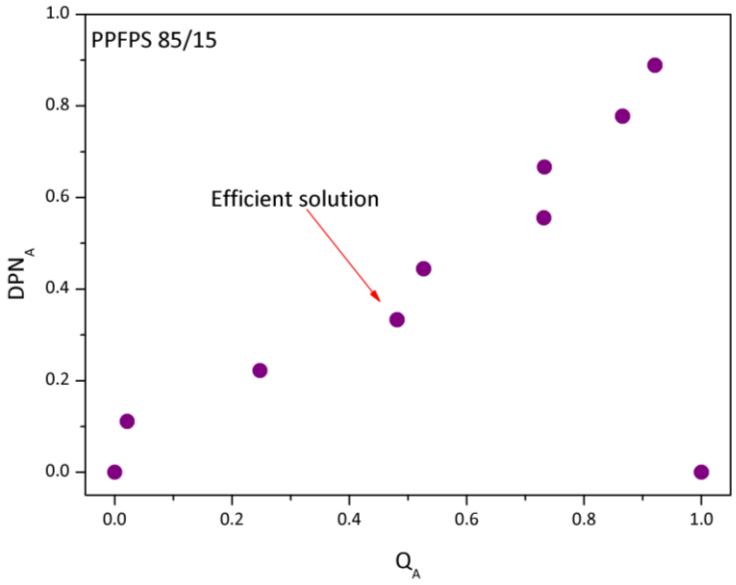

Figure 185. Batch Pareto frontier PPFPS 85/15.

E.8 Segments' concentration profiles

E.8.1 PPeS

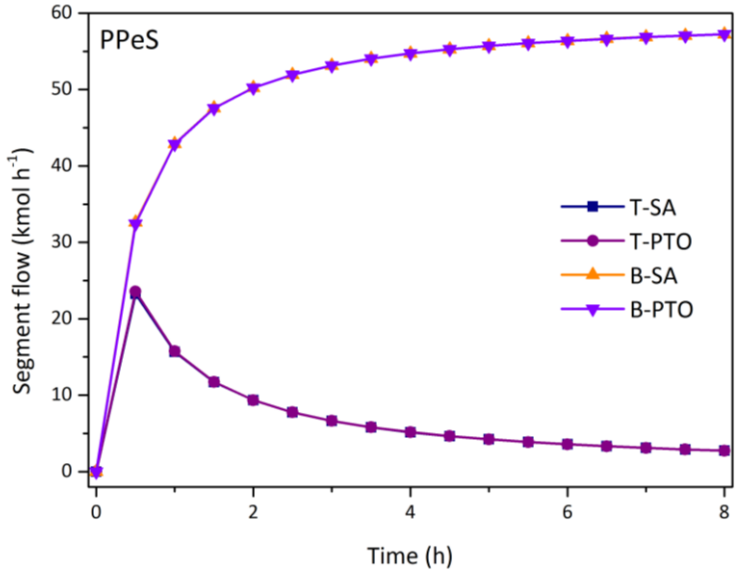

Figure 186. Batch segments' concentration profiles for PPeS.

E.8.2 PPeFS 15/85

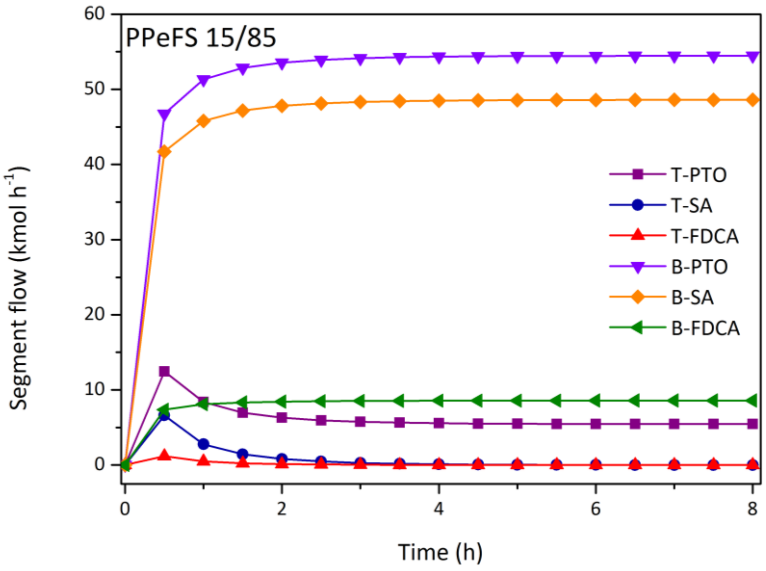

Figure 187. Batch segments' concentration profiles for PPeFS 15/85.

E.8.3 PPeFS 30/70

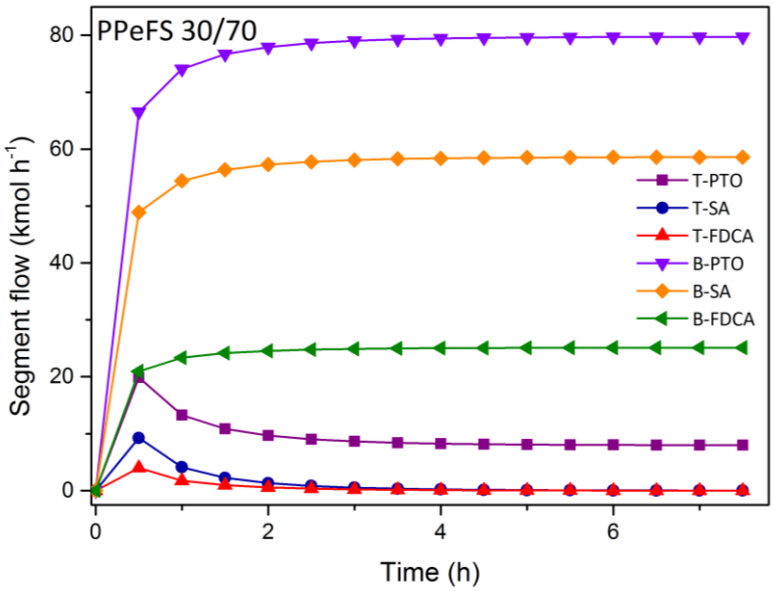

Figure 188. Batch segments' concentration profiles for PPeFS 30/70.

E.8.4 PPeFS 85/15

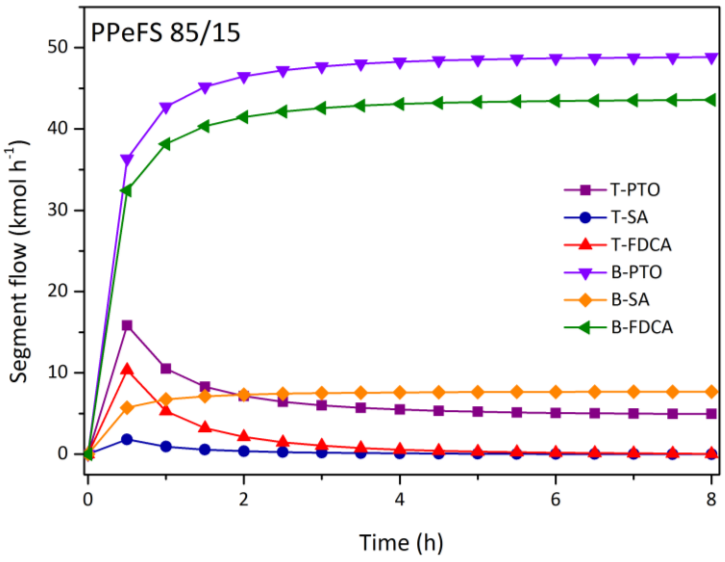

Figure 189. Batch segments' concentration profiles for PPeFS 85/15.

E.8.5 PPeF

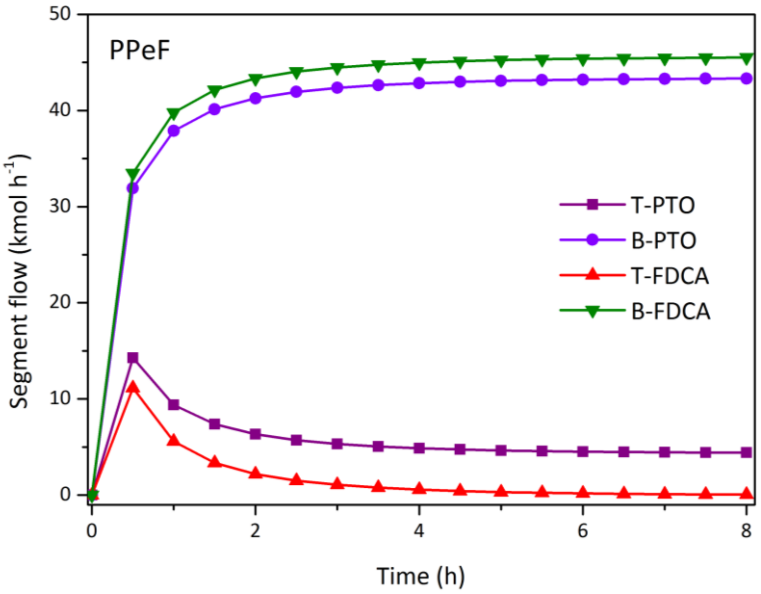

Figure 190. Batch segments' concentration profiles for PPeF.

E.8.6 PPS

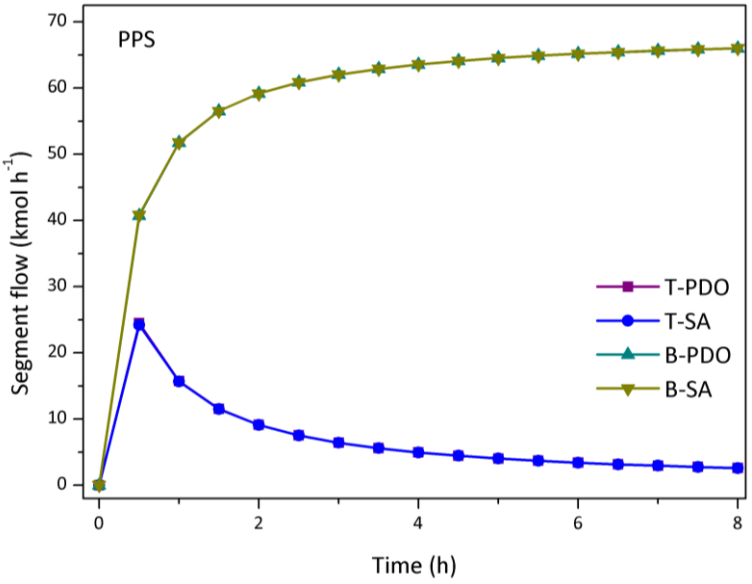

Figure 191. Batch segments' concentration profiles for PPS

E.8.7 PPFPS 30/70

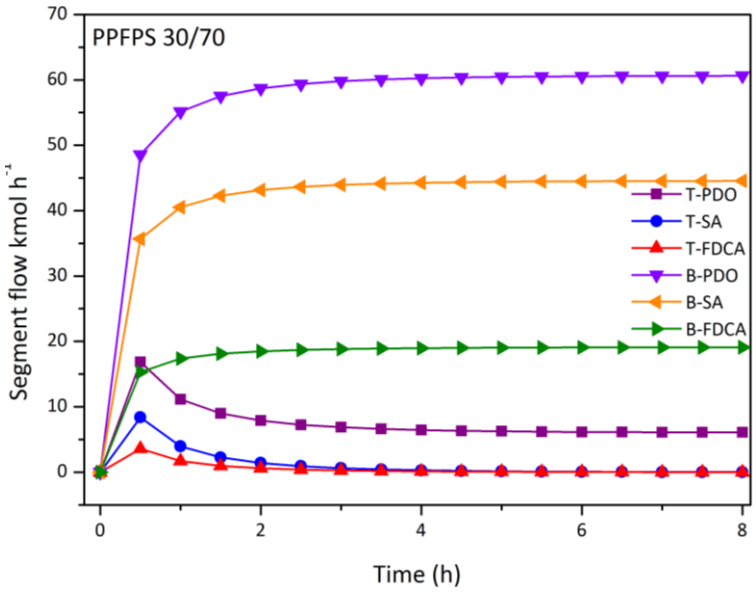

Figure 192. Batch segments' concentration profiles for PPFPS 30/70.

E.8.8 PPFPS 70/30

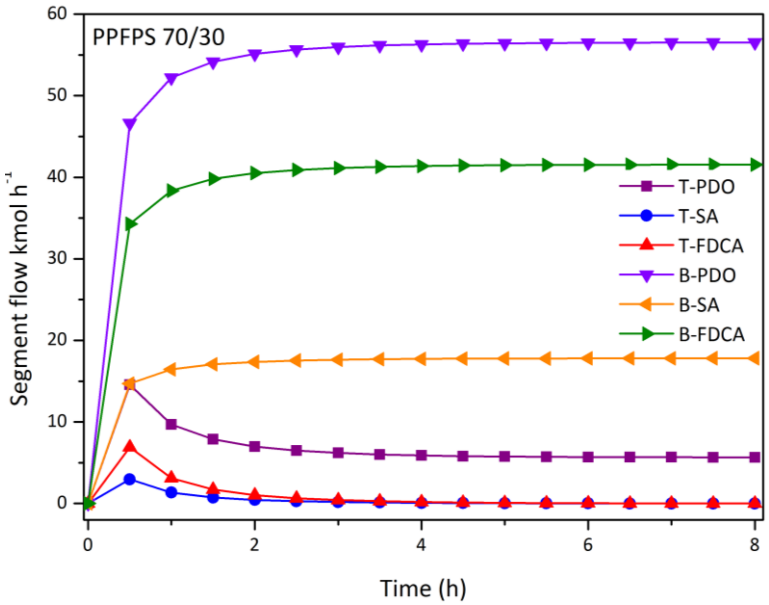

Figure 193. Batch segments' concentration profiles for PPFPS 30/70.

E.8.9 PPFPS 85/15

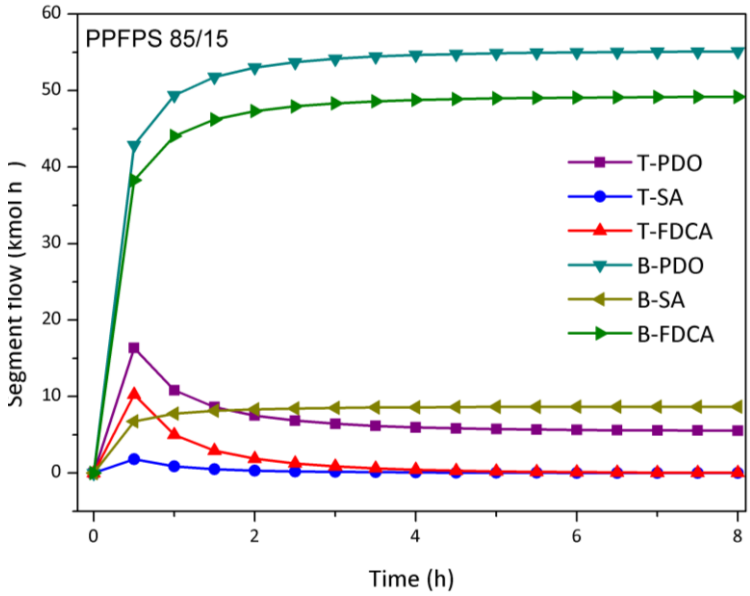

Figure 194. Batch segments' concentration profiles for PPFPS 85/15.

E.8.10 PET

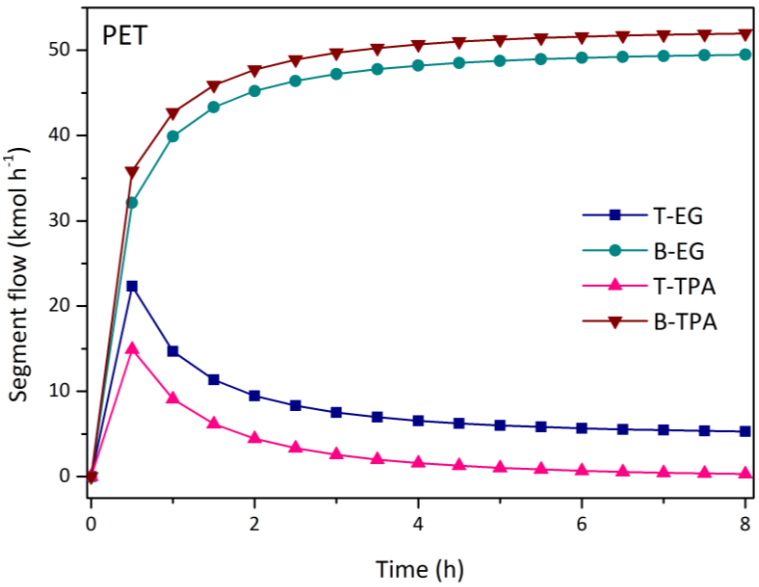

Figure 195. Batch segments' concentration profiles for PET.

E.9 M_n and DPN profiles

E.9.1 PPeS

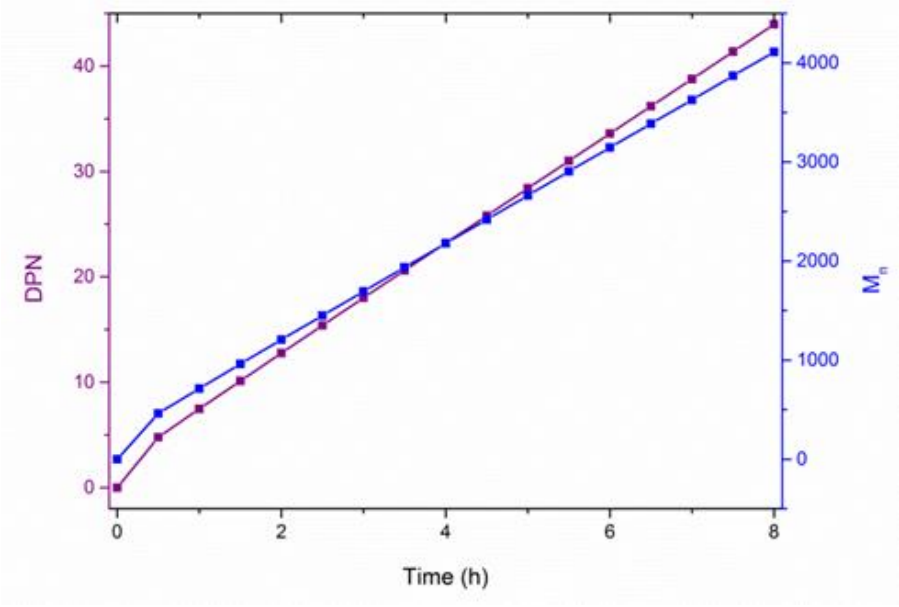

Figure 196. Batch M_n and DPN profiles for PPeS.

E.9.2 PPeFS 15/85

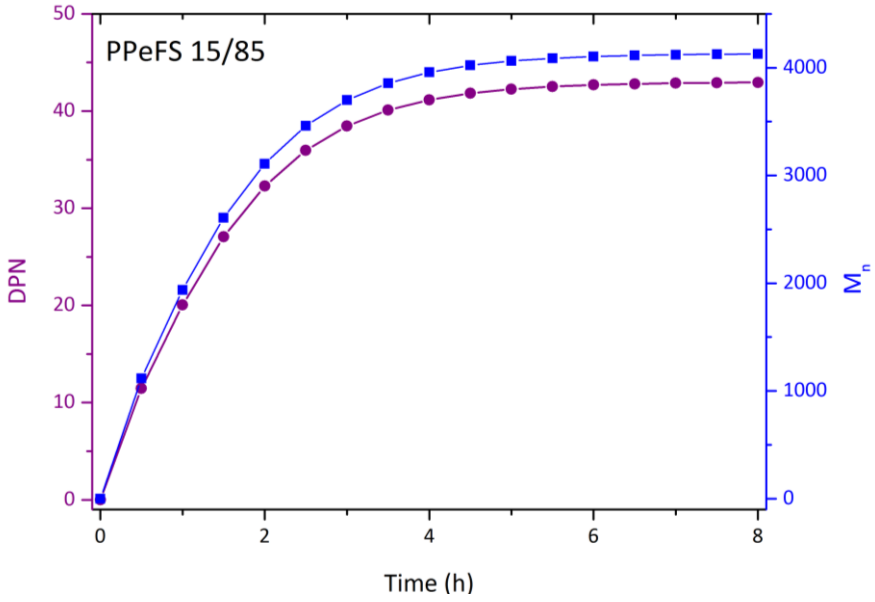

Figure 197. Batch M_n and DPN profiles for PPeFS 15/85.

E.9.3 PPeFS 70/30

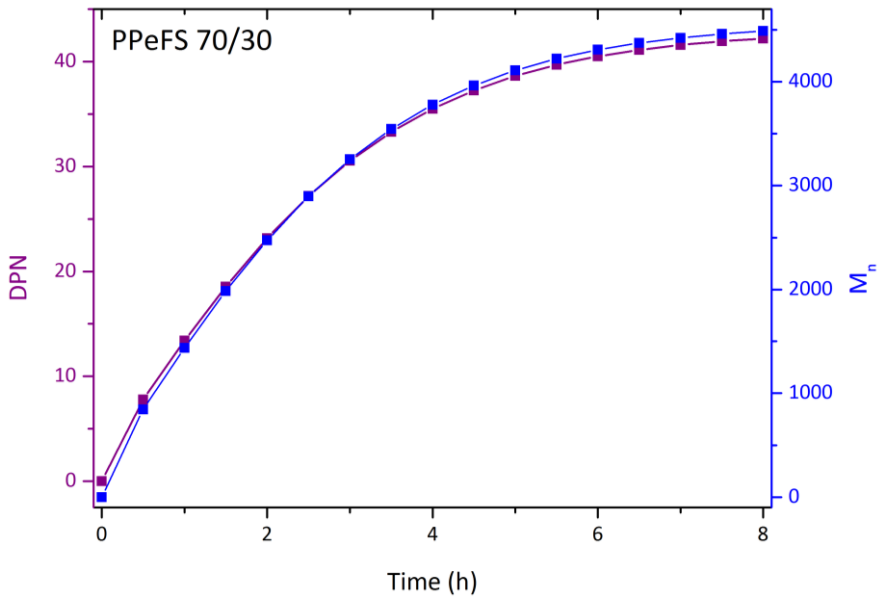

Figure 198. Batch M_n and DPN profiles for PPeFS 70/30.

E.9.4 PPeF

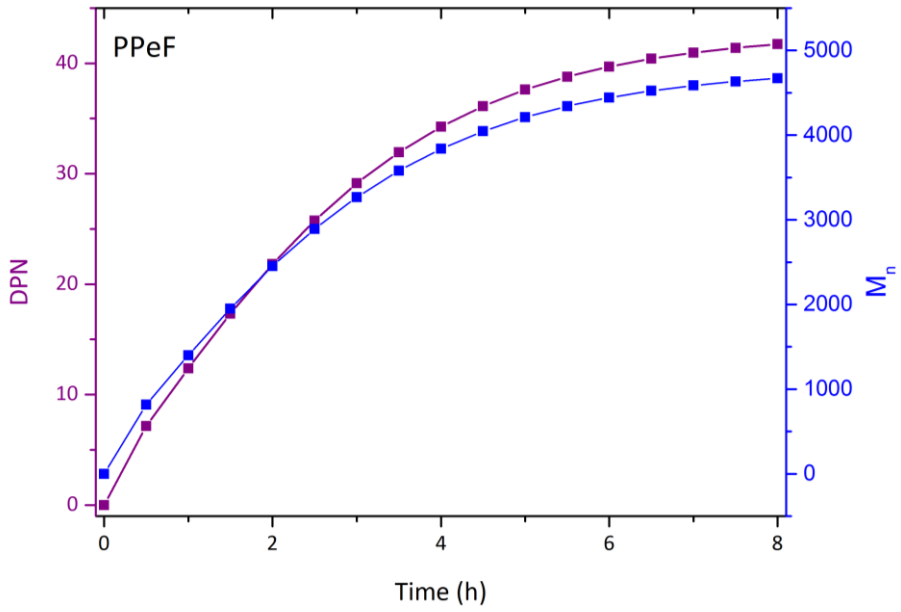

Figure 199. Batch M_n and DPN profiles for PPeF.

E.9.5 PPS

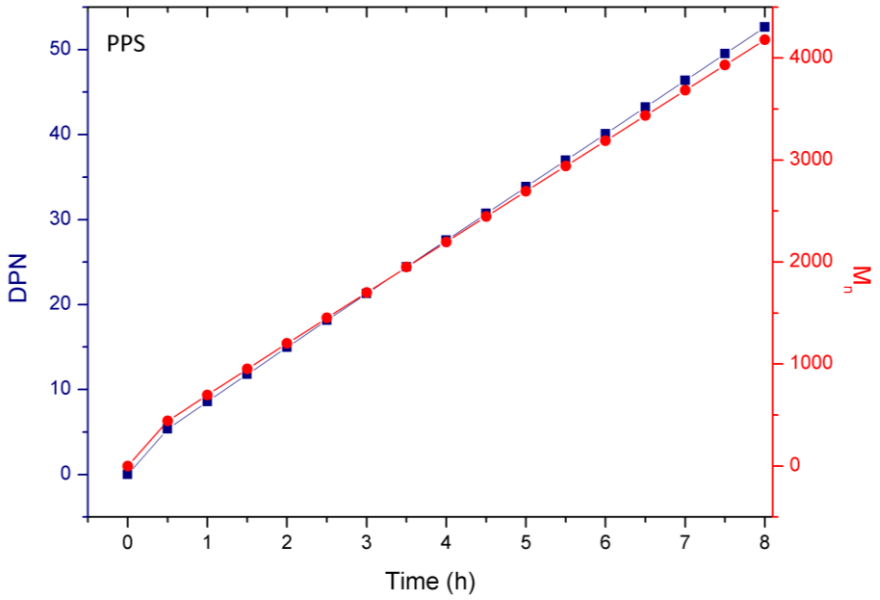

Figure 200. Batch M_n and DPN profiles for PPS.

E.9.6 PPFPS 15/85

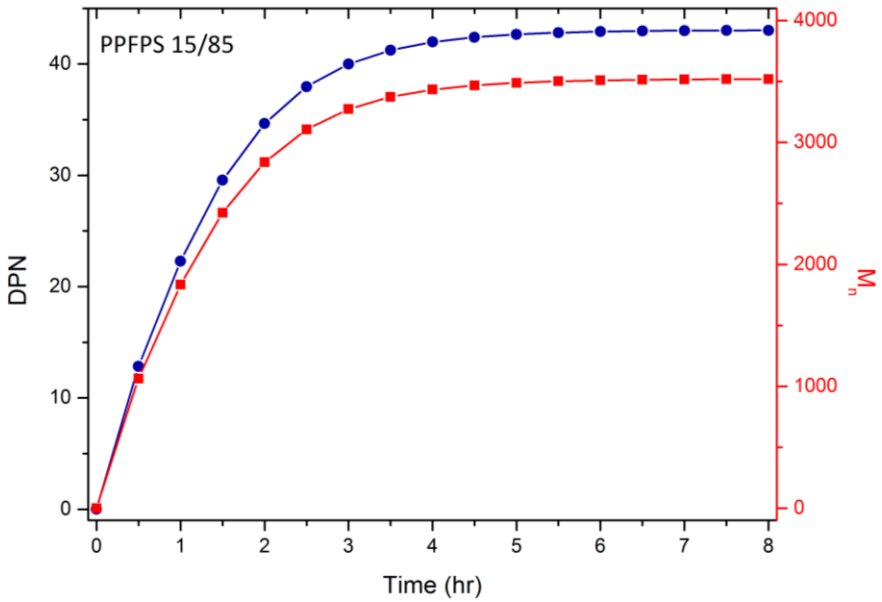

Figure 201. Batch M_n and DPN profiles for PPFPS 15/85.

E.9.7 PPFPS 30/70

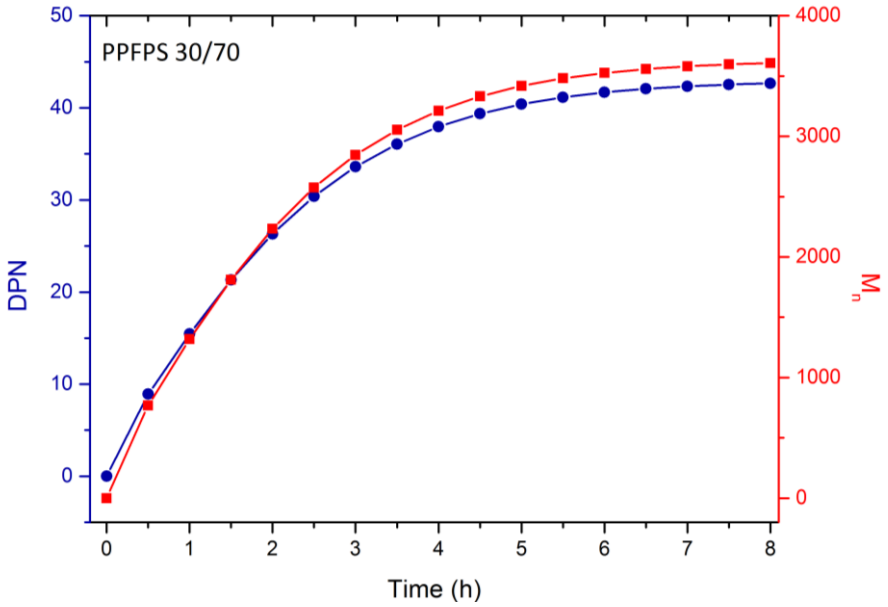

Figure 202. Batch M_n and DPN profiles for PPFPS 30/70.

E.9.8 PPFPS 70/30

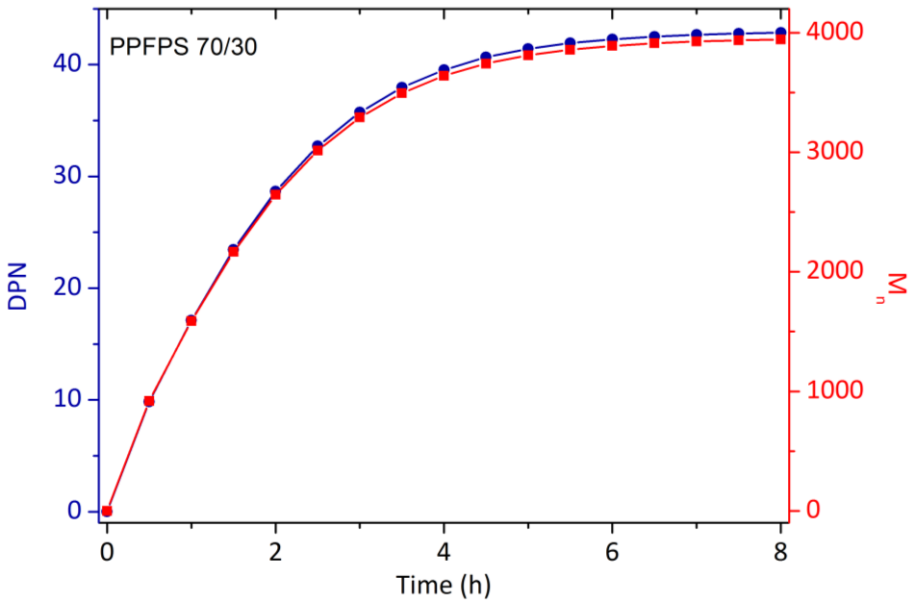

Figure 203. Batch M_n and DPN profiles for PPFPS 70/30.

E.9.9 PPFPS 85/15

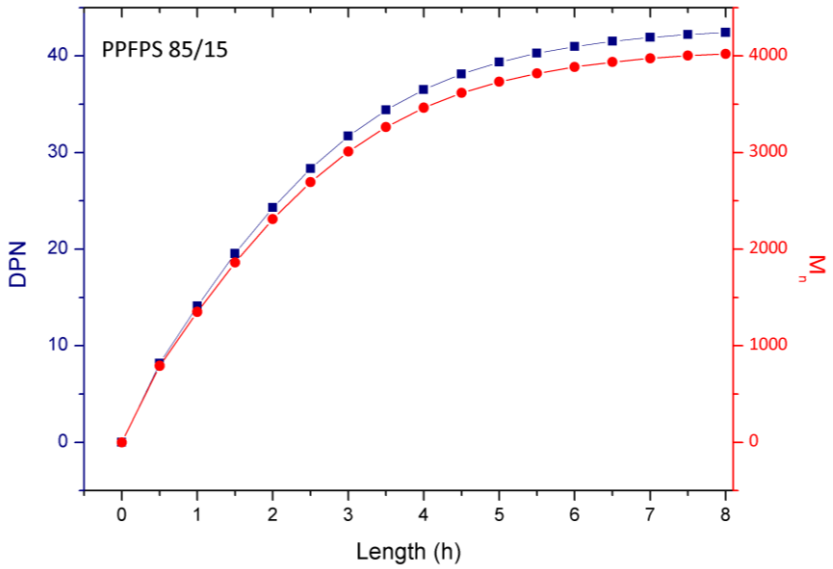

Figure 204. Batch M_n and DPN profiles for PPFPS 85/15.

E.9.10 PET

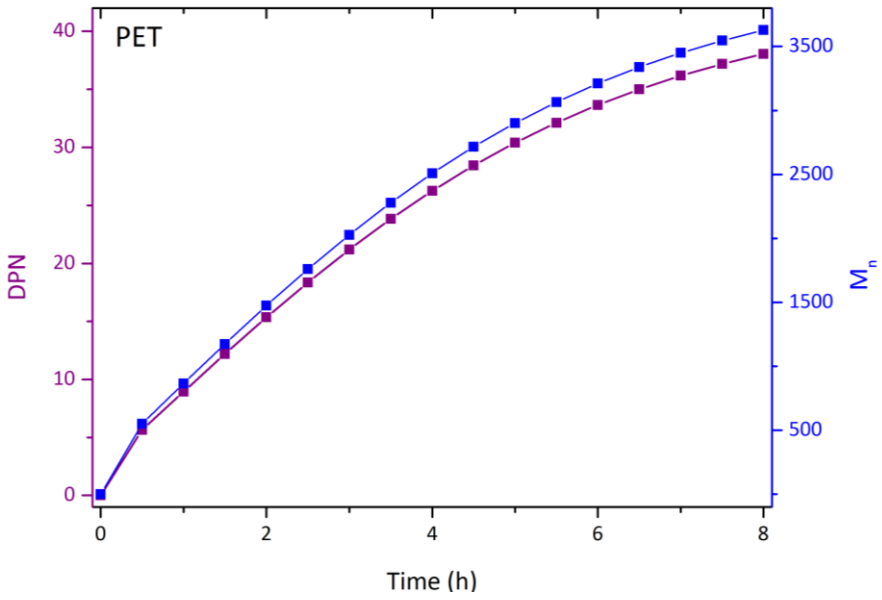

Figure 205. Batch M_n and DPN profiles for PET.

E.10 Sustainability Indicators for PPS and PPFPS (Batch)

Table 79. Sustainability Indicators for PPS and PPFPS (Batch)

Polyester	$GWP_{natural\ gas}$ $kg \cdot kg^{-1}$	GWP_{coal} $kg \cdot kg^{-1}$	R_{SEI} $kBTU \cdot kg^{-1}$	RME $kg \cdot kg^{-1}$	MI $kg \cdot kg^{-1}$
PPS	0.12	0.22	1.71	0.82	1.22
PPFPS 15/85	0.12	0.22	1.75	0.82	1.22
PPFPS 30/70	0.12	0.22	1.72	0.83	1.21
PPFPS 70/30	0.10	0.18	1.65	0.84	1.19
PPFPS 85/15	0.11	0.20	1.60	0.84	1.19

E.11 Total mass of product and reagents for the calculation of the reaction mass efficiency and mass intensity

Polymer	Mass of reagents, $kg \cdot h^{-1}$	Mass of polymer, $kg \cdot h^{-1}$
PPeS	1666.67	1401.42
$PPeF_{15}S_{85}$	1666.67	1407.33
$PPeF_{30}S_{70}$	1666.67	1413.52
$PPeF_{70}S_{30}$	1666.67	1428.75
$PPeF_{85}S_{15}$	1666.67	1434.00
PPeF	1511.98	1305.43
PPS	1666.67	1362.78
$PPS_{15}PF_{85}$	1666.67	1370.37
$PPS_{30}PF_{70}$	1511.98	1250.50
$PPS_{70}PF_{30}$	1666.67	1397.96
$PPS_{85}PF_{15}$	1666.67	1404.67
PET	1511.98	1276.16

Appendix F (Chapter 7)

F.1 ε-Constraint Optimisation Results for PPS and PPFPS during the PFR Synthesis

Table 80. ε-Constraint Optimisation Results for PPS and PPFPS during the PFR Synthesis

Polyester	Temperature, °C	M_n, Da	DPN	Polymer produced, kg·hr^{-1}	Heat Duty, kBTU·hr^{-1}
PPS	214	9077	53	1360	2447
PPFPS 15/85	215.6	3517	43	1370	2410
PPFPS 30/70	214	3636	43	1250	2146
PPFPS 70/30	217	3956	43	1398	2287
PPFPS 85/15	219.5	3999	42	1408	2268

F.2 Sensitivity Analysis for the Reactive Distillation Configuration for PPS and PPFPS

Table 81. Sensitivity Analysis for the Reactive Distillation Configuration for PPS and PPFPS

Polyester	Temperature (T_3-T_5), °C	M_n	DPN	Polymer produced, kg·hr^{-1}	Heat Duty, kBTU·hr^{-1}
PPS	215,215,215	2103	26	1363	1426
PPFPS 15/85	220,230,23	2658	32	1372	2232
PPFPS 30/70	220,220,230	2118	25	1381	2182

PPFPS 70/30	230,230,230	2359	26	1381	2182
PPFPS 85/15	225,220,230	2330	25	1407	2085

F.3 Temperature Distribution for Reactive Distillation

Table 82. Temperature Distribution for Reactive Distillation

CSTR	PPS	PPFPS 15/85	PPFPS 30/70	PPFPS 70/30	PPFPS 85/15
$T_{condenser}$, °C	121	121	121	121	121
T_1, °C	215	230	230	230	230
T_2, °C	215	230	230	210	230
T_3, °C	215	220	220	230	225
T_4, °C	215	230	220	230	220
T_5, °C	215	230	230	230	230
T_6, °C	185	210	210.5	210	211
$T_{reboiler}$, °C	230	230	230	230	230
Split fraction	0.30	0.30	0.30	0.35	0.35

F.4 Sensitivity Analysis for the Divided Wall Configuration for PPS and PPFPS

Table 83. Sensitivity Analysis for the Divided Wall Configuration for PPS and PPFPS

Polyester	Temperature (T_3-T_5), °C	M_n	DPN	Polymer produced, kg·hr^{-1}	Heat Duty, kBTU·hr^{-1}
PPS	210,220,230	851	11	1363	1200
PPFPS 15/85	210,220,230	3024	37	1372	1233
PPFPS 30/70	225,210,230	2639	31	1380	1201
PPFPS 70/30	230,220,225	2873	31	917	1168
PPFPS 85/15	225,220,230	2965	31	1406	1160

F.5 Temperature Distribution for Divided Wall

Table 84. Temperature Distribution for Divided Wall

CSTR	PPS	PPFPS 15/85	PPFPS 30/70	PPFPS 70/30	PPFPS 85/15
$T_{condenser}$, °C	121	121	121	121	121
T_1, °C	230	230	230	230	230
T_2, °C	230	230	230	210	230
T_3, °C	210	210	225	230	225
T_4, °C	220	220	210	220	220
T_5, °C	230	230	230	225	230
T_6, °C	225	225	230	230	230
T_7, °C	210	210	210	210	211
$T_{reboiler}$, °C	230	230	230	230	230
Split fraction	0.40	0.30	0.35	0.35	0.35

F.6 Sustainability Indicators for PPS and PPFPS

Table 85. Sustainability Indicators for PPS and PPFPS

Polyester	R_{SEI}[a] kBTU·kg^{-1}	RME[b] kg·kg^{-1}	MI[c] kg·kg^{-1}	$GWP_{natural\ gas}$[d] kg·kg^{-1}	GWP_{coal} kg·kg^{-1}
PFR					
PPS	1.80	0.82	1.22	0.12	0.23
PPFPS 15/85	1.76	0.82	1.22	0.12	0.22
PPFPS 30/70	1.71	0.83	1.20	0.12	0.22
PPFPS 70/30	1.64	0.84	1.19	0.09	0.19
PPFPS 85/15	1.61	0.84	1.19	0.11	0.20
Polyester	**R_{SEI}**	**RME**	**MI**	**GWP**	**GWP**
Reactive Distillation					
PPS	1.05	0.82	1.22	0.74	1.34
PPFPS 15/85	1.63	0.82	1.22	0.20	0.37
PPFPS 30/70	1.58	0.83	1.20	0.19	0.34
PPFPS 70/30	1.58	0.83	1.21	0.19	0.34
PPFPS 85/15	1.48	0.84	1.18	0.18	0.32
Polyester	**R_{SEI}**	**RME**	**MI**	**GWP**	**GWP**
Divided Wall					
PPS	1.81	0.82	1.22	0.22	0.40
PPFPS 15/85	1.69	0.97	1.02	0.21	0.40
PPFPS 30/70	1.69	0.83	1.21	0.25	0.45
PPFPS 70/30	1.05	0.55	1.82	0.32	0.58
PPFPS 85/15	1.34	0.84	1.18	0.21	0.38

F.7 Pareto frontiers PFR

F.7.1 PPeS

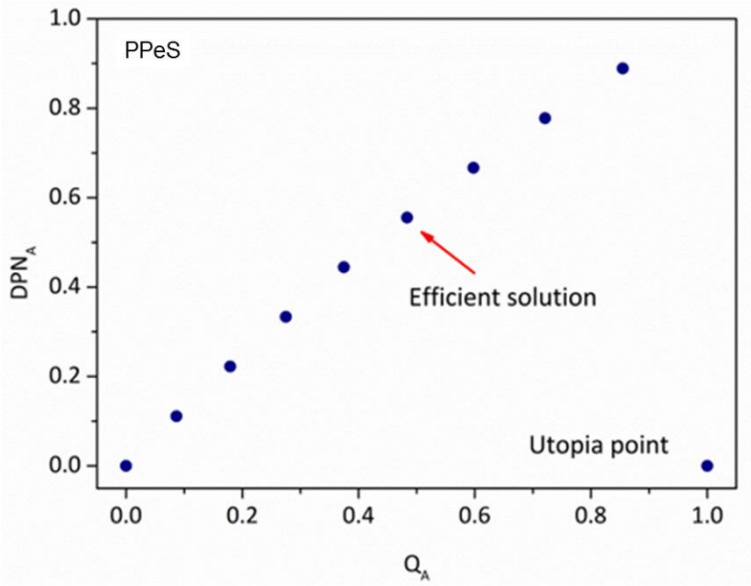

Figure 206. PFR Pareto frontier for PPeS.

F.7.2 PPeFS 30/70

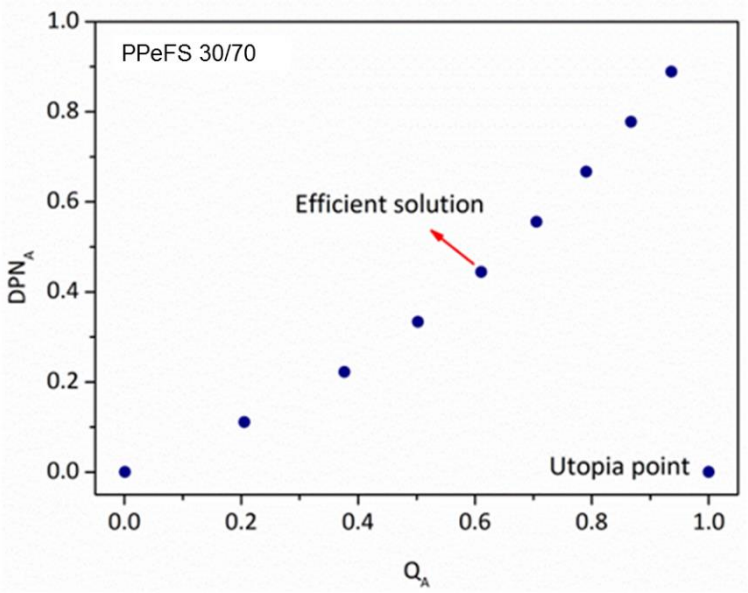

Figure 207. PFR Pareto frontier for PPeFS 30/70.

F.7.3 PPeFS 70/30

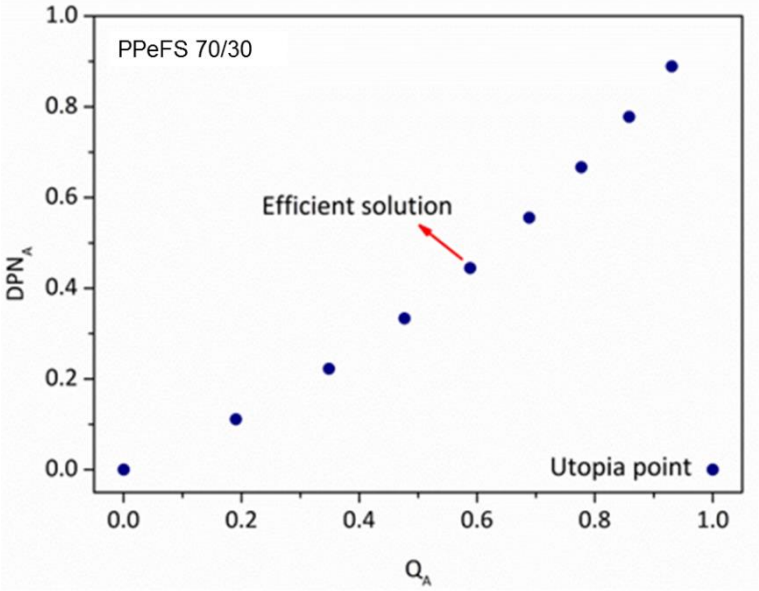

Figure 208. PFR Pareto frontier for PPeFS 70/30.

F.7.4 PPeF

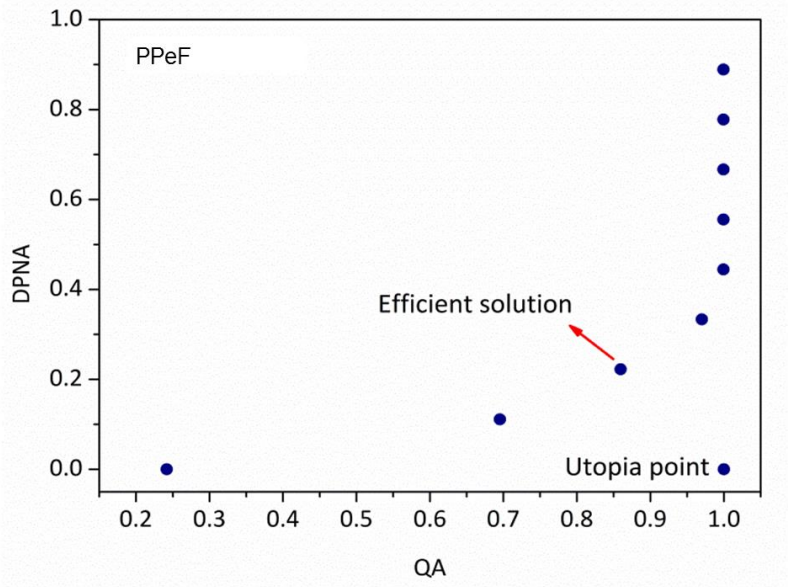

Figure 209. PFR Pareto frontier for PPeF.

F.7.5 PPS

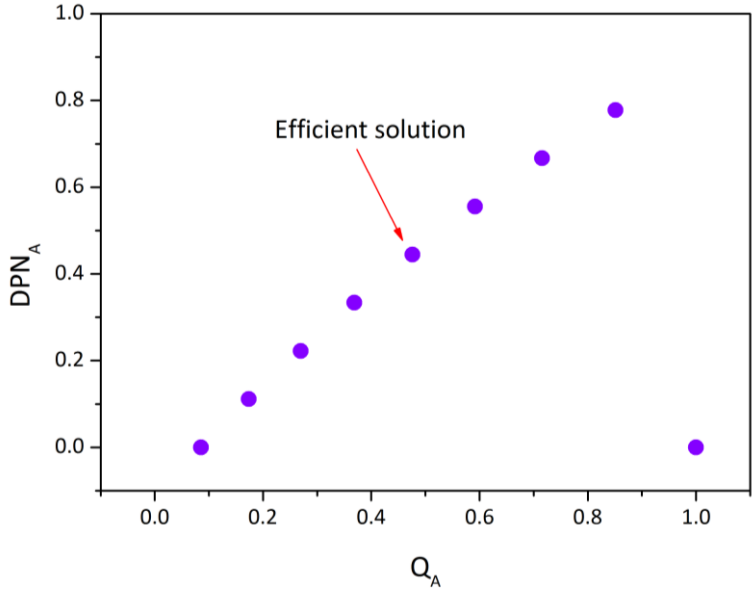

Figure 210. PFR Pareto frontier for PPS.

F.7.6 PPFPS 15/85

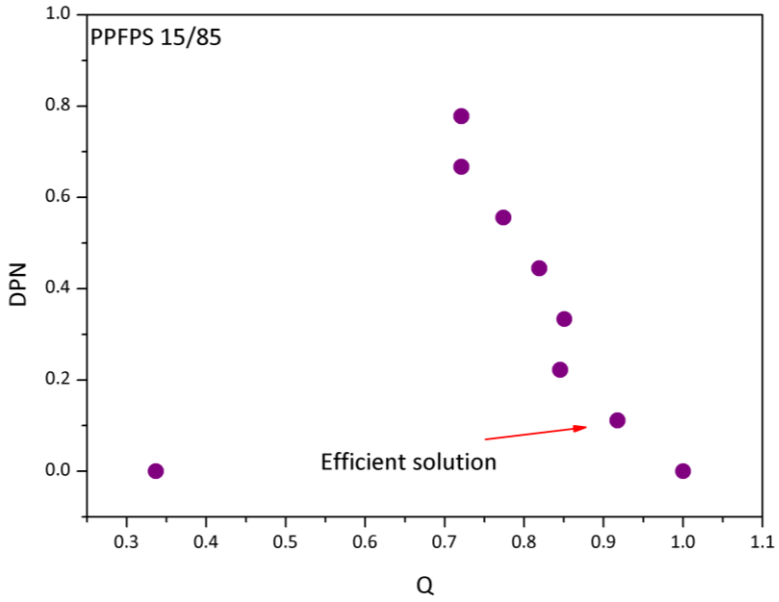

Figure 211. PFR Pareto frontier for PPFPS 15/85.

F.7.7 PPFPS 30/70

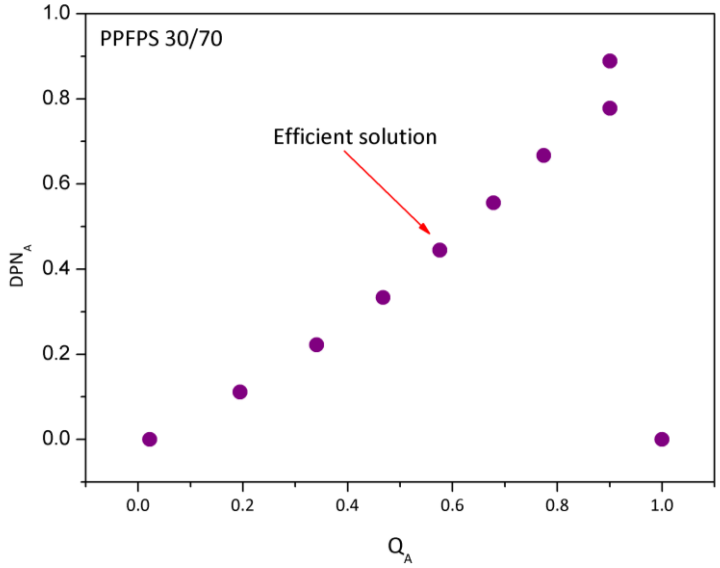

Figure 212. PFR Pareto frontier for PPFPS 30/70.

F.7.8 PPFPS 70/30

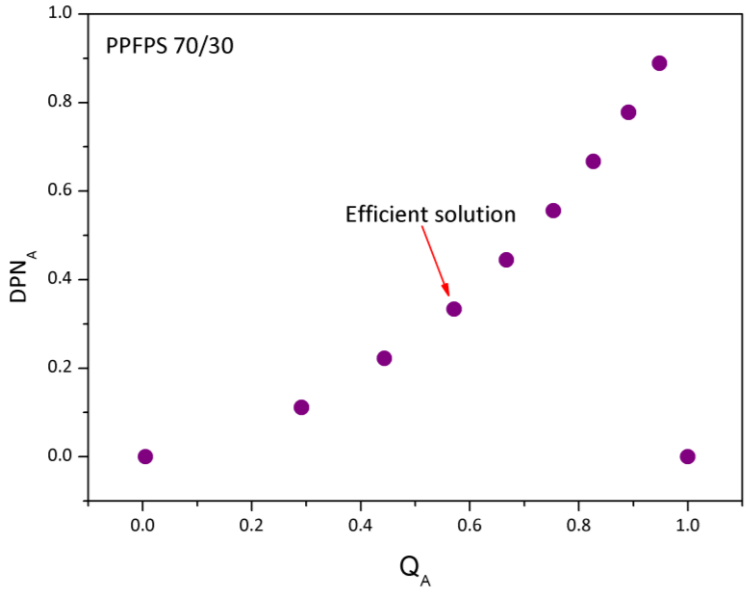

Figure 213. PFR Pareto frontier for PPFPS 70/30

F.7.9 PPFPS 85/15

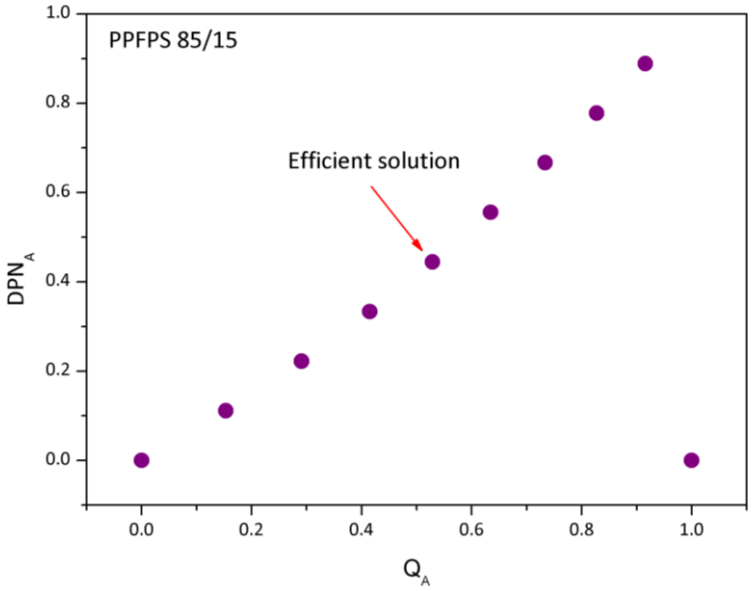

Figure 214. PFR Pareto frontier for PPFPS 85/15.

F.7.10 PET

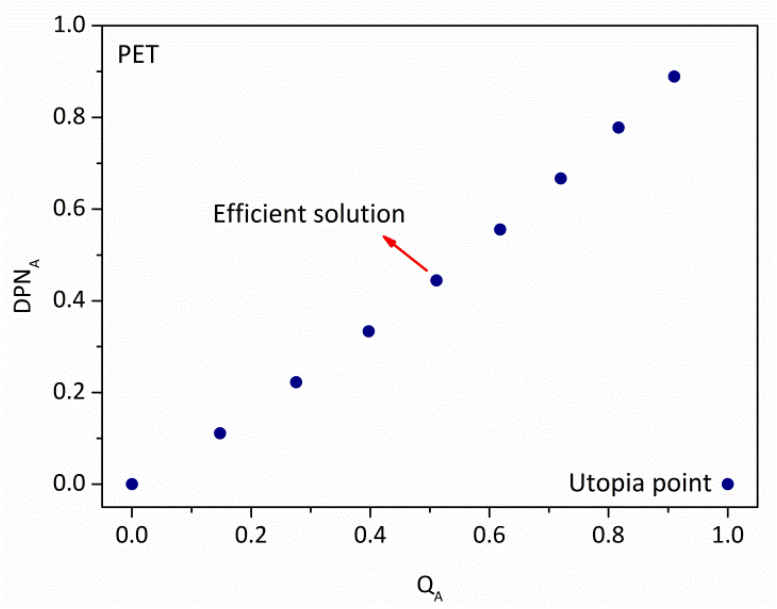

Figure 215. PFR Pareto frontier for PET.

F.8 M_n, DPN and segments' concentration profiles for PFR

F.8.1 PPeS

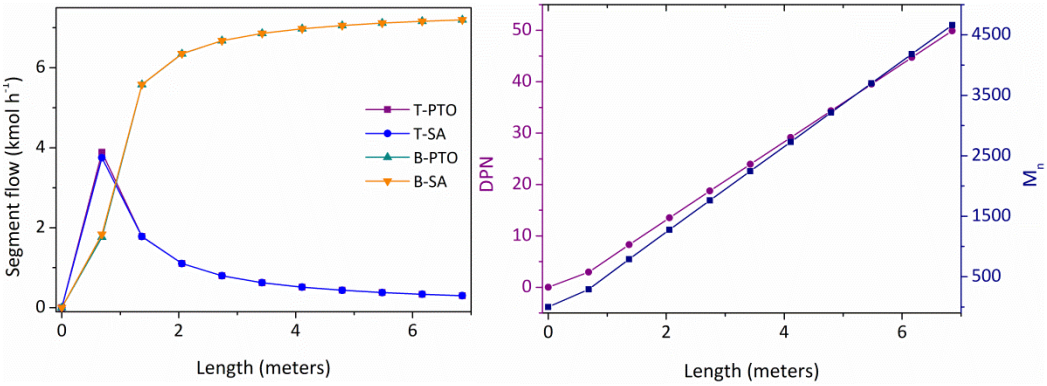

Figure 216. Segments' concentration, M_n and DPN profiles for PPeS (PFR).

F.8.2 PPeFS 15/85

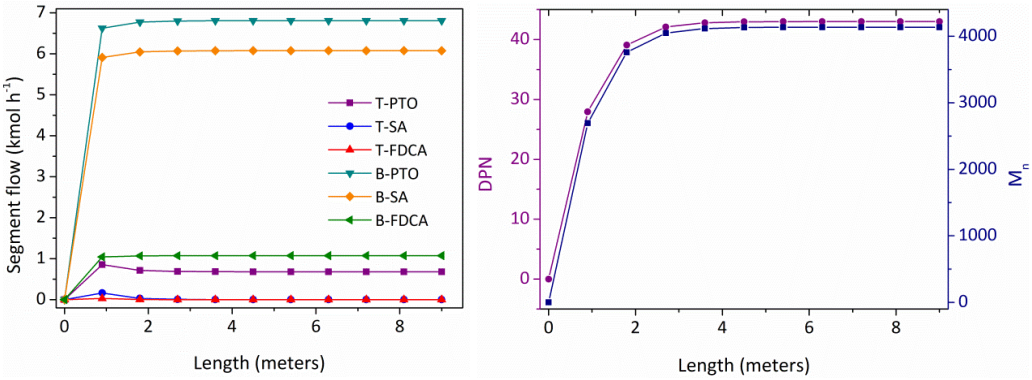

Figure 217. Segments' concentration, M_n and DPN profiles for PPeFS 15/85 (PFR).

F.8.3 PPeFS 70/30

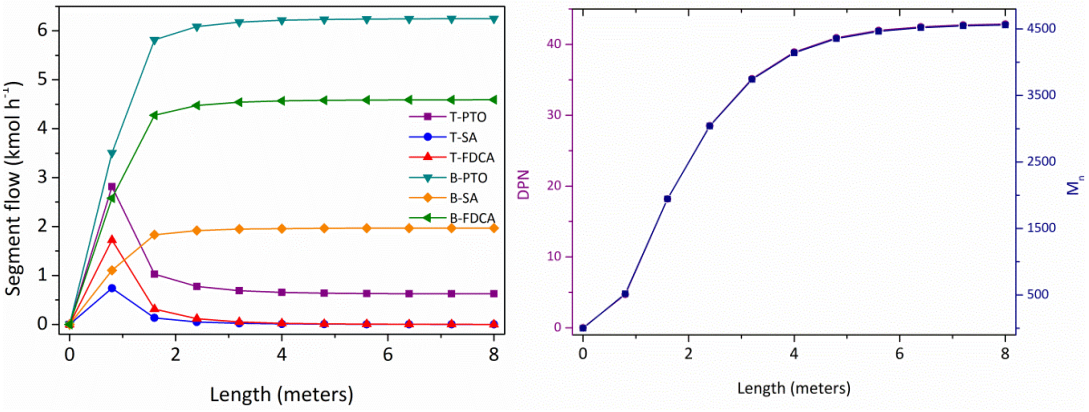

Figure 218. Segments' concentration, M_n and DPN profiles for PPeFS 70/30 (PFR).

F.8.4 PPeF

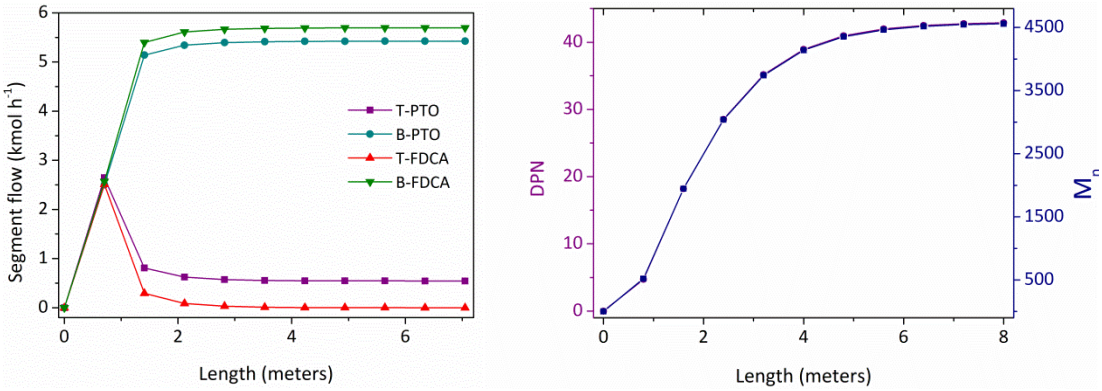

Figure 219. Segments' concentration, M_n and DPN profiles for PPeF (PFR).

F.8.5 PPS

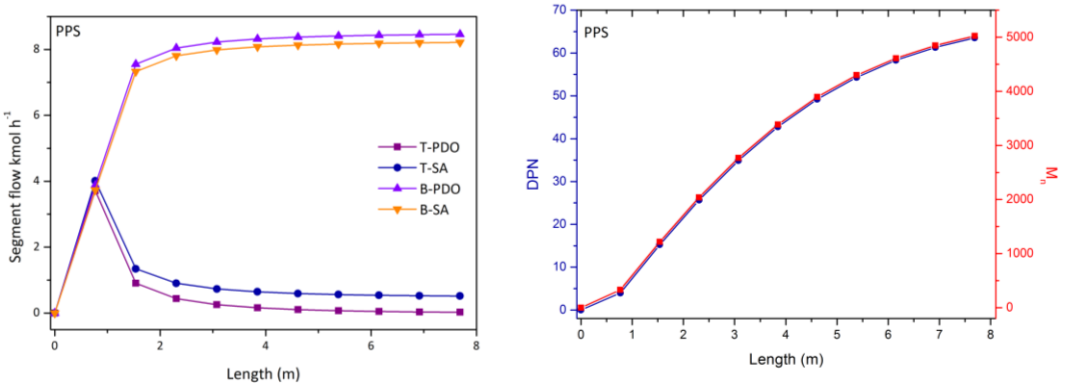

Figure 220. Segments' concentration, M_n and DPN profiles for PPS (PFR).

F.8.6 PPFPS 15/85

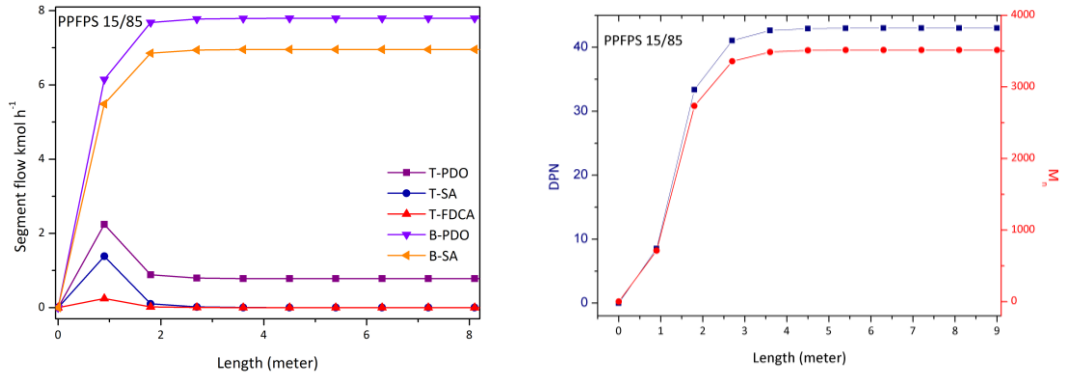

Figure 221. Segments' concentration, M_n and DPN profiles for PPFPS 15/85 (PFR).

F.8.7 PPFPS 30/70

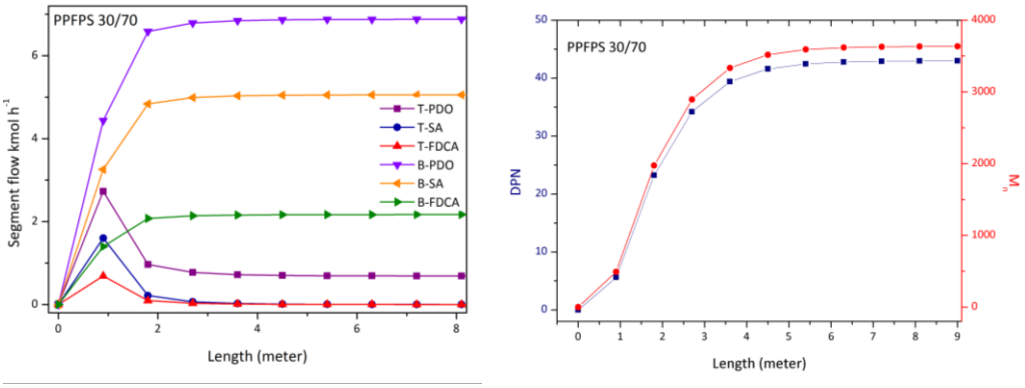

Figure 222. Segments' concentration, M_n and DPN profiles for PPFPS 30/70 (PFR).

F.8.8 PPFPS 70/30

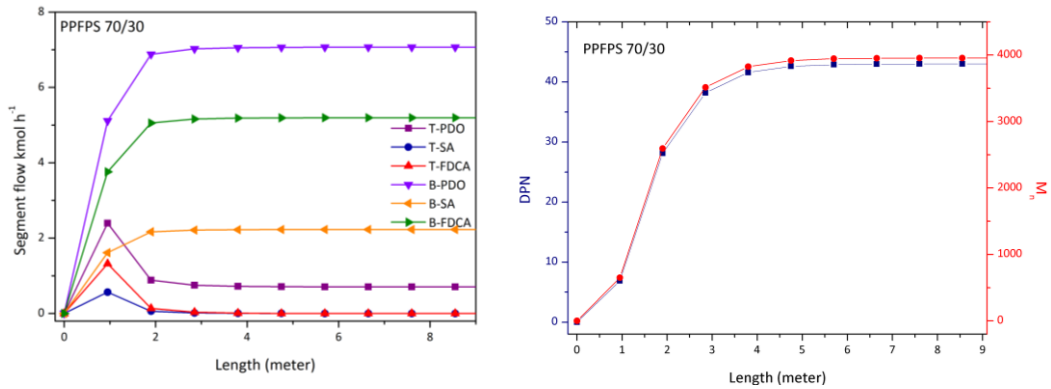

Figure 223. Segments' concentration, M_n and DPN profiles for PPFPS 70/30 (PFR).

F.8.9 PPFPS 85/15

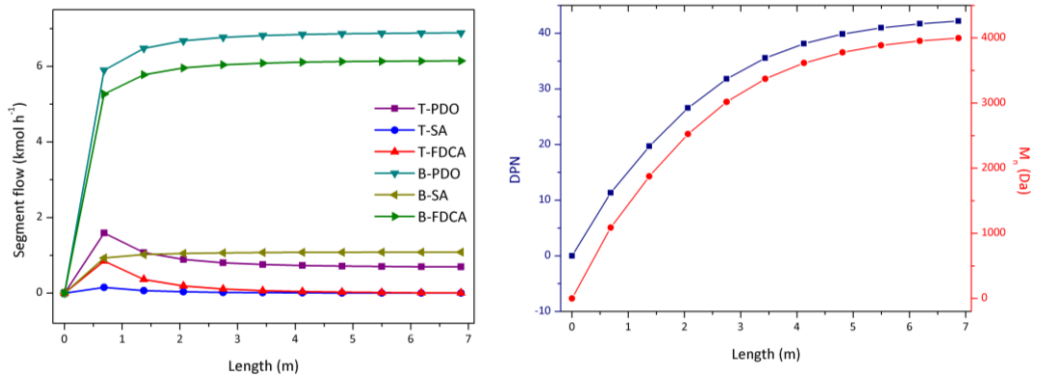

Figure 224. Segments' concentration, M_n and DPN profiles for PPFPS 85/15 (PFR).

F.8.10 PET

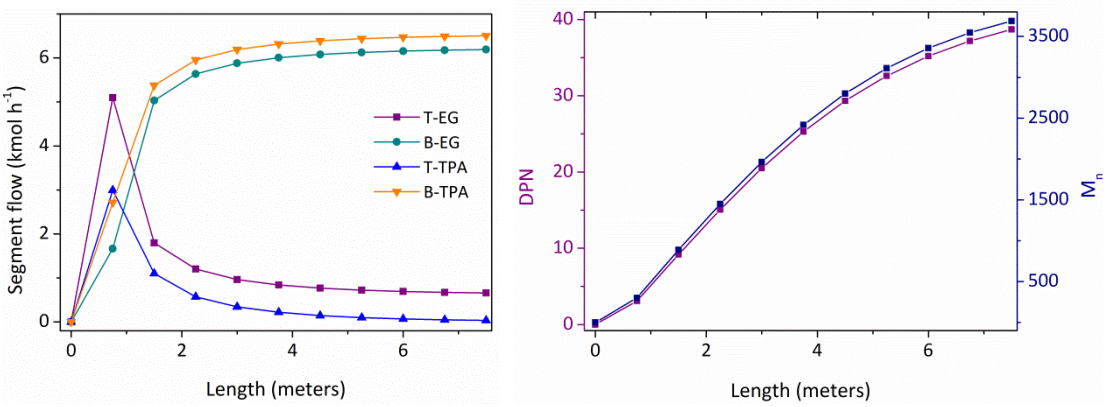

Figure 225. Segments' concentration, M_n and DPN profiles for PET (PFR).

F.9 M_n, DPN and segments' concentration profiles for reactive distillation

F.9.1 PPeS

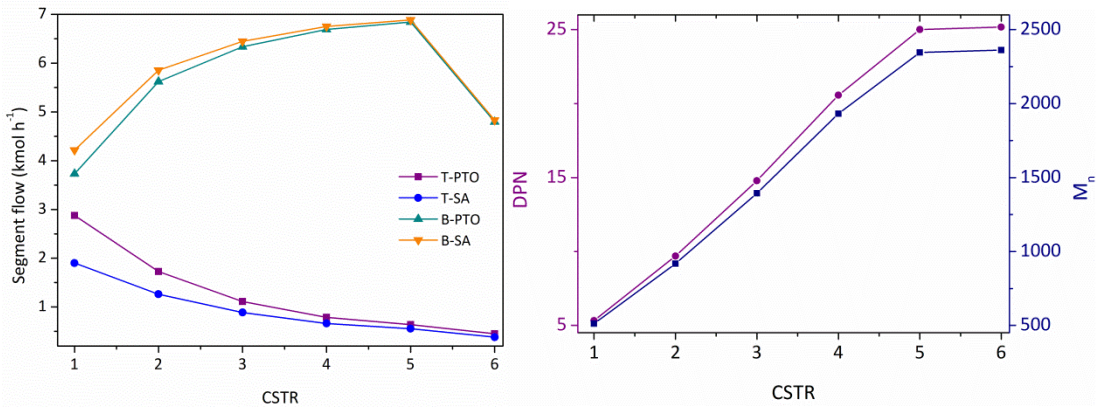

Figure 226. Segments' concentration, M_n and DPN profiles for PPeS (Reactive distillation).

F.9.2 PPeFS 15/85

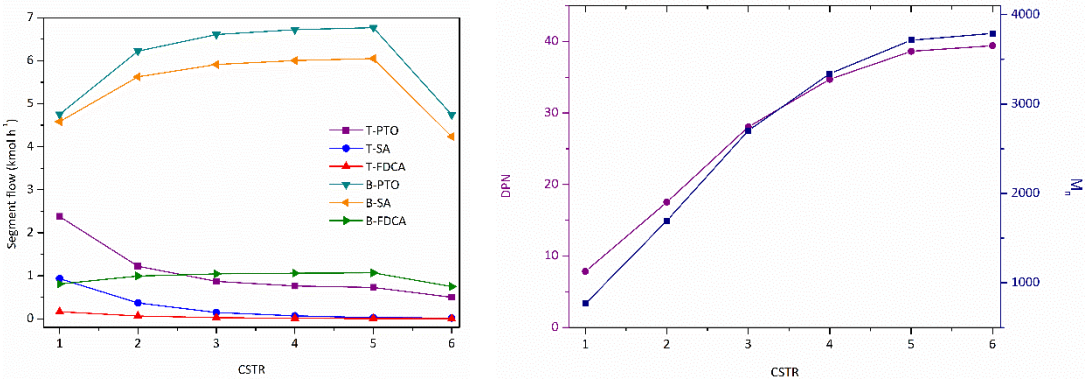

Figure 227. Segments' concentration, M_n and DPN profiles for PPeFS 15/85 (Reactive distillation).

F.9.3 PPeFS 30/70

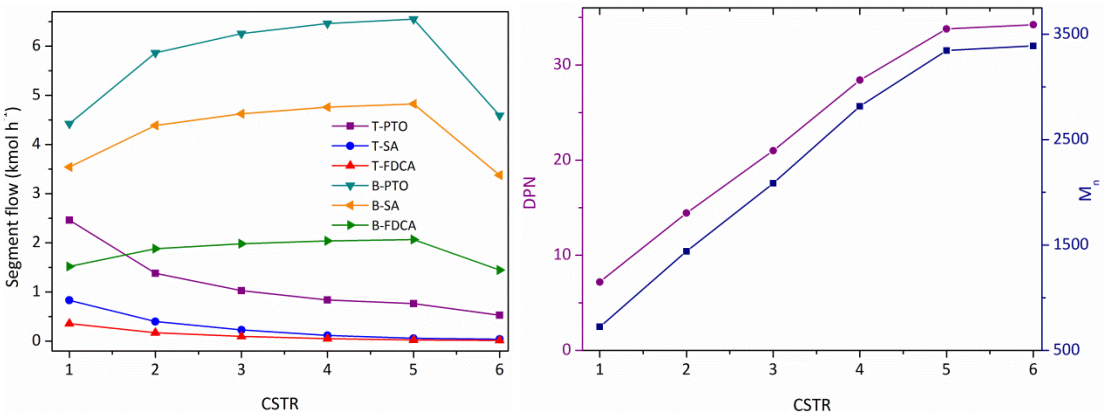

Figure 228. Segments' concentration, M_n and DPN profiles for PPeFS 30/70 (Reactive distillation).

F.9.4 PPeFS 85/15

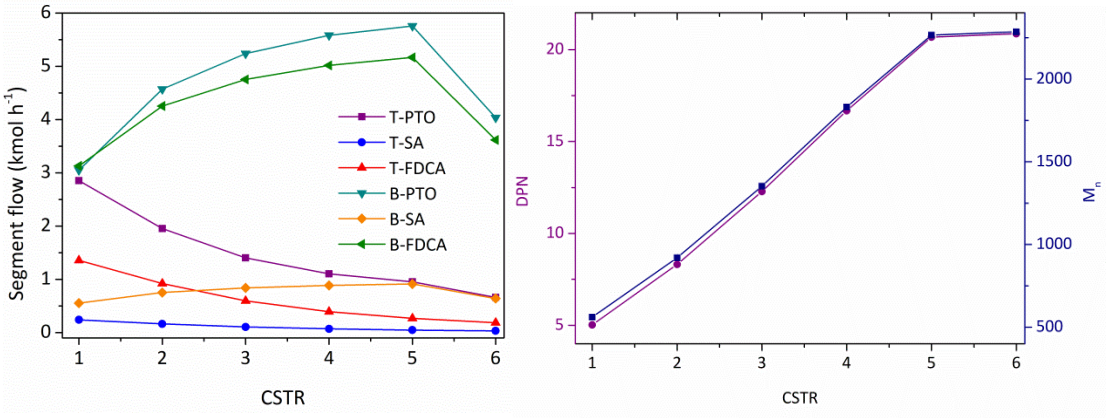

Figure 229. Segments' concentration, M_n and DPN profiles for PPeFS 85/15 (Reactive distillation).

F.9.5 PPeF

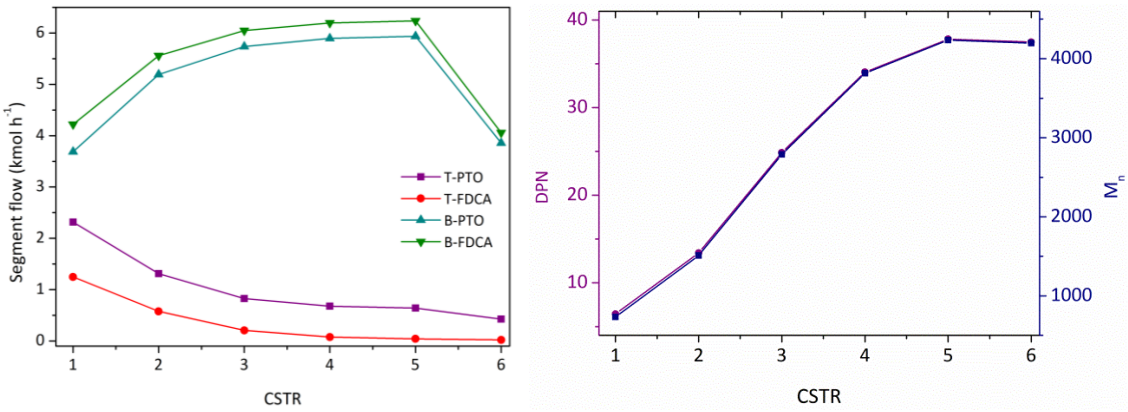

Figure 230. Segments' concentration, M_n and DPN profiles for PPF (Reactive distillation).

F.9.6 PPS

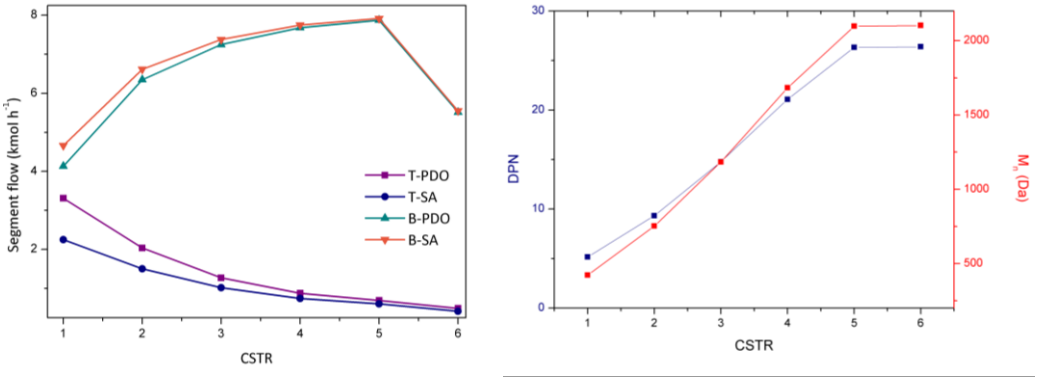

Figure 231. Segments' concentration, M_n and DPN profiles for PPS (Reactive distillation).

F.9.7 PPFPS 15/85

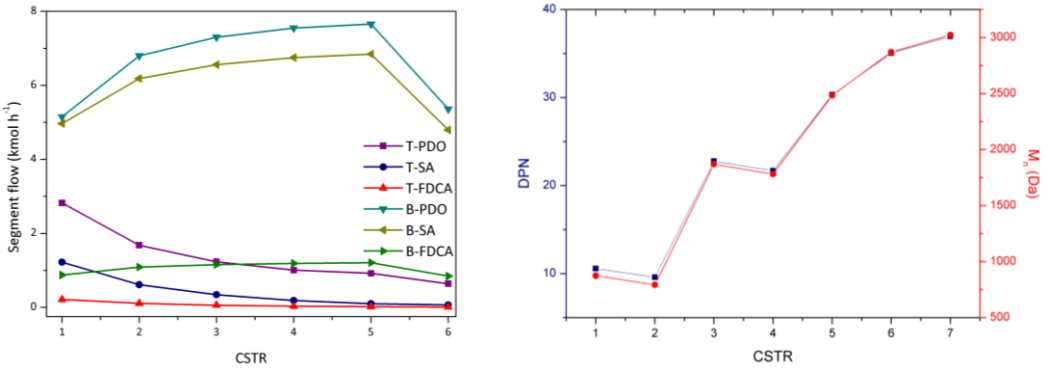

Figure 232. Segments' concentration, M_n and DPN profiles for PPFPS 15/85 (Reactive distillation).

F.9.8 PPFPS 30/70

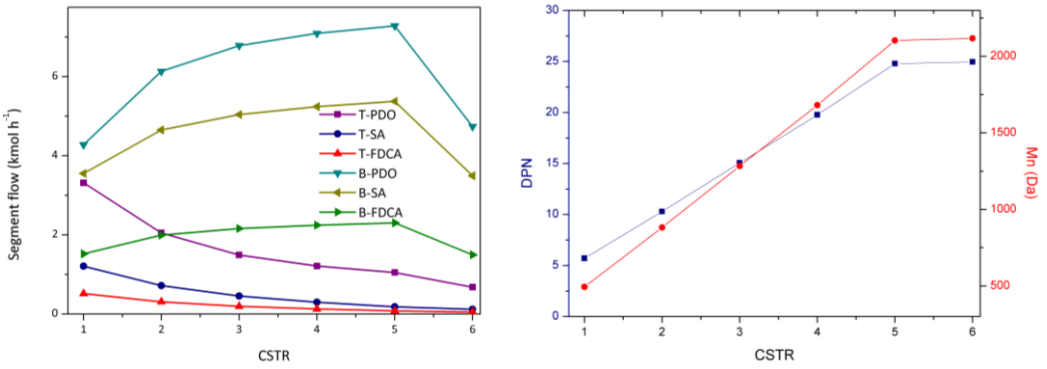

Figure 233. Segments' concentration, M_n and DPN profiles for PPFPS 30/70 (Reactive distillation).

F.9.9. PPFPS 70/30

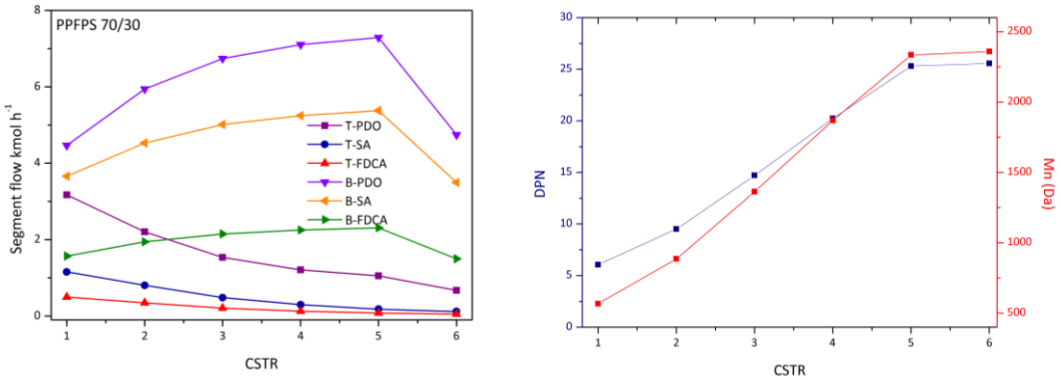

Figure 234. Segments' concentration, M_n and DPN profiles for PPFPS 70/30 (Reactive distillation).

F.9.10 PPFPS 85/15

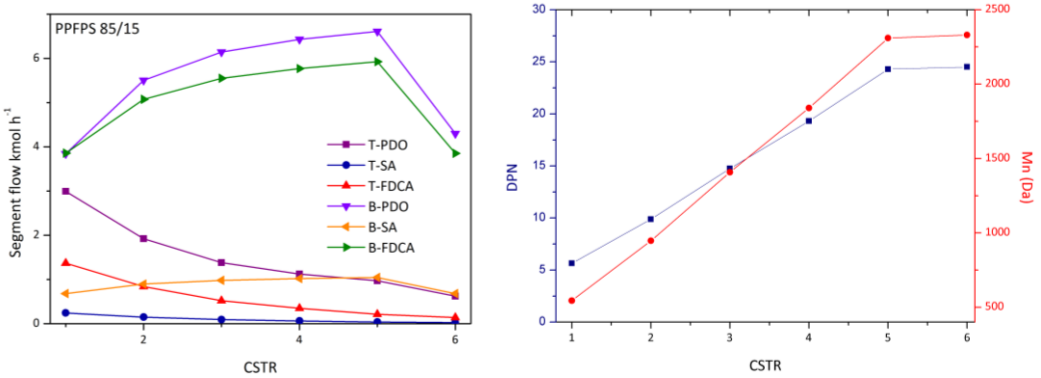

Figure 235. Segments' concentration, M_n and DPN profiles for PPFPS 85/15 (Reactive distillation).

F.9.11 PET

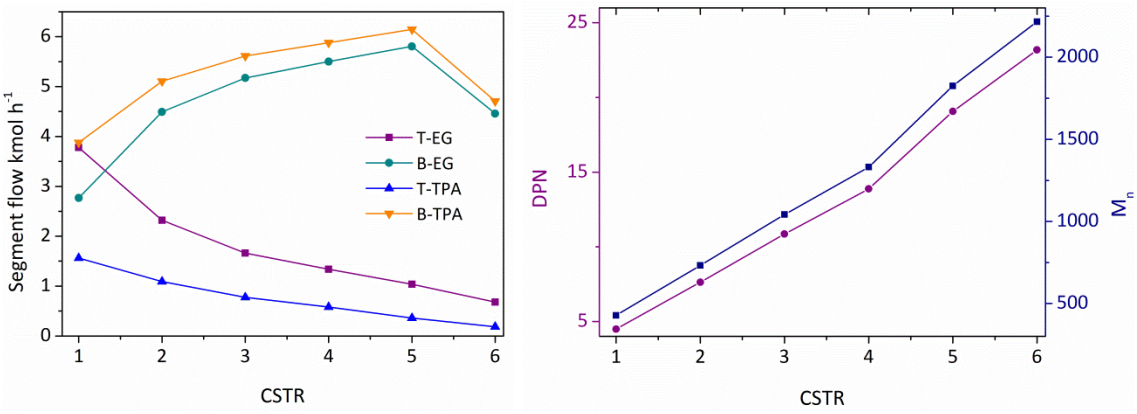

Figure 236. Segments' concentration, M_n and DPN profiles for PET (Reactive distillation).

F.10 Segments' concentration profiles for divided wall

F.10.1 PPeS

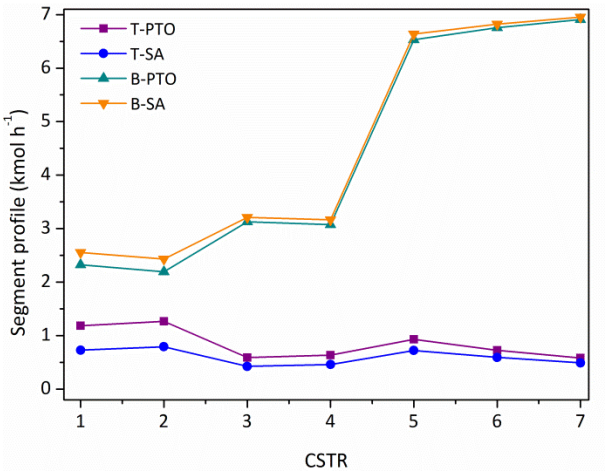

Figure 237. Segments' concentration profiles for PPeS (divided wall).

F.10.2 PPeFS 15/85

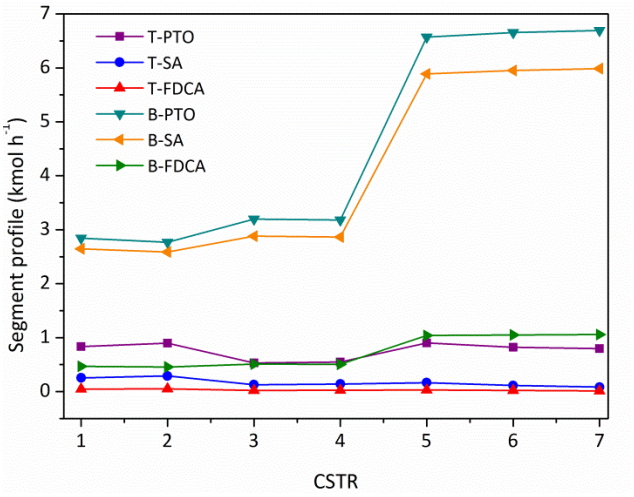

Figure 238. Segments' concentration profiles for PPeFS 15/85 (divided wall).

F.10.3 PPeFS 30/70

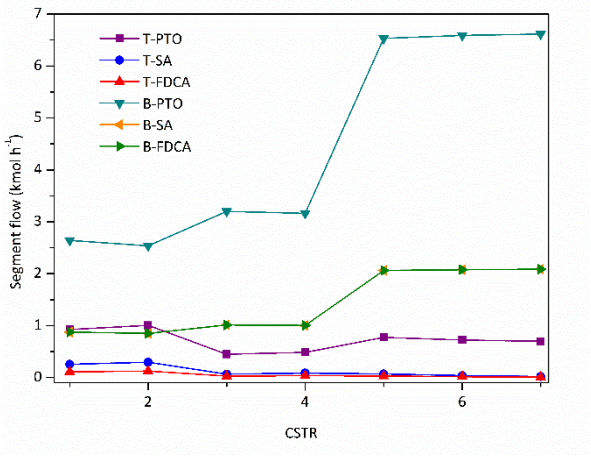

Figure 239. Segments' concentration profiles for PPeFS 30/70 (divided wall).

F.10.4 PPeFS 85/15

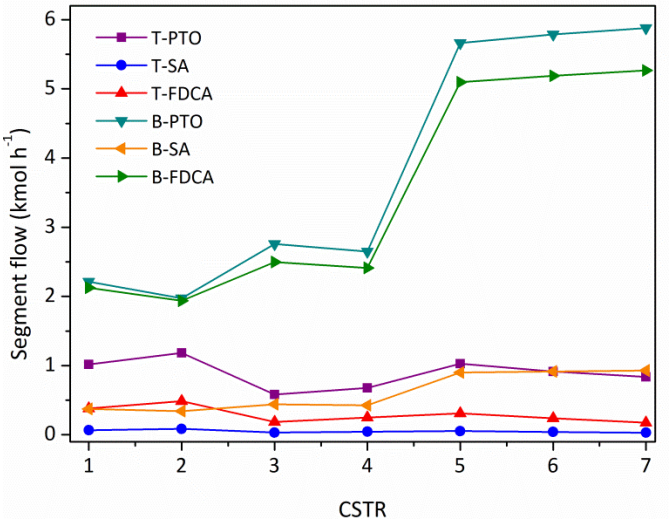

Figure 240. Segments' concentration profiles for PPeFS 85/15 (divided wall).

F.10.4 PPeF

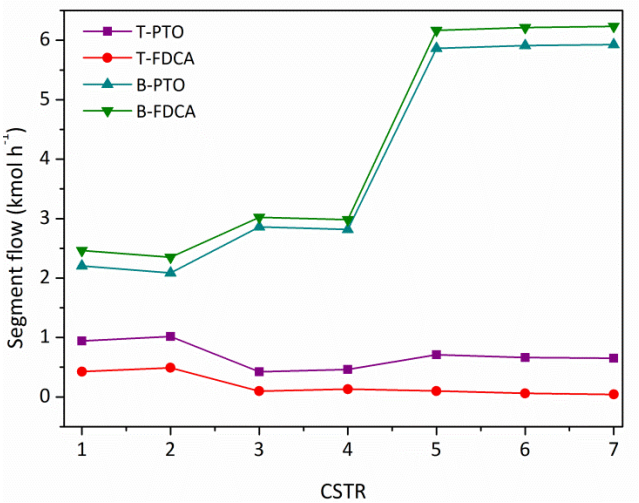

Figure 241. Segments' concentration profiles for PPeF (divided wall).

F.10.5 PET

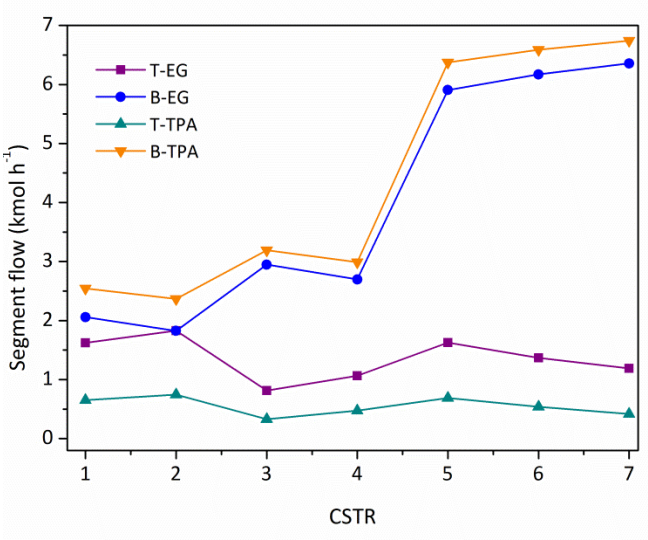

Figure 242. Segments' concentration profiles for PET (divided wall).

Appendix G (Chapter 8)

G.1 ^{13}C NMR and HSQC of polyester 12c

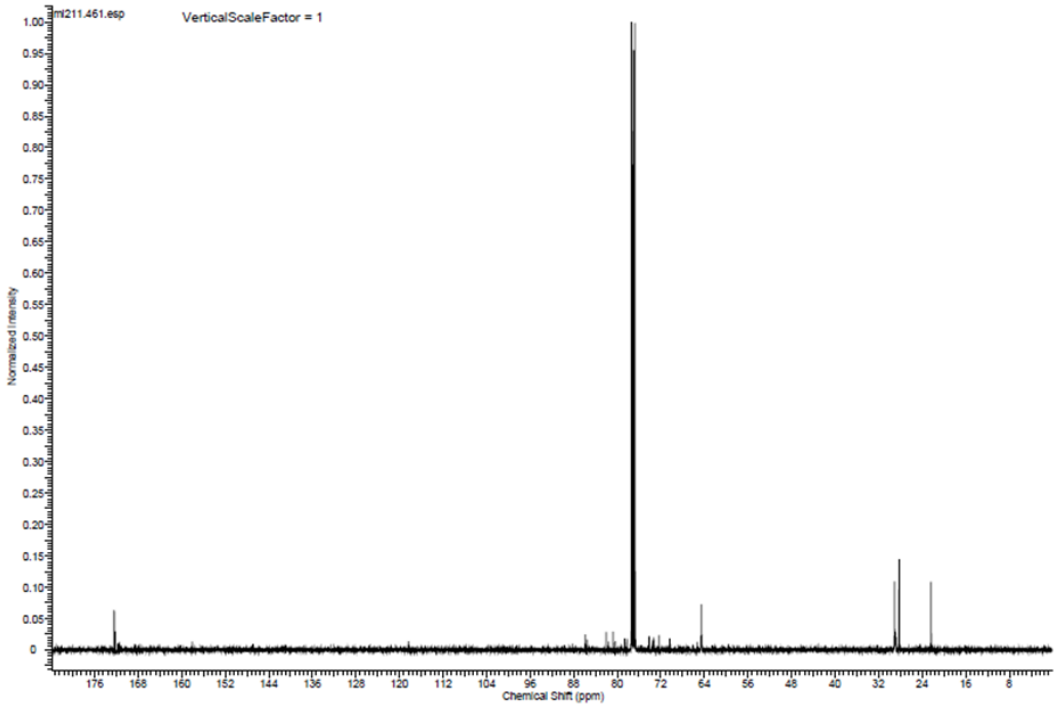

Figure 243. ^{13}C NMR of polyester **12c**.

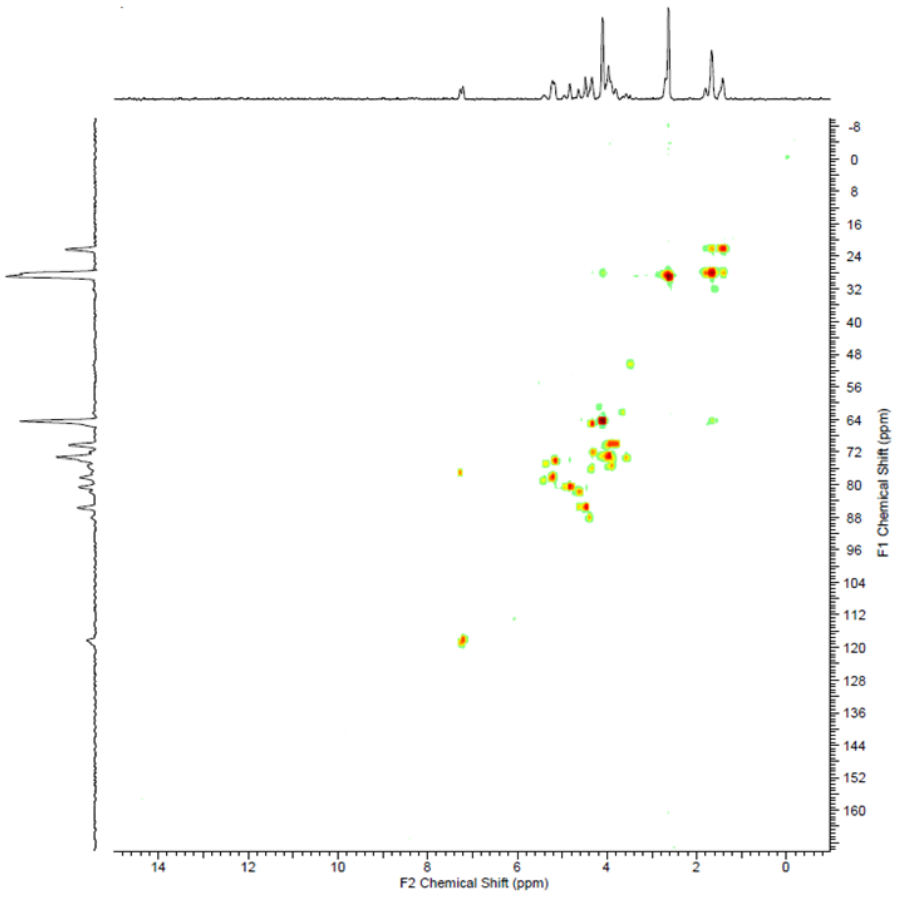

Figure 244. HSQC of polyester **12c**.

G.2 ^{13}C NMR and HSQC of polyester 14c

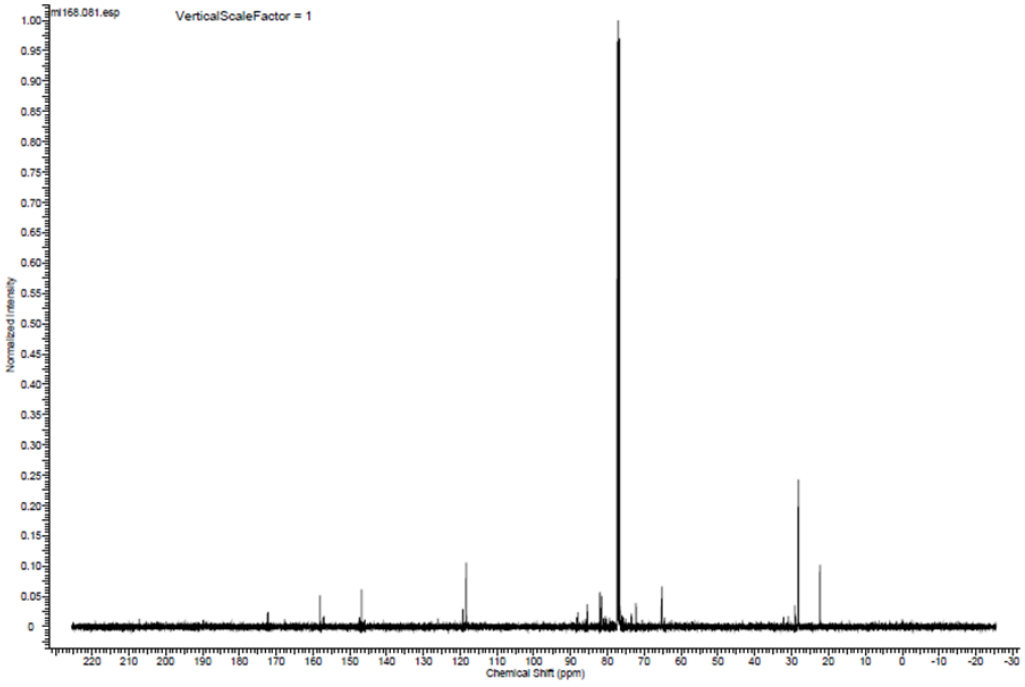

Figure 245. ^{13}C NMR of polyester **14c**.

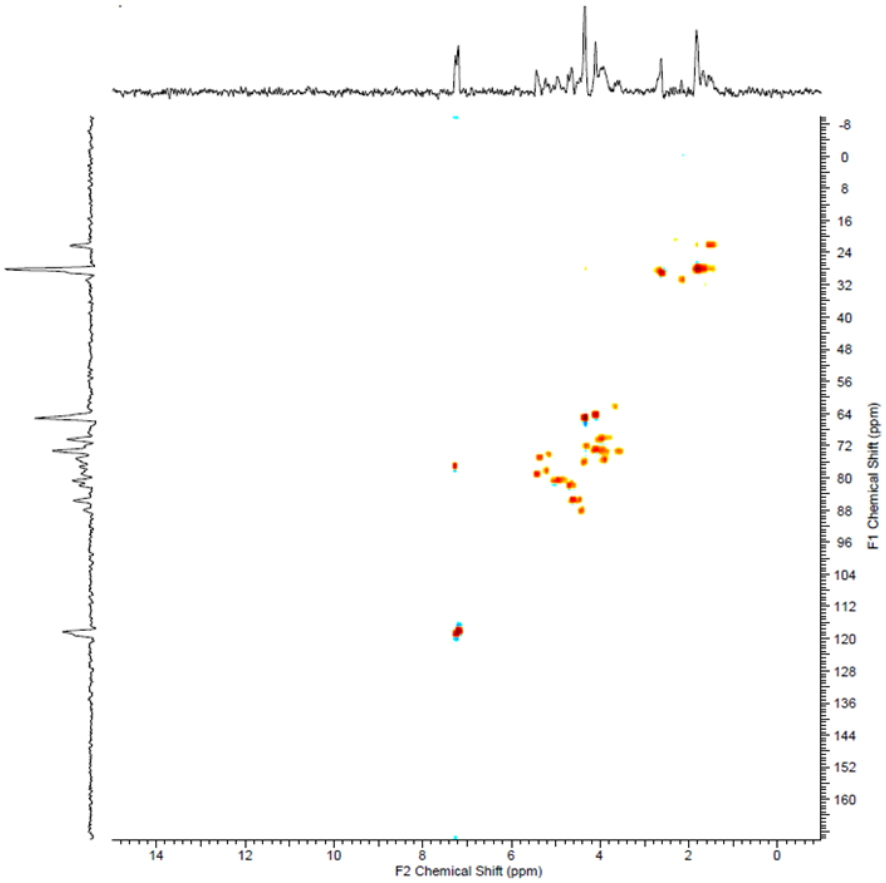

Figure 246. HSQC of polyester **14c**.

G.3 GPC chromatogram of polyesters PPeFIS (12b-15b) with 30 mol% IS

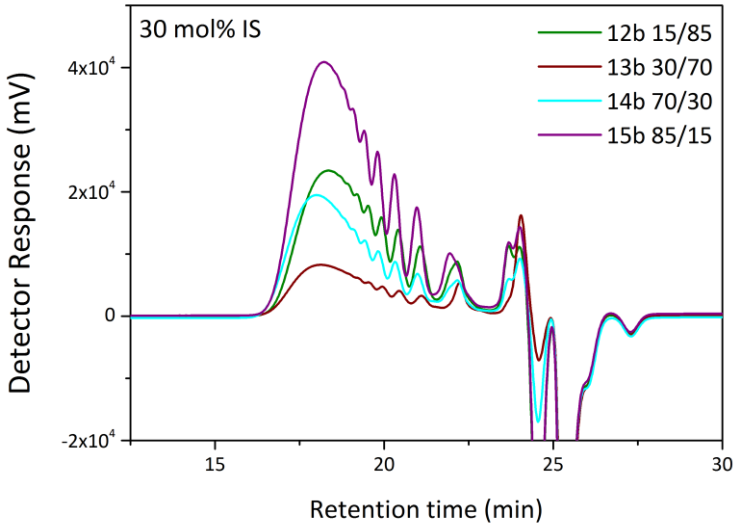

Figure 247. GPC chromatogram of polyesters PPeFIS (**12b-15b**) with 30 mol% IS.

G.4 GPC chromatogram of polyesters PPeFIS (12c-15c) with 50 mol% IS

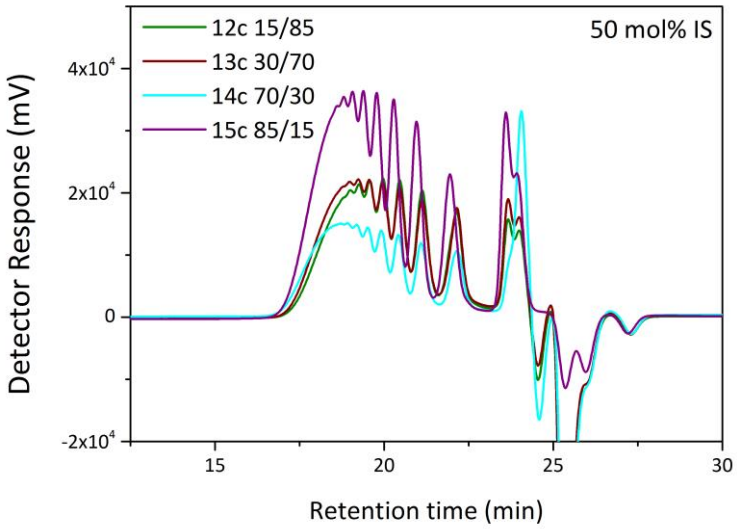

Figure 248. GPC chromatogram of polyesters PPeFIS (**12c-15c**) with 50 mol% IS.

G.5 GPC chromatogram of polyesters PPeIS (11)

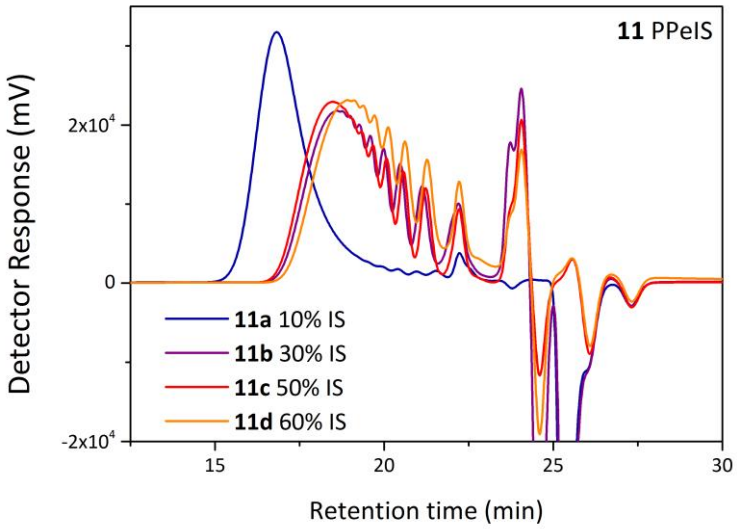

Figure 249. GPC chromatogram of polyesters PPeIS (**11**).

G.6 GPC chromatogram of polyesters PPFIS (8)

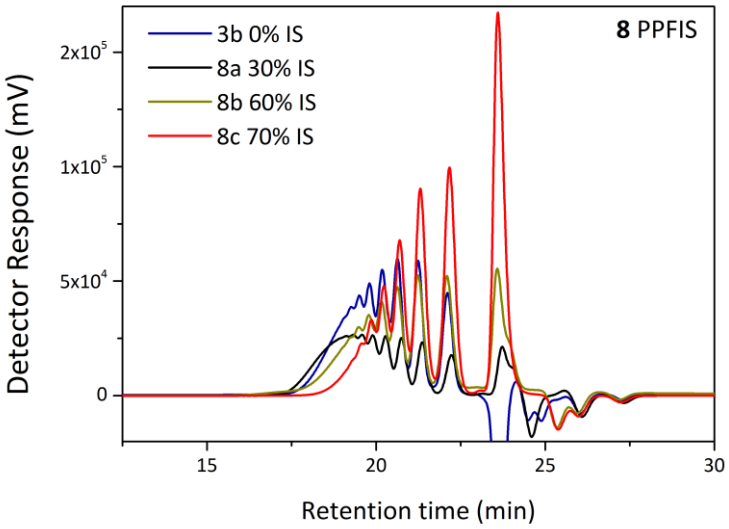

Figure 250. GPC chromatogram of polyesters PPFIS (**8**).

G.7 DSC first heating scan of polyesters PPeIS (11)

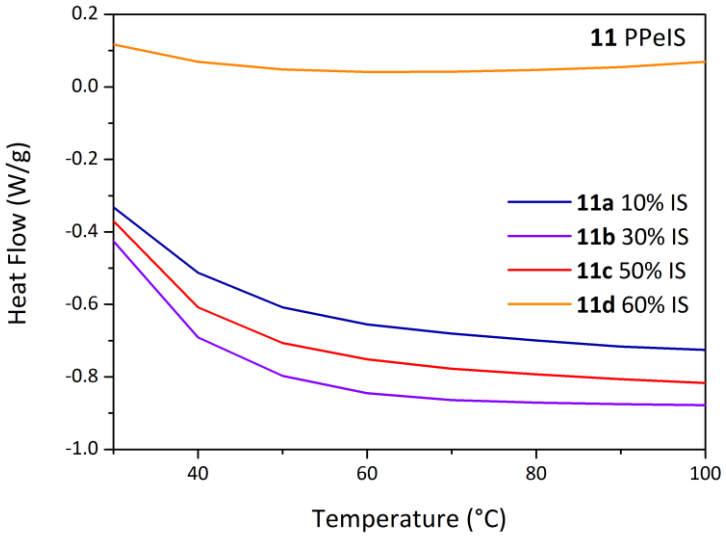

Figure 251. DSC first heating scan of polyesters PPeIS (**11**).

G.8 DSC second heating scan of polyesters PPeIS (11)

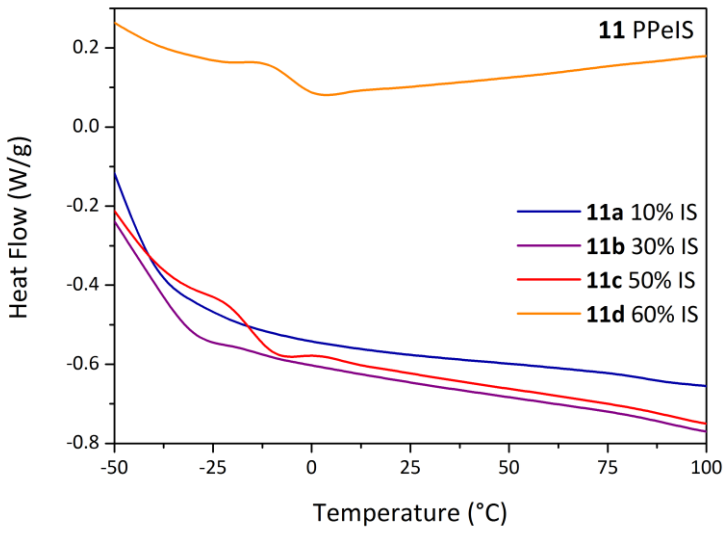

Figure 252. DSC second heating scan of polyesters PPeIS (**11**).

G.9 T_g-M_n-IS relationship for PPeFIS 15/85 (12)

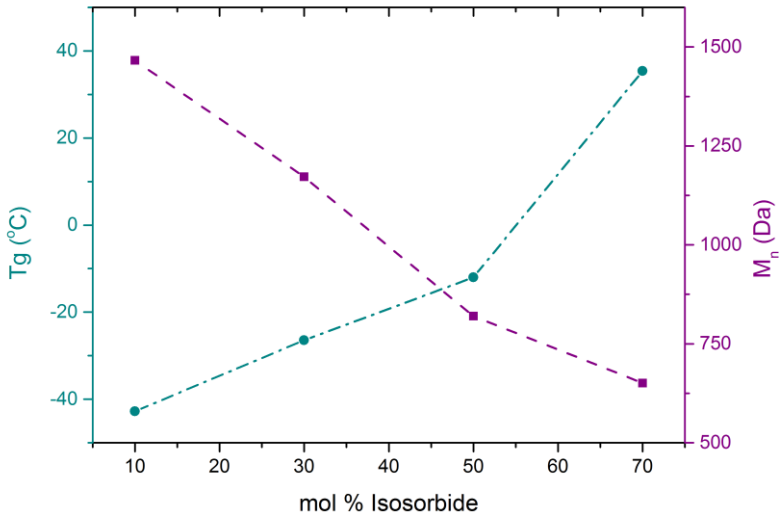

Figure 253. T_g-M_n-IS relationship for PPeFIS 15/85 (**12**).

G.10 T_g-M_n-IS relationship for PPeFIS 30/70 (13)

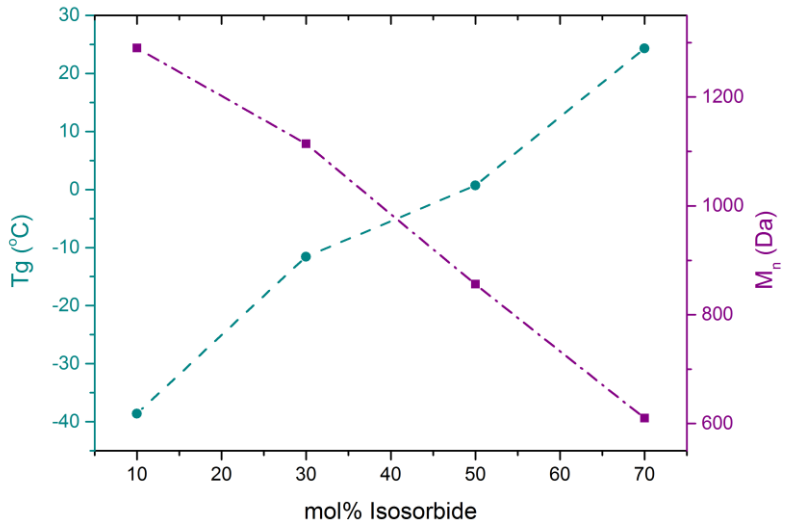

Figure 254. T_g-M_n-IS relationship for PPeFIS 30/70 (**13**).

G.11 DSC second heating scan of polyesters PPFIS 30/70 (8)

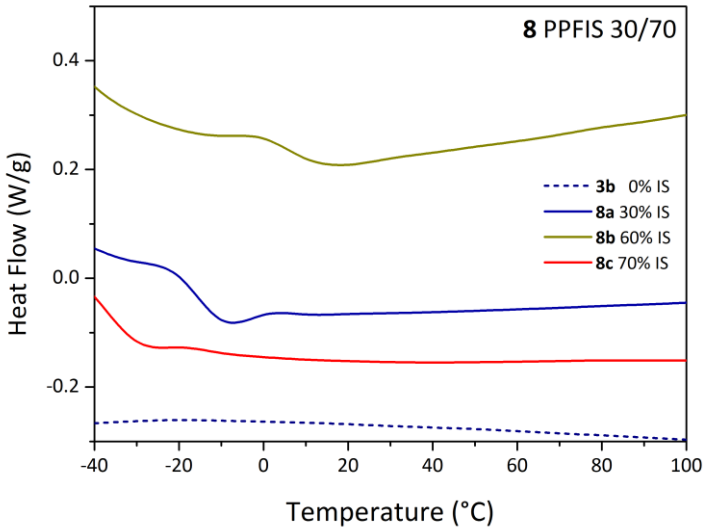

Figure 255. DSC second heating scan of polyesters PPFIS 30/70 (**8**).

G.12 DSC first heating scan of polyesters PPFIS 70/30 (9)

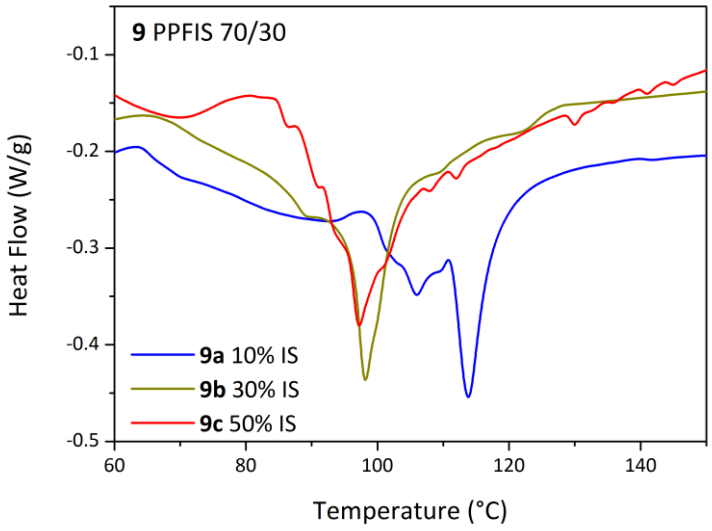

Figure 256. DSC first heating scan of polyesters PPFIS 70/30 (**9**).

G.13 DSC second heating scan of polyesters PPFIS 85/15 (10)

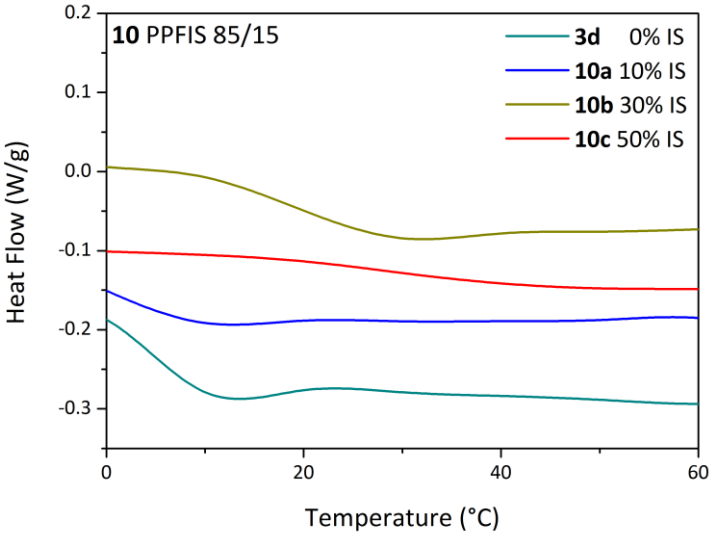

Figure 257. DSC second heating scan of polyesters PPFIS 85/15 (**10**).

G.14 GPC chromatogram of polyester PPeIa (17)

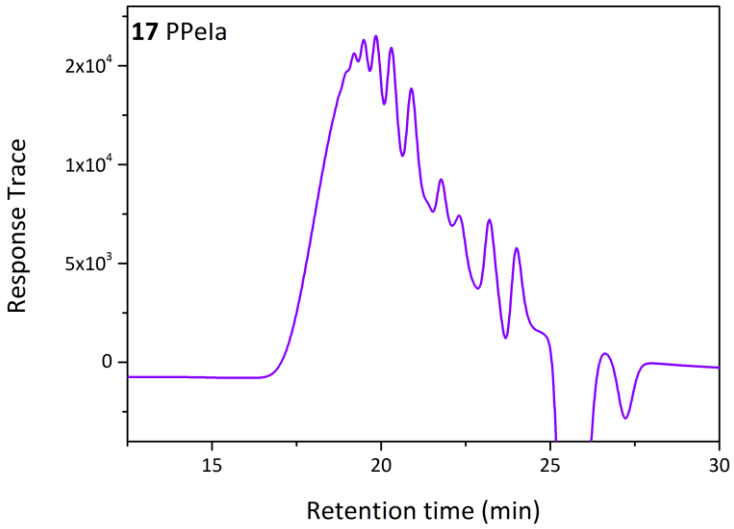

Figure 258. GPC chromatogram of polyester PPeIa (**17**).

G.15 DSC second heating scan of polyester PPeIa (17)

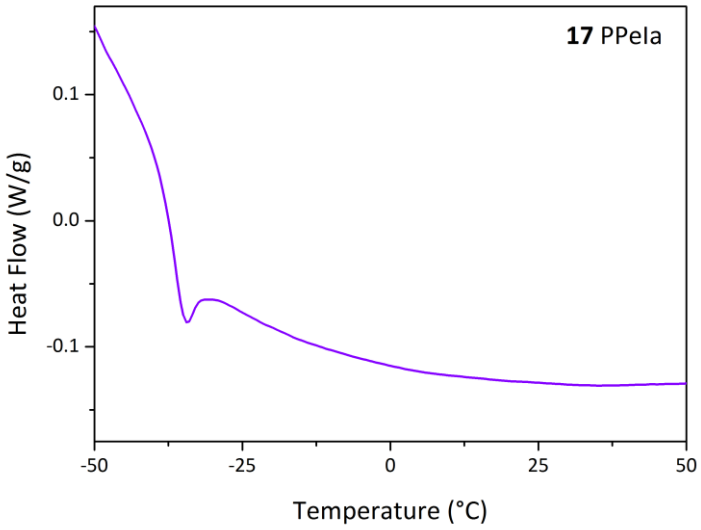

Figure 259. DSC second heating scan of polyester PPeIa (**17**).

Appendix H (Chapter 8)

H.1 Acid value for PPFIS ($mg_{KOH} \cdot g_{resin}^{-1}$)

Table 86. Acid value for PPFIS polyesters

PPFIS 15/85			
Time, h	**7a**	**7b**	**7c**
0	64.99	102.49	119.18
0.5	41.35	60.32	75.61
1	25.05	46.91	59.4
1.5	19..97	32.06	45.92
2	16.29	34.64	44
2.5	13.48	34.89	38.32
3	8.65	20.97	26.53
3.5	6.82	18.19	
4	6.52	17.49	22.62
4.5	6.46	12.36	-
5	6.21	11.79	15.68
5.5	5.57	14.54	-
6	4.38	13.07	9.49
6.5	4.99	9.29	-
7	4.97	8.51	10.49
PPFIS 30/70			
Time, h	**8a**	**8b**	**8c**
0	69.31		102.94
0.5	40.11		75.4
1	28.05		60.24
1.5	21.06		52.2
2	17.77		40.18
2.5	13.46		36.78
3	10.49		44.27
3.5	9.52		41.84
4	4.67		39.20
4.5	5.71		31.06
5	4.61		29.5
5.5	4.14		29.05
6	4.01		28.10
6.5	2.79		27.06
7	-		25.44
PPFIS 70/30			
Time, h	**9a**	**9b**	**9c**
0	118.52	73.68	95.07
0.5	72.13	46.41	68.74
1	48.52	33.94	51.69
1.5	40.52	23.29	45.68
2	31.52	19.55	34.98
2.5	27.50	15.05	24.74
3	26.18	-	15.07
3.5	20.64	10.75	9.89
4	17.09	10.63	8.63
4.5	14.02	7.33	2.66
5	10.95	5.0	1.69
5.5	7.93	4.38	-
6	5.91	4.16	-
6.5	4.88	-	-
7	2.18	-	-

PPFIS 85/15

Time, h	10a	10b	10c
0	109.8	65.65	136.71
0.5	35.78	47.25	-
1	-	34.38	-
1.5	14.11	26.55	-
2	-	21.69	-
2.5	8.66	18.12	27.88
3	7.89	-	-
3.5	-	-	-
4	4.25	20.94	-
4.5	4.13	15.06	-
5	3.15	6.3	-
5.5	-	8.58	-
6	1.98	-	-
6.5	-	-	-
7	1.89	4	-

H.2 Acid value for PPeIS and PPeFIS ($mg_{KOH} \cdot g_{resin}^{-1}$)

Table 87. Acid value for PPeIS and PPeFIS polyesters

		PPeIS		
Time, h	**11a**	**11b**	**11c**	**11d**
0	106.50	137.13	155.62	167.69
0.5	67.82	64.19	78.6	117
1	53.83	46.17	57.85	78.13
1.5	41.99	33.77	42.3	62.79
2	37.15	25.42	35.86	51.47
2.5	30.71	20.35	25.81	48.49
3	28.28	17.24	17.4	41.81
3.5	19.58	15.38	11.34	41.36
4	18.07	7.97	9.54	34.76
4.5	16.78	14.26	3.31	33.37
5	14.20	12.64	2.96	32.39
5.5	11.69	10.92	1.99	33.17
6	-	9.21	2.64	32.15
6.5	-	8.99	1.4	29.7
7	-	7.61	1.6	24.76
		PPeFIS 15/85		
Time, h	**12a**	**12b**	**12c**	**12d**
0	86.64	90.83	87.47	99.10
0.5	56.75	57.45	62.65	62.92
1	29.75	45.8	49.09	50.35
1.5	22.14	41.2	30.37	38.06
2	19.43	33.72	23.28	34.94
2.5	17.70	26.32	20.28	24.93
3	16.21	19.02	19.88	17.98
3.5	11.54	17.68	16.52	13.42
4	9.30	14.98	13.95	12.17
4.5	4.49	11.87	0.17	7.79
5	2.78	7.24	10.31	4.64
5.5	2.49	6.53	9.65	3.60
6	2.38	5.34	7.65	2.99
6.5	2.29	4.34	7.52	2.44
7	0.87	4.57	7.08	-

	PPeFIS 15/85	PPeFIS 30/70		
Time, h	**12e**	**13a**	**13b**	**13c**
0	113.95	90.83	95.65	116.59
0.5	80.14	57.45	68.77	70.49
1	56.81	45.80	48.62	59.14
1.5	39.42	41.20	38.24	42.08
2	35.23	33.73	27.43	37.63
2.5	29.96	26.32	23.38	31.39
3	28.65	19.02	19.65	26.79
3.5	24.34	17.68	17.02	24.96
4	21.74	14.98	20.90	19.73
4.5	17.77	11.87	16.66	15.57
5	17.49	7.26.534	16.46	12.95
5.5	16.61	5.34	12.41	11.16
6	10.55	4.35	11.04	8.63
6.5	9.44	4.57	-	-
7	-	-	-	-

	PPeFIS 30/70		PPeFIS 70/30	
Time, h	**13d**	**13e**	**14a**	**14b**
0	88.91	-	52.36	61.13
0.5	58.22	-	29.75	50.17
1	34.91	-	19.88	34.23
1.5	16.83	-	11.84	17.50
2	14.48	-	7.76	14.36
2.5	8.98	-	4.63	
3	6.06	-	4.14	10.28
3.5	14.48	-	3.40	10.13
4	5.80		2.63	9.12
4.5	11.22	-	2.45	8.82
5	4.55	-	1.62	6.76
5.5	7.01	-		5.49
6	5.10	-	1.33	3.13
6.5	3.70	-	1.30	-
7	3.91	-	-	-

	PPeFIS 30/70		PPeFIS 85/15	
Time, h	**14c**	**15a**	**15b**	**15c**
0	83.59	58.61	81.03	86.56
0.5	42.9	30.43	53.96	78.01
1	34.93	21.60	38.55	44.24
1.5	25.09	16.77	28.76	20.43
2	21.97	9.45	25.96	16.49
2.5	19.54	8.10	17.42	14.48
3	17.09	7.48	15.32	14.2
3.5	25.48	6.50	14.52	15.31
4	18.94	3.45	11.76	13.18
4.5	12.99	2.99	8.11	10.85
5	8.71	2.00	8.72	12.4
5.5	7.68	1.10	6.23	-
6	7.18	-	5.9	-
6.5	7.11	0.81	4.91	-
7	5.91	-	3.21	8.24